AMC PAMPHLET AMCP 706-160

RESEARCH AND DEVELOPMENT OF MATERIEL

ENGINEERING DESIGN HANDBOOK

ELEMENTS OF TERMINAL BALLISTICS

PART ONE, INTRODUCTION, KILL MECHANISMS AND VULNERABILITY

See inside back cover for information on previous publications.

HEADQUARTERS, U.S. ARMY MATERIEL COMMAND NOVEMBER 1962

AD389219

Elements of Terminal Ballistics. Part One. Introduction, Kill Mechanisms and Vulnerability. Engineering Design Handbook

ARMY MATERIEL COMMAND ALEXANDRIA VA

NOV 1962

Redistribution Of DTIC-Supplied Information Notice

As a condition for obtaining DTIC services, all information received from DTIC that is not clearly marked for public release will be used only to bid or perform work under a U.S. Government contract or grant or for purposes specifically authorized by the U.S. Government agency that sponsored the access. Furthermore, the information will not be published for profit or in any manner offered for sale.

Reproduction Quality Notice

We use state-of-the-art, high-speed document scanning and reproduction equipment. In addition, we employ stringent quality control techniques at each stage of the scanning and reproduction process to ensure that our document reproduction is as true to the original as current scanning and reproduction technology allows. However, the following original document conditions may adversely affect Computer Output Microfiche (COM) and/or print reproduction:

- Pages smaller or larger than 8.5 inches x 11.0 inches.
- Pages with background color or light colored printing.
- Pages with smaller than 8 point type or poor printing.
- Pages with continuous tone material or color photographs.
- Very old material printed on poor quality or deteriorating paper.

If you are dissatisfied with the reproduction quality of any document that we provide, particularly those not exhibiting any of the above conditions, please feel free to contact our Directorate of User Services at (703) 767-9066/9068 or DSN 427-9066/9068 for refund or replacement.

Do Not Return This Document To DTIC

UNCLASSIFIED

AD NUMBER

Ø389 219

CLASSIFICATION CHANGES

TO UNCLASSIFIED

FROM CONFIDENTIAL

AUTHORITY

USAMDRC Ltr, 16 Mar 1976

THIS PAGE IS UNCLASSIFIED

UNCLASSIFIED

HEADQUARTERS
UNITED STATES ARMY MATERIEL COMMAND
WASHINGTON 25, D. C.

30 November 1962

AMCP 706-160 (S), Elements of Terminal Ballistics, Part One, Introduction, Kill Mechanisms, and Vulnerability (U), forming part of the Army Materiel Command Engineering Design Handbook Series, is published for the information and guidance of all concerned.

FRED P. CAMPBELL
Brigadier General, USA
Chief of Staff

OFFICIAL:

H. E. ALPHIN
Colonel, GS
Chief, Administrative Office

DISTRIBUTION: Special

UNCLASSIFIED

FOREWORD

The three handbooks devoted to Elements of Terminal Ballistics are part of a group of handbooks covering the engineering information and quantitative data needed in the design and construction of Army materiel, which (as a group) constitutes the Engineering Design Handbook Series.

The handbooks on Elements of Terminal Ballistics present information on the fundamental principles governing the behavior of ammunition in its final phase. Ammunition is produced with a great variety of final purposes in mind, and the designer must direct his endeavors toward obtaining the desired effects to the greatest possible degree within the limitations which consideration of weight, bulk, and safety impose. Any improvement in the effectiveness of ammunition will be reflected directly in reduction in the time and quantity required for accomplishment of any mission, and may be sufficient to make the difference between defeat or victory.

Because of the great variety of purposes for which ammunition is designed, and the complexity of the theories and engineering principles associated with each type, and which differ between these types in great degree, it has not been possible to present within practicable limits all of the factors of design or to give illustrative designs showing the applications in existing ammunition. In some cases the necessity of maintaining a reasonable security level has also been a controlling factor.

To offset these recognized limitations, both a reference and a bibliography have been prepared as a part of each major subdivision. The reference includes material for supporting statements made in the handbook text, and the bibliography provides for extended reading on the subject to improve and simplify the understanding of principles involved.

The handbooks are presented in three PARTS, each of which constitutes a volume. PART ONE (AMCP 706-160) covers introductory information, mechanisms for accomplishing the desired effects, the character of the target as it influences the effect, and collection and analysis of data covering the mechanism of effect. Chapter 1 provides a short history of terminal ballistics and briefly outlines current programs. Chapter 2 discusses the physical mechanisms by which damage may be inflicted upon targets; that is, it describes the various means of obtaining terminal ballistic effects. The emphasis is on the phenomenology involved, without application of the mechanisms to specific targets. Qualitative information is presented in order to identify those parameters associated with each mechanism which influence its effectiveness or damage capability.

Chapter 3 discusses the ways in which various targets can be killed, incapacitated, or rendered incapable of performing their functions. The vulnerability of various target classes to appropriate kill mechanisms is described in detail, and particular emphasis is placed on the various features of each that are most susceptible to attack. Target parameters which influence the target vulnerability or damage-resistance capability are identified. A separate section is devoted to each of the following target classes: personnel, ground vehicles, ground structures, and aircraft.

Chapter 4 presents detailed technical information concerning the physical processes involved in various kill mechanisms. The processes are first described from the theoretical point of view which forms the basis for scaling laws. Discussion of scaling laws is then presented, followed by a description of the experimental techniques used in collecting data which are not specifically related to a particular [redacted] type. A separate section is devoted to

each of the following: blast, thermal and nuclear radiation, fragmentation and penetration, and detonation physics.

PART TWO (AMCP 706–161) is devoted to the collection and analysis of data concerning the target toward which the mechanism of effect is directed. Methods of collecting terminal ballistic data are described that are specifically related to the incapacitation or defeat of particular targets. Also discussed is the synthesis of these data as necessary for the prediction of kill probabilities. A great deal of ballistic data is presented, with most of the information included for the purpose of showing how raw data from ballistic tests are organized and presented. Some of the data, such as penetration curves and component damage data, should prove useful for general reference purposes.

Of the four chapters constituting PART TWO, Chapter 5 is concerned with the incapacitation and mortality of personnel due to projectiles, blast, thermal and nuclear radiation, and chemical and biological agents. Chapter 6 is concerned with the incapacitation and defeat of ground vehicles in terms of test parameters for projectiles, armor material, and penetration formulas, and in terms of test and data generation and analysis, lethality evaluation methods, and in the synthesis of kill probability from nuclear weapons. Chapter 7 deals with ground structural targets of various types in terms of full-scale experiments, model loading tests, analyses and tests to obtain response data, analysis of wartime bomb damage and of catastrophic accidents, and with the synthesis of probabilities of ground target damage. Chapter 8 is a discussion of kill mechanisms in terms of aircraft damage, a consideration of damage to various aircraft components in both operational and test environments, methods of test and data generation, and the synthesis of data.

PART THREE (AMCP 706–162) discusses the targets of the future, missiles and satellites, and the application of the principles discussed in PARTS ONE and TWO to the attack of these targets. Of the three chapters in PART THREE, Chapter 9 describes in a general manner such kill mechanisms as nuclear effects, particle beams, fragmentation, rendezvous type mechanisms, and electronic countermeasures. It also briefly describes certain currently unfeasible mechanisms. Chapter 10 provides a qualitative discussion of the major sources of vulnerability of missiles and of satellites. The characteristics of both, and of their components, are briefly described in terms of some of the means by which they may be defeated. Chapter 11 discusses methods for obtaining terminal ballistic data on missile and space targets, as well as the means of using data for quantitative results.

The handbooks were prepared under the direction of the Engineering Handbook Office, Duke University under contract to the United States Army. The material for the handbooks was prepared by Aircraft Armaments, Inc., with the technical assistance of the Ballistic Research Laboratories. Reviews and valuable contributions were made by personnel of the Frankford, Picatinny and Edgewood Arsenals (now of the Munitions Command); the Engineer Research and Development Laboratory (now of the Mobility Command); and the Redstone Arsenal of the Missile Command.

Comments and inquiries on these handbooks should be addressed to Army Research Office (Durham), Box CM, Duke Station, Durham, N. C.

Since preparation of the text of this handbook, responsibility for design and for all other functions pertaining to Army materiel, including publication of this series of handbooks, has been assumed by the Army Materiel Command. Any indicated responsibility of the Ordnance Corps in this regard should be understood as the responsibility of the Army Materiel Command.

Information on resulting changes in handbook designation, together with a current list of handbooks, is contained on the inside back cover.

PREFACE

Introduction, Kill Mechanisms, and Vulnerability, forming PART ONE of Elements of Terminal Ballistics, contains Chapters 1 through 4. Chapter 1 provides a brief history of terminal ballistics and a summary of current areas of interest in Terminal Ballistics.

Chapter 2 describes the various kill mechanisms, that is, the mechanisms for obtaining terminal ballistic effects. Chapter 3 covers target vulnerability for targets consisting of personnel, ground vehicles, aircraft, and surface and underground structures. Chapter 4 covers the collection and analysis of data concerning kill mechanisms.

A glossary and an index are included as part of this handbook.

The other handbooks which, together with this volume, comprise Elements of Terminal Ballistics are:

AMCP 706–161 (S)	PART TWO, Collection and Analysis of Data Concerning Targets (U)
AMCP 706–162 (S–RD)	PART THREE, Application to Missile and Space Targets (U)

[redacted]

TABLE OF CONTENTS

[redacted]

TABLE OF CONTENTS (cont)

TABLE OF CONTENTS (cont)

TABLE OF CONTENTS (cont)

TABLE OF CONTENTS (cont)

TABLE OF CONTENTS (cont)

TABLE OF CONTENTS (cont)

TABLE OF CONTENTS (cont)

TABLE OF CONTENTS (cont)

TABLE OF CONTENTS (cont)

LIST OF ILLUSTRATIONS

LIST OF ILLUSTRATIONS (cont)

LIST OF ILLUSTRATIONS (cont)

LIST OF ILLUSTRATIONS (cont)

LIST OF ILLUSTRATIONS (cont)

LIST OF ILLUSTRATIONS (cont)

LIST OF ILLUSTRATIONS (cont)

LIST OF ILLUSTRATIONS (cont)

LIST OF ILLUSTRATIONS (cont)

LIST OF TABLES

LIST OF TABLES (cont)

Chapter 1 (U)

INTRODUCTION

Section 1—Brief History of Terminal Ballistics

1–1. PRE NINETEENTH CENTURY

It can be speculated that man has always had a deep interest in increasing the effectiveness of the weapons he employed in his battle for survival. It was not until the time of Galileo and Newton, however, that scientific principles were developed and applied to problems associated with weapons and projectiles. The earliest problem to receive attention was that of determining the variation of range with the change of elevation angle, for a given gun, charge, and projectile. This may be considered the beginning of the general field of ballistics and, in particular, of what is now called "exterior ballistics". Science in the eighteenth century was occupied mainly with the development of mathematics, physics, and mechanics. The further application of these sciences to weapon problems was made in 1829 by the French engineer, J. V. Poncelet (1788-1867). Poncelet postulated a law of resistance for the penetration of projectiles into targets and conducted experiments to determine values for the two parameters involved. Poncelet's resistance law is still used today, as are experiments to determine the parameters for new target materials and projectile configurations. The work of Poncelet would appear to mark the beginning of what is now known as "terminal ballistics".

The general field of ballistics must be classified as an applied rather than a pure science. Developments in most applied sciences seem to be compressed into relatively short periods of time wherein a particular external stimulus produces rapid advances in the field. It is perhaps unfortunate, but true, that the applied science of ballistics is stimulated by national or international situations of war.

1–2. THE NINETEENTH CENTURY

1–2.1. General

During the nineteenth century, British military engineers were much concerned with the design and construction of ships and land fortifications to withstand penetration of solid projectiles. The first recorded instance in which a projectile was fired from a rifled gun at armor for land fortifications was in 1860, when an 80-pounder Armstrong gun fired wrought-iron, flat-headed shot, and a 40-pounder fired cast-iron shot, at two iron embrasures 8 inches and 10 inches thick fixed in masonry work at Shoeburyness (Ref. 1). Experiments with projectile effect on armor occurred rapidly after this. A selection of these experiments follows.

1–2.2. 1861—Armor Backed with Various Materials

Trials were conducted with wrought-iron armor backed with rigid materials, such as cast iron and granite, and backed with resilient materials, such as timber, cork, and rubber. The results indicated that the hard backing increased the resistance to penetration but led to cracking and to failure of fasteners.

1–2.3. 1862–1864—Simulated Ship Targets

Ship hulls were simulated, and trials were conducted with a 10½ inch gun firing 300-pound cylindrical shot at 1,320 ft/sec. There appears to have been a controversy at this time as to whether flat-nose or ogival-nose shot was more effective against armor. It was reasoned that the ogival shape would be deflected more readily by sloped armor.

1–2.4. 1865—Land Fortifications

Masonry targets 14 feet thick were fired on with 7-, 8-, 9.22-, and 10-inch guns at ranges

of 600 and 1,000 yards. Steel and cast-iron shot with hemispherical and elliptical (ogival) heads were used. The damage was assessed as follows:

1. 33 hits did serious damage.
2. 54 hits would have silenced return fire.
3. 86 hits destroyed the walls.

Other trials at this time brought out the excellent qualities of chilled cast iron for shot. This type of shot became known as Palliser shot, after Sir W. Palliser who suggested the idea. The trials also established the superiority of the ogival head over the blunt head.

1–2.5. 1871—Simulated Ship Targets with Spaced Armor

Two ship targets were simulated. The first was protected by a single plate built up to a thickness of 14 inches. The second target was protected by an 8-inch plate and a 6-inch plate separated by 9 inches of timber. The trials showed the superiority of the spaced armor. A series of trials was then conducted to determine the optimum spacing and filler material. It was concluded that a 5-inch space filled with cement was optimum. Apparently the spaced-armor technique was not widely used because no one knew quite how to employ it in the construction of fortifications. An interesting observation was made during these trials, however, as quoted directly from Ref. 1.

"It may be well to mention here a very remarkable result that was obtained in the course of the early trials with plate-upon-plate structures. When void spaces were left between the plates of these structures, it was found that the heads of the Palliser shells collapsed completely under the work they had to do in penetrating them, and, naturally, the effect produced upon the target was thereby very much reduced."

1–2.6. 1872—Ship Turret Tests

Trials were conducted at Portland using the turret of the HMS Glatton as the target and the 12-inch, 25-ton gun of the HMS Hotspur, at 200 yards range, as the weapon. The turret armor was 14 inches thick. Two Palliser shots were fired with 35-pound charges. The results reported (Ref. 3) were that ". . . there was some damage done inside the turret, but the goat, rabbit, and fowl emerged unharmed."

1–2.7. 1876—Early Use of a Massive Explosive Charge

An item of allied interest during this period was the use of a large quantity (52,000 pounds) of explosives to remove reefs in the East River in New York. There was apparently much speculation as to the effect the detonation of this quantity of explosives might have on structures in the surrounding area. It was reported that many people left their homes fearing possible collapse. Curiosity apparently overcame fear, however, because an estimated 250,000 people lined the river bank on the day of the blast. The charge was set off in September 1876, shattering millions of tons of rock. Eyewitnesses reported a rumbling or shaking of the ground, the rising of a great mass of water to a height of 20 to 40 feet, followed by an immense mass of smoke. There was no report of damage to any of the nearby structures.

1–3. THE TWENTIETH CENTURY THROUGH WORLD WAR II

During the early part of the twentieth century, military engineering interest was still centered in the field of penetration ballistics. However, during World War I several innovations were introduced which were the forerunners of new areas of interest. The airplane was introduced as a weapon carrier, and air-to-air combat led to interest in what is now called aircraft vulnerability. Chemical agents were introduced as damage mechanisms, ultimately leading to interest in personnel incapacitation by chemical and other means. Interest in damage to structures by blast, rather than penetration, arose from the possibility of aerial bombardment and from the realization that not all military targets could be fortified.

Pertinent developments in other fields provided facilities and instrumentation for much more exacting work in terminal ballistics. It was during this period that the major ballistics

research establishments were organized. In the United States, the Naval Ordnance Laboratory was formally established in 1929 and the Army Ballistic Research Laboratory was formally established in 1937. (Both of these had been functioning for a number of years prior to their formal activation under their present names.)

During World War II many new ordnance items were developed and introduced (Ref. 2). Some of these items were the proximity fuze, shaped charge ammunition, guided missile, aircraft rocket, flame thrower, and atomic bomb. Each of these new developments opened vast new areas for investigations in terminal ballistics.

1–4. POST WORLD WAR II THROUGH 1960

The largest area of terminal ballistic activity since World War II has been the atomic and nuclear weapons effects program. These operations were managed by the Armed Forces Special Weapons Project (AFSWP), and were participated in by all military services, as well as by numerous educational and industrial organizations. The new damage mechanisms of blast, and thermal and nuclear radiation have received a great amount of theoretical and experimental attention.

Second only to the nuclear weapons effects program has been the aircraft vulnerability program. For example, the development of the guided missile, capable of carrying various kinds of warheads, led to a terminal ballistic program concerned with the means of determining aircraft and missile vulnerability. This program has also been actively involved with such studies as the effects of explosive charges, delay fuzes, incendiaries, and high explosive loading in projectiles.

The introduction of the shaped charge has led to extensive analysis and testing of the shaped charge versus armor plate. In addition, the explosive launching of fragments has revived interest in the field of penetration ballistics.

The launching of earth satellites and the development of the ICBM have caused much interest and speculation in the possibility of new damage mechanisms. The investigation of these mechanisms is presently somewhat limited because facilities for controlled experimentation have not yet been perfected.

Section II—Current Programs in Terminal Ballistics

1–5. GENERAL

Virtually every world power is currently active in some aspect of the field of terminal ballistics. In the United States all of the military services have active programs, which taken together involve dozens of laboratories, research institutions, and industrial contractors. No attempt will be made in the following paragraphs to credit individual programs to the proper investigating or sponsoring agency. Rather, a summary of current areas of activity (Ref. 3) will be presented which is believed to be representative of all the various interests.

1–6. PERFORMANCE OF EQUIPMENT IN A NUCLEAR ENVIRONMENT

Because adequate shielding cannot always be provided for protection of vital components from nuclear radiation, attempts are being made to develop components and systems with greater radiation resistance. In addition, various agencies are engaged in efforts to provide procedures and data whereby the capability of current military equipment to survive nuclear radiation may be predicted. It is anticipated that these programs will lead to the development of new design procedures and concepts to improve the radiation resistance of equipment.

1–7. DETONATION

Programs in this area are concerned with various aspects of the physics of the detonation process. The initiation of high explosives by pressure waves transmitted across air gaps or metal barriers is of particular interest. Other programs are concerned with the effects of externally applied electric and magnetic fields

upon detonation, and with the development of explosive-electric transducers.

1–8. HYPERVELOCITY IMPACT

Impact between small fragments and structural targets is currently of interest for velocities up to 50,000 ft/sec. Satellite and ICBM vehicles make this order of magnitude of velocity technically feasible. Current activities in this field are directed toward means for attaining such velocities in the laboratory. Velocities of 20,000 ft/sec. are presently attainable, and efforts are being expended in developing a better understanding of the phenomena exhibited in this hypervelocity range.

1–9. SHAPED CHARGES

Current interest in the shaped charge field is centered in efforts to improve the theory relating design and performance of this type of weapon. One problem receiving attention, for example, is the design of liners to compensate for the deleterious effects produced by the spin of the projectile.

1–10. GROUND SHOCK

Research in ground shock phenomena is continuing, utilizing both laboratory and field test techniques. Efforts are being made to improve both measurement and scaling techniques, as well as to determine the dynamic stress-strain properties of various transmission media.

1–11. AIR BLAST

Extensive programs are currently active in order to determine the effect of blast waves on structures. Shock tube facilities are being used to study diffraction loading and target dynamic response. High-speed track facilities are being used to realistically simulate the interaction of blast waves and the transonic and supersonic flow fields of airfoils.

1–12. WOUND BALLISTICS

The objective of this continuing program is to provide a knowledge of the wounding potential of fragments, bullets, and other damage mechanisms. A quantitative basis for the assessment of wounding potential is necessary for the design of effective antipersonnel weapons.

Section III—References

1. E. S. Farrow, *Military Encyclopedia*, published by the author in 1885, (Unclassified).
2. L. H. Campbell, Jr., *The Industry-Ordnance Team*, Whittlesey House, 1946, (Unclassified).
3. —— *Annual Report 1959*, BRL, Aberdeen Proving Ground, Maryland, (Confidential), ASTIA No. AD316 874.

Chapter 2 (S)

KILL MECHANISMS

Section I (C)—Fragments

2–1. (U) INTRODUCTION

Fragmentation is the disruption of a metal container by a high explosive filler. Its purpose is to produce the optimum distribution of a maximum number of high velocity lethal fragments. Due to the use of the high explosive filler, fragmentation is always accompanied by blast.

The fragment acts as a kill mechanism by impacting the target at high velocity with its mass and forcing its way through the target material. The kinetic energy of the fragment at the time it strikes the target is one measure of its lethality. However, what constitutes the optimum fragment mass, velocity, and distribution of fragments will vary according to the target, be it a human, truck, airplane, building, satellite, etc.

It is generally desirable to have a shell or bomb body break up into pieces no larger than are required to "kill" the particular target. This arrangement provides the maximum number of effective fragments, by avoiding fragment sizes that are larger than necessary. Fragments are employed in projectiles in three different ways, as uncontrolled fragments, controlled fragments, and preformed fragments. Each of these three different types is discussed in following paragraphs. Special attention is also given to the effects of changes of velocity.

2–2. (U) PRINCIPLES OF OPERATION

To understand the mechanism involved in a fragmentation weapon, it is necessary to know what happens to the fragment between the time of weapon detonation and the time of fragment arrival at the target. Upon detonation of the explosive charge, the detonation wave causes the explosive and its case to swell until the failure point is reached. The case then fails in shear and tension, and fragments are ejected at high velocity. The fragments achieve an initial velocity and form a pattern (or beam) dependent primarily upon the physical shape of the casing. Aerodynamic drag forces slow the fragments during their flight to the target, as do the retardation effects of any target shielding penetrated prior to impact with the target. The area effectively covered by the beam of fragments depends to a large extent on the angle of fall of the projectile and the range to the target.

The fragments produce damage by penetration of a target. Upon impact with a hard target, such as steel or concrete, the kinetic energy of the fragment is transferred to the target material. If the energy transferred by the fragment is great enough to stress the target beyond its limit, penetration takes place. The kinetic energy is transmitted to the target from the fragment through the contact area, or presented area, of the fragment. For fragments of equal mass and velocity, the one with the least presented area will penetrate more extensively, due to the higher concentration of energy transfer.

Upon impact with a soft target, such as the human body, the fragment penetrates with much less loss of energy and often passes completely through the body. The effectiveness of the fragment depends upon the amount of energy lost to the target during fragment travel within the target. The shape of the fragment may be more significant in a soft target than within a hard target, because the shape will influence the path of the fragment and the rate of energy transfer. Relative to a given target, the penetrating power of a fragment is dependent, therefore, upon its mass,

shape, and striking velocity. A discussion of the effectiveness of fragments against soft targets is included in Ch. 3, Par. 3–3. The discussion of basic fragmentation and penetration data is found in Ch. 4, Sec. III.

2–3. (U) UNCONTROLLED FRAGMENTS

2–3.1. Description

Many items of explosive ordnance are designed to produce uncontrolled fragments as the primary kill mechanism. When the casing of a bomb, shell, warhead, or grenade is ruptured by the detonation of its high explosive filler, portions of the casing are propelled outward at high velocity. These segments of the casing are known as fragments. When no provision is made in the design of the projectile to control the size and shape of the segments, the segments are termed uncontrolled (or natural) fragments. The casting and explosive materials, charge-to-metal ratio, casing thickness and configuration, point of detonation, etc., determine the characteristics of the fragments.

Within some degree of probability, the fixed characteristics of the fragments are the number of fragments, initial velocity, weight distribution, and spatial characteristics. Those characteristics which differ with ambient conditions are blast and the retardation of fragments.

2–3.2. Examples

Two typical examples of uncontrolled fragmentation devices are a high explosive (HE) artillery shell and a general purpose (GP) bomb. The high explosive capacity of a bomb or shell will vary according to its mission and method of projection. A shell designed to be fired from a high-velocity tank gun must have thicker shell body walls, and consequently less explosive content, than one designed for use in a low-velocity howitzer or mortar (Ref. 1). The thicker walls are required to withstand the higher acceleration forces encountered at the time of firing. The bursting charge capacity of a bomb will depend upon its mission: an armor-piercing bomb must have much thicker walls than a general purpose bomb. A light-case bomb has thinner walls than the GP bomb, and sacrifices fragmentation effect for increased blast effect.

Shells, bombs, and fragmentation grenades basically consist of a metal casing, a high explosive filler, and a fuze. The casing is usually steel, and an explosive such as trinitrotoluene (TNT) may be used as the high explosive. Various fuzes are employed, depending on the delivery mechanism and the target characteristics. Since fragmentation devices are designed to be detonated near, rather than upon striking, the target, proximity (VT) fuzes are often employed.

2–4. (U) CONTROLLED FRAGMENTS

2–4.1. Description

Controlled fragments are produced by warhead casings designed to break up in specific patterns. The fragment takes on its final individual shape during the expansion of the products of explosive detonation. Some of the methods employed to achieve various degrees of control consist of: multiple wall casings; casings made of a series of rings, or helically wrapped wire, where the rings or wire may or may not be notched (grooved); casings that are scored (grooved) in one or two directions; and fluted liners inserted between the charge and the casing to focus the detonation on the casing in a desired pattern.

2–4.2. Advantages

Through the use of controlled fragments, the amount of casing metal that is wasted in fragments too small to be effective, or larger than necessary, is kept to a minimum. The most efficient fragment size and shape for use against a specific target can be selected, and optimum fragment pattern and initial velocity can be approached within practical limits.

The mechanics of kill by a controlled fragment is identical to that of an uncontrolled fragment; however, controlled fragments offer the advantages listed below:

1. The performance of controlled fragments can be predicted more accurately.
2. When the parameters affecting penetration (velocity, mass, and shape) are con-

trolled, greater damage will be inflicted to a target for which the weapon is designed.

3. Fragments with better aerodynamic characteristics can be employed, resulting in higher impact velocities and greater penetration.

2–5. (U) PREFORMED FRAGMENTS

The most complete control of fragment size and shape is achieved by the use of preformed, or precut, fragments. Preformed fragments, formed during weapon fabrication, exist in their final shape before detonation of the explosive charge, and they are mechanically held in their proper orientation around the charge. When preformed fragments are used in a properly designed warhead, breakage of fragments upon expulsion and adhesion of fragments to each other may be considered negligible, and nearly 100 per cent fragmentation control is achieved.

Typical shapes used for preformed fragments are cubes, rods, spheres, and flechettes (fin-stabilized darts or needles). They cause damage by penetration, as is the case with all fragments. In the same manner in which controlled fragments offer advantages over uncontrolled fragments, preformed fragments may closely approach optimum fragmentation effects for a specified target, because nearly complete control of fragment mass, shape, and velocity can be designed into the weapon.

2–6. (U) SECONDARY FRAGMENTS

Secondary fragmentation results from break-up of either controlled or uncontrolled fragments upon impact, or from the creation of fragments from the target material when it is impacted by a projectile. One important example of secondary fragmentation is the spalling of armor plate when it is pierced by armor-piercing shot. The fragments or spalls are broken off the back of the plate and become significant kill mechanisms within the armored enclosure. Another example of secondary fragmentation is the break-up of human bone structure upon the impact of a penetrating missile. The bone splinters or fragments may cause more overall damage within the human body than did the original missile.

2–7. (C) CONTINUOUS RODS

Continuous rods represent a specialized extension of fragmentation techniques, in which discrete rod fragments are replaced by a bundle of metal rods. The rod bundle is arranged in the form of a hollow cylinder with the rod axes parallel to the cylinder axis. Alternate rod ends are welded together to form a continuous expanding ring when the rods are launched at high velocity by a central cylindrical, or annular, high explosive charge. As the bundle of rods expands outward from the point of detonation it forms a continuous and expanding hoop, which eventually breaks up into several pieces as the hoop circumference approaches and exceeds the total of the rod lengths. The cutting ability of the rods is a function of the rod hoop weight and its velocity. A warhead of this type can produce severe structural and component damage against a large light-frame target. For this reason, its considered use is against aircraft targets (Ref. 2).

2–8. (C) HYPERVELOCITY FRAGMENT IMPACT (Refs. 3 and 4)

2–8.1. (U) Description

Observations of the effects of increases in fragment velocity have revealed three general conditions of impact, characterized by the behavior of the fragment and target material. In the low velocity condition, the fragment remains intact and the cavity produced in the target may be only slightly larger in diameter than the fragment. As the striking velocity increases, the dynamic pressures encountered exceed the strength of the fragment, which begins to break up, initiating the transitional condition. This causes the penetration to increase more slowly with increasing velocity; in some cases it causes an actual reduction in the penetration with increasing velocity. As the striking velocity increases further, the penetration again increases, proportional to a fractional power of the velocity (usually between $\frac{1}{3}$ and $\frac{1}{2}$). The crater formed approaches a hemi-

spherical shape, and the hypervelocity or fluid-impact condition begins.

The term hypervelocity, when used in the terminal ballistics sense, is applied to the crater-formation phenomenon, rather than to a specific impact velocity. One criterion for the onset of hypervelocity is that the cavity shape must be approximately that of a hemisphere. No single numerical value can be assigned for the beginning of this velocity range, as the velocity is a function of the strength characteristics of both the target and the fragment materials. Hypervelocity fragments and cratering are discussed in detail in Ch. 4, Par. 4–13.

2–8.2. (U) Effect of Hypervelocity Impact

The transition condition of hypervelocity impact is clearly demonstrated in the case of a steel projectile impacting on a thick lead target. The penetration increases roughly as the first power of the velocity up to about 0.5 km/sec. (1640 ft/sec.), and then decreases as the inverse first power of velocity up to about 0.8 km/sec. (2600 ft/sec.). Penetration of the steel projectile into the lead then increases again, proportional to the ⅓ power of velocity. It is interesting to note that the penetration does not rise to its earlier maximum value until the impact velocity reaches 2 km/sec. (6560 ft/sec.), which is a fourfold increase. The actual cavity volume continues to increase with velocity increase, but its shape is changing to become more nearly hemispherical. The velocity boundaries and detailed character of the transitional condition are not well defined, and differ markedly with target and projectile material. The transitional condition has been associated with the plastic wave velocity for the target material, but it would seem that a more important factor would be the impact pressures determined by the velocity and target density as well as the strength of the projectile.

In the true hypervelocity impact condition, it is expected that the crater formed in a semi-infinite target will be hemispherical, independent of the ratio of projectile and target densities and, to a considerable extent, independent of the projectile shape except in the case of large length/diameter ratios. These features seem to be confirmed by experimental results, to date.

2–8.3. (C) Stages of Crater Formation

(C) Three stages have been identified in the formation of the crater in the hypervelocity condition, as a result of experimental work in which flash X-ray photography is employed. Initially, the mechanism appears to be a hydrodynamic one in which both the target and the projectile flow plastically during the primary stage, and the kinetic energy of the projectile is transferred to the target. This primary stage persists for only a small fraction of the total time of crater formation. During the primary stage, the pressures generated are of the order of millions of atmospheres, and the density of the target and projectile behind the shock front may be appreciably increased. For example, calculations for the impact of iron on iron at 5.5 km/sec. indicate that the maximum pressure is about 2 megabars, which corresponds to a density ratio of about 1.4.

(C) After the pellet has been completely deformed and lost its integrity, the energy is transferred to the target in the form of a plastic deformation wave. The cavitation continues for a period that depends on the amount of energy transferred.

(U) Finally, there is a plastic and elastic recovery stage which follows the immediate crater formation. Craters in 2SO aluminum have been observed to recover about 30 per cent by volume.

(U) The great bulk of experimental work in hypervelocity impact has been devoted to the study of crater formation in essentially semi-infinite targets, in an effort to develop an understanding of the basic phenomena. However, studies have indicated that, if the penetration in a semi-infinite target is p, complete penetration of a plate of thickness up to 1.5 p may be obtained with the same projectile and impact velocity. In a marginal hypervelocity penetration, however, the projectile or fragment itself does not carry through, but spalling and some flow of the target material will be produced and may be sufficient to cause damage to internal components.

Section II (C)—Solid Projectiles

2–9. (U) INTRODUCTION

Solid projectiles, like fragments, act as kill mechanisms by their penetration of a target. The term "kinetic energy (KE) projectiles" is often used to refer to solid projectiles, because their terminal effects are dependent upon the kinetic energy of the projectile at the time it strikes the target. Examples of solid projectile types are: bullets, armor-piercing shot, single flechettes, knives, and arrows.

Unlike the fragment, the solid projectile is usually fired singly (one projectile per round fired), has a sharp or relatively sharp tip, and is launched in a path directly at the target. In contrast to this, the fragment is produced multiply as a result of an explosion, has no particular penetrating surface, and reliance is placed upon a number of fragments, distributed in space, to hit the target. The solid projectile is also differentiated from the explosive "shell," whose terminal ballistic effects depend on blast and fragmentation, rather than the kinetic energy of the projectile.

2–10. (U) BULLETS

Bullets are classed as solid projectiles fired from small arms weapons, usually limited to caliber .50 and below. There are several types of bullets, used for various purposes, the service types being ball, armor-piercing, tracer, incendiary, and armor-piercing incendiary. Special purpose types are used for testing and practice, but will not be considered here. Bullets have a metal core and a gilding metal jacket, and some have a filler in the point or base, or both. Fig. 2–1 illustrates some typical bullet types.

Ball ammunition is effective against personnel or light materiel. The bullet is usually comprised of a core, composed of an antimony-lead alloy, and a gilding metal jacket. Caliber .50 ball ammunition bullets, however, use a core of soft steel to provide ballistic properties similar to the armor piercing bullet (Ref. 6).

The kill mechanism of ball ammunition against both hard and soft targets is the same as that previously described for fragments. That is, the penetration and amount of damage is a function of the shape, weight, and striking velocity of the bullet. When used against light target materials, ball ammunition may produce secondary fragments that are effective against personnel located behind the target.

Armor-piercing bullets contain a hardened steel core and a point, or base, filler of lead or aluminum between the core and the jacket. They are designed for use against armored aircraft and lightly armored vehicles, concrete shelters, and other bullet-resisting targets. Armor-piercing bullets employ the same kill mechanisms as ball type ammunition, that is, penetration into hard and soft targets and the production of secondary fragments. Armor-piercing bullets have greater penetrating power than other types of standard ammunition due to the presence of the hardened steel core. This core resists deformation upon impact with the target and thus maintains a smaller impact area, resulting in a longer duration of highly concentrated forces.

Tracer bullets contain a chemical composition in the rear which is ignited by the propellant charge and which burns in flight. The forward half of the bullet contains a lead slug. Tracer ammunition is primarily used for observation of fire. Secondary purposes are for incendiary effect and for signaling.

Incendiary bullets contain an incendiary which is ignited upon impact. Armor-piercing incendiary (API) bullets are designed to "flash" on impact and to then penetrate armor plate. The main kill mechanism is the penetration of fuel cells and the ignition of the fuel in the target. Destruction is accomplished by the combined use of kinetic-energy impact and fire.

2–11. (C) FLECHETTES

Flechettes are fin-stabilized solid projectiles with a length to diameter ratio much greater than that of a bullet. The general configuration and nomenclature are shown in Fig. 2–2. Fle-

Official U. S. Army Photograph

BULLET, BALL, CAL..50, M2

BULLET, ARMOR-PIERCING, CAL..50, M2

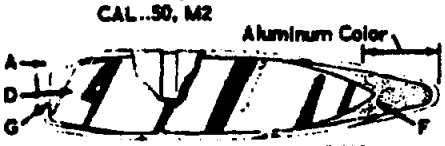

BULLET, ARMOR-PIERCING-INCENDIARY, CAL..50, M8

BULLET, ARMOR-PIERCING-INCENDIARY, CAL..50, T49

BULLET, ARMOR-PIERCING-INCENDIARY-TRACER, CAL..50, M20

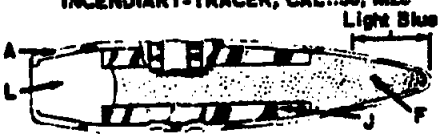

BULLET, INCENDIARY, CAL..50, M1

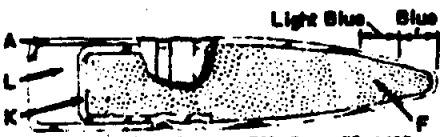

BULLET, INCENDIARY, CAL..50, M23

A - Gilding Metal Jacket
B - Steel Core
C - Lead - Antimony Point Filler
D - Hardened Alloy Steel Core
E - Lead - Antimony Base Filler
F - Incendiary Mixture
G - Igniter Composition
H - Tracer Composition
J - Steel Body
K - Gilding Metal Clad Steel Container
L - Lead - Antimony Slug

Figure 2–1. Bullets

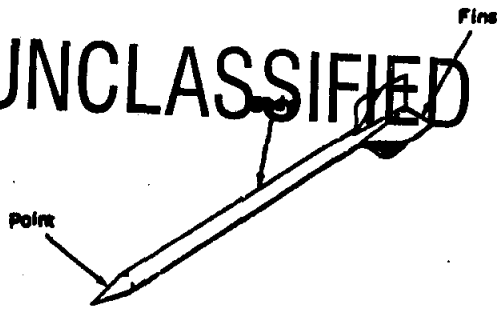

Figure 2–2 (C). Flechette Configuration (U)

chettes, sometimes called darts or needles, are made in a variety of materials, sizes, and shapes. Fin forms vary widely with manufacturing techniques and application, and may be straight, or canted to provide spin in flight, or on-center or offset to conform to special packing requirements. Many point shapes are utilized for improving terminal ballistics effects against specific targets (*Ref. 6*).

Flechette employment may be divided into two major categories: as used in antipersonnel warheads; and as used in small arms ammunition, in either scatter-pack cartridges or individual projectile rounds. In antipersonnel warheads, the flechettes offer advantages over cubes and similar fragments by their superior aerodynamic characteristics and penetrating power. Damage is achieved by penetration and perforation, and is enhanced by the higher long-range striking velocity of the flechette. This permits more fragments of lower unit mass to be incorporated in a fragmentation warhead, providing better area coverage.

In small arms ammunition a pack of flechettes may be used in what is known as a scatter or salvo round, or a single flechette can be employed to provide a cartridge of small size and light weight. The scatter rounds are foreseen as particularly adaptable to short range weapons, such as shotguns or caliber .45 hand arms, to provide increased probabilities of hit. The single flechettes provide a relatively flat trajectory projectile for long ranges.

The flechette may be made lighter in weight than a bullet, yet obtain comparable lethality, because the light flechette can be launched at

higher velocities than the bullet for the same gun pressure and will retain its velocity for longer ranges. The smaller frontal area of the flechette enhances its penetrating power and, if its remaining velocity is sufficiently high, it will tumble within a soft target and transfer its energy to the soft target at a greater rate than a bullet. For impacts at velocities below that at which tumbling occurs, the flechette wounds by cutting permanent slits that are comparable in size to the lateral dimensions of the fins.

Flechettes appear to have good characteristics with respect to penetration of hard targets, but additional studies are required for a complete analysis. Additional studies are also required on the action of flechettes within soft targets, and on the factors affecting tumbling.

2–12. (U) ARMOR-PIERCING (AP) PROJECTILES

Armor-piercing projectiles achieve their terminal effect by forcing their way through the target material under the impetus of kinetic energy, as do fragments, bullets, and flechettes. Armor piercing "shot," for example, is a solid projectile without a bursting charge, for use with cannon, and thus differs physically from bullets, even though both may be armor-piercing.

Armor-piercing projectiles are designed specifically to attack hardened targets such as armored vehicles, and are sometimes used against reinforced structures. For this reason they are characterized by high accuracy and high velocity (a flat trajectory resulting from short time of flight), because of the importance of achieving a first-round hit (Refs. 1 and 7). Armor-piercing projectiles are discussed in more detail in Ch. 6, Par. 6–5.2.

2–13. (U) HIGH EXPLOSIVE PLASTIC (HEP) ROUNDS

High explosive plastic rounds achieve their terminal effect by spalling the interior surface of armor plate. This type of round is discussed in detail in Ch. 6, Par. 6–5.4.*b*.

2–14. (U) KNIVES, BAYONETS, AND ARROWS

Knives, bayonets, and arrows are sometimes used in combat. They are suitable for use against personnel, but require considerable skill in handling in order to achieve a kill.

Knives and arrows have been used in recent times in order to attack sentries and outposts when silence has been necessary. Bayonets have been used in hand-to-hand combat, but remain a weapon of last resort. It may be necessary for a soldier to resort to the bayonet in close combat should he not have time to reload his rifle.

Section III (5)—Shaped Charges

2–15. (U) INTRODUCTION

The performance of the shaped charge missile in no way resembles that of the kinetic energy projectile. Its effect is due entirely to the formation of a high velocity jet of gases and finely divided metal, which becomes the penetration medium. The thickness of material that can be penetrated is essentially independent of the projectile's striking velocity. The projectile case remains at the outer face of the target.

A shaped charge missile consists basically of a hollow liner of inert material, usually metal, that is a conical, hemispherical, or other shape, backed on the convex side by explosive. A container, fuze, and detonating device are included (Fig. 2–3).

Shaped charge projectiles intended for use against armored vehicles are often designated by the letters "H.E.A.T.," which stand for "*H*igh-*E*xplosive *A*ntitank." The abbreviation is often reduced to "HEAT," which has been interpreted by some to infer that the projectile burns its way through the armor. This is not a correct assumption; the letters are simply an abbreviation which, by coincidence, spells out a common word.

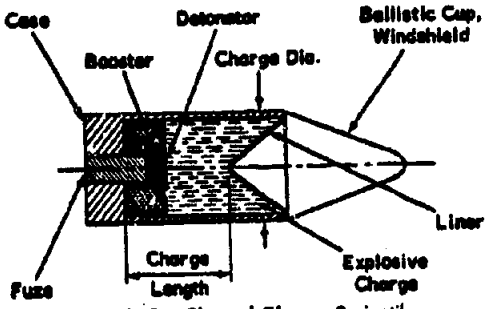

Figure 2–3. *Shaped Charge Projectile, Schematic Diagram*

2–16. (U) PRINCIPLES OF OPERATION

When the shaped charge missile approaches or strikes a target, the fuze (proximity or contact) detonates the charge from the rear. A detonation wave travels forward and the metal liner is collapsed, starting at its apex. The collapse of the liner cone results in the ejection of a long, narrow jet of metal particles from the liner, at velocities from 10,000 to 39,000 ft/sec.

This process is illustrated in Fig. 2–4 by the series of ultra-high speed radiographs of an experimental shaped charge lined with a 45-

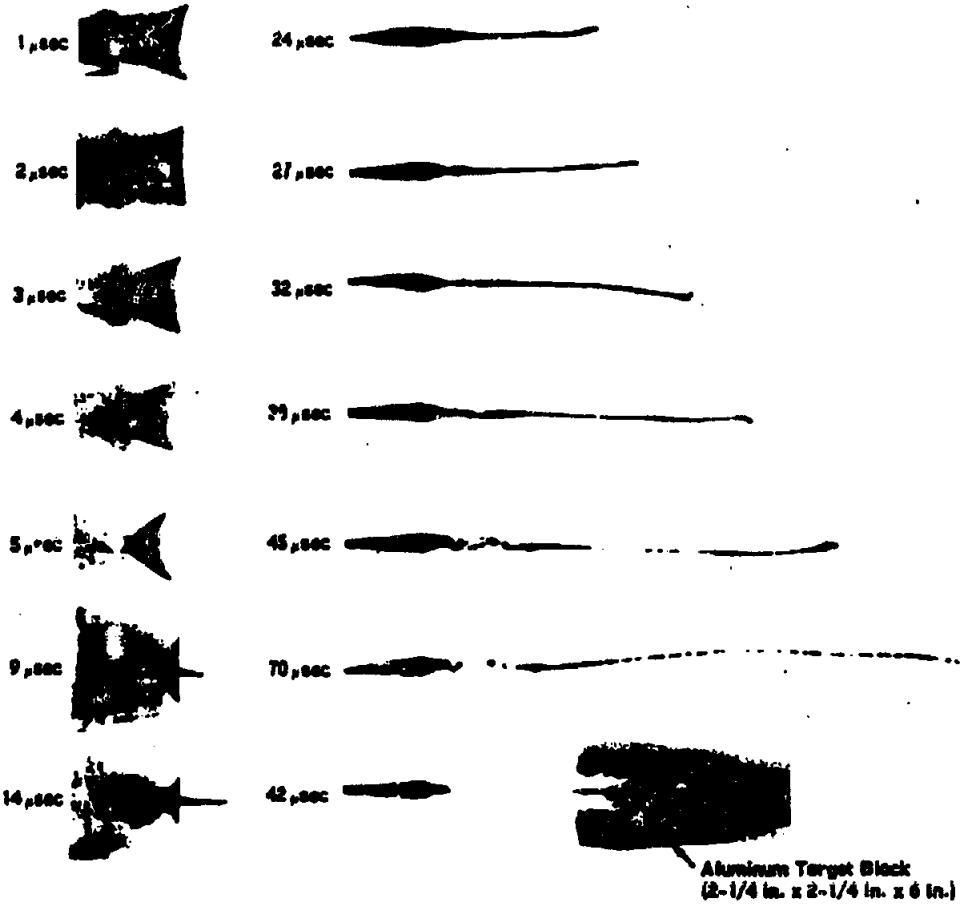

Figure 2–4. *Ultra-High Speed Radiograph of Shaped Charge Detonation*

degree steel cone, radiographed at successive times to depict the mechanism of cone collapse. The charge was 50/50 Pentolite, having a base diameter of ¾ inch. The time, noted in microseconds for each radiograph, denotes the time after the detonation wave passed the apex of the liner cone. There is a gradient in the velocities of the elements of length along the jet. The elements in front move faster than those in the rear, thus causing the jet to lengthen, thereby reducing its average density with time. The jet is followed by the major portion of the now completely collapsed cone. The latter is often referred to as the "slug," or "carrot," because of its peculiar shape.

The description of the principles of operation of the shaped charge, given above, is general in nature. Shaped charge design involves numerous, variable parameters. It should be recognized that considerable latitude exists in the choice of these parameters; but also that many permutations of these could (and should) result in the same net effect.

2–17. (U) JET PENETRATION

When a jet strikes a target of armor plate or mild steel, pressures approximating 250,000 atmospheres are produced at the point of contact. This pressure produces stresses far above the yield strength of steel; consequently, the target material flows out of the path of the jet as would a fluid. There is so much radial momentum associated with the flow that the diameter of the hole produced is considerably larger than that of the jet. The difference in diameter between the jet and the hole it produces depends upon the strength characteristics of the target plate. Thus, a larger hole is made in mild steel than in armor plate, and the penetration depth in a very thick slab of mild steel can be as much as 30 per cent greater than in homogeneous armor.

As the jet particles strike, they are carried radially with the target material. Thus, the jet is used up from the front, becoming shorter and shorter, until finally the last jet particle strikes the target and the primary penetration process stops. The actual penetration continues for a short time after cessation of jet action, because the kinetic energy imparted to the target material by the jet must be dissipated. The slight additional penetration caused by this afterflow is called secondary penetration. Its magnitude depends upon target strength, and accounts for the differences observed between the depths of penetration in mild steel and in homogeneous armor, although there is probably some difference in the primary penetration as well.

While some exceptions will be found to the following rule, the depth of primary penetration, P′, depends mainly on several factors: the length of the jet, L; the density of the target material, ρ_t; and the average density of the jet, ρ_j. It has been found that P′ is proportional to $L\sqrt{\rho_j/\rho_t}$, giving

$$P' \propto KL\sqrt{\rho_j/\rho_t} \qquad (2\text{–}1)$$

The jet density, ρ_j, is proportional to the density of the cone liner material, particles of which are dispersed throughout the primary jet.

2–18. (C) PENETRATION FACTORS (Ref. 1)

2–18.1. (C) Type, Density and Rate of Detonation of Explosive Charge

While the depth of penetration is indicated to be more closely related to detonation pressure than to the rate of detonation, because of interdependence of effects it may be said that the greatest effect will be produced by that explosive having the highest rate of detonation. Table 2–1 illustrates the relative effect of four different castable explosives.

Although the rate of detonation is of prime importance in selecting a high-explosive filler,

TABLE 2–1 (C). DETONATION RATE COMPARED TO PENETRATION FOR FOUR CASTABLE EXPLOSIVES (U)

Explosive	Density (grams/cc)	Detonation Rate (m/sec.)	Relative Standing in Penetration Efficiency
Comp B	1.68	8,000	1
Pentolite	1.64	7,640	2
Ednatol	1.62	7,500	3
TNT	1.59	6,900	4

other properties of the explosive must be taken into consideration. Among these are sensitivity to initiation, pourability, and thermal stability.

2–18.2. (C) Confinement of Charge

Confinement is inherent in a military projectile, whether it be the relatively heavy confinement found in the shell thickness of the 105-mm Howitzer, or the thin-gage wall of the bazooka rocket. Also, the confinement effect is noted whether the confinement is provided by an increased wall thickness or by a "belt" of explosive. Its effect on shaped charge action is to decrease lateral loss of pressure, and to increase the duration of application of pressure. This results in a more efficient shaped-charge collapse, and, therefore, increased hole volume or depth in the target material. As a matter of design compromise the wall may be quite thin in order to provide a lighter projectile, thus obtaining a higher muzzle velocity, which should increase the hit probability. However, the thinner wall results in less depth of target penetration.

2–18.3. (C) Shape, Diameter, and Length of Charge Back of Liner

The length of the projectile body, and hence of the charge, is most frequently limited by aerodynamic performance and projectile weight specifications. In general, the penetration and the hole volume obtained increase with increasing charge length, but reach a limit at about 2 or 2.5 charge diameters. (Charge length is measured from the apex of the liner to the rear of the explosive charge.) Existing shaped charge designs usually have one of the shapes shown in Fig. 2–5. Although each can be made to perform satisfactorily, type (A) has the advantages of increased amount of high-explosive, which could result in increased secondary effects of blast and fragmentation. Types (B) and (C) are sometimes necessitated by the requirements for a lighter projectile weight, in order to increase muzzle velocity and accuracy.

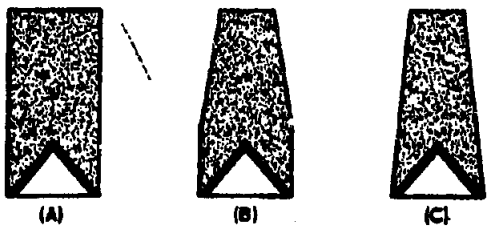

Figure 2–5. Shaped Charge Body Designs

2–18.4. (C) Liner Material and Thickness of Liner

The shaped charge effect is not dependent on the presence of a liner, but because the penetration of the jet is proportional to the square root of its density, the material of the liner enhances the effect by increasing the density of the jet. Increased depth of penetration is obtained as the liner is made thinner, but thin liners require much closer manufacturing tolerances than the thicker ones. The net effect of these contradictory factors is that the penetration depth will increase up to a maximum as the liner thickness is decreased (Fig. 2–6), at which point the manufacturing imperfections will become more important, and

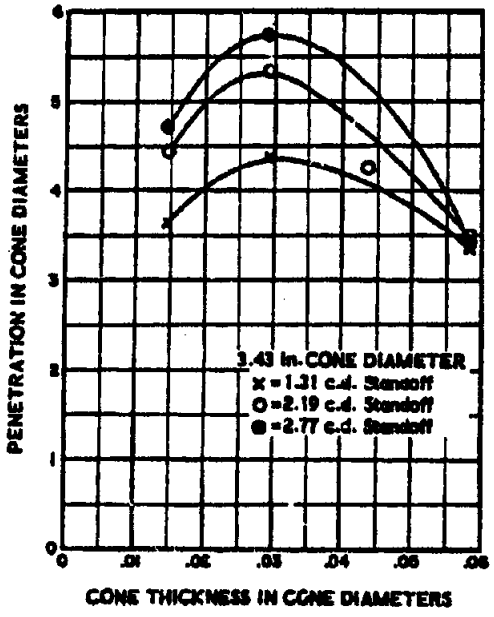

Figure 2–6 (C). Penetration vs Standoff and Liner Thickness (U)

further decreases in liner thickness result in less penetration. The alloy of the metal to be specified for the cone should generally be that which has the greatest ductility. Copper, steel, and aluminum have all been used. Fig. 2–7 shows the variation in penetration, as a function of standoff, obtained with liners made of these materials. (Refer to Par. 2–18.8 for a definition of "standoff ")

2–18.5. (C) Liner Shape

Differently shaped liners and cavities react in different ways. For example, a conical liner (Fig. 2–8) collapses from the apex and approximately 70 per cent to 80 per cent of the liner follows behind the jet as a slug. Hemispherical liners appear to turn inside out, most of the liner being projected in the jet. However, the best and most consistent results have been obtained with conical liners. This may be because it is more difficult to maintain close tolerances with shapes other than conical. Double-angle conical liners are also being investigated. Firings early in the study of double-angle cones, with cones in which the change from one angle to another was made abruptly, did not show any increase in penetration. However, with cones in which the change from one angle to another was made smoothly, and the liner wall was tapered, peak performance was obtained at normally available standoffs.

2–18.6. (C) Effects of Rotation Upon Jets

The rotation in flight of a spin-stabilized, shaped-charge projectile with a simple liner, as previously described, causes a large decrease in penetration. This effect is especially noticeable at large standoff. In the process of jet formation from a rotated liner, there is induced not only the typical, linear velocity gradient found in all shaped charges, but an additional rotational velocity gradient as well. The base of the cone has a higher tangential velocity than the apex. Consequently, when the cone col-

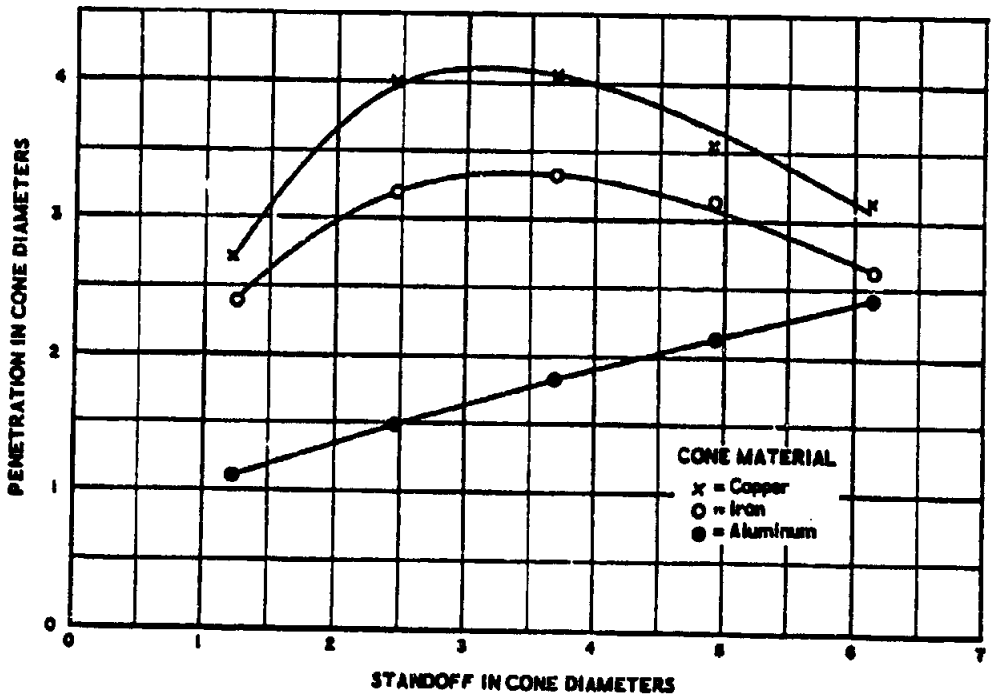

Figure 2–7 (C). Penetration Obtained with Different Liner Materials (U)

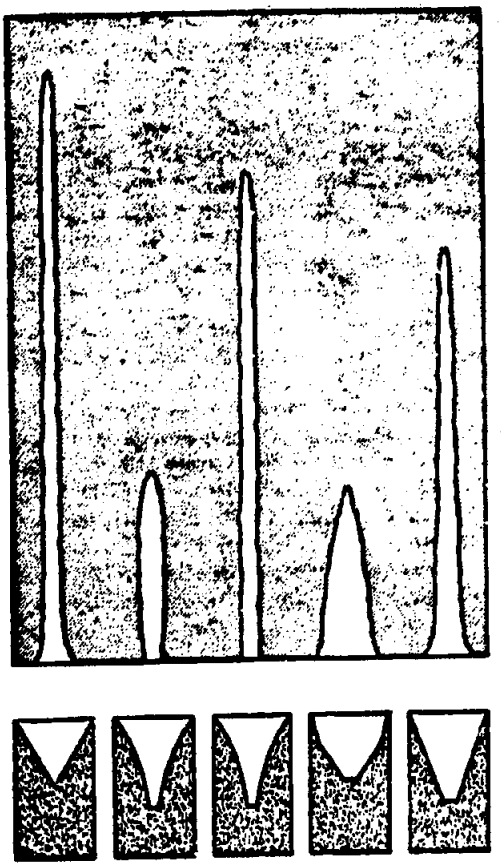

Figure 2–8 (C). Typical Liner Shapes and Hole Profiles (U)

lapses, the faster-moving particles of the cone base form the tail end of the jet. The rear end of the resultant jet is, therefore, rotating faster than the forward end, and the rotational velocity should show a continuous decrease from the rear of the jet to the forward tip. As long as the jet is continuous, therefore, it may be considered as being subjected simultaneously to tension resulting from the linear velocity gradient, and to torsion produced by the rotational velocity gradient (Ref. 8).

It is possible to study in detail the deterioration of the jet by the use of triple-exposure flash X-ray pictures of detonated, shaped charges. The observed, detailed effects of rotation are illustrated by the radiographs shown in Fig. 2–9. Part (A) of the figure shows three views, 60 degrees apart, of the normal jet from an unrotated, 105-mm, smooth, copper liner of good quality. Part (B) shows three views of a jet from a similar liner rotating at 15 rps. These show the marked tendency toward ellipticity of the transverse cross-section of the jet, as well as an early incidence of jet break-up.

Part (C) of the figure shows, at 30 rps, the incidence of the "bifurcation" phenomenon. (Bifurcation is the radial break-up of the jet

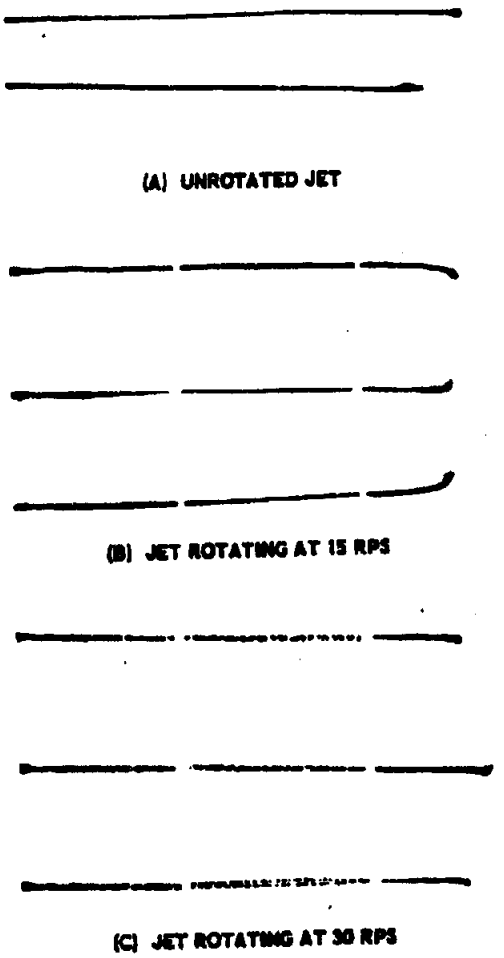

Figure 2–9 (C). Effects of Rotation upon Jets (U)

into two distinct jets.) The two separate portions of the bifurcated jet appear to lie in a plane. The same charge, detonated at 45 rps, produces bifurcated portions which no longer lie in a plane but appear to lie along a helical surface. Experimental observations indicate that at rotational frequencies considerably in excess of 60 rps, the process of bifurcation gives way to "polyfurcation." (Polyfurcation is the radial break-up of the jet into more than two distinct jets.)

In order to counteract the rotational frequencies of the jet, it is necessary to impart to each element of the liner, by some means, a tangential component of velocity which is equal in magnitude but opposite in direction to that set up by the initial spin of the liner. The simplest means of accomplishing this is to find a way of using the energy of the explosive to produce a counter-torque on the liner.

Attempts have been made to improve the performance of spin-stabilized shells by using various non-conical, axially-symmetric liners. However, such attempts have not been promising at high rates of spin; therefore, the major emphasis has been on the design of fluted liners not having axial symmetry.

The idea underlying the use of fluted liners is that of spin compensation to destroy the angular momentum of the liner, to inhibit jet spreading. The fluted-liner method of spin compensation is based on two phenomena. One, sometimes called the "thick-thin" effect, is the observed dependence upon the thickness of the liner of the impulse delivered to a liner element by the product gases of detonation. The second, named the "transport" effect, is the dependence of the impulse delivered to the liner upon the angle at which the detonation products impinge on the liner.

Application of the thick-thin effect to a fluted liner is illustrated in Fig. 2–10. The impulse per unit area is always greater on the offset surface, because the thickness normal to that surface is greater. Furthermore, the impulse is directed along the surface normal. When the impulses delivered at all surface elements are resolved into radial and tangential components, and summed, the total tangential component has a net resultant which produces a torque, in

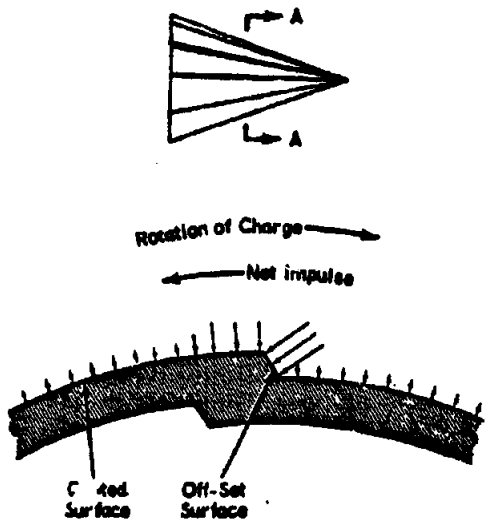

Figure 2–10 (C). Fluted Liner Configuration and Active Forces (U)

the direction shown, which can be used for spin compensation.

Also shown in Fig. 2–10 is the effect of the impulse delivered to the canted surface. The effect is significant in spin compensation because a torque is produced in the direction opposite to that produced by the thick-thin effect. However, because the angle at which the detonation wave strikes the canted surface is usually less than that for the offset surfaces, the net torque produced is in the direction of the forces acting on the offset surface.

A fluted liner is designed to compensate for the angular momentum of a particular projectile, thus, the caliber, charge diameter, and spin rate of the projectile are determining factors in selecting flute characteristics. A fluted liner spun at its designed optimum frequency produces a jet like that produced by an equivalent smooth liner fired statically. When fired statically, the fluted liner produces a jet like that from a rotated smooth liner.

Other methods of spin compensation have been tried, such as spiral detonation guides, fluting the explosive instead of the liner, and the "built-in" compensation found in smooth,

spun liners. These techniques have been found to produce some degree of spin compensation, but only the fluted liner has been found to hold much promise.

The elimination of spin degradation by means other than spin-compensation has also been the subject of experimentation. One method has been to design a shell so that it will be stable with a very low spin. This type of shell has increased drag, requires a special weapon with low-twist rifling, and still needs some kind of spin compensation.

The concept has been proposed of using peripheral jet engines on the shell to stop its spin before the target is reached. Computations of the required torque offer little hope that this method will prove practical.

Bearing-mounted charges that permit part of the shell to spin, for stability, while the charge itself spins only slowly, have been proven practical. However, a means is required to compensate for the low spin rate, as is a means to assure the uniformity of projectile spin rate.

Fin-stabilized rounds are commonly used as a means to avoid spin degradation. Even these types are often given a small amount of spin in order to improve their stability in flight; therefore, spin compensation is still required.

Any technique for reducing the rate of spin of a given projectile provides only an interim solution. As soon as a fluted liner can be designed to compensate for the frequency of spin of a standard round of the given caliber, it provides the most convenient and economical solution to spin-degradation for that caliber (Ref. 9).

2-18.7. (C) Fuze Action

The use of a suitable fuze is a major factor in the effective use of shaped charges that are to be activated on impact. The contact fuze must function quickly enough to detonate the charge before the cone liner becomes deformed, and before the projectile is deflected. This is vitally important when shaped charge projectiles strike high obliquity armor, because the speed of fuze action will affect the relative amount of surface armor area that is perforable. If the projectile is fuzed with an inertial-type base fuze, as shown in views (A) and (B) of Fig. 2-11, the inherent delay action of the fuze plunger may allow the projectile to ricochet before detonation, or permit collapse of the ballistic cap under forward inertia and cause an appreciable decrease in the standoff distance (Par. 2-18.8, below).

It is desirable to start initiation at the front end, at the instant of impact, and to transmit the impulse to the rear end so that the detonating charge may be initiated from the rear. However, this must take place much faster than occurs with the use of the inertia-type base fuze. There are two principal means of accomplishing this desired result. One uses the so-called "spit-back" (flash-back) fuze. In this fuze a small, shaped-charge explosive in the nose of the projectile is initiated by a percussion primer and fires a jet backwards, through a passage provided in the main charge, into a base booster. Because the velocity of such a small jet is very high, this fuze provides an extremely rapid method of transmitting the trigger action from the front to the rear. The other type of nose-initiated fuze is electrically actuated. In this type, often referred to as the "point-initiating base-detonating" (PIBD) type, crushing of the nose sets off an electrical impulse which is carried by wires to an electrical detonator at the rear of the projectile.

2-18.8. (U) Standoff Distance

One of the most important factors governing depth of penetration by shaped charges is the standoff distance. Standoff distance is the distance between the base of the liner and the surface of the target, at the instant of explosive initiation. This distance may be given in absolute terms, such as inches or millimeters, or may be expressed in terms of the charge diameter (i.e., 1½ charge diameters, 2 charge diameters).

Proper projectile design provides a standoff distance that allows time for the fuze to function properly and the cone to collapse, forming a jet of proper density, thus realizing the maximum capabilities of the projectile. View (C) of Fig. 2-11 illustrates the shaped charge technique as used in an anti-vehicle land mine. The distance from the top of the mine to the bottom

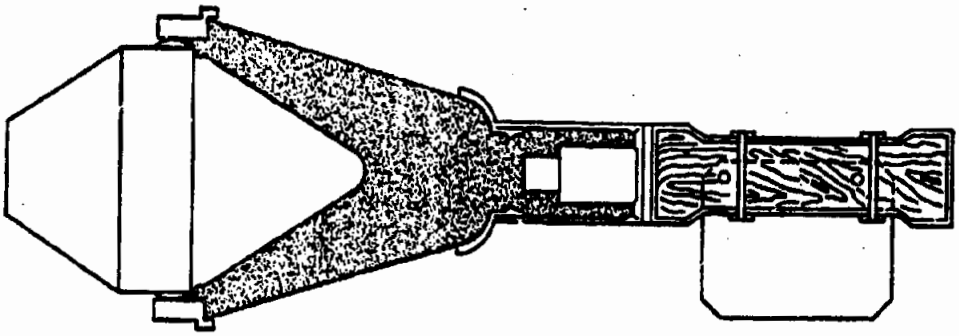

(A) "PANZERFAUST" H.E.A.T. ROCKET (GERMAN & SOVIET)

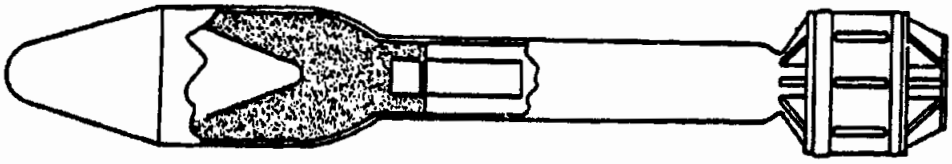

(B) 3.5 in. H.E.A.T. ROCKET (U. S.)

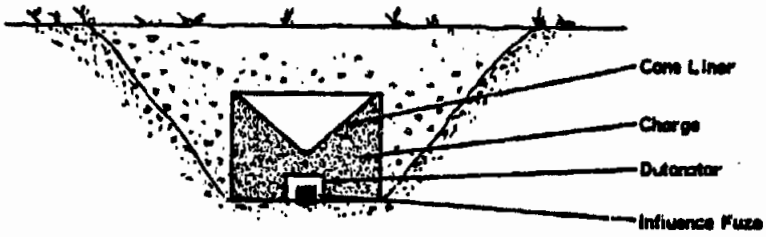

(C) SHAPED CHARGE LAND MINE

Figure 2–11. Typical Shaped Charge Anti-Vehicle Applications

of the vehicle hull is the standoff distance provided. The dependence of penetration depth on standoff is illustrated in Fig. 2–12, which shows typical craters produced in mild steel by static charges fired at various standoff distances.

2–19. (S) DAMAGE MECHANISMS

2–19.1. (C) General

In general, there are two primary damage mechanisms which act to produce a shaped charge kill: perforation by a jet of high and hyper-velocity particles; and vaporific effect. The types of damage produced by the two mechanisms are quite distinct. The perforating jet produces holes in the structure, and also produces internal target damage by the jet and target fragments. The vaporific effect produces damage mainly by what appears to be internal blast. Which damage mechanism will be primarily operative in a given case will depend on such factors as the shaped charge size, cone geometry and material, standoff distance, and target characteristics.

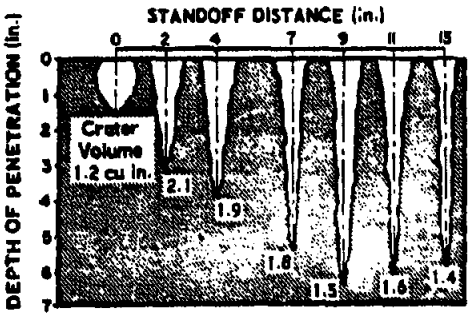

Figure 2–12. Penetration vs Standoff

2-19.2. (S) Perforation Damage

(U) Shaped charges which can produce perforation damage can also ignite or detonate fuel and explosives inside the target, be it a vehicle, building, or aircraft. Aside from the above effects, the perforation type damage mechanism becomes important against aircraft only when the size and density of the fragment jet are sufficient to produce an entrance hole diameter which is significant when compared to the linear dimensions of the target. Perforation damage is the primary damage mechanism of shaped charges made with steel or copper liners, and is an active (although not necessarily the primary) damage mechanism of shaped charges with zinc or aluminum liners.

(U) Increasing the depth of penetration is not necessarily the same as increasing the effectiveness of the shaped-charge against the target. Aside from the internal damage done to the target by the residual penetration of the jet, the spatial distribution, mass, and velocity of spall fragments all affect the lethality of the shaped charge. Those particles spalled from the inner surface of the target are largely responsible for the damage inflicted by a perforating jet.

(C) It is desirable to obtain some measure of probable damage after perforation. Examination of a body of test data shows that the total number of spall particles observed is directly proportional to the cross-sectional area of the hole, formed by the jet, at the exit surface of the target. Since the hole diameter is proportional to the rate of transfer of energy from jet to target, it is implied that the total number of spall particles formed is in proportion to the rate of transfer of energy as the jet penetrates the last element of target material. (Ref. 10).

(C) The above statement may be illustrated by Fig. 2-13, which represents the perforation obtained by the shaped charge, as shown, in a stack of twelve, one-inch-thick, metal plates. The hole diameter becomes less as the hole depth increases. It should be clear that this is due to the decrease in residual energy of the jet as it penetrates. The area of the hole at each increment of depth is in proportion to the residual penetration available at that depth, and also in proportion to the total number of spall particles produced by a penetration of that thickness of armor.

(S) Keeping in mind the fact that the number of spall particles is proportional to the area of the hole at the back of the target per-

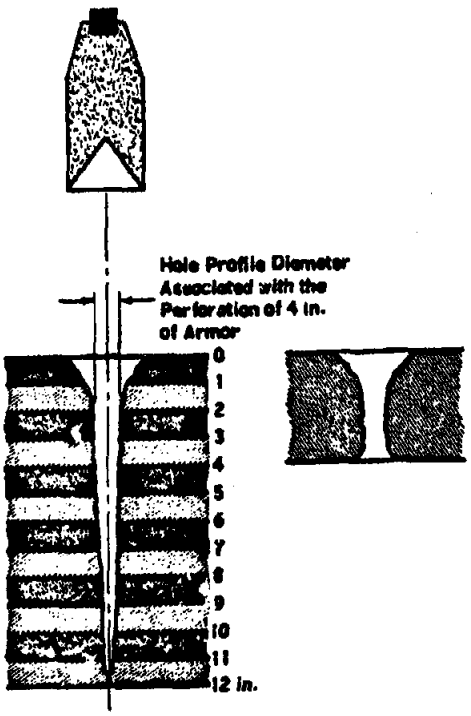

Figure 2–13 (C). Measurement of Hole Profile Diameter (U)

forated, the relative lethality of a charge can be varied by using some of the cone shapes illustrated in Fig. 2–8, which shows the hole profiles obtained with the cones.

(S) The first profile on the left (Fig. 2–8) is that produced by the ordinary 42-degree copper cone; it is shown for purposes of comparison. The second profile shows the effect of a very simple change in geometrical configuration, one useful in the design of warheads for large weapons, where penetration can be sacrificed in favor of increased lethality. The third profile shows the effect of another simple geometrical modification (a copper trumpet). This design not only yields somewhat greater penetration than a simple cone, at short standoffs, but also affords a hole of almost uniform diameter. Thus, at the expense of some lethal effect against thinly armored targets, increased effectiveness has been achieved against thicker ones. A liner of similar geometry, but of low-density metal (aluminum is illustrated), produces the fourth hole profile, which would be useful under the same circumstances as the second. The fifth hole profile is that produced by a 60-degree cone of lead-antimony. The greatest depth of penetration is attained by this type, but with decreased lethality against thin targets (Ref. 11).

(S) Further experiments are now being conducted on methods of enhancing the lethality by propelling a follow-through projectile through the jet hole. The projectile is intended to have a high-explosive filler. Other experiments are being conducted with chemicals which are focused into a jet, oriented on the axis of the hole, at the appropriate time for entering the hole without being obstructed by the slug.

2–19.3. (C) Vaporific Effects

The vaporific effect exhibits many of the same characteristics as the detonation of a high explosive charge inside an aircraft structure. Separate aircraft subjected to the two types of damage (detonation of a high explosive charge, and vaporific) show the same effects of internal blast.

It is concluded that the primary mechanism that is active in the vaporific explosion is the capture of the kinetic energy from the impacting particles (Ref. 12). Confinement is necessary. The tighter and more rigid the structure penetrated, the greater the resulting damage appears to be. The material being affected is also of significance. The degree of vaporic effect suffered by the following metals is indicated by the order of their listing, with the first named metal being most affected: magnesium, alclad aluminum, 24S aluminum, 75S aluminum, and 18–8 stainless steel. The thickness of the target material is another determining factor, because thicker materials contribute more finely-divided material (Ref. 13).

Section IV (C)—Blast

2–20. (U) INTRODUCTION

When a conventional or nuclear explosive charge is detonated in air, it is accompanied by the release of a large amount of energy in a small time-space environment. Most of the materials in the charge are immediately converted to gaseous form at high temperature and begin to expand rapidly, compressing the surrounding air and thus initiating a shock wave. This shock (or blast) wave, propagates through the surrounding atmosphere in a manner somewhat similar to a sound wave. However, the shock wave, unlike a sound wave, travels at supersonic velocity and causes appreciable increases in pressure, density, temperature, and air particle velocity.

The blast wave thus formed is capable of effecting considerable damage on many types of targets. The degree of damage is dependent upon the charge size, distance from the explosion to the target, atmospheric conditions, altitude, and the ability of the target to resist the loads imposed by the blast wave. The blast wave has several characteristics which may be related to damage: peak pressure, impulse, and dynamic pressure (Ref. 14). These are briefly described in following paragraphs, and are analyzed in detail in Ch. 4, Sec. I.

In general, the characteristics of the blast wave from a nuclear explosion are similar to those from conventional explosions. However, there are several quantitative differences which affect the blast wave properties. These differences and their effects are discussed in Ch. 4, Sec. I.

2–21. (U) PEAK PRESSURE

The shock wave is bounded by an extremely sharp front, called the shock front, which represents a discontinuity in density, pressure, and temperature of the medium through which it passes. Here, the pressure rises abruptly from atmospheric pressure to a peak pressure, generally referred to as peak overpressure, which is measured in psi over the atmospheric pressure (Ref. 15).

When the shock front passes a given point it causes an abrupt rise in overpressure, which is followed by a gradual decline to ambient, a further decline below ambient, and, finally, a return to normal atmospheric pressure. The portion of the wave in which the overpressure is above ambient is termed the positive overpressure phase; the remaining portion, where the pressure is below atmospheric, is referred to as the negative pressure phase. The decrease in pressure below ambient is usually small when compared with the increase during the positive phase.

The blast wave decreases in amplitude (peak overpressure) and lengths (increases in duration of overpressure) as it propagates. At a given distance from a blast source, the peak overpressure and duration both increase with increase in energy of the explosive source (Ref. 3).

When an incident air blast strikes a more dense medium, such as the earth's surface, the wave is reflected. Under proper conditions, the reflected wave overtakes the incident wave and the two merge to form a single shock front of higher pressure than either original wave. The combined front is called the Mach stem, and the region where the two shocks have merged is referred to as the region of Mach reflection (Ref. 17). Reflection and Mach characteristics are discussed in Ch. 4, Par. 4–2.2.6.

When the shock front strikes the face of an object, reflection occurs. As a result, the overpressure builds up rapidly to at least twice (and generally several times) that in the incident shock front. This reflected pressure, caused by arresting the moving air particles behind the shockfront, is referred to as face-on overpressure. The pressure at the side of the object, where little or no reflection or dynamic pressure effect occurs, is generally called the side-on overpressure. A measure of side-on overpressure plus dynamic pressure is referred to as total pressure.

Under conditions where the wave front has not completely surrounded the object, a considerable pressure differential will exist between the front and rear. This pressure differential will produce a lateral (translational) force, tending to cause the object to move bodily in the same direction as the blast wave. The translational force is known as diffraction loading, because it operates while the blast wave is being diffracted around the object. The extent and nature of the motion will depend upon the physical characteristics of the object and on the time history of the overpressure.

When the blast wave has completely engulfed the object, the pressure differential no longer exists. However, the pressures applied are still in excess of normal, and the diffraction loading is replaced by an inwardly directed pressure tending to compress or crush the object. For an object with no openings, this crushing action will cease only when the overpressure has decayed to zero (Ref. 17).

If the object under consideration is large, the diffraction loading will operate for a longer time. For small objects, the diffraction period is so short that the corresponding loading is usually insignificant. For objects with openings, the internal and external pressures will tend to equalize, thus nullifying both diffraction and compression forces.

2–22. (U) DYNAMIC PRESSURE

For a large variety of target types, the degree of damage may depend on the dynamic pressure associated with the explosion. The dynamic pressure is a function of the wind (particle) velocity and the density of the air

behind the shock front. For very strong shocks the peak dynamic pressure is greater than the overpressure (Ref. 15).

Like the overpressure, peak dynamic pressure decreases with increasing distance from the explosion center, although at a greater rate. The duration over which the dynamic winds act in the direction of shock motion, at a given location, is slightly longer than the positive phase of the overpressure. However, by the time the overpressure has decayed to zero, the dynamic pressure is usually insignificant.

Reflection phenomena cause certain changes in the dynamic pressures, as they do with peak overpressures. Under such conditions, the classical shock front disappears and peak values of dynamic pressure occur at different times for a given range. Both thermal and mechanical (surface) effects contribute to these variations (Ref. 15).

During the entire period that the positive phase of an airblast wave is passing, an object is subjected to dynamic pressure loading (or drag loading) caused by the strong transient winds behind the shock front. Like the diffraction loading, the drag loads produce a translational force in the direction of shock motion. However, drag loading usually persists for a relatively long period of time in comparison with diffraction loading. It is the effect of drag loading which constitutes an important difference between nuclear and conventional detonations. For equivalent peak overpressures, the duration of the drag phase is much longer for a nuclear explosion than for a conventional one. Correspondingly, the dynamic pressure impulse from a nuclear detonation is of much greater magnitude. For conventional high explosive, the duration of the drag phase is usually so short that the dynamic pressure impulse may be considered negligible.

In many cases, damage to targets by conventional explosives is a function of both the positive phase overpressure and its duration (known specifically as the overpressure impulse) rather than a function of peak overpressure alone. Overpressure and dynamic pressure impulse are discussed in Ch. 4, Par. 4-2.2.

2-23. (C) WAVE PERTURBATIONS

2-23.1. General

When a nuclear weapon is burst over a real target area, the condition and nature of the surface must be considered, since under some circumstances, severe modifications of the blast wave may occur. These modifications are due to the physical characteristics of the surface.

For relatively low-scaled heights of burst, the earth's surface absorbs sufficient thermal energy to reach a temperature of several thousand degrees in a relatively short period of time. If certain surface conditions exist, a hot layer of air or other gases will form with explosive rapidity above the earth's surface. If this thermal layer is sufficiently intense, a separate pressure wave forms and moves ahead of the incident and reflected blast waves. This detached wave is known as the precursor.

The surface characteristics necessary for the formation and development of the precursor are not completely understood. However, precursors have been observed over coral and desert type soils, forest areas, and asphalt, and are expected over other surfaces such as agricultural and urban areas. It is not expected that precursors will occur over water, snow, ice, or ground covered with a white smoke layer.

The precursor produces non-classical wave forms. The rise in pressure at shock arrival is not nearly as instantaneous as in free air. The positive phase duration is somewhat longer in the presence of a precursor, and the impulse is correspondingly greater. It is believed that the increased dynamic pressures which result from precursor formation are caused by increased particle velocity and the addition of dust particles to the transient winds.

It has been found convenient to divide the variations of non-ideal wave forms into five major classifications, as illustrated in Fig. 2-14 for overpressure and in Fig. 2-15 for dynamic pressure. The illustrated wave forms, with types A through E indicating waves encountered while progressing outward from ground zero, are discussed in following sub-paragraphs (Ref. 16).

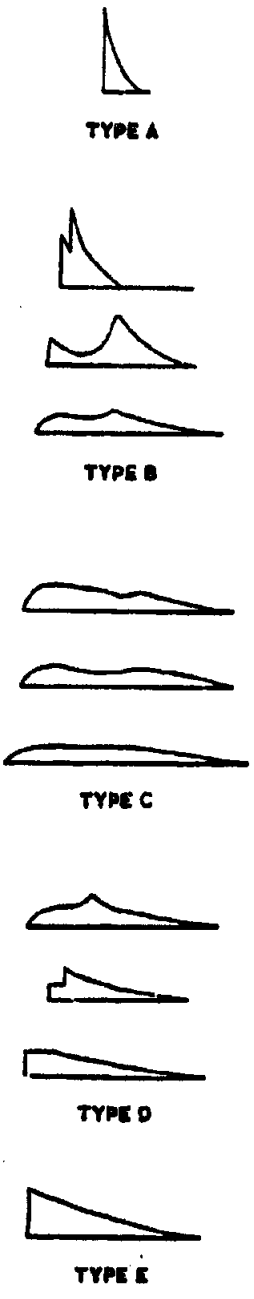

Figure 2–14 (C). Non-Ideal Wave Forms, Overpressure (U)

2–23.2. Overpressure Wave Forms (Fig. 2–14)

2–23.2.1. *Type A*

This type is a relatively ideal wave form, with a sharp rise to a peak value, followed by a rapid exponential decay. Usually the peak pressure is rather high, and the duration is rather short, in comparison with the other four wave forms.

2–23.2.2. *Type B*

This wave form, with two distinct peak values, becomes increasingly non-ideal with increasing range. Usually shock-type rises are evident at the closer ranges. However, as the distance from ground zero increases, the separation of the two peaks as well as the rise time for the main shock increases, while the first peak attenuates more rapidly than the second. At midrange, the wave form is characterized by a shock-type rise to a first, low peak, followed either by a plateau or a slow decay, with a longer rise to a higher, second peak preceding a more rapid decay. As the ground range continues to increase, the first peak becomes round and the second peak attenuates more rapidly than the first. This wave form is typical of the early stages of development in the precursor cycle.

2–23.2.3. *Type C*

This is a wave form whose peaks and valleys become poorly defined with increasing range. At the closer ranges, the wave form shows a first, large, rounded maximum followed by a slow decay, then a later, smaller, second peak. As the distance from ground zero increases, the first peak attenuates more rapidly than the second, so that the two peaks become comparable in magnitude, while the rise times become longer. The second peak disappears at the farther ranges, resulting in a low, rounded, flat-topped wave form with a long initial rise and a rather slow decay marked by considerable turbulence. This wave form is typical of strong precursor action.

2–23.2.4. *Type D*

This wave form progressively loses its nonclassical characteristics with increasing range.

At the closer ranges, the wave form shows a compression-type rise to a rounded plateau, followed by a slow rise to a second, higher peak. As the distance from ground zero increases, the rise times decrease, so that the front of the wave form develops a step-like appearance, and the time separation between the two peaks becomes less. At the farther ranges, the second peak overtakes the first peak, to form an almost classical form with a sharp rise to a more or less level plateau, followed by an essentially regular decay. This wave form is typical of the clean-up portion of the precursor cycle.

2–23.2.5. *Type E*

This is a classical or ideal wave form with a sharp rise to a peak value, followed by an exponential decay. The duration is rather long in comparison with the type-A wave form, and the rate of decay is slower.

2–23.3. Dynamic Pressure Wave Forms (Fig. 2–15)

2–23.3.1. *General*

A tentative classification of the various dynamic pressure wave forms has been made. It is not possible to make a direct correlation of these with the five general types of overpressure wave forms, due to the lack of experimental data for dynamic pressure, particularly in the close-in region. Nor is it possible to draw a wave form height-of-burst chart for dynamic pressures, at this time, because of the lack of experimental data.

2–23.3.2. *Type A*

This is a relatively ideal wave form, with a sharp rise to a peak value followed by a very rapid decay. The duration is usually rather short in comparison with the other four wave forms.

2–23.3.3. *Type B*

This double-peaked wave form has a shock-type initial rise in most cases. The second peak is larger at the closer ranges, but becomes comparable in magnitude with the first as the distance from ground zero increases.

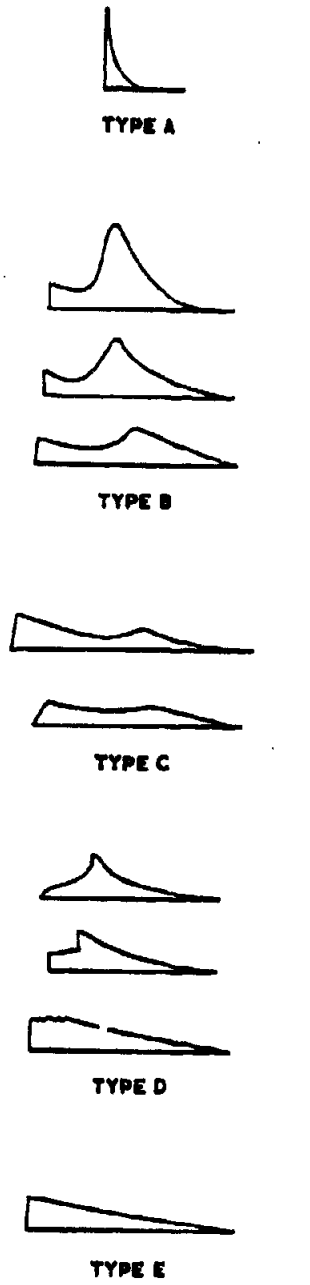

Figure 2–15 (C). Non-Ideal Wave Forms, Dynamic Pressure (U)

[redacted]

2-23.3.4. Type C

This is a transitional double-peaked wave form with longer initial rise time. Actual record traces have a very turbulent appearance. The second peak is smaller than the first and becomes somewhat indefinite with increasing range.

2-23.3.5. Type D

This essentially single-peaked form is characterized by a low amplitude plateau with a slow, smooth rise at the closer ranges. Actual traces have a very turbulent appearance. As the distance from ground zero increases, the turbulence becomes less and the plateau develops a shock rise with a flat top, or a slow steady increase to a second shock rise followed by a smooth decay. The initial disturbance at the front of the wave form eventually dies out at the farther ranges, leaving a smooth, clean record with a slight rounding after an initial shock-type rise.

2-23.3.6. Type E

This is a classical or ideal wave form with a sharp rise to a peak value followed by an exponential decay. The duration is rather long in comparison with type-A wave forms, and the rate of decay is slower.

Section V (C)—Mine Clearing Devices

2-24. (C) DESCRIPTION

(U) It is possible to detonate land mines by the blast wave from a nuclear or conventional explosion. The capability of the blast wave to detonate the mine is usually stated in terms of the overpressure required for detonation, which is dependent upon the mine type, burial depth, mine spacing, and soil characteristics. Only nuclear explosions, however, have a sufficiently wide radius of lethal overpressure to be able to clear entire minefields.

(U) Although mines can be detonated by explosions acting directly on either the main explosive or the more sensitive primer, or booster, the overpressures required are so high that blast action on mine pressure plates is always the controlling effect. Buried mines are insensitive to the thermal and nuclear radiation associated with the explosion.

(C) In general, land mines are sensitive to the rise time of the blast wave; i.e., if the rise time is long, greater pressures are needed to actuate a given mine than if the rise times are short. Long rise times are characteristic of the precursor zone. Therefore, in the criteria given for detonation, two sets of data must be specified for each mine type, depending upon whether or not the mine is expected to be in a precursor zone. On the other hand, all explosions having overpressures of less than about 8 psi have fast rise times. Therefore, for mines which require actuation pressures of less than about 8 psi, the criteria are the same for explosions which produce a precursor as for those that do not. This is also true for mines with fuzes which are insensitive to rise times (Ref. 16).

(U) The criteria for mine detonation do not usually include any sympathetic actuation effects. Sympathetic detonation of a mine is caused by the transmission of a detonation wave through the air from the explosion of another mine. Mines are usually spaced so that the pressures from the detonation of one mine do not sympathetically detonate adjoining mines. However, if the spacing of mines is close enough, it is possible for the combined overpressures of a nuclear blast and an actuated mine to effect sympathetic detonation of an adjacent mine that was not actuated by the nuclear blast. Gaps in mine fields, if sufficiently large, halt this process. Therefore, extensive clearance by sympathetic actuation cannot be depended upon.

2-25. (U) COMMON EXPLOSIVE DEVICES

It is feasible for a conventional artillery shell to detonate a mine if the shell has a sufficiently large bursting capacity, and if the distance

[redacted]

between exploding shell and mine is sufficiently small. It is not, however, an economical means of clearing mine fields because of the excessive number of shells that would be required. Conventional artillery shells are of some limited value in attacking a mine field because they can damage some of the mines (buried and/or unburied) by fragments, displace and damage surface mines, and cut trip wires attached to antipersonnel mines.

Conventional explosives have also been adapted to linear type charges, wherein the explosive is placed within a long steel tube (the bangalore torpedo) or a flexible cord. The linear charge is then pushed into the minefield, or, in the case of the flexible cord, pulled across by a small rocket, and then detonated (Ref. 18). The resulting blast will clear antipersonnel mines within narrow limits along the length of the charge. Whether or not the charge will be effective against antitank mines depends upon the amount of explosive per unit of length, the mine type, mine emplacement technique, and soil characteristics.

Section VI (C)—Ground Shock

2-26. INTRODUCTION

The production of ground shock by an explosion is extremely complex, and, in some respects, not completely understood. Basically, ground shock may be produced by two separate mechanisms. One mechanism is the sudden expansion of the bubble of gas, from a surface or underground explosion, which generates a pulse or oscillation in the ground. This is termed direct ground shock. As this direct shock propagates through the ground, it may be modified by reflections and refractions from underlying bedrock or hard strata, or rarefaction from the air-ground interface. The second mechanism is the production of a ground shock by the air blast wave from an explosion striking and moving parallel to the ground surface. This is termed air-induced ground shock (Ref. 19). For a given burst geometry, except at extremely short ranges, these two forms of ground shock are separated in time. Because the direct ground shock is usually attenuated very rapidly, air-induced ground shock is more important as the cause of damage to underground installations, except for extremely close ranges and for deep underground bursts.

2-27. PHYSICAL MECHANISMS

The physical mechanisms of major interest in regard to damage produced by ground shock are ground pressure (or stress), acceleration of soil particles, and displacement of soil particles. Collection and analysis of data for these mechaniams is covered in detail in Ch. 4, Par. 4-3.3.2.

Ground pressure is changed into directional components, which differ in magnitude, by the shear and cohesive strength of the soil. These directional pressure components are termed stresses. Under the dynamic loading from a nuclear explosion, the direct ground stresses rise most abruptly in the ground nearest the explosion, whereas at greater distances, the peak stresses at any specific point are reduced and the rise times are increased. Air-induced ground pressure (stress) is closely related to direct ground stress. Just below the surface, the air-induced shock stresses, and durations, are approximately equal to the changing air-blast positive pressure, and duration.

Vertical acceleration of soil particles is caused by both types of ground shock, direct and air-induced. The air-induced, occurring later, causes a sudden increase in the particle acceleration. Displacement of soil particles will be both permanent and transient. In addition to the obvious displacement resulting from cratering, both types of displacement occur, to a lesser degree, beneath the ground surface. Displacement is affected to a considerable extent by the soil types and moisture content.

[redacted]

Section VII (U)—Fire

2–28. INTRODUCTION

Fire usually implies combustion or burning of a fuel. The term combustion implies a more or less rapid chemical reaction between the fuel and an oxidizer (usually oxygen). This reaction produces heat and light, these being emitted primarily from a zone called the flame (Ref. 20). For a burning fuel in solid or liquid form, the vapors from the fuel support the flame.

The combustible constituents of conventional fuels are carbon, hydrogen, sulphur and hydrocarbons. Other constituents are oxygen, nitrogen, moisture, and ash. (In incendiaries, other constituents such as magnesium and aluminum may be used.) In burning, the combustibles combine with oxygen in the air and in the fuel to form carbon dioxide (CO_2), carbon monoxide (CO), sulphur dioxide (SO_2), and water (H_2O). The ash includes all non-combustible matter. The nitrogen in the air is inert and is not burned. Generally, ignition occurs when the body temperature rises sufficiently for a self-propagating reaction to occur at some elevated temperature; that is, when the heating effect of the oxidation reaction overcomes the loss of heat at some point in the object. This elevated temperature is referred to as the ignition temperature.

The requirements for combustion are:

1. The presence of a fuel and oxidizer in proper proportions. Some fuels may contain the oxygen.
2. Exposure of fuel particles to the oxidizer throughout a period of time sufficient for their combustion.
3. Maintenance of the combustion zone at a temperature above the ignition temperature (Ref. 21).

For fuel in a gaseous state subjected to the action of an ignition source, the small local volume around the source begins to burn, and if the mixture is flammable, the reaction proceeds to the next layer, which begins to burn. Eventually the flame propagates throughout the gaseous mixture. The flame surface at any instant is referred to as the flame front, and the conditions which determine the velocity of the flame front also distinguish a fire from an explosion.

2–29. FIRE DAMAGE

Damage resulting from fire includes destruction of the utility or structural integrity of structures and vehicles, detonation of explosives or engine fuel, physical or psychological incapacitation of personnel, and the disabling of equipment components. Anything which is flammable is subject to destruction by burning. In addition to the actual consumption of material, the properties of structural materials are adversely affected by the elevated temperatures encountered with fire.

Fire may be caused by direct sources such as fire bombs, napalm, white phosphorus, incendiary grenades, incendiary bullets, etc. Fire may also be induced as a secondary effect of fragments, projectiles, or other primary kill mechanisms when they act upon target components. When the cause of burning is radiant energy (produced by the thermal radiation from a neuclear explosion), the effects can be catastrophic to urban areas, because many fires are started over a wide area.

Fire, or flame, as an agent for incapacitation of personnel, differs from nuclear thermal radiation in several ways. First, because it is not exclusively electromagnetic radiation, it can pass around corners to burn otherwise shielded personnel. Secondly, it can consume the available oxygen, causing death by suffocation. Thirdly, it may bring on shock from paralyzing fear. In addition, it may destroy those things (food, clothing, and shelter) which are essential to the maintenance of life. Of these several damage effects, the immediately important ones are burns and suffocation. The particular burning agent might be white phosphorus or napalm, or some target material ignited by the burning agent.

[redacted]

2–30. (U) INTRODUCTION

2–30.1. General

The large scale use of chemical agents to influence battlefield success originated during World War I. In the early stages, many chemical compounds were proposed, and some of them were actually employed on the battlefield. Since World War I, however, the requirements of modern warfare, involving the problems of large area coverage and large scale production and supply, have reduced the number of militarily practicable chemical agents to a small group. The nerve gases, outstanding because of their high lethality, may well represent the most important group of chemical agents.

Attention has recently been focused on the possible use of non-lethal incapacitating agents to influence military affairs. Such agents may produce temporary blindness, mental or physical incapacitation, or anesthesia.

The chemical agents may best be separated or classified for tactical use according to the seriousness of their effects, using a scale with death as one limit and temporary incapacitation as the other limit. The five primary agents discussed in detail in Ch. 2, Par. 2–31 represent varying effects on this scale.

Chemical agent employment is the intentional use of various gaseous, liquid, and solid agents to achieve the occupation of territory and the disabling of enemy personnel. In attaining these ends by any form of warfare, it is desirable that a minimum of men and materiel be expended, and that the least possible damage be inflicted upon objects of probable value. In this regard, the chemical agents are outstanding. A chemical attack, in contrast to a conventional ballistic attack, begins only when the agent is released and may continue for hours, days, or even weeks, depending upon the particular agent and the prevailing weather conditions.

Although chemical agents are used primarily for their effects on personnel, some agents will have a deleterious effect on specific materials. This property could be utilized effectively, for example, against targets such as satellites and missiles by the destruction of thermal balance systems, through the changing of the structural emissivity (Ch. 9, Par. 9–7.3.).

2–30.2. History of Chemical Agent Use

The beginnings of the use of chemicals in warfare are lost in antiquity. The earliest recorded attempt to overcome an enemy by the use of poisonous and suffocating gases occurred in the year 428 B.C., during the wars between the Spartans and Athenians (431-404 B.C.). At the siege of Clataea, wood saturated with pitch and sulphur was burned under the walls of the city. This operation was unsuccessful, but five years later, at the siege of Selium, a similar operation was completely successful.

The North American Indian produced a toxic gas by burning poison ivy saturated with fish oil. Poison gas is known to have been proposed for use in the Crimean War, against the Russians, and in the Civil War, against the Confederates, but neither suggestion was carried out (Ref. 22). Tear gases for harassment purposes were used by the French in August of 1914, followed shortly afterward by German and British use of similar agents.

The employment of chemical agents as a weapon of modern warfare dates to the early spring of 1915. This period brought the Germans in World War I to the realization that they had arrived at a deadlock which conventional warfare could not resolve. The situation was particularly grave because supplies were low and logistics had become a serious problem. Accordingly, Germany mobilized her industrial and scientific talent, and on the afternoon of April 22, 1915, unveiled a new weapon: the toxic gas chlorine (Ref. 22).

By modern standards, chlorine is an ineffective agent, yet within a few hours after it was first released, it caused complete demoralization among Allied troops. In the months that followed, both sides, taking advantage of the World War I static-type warfare, employed toxic chemical agents. The British, for example, retaliated with chlorine gas at Loos, six months after its first use, and the French

and Germans tried several other casualty producing gases. A major instance of this occurred in December of 1915, with the German introduction of phosgene, a choking gas which could penetrate the crude protective masks then in existence.

In the following months, protective masks were improved. To counteract this, the Germans developed an agent which, even though not highly poisonous, would cause nausea and vomiting. The effects of this agent made the troops remove their gas masks, which left them subject to the more lethal agents accompanying the vomiting agent. In 1917, the Germans first employed a chemical agent that attacked all parts of the body, thereby rendering the use of gas masks less effective. This agent was mustard, a poisonous, multiply effective agent which could penetrate almost any ordinary type of clothing. It proved to be extremely effective and was used throughout the remainder of the war.

In World War I, over 3,000 substances were investigated for possible use in toxic warfare, but only 32 were actually tested in combat, and only 12 obtained noteworthy results. Both sides employed a total of approximately 17,000 chemical troops and caused 1,297,000 casualties, but only 91,000 of these were deaths. This is about one-third to one-fourth the per cent of deaths obtained with other weapons. (Gas casualties are compared with casualties by all other mechanisms in Table 2-2.) Approximately 9,000,000 artillery shells filled with mustard gas were fired, producing 400,000 casualties, being nearly five times as effective as shrapnel or high-explosive shells. One-third of the United States casualties were caused by gas, but only 2 per cent of these were fatal, as compared with the 25 per cent fatality of non-gas victims (Ref. 24).

The major participants in World War II carried chemical agents with them, but did not use them. However, a startling discovery was made at the end of the war, when it was found that Germany had stocks of a new gas of the nerve type, far more deadly than the standard gases of the Allies. The German supplies of these organic phosphates were seized by both the Western and Soviet forces. It must be assumed, then, that a chemical attack by the enemy using agents of the types described in this chapter is within the realm of possibility.

2-31. (C) PHYSICAL CHARACTERISTICS OF THE PRIMARY CHEMICAL AGENTS

2-31.1. (U) General

In the military use of chemical agents, there are four, predominant, operational factors to be considered in determining the most appropriate agent and method of application for a given tactical situation. These are:

1. Availability of protection against chemical agents, for enemy personnel.
2. The nature of physical protection available to the enemy.
3. The urgency, with respect to time, of casualty production.
4. Degree of acceptability to residual hazards.

There is no complete protection against a specific weapons system, whether it be high explosives, chemical agents, biological agents, or nuclear weapons. Physical protection greatly increases the high-explosive munition expenditure rates to produce a given casualty

TABLE 2-2. WORLD WAR I CASUALTIES

	Battle Casualties	Deaths	Non-Fatal Injuries	Per Cent of Deaths Among Casualties
Gas	1,297,000	91,000	1,206,000	7.0
Other Mechanisms	28,010,000	6,891,000	21,119,000	24.6
Total	29,307,000	6,982,000	22,325,000	—

level. Likewise, chemical protection (protective masks and clothing, and collective protection) will degrade the effectiveness of toxic attacks. However, under field conditions, neither physical nor chemical protection can be expected to prevent significant casualty effects.

Suitable targets for chemical weapons include enemy troop and artillery concentrations, reserves, logistical installations, and any other areas where enemy personnel may be concentrated.

Because chemical agents attack the body and produce specific damages according to the nature of the particular agent employed, the primary agents in this country's chemical arsenal are designed to range from the extremely lethal to the mildly incapacitating. The basic types of agents, and their relative position on this effects scale, are described in following paragraphs.

2-31.2. (C) Nerve Agents

The nerve agents represent the most recent development in the use of offensive warfare chemicals. Their two outstanding characteristics are that they cannot be detected by sensory means, and they attack the body through the multiple routes of ingestion, inhalation, and absorption through the skin. Their effects are to attack the nerve ends which control the muscles, thereby disrupting bodily functions. The time required for incapacitation is very short, usually only a few minutes after a casualty dose is received; and death swiftly follows.

The primary nerve agents are GB and VX. The former is a non-persistent agent which is most effective against unmasked personnel, because of its high lethality through the inhalation of very small amounts of agent. It can also cause casualties by its absorption through the skin, but the incapacitating and lethal dosages required are quite high. VX is a persistent agent which is designed to attack primarily through the percutaneous route. It is extremely effective in causing casualties among masked personnel, as only small amounts of agent need to contact the skin. Its long persistency makes it a continuing hazard to personnel traversing terrain and contacting materiel which has been contaminated. Development work is in progress to obtain a capability of dissem inating this agent as an aerosol, which wi. greatly increase the effectiveness of a given munition. VX also attacks through the inhalation route, but its primary value as a chemical agent is its characteristic of per·cutaneous action (Ref. 25).

2-31.3. (U) Blister Agents

The original blister agent introduced into modern warfare w· · mustard gas. The primary mustard agent is distilled mustard (symbol HD). In vapor form this is quite dense, and it can be initially detected by its garlic or horseradish odor. This agent quickly anesthetizes the olfactory senses, making subsequent sensory detection difficult, if not impossible.

As a vapor, HD may be used primarily for the attack of masked, dug-in (in bunkers) individuals through skin absorption. For attack of masked personnel in the open or protected by hasty field fortifications, it should be used primarily as a liquid, for skin absorption. This agent is primarily incapacitating and rarely results in death. Its primary effect is to cause deep burns on the skin and in the lungs, nose, throat, and eyes. Casualties require considerable medical care and nursing, and the severe burns are slow to heal.

2-31.4. (U) Riot-Control Agents

This family of nonlethal incapacitating agents find their main employment, in controlling unruly crowds of persons, such as in prison camps, or in dispersing refugees who are interfering with tactical operations. The agents may be disseminated in aerosol form, with vehicle-mounted or portable dispensers, or by hand grenades.

The primary riot control agent is CS, which is a white, crystalline solid. It causes an extreme burning sensation in the eyes and a copious flow of tears, coughing, difficult breathing and chest tightness, involuntary closing of the eyes, stinging action on moist skin areas, sinus and nasal drip, and nausea and vomiting on exposure to extreme concentrations via in-

gestion. The attacked individuals entirely lose their will to do anything but get fresh air. Generally, after several minutes in the fresh air (15 to 20), the fresh air will restore them to normal.

2-31.5. (C) Nonlethal Agents

These agents are still under development; however, they seem to possess considerable potential as incapacitating agents. They affect human beings by producing severe mental and muscular incoordination, and perhaps even temporary paralysis. They seem most applicable against quasi-military forces, such as might be encountered in an international police action, and may have tactical significance in addition to their potential for mass population control.

The primary incapacitating agent of this type currently under development is EA 2277. This agent is probably best disseminated in the form of a fine dust or smoke by large-caliber, medium-range missiles. In addition to physical incapacitation, most of the casualties from this agent will experience psychic abberrations, such as marked confusion, disorientation as to time and space, various hallucinations and delusions, and loss of memory for periods of at least 24 to 48 hours. With larger dosages, the onset of symptoms will be more rapid, and the effects will be more pronounced and will last longer.

It is believed that if a small amount of EA 2277 is inhaled (.5 to 1.0 mg), 50 percent of the personnel exposed will become incapacitated within three hours. due to lack of muscular coordination and decreased visual acuity. Physical incapacitation will probably continue from five to fifteen hours after the onset of symptoms.

2-32. (C) DISSEMINATION SYSTEMS

2-32.1. (C) General

(U) In order to accomplish the objectives of chemical munition systems (personnel control, incapacitation, or destruction), the agents must be effectively disseminated over the intended targets. Various delivery systems are available, depending on the tactical situation. A somewhat detailed presentation of these systems is given in Ref. 25. (This reference source is doubly valuable, in that it also gives a more detailed treatment of the characteristics of chemical agents—summarized in Ch. 5, Section VI of the present publication.)

(C) The main criterion which dictates the required type of dissemination hardware or munition is whether the agent is to produce its effects through the inhalation or percutaneous route. Agents disseminated primarily in the form of aerosol or, in the case of a solid agent, fine particles of dust, produce their effects through inhalation. Agents in liquid form are designed to attack through the percutaneous route.

(C) Conventional artillery, rocket, and missile systems and munitions have been modified to provide agent delivery and dissemination capabilities. In this form, their use by field troops is simplified, and the shells, warheads, etc., are generally unrecognizable as chemical-carrying or dispersing munitions, providing an element of surprise to their employment in a tactical situation.

2-32.2. (C) GB Systems and Munitions

This agent is extremely effective against unmasked personnel. Its primary delivery systems are artillery weapons, rockets, missiles, and spray tanks. When GB is used in howitzer and mortar shells, it is considered to be a combination toxic-HE round, with the fragmentation effect about one-half that of a comparable straight HE shell. The inability of personnel, under fire from this type of munition, to determine by sensory means that the round contains GB, makes this delivery system very effective against personnel without protective masks.

This agent is also disseminated by explosive bomblet munitions which are carried in missile and rocket warheads. These delivery systems provide a greater range and wider area-coverage capability, with fewer individual weapons batteries. The bomblets are deployed at some position in the air above the target by separating the warhead skin with primacord. The submissiles, or bomblets, then are made to spin

about a selected axis. This arms a fuze in each bomblet, which detonates a small explosive charge on impact with the ground. The explosion bursts the bomblet casing and causes the liquid agent to form a cloud of fine droplets. The particular aerodynamic characteristics of a spinning object causes a phenomenon called the Magnus Effect. This phenomenon causes the bomblets to glide at some small angle, thus allowing them to be dispersed over a larger area.

Meterological conditions such as wind velocity and direction, and temperature and temperature gradient, have some effect on the area coverage by the agent; however, the subject will not be considered here. The interested reader may consult Ref. 25 for more information on this particular aspect.

Specific munitions which utilize GB as a chemical agent are the 4.2-inch shell, the 90-, 105-, 115-, 120-, 155-, and 175-millimeter shells, and the E130R2 bomblet. Delivery systems are howitzers, mortars, guns, and recoilless rifles, and the BULLPUP, SERGEANT, LITTLE JOHN, and improved HONEST JOHN rockets. This agent can also be disseminated by the Aero 14-B aircraft spray tank.

2–32.3. (C) VX Systems and Munitions

The fact that this agent is absorbed through the skin makes it extremely effective against personnel in the open, even though they may be wearing protective masks. Also, its high persistency creates a continuous hazard for personnel who may come in contact with contaminated terrain and materiel.

At present, this agent is capable of being disseminated mainly by artillery shells, rockets, and land mines. Aircraft spray tanks are also considered standard agent delivery systems. There is currently underway a considerable amount of development work to obtain a bomblet munition to be carried in missile warheads, the bomblet to be capable of disseminating VX agent as an aerosol. This system has great potential because larger area coverage and high lethality can be obtained with a lower missile expenditure rate.

Specific VX munitions currently available are the 155-mm standard-wall howitzer shell, the 8-inch T170 howitzer shell, the 155-mm rocket, and the M23(E5) chemical land mine. The Aero 14–B aircraft spray tank is also available for disseminating this agent (Ref. 25).

2–32.4. (C) HD Systems and Munitions

The principal use of this agent is to cause delayed casualties by circumventing the mask. Delayed casualties will also be caused if the protective mask is not worn, by means of inhalation. HD in liquid form may be used to contaminate terrain and materiel, so as to cause casualties among troops encountering these contaminated surfaces. (It is especially effective against dug-in personnel in bunkers and in conjunction with barriers.)

This agent is disseminated by howitzer shells, bombs, mortars, aircraft spray tanks, and land mines. Specific munitions and delivery systems for HD are the 105- and 155-mm howitzer shells, the 4.2-inch M2 and M2A1 mortar shell, the 115-pound M70A1 gas bomb, the one-gallon chemical land mine, and the Aero 14–B aircraft spray tank.

2–32.5. (U) CS Systems and Munitions

Because of the nature of the employment of this non-lethal riot control agent, relatively short range disseminating systems and munitions are required. It is possible that the agent may be used mainly at close quarters, to control crowds of disorderly or milling persons; hence, hand grenades and gas dispersers are the logical methods of disseminating the agent. Munitions available are the M7A1 and M25A2 hand grenades. Dispersing systems are the portable M3 unit, the helicopter- or vehicle-mounted M4(E16R1), and the skid-mounted GED 5000 CFM M2. More detailed information on these systems and munitions are given in Ref. 25.

2–32.6. (C) EA 2277 Systems and Munitions

This agent is not yet fully developed as an operational, non-lethal, chemical weapon, hence

little detail work has been done on specific dissemination or delivery systems. Probably the best means of dissemination will be in the form of dust or smoke by large-caliber, medium-range rockets with minimal fragmentation. Its potential for the control of large groups of people, however, may be so great that delivery and dissemination systems of other types might have to be developed.

2–33. (S) AGENT EXPENDITURE RATES AND AREA COVERAGE ESTIMATES

(C) Tables 2–3 and 2–4 provide typical data available on agent expenditure rates of the primary toxic chemical agents, and of incapacitating agent EA 2227, respectively. Table 2–5 charts the area coverage for various riot-control agent dissemination systems and munitions (Ref. 25).

Section IX (C)—Biological Agents

2–34. (U) INTRODUCTION

This section discusses the characteristics of biological agents in general terms. A discussion of the effects of the agents is presented in Ch. 5, Paras. 5–21 and 5–23. Because of the nature of the material, some overlapping of data exists.

Biological agents may be selected to achieve many strategic objectives and certain tactical objectives. However, these agents are primarily strategic weapons because they provide no quick-kill effects and their optimum effectiveness accrues from the possibility of covering very extensive target areas (Ref. 29). The general purpose of biological agents for tactical consideration is to cause casualty effects in the enemy's forces in the field, at all possible ranges, for the purpose of weakening or destroying their capability to carry out their long-range combat mission. Biological agent weapon systems are characterized by the following (Ref. 28):

1. Small quantities of agent are required. For example, a small bomblet may contain several billion effective doses. Two or three such bomblets can produce a satisfactory casualty level over an area of about one square mile.

TABLE 2–3 (S). STANDARD EXPENDITURE RATES FOR PRIMARY TOXIC CHEMICAL AGENTS[a] (U)

Agent	Men In Open		Men With Overhead Cover	
	No Masks Available	Masks Available	No Masks Available	Masks Available
GB	3.0	36 [d]	3.0	36 [d]
GB spray	6.0	—	6.0	—
VX aerosol	3.0	12	6.0	24
VX liquid [d]	4.5	4.5	—	—
HD [c]	20.0	140.0	20.0	140.0

NOTES:

[a] Values given are based on the standard criteria enumerated in Ref. 26, and may not apply to very small targets. Rates are in pounds of agent per hectare to achieve 30 per cent casualties.

[b] Casualty level of 5 to 15 per cent. For this situation, no higher level of casualties can be assured, due to GB effects.

[c] These values apply to air burst or spray munitions.

[d] These are median values for the various types of munitions.

SECRET

TABLE 2-4 (C). ESTIMATED EXPENDITURE RATES AND DELIVERY REQUIREMENTS FOR 50 PER CENT CASUALTIES ON UNPROTECTED PERSONNEL, USING NONLETHAL AGENT EA 2277 (Ref. 25)[1] (U)

Munition, with Average Agent Content	Expenditure Rate per Hectare: Random Dispersal in Target Area (30 lb/hectare)	Expenditure Rate per Hectare: Upwind Target Edge Release on Target Less Than 2 Hectares[2] (50 lb/hectare)	Large Area Delivery Requirements (1 sq mile)
4.2-inch mortar (1 lb agent)	30 rounds	50 rounds[3]	Not feasible
155-mm howitzer (1.8 lb agent)	17 rounds	28 rounds[3]	Not feasible
M55 type area rocket (4 lb agent)	8 rounds	12 rounds[3]	46 launchers (45 rounds)
E42 type area rocket (10 lb agent)	3 rounds	5 rounds[3]	31 launchers (25 rounds)
Mechanical smoke generator	—	1 generator for 30 minutes	392 generators for 20 minutes
Mars type turbine generator (500 lb agent per hour)	—	1 generator for 6 minutes	104 generators for 15 minutes
Cargo aircraft w/ 10,000 lb payload:			
Bomb (15% agent payload)	—	—	9 aircraft
Dust spray (8,000 lb agent)	—	—	1½ aircraft
Fixed-wing aircraft:			
Fighter-bomber spray (500 lb agent payload)	—	1 per 10 aircraft	26 aircraft
L20 type spray (400 lb agent payload)	—	1 per 8 aircraft	32 aircraft
30-lb smoke-pot type munition (6 lb agent)	—	9 pots	2,160 pots

SECRET

TABLE 2-4 (C). (cont)

Munition, with Average Agent Content	Expenditure Rate per Hectare: Random Dispersal in Target Area (30 lb /hectare)	Upwind Target Edge Release on Target Less Than 2 Hectares [c] (50 lb /hectare)	Large Area Delivery Requirements (1 sq mile)
Irritant gas disperser:			
M3 type (15 lb agent)	Point target only	Not feasible	Not feasible
M4 type (80 lb agent)	—	1 disperser	Not feasible
Grenade:			
Burning type (9 grenades per lb agent)	Point target only	—	—
Bursting type (22 grenades per lb agent)	Point target only	—	—

NOTES:

[a] Rates and values are based on a conservative, preliminary estimate. Meteorological conditions are standard, with 5 mph wind and neutral temperature gradient. Casualty rate is 50 per cent. For 30 and 80 per cent casualties, multiply expenditure rates by 0.6 and 1.6, respectively.

[b] Includes ground release and direct aerosol release from fixed-wing aircraft flying 100 feet above ground.

[c] Applies to target less than 2 hectares.

2. Large areas can be covered at low cost. As an example, one bomber aircraft flight can cover about 1,000 square miles, producing a casualty rate as high as 70 per cent.
3. Biological attacks are insidious. They cannot be detected by any sensory means, nor are warning or detection devices satisfactory or available for field use.
4. Biological agents in aerosol form will penetrate fortifications and other structures.
5. The agents can be selected to provide gradation of effects, from mildly incapacitating to highly lethal.
6. Biological effects are delayed. For some agents, the time to take effect may be one to three days; for others, as much as three weeks may be required.
7. Except for biological agents disseminated by insect vectors, personnel are infected by breathing the agent.
8. For a few agents, immunization is available. In some instances it may be possible to overwhelm this immunity by increasing the amount of agent used, but the logistical requirement for a given strike will be greatly increased.
9. Biological agents, being living organisms, tend to die off at predictable rates, both in storage and after release as an aerosol.
10. Biological agents, once released, are affected by the climatic conditions. Sun-

light and relative humidity greatly affect the survival time of certain agents.

These characteristics apply, in most part, to attacks on human beings. A discussion of biological agents as used against animals and crops is presented later in this section.

In addition to being classified according to their lethality, and by the form in which they are disseminated, biological agents can be grouped under various microorganism types. A discussion of these types of microorganisms is presented in this section.

Biological agents can be delivered by various weapons systems and disseminated over the target by various munitions. Some of these systems and their corresponding munitions are listed later in this section.

The complex nature of the field of biological agents and of their employment as weapons necessitates the rather brief treatment given in this publication. The interested reader should consult References 28 and 30.

The real potential of biological agents lies in the future; if they are fully exploited, they can become one of the most potent and selective weapons available. Because they have not been tested under actual field conditions against personnel, their effects are difficult to assess positively with regard to such characteristics as their sensitivity to climatic conditions, level of casualty production, persistency, and epidemiological capabilities. Biological agents disseminated in aerosol form cannot be detected by sensory means. Insect vectors cannot be readily identified from normal arthropods without adequate sampling and laboratory testing. These factors make early detection extremely difficult. By the time insect incubation has been completed, wide dissemination of biological agents could present an acute medical problem to the target community. The potentials of biological weapons are thus considerably greater than those resulting from the natural or accidental spread of disease. On a small scale, their use might represent simply a sup-

TABLE 2-5 (C). AREA COVERAGE DATA FOR VARIOUS CS TYPE GRENADES AND DISPERSERS (U)

Munition	Number Employed	Wind Speed (mph)	Area Covered (sq m)	Effective Distance Downwind (m)
M7 Burning-type grenade	1	9–15	250 (approx)	35+
M25A2 Bursting-type grenade	3	12–18	1200 (approx)	90+
M3 Portable irritant gas disperser	Single filling (25 lb of agent)	4–6	2300–3900	200+
M2 skid-mounted irritant gas disperser (mounted on vehicle)	40 lb of agent— Vehicle speed 9 mph	12–15	Discharge distance— 500 meters	500
M4 helicopter-mounted irritant gas disperser (mounted in H-19 or larger helicopter)	100 lb of agent— Helicopter speed 50 mph— Helicopter height 50 feet	15	Discharge distance— 500 meters	500

plement to the ever present health hazards, but on a large scale the employment of biological agents can have a devastating effect, not only on the troops in the field, but on the civilian population in areas nearby and quite removed from the zone of military operation.

2-35. (U) TYPES OF BIOLOGICAL AGENTS

2-35.1. General (Ref. 27)

Biological agents, when used militarily, can be classified on the basis of persistence, contagious ability, or virulence. An agent able to resist unfavorable conditions of environment for long periods of time is classed as a persistent agent. Most organisms, however, are nonpersistent agents, since they are sensitive to changes in temperature, food, moisture, light, or air. A contagious disease is one which will spread rapidly from person to person, either by direct or indirect contact. These are the diseases responsible for epidemics of all forms. Virulence, or potency, is a measure of the disease producing ability of a particular agent. The resulting degree of illness varies considerably, not only with the agent, but with the route of entry into the body, the site of attack, and the strain of the particular organism. The effect of different strains of the same organism may range from mild infection to fatal illness.

Agents may be biologically identified as bacteria, rickettsiae, viruses, fungi, and protozoa. Toxins produced by certain microorganisms, plants, insects and animals are also considered as a biological grouping for agent identification.

The broad groups of organisms from which biological agents may be selected are described briefly in the following sub-paragraphs (Ref. 23). Additional details are found in Ch. 5, Par. 5-23.3.

2-35.2. Bacteria

The bacteria are a widely distributed group of typically one-celled microorganisms, chiefly parasitic or saprophytic, ranging in size from 1/50,000 to 1/2,500 of an inch. They exhibit three chief typical shapes: spherical (coccus), rod-shaped (bacillus), and comma- or spiral-shaped (spirillum). They are present everywhere in nature, being found in soil, water, air, and animal and plant bodies, both living and dead. Some bacteria are disease producers; the powerful toxins produced by some are also utilized as biological agents.

Most bacteria can be grown very easily in simple broth; they do not need living tissue for their cultivation. Examples of diseases caused by bacteria are typhoid fever, meningitis, tuberculosis, anthrax, brucellosis, glanders, tularemia, plague, bacillary dysentery, and cholera.

2-35.3. Rickettsiae

Rickettsiae are usually somewhat smaller in size than the bacteria, but are still visible under the ordinary microscope. They grow only within living cells, which makes production somewhat complicated. They are potent disease producers in man and are usually transmitted naturally by lice, ticks, and insect bites. Examples of diseases caused by rickettsiae are rocky mountain spotted , typhus, Q fever, and trench fever.

2-35.4. Viruses

The viruses are minute enough to be undetectable under the ordinary microscope, although some have been photographed with the aid of the electron microscope. Like the rickettsiae, they will grow only within the living cell; but it is known that they can survive for various periods of time in the air. There is some indecision existing as to whether these agents are living organisms or complex proteins capable of reproduction in living cells.

Viruses cause a number of diseases in humans, animals, and plants. Mumps, smallpox, psittacosis (parrot fever), influenza, foot-and-mouth disease, fowl plague, Newcastle disease, Venezuelan equine encephalomyelitis, rabies, tobacco mosaic, East African swine fever, hog cholera, Rift Valley fever, and rinderpest are examples of virus infections.

2-35.5. Fungi

Fungi include such plants as the yeasts, molds, mildews, and mushrooms. These organisms are well known for their ability to cause

spoilage of foods and fabrics. The fungi are plants which are generally destitute of chlorophyll. They reproduce primarily by means of asexual spores. Several plant diseases are caused by fungi. Among these are potato blight, cotton root rot, corn smut, and wheat rust. Should attacks be made on food crops, certain of the agents used might be in this class.

Generally speaking, diseases caused by fungi in humans are less severe than those produced by other microorganisms. They usually produce mild, but often chronic diseases such as ringworm, athlete's foot, and San Joaquin Valley fever. However, a few fungi are capable of producing serious diseases, such as blastomycosis (a chronic infection affecting the skin, lungs, liver, bones, spleen, and kidneys) in humans.

2-35.6. Protozoa

Protozoa are single-celled, animal-like forms occurring in a great variety of shapes, and in many cases having complicated life cycles. They range in size from 1/25,000 to 1/250 of an inch. The protozoans are mostly aquatic and reproduce by fission. A few types are parasitic. Examples of diseases caused by these organisms are amoebic dysentery and malaria.

Their complicated life cycles and reproduction method cause problems of mass production and transmission, which at the present time limit the application of this class as biological agents.

2-35.7. Toxins

Toxins, which are poisons produced by certain microorganisms, and by certain fish, jelly fish, shell fish, and insects, must be considered as possible agents for biological weapons. They might be used in two ways: either they could be produced outside the body and introduced into food and wounds; or the organisms producing them could be used as agents. In the case of botulism (a form of food poisoning), for example, the toxin is produced outside the body and is eaten. The toxin produced by the botulism organism is the most potent known to be produced by nature. It is hundreds of times more poisonous than phosgene, mustard gas, or cyanide, and it is several times more toxic than rattlesnake or cobra venom.

2-36. (U) AGENTS USED AGAINST NON-HUMAN TARGETS

Foreign pathogenic organisms appear as the agents most likely to be used as weapons in an attack on animals or plants. Unusual organisms which can be employed as biological weapons against man are fewer in number, and it is probable that the common species will be favored. However, all of the lower forms which will attack both man and animals have potential characteristics for biological agents, because they have two possible targets, and a large number of secondary human cases might follow an epizootic (epidemic among animals).

In the list of animal infections where man may be involved are such diseases as brucellosis, anthrax, glanders, Rocky Mountain spotted fever, tularemia, and plague. For many of them, eradication or control within the animal population is the only effective method of preventing human infection. Veterinarians and inspectors of meats and other animal food products may be the first to see the initial indication of anti-animal biological agents.

Pathogens or pests suitable for biological agent attack against plants could be either of foreign origin or those confined to limited areas in the country attacked. To be most effective, biological agents used against plants should be capable of severely damaging important crops, under the conditions that there are no immediately available control measures. These agents must also be capable of persisting, accumulating, and spreading under prevailing climatic conditions.

A number of diseases and insects meet these requirements for employment against important field crops such as rice, corn, wheat, oats, cotton, potatoes, and so forth. Losses caused by the introduction of several pathogens and pests might have serious attritional effects, and might curtail the ability to export food and materials of plant origin.

In countries such as China, where rice is the primary food crop and the supply of it is always

s..., the use of anticrop agents could wipe out the limited food supply by attacking this plant. Without rice, a great majority of the civilian population would suffer extreme hardship through lack of the diet mainstay. This would be certain to greatly damage the economy, and to result in famine. During the course of such a famine, the ability to maintain military operations would be drastically weakened, if not halted altogether.

Indications of animal infection, even though the general symptoms are not noticeable, might be deviations in the normal behavior of animals, such as undue drowsiness or restlessness. Other symptoms which might appear with specific diseases in animals include lameness, diminished milk secretion, ulcers, marked and rapid loss of weight, lowered reproduction capacity, bloody diarrhea, erosion or eruptions of the mucous membranes of the mouth, discharges from the eyes, hemorrhages, and paralysis.

Plant disease agents attack food, feed, fiber, oil, medicinal, or industrial crops in a number of ways. They may attack the conducting tissues of plants and interfere with water movement, or they may invade the soft tissues of leaves and roots. They may inhibit growth or cause lesions, rusts, or galls on specific parts of the plants.

The symptoms which indicate that a crop has been attacked or infected will vary with the type of pest or the specific disease. Some of these symptoms include: water-soaked injuries to the foliage; shriveled and blighted kernels; injuries of the leaf sheaths and stems; orange colored blisters on stems and leaves; lumps on stems, leaves, buds and ears; mottled and wrinkled leaves; yellowing of leaves and blackening of the veins; and general wilting and rotting.

2-37. (C) DISSEMINATION SYSTEMS AND MUNITIONS (Ref. 28)

Biological agents may be delivered by various weapon systems. These include missiles, bomber aircraft, and spray tanks. The 3.4-inch E134 sphere is a submissile munition used to disseminate liquid agents. This munition might be delivered by the A/B, the C, the Sergeant, and the XM-50 missiles, or by bomber aircraft. The 4½-inch E120R1 and E120R2 spherical bomblets can be used to disseminate liquid agents. These bomblets might be delivered by bomber aircraft.

Flettner rotor-type munitions can be used to disseminate both liquid and dry agents. The 5-inch version is used for dry fill. It might be delivered by missiles such as the A/B, B, C, Sergeant and XM-50. The 7-inch Flettner rotor is used for disseminating liquid agents. It is primarily delivered by bomber aircraft.

There are under de... ...nt spray tanks to be used for the dissemin...on of liquid agent. The Aero 14-B aircraft spray tank is currently available for use with the A4D, F54-B, AD5, AD6, and AD7 Naval aircraft for disseminating biological agents.

Section X (U)—Other Chemical Means

2-38. INTRODUCTION

In addition to the chemical agents, both casualty and harassing, there are various other chemical weapons. These may be placed in either of two major groups: offensive weapons, composed of the various types of incendiary weapons; and defensive weapons, primarily composed of the various types of screening smokes. Although incendiary and smoke weapons are now firmly entrenched in the chemical weapons system, their presence there is probably an accident of history, or a convenient lumping together of weapons which were at one time odd or unusual (Ref. 23).

Both incendiary and smoke weapons are known to have been employed as implements of warfare for thousands of years. Incendiary chemicals were used by the Greeks as early as 1200 B.C., and they also were used in India and by the Romans at a very early date. An early weapon was "Greek fire," invented about 600 B.C. This has the property of spontaneously

bursting into flame on contact with water. Smoke has also been used since early times, as a screen for personnel and cavalry movements (Ref. 22). In more recent times, incendiaries and screening smokes were employed successfully and extensively in both World War II and the Korean conflict.

2-39. THE INCENDIARIES

Incendiary weapons, unlike the chemical agents, are primarily concerned with the destruction of equipment and material, rather than with the infliction of casualties. The incendiaries have also been used against personnel with considerable success, especially against massed troop movements. However, a broad survey indicates that incendiaries have found greatest application in the destruction of industrial installations, housing, fuel dumps, ammunition depots, etc.

Modern military incendiaries may be grouped according to three types of material used: oil, metal, and a combination of oil and metal. They may also be grouped according to ignition characteristics, as: the spontaneously flammable materials, such as phosphorus; and those agents which require ignition, such as magnesium.

The oil incendiaries contributed materially to our success against the Japanese in the Pacific during World War II. In 1942, the Japanese had entrenched themselves in coconut-palm log bunkers and had completely halted our advance on Guadalcanal. These bunkers were nearly impregnable and ordinary high-explosive shells had failed to dislodge the enemy. With relatively little training and experience in the use of the flame thrower, the Marines successfully attacked and destroyed bunker after bunker with this weapon.

The flame throwing technique was so successful in the Pacific, its use was extended to the European Theatre of Operations. Here it was not as successful, at first, principally because of the limited range of the available flame throwers, but also because the incendiary was largely consumed during its passage to the target. These defects were remedied to an extent by the use of heavier oil, but the problem was not completely solved until M1 thickener (Napalm) was developed. When mixed with gasoline, this agent forms a jelly which holds the gasoline mechanically. By its use, the gasoline may be ejected from a flame thrower and be only slightly consumed before it reaches the target. On arriving at the target the fuel scatters in "blobs" which burn sufficiently slowly to assure a maximum incendiary effect. The oil incendiaries were not confined to flame throwers, but were used in incendiary bombs as well. More than 750,000 Napalm bomb clusters were dropped on Japan, alone, during the Second World War.

Another agent, filling approximately the same role as M1 (Napalm) thickener was IM. This substance, a derivative of a synthetic rubber, provides a better burning composition than M1. In addition, newer, improved thickeners are now available.

In most cases, oil incendiaries are equipped with white phosphorus igniters to insure ignition, because the bursting charge may or may not serve this function. Because the ignition of white phosphorus is prevented by water, a sodium igniter is used in oil incendiaries that are to be dropped over water.

Metal incendiaries include those consisting of magnesium in various forms, and those composed of powdered or granular aluminum mixed with powdered iron oxide. Magnesium is a soft metal which, when raised to its ignition temperature of 623°C, burns vigorously in air. In either solid or powdered form it is used as an incendiary filling; in alloyed form it is used as a casing for small incendiary bombs. Thermite and Thermate are examples of aluminum and iron oxide mixtures which find employment as incendiary weapons.

The incendiary grenade produces its effect by the burning of Thermate. Thermate is essentially a mixture of approximately 73 per cent powdered iron oxide (Fe_2O_3) and 27 per cent powdered or granular aluminum. The aluminum has a higher affinity for oxygen than iron; therefore, if a mixture of iron oxide and aluminum powder is raised to the combustion

temperature of aluminum, an intense reaction occurs (Ref. 3):

$$Fe_2O_3 + 2Al \rightarrow Al_2O_3 + 2\,Fe + Heat$$

Under favorable conditions, the Thermate reaction produces temperatures of about 4,000° F. This is high enough to turn the newly formed metallic iron into a white-hot liquid, which acts as a heat reservoir to prolong and to spread the heating or igniting action. An ignition-type fuze with delay element is used with this type of grenade.

Incendiary mixtures of oil and metal produce the same type of dispersed effect as that obtained with oil incendiaries. These mixtures are usually in the form of a paste composed of magnesium dust, powdered iron oxide, and carbon, with a sufficient amount of petroleum distillate and asphalt to form the paste. PT–1 incendiary is the major weapon of this type in use. The number of combustible elements in a bomb of this type assures ready ignition by standard nose and tail fuzes.

2–40. THE SCREENING SMOKES

2–40.1. General

The functions of the screening smokes are to obscure the enemy's vision and to conceal friendly troop movements and installations. These smokes are not considered to be toxic in the concentrations which are normally used for concealment purposes. However, exposures to heavy smoke concentrations for extended periods, particularly if near the source of emission, may cause illness or even death. In confined spaces or closed compartments, the screening smokes are poisonous.

Technically, a smoke is a dispersion of extremely fine solid or liquid particles suspended in the air. Such particles reflect and absorb light, and result in typical smoke clouds. White phosphorus (symbol—WP) and plasticized white phosphorus (PWP) are examples of substances used to produce screening smokes.

2–40.2. White Phosphorus

White phosphorus is used both as an incendiary and a screening smoke, and is characterized by pillaring and rapid burning (Ref. 31). When hot smoke rises rapidly, it produces the effect known as pillaring. In still air, the pillaring of WP nullifies its screening effect. WP pillars because it has such a high heat of combustion. Because WP is very brittle, the explosion of the bursting charge in the munitions in which it is used cause it to be broken into small particles, which burn very rapidly. This may enhance its usefulness as an incendiary, but also increases the pillaring.

Direct physical contact with solid phosphorus will result in painful, slow-healing burns. The smoke produced by the combustion of white phosphorus will irritate the eyes, nose, throat, and lungs. These symptoms are rarely pronounced, however. White phosphorus smoke is corrosive toward metals. It has no ability to poison foodstuffs.

WP is a standard smoke filler for hand grenades, rifle grenades, the 4.2-inch mortar shell, rockets, and artillery shells.

2–40.3. HC Mixture

HC mixture uses hexachloroethane (CCl_3·CCl_3) for the production of smoke. The physiological effects of HC are somewhat more drastic than white phosphorus, for this smoke has toxic characteristics in high concentrations.

2–40.4. FS Mixture

Sulphur trioxide-chlorosulfonic acid solution (FS), is another very effective mixture that has been adopted as a smoke agent. FS is irritating to the eyes, nose, throat, and lungs as ordinarily used, but it is non-poisonous. The liquid agent is highly corrosive, especially so to the skin.

2–40.5. The Oil Smokes

During World War II, a new method of smoke generation was developed, based on production of minute oil particles by purely physical means. The oils used are straight, non-additive petroleum oils of high flash-point, similar to light lubricating oils, and are generally known as fog oils. The chemical agent symbols are SGF–1 and SGF–2. Oil fog generators burn gasoline or other fuels, and the fog oil is vaporized in the hot exhaust gases.

As the gases expand into the surrounding air, the oil vapor cools and condenses into a white smoke or fog of high density, thus obscuring the vision.

The oil smokes are the least poisonous of the screening smokes. Although there is evidence that petroleum oil smoke is carcinogenic, breathing or working in it for extended periods seldom produces any ill effects. Since these smokes are petroleum oils, they are non-corrosive. In fact, any condensation would have a lubricating or protective effect on metals.

Section XI (U)—Thermal Radiation

2-41. INTRODUCTION

Associated with a nuclear explosion are a number of characteristic phenomena, some of which are visible, while others are not directly apparent. Certain aspects of these phenomena will depend on the type of burst (air, surface, or subsurface). In addition, meteorological conditions, such as temperature, humidity, wind, precipitation, and atmospheric pressure, may influence some of the observable effects, although the overall characteristics remain unchanged. This section is concerned with thermal radiation and the phenomena associated with it. The ball of fire, the mechanism of thermal radiation, attenuation, the effects of meteorological conditions and shielding, primary and secondary fires, the phenomena of fire storm, and the effect of the type of burst will be discussed in sequence.

2-42. PRODUCTS OF THE NUCLEAR EXPLOSION

The fusion or fission of nuclear material in an atomic weapon leads to the liberation of a large amount of energy in a very small period of time within a limited quantity of matter. As a result, the nuclear products, bomb casing, weapon parts, and the surrounding air are raised to extremely high temperatures, approaching those in the center of the sun.

The maximum temperature attained in a nuclear explosion is probably several million degrees. This may be compared with a maximum of approximately 9,000° F in a conventional high-explosive bomb. The great heat of the nuclear explosion instantly converts the materials into gaseous form. Since these gases, at the instant of explosion, are restricted to the region occupied by the original constituents of the bomb, tremendous pressures are produced in the order of magnitude of several millions of pounds per-square-inch.

Within a few millionths of a second, these intensely hot gases appear in a roughly spherical, highly luminous mass. This is known as the fireball. Although the brightness decreases with time, after about seven-tenths of a millisecond the fireball from a one megaton (MT) bomb would appear to an observer 60 miles away to be thirty times as brilliant as the sun at noon. In several of the nuclear tests conducted at the Nevada Test Site, in all of which bombs of less than 100 kilotons (KT) were employed, the glare at dawn has been visible more than 400 miles away. As a general rule, the luminosity does not vary greatly with the yield of the bomb. Therefore, the surface temperatures attained, upon which the brightness depends, cannot be very different despite the differences in the total amounts of energy released (Ref. 17).

Immediately after its formation, the ball of fire begins to grow in size, engulfing the surrounding area. This growth is accompanied by a decrease in temperature and pressure and, hence, in luminosity. At the same time, the fireball rises, like a hot-air balloon. After about one minute, the fireball has cooled to an extent where it is no longer visible. It has then risen approximately 4.5 miles from the point of burst.

2-43. EMISSION OF THERMAL RADIATION

Immediately upon formation, the fireball begins to emit thermal radiation. Because of the extreme temperatures, this radiation consists of ultraviolet rays as well as visible and infrared rays. Certain phenomena associated

with the absorption of thermal radiation by the air in front of the fireball (Ch. 4, Par. 4–7.5.2) cause the surface temperature to undergo a curious change. Although the temperature of the interior falls steadily, the temperature of the surface at first decreases more rapidly than this, then increases again, and, finally, falls off continuously. Thus, there are essentially two surface-temperature pulses: the first is of very short duration; the second lasts for a much longer period. This phenomenon is characteristic of all nuclear explosions, although the duration of the pulses increases with an increase in the energy yield of the explosion.

Corresponding to the two temperature pulses, there are two pulses of thermal radiation from the fireball (Ref. 17), as shown in Fig. 2–16. In the first pulse, the temperatures are extremely high, which results in a large portion of the radiation being in the ultraviolet range. Moderately large doses of ultraviolet radiation can cause painful blisters, and even small doses can cause reddening of the skin. However, the first pulse of thermal radiation is not considered a significant skin-burn hazard for several reasons. One reason is that only about one per cent of the total radiation appears in the initial pulse because of its short duration. In addition, the ultraviolet rays of this pulse are attenuated by the intervening air, making the ranges at which the thermal radiation could cause significant damage so short that other radiation effects are much more serious.

The second pulse may last for several seconds. This emission carries approximately 99 per cent of the total thermal radiation energy from the bomb. Because the temperatures are lower than in the first pulse, most of the rays lie in the visible and infrared spectrum. It is this radiation which is responsible for most skin-burns of exposed personnel, and which causes the ignition of a large number of secondary fires.

Of the total energy yield of a nuclear air burst at low altitude, approximately one third is emitted in the form of thermal radiation. Hence, for every 1-kiloton yield of the explosion, approximately 3.3×10^{11} calories of thermal energy are liberated, an amount sufficient to convert over a million pounds of water into steam.

2–44. DISTRIBUTION AND ATTENUATION OF THERMAL RADIATION

The extent of injuries or the amount of damage caused by thermal radiation depends upon the total amount of energy received by a unit area of skin, or exposed, combustible material. The thermal energy per-unit-area will decrease with distance from the ground zero (the point on the surface directly above which the bomb is detonated) for two reasons: The dispersal of the radiation over a constantly increasing area as it moves away from the fireball; and the attenuation of the radiation in its passage through the air.

If a uniform distribution of radiation and no attenuation are assumed at a distance R from ground zero, then the same amount of energy will fall upon each unit portion of the surface of a sphere of radius R. The total surface area of this sphere is $4\pi R^2$, and the energy received per unit area is, therefore, $\frac{E}{4\pi R^2}$, where E is the total thermal energy yield of the explosion. It is clear, then, that under the assumed conditions the energy received per unit area therefore varies inversely as the square of the distance from the explosion.

In order to obtain a more realistic estimate of the quantity of thermal radiation arriving

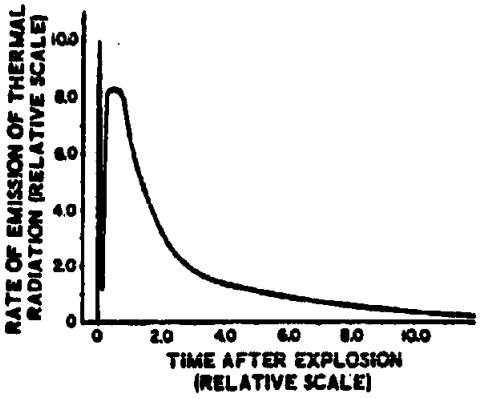

Figure 2–16. Emission of Thermal Radiation

at a particular unit area, however, the effect of atmospheric attenuation must be considered. Attenuation is due in part to absorption by the molecules present in the air, and partly to the scattering or diversion of the rays from their original path.

The absorption, or removal, of thermal energy rays by air molecules is most effective for the short wavelength (ultraviolet) rays. Oxygen molecules and ozone are quite significant in achieving this effect. Although the proportion of ozone present in the atmosphere is normally quite small, considerable quantities are released by the interaction of oxygen with the gamma radiation from the nuclear explosion. Because of this absorption quality of the atmosphere, the amount of ultraviolet radiation decreases rapidly with the distance from ground zero. At distances such that thermal radiation effects are more significant than the effects of blast and nuclear radiation, the proportion of ultraviolet radiation present has become quite small.

Attenuation as a result of scattering (the diversion of rays from their original path) occurs with radiation of all wave lengths. Scattering can be caused by collison with molecules present in the atmosphere, or, more importantly, by the reflection and diffraction of light rays by particles of dust, smoke, or fog. This diversion from the original path results in a diffused, rather than a direct, transmission of the thermal radiation.

The decrease of thermal radiation energy due to scattering depends upon the wave length of the radiation and upon the prevailing atmospheric conditions. The different wave lengths, ultraviolet, visible, and infrared, will attenuate at different rates. For most practical purposes, however, it is reasonably satisfactory, although certainly less precise, to utilize a mean attenuation averaged over all the wave lengths present.

The state of the atmosphere as far as scattering is concerned will be represented by what is known as the visibility range. This is defined as the horizontal distance at which a large dark object can be seen against the horizon sky in daylight. A rough correlation between the visibility and the clarity of the atmosphere is given in Table 2–6.

TABLE 2–6. VISIBILITY AND ATMOSPHERIC CLARITY (Ref. 17)

Atmospheric Condition	*Visibility (miles)*
Exceptionally clear	More than 30
Very clear	12—30
Moderately clear	6—12
Light haze	2.5— 6
Haze	1.2—2.5
Dense haze or fog	Less than 1.2

The attenuation is believed to increase continuously with increasing distance. At any given distance the degree of attenuation does not vary considerably with the visibility, provided the following conditions are met: the visibility range is between two and fifty miles (atmospheric condition ranging from light haze to exceptionally clear); the distance is half the visibility range or less; and the explosion does not occur beneath a cloud layer.

The ineffectiveness of the atmosphere as an attenuator, when the above conditions are adhered to, can be directly ascribed to the effect of scattering. The thermal radiation received at a particular point can be attributed to both direct and scatter transmission. If the air is clear, there are very few suspended particles, and the effect of scattering is small. In this case, the radiation received is essentially only that which has been transmitted directly. If the air contains a moderately large number of particles, more radiation will be scattered and, consequently, a smaller amount of direct radiation will reach the target. However, subsequent scattering of already deflected rays (multiple scattering) generally results in sufficient scattered radiation arriving at the target to compensate for the loss of directly transmitted energy.

However, it should be noted again that this general condition applies only when the restrictions previously mentioned are adhered to. In the event the visibility range is less than two miles, only a small portion of the thermal radiation will escape scattering. If this condition exists, the tremendous loss in direct transmis-

sion cannot be compensated for by multiple scattering. Consequently, there is a definite decrease in the radiant energy received at a specified distance from the explosion.

Attention should also be drawn to the distance limitation; the target in question is at less than half the visibility range. At greater distances, loss of radiation to the atmosphere cannot be neglected. In this circumstance, the assumption that the energy attenuation is independent of the visibility leads to estimates of thermal energy which are too high.

Should the explosion occur in moderately clear air but beneath a layer of cloud or fog, the assumption is also invalid. Some of the radiation which would normally proceed outward into space will be scattered back to earth, resulting in a greater amount of energy received than would normally be expected.

A nuclear bomb detonated above a dense cloud, fog, or smoke layer has just the opposite result. An appreciable portion of the energy will be reflected upward and must be regarded as lost, as far as the ground target is concerned. In addition, almost all of the radiation penetrating the cloud will be scattered; very little will reach the target by direct transmission. These two effects result in a considerable decrease in the amount of radiation reaching the target. Chemical smoke acts exactly like a cloud or fog. A dense smoke screen between the point of burst and a given target can reduce the thermal radiation received as much as 90 per cent.

Unless scattered, thermal radiation travels in straight lines from its source like ordinary light. Any solid, opaque material will serve as an adequate shield against directly transmitted rays, provided it is between the target and the source. Transparent materials such as glass and plastics, however, allow the passage of thermal energy with only slight attenuation.

Under hazy atmospheric conditions, a shield which merely intervenes between the target and fireball may not be sufficient. The large proportion of scattered radiation will arrive from all directions, not from the point of burst alone. This situation should be borne in mind in connection with the problem of protection against thermal radiation.

2-45. DAMAGE EFFECTS

Generally, two types of fires may result from a nuclear detonation. These are usually referred to as primary and secondary fires. Primary fires are those which are ignited by the thermal radiation from the bomb, and secondary fires are those which indirectly result from the effects of blast.

When thermal radiation strikes an exposed surface, it is partially absorbed and is immediately converted into heat. Since nearly all the radiation is delivered in a few seconds, there is not sufficient time for conductive heat transfer to take place. Consequently, exceptionally high surface temperatures result. These high surface temperatures, dependent upon the color and nature of the substance, and the amount of thermal radiation received, may cause the material to scorch, char, or burst into flames (Ref. 23).

Thermal radiation also results in injuries to personnel by means of painful skin burns and eye injuries. Again, the amount of radiation received and, therefore, the distance from ground zero, determine the extent of the damage.

Usually, a great number of fires, both primary and secondary, accompany nuclear explosion. This simultaneous burning effect may produce the phenomena known as fire storm. As a result of the huge masses of hot air and gases rising from the burning area, air is sucked in on all sides with great force, producing a strong wind which blows toward the center of the fire. The effect is similar to the draft in a chimney, except on a much larger scale. At Hiroshima, the winds produced reached velocities of 30 to 40 miles an hour. The fire storm was a decisive factor in limiting the spread of fire, and caused an almost uniform burn-out area in which almost everything was destroyed. It should be noted that a fire storm does not always accompany a nuclear explosion, and it could occur with fires resulting from other origins.

In addition to the damage produced by the primary and secondary fires, thermal radiation may be an effective kill mechanism in a quite different manner. When a structure such as a bridge, building, or aircraft is exposed to a substantial increase in temperature, a corresponding decrease in the strength characteristics of the materials composing the structure results. This decrease in structural strength causes the structure to become more vulnerable to the blast mechanism associated with the detonation of a nuclear weapon. Should the increase in temperature be of sufficient magnitude, it is possible for collapse to occur without the addition of any loads other than those normally imposed on the structure.

The foregoing discussion has referred in particular to thermal radiation from an air burst. For other types of bursts the results are the same, in general, but they differ in degree. For a surface burst on land or water, the amount of thermal radiation is less than for an air burst. This is due in part to a portion of the thermal energy being absorbed by the earth and water, and partly to additional scattering caused by the greater density of atmospheric particles at the earth's surface. In subsurface bursts, nearly all the radiant energy is absorbed by the soil or water. The thermal effects are then consumed in the vaporizing of the soil or water, as the case may be.

Section XII (C)—Nuclear Radiation

2–46. (U) INTRODUCTION

Nuclear radiation may be conveniently separated into initial radiation and residual radiation. The initial radiation is defined as that produced within the first minute after detonation of a nuclear weapon. All of the residual radiation, which arises from several sources, is produced after the first minute has elapsed. (Refer to Ch. 4, Par. 4–8.)

As a hazard, radiation is primarily dependent upon the yield of the weapon and the type and height of burst. As might be expected, an increase in energy yield causes an increase in the nuclear radiation emitted. This, however, causes an enlargement of the area over which a given dose is received. For a weapon air burst (fireball does not touch the ground) essentially all the harmful radiation is produced during the initial phase (first minute after detonation).

Such is not the case for underwater, underground, or surface bursts. In these instances, a large quantity of matter is pulled into the explosion and, consequently, is made radioactive. This material, coupled with the radioactive bomb residues, presents a significant residual radiation problem. The mechanics of nuclear radiation, both initial and residual, the type of radiations present, the distances at which they are effective, and the units with which they are measured, are presented in Ch. 4, Par. 4–8.2. It is not necessary for this discussion that they be repeated in detail here.

Essentially, all types of nuclear radiations produce the same end effects in, or on, various materials. The different types of radiation may produce variations in the magnitude of the effects for equivalent exposures, but this is relatively unimportant when considering only the actual mechanism of kill.

2–47. (U) PHYSIOLOGICAL EFFECTS

Excessive exposure to nuclear radiations, such as X-rays, alpha and beta particles, gamma rays, and neutrons, can cause injury to living organisms. The harmful effects of radiation seem to be due to the ionization and excitation produced in the cells composing living tissues. As a result of ionization, some of the constituents of the cells which are essential to normal functioning, are destroyed. In addition, the products formed during the cell destruction process often act as cell poisons. Among the observed consequences of the action of ionizing radiations on cells are: breaking of the chromosomes, swelling of the nucleus, complete destruction of the cell, an increase in the viscosity of the cell fluid, and increased permeability of the cell membrane. In addition, the process of cell division (mitosis) is delayed by exposure

to radiation. Frequently, the ability of the cell to undergo mitosis is completely inhibited. The effect of nuclear radiation on living organisms is dependent not only on the total dose received but on the rate of delivery. The majority of living cells have the ability to recover at least partially if some time is allowed to elapse between doses. The expected initial effects on living organisms are visible in the physiological symptoms produced: vomiting, nausea, diarrhea, inflammation, fever, emaciation, and death.

In addition to the initial effects, there are several consequences which do not become evident for some years after exposure. Several of the more important retarded effects are discussed in the following paragraphs.

The incidence of cataracts seems to be greatly increased in persons who were exposed to relatively large doses of radiation, but managed to survive the initial effects. Along the same line, a study of mortality rates in Japan indicates an enormous increase in the occurrence of leukemia among survivors of the bombings at Hiroshima and Nagasaki. The incidence of leukemia among these survivors was, on the average, about one in 500, compared with one in 50,000 among the unexposed population of Japan (Ref. 17).

There was also a marked increase over normal in the number of stillbirths and in the deaths of newly-born infants. A study of the surviving children made four or five years later showed an increased frequency of mental retardation.

The genetic effects of radiation are those of a long-term character which produce no visible injury in the exposed generations, but may have significant consequences to future generations. These effects differ from most radiation injuries in that they appear to be cumulative and, to a great extent, do not depend on the dose rate, but only on the total dose.

The harmful effects of mutation may be quite varied, ranging from a decrease in life expectancy by a few months, to death in the embryonic stage. Sterility is another common result. The increase in genetic mutations seems to be in direct proportion to the amount of radiation absorbed by the parents. There seems to be no amount of radiation, however small, that does not produce some genetic change.

2-48. (C) PHYSICAL EFFECTS

Except for photographic film, which is clouded by neutron interaction with the particles in the emulsion, and for electronic equipment which utilizes transistors, no permanent damage to equipment results from neutron radiation. There is evidence that exposure to a neutron flux in excess of 10^{14} neutrons per square centimeter permanently alters the characteristics of transistors. However, any electronic equipment exposed to this flux of neutrons from a nuclear weapon detonation is likely to be destroyed or severely damaged by other aspects of the explosion. Discoloration of glass does not occur for neutron fluxes less than about 10^{18} neutrons per square centimeter, and thus can be disregarded as a significant effect (Ref. 16).

If the neutron flux is sufficiently high, a certain amount of neutron-induced gamma activity (Ch. 4, Par. 4-8.4), results for most articles made of steel. The induced activity presents no significant hazard except for articles almost within the fireball. Even then, the activity decays so rapidly as to be negligible less than a day after exposure. Significant neutron-induced, beta-particle radiation occurs in articles made of brass or other copper alloys. Again, radioactive decay reduces the activity to negligible levels in a short time.

In general, damage to materials by gamma radiation requires massive quantities to be effective. Damage from some other weapon phenomena is almost always more significant. Gamma radiation in excess of 10,000 roentgens can cause deterioration of rubber and other polymers, as evidenced by a decrease in tensile strength. Like neutron radiation, large quantities of gamma rays can cause discoloration of glass. Since gamma rays induce negligible radioactivity in materials, no residual radiation hazard is caused.

In the absence of atmosphere, perhaps the most damaging aspect of a nuclear detonation is the X-ray effect. A large amount of energy

is released from the bomb as soft X-rays in an extremely short time period. Those which strike a solid surface deposit their energy within a thin surface layer. Although the total incident X-ray flux may be very low, the material in this thin layer becomes extremely hot, vaporizes, and blows off at a high velocity. This blow-off causes an impulse that develops a shock wave in the remaining material. The shock wave then travels through the material layer and is reflected from the opposite side, which results in spalling from the rear surface. This effect is similar to the effect of fragments, in that damage is caused by the kinetic energy of internal particles within the target. In addition, exposed optical devices and other fragile components are immediately destroyed.

One other radiation phenomenon should be mentioned as a possible kill mechanism. A large electrical signal is produced by the detonation of a nuclear weapon. This signal consists of a sharp transient wave, with a strong frequency in the neighborhood of 15 kilocycles. Field strengths greater than one volt per meter have been detected at distances of 2,000 miles from the detonation of megaton-yield weapons. It can be expected that electronic equipment which responds to rapid, short-duration, transients will be actuated by the pick-up of this phenomenon (Ref. 16).

Section XIII (U)—Target Illumination

2-49. INTRODUCTION

The purposes of terminal effects fall into two broad categories: the actual defeat of a target; and the production of an effect (signaling, illuminating, screening) that will aid in the ultimate defeat of the target. Target illumination, then, is a means by which the protection of darkness is decreased and the target is rendered more vulnerable to the various kill mechanisms (Ref. 32). The illumination may be provided by pyrotechnic devices (shells, trip flares, etc.), searchlights, or electronic aids.

2-50. PYROTECHNIC DEVICES

Some common pyrotechnic devices which provide target illumination are illuminating shells, aircraft-dropped bombardment flares, and land-mine trip flares (Ref. 35).

Illuminating shells are essentially parachute flares specially housed in shell casings for launching from artillery weapons (Ref. 33). Aircraft bombardment flares are designed to provide illumination for night bombardment (Ref. 34). They, too, are essentially parachute flares, but are housed in a bomb-like casing. In both the shell and bomb flare, a time fuze sets off an ejection charge which expels the parachute flare. Trip flares are constructed like a "bounding" type of antipersonnel mine; or are similar to a hand grenade and fitted with a mounting bracket for attachment to trees, poles, etc. Both types of trip flares are usually set off by trip wires or foot contact (Refs. 33 and 34). They are intended to give warning of enemy infiltration, and to silhouette the infiltrators so that they may be fired at. The "bounding" type is propelled into the air by a small ejection charge when the flare is actuated. This flare has a parachute to delay its fall. The grenade type flare is stationary and simply burns when actuated by the trip wire.

2-51. SEARCHLIGHTS

Searchlights can also provide target illumination. The large 60-inch diameter searchlight and the new 30-inch general purpose searchlight can provide direct illumination, particularly in hilly terrain. Although these lights are not armored, they are relatively invulnerable to enemy small-arms fire and high-explosive attack because of the extreme difficulty in estimating range to the source of the light (Ref. 36). Large, battlefield-illumination searchlights are most frequently used for indirect illumination, either by diffusion of a slightly elevated beam by atmospheric particles, or by reflection from low lying clouds. In this indirect mode, the 30-inch searchlight can provide illumination equivalent to quarter moonlight at a range of 10,000 meters.

A new tank-mounted xenon searchlight replaces the 18-inch fighting light (visible light).

It will be used in conjunction with new infrared-visible periscopes and binoculars. The xenon searchlight is mounted on the gun mantlet and is boresighted with the main armament. This searchlight has several lenses and filters concentric about the 2,500-watt xenon lamp. These elements rotate upon command from controls within the tank. The resultant five modes of operation are: visible light, compact or spread; infrared light, compact or spread; or blackout (the lamp operating but completely obscured). This searchlight has 100-million, peak-beam candlepower. Its light beam produces a dazzling or blinding effect in the eyes of the enemy, which hampers his aim and movement, and temporarily destroys his night vision. The dazzling effect of the light also can provide concealment for movement of friendly units.

2–62. ELECTRONIC DEVICES

Electronic means to provide night vision for target acquisition and engagement are also available. These utilize near-infrared, low-light-level image intensification, and far-infrared. Near-infrared systems employ projected, invisible, near-infrared light, and a viewer which convert the reflected infrared rays to a visible image. Low-light-level, image-intensification equipments greatly amplify the reflected natural night illumination to the extent that a useful visible image is obtained. Far-infrared devices utilize the far-infrared (or heat-energy) which is emitted by all objects to a degree dependent upon their temperature and surface characteristics. The body warmth of a man, and the heat from the engine compartment of a vehicle or aircraft, have a significant infrared signature to a far-infrared detector.

Near-infrared systems have the advantage of very long range viewing and instantaneous imaging. However, the projected, near-infrared radiations may be detected by a properly equipped enemy. The low-light-level image-intensification and far-infrared equipments are passive, but have less instantaneous viewing ranges than comparable near-infrared devices.

The only currently operational, electronic-imaging, night-vision equipments are near-infrared devices. These vary from the hand held Infrared Weaponsight for the M-14 rifle to the Night Vision Kit for the M-60 tank. The latter consists of two similar periscopes for the gunner and commander, each having both visible and infrared viewing channels, an infrared hand held binocular, and the xenon tank-mounted searchlight. All of the viewers use a small, single-stage, image-converter tube.

The next-generation, night-vision equipment for tanks will consist of low-light-level, image-intensification viewers. These viewers will use three or more image tubes in series, in order to realize brightness gains of 100,000 or more times. They will be designed as periscopes or articulated telescopes, as the particular application warrants. Remote-view, closed-circuit, television-type, systems will also be available for use in those situations requiring image transfer. Special features such as selective, dual-capability, passive-and-active viewing modes, using either ambient night illumination or projected near-infrared, or using image integration or storage for a brief time exposure, may be used to greatly increase viewing ranges.

Section XIV (S)—Radar Jamming

2–63. INTRODUCTION

Radar jamming, in its broadest sense, may consist of any method of denial of radar-derived information by the opponent. The method of denial may take the form of deception or confusion and, in general, is limited only by the ingenuity of the designer.

The ability to perfom successful jamming is dependent on several factors. The first, of course, is detection. This involves the locating, examination, and analysis of electromagnetic radiation to gain information about the opponent's actions and intentions. Methods, here, can include ground monitor receivers, reconnaissance receivers, passive tail warning sys-

tems, and passive radar warning systems. In any event, an *a priori* knowledge of precisely what i that one wishes to jam is required.

The second factor is power. Whether deception, the generation of false signals to simulate real ones and so mislead the opponent, or denial, the radiation of spurious signals to mask the signals needed by the opponent's system for proper operation, is selected as the desired countermeasure, it is necessary that the jamming signal be dominant.

Successful operation of a radar requires the detection of the energy reflected from the desired target. The power, S, received from a target is found from the radar equation

$$S = \frac{P_t G_t \sigma A}{(4\pi)^2 R^4} \qquad (2\text{-}2)$$

where

P_t = peak power transmitted by the radar

G_t = on-axis gain of the radar antenna

σ = back-scattering cross-section of the target

A = effective aperture of the radar antenna

R = range from radar to target.

A jamming transmitter located in the target, if it is assumed that the total power will fall in the radar pass band, will deliver to the radar a power J, given by

$$J = \frac{P_j G_j A}{4\pi R^2} \qquad (2\text{-}3)$$

where P_j = jammer power

G_j = jammer gain.

The ratio of jamming power to signal power J/S becomes a significant parameter, and can be seen to be

$$J/S = \frac{P_j G_j 4\pi R^2}{P_t G_t \sigma} \qquad (2\text{-}4)$$

Since J/S varies with range squared, it is apparent that, for J/S greater than unity, the jammer rapidly gains advantage over the radar with increasing range. For J/S less than one, the converse is true. We may then take the range for which the jamming-to-signal ratio is unity as the maximum effective range of the radar. Beyond this range, the jammer will effectively deny the use of the radar. This particular value of range is often termed the "self-screening range" of the jammer.

Granting that the jammer has the ability to deliver a significantly greater power to the radar receiver than that received from the target, the particular *form* that the jamming power takes becomes of interest.

The following paragraphs of this chapter discuss radar jamming methods and present very generalized examples of presently conceived jamming equipment.

2–54. RADAR JAMMING METHODS

2–54.1. General

All forms of jamming can be classed as either active or passive. Active jamming requires the generation and transmission of energy by the jamming source. Passive jamming takes advantage of the radiated energy of the radar that is to be jammed, in some manner calculated to produce confusion.

2–54.2. Passive Jamming

Passive methods of jamming may consist of atmospheric effects, chaff, decoys, anti-radar coatings, or reflectors (Fig. 2–17). The atmospheric effects are simply fortuitous meteorological effects which may serve to occlude targets. Because these effects can, at best, only happen to be operative on the radar frequency, and because they are not under control of the jammer, little consideration need be given them.

Chaff is the most common and effective material and will probably still be employed in the coming decade. Chaff consists simply of thin metallic strips or metalized dielectric filaments, cut to a length so as to resonate in the desired radar band. They are dispensed in mid-air, either in a continuous flow or in bursts. Continuous flow methods are used to provide a corridor or shield (to provide a screen) behind which deployment of aircraft may be carried out unobserved. Discrete bursts are generally used to saturate a defense with false targets.

Decoys will employ some form of solid reflector, either corner reflectors, Luneberg lenses, or the like, and may be self-powered, towed, or dispensed in a manner similar to de-

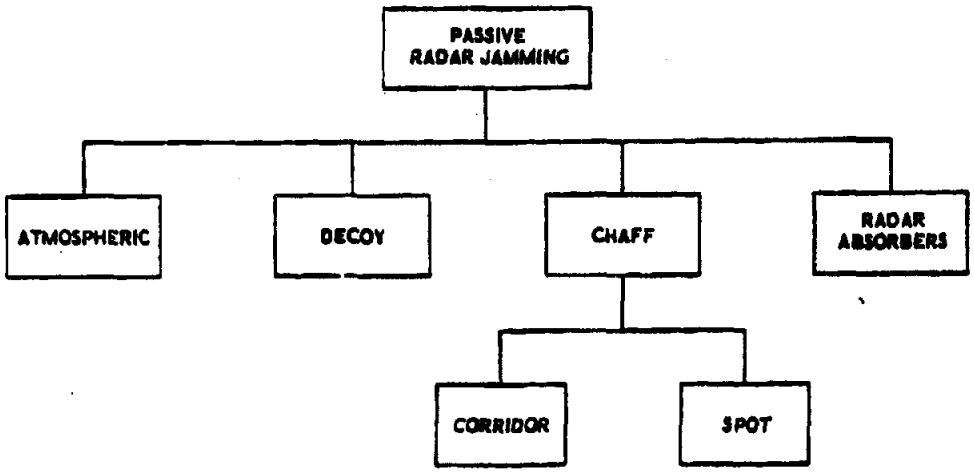

Figure 2–17 (S). Passive Jamming Methods, Block Diagram (U)

layed-opening chaff. The possibility exists that some form of mechanical shuttering or blinking may be used for angle-tracking confusion; but size, weight, and drag disadvantages make them of questionable value. Essentially the same tactics as for chaff may be employed in this case.

Radar-absorbent materials have existed since World War II, and development work with them continues. Their principle is simple; the target object is covered or coated with a material that is transparent to radar or that does not re-radiate significant energy back to the radar. All forms of radar-absorbent material developed to date have not been completely satisfactory for one of two reasons: they are effective only over a limited frequency range (resonant effects); or significant absorption can be obtained only with coatings several wavelengths thick. These considerations have limited their use on aircraft, and the presently available coatings have little practical use as a countermeasure.

2–54.3. Active Jamming

2–54.3.1. *The Two Basic Methods*

Active jamming requires the generation (or amplification) and the transmission of energy by the jamming source. Two broad categories can be established, depending on the frequency band occupied by the jamming signal. A wide band system would be that radiating energy over a bandwidth greater than that of the radar being jammed. A narrow band system would be one radiating in a bandwidth equal to or less than the bandwidth of the radar being jammed. The narrow band systems have the advantage of high power density (watts/megacycle) for a relatively small total output power. The wide band systems have the capability to jam a wide range of frequencies and several radars simultaneously. Considerably more jamming energy is required to disrupt the radar than in the case of the narrow band jammer.

2–54.3.2. *Wide Band Jamming*

Wide band active jamming may consist merely of the generation of random noise, either white or colored, having an inherently large bandwidth, or it may consist of the generation of special waveforms having many frequency components. The possible wideband active jamming methods are indicated in Fig. 2–18.

An impulse is an outstanding case of a waveform requiring a wide frequency band. The impulse function, sometimes called the Dirac

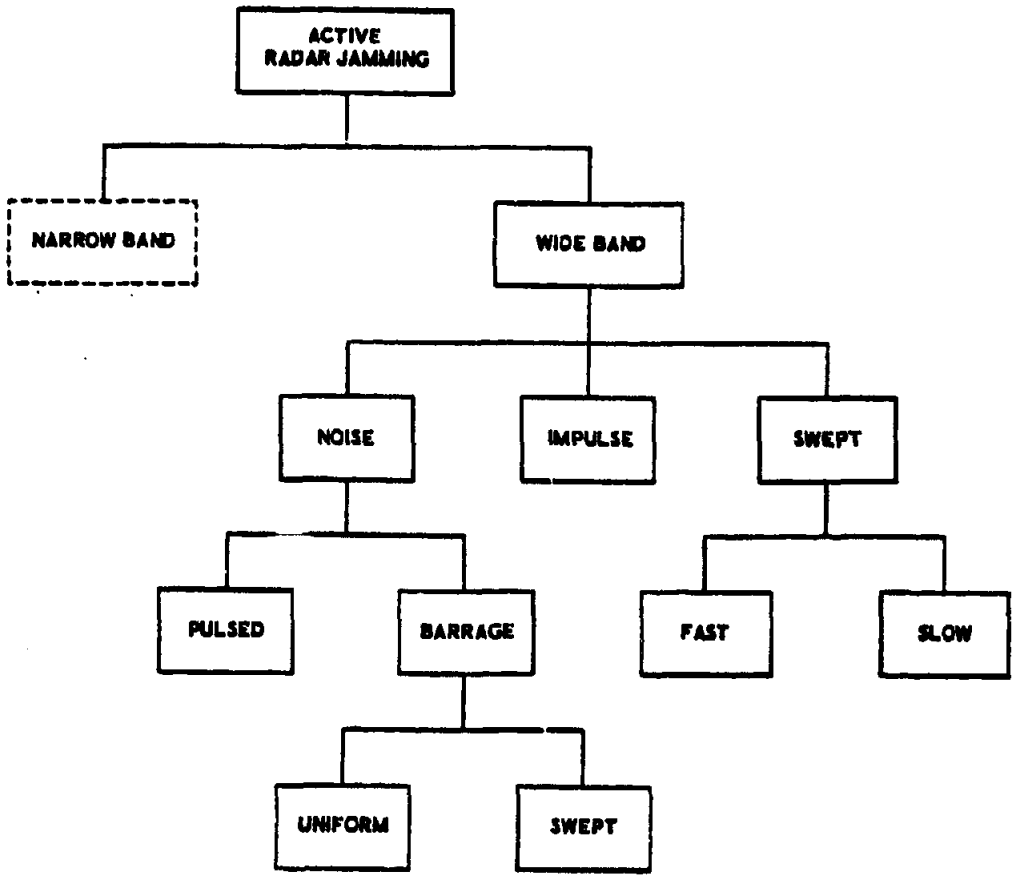

Figure 2–18 (S). Wide Band Active Radar Jamming Methods, Block Diagram (U)

or delta function, is an extremely narrow pulse in the time domain, tending to zero width in the limit. This function, when transformed to the frequency domain by the Fourier integral, will show frequency components extending from zero to infinity in the limit. While a pulse having a zero width in time is not realizable, it may be approached to the extent of having a significantly greater bandwidth than the acceptance bandwidth of the radar to be jammed.

Wideband swept jamming may consist of a narrow band of noise whose center frequency is swept over a wide band, or it may consist of a simple continuous wave which is swept in frequency. In general, the slowly swept systems will use noise as the jamming signal, while the rapidly swept systems will use a continuous wave. The advantage of the latter lies in the fact that, if the continuous wave is swept through the radar pass band at a sufficiently rapid rate (megacycles/second/second), a signal will be generated in the pass band having a time duration shorter than that normally used by the radar. This approaches the impulse function case, with the result that the radar pass band is essentially filled with energy delivered by the jammer.

The basic, wideband, noise jammer is the barrage jammer, one which simply radiates wide band noise at high power levels.

2-54.3.3 *Narrow Band Jamming*

a. Basic Techniques

The narrow band active jammers (Fig. 2-19) allow greater sophistication in application and in jamming results. Their use makes available to the jammer the techniques of deception, as contrasted with the confusion tactics generated by the wide band systems. Because the frequency band occupied by the narrow band jammers is no greater than the acceptance bandwidth of the radar, and because deception may be the desired result of the jamming, fairly detailed characteristics of the radar must be known to the jammer.

The narrow band jamming methods may use continuous wave signals, either modulated or unmodulated, or continuous random noise, with the objective of saturating the radar amplifiers. The area of greatest sophistication in this field lies in methods of pulse modulation. Random pulses may be used with effects similar to those of an adjacent, friendly radar; or true, deceptive-modulation methods may be employed.

b. Deception Repeaters

(1) Basic Techniques

The deception jammers are all repeater type devices; that is, they receive the radar signal, operate on the signal in some fashion, and retransmit the modified signal back to the radar. The purpose of repeater countermeasures is to disrupt or degrade the tracking capabilities of automatic tracking radars, to the extent that precise tracking data are denied. This renders ineffective, to some extent, those weapons that require precise data for weapon control. The following sub-paragraphs describe some of the more commonly used repeater jammers.

(2) Range Gate Stealer

This repeater jammer samples the radar interrogating impulse instantaneously, stores the frequency, and repeats a synthetic signal that is several times stronger than that of the interrogating signal and is in time coincidence with the radar echo. On subsequent interrogations, the returned signal is progressively delayed in time. When the radar range gate has been displaced sufficiently from the target, the jammer is shut off and lock-on is lost. The radar must then go through the range acquisition program again, at which time the jammer repeats the gate stealing cycle. By this method, range information is denied to the radar, and weapon attack computations cannot be made.

(3) Angle Track Breaker

Several modulation techniques are possible for this purpose. One consists simply of repeating the interrogation signal with a superimposed amplitude modulation at low frequencies, thus causing noise in the radar angle tracking channels. This, in turn, will increase the average tracking error, and possibly cause antenna deflections sufficient to cause loss of the target signal. Other modulation methods, effective against conical tracking radars, may consist of "inverse gain" modulation, or phase shift, to prevent the tracking radar from nulling on the true target position. Under the proper conditions, a phase shift repeater can entirely prevent a tracking radar from determining a tracking error.

(4) Velocity Gate Stealer

These repeaters, designed for employment against Doppler radars, operate somewhat in the manner of the range gate stealers. In this case, the repeated signal is progressively shifted in frequency, so that the velocity gate of the Doppler radar is pulled off target.

2-55. IMPLEMENTATION

2-55.1. General

As has been shown in preceding paragraphs, there are numerous, possible methods of radar jamming. However, careful investigation of the pay-off for various radar-countermeasure games indicates that certain approaches and methods are more attractive than others. The designers of countermeasures equipment are well aware of these areas; a survey of operational equipment will show that the majority of jammers are specifically intended to capitalize on the vulnerable aspects of the radars. In addition, although countermeasures is an active, changing field, it is limited by component availability. For these reasons, it is possible to establish very generalized jamming equipment characteristics, based on components presently available, and on components

"SECRET"

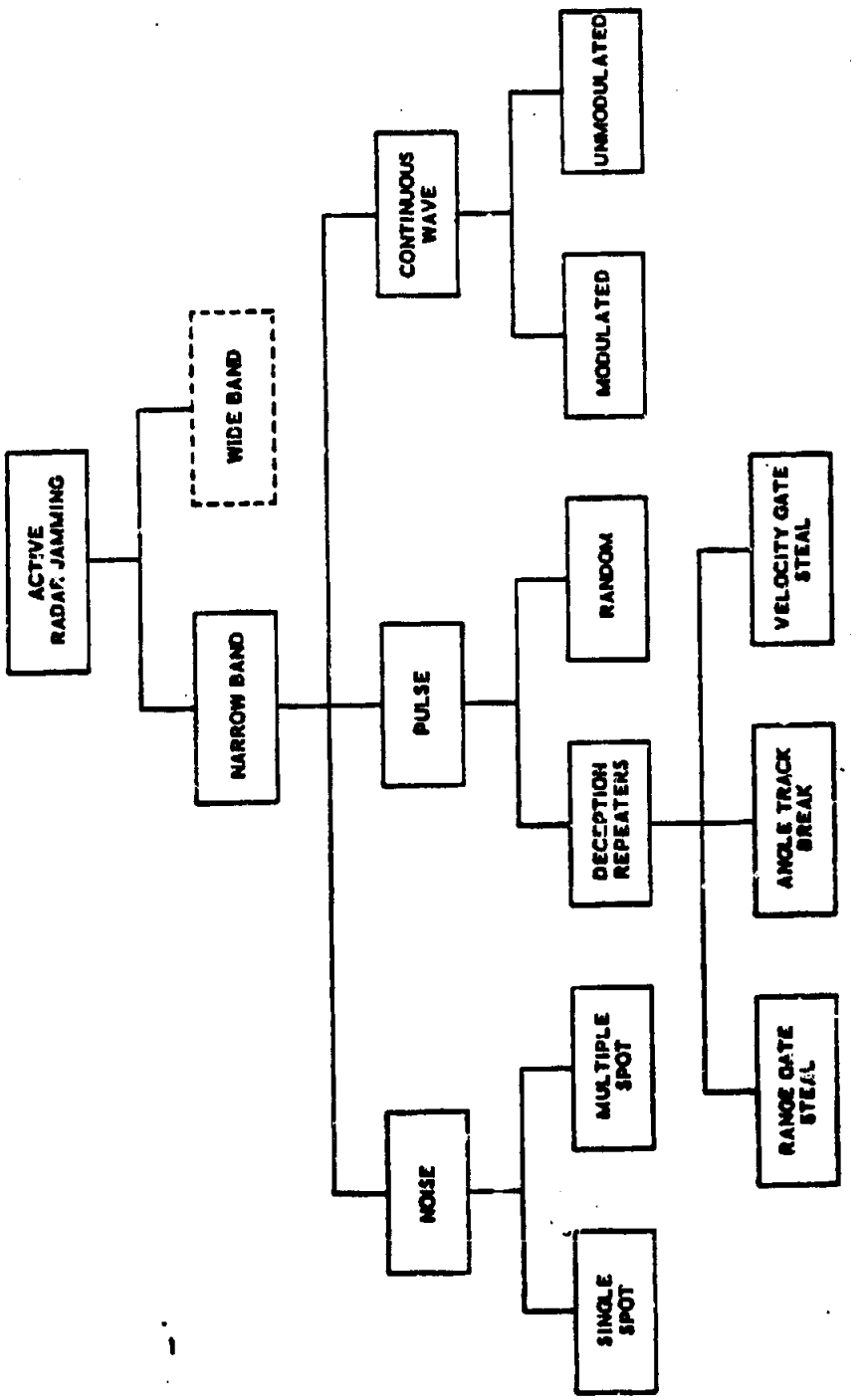

Figure 2-19 (S). Narrow Band Active Radar Jamming Methods, Block Diagram (U)

SECRET

2-61

that are in the development stage but will be available in the near future. The equipments that will probably be used in the early part of the 1960-1970 decade are discussed in the following sub-paragraphs, and are illustrated by generalized circuits.

It is to be noted that the following descriptions and illustrations represent highly conventionalized jammers, as indicative of design trends and equipment capabilities. The actual realization of the equipments is a considerably more complex undertaking than the diagrams might indicate. In addition, the frequencies and bandwidths indicated are predicated on operation between 500 and 1,000 mc/s. A change of operating frequencies will require some readjustment of parameters. For example, if the operating frequencies are doubled, either the number of filters in the banks must be doubled, if the same frequency resolution is to be obtained, or, if the same number of filters is used, the frequency resolution becomes one-half that indicated. These factors are the normal engineering compromises that must be made in any situation, but they should be kept in mind.

2-55.2. Uniform Barrage Jammer

This unit will have a total power output capability of 1,000 watts over an octave bandwidth. A programmer will allow the selection of any 5 mc/s band, or any combination of bands, at the discretion of the operator. The power density will vary with the number of bands in use, ranging from 200 w/mc in a single band down to 2 w/mc if all bands are used. A block diagram of this unit is shown as Fig. 2-20. Characteristics of this unit, and those that follow, are based on a 500-1,000 mc/s frequency range. Changes in this basic range will cause variations in the indicated values for power density and filter widths.

2-55.3. Swept Barrage Jammer

This unit will utilize an output tube similar to that used in the uniform barrage jammer. An output power of 1,000 watts will be available which, with a noise bandwidth of 50 mc/s, will yield a power density of 20 w/mc. The sweep width will be under the control of the operator and will extend from zero to 500 mc/s. The sweep rate may be varied between the limits of one sweep per minute to 5,000 sweeps per second. Fig. 2-21 is a block diagram of this unit. The voltage tuned oscillator will be a backward wave tube, to provide an octave tuning capability.

2-55.4. Composite Spot Jammer

This unit will have the capability of either single spot or multiple spot jamming, at the operator's demand. In addition, various automatic modes will be available in either the single spot or multiple mode. In operation, the received radar signal will be processed in a filter-detection bank and, based on that analysis, the appropriate filter-gates will open to jam the frequency band which contained the received signal. Look-through provisions will be provided to allow observation of the band being jammed, permitting the decision to continue, or not continue, jamming. In single spot operation, a sequential mode will be available as well as the automatic mode. A simultaneous capability will provide multiple spot operation as well as automatic modes.

The equipment will utilize 1,000-watt final amplifiers, with a modulation bandwidth of 5 mc/s providing a power density of 200 watts/mc, in single spot operation, or 200 watts/mc/radar when operated as a multiple spot jammer. In either case, the frequency set-on will be automatic in 5 mc/s increments. Fig. 2-22 is a block diagram of this unit.

2-55.5. Swept Frequency Transponder

This repeater type unit will provide a swept, continuous wave across the frequency band of any radar signal received. The sweep will be sufficiently rapid to simulate impulse response in the radar pass band, and a variable delay will be provided to simulate targets at ranges other than that at which the jammer is located. The peak output power will be 5,000 watts, with a signal swept over 50 mc/s at a rate of 40-mc per microsecond. The unit will have a multiple radar capability, limited by the average power capability of the output traveling wave tube, and by the design capability of the program-

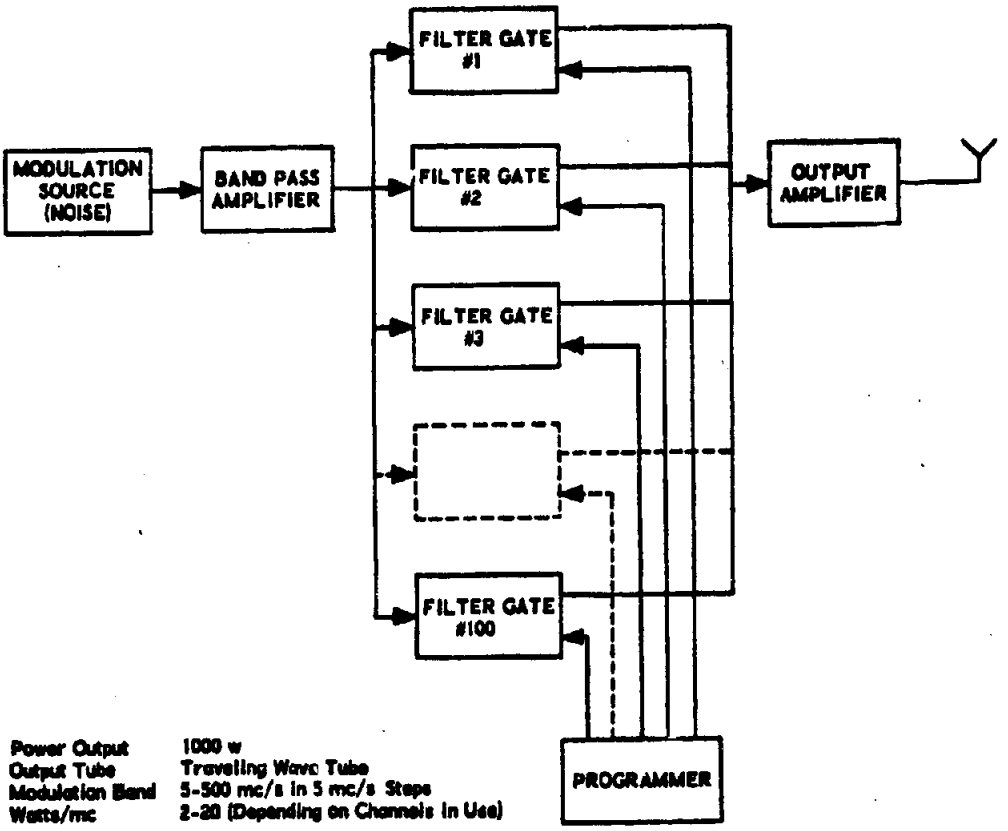

Figure 2–20 (S). Uniform Barrage Jammer, Block Diagram (U)

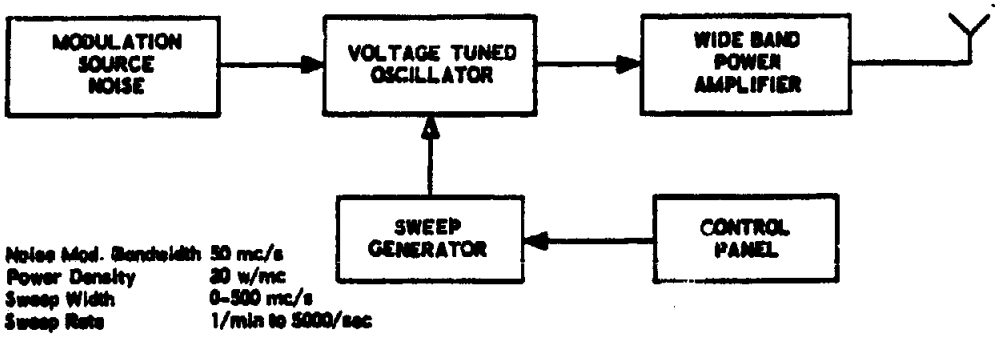

Figure 2–21 (S). Swept Barrage Jammer, Block Diagram (U)

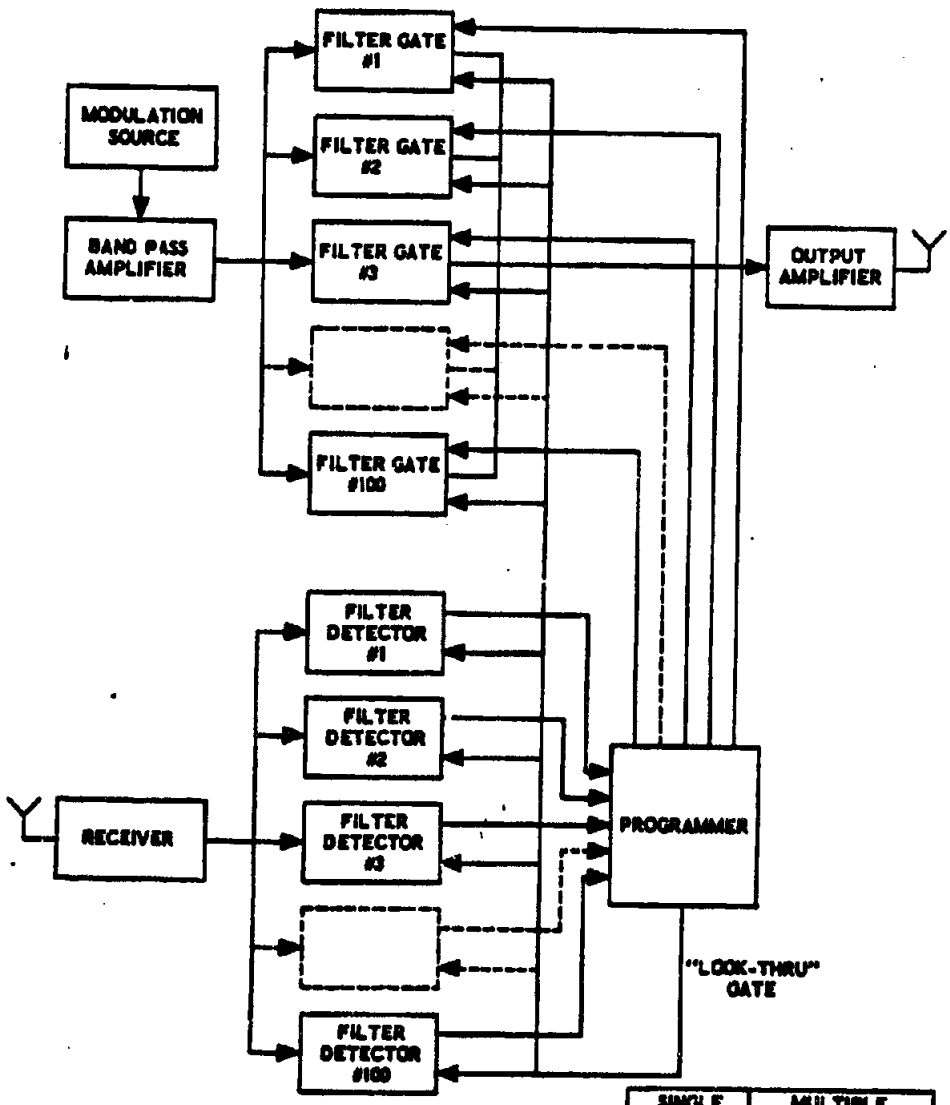

	SINGLE SPOT	MULTIPLE SPOT
Power Output	1 kw	1 kw
Mod. Bandwidth	5 mc	5 mc/radar
Power Density	200 w/mc	200 w/mc/radar
Set-On	Automatic	Automatic
Modes	Manual	Manual
	Sequential	Simultaneous
	Automatic	Automatic

Figure 2-22 (S). Composite Spot Jammer, Block Diagram (U)

mer. The probable capability will be from 1 to 10 radars. Fig. 2-23 is a block diagram of the unit.

2-55.6. Noise Pulse Repeater.

This unit will be automatic in operation. The received signal will cause a return signal consisting of a large noise pulse at the radar frequency. The peak power output will be 5,000 watts, with a noise bandwidth of 50 mc/s. The power density will then be 100 w/mc. The unit will employ variable pulse width, with delay on return, and will be capable of responding to at least ten radars. A block diagram of this unit is included as Fig. 2-24.

2-55.7. Composite Repeater

This unit is typical of countermeasures devices used for range gate stealing, or, by change of modulation methods, for angle track breaking, etc. The unit shown in Fig. 2-25 is equipment which would be used for range gate stealing. As can be seen, it will simply provide a means of delaying the received radar signal for a variable period. In addition, the provision for variable gain is shown. This would permit the equipment to operate as an angle track breaker, if inverse gain modulation were used. The equipment will deliver a peak power of 1,000 watts at the exact radar frequency. It would be completely automatic in operation.

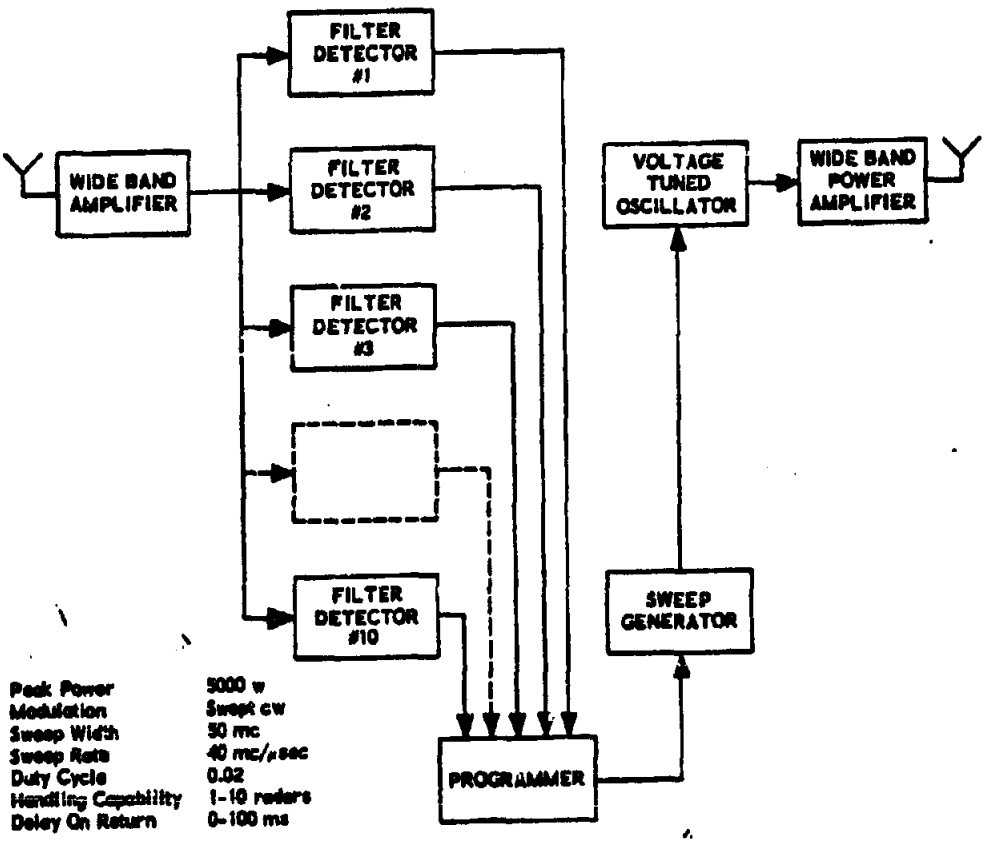

Figure 2-23 (S). Swept Frequency Transponder, Block Diagram (U)

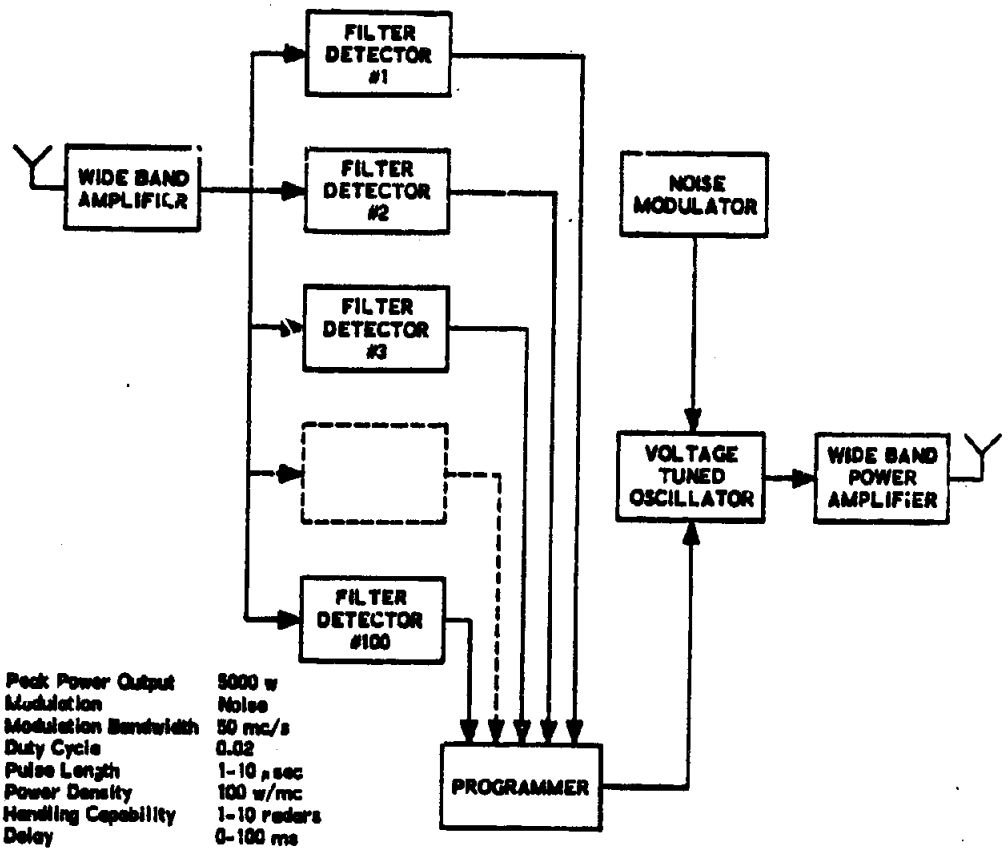

Figure 2-24 (S). Noise Pulse Repeater, Block Diagram (U)

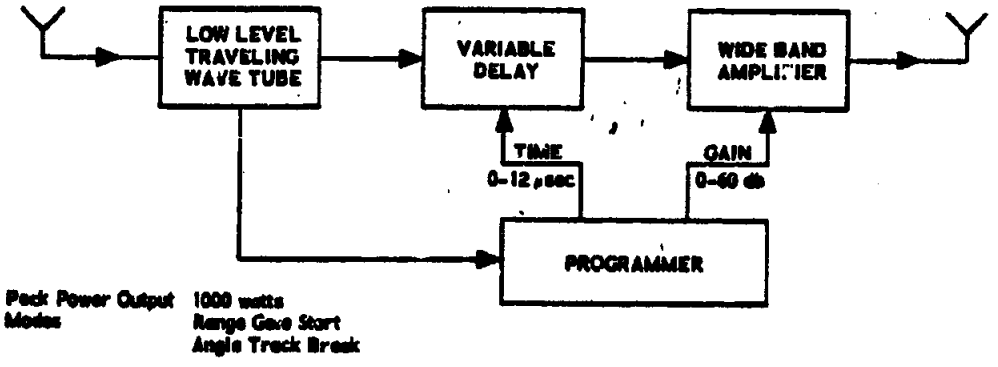

Figure 2-25 (S). Composite Repeater, Block Diagram (U)

Section XV (U)—List of References and Bibliography

2–56. REFERENCES

1. —— *Artillery Ammunition Series, Section 2, Design for Terminal Effects*, ORDP 20–245, Ordnance Corps Pamphlet, May 1957, (Confidential).
2. —— *Warheads—General*, ORDP 20–290, Ordnance Corps Pamphlet, July 1959, (Confidential).
3. —— *Fourth Symposium on Hyper-Velocity Impact*, Vols. I through III, Report No. APGC–TR–60–39, Air Proving Ground Center, Eglin AFB, Florida, September 1960, (Unclassified).
4. —— *Seminar on Hypervelocity Impact*, BRL Report No. 1101, BRL, Aberdeen Proving Ground, Maryland, February 1960, (Secret–RD).
5. —— *Small-Arms Ammunition*, Department of the Army Manual, TM9–1990, September 1947, (Unclassified).
6. R. A. Muldoon, *Terminal Ballistic Study of FL–17 Flechette*, WAL TR 763/899, Watertown Arsenal, Watertown, Massachusetts, (Confidential), ASTIA No. AD–153 037.
7. B. R. Killian, *Empirical Analysis of the Perforation of Rolled Cast Homogeneous Armor by Conventionally Shaped Kinetic Energy Projectiles of Calibers 37 mm thru 155 mm*, BRL Memorandum Report No. 1083, BRL, Aberdeen Proving Ground, Maryland, June 1957, (Confidential), ASTIA No. AD–143 533.
8. L. Zernov, J. Regan and I. Lieberman, *A Survey of the Effects of Rotation Upon Jets from Smooth Liners*, Transactions of Symposium on Shaped Charges, BRL Report No. 909, BRL, Aberdeen Proving Ground, Maryland, (Confidential), ASTIA No. AD–58 899.
9. R. J. Eichelberger, *Spin Compensation*, Chapter VIII, "Critical Review of Shaped Charge Information," BRL Report No. 905, BRL, Aberdeen Proving Ground, Maryland, (Confidential), ASTIA No. AD–48 311.
10. J. Regan and R. J. Eichelberger, *Prediction of Effectiveness of Shaped Charge Warhead Designs*, BRL Technical Note No. 1296, BRL, Aberdeen Proving Ground, Maryland, January 1960, (Confidential.)
11. R. J. Eichelberger, "Recent Progress in Shaped Charge Design, Paper No. 1, Delivered at the 9th Tripartite AXP Research Conference," Canada, April 1959, (Secret), ASTIA No. AD–316 792.
12. R. Sewell, et al, *Vaporific Explosions in Inert and Active Atmospheres*, The Ordnance Corps Shaped Charge Research Report No. 2–56, BRL, Aberdeen Proving Ground, Maryland, April 1956, (Confidential).
13. F. Triffet, *The Mechanism of Vaporific Damage to Aircraft Structures*, NAVORD Report 3490, U. S. Naval Ordnance Test Station, China Lake, California, June 1955, (Confidential).
14. H. A. Bethe, et al, *Blast Wave*, Los Alamos Scientific Laboratory, LA–2000, August 1947, (Unclassified).
15. —— *Elements of Armament Engineering*, Parts 1, 2, and 3, Ordnance Engineering Design Handbook ORDP20–106, 107, and 108, U. S. Army Ordnance Corps, August 1960, (Unclassified).
16. —— *Capabilities of Atomic Weapons*, Department of the Army Manual, TM 23–200, 1957, (Confidential).
17. S. Glasstone, *The Effects of Nuclear Weapons*, United States Atomic Energy Commission, June 1957, (Unclassified).
18. —— *Land Mines*, Department of the Army Manual, TM 9–1940, May 1956, (Unclassified).
19. C. Thompson, *Final Report on Effects of Underground Explosions*, NDRC Report No. A–479, OSRD Report No. 6645, OSRD, 1946, (Unclassified).
20. —— *Van Nostrand's Scientific Encyclopedia*, Third Edition, D. Van Nostrand Co., Inc., Princeton, New Jersey, 1958, (Unclassified).

21. O. A. Hougen, et al, *Chemical Process Principles*, Part II, Second Edition, John Wiley & Sons, Inc., New York, 1959, (Unclassified).

22. —— *Research in CBR*, Report of the Committee on Science and Astronautics, U. S. House of Representatives, Eighty-Sixth Congress, First Session, No. 23, August 18, 1959, (Unclassified).

23. —— *ABC Warfare Defense*, NAVPERS 10099, Bureau of Naval Personnel, Navy Training Course, (Unclassified).

24. M. Prentiss, *Chemicals in War*, McGraw-Hill Book Company, Inc., New York and London, 1937, (Unclassified).

25. —— *Chemical and Biological Warfare Materiel Characteristics*, Chemical Corps Board Report, Revised December 1960, (Secret).

26. —— *Casualty Effectiveness of Toxic CW Munitions*. Chemical Corps Board, unnumbered report, 27 June 1958, (Confidential).

27. —— *Military Biology and Biological Warfare Agents*, Department of the Army Manual, TM 3-216, January 1956, (Unclassified).

28. —— *Chemical and Biological Warfare Materiel Characteristics*, Chemical Corps Board Report, Revised April 1961, (Secret).

29. —— *Non-Military Defense, Chemical and Biological Defenses in Perspective*, American Chemical Society, Advances in Chemistry Series, Number 26, July 1960, (Unclassified).

30. —— *Operational Effectiveness of Biological Warfare*, Operations Research Group Study No. 21, August 1958, (Secret).

31. —— *Military Chemistry and Chemical Agents*, Department of the Army Manual, TM 3-215, August 1956, (Unclassified).

32. —— *Battlefield Illumination*, Department of the Army Manual, FM20-60, January 1958, (Unclassified).

33. —— *Bombs for Aircraft*, Department of the Army Manual, TM 9-1980, November 1944, (Unclassified).

34. —— *Artillery Ammunition*, Department of the Army Manual, TM 9-1901, September 1950, (Unclassified).

35. —— *Grenades and Pyrotechnics*, Department of the Army Manual, FM23-30, October 1959, (Unclassified).

36. —— *The Field Artillery Searchlight Battery*, Department of the Army Manual, FM6-115, August 1956, (Unclassified).

2-57. BIBLIOGRAPHY

1. G. Birkhoff, et al, "Explosives With Lined Cavities," Journal of Applied Physics, Vol. 19, No. 6, pp. 563-582, June 1948.

2. E. M. Pugh, R. J. Eichelberger and N. Rostoker, "Theory of Jet Formation by Charges With Lined Conical Cavities," Journal of Applied Physics, Vol. 23, No. 5, pp. 532-536, May 1952.

3. R. J. Eichelberger and E. M. Pugh, "Experimental Verification of the Theory of Jet Formation by Charges With Lined Conical Cavities," Journal of Applied Physics, Vol. 23, No. 5, pp. 537-542, May 1952.

4. R. J. Eichelberger, "Re-Examination of the Nonsteady Theory of Jet Formation by Lined Cavity Charges," Journal of Applied Physics, Vol. 26, No. 4, pp. 398-402, April 1955.

5. R. J. Eichelberger, "Experimental Test of the Theory of Penetration by Metallic Jets," Journal of Applied Physics, Vol. 27, No. 1, pp. 63-68, January 1956.

6. —— *Critical Review of Shaped Charge Information*, BRL Report No. 905, BRL, Aberdeen Proving Ground, Maryland, May 1954, (Confidential), ASTIA No. AD-48 311.

7. —— *The Ordnance Corps Shaped Charge Research Report*, formerly published periodically by BRL, Aberdeen Proving Ground, Maryland, sponsored by the Ordnance Corps Shaped Charge Research and Development Steering and Coordinating Committee, (Confidential — most numbers).

8. J. Simon. *A Flash Radiographic Study of Special Armor*, BRL Memorandum Report No. 909, BRL, Aberdeen Proving Ground, Maryland, July 1955, (Confidential), ASTIA No. AD-76 128.

9. G. Birkhoff, *Mathematical Jet Theory of Lined Hollow Charges*, BRL Report No. 370, BRL, Aberdeen Proving Ground, Maryland, June 1943, (Confidential).

10. M. W. Ayton, J. R. Gibson, C. B. Gurtowski and B. Bledsoe, "Shaped Charges, An Annotated Bibliography," Library of Congress, Technical Information Division, May 1955.

11. —— *Collection and Arrangement of Shaped Charge Data*, Final Report, Vols. I, II, and III, Arthur D. Little, Inc., 1959.

12. J. M. Regan, R. J. Eichelberger, G. E. Hauver and A. Merendino, *A Critique on the Design of the T42 Warhead*, BRL Memorandum Report No. 1212, BRL, Aberdeen Proving Ground, Maryland, June 1959.

13. J. M. Regan and R. J. Eichelberger, *Prediction of Effectiveness of Shaped Charge Warhead Designs*, BRL Technical Note 1296, BRL, Aberdeen Proving Ground, Maryland, January 1960, (Confidential).

14. —— *Protection Against Shaped Charges*, NDRC Report No. A-384, Final Report, Carnegie Institute of Technology, under OSRD Contract DEMar-950, (Confidential).

15. F. E. Allison, *Defeat of Shaped Charge Weapons*, Final Report, Ordnance Corps Contract No. DA-36-061-ORD-507, Carnegie Institute of Technology, April 1960.

16. N. Rostoker and R. J. Eichelberger, *Rotated Charges*, Carnegie Institute of Technology, Fourth Bimonthly Report, Ordnance Corps Contract No. DA-36-061-ORD-122, CIT-ORD-R-24, June 1952.

17. J. Simon and T. Martin, *Spin Compensation of Shaped Charge Liners Manufactured by Rotary Extrusion Process*, BRL Memorandum Report No. 1181, BRL, Aberdeen Proving Ground, Maryland, December 1958.

18. R. J. Eichelberger, J. Simon and R. DiPersio, *Shaped Charge Performance in the New Tank Main Armament Concept*, BRL Memorandum Report No. 1186, BRL, Aberdeen Proving Ground, Maryland, February 1959, (Confidential).

19. J. Simon, R. DiPersio and R. J. Eichelberger, (Classified Title), BRL Memorandum Report No. 1231, BRL, Aberdeen Proving Ground, Maryland, September 1959.

20. R. DiPersio and J. Simon, *An Empirical Approach to the Design of Spin Compensating Shaped Charge Liner*, BRL Memorandum Report No. 1251, BRL, Aberdeen Proving Ground, Maryland, February 1960.

21. —— *Fundamentals of Shaped Charges*, Carnegie Institute of Technology, CIT-ORD-38, Contract DA-36-061-ORD-122, April 30, 1956.

22. —— *Fundamentals of Shaped Charges*, Carnegie Institute of Technology, CIT-ORD-37, Contract DA-36-061-ORD-122, February 29, 1952.

23. —— *Fundamentals of Shaped Charges*, Carnegie Institute of Technology, Status Report No. 1, Contract DA-36-061-ORD-394, January 31, 1954.

24. —— *Fundamentals of Shaped Charges*, Carnegie Institute of Technology, 4th Quarterly Progress Report, Contract DA-36-061-ORD-513, October 31, 1956.

25. —— *Fundamentals of Shaped Charges*, Carnegie Institute of Technology, 7th Quarterly Progress Report, Contract DA-36-061-ORD-513, July 31, 1957.

26. —— *Theory of Signal Detectability*, University of Michigan, Engineering Research Institute TR-13, (Unclassified), ASTIA Nos. AD-16 786 and 16 787.

27. —— *Electronic Countermeasures*, Bibliography, ASTIA Reference Center, ARC 1163, (SECRET), ASTIA No. AD-49 537.

28. —— *Radar Reflections*, Bibliography, ASTIA Reference Center, ARC 1719, (SECRET), ASTIA No. AD-49 980.

29. —— *Clutter*, Bibliography, ASTIA Reference Center, ARC 1647, (SECRET). ASTIA No. AD–50 260.

30. —— *Effects of Noise on Automatic Tracking Systems*, General Electric Report 2–202–262, (SECRET). ASTIA No. AD–56 491.

31. —— *Electronic Countermeasures*, Bibliography, ASTIA Reference Center, ARC 1163, Sup. 1, (SECRET). ASTIA No. AD–60 320.

32. —— *Synchronous Sweep Jamming of Conical Scan Radar—Aerial Rec. Lab.*, WADC TN–55–113, (SECRET), ASTIA No. AD–67 019.

33. —— *Bibliography of Bibliographies*, ASTIA Reference Center, ARC 1721, (SECRET). ASTIA No. AD–74 436.

34. —— *Susceptibility of Doppler Navigator Systems to Detection and Jamming*. Airborne Instrument Lab. Report 8225–1, (CONFIDENTIAL), ASTIA No. AD–83 802.

35. —— *Signal Analysis and Data Processing in Electronic Countermeasures*, Tri-Service Symposium, May 1955, (SECRET), ASTIA No. AD–86 183.

36. —— *Studies in Radar Cross-Sections XVIII: Airborne Passive Measures and Countermeasures*, University of Michigan, (SECRET), ASTIA No. AD–90 201.

37. —— *Electronic Countermeasures Equipment for Aircraft Defense*, Stanford Research Inst. Sci. Report 4, (SECRET), ASTIA No. AD–110 130.

38. —— *Electronic Countermeasures*, Bibliography, ASTIA Reference Center ARC 1163, Sup. 2, (SECRET), ASTIA No. AD–111 574.

39. —— *Proceedings of the Annual RADAR Symposium*, University of Michigan, Willow Run Labs., annually since 1955, (SECRET).

40. —— *Symposium, Next Decade in Countermeasures*, Johns Hopkins University, Radiation Lab., Tech. Report AF–62, February 1959, (SECRET). ASTIA No. AD–305 370.

41. —— *Electronic Warfare Systems Study*, Motorola, Inc., (SECRET), ASTIA No. AD–304 674.

42. —— *Study and Development of Deception Countermeasures for Tracking Radars*, RCA West Coast Elec. Products Dept. 59–4819, (SECRET), ASTIA No. AD–304 205.

43. —— *Proceedings: Pulse Compression Symposium*, Radar Lab., Rome Air Development Center, June 1957, RADC–TR–58–6, (SECRET). ASTIA No. AD–148 551.

44. —— *Transactions of Annual Electronic Warfare Symposium*, University of Michigan Research Institute, annually since 1956, (SECRET).

45. —— *Defense Aginst Electronic Jamming*, Dept. of the Army Manual, FM 11–151, June 1955, (Unclassified).

46. L. P. Brophy and G. J. B. Fisher, *The Chemical Warfare Service: Organizing for War*, Office of the Chief of Military History, Department of the Army, Washington, D. C., 1959, (Unclassified).

Chapter 3 (S)

TARGET VULNERABILITY

Section I (U)—Personnel

3–1. INTRODUCTION

Personnel are vulnerable to numerous kill mechanisms, the most important of which are fragments, bullets, flechettes, blast, toxic and biological agents, and thermal and nuclear radiation. Although personnel are vulnerable to each of the kill mechanisms in different ways, the end effect is to render the individual incapable of performing his intended function.

Fragments, bullets, and flechettes are considered as a single class of kill mechanism because all cause their results by penetration and/or perforation. These projectiles can penetrate into the major body cavities and limbs to cause damage to the critical tissues such as the heart, lungs, and brain, etc., thus causing loss of fine and coarse muscular coordination of the extremities. Their effects range from immediate death, to incapacitation through loss of the use of one or more limbs, to minor wounds which produce little immediate effect, but which can become incapacitating if no medical treatment is available.

3–2. INCAPACITATION CRITERIA

As defined by current lethality criteria, the incapacitation of a soldier refers to his inability to carry out his assigned duties. A soldier's combat duties are various and depend upon the tactical situation as well as his military assignment. Four military tactical situations have been chosen for defining incapacitation. These situations are assault, defense, reserve, and supply. The ability to see, hear, think, and communicate is considered as a fundamental necessity in all of the situations; loss of these abilities is assumed to be incapacitating.

Infantry soldiers in assault situations are considered to require the use of their arms and legs. The ability to run and to use both arms is desirable, and the ability to move about and to use at least one arm is necessary. A soldier cannot effectively participate in an assault if he cannot move about and if he cannot use hand-operated weapons. Thus, incapacitation is defined for the assault situation.

In a defense situation a soldier's need to move is considered minimal as long as he can operate hand weapons. His ability to relocate himself, although desirable, is not necessary to the performance of some valuable duties.

The third situation considered is that of troops held in reserve close to the combat zone, and ready to be committed to the assault or defense. They are considered to be more vulnerable to incapacitation than active combat troops, because they probably would not be committed to action even if the wounds received were relatively minor.

The final military situation is that of supply, which includes vehicle drivers, ammunition handlers, and a variety of other personnel, possibly far from combat. These troops would be hospitalized upon the loss of use of an arm or leg, or for even less severe causes, and are considered to be very vulnerable to incapacitation.

The time factor used in the incapacitation criteria is the length of time from the wounding to the occurrence of loss of muscular coordination sufficient to render a man ineffective in performing his mission. To illustrate the need for a time factor, consider a soldier in a defense position where it is not necessary that he move about. He is hit in the leg by a fragment which penetrates into the muscle and severs a peripheral artery. Although he may be limited in his ability to move, he is not considered incapacitated. However, if he has no

medical attention the loss of blood will, in time, prevent him from functioning effectively, and he must then be considered a casualty.

Psychological factors will have a definite effect on incapacitation and may even void the entire organic approach. Among these factors are the fear of the unknown, as experienced by "green" troops, the effect of enemy propaganda, apprehension caused by personal problems, and excessive loss of mental capabilities or of emotional stability due to prolonged exposure to physical danger or to an abnormally hot, cold, or wet battlefield environment. Owing to a lack of measurement standards, these factors are not discussed in this section.

Current lethality criteria relate the effects of wounds to the functioning of the extremities; therefore, the analyses of a soldier's ability to carry out his mission are based primarily on the use of the extremities. However, direct wounds of some vital organ, such as an eye or the heart could be immediately incapacitating for all military situations.

3–3. FRAGMENTS, BULLETS, AND FLECHETTES

The vulnerability of personnel to fragments, bullets, and flechettes (Refs. 1 and 2) has been discussed, thus far, only in relative terms; that is, a soldier in a given situation is either more or less vulnerable than another soldier in a different situation. To discuss personnel vulnerability quantitatively, requires a more concrete expression of what vulnerability is. The expression now used is the conditional probability, given a hit, that the target is incapacitated. This probability is based on the mass, area, shape, and striking velocity of the projectile, because these factors govern the depth, size, and severity of the wound. These factors are evaluated for various tactical situations and elapsed times from wounding to incapacitation, as described earlier. The experimental procedures and the analytical means of quantitatively determining the conditional probability of incapacitation by fragments is given in Ch. 5.

Although natural or man-made cover, such as trees or foxholes, has a definite influence on the actual probability of being hit, it has no bearing on the conditional probability, which assumes a hit. However, any combat clothing (i.e., body armor, helmet) reduces the striking velocity of the projectile, and hence influences the depth of penetration and the conditional probability that the target is incapacitated.

3–4. BLAST

The vulnerability of personnel to blast is dependent primarily upon the magnitude and duration of the peak overpressure and the transient winds (dynamic pressure) which accompany an explosion. Blast effects may be conveniently separated into three phases, designated primary, secondary, and tertiary (Refs. 3 and 4).

The injuries associated with primary blast effects are directly related to the peak overpressure at the shock front. The arrival of the shock front is accompanied by a sudden increase in pressure which may produce considerable damage to the human body by crushing, damage to the central nervous system, heart failure due to direct disturbance of the heart, suffocation caused by lung hemorrhage, damage to the gastro-intestinal tract, or ruptured eardrums. In general, damage is most definite in those body regions with the greatest variation in tissue density and, particularly, in the air-containing organs of the body. Use of cover such as foxholes may not have much effect as a protective measure because the reflected shock waves usually magnify the overpressure and, hence, the damage.

Secondary blast effects are those caused by the impact of penetrating and nonpenetrating missiles which are propagated by the transient winds. The effects depend on the missile velocity, mass, size, shape, composition, and density, and on the specific regions and tissues of the body involved. The lethality criteria associated with this type of penetrating missile are the same as those encountered with fragments, bullets, and flechettes. Nonpenetrating missiles impacted against the chest can cause early fatality by bilateral lung lesions very similar to those caused by primary blast. Skull fracture, concussion, rupture and hemorrhage of the liver and spleen, and skeletal fracture can

result, as can crushing injuries from heavy masses of masonry and other building materials

The use of armor and protective equipment serve a purpose against secondary blast effects by reducing the velocity of the missiles, thus lowering the probability of damage.

Tertiary blast effects are defined as damage which is a consequence of physical displacement of the target by the shock wave and the transient winds. Damage from displacement can be of two general types. One type involves the separation of a limb or other appendage from the body. The other type results from a total displacement of the body, with the injury usually occurring during the decelerative phase of the translation. These injuries are comparable to those resulting from automobile and aircraft accidents. The extent of the damage depends on the portions of the body subjected to accelerative and decelerative loads, the magnitude of the loads, and the ability of the body to withstand these loads. In the case of nuclear explosions, the hazards of violent impact are of considerable importance, because of the great range and long duration of the blast winds.

Miscellaneous effects of blast can involve exposure to ground shock, dust, temperature phenomena, contact with hot dust and debris, and conflagration heat from blast-produced fires.

The nature of damage from ground shock concerns injuries from displacement, and impact with heavy objects, as noted above. A sufficiently high concentration of dust, under certain circumstances, has proved fatal simply through deposits in, and obstruction of, the small airways of the lungs. The danger depends upon time of exposure and the concentration of appropriately sized dust particles. Thermal injuries involve burns from thermal radiation and other sources (Par. 3–5).

When considering damage resulting from blast, it is not the rule, nor is it practical, to consider the injuries on the basis of only one of the three phases. Injuries from explosions, nuclear explosions in particular, are caused by a combination of all the blast damage mechanisms. An example of combined blast injury may be quoted directly from the report on the Texas City explosion (Ref. 5).

"A man, age thirty-nine, had just come from loading one of the ships and was standing on the pier facing the ship. When the explosion occurred, he was blown into the sky so high that he could see over a warehouse and then he was blown laterally into the water. He did not lose consciousness and was able to swim to land. The injuries sustained were perforation of both eardrums, severe scalp lacerations, severe lacerations of left upper arm with extensive infection, left ulnar (forearm) paralysis, and laceration of the right foot." All three damage phases were involved in this accident. The perforation of the eardrums resulted from the primary blast effects, and a combination of secondary and tertiary effects caused the lacerations and paralysis.

3–5. FIRE AND THERMAL RADIATION

The vulnerability of personnel to fire and thermal radiation probably can be described best in terms of their effects, as flame and flash burns, respectively. The two types of burns can usually be distinguished by the characteristic-profile nature of the flash burns as compared with overall burning by flame burns. Usually flash burns are limited to small areas of the body not covered by shielding, such as clothing. Flame burns, on the other hand, will cover large areas of the body, because the clothing will catch on fire.

The severity of flash burns will range from mild erythema (reddening) to charring of the outermost layers of the skin, with the severity being determined by the thermal energy received and the rate at which the energy is delivered. With flash burns, there is no accumulation of fluid under the skin, as there is with flame burns. In addition, the depth of penetration is considerably less than that associated with injuries caused by direct flames.

The degree and type of cover that the individual affords himself will for the most part determine the amount of burns resulting from thermal radiation. Cover, however will not have much effect in reducing flame burns if the

combustible material around the individual is burning.

When fire or thermal radiation are the products of bombs, the incapacitating effects of any burn sustained will be magnified because many of the medical facilities will be either damaged or destroyed. As a result, medical attention will not be available.

3–4. BIOLOGICAL AND CHEMICAL AGENTS

Biological and chemical warfare agents are designed primarily as anti-personnel agents. Biological warfare is the military use of living organisms, or their toxic products, to cause death, disability (either temporary or permanent), or damage to man, his animals, or his crops. Chemical warfare is the military use of toxic gases, liquids, or solids to produce casualties (Refs. 6 and 7).

Biological warfare agents are selected to produce many results, from brief but crippling disease to widespread serious illness resulting in many deaths, depending on the effects desired. Chemical warfare agents cause incapacitation by choking, blood poisoning, destruction of the nervous system, shock, vomiting, and various other effects.

Due to the seriousness of the effects, and because these agents are designed primarily for use against personnel, it is sufficient to say that personnel are vulnerable, and that the effects depend upon the particular agent, the concentration, and the duration of exposure. Any undisciplined group, particularly without protective gear such as masks, would be especially vulnerable to casualties and to panic, with complete demoralization resulting as a secondary effect.

3–7. NUCLEAR RADIATION

Most effects of nuclear radiation on living organisms depend not only on the total dose absorbed, but also on the rate of absorption, and the region and extent of the body exposed. However, a few radiation phenomena, such as genetic effects, apparently depend only upon the total dose received and are independent of the rate of delivery. In other words, the damage caused to the reproductive cells by radiation is cumulative. In the majority of instances the rate of delivery is the important factor; that is, biological effect of a given total dose of radiation decreases as the rate of exposure decreases. For instance, if the whole body were exposed, 800 roentgens in a single dose would have a high probability of being fatal, but it would not cause death or have any noticeable clinical effects if supplied evenly over a period of 25 to 30 years.

Different portions of the body show different sensitivities to radiation, although there are undoubtedly variations of degree among individuals. In general, the most radio-sensitive parts include the lymphoid tissue, bone marrow, spleen, organs of reproduction, and gastrointestinal tract. Of intermediate sensitivity are the skin, lungs, kidney, and liver; whereas muscle and full-grown bones are the least sensitive. Those parts that are the most radio-sensitive are not able to replace the damaged cells, or the rate of replacement is so slow that the functional ability is impaired.

Although a large dose (450 roentgens or greater) will generally be fatal if administered over the whole body, the same dose received in a small area may result in considerable damage to that area, but the overall health of the individual may not be seriously affected. One of the reasons for this difference is that when the exposure is restricted, the unexposed regions can contribute to the recovery of the injured area. The effects of cover will, therefore, influence the amount of exposure, and thus the number of incapacitations.

Section II (U)—Ground Vehicles

3–8. INTRODUCTION

Ground vehicles are vulnerable to a variety of kill mechanisms, with the most effective kill mechanism depending on the type of vehicle. A customary method of classing vehicles is according to armor protection, as armored vehicles or unarmored vehicles. The presence or absence of armor on a vehicle does not in it-

self determine the function or battlefield role of the vehicle. For example, a cargo-carrying vehicle, wheeled or tracked, armored or unarmored, has logistic support as its role.

In general, ground vehicles are vulnerable in varying degrees to shell fragments and armor-piercing projectiles, blast, fire, thermal and nuclear radiation, shaped charges, electronic jamming of communications equipment, and to any of these or other kill mechanisms which can affect the crew. Vulnerability to fragments and projectiles depends on the type, amount, and obliquity of the armor (if any), and on the mass, shape, and striking velocity of the impacting projectile or fragment.

In any vehicle vulnerability assessment the crew must be considered as a factor. The crew of a soft (unarmored) vehicle, unlike an aircraft or armored vehicle crew, are not normally considered to be a vulnerable part of the vehicle, because replacements should be available from the other parts of the vehicle convoy. On the other hand, it might be possible to immobilize an armored vehicle simply by incapacitating the crew.

Nuclear weapon effects include: initiation of fires and destruction of protective coatings by thermal radiation; crushing of external equipment, and overturning by blast; and radiation damage to organic compounds, optical elements and electronic components. Vulnerability is usually related to weapon yield, distance from detonation, type of burst, and environmental and terrain conditions.

Tank tracks and running gear, and light vehicles with their cargo and crew, are vulnerable to conventional high explosive blast. Shaped charges can provide penetration of heavy armor and cause damage, by the residual jet and back spall, to internal components such as fuel, ammunition, engine, crew, steering controls, and fire control equipment. Armored vehicles (as well as others) are also vulnerable to other specialized high explosive weapons such as plastic charges, which, when detonated on the outer surface of the armor, cause severe spalling of the inner surface. The spalling produces large numbers of high velocity fragments, damaging to crew and internal components.

3–9. ARMORED VEHICLES (Ref. 8)

3–9.1. General

Armored vehicles can be divided into two basic groups: those meant to participate in the assault phases of offensive combat, the armored fighting vehicle (AFV); and those intended to participate in offensive combat, but not ordinarily in the assault, of which type the armored infantry vehicle (AIV) and the armored self-propelled artillery piece (AAV) are examples. Assault, in this context of offensive combat, is the final step in the attack during which the objective is physically overrun and taken.

The relative amount of armor protection of the AFV, as compared to the AIV and armored artillery vehicle (AAV), is a distinguishing feature because the AFV is the only vehicle specifically designed to defeat armor-piercing projectiles and shaped charges.

The AIV represents a class of armored, tracked vehicles which is adaptable to a wide variety of uses on the battlefield. A few examples are armored personnel carriers, mortar carriers, ambulances, and command post vehicles. Increased mobility and limited protection to the infantry are provided by the armored personnel carrier type of AIV, and to artillery weapons and crews in the case of the AAV (Refs. 9 and 10).

3–9.2. Armored Fighting Vehicles (Ref. 11)

The AFV is typified by the tank, which combines the favorable assault characteristics of great firepower, mobility, shock action, and armor protection. In the normal combat situation destruction of the AFV is not required, some degree of incapacitating damage usually being sufficient.

As a reference basis, certain damage categories have been established for the AFV. "M" damage will cause complete or partial immobilization of the vehicle. "F" damage causes complete or partial loss of the ability of the vehicle to fire its main armament and machine guns.

"K" damage will cause the vehicle to be destroyed (Ref. 12). These levels of damage, considered to be levels of functional impairment, are described fully in Ch. 6.

The vulnerability of an AFV is usually thought of in terms of its resistance to perforation by armor-piercing projectiles, shell fragments, and shaped charges, and by its structural resistance to blast from nuclear detonations or HE projectiles. In actuality, the vehicle or its internal components may be damaged to some degree by mechanisms which will not ordinarily destroy or cripple the vehicle.

For example, bullet splash from small arms projectiles may enter small, exposed openings and clearances. (Bullet splash is defined as the dispersion of finely divided or melted metal which is produced upon the impact of a projectile on armor plate or other hard objects). The splash particles have been known to enter openings and make two or three right-angle turns before losing enough energy to be non-lethal. The air grilles of engine compartments are normally susceptible to the passage of splash, because they are designed to allow the entrance of sufficient air to cool the engine. The clearance around a gun shield is still another location where splash may enter.

When the AFV is attacked with projectiles of various calibers, it is possible for movable components to become wedged, burred, or deformed in such a manner that their usefulness is impaired. This is termed immobilization of the part (as contrasted with immobilization of the complete vehicle). Movable components include such items as hatch covers, gun shields, complete tank turrets, and the main gun tube.

High explosive blast (or nuclear blast) damage may be incurred in AFV armor structure, especially where the blast effect is confined. The impacting wave front will cause the armor plate to act like a flexible membrane so that it vibrates back and forth like a drumhead. This same phenomenon may also be induced by the impact of armor-piercing projectiles. The resulting high- and low-frequency vibrations of the structure impose a shock, which is a sudden change in the motion of the system that varies with the magnitude and duration of the forces imposed. Even in those cases where the armor structure itself can resist the shock, interior components fastened to the armor structure may be severely damaged. Some of these components may even become detached and act as secondary missiles. Traversing mechanisms, control and instrument panels, sighting systems, radios, turret bearings, and turret traversing gear rings are all important components that are apt to be damaged by shock (Ref. 13).

The armor distribution of the AFV is based upon resistance to ground attack, consequently the vehicle is more vulnerable to air attack. Overhead armor protection (turret top, hull top, engine grilles) is usually considerably less than that found on the front and sides. Air attack can include strafing fire from small arms, small caliber guns (20 mm, and U. S. S. R. 23 mm and 37 mm cannons), rockets, and aerial bombs. Actual test data pertaining to the vulnerability of various components of armored vehicles, and suggested means for reducing their vulnerability, are to be found in Refs. 13 and 14.

A successful means of attack upon the AFV is usually not found in some ideal weapon or kill mechanism, but rather in the proper tactical use of many available devices which will exploit the weaknesses of the AFV. Some of these weaknesses are its considerable weight, exposed suspension and weapons, and poor vision when buttoned-up.

Tactical defensive positions will be protected against the AFV by mine fields capable of damaging or destroying vehicles by blast, shaped charges, Napalm (buried), or any combination of these. As hostile tanks approach the position, small arms (bullets) and artillery fire (blast and fragments) employed against the tanks will force the tank crews to button-up and will hamper the vehicle commanders (by an impairment of vision) in controlling the movement of the vehicles. Armor-piercing and incendiary bullets, together with shell fragments, will damage some vision mechanisms, and make the tanks more vulnerable to anti-tank weapons. While buttoned-up, the ve-

hicles are more likely to veer into mine fields, where many vehicles will at least become "M" damaged. Many of those tanks not immobilized by mines will be made so by direct blast effect from HE shells against the vehicle suspension system. Once the vehicle is a stationary target, it is more likely to be hit by direct-fire anti-tank weapons, where an "F" or "K" kill can be more easily accomplished. In addition, the stowed ammunition and fuel in the vehicle provide a source of destructive energy which can be ignited, thereby damaging the vehicle.

3–9.3. Armored Infantry and Armored Artillery Vehicles

The AIV and the AAV are provided with limited armor protection, consistent with their weight limitations and tactical roles. Such armor is resistant (at some given range) to small arms fire of caliber .50 or less, high explosive shell fragments, and blast (up to a certain size shell as specified for the vehicle). The AIV and AAV are generally vulnerable to any anti-tank weapon. This includes such devices as small caliber anti-tank weapons which fire AP projectiles (U. S. S. R. 14.5 mm, for example), the smallest shaped charges currently used by infantry troops, and almost any anti-vehicle land mine.

The function of these vehicles does not require that they seek anti-tank weapons; rather, they attempt to avoid them. For example, an armored artillery vehicle does not normally encounter enemy gun positions; therefore, its armor is based upon providing protection only against shell fragments and some HE blast from counter-battery fire. Nor is the armored infantry vehicle intended to assault hostile gun positions. The armored infantry advance as far as possible in their personnel carriers, dismounting when forced to by enemy fire or when making the final assault upon the objective. The vehicular weapons of the personnel carriers, either mounted or dismounted, may then be used to support the attack from appropriate positions (Refs. 9 and 10). The AIV thus provides support but avoids direct fire upon itself, because it is protected only by thin armor.

3–10. UNARMORED VEHICLES

The category of unarmored vehicles includes two basic types: those transport-type vehicles (trucks, tractors, jeeps, etc.) which have logistical support of combat forces as their primary mission; and unarmored wheeled or tracked vehicles serving as weapons carriers. Unarmored vehicles are often referred to as "soft" vehicles.

An unarmored vehicle is not only vulnerable to all the kill mechanisms which can be used against armored vehicles, but also is vulnerable to most anti-personnel weapons (small-caliber ball ammunition, anti-personnel mines, many shell fragments which cannot perforate light armor, HE blast, etc.). A quantitative measure of minimum-damage vulnerability for such a vehicle is to consider it a casualty if a part necessary for its operation is damaged to a degree which causes the vehicle to stop within a specified time limit. Although most of the presented area of such a target, at some given aspect, may be perforated by projectiles or fragments without their striking a component required for operation, some of the components essential to operation (electrical, fuel, lubricating, and cooling system) are especially vulnerable to impacting objects. These components are considered to be the parts most likely to fail under attack.

Section III (C)—Ground Structures

3–11. (U) INTRODUCTION

An accurate knowledge of the response of structures and structural components to the various mechanisms of attack is of vital interest to the structural designer, military planner, and those agencies concerned with military and civil defense. The nature of target loading and response, and the parameters governing this response, are required to establish design and damage criteria and, hence, the vulnerability of the structure to a specific damage mechanism.

The effects of each of the possible damage mechanisms are produced by different means. Therefore, any study associated with a particular class of structure must be conducted with respect to a particular damage mechanism. When a target is exposed to a weapon which produces several damage mechanisms, such as those produced by a nuclear weapon, the possible synergistic effects are ignored because the problem becomes too complicated. Only the mechanism most effective against the particular target is employed in the vulnerability analysis.

Although structures are vulnerable to the great majority of kill mechanisms, only air blast, ground shock, and fire will be considered in the discussion of vulnerability which follows. These phenomena are considered as the most probable mechanisms which will completely destroy or severely damage the structure. Both surface and subsurface structures will be considered in the discussion.

With respect to air blast, the loading, in magnitude and duration, and the deflection and elasticity of the target element are the prime variables affecting the degree of damage. The target size and composition influence the loading transmitted to the structure, by making it primarily either more susceptible to diffraction loading or to the drag forces produced by the dynamic pressures. Surface structures are usually most vulnerable to air blast.

Ground shock is primarily effective against structures located underground. The intensity of the shock wave, the type of soil formation, and the flexibility of the structure are most significant in determining the degree of damage.

Structural fires are usually a secondary result of some other damage mechanism. (For nuclear weapons, primary thermal radiation may produce the fires.) Nevertheless, in many cases, the fire will spread sufficiently to cause severe damage well outside the lethal radius of the primary effect. The vulnerability of a structure to fire is largely dependent upon the combustibility of the building and its contents.

Detailed information concerning the vulnerability of ground structures to the above mentioned damage mechanisms is presented in the following pages. Additional information on target response may be found in Ch. 7, Par. 7–17. Data related to target vulnerability analysis and computation of damage probabilities is found in Ch. 7, Par. 7–20.

3–12 (C) SURFACE STRUCTURES

3–12.1. (C) Air Blast

3–12.1.1. (C) *Loading*

a. (U) *General*

The loading on an object exposed to air blast is a combination of the forces exerted by the overpressure and the dynamic pressure of the incident blast wave. The loading at any point on a surface of a structure can be described as the sum of the dynamic pressure, multiplied by a local drag coefficient, and the overpressure after any initial reflections have cleared the structure. Since the loading changes rapidly during the time the blast wave is reflecting from the front surfaces and diffracting around the structure, loading generally comprises two distinct phases. They are: loading during the initial diffraction phase (Ch. 2, Sec. IV); and loading after the diffraction is complete, or drag loading (Ref. 15).

Air blasts originate from two sources, namely conventional high-explosive weapons and nuclear weapons. The loadings that result from the two sources differ due to the difference in overpressures and duration of the positive phase of the blast wave. Air blasts from conventional high-explosives have relatively short positive phases; therefore, the resulting loadings are more important during the diffraction phase. The considerably longer positive phases of the blast waves of nuclear explosions make the resulting loadings significant during both the diffraction and drag phases. Figure 3–1 shows the effects of the nuclear bomb explosion at Nagasaki.

b. (C) *Loading During the Diffraction Phase*

(U) A large closed structure with walls that remain intact throughout most of the load duration is primarily sensitive during the diffraction phase, since most of the translational load is applied during this period. As the blast wave strikes this type of structure, it is reflected, creating overpressures greater than those inci-

Official U. S. Army Photograph

Figure 3–1. Area Around Ground Zero at Nagasaki, Before and After the Atomic Explosion

dent thereon. Subsequently, the reflected overpressure decays to that of the blast wave. As the blast wave progresses, it diffracts around the structure, eventually exerting overpressures on all sides. Before the blast wave reaches the rear face, overpressures on the front exert translational forces in the direction of blast wave propagation. After the blast wave reaches the rear face, the overpressures on the rear tend to counter the overpressures on the front. For smaller structures, the blast wave reaches the rear face more quickly, so that the pressure differential exists for a shorter time. Thus, the net translational loading resulting from overpressures during the diffraction phase depends primarily on structural dimensions. For some structures where wall failure takes place early in the diffraction phase, only the structural frame may remain, and essentially no load is transmitted to the structural frame during the remainder of the diffraction process. A longer duration blast wave does not materially change the magnitude of the net translational loading during the diffraction phase, or the resulting damage. In other words, the structure is primarily sensitive to the peak blast wave overpressure. Table 3–1 lists those types of structures which are generally affected primarily by blast wave overpressure during the diffraction phase (Ref. 15).

c. (C) ***Loading During the Drag Phase***

(U) During the diffraction phase, and until the blast wave has passed, dynamic pressures are also exerted on structures. Dynamic pressure loading is commonly referred to as drag loading. In the case of a large, closed structure the drag phase loading is small relative to the overpressure loading during the diffraction phase. For smaller structures, the drag phase assumes greater relative importance. For small area components such as the frame of a structure after removal of siding, the translational load applied as a result of the drag phase is much greater than the net translational loading from overpressures during the diffraction phase. For frame buildings with siding removed during the diffraction phase, the drag phase is the predominant factor in producing further damage. Likewise, for bridges the net load during the diffraction phase is applied for an extremely short time, but the drag phase continues until the entire blast wave passes the structure. Because the drag phase duration is closely related to the duration of the blast wave overpressure, rather than to the overall dimensions of the structure, damage is dependent not only on peak dynamic pressure but also on the duration of the positive phase of the blast wave. Thus, damage to this type of structure is dependent on weapon yield as well as peak target loading.

(U) Table 3–2 lists those types of structures which are sensitive primarily during the drag phase. Some elements of a structure may be damaged more by loading during the diffraction phase, other elements of the same structure may be damaged more by the drag phase. The dimensions and orientation of a structure, together with the number and area of the openings and the rapidity with which wall and roof

TABLE 3–1 (C). DAMAGE TO TYPES OF STRUCTURES PRIMARILY AFFECTED BY BLAST-WAVE OVERPRESSURE DURING THE DIFFRACTION PHASE (U)

Description of Structure	Description of Damage		
	Severe	Moderate	Light
Multistory reinforced concrete building with reinforced concrete walls, blast resistant designed, no windows, three story.	Walls shattered, severe frame distortion, incipient collapse of first floor columns.	Walls cracked, building slightly distorted, entranceways damaged, doors blown in or jammed. Some spalling of concrete.	
Multistory reinforced concrete building, with concrete walls, small window area, five story.	Walls shattered, severe frame distortion, incipient collapse of first floor columns.	Exterior walls badly cracked. Interior partitions badly cracked or blown down. Structural frame permanently distorted; spalling of concrete.	Windows and doors blown in. Interior partitions cracked.
Multistory wall-bearing building, brick apartment house type, up to three stories.	Bearing walls collapse, resulting in total collapse of structure.	Exterior walls badly cracked, interior partitions badly cracked or blown down.	Windows and doors blown in. Interior partitions cracked.
Multistory wall-bearing building, monumental type, four story.	Bearing walls collapse, resulting in collapse of structure supported by these walls. Some bearing walls may be shielded enough by intervening walls, so part of structure may receive only moderate damage.	Exterior walls facing blast badly cracked, interior partitions badly cracked, although toward far end of building damage may be reduced.	Windows and doors blown in. Interior partitions cracked.
Wood frame building, house type, one or two stories.	Frame shattered so that structure is for the most part collapsed.	Wall framing cracked. Roof badly damaged. Interior partitions blown down.	Windows and doors blown in. Interior partitions cracked.
Oil tanks, 30 feet in height, 50 feet in diameter. (Tanks considered full; more vulnerable if empty.)	Large distortion of sides, seams split, so that most of contents are lost.	Roof collapsed, sides above liquid buckled, some distortion below liquid level.	Roof badly damaged.

panels fail, determine which type of loading is predominant in causing damage.

3–12.1.2. (U) Response (Refs. 17, 18 and 19)

Structural characteristics determining response and damage are ultimate strength, period of vibration, ductility, dimensions, and mass. Ductility increases the ability of a structure to absorb energy, and increases its resistance to failure. Brittle structures, such as those of masonry construction, have little ductility and fail after relatively small deflections. Ductile structures, such as steel frame buildings, have the ability to withstand large and even permanent deflections without failures (Ref. 4). For each representative structural type listed in Tables 3–1 and 3–2, structural characteristics are similar enough that structures of a given type are considered to respond to approximately the same degree, under identical loading conditions, despite a recognized variability of unknown amount for each type.

The direction of the imposed load may have considerable effect on response. Most structures are able to withstand much larger verti-

cal than horizontal loads. Consequently, they are more resistant to a load imposed on the top of a structure than to an equal load imposed against a side. Thus, in the early regular-reflection region, damage from the same peak loading is likely to be less than damage to a similar structure in the Mach reflection region (Ch. 4, Sec. I).

TABLE 3–2 (C). DAMAGE TO TYPES OF STRUCTURES PRIMARILY AFFECTED BY DYNAMIC PRESSURES DURING THE DRAG PHASE (U)

Description of Structure	Description of Damage		
	Severe	Moderate	Light
Light steel frame industrial building, single story, with up to 5-ton crane capacity. Light-weight, low-strength walls fail quickly.	Severe distortion of frame (one-half column height deflection).	Some distortion of frame; cranes, if any, not operable until repairs made.	Windows and doors blown in. Light siding ripped off.
Heavy steel frame industrial building, single story, with 50-ton crane capacity. Light-weight, low-strength walls fail quickly.	Severe distortion of frame (one-half column height deflection).	Some distortion of frame; cranes, if any, not operable until repairs made.	Windows and doors blown in. Light siding ripped off.
Multistory steel frame office type building, five story. Light-weight, low-strength walls fail quickly.	Severe frame distortion. Incipient collapse of lower floor columns.	Frame distorted moderately. Interior partitions blown down.	Windows and doors blown in. Light siding ripped off. Interior partitions cracked.
Multistory reinforced concrete frame office type building, five story. Light-weight, low-strength walls fail quickly.	Severe frame distortion. Incipient collapse of lower floor columns.	Frame distorted moderately. Interior partitions blown down. Some spalling of concrete.	Windows and doors blown in. Light siding ripped off. Interior partitions cracked.
Highway and railroad truss bridges, spans of 150 feet to 250 feet.	Total failure of lateral bracing, collapse of bridge.	Some failure of lateral bracing such that bridge capacity is reduced about 50 per cent.	Capacity of bridge unchanged. Slight distortion of some bridge components.
Highway and railroad truss bridges, spans of 250 feet to 550 feet.	Total failure of lateral bracing, collapse of bridge.	Some failure of lateral bracing such that bridge capacity is reduced about 50 per cent.	Capacity of bridge unchanged. Slight distortion of some bridge components.
Floating bridges, U. S. Army standard M–2 and M–4, random orientation.	All anchorages torn loose, connections between treadways or balk and floats twisted and torn loose, many floats sunk.	Many bridle lines broken, bridge shifted on abutments, some connections between treadways or balk and floats torn loose.	Some bridle lines broken, bridge capacity unimpaired.
Earth covered light steel arch with 3-foot minimum cover (10-gauge corrugated steel with 20–25 foot span).	Total collapse of arch section.	Slight permanent deformation of arch.	Deformation of end walls, possible entrance door damage.
Earth covered light reinforced concrete structures with 3-foot minimum cover (2 to 3 inch panels with beams on 4-foot centers).	Total collapse.	Deformation, severe cracking and spalling of panels.	Cracking of panels, entrance door damage.

In the case of earth-covered surface structures, the earth mounding reduces the reflection factor and improves the aerodynamic shape of the structure. This results in a large reduction in both horizontal and vertical translational forces. It is estimated that the peak force applied to the structural elements is reduced by a factor of at least 2 by the addition of earth cover. The structure is somewhat stiffened against large deflections by the buttressing action of the soil, when the building is sufficiently flexible.

Air blast is also the determining factor in the damage to surface structures resulting from relatively shallow underground bursts. However, the distances from weapon burst to target, for a given degree of damage, are reduced from those for a surface burst.

3–12.1.3. (C) Classification of Damage

a. Basis of Classification

A major factor to consider in assessing structural damage is the effect of the damage on continued operations within the structure. If rugged equipment is mounted on a foundation at ground level, major distortion or even collapse of a structure may not preclude operation of the equipment. Conversely, if the equipment is tied in with the structural frame, distortion of the structure may prevent or seriously affect operability. No satisfactory general method has been developed for relating damage of structures to the damage to operational equipment contained in the structures. This relationship may be established for particular cases of interest on an individual basis. In general, severe structural damage approaching collapse entails a major reduction in operating capability.

b. Conventional Bomb Damage Classification

Due to the differences between conventional and nuclear bombs, their damage classifications are different. Since the effects of conventional bombs are usually local on a large structure, or around the point of burst, there are two damage classifications: "structural"; and "superficial." The damage descriptions of these two classes are similar to the last two classes for nuclear explosions, as indicated below. In the case where the structure is small, the structural classification for conventional bombs may extend into the first class listed below.

c. Nuclear Bomb Damage Classification

There are three damage classifications for nuclear explosions, described in following subparagraphs. A more detailed description of the application of these classifications to specific targets is given in Tables 3–1 and 3–2 (Ref. 16).

(1) Severe Damage

That degree of structural damage which precludes further use of a structure for the purpose for which it is intended, without essentially complete reconstruction. Requires extensive repair effort before being usable for any purpose.

(2) Moderate Damage

That degree of structural damage to principal load carrying members (trusses, columns, beams, and load carrying walls) that precludes effective use of a structure for the purpose for which it is intended, until major repairs are made.

(3) Light Damage

That degree of damage which results in broken windows, slight damage to roofing and siding, blowing down of light interior partitions, and slight cracking of curtain walls in buildings, and as described in Tables 3–1 and 3–2 for other structures.

3–12.2. (U) Ground Shock

Ground shock has to be so intense in order to cause serious damage to foundations of surface structures that the damage area for these structures is confined closely to the crater area of a surface or underground burst. Since the air blast at these ranges will be most devastating, the ground shock damage is neglected.

3–12.3. (U) Fire

The vulnerability of a structure to fire is dependent upon many factors. Some of these factors are: the combustibility of the building and its contents; the existance and adequacy of fire-stop partitions, etc; the weather conditions; etc.

Fires caused by high-explosive and nuclear bombs are for the most part, except possibly in the case of high-megaton yield nuclear weapons, due to secondary blast effects. The majority of such fires are caused by the breaking open or upsetting of tanks, drums, pipes, ovens or furnaces containing hot or highly inflammable materials, or by electrical short circuits.

In the case of the nuclear bomb, damage also may result from thermal radiation. Primary thermal radiation is seldom a factor in damage to structures. However, since exterior and interior surfaces of many structures are covered with protective coatings (paint), these coverings may be scorched at moderate levels of thermal radiation from the fireball. All structures, whether principally of steel and concrete construction, or of wood, contain some combustible material, and it is likely that some kind of kindling fuels will be present. Therefore, the possibility must always be considered that fire may be initiated in kindling fuels and spread to other components.

Certain classes of surface structures, such as badly weathered or rotted wooden buildings, buildings with thatched roofs, houses with lacquered paper windows, etc., may be ignited by direct thermal radiation, with resultant self-sustaining fires (Ref. 15).

3–13. (C) UNDERGROUND STRUCTURES

3–13.1. Air Blast

Air blast is the controlling factor for damage to lightweight soil-covered structures and shallow-buried underground structures. The soil cover provides surface structures with substantial protection against air blast and also with some protection against missiles.

Light-weight shallow-buried underground structures are those constructed deep enough for the top of the soil cover to be flush with the original grade. However, they are not sufficiently deep for the ratio of span to depth-of-burial to be large enough for any benefit to be derived from soil arching. For depths of cover up to about 10 feet in most soils, there is little attenuation of the air blast pressure applied to the top surface of a shallow-buried underground structure. Also, there is apparently no increase in pressure exerted on the structure due to ground shock reflection at the interface between the soil and the top of the structure.

Soil-covered structures are those that have a mound of soil over the portion of the structure that is above normal ground level. The soil mound reduces the blast reflection factor and improves the aerodynamic shape of the structure. This results in a considerable reduction in the applied translational forces. An additional benefit of the soil cover is the stiffening of the structure, or the additional inertia, that the soil provides by its buttressing action.

The lateral pressures exerted on vertical faces of a buried structure have been found to be about 15 per cent of the pressures on the roof in dry, silty soil. This lateral pressure is likely to be somewhat higher in general, and may approach 100 per cent in a porous, moisture saturated soil. The pressures exerted on the bottom of a buried structure in which the bottom slab is a structural unit integral with the walls may be as low as 75 per cent of the roof pressure, but may range up to 100 per cent of that pressure.

The damage that might be suffered by a shallow buried structure will depend on a number of variables, including the structural characteristics, the nature of the soil, the depth of burial, and the downward pressure (i.e., the peak overpressure) of the air blast wave (Ref. 15).

3–13.2. Ground Shock

An underground structure can be designed to be practically immune to air blast, but such structures can be damaged or destroyed by cratering or by ground shock due to a near-surface, true-surface, or an underground burst.

The mechanism of damage to underground structures from ground shock and cratering is dependent upon several more or less unrelated variables, such as the size, shape, flexibility, orientation of the structure with respect to the explosion, and the characteristics of the soil or rock.

The criteria for damage caused by cratering and ground shock may be described in terms of three regions, namely:

1. The crater itself.
2. The region extending roughly out to the

limit of the plastic zone (roughly 2½ times the crater radius).

3. The zone in which transient earth movement occurs without measurable permanent deformation.

The shock parameter mainly responsible for damage has not been defined either theoretically or empirically. However, there is considerable evidence that the degrees of damage can be related, without serious error, to the crater radius. Some examples of this type of relationship are given in Table 3–3 (Ref. 16).

For purposes of estimating earth shock damage from surface or subsurface bursts, underground structures are divided into various categories as follows:

1. Relatively small, highly resistant targets in soil. This type, which includes reinforced concrete fortifications, can probably be damaged only by acceleration and displacement of the structure in its entirety.
2. Moderate size, moderately resistant targets. These targets are damaged by soil pressure as well as acceleration and bodily displacement.
3. Long, relatively flexible targets. These include buried pipes and tanks, which are likely to be damaged in regions where large soil strains exist.
4. Orientation sensitive targets. Targets such as gun emplacements may be susceptible to damage from small permanent displacements or tilting.
5. Rock tunnels. Damage to such targets from an external explosion is caused by the tensile reflection of the shock wave from the rock-air interface, except when the crater breaks through into the tunnel. Larger tunnels are more easily damaged than smaller ones. However, no correlation between damage and tunnel size or shape is known.
6. Large underground installations. Such installations can usually be treated as a series of smaller structures.

TABLE 3–3 (C). DAMAGE CRITERIA FOR UNDERGROUND STRUCTURES (U)

Structure	Damage	Damage Distance	Remarks
Relatively small, heavy, well designed underground targets.	Severe	$1\frac{1}{4}R$	Collapse.
	Light	$2R$	Slight cracking, severance of brittle external connections.
Relatively long, flexible targets, such as buried pipelines, tanks, etc.	Severe	$1\frac{1}{4}R$	Deformation and rupture.
	Moderate	$2R$	Slight deformation and rupture.
	Light	$2\frac{1}{2}$ to $3R$	Failure of connections. (Use higher value for radial orientation of connections.)

Note. R—Apparent Crater Radius.

Section IV (S)—Aircraft

3–14. (U) INTRODUCTION

Aircraft vulnerability concerns the many factors which determine the ability of an aircraft to withstand combat damage. In particular, it indicates the means for improving the chances for survival of aircraft in battle and, by inference, indicates weapons which show the greatest promise of inflicting critical damage on an aircraft. Thus, aircraft vulnerability and weapon lethality are closely interrelated subjects of comparable importance; they are the defensive and offensive aspects of the same phenomena. It is the expressed desire of the procuring agencies for manned military aircraft to incorporate the principle of minimum vulnerability in new design concepts, within the limitations of the overall design requirements.

3–15. (C) BASIC CONSIDERATIONS

3–15.1. (C) Initial Studies of Aircraft Vulnerability

Prior to 1939, consideration of aircraft in terms of target vulnerability and weapon lethal-

ity received little coordinated study. The results of this neglect soon became evident when battle experience was gained, but it was then found that any major design changes needed to reduce the vulnerability of aircraft were not easily introduced into the production line, and were consequently late appearing in service aircraft. Considerable losses were undoubtedly suffered due to the late introduction of such changes.

Shortly after World War II, a firing program (Ref. 20) was initiated at the Ballistic Research Laboratories (BRL), Aberdeen Proving Ground, Maryland, in order to determine the vulnerability of aircraft and their components to various aircraft weapons. This effort, based in part on work by the New Mexico Institute of Mining and Technology, under contract to the Bureau of Ordnance, was supplemented by a progress report (Ref. 21) relating to the two complementary aspects of the so-called "Optimum Caliber Program." The objects of this program were: first, to determine the probability that a single round of existing ammunition striking an airplane would cause a certain level of damage; and, second, to assess the overall effectiveness of complete armament installations, with the object of indicating the answer to the whole problem of what armament should be carried by aircraft to meet various tactical situations. The report of this work represents the beginning of a considerable amount of literature available on the subject of aircraft vulnerability and, in particular, the subject of aircraft "terminal vulnerability."

3–15.2. (C) Vulnerability Definitions

(U) The word "vulnerability," as it appears in the literature, has two common usages. Vulnerability in the overall or "attrition sense" is the susceptibility of an item to damage, which includes the considerations of avoiding being hit. Vulnerability in the restricted or "terminal sense," is the susceptibility of an item to damage, assuming that it has been hit by one or several damaging agents. Therefore, the probability of obtaining a kill on an aircraft target is found equal to the probability of obtaining a hit times the probability that the hit results in a kill (Ref. 22). This chapter considers only the latter factor, or the terminal ballistic vulnerability of aircraft.

(C) The chance of survival of an aircraft in battle is influenced by many factors, including its flight performance and maneuverability, its defensive armament and offensive equipment, and the skill and morale of its crew. The term aircraft vulnerability, however, is restricted in meaning. It is commonly used to refer to the extent to which an aircraft is likely to suffer certain specified categories of damage, when the weapon used to attack it either strikes the aircraft or bursts in some desired zone around it.

3–15.3. (C) Vulnerability Factors

The major factors which influence the chance of survival of an aircraft are in most instances the inherent safety (or invulnerability) of the airframe and components, which together make up the basic aircraft, and the efficiency of any protective devices with which it may be fitted. Evidence on these factors can usually be obtained by experiment. When this evidence is related to an attack of a specified nature and from a specified direction, it forms the usual basis of aircraft vulnerability assessments. The vulnerability of components such as the power plants can be assessed separately in a similar manner, and can be included in an overall assessment. Care must be exercised in making the overall assessment, however, because the individual damage effect may be quite different from the overall effects. For example, in the case of a single-seated aircraft, 100 per cent probability of lethal injury to the pilot will give a similar probability for the loss of the system; whereas, damage which is 100 per cent lethal to one engine of a four-engine aircraft may not be lethal to the entire aircraft. These individual components are usually referred to as singly and multiply vulnerable, which terms are discussed in Ch. 8, Par. 8–22.

It is useful at this point to define two terms which are used in the collection and analysis of aircraft target vulnerability (Ch. 8, Par. 8–22). Presented Area: the area of the projection of the configuration of a given component

upon a plane perpendicular to the line of flight of the attacking projectile or warhead. Vulnerable Area: the product of the presented area and the conditional probability of a kill for a random hit on the presented area. (It is assumed that all projectiles approach the presented area on parallel paths.)

3–15.4. (C) Use of the Empirical Approach

A synthesis of the vulnerability characteristics of aircraft targets is based mainly on empirical relationships for the vulnerability of the major aircraft components. A large part of these data are obtained from firings against aircraft conducted at the various proving grounds. These include firings of selected weights of bare and cased charges about, in contact with, and within aircraft structures, filled fuel tanks, and both reciprocating and jet engines; also the firing against all major aircraft components by various projectiles. Damage caused in field firings against aircraft is assessed by qualified military or civilian personnel (sometimes in conjunction with the manufacturer), who prepare a detail description of the damage in addition to numerical estimates for the various damage categories.

This empirical approach is subject to strong economic and humane restrictions and limitations; as a result, the test aircraft is usually on the ground with no personnel aboard. (The effects of altitude and aerodynamic and inertial forces on the airframe are usually estimated.) Firing trials may be made against stressed structural members, against engines running under cruising conditions, or against canopies which are subject to realistic conditions of temperature and pressure. In-flight vulnerability investigations are naturally difficult to stage, but are sometimes essential. An example is the investigation of the probability of causing fires in the fuel systems, at altitudes which demand conditions of air temperature, air density, and high-speed air flow not easily reproduced simultaneously on the ground. An additional limitation on this empirical approach is that the sample sizes obtained are usually small, restrictions on the sample size being especially stringent for the more recent aircraft.

The test aircraft may then be considered as collections of components, rather than as entities in themselves. Since the "aircraft of the future" that are under study are composed of structures, fuel cells, or engines physically similar to corresponding components in the test aircraft, the information obtained can be applied directly in some cases, with due correction for changes in areas and physical arrangements.

3–15.5. (C) Damage Categories

In order to classify damage effects, several kill or damage categories are in common use, as follows:

- **KK** — The aircraft disintegrates immediately after being hit (in addition, denotes complete defeat of its attack).
- **K** — The aircraft falls out of control immediately, without any reasonable doubt (usually specified as 1/2 minute, or less).
- **A** — The aircraft falls out of control within 5 minutes.
- **B** — The aircraft will fail to return to its base. This is commonly taken as being 1 hour away for a jet, or 2 hours away for a piston-type engine aircraft.
- **C** — The aircraft does not complete its mission after being hit.
- **E** — The aircraft could complete its mission after being hit, but is damaged to the extent of not being able to go on the next scheduled mission (usually denotes a bad crash on landing).

It is important to note that in order to assess B or C damage, it is necessary to define the mission on which the aircraft is engaged. Frequently in the literature, the K and KK categories are grouped as sub-categories under the A-damage assessment. In addition, reference is sometimes made to an R-damage category, which is "detectable by radar facilities." For the most part, damage is usually assessed in the K, A, and C categories.

3–15.6. (C) Damage Assessment

In tests on aircraft vulnerability, a basic method of determining the degree of damage is by assessment. After a test aircraft is damaged, assessors are asked to estimate the probability that the damage produced would incapacitate the aircraft to a specified degree (damage category) assuming a certain mission, crew reaction, etc. Thus, an assessment of 0, 0, 0, 0 may be given for A, B, C, and E categories, respectively, meaning that the damage would not cause a crash within 2 hours, would not interfere with the mission, and would not cause a crash on landing. An assessment of 0, 100, 0, 0 means that the assessors believe that the damage would cause a crash within 2 hours, although not within 5 minutes. For example, such an assessment may be made for damage causing oil loss to the engine of a single piston-engine aircraft. To enable the assessors to express their uncertainty as to the outcome of damage, intermediate numbers between 0 and 100 are used. Thus, a 20A assessment means that the assessor is inclined to believe that the damage would not result in a crash within 5 minutes, although he is not sure of this. Wherever possible, independent assessments of the same damage are obtained from two or more assessors. Detailed descriptions of the conduct of the field trials and of the assessment procedure are provided in the many BRL reports dealing with analyses of firing data. (A and B assessments, made for damage to the engine of a multi-engined aircraft, refer to the ability of that engine to deliver power, rather than to a crash.)

A comment of interest on the assessment procedures has been made by Arthur Stein, formerly of BRL (Ref. 20).

"It will be noted that the numbers used to describe the various categories of damage are described as probabilities often written as percentages. Strictly speaking, however, this is not correct, since the particular damage suffered by the aircraft will generally either cause a crash or it will not in the stated interval of time, assuming a set of standard conditions under which the aircraft is operating. The numerical assessment, therefore, chiefly represents the uncertainty of the assessor as to whether the damage would result in a kill or not. If the individual assessment is 20A, for example, the assessment is in error by 20 per cent or 80 per cent, since the damage would actually have produced a kill or no kill within 5 minutes. If assessments are not biased, however, the expected value of many such assessments on various parts of the plane would be the correct value and in the 'long run' one would arrive at a correct value for the vulnerability of the plane. The parameters of the error distribution can be estimated if one has a large number of cases in which the same damage has been assessed independently by different assessors. Such information would also yield information as to the assessibility of various aircraft components."

It must be strongly emphasized that assessment represents the basic measure of aircraft terminal vulnerability.

3–15.7. (C) Categories of Associated Data

3–15.7.1. (C) *Modes of Damage*

There are numerous modes of damage which can effect aircraft kills. Some of these are given in the following list:

1. The detonation of the aircraft bomb load.
2. The killing of a sufficient number of essential crew members.
3. The ignition of a lethal fire.
4. The killing of a sufficient number of engines.
5. Lethal damage to the airframe.
6. Lethal damage to the armament system.

3–15.7.2. (C) *Typical C-Damage Factors*

The word lethal, as used in the above paragraph, implies that only a specified category of kill results, and does not imply any fixed degree of damage severity. It should also be noted that the determination of what constitutes a kill, in a given situation, can often require the use of simplifying assumptions for a feasible analysis procedure. For example, listed below are some of the factors to be considered in a typical C damage situation:

1. Aircraft position along the flight profile at the time damage occurs.

2. The assigned mission of the particular aircraft.
3. The crew (number, skill, individual specialties, and determination to complete the mission).
4. Item(s) damaged.
5. Alternate equipment available.
6. Type and intensity of enemy action.

3–15.7.3. (U) *Significant Aircraft Components*

In determining aircraft vulnerability, the aircraft may be defined by the sum of the following components, which in turn include subcomponents:

1. Airframe.
   a. Structure (Fig. 3–2).
   b. Controls (flight).
2. Fuel system.
3. Power plant.
4. Personnel (only crew necessary for mission).
5. Armament system.
   a. Guns.
   b. Bombs.
   c. Fire control.
   d. Bomb sight.
   e. Radar.
6. Miscellaneous (tires, flaps, etc.).

3–15.7.4. (C) *Damaging Agents*

The many different types of damaging agents in use against aircraft can be placed under three basic categories of armament:

1. External blast weapons.
   a. Conventional rounds.
   b. Nuclear rounds (including thermal and nuclear radiation).
2. Direct contact weapons.
   a. Bullets: armor-piercing (AP) and armor-piercing incendiaries (API).
   b. Shells: high explosives (HE) and high-explosive incendiaries (HEI).
   c. Fragments: shaped charges, rods, etc.
3. Fragmentation/blast weapons (controlled fragmentation burst combined with a high explosive charge).

3–15.7.5. (C) *Relative Vulnerability of Components*

Although no such listing can be correct in all cases, Table 3–4 affords a general idea of the terminal vulnerability of the various components to the several (non-nuclear) damaging agents (Refs. 23 and 24).

3–16. (S) AIRCRAFT BY TYPE AND LOCATION

3–16.1. (U) General

The vulnerability of an aircraft target as an entity (in contrast to the test aircraft which were considered as collections of components) depends upon the location and type of aircraft target. Normally the aircraft is in flight, but when parked it may become a ground target. Aircraft may be further defined by two general types, combat and non-combat, with various

TABLE 3–4 (C). RELATIVE VULNERABILITY OF AIRCRAFT COMPONENTS (U)

	Personnel	Fuel System	Power Plant		Airframe	Armament & Misc.
			Turbojet	Piston		
Incendiary bullets	High	Uncertain	Moderate	Low	Negligible	High
HE & HEI shells	High	Uncertain	High	High	Varies	High
Fragments & non-incendiary bullets	High	Uncertain	Moderate	Low	Negligible	Moderate
Rods	High	Uncertain	High	High	High	High
External blast	Negligible	Negligible	Negligible	Negligible	Moderate to high	Moderate

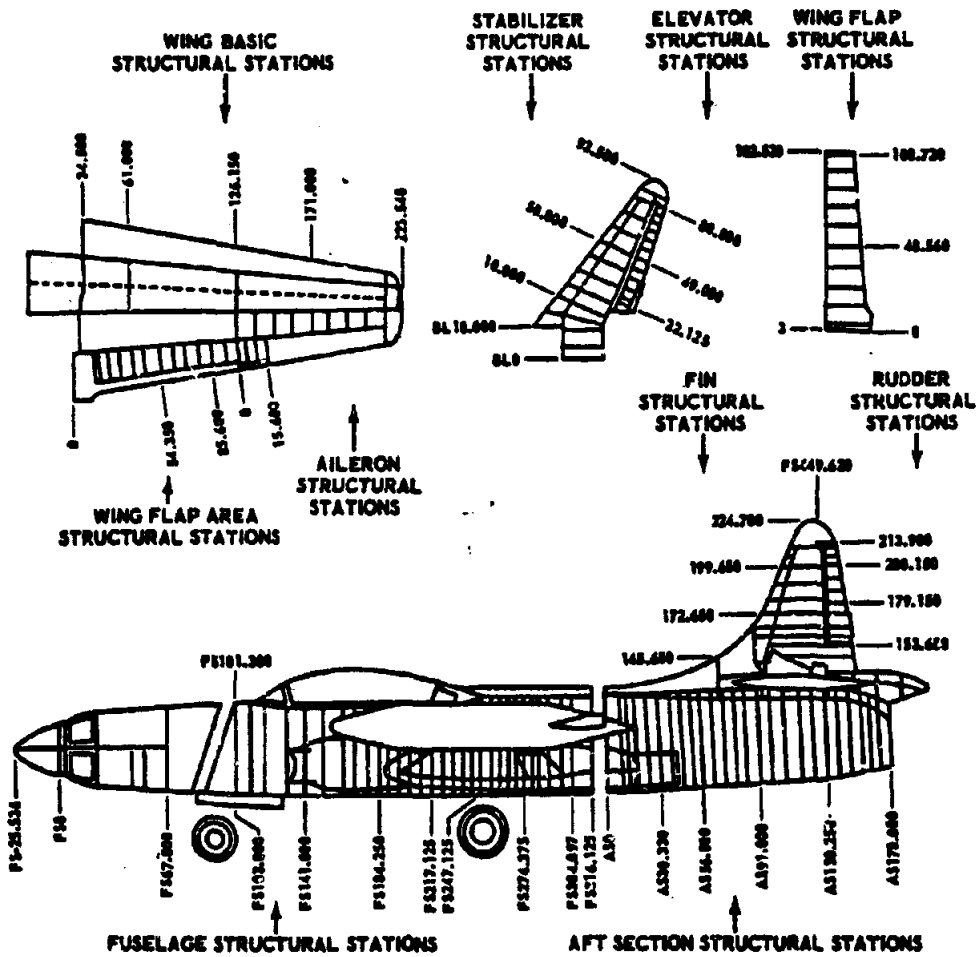

Figure 3–2 (C). Stations Diagram, F94C Aircraft (U)

classes of aircraft falling into these two categories according to their mission or function. A corollary grouping is in terms of the fixed-wing, the rotary-wing (helicopter), the new STOL (short takeoff and landing), and new VTOL (vertical take off and landing) types of aircraft.

3–16.2. (S) *Aircraft in Flight*

3–16.2.1. (S) *Combat Aircraft*

(U) Combat aircraft are generally classed as bomber, fighter, or attack aircraft, depending primarily on the mission of the aircraft, and to a lesser degree on the design configuration. World War II aircraft were characterized within these classes by size, weight, and speed; but the character of later day aircraft are such that these characteristics are not as obvious. An excellent source of physical data on the characteristics of aircraft is *Jane's All the World's Aircraft* (Ref. 25).

(S) The greatest combat risk to a bomber force during the past few years has been from fighters armed either with 20- to 40-mm cannon

or with small (2- to 3-inch) unguided rockets; the attacks being almost wholly from the rear or off by small angles. The projectiles have usually been impact-fused explosive or explosive/incendiary types.

(S) An aircraft is likely to suffer severe structural damage if hit by a small rocket; and with either cannon or rocket there will be a high probability of damage to fuel systems and power plant, with a corresponding chance of delayed kill.

(S) With the 2- to 3-inch rocket, the structural and mechanical damage (internal blast) from a hit is likely to be so great that the possible additional effects due to fire need scarcely be considered. Incendiary effects from the small, gun-fired shell could be very severe, and would depend largely on the type of fuel system used.

(S) Both surface-to-air and air-to-air guided missiles are now available in addition to the conventional fighter weapons just mentioned. If the guided missile warheads are of the large, blast type, structural damage can result. For the fragmenting type warheads, there will be a large increase in the vulnerability of the pilots of the bomber, a high probability of leakage from fuel tanks, damage of radar equipment, and possibly a high fire risk, due to the high-velocity fragmentation given by the warhead.

(S) The main combat hazards to the fighter have been the attack from ahead by bomber return fire, and the attack from the rear by enemy fighters. Missiles in either case have been explosive shells from aircraft cannon, or small rockets. Hits against high performance jet fighters are likely to cause severe structural damage, engine failure, or pilot injury. Even superficial damage at the time of hit can result in a lethal situation, subsequently, due to a high-g maneuver such as LABS (Low Altitude Bombing System). Owing to the rapid changes in altitude by the fighter during combat, there may be difficulty in maintaining an inert atmosphere (purging) above the fuel in the tanks, and unless new methods are employed there will be a risk of fuel tank explosion and fire. The introduction of guided missile warheads with blast and fragmentation effects now produce the possibility of structural damage to the fighter by external blast, in addition to increasing pilot vulnerability and the risk of fire due to high velocity fragments.

(S) The main risk to attack aircraft has been from ground or ship weapons (mainly conventional guns and rockets) firing impact fuzed explosive projectiles of up to about 3 inches, and from small arms fire with either armor-piercing or incendiary bullets. The damage effects will be generally similar to those described for the fighter aircraft, but the emphasis will be mainly on attacks from the front hemisphere. Wartime evidence has indicated the importance, to aircraft engaged on ground-attack missions, of self-sealing protection for fuel tanks and armor protection for pilots and items such as oil coolers. The value of such equipment is, however, a subject of great debate. Small surface-to-air missile weapons presently in development will create an additional threat to attack aircraft at low altitudes.

(C) It is possible during the time of war to obtain a fair indication of the vulnerability characteristics of military aircraft, and the frequency and effects of different types of combat damage, by making detailed investigations of air casualties in action. From this evidence, it is possible to determine the main causes of enemy and friendly losses in air warfare, and the relative vulnerability of the various parts of each aircraft.

(S) Evidence of the causes of aircraft losses in World War II was gathered by the British Operational Research Sections attached to the Royal Air Force and the United States Army Air Force (Ref. 23). For example, it was found that the Bomber Command's losses in night operations during the latter part of the war were caused approximately as follows:

1. 75 per cent by fighter attack.
2. 20 per cent by antiaircraft gunfire.
3. 5 per cent by accidents, including navigational errors, collisions, fuel shortage, engine failure, etc.

Of these bomber losses due to enemy action, by far the greatest number either resulted from fire or suffered fire as a secondary effect.

(S) From the best evidence available, it is estimated that the significantly vulnerable parts of the bomber are:

1. Engines (piston type)—by mechanical damage and fire.
2. Fuel systems—by fire, internal explosion, or loss of fuel.
3. Flight control systems and surfaces—by mechanical damage from multiple hits causing break-up and loss of control.
4. Hydraulic and electrical services—mainly by fire.
5. Bombs and pyrotechnic stores—by explosion or fire.
6. Pilots—by incapacitation (an infrequent cause of loss).

(S) For the single-engined fighter types, the order of vulnerability due specifically to light anti-aircraft fire from the ground was estimated to be:

1. Engine—by mechanical damage and fire.
2. Pilot—by injury or death.
3. Fuel system—by loss of fuel or fire.

Although fire is not stated as the major risk because the damage would generally cause loss whether combined with fire or not, a substantial proportion of the losses was undoubtedly accompanied by fire. In air-to-air engagements, the single-engined fighter was believed to be most frequently destroyed by the cumulative effects of multiple hits on the structure and main flight control surfaces.

(S) Information from air operations in the Korean war has been small as regards evidence on causes of losses in combat. This appears to be due to the small percentage of actual losses caused by enemy action, and to the overwhelming emphasis on ground-attack sorties by the air forces of the United Nations. However, there is some evidence, obtained by the United States Air Force, from which the following facts appear to emerge. Based on combat hours of duty, and for the same type of ground-attack mission, the single-engined jet aircraft receives only about 50 per cent as many hits from anti-aircraft projectiles (bullets or small shells) as the single-engined piston aircraft. This difference in the number of hits appears to be related to the different tactics employed during the dive and pullout. For example, the jet aircraft attacks at a much higher speed and thus spends far less time than the piston aircraft at altitudes subjected to accurate gunfire. When hit, the piston aircraft is 50 per cent more likely to be lost than the jet aircraft. A large proportion of the vulnerability of the piston aircraft can be attributed to the vulnerability of its engine oil coolers. These observations relate only to the particular conditions and particular types of attacking projectiles (now possibly outdated) which were encountered by the United Nations' forces in Korea.

(S) The actual vulnerability of any potentially vulnerable part of an aircraft depends to a great extent on its area of presentation. For example, a medium-range, four-engined bomber with gross weight of about 120,000 pounds may have an average presented area of 1,500 square feet. The average areas of some of the potentially vulnerable components might be approximately as follows:

1. Structure (*including fuel tanks*)—1,200 square feet (80%).
2. Fuel with tanks at ⅔ capacity—340 square feet (23%).
3. Pressure Cabin—130 square feet (9%).
4. Power plants—90 square feet (6%).
5. Pilot—7 square feet (½%).

It will be seen that the structure is by far the largest of the potentially vulnerable items, while the fuel tanks, pressure cabin, and power plants also present relatively large areas. For the long range bomber of the near future, the fuel may have a considerably larger presented area than the value just quoted.

(C) Aircraft in flight are relatively vulnerable to the blast and thermal effects of nuclear detonations. Since aircraft are designed within narrow limits for flight and landing loads, the structure can withstand only small additional loads imposed by weapon effects. Blast overpressure, on striking an aircraft surface, may cause dishing of panels and buckling of stiffeners and stringers. On the side struck by the blast wave the pressure is increased, above the incident intensity, by reflection, and a diffractive force of short duration is generated. As the wings, empennage, and fuselage are completely enveloped by the blast, further dishing and buckling of skins and structure

may result from the crushing effect of the differential pressure between the outside and inside of the aircraft components. Additional damaging loads are also developed by the particle velocity accompanying the blast wave. The particle velocity results in drag loading in the direction of the wave propagation (usually termed "gust loading" with reference to aircraft). The duration of the gust loading is many times that of the diffractive loading, and it develops bending, shear, and torsion stresses in the airfoil and fuselage structures. These are usually the major stresses on an aircraft in flight.

(C) The weapon thermal energy which is absorbed by aircraft components can also produce damaging effects. Very thin skins are rapidly heated to damaging temperatures by exposure to the short-period thermal flux, because the energy is absorbed by the skin so much more rapidly than it can be dissipated by conduction and convective cooling. Exposed fabric, rubber, and similar materials with low ignition and charring temperatures, are vulnerable items which may also initiate extensive fire damage at even very low levels of radiant exposure. In recent years, designers of military aircraft have reduced aircraft vulnerability to thermal effects by coating thin-skinned materials with low absorptivity paints, by eliminating ignitable materials from exposed surfaces, and by substitution of thicker skins for very thin skins. With these protective measures and design modifications, aircraft can be safely exposed at radiant exposure levels several times those which formerly caused serious damage.

3–16.2.2 (U) *Non-combat Aircraft*

Non-combat aircraft include the following types: cargo, transport, utility, and observation and reconnaissance. The latter two types are often converted combat aircraft. These aircraft are characterized by their function, size, and speed, and by the type of their construction, which is a conventional, World-War-II type of design. This is a semi-monocoque fuselage and full cantilever wings with a stressed aluminum skin. The collection of terminal ballistic vulnerability data for this type of aircraft has received little specialized attention in the past. However, because most of the testing on combat aircraft has been with targets reflecting this type of construction, there is in fact considerable information available for those who may be interested.

3–16.2.3. (C) *Rotary Wing and Other Aircraft*

(U) It is necessary to distinguish rotary-wing (helicopter) aircraft from conventional fixed-wing aircraft, and also the new STOL and VTOL vehicles. The vulnerability of rotary-wing aircraft is similar in many respects to the fixed-wing aircraft, but the following items may not be similar and require individual attention:

1. Relative location of fuel, and personnel.
2. Complex control system.
3. Rotor drive system and gear boxes.
4. Main and tail rotor blades.
5. Unconventional airframe (slender tail cone, etc.).

(C) Firing tests have been conducted at the Wright Air Development Center (WADC) against rotor blades, using caliber .30 and caliber .50 projectiles. The blades were fired on so as to obtain damage to the structural or spar portion of the blade and then whirl-tested to determine the effects of damage. The damage caused by these projectiles was found not to be serious. This agrees with Korean combat results, which show that small caliber holes in portions of the blades are not serious. However, a perforation by a larger projectile, such as a 37-mm AP or HE projectile, could cause the loss of a blade, which would be most serious.

(C) The problem of the vulnerability of low flying aircraft in the forward area has recently been given higher priority by the Army, due to new tactics and organizations developed by the Army, new reconnaissance drones and aircraft being developed by the Signal Corps, and new STOL and VTOL vehicles being studied for air transport by the Transportation Corps. Because of the missile threat at medium and high altitudes, most Army air tactics envision low flying aircraft. In the region below 500 feet, light arms (40-mm AA, and smaller caliber) will be a threat to these aircraft in forward areas. In the near future, small surface to-air weapons

now in development may be included. Vulnerability testing for these special-purpose aircraft has been initiated.

3–16.3. (C) Parked Aircraft

(U) Considerable interest has been shown in the vulnerability of parked aircraft in the vicinity of a nuclear air blast. Nuclear weapon tests have included parked aircraft placed at various locations and orientations with respect to the burst point.

(C) The diffraction phase loading and the drag phase loading have varying relative importance in producing damage to parked aircraft. In general, the diffraction phase is of primary importance in the zones of light and moderate damage. In the zone of severe damage, the drag phase assumes more importance. Orientation of the aircraft with respect to the point of burst affects vulnerability considerably. With the nose of the aircraft directed toward the burst, higher weapon-effects inputs can be absorbed without damage than for any other orientation. The longer duration of the positive phase of the blast from a large yield weapon may result in some increase in damage over that expected from small yields at the same overpressure level. This increase is likely to be significant at input levels producing severe damage, but is not likely to be important at the levels of moderate and light damage. Experiments have shown that revetments provide only slight shielding against blast overpressure, and under some conditions reflected pressures within the revetment are higher than corresponding incident pressures. Revetments do provide significant shielding from damage due to flying debris born by the blast wave.

(C) Aircraft properly prepared with reflective paint, and with all vulnerable materials shielded from direct thermal radiation, will not be damaged by thermal inputs at distances where damage from blast inputs is not severe. Aircraft not so prepared may sustain serious damage at very low thermal levels, as a result of ignition of items such as fabric-covered control surfaces, rubber and fabric seals, cushions, and headrest covers. Aircraft painted with dark paint are especially vulnerable to thermal radiation damage, because the dark painted surfaces absorb three-to-four times the thermal energy that is absorbed by polished aluminum surfaces or surfaces protected with reflective paint. Temporary emergency shielding such as that provided by trees, buildings, embankments, or similar barriers may be useful for thermal protection of unprepared aircraft, but any of these may increase the blast damage by adding to the flying debris or by multiple reflection of incident overpressures.

Section V (U)—List of References and Bibliography

3–17. REFERENCES

1. T. Sterne and A. J. Dziemian, *Provisional Probabilities of Incapacitation by a Caliber .30 Rifle Bullet*, BRL Memorandum Report No. 949, BRL, Aberdeen Proving Ground, Maryland, December 1955, (Secret).
2. J. Sperrazza and F. Allen, *New Casualty Criteria for Wounding by Fragments*, BRL Report No. 996, BRL, Aberdeen Proving Ground, Maryland, October 1956, (Secret).
3. C. S. White, *Biological Blast Effects*, Lovelace Foundation for Medical Education and Research, Albuquerque, New Mexico, September 1959, United States Atomic Energy Commission, Technical Information Service, TID–5564, (Unclassified).
4. S. Glasstone, *The Effects of Nuclear Weapons*, United States Atomic Energy Commission, June 1957, (Unclassified).
5. V. Blocker and T. G. Blocker, "The Texas City Disaster—A Survey of 3000 Casualties," Air Force Surgeon, Vol. LXXVIII: pp. 756–771, 1949, (Unclassified).
6. —— *ABC Warfare Defense*, Bureau of Naval Personnel, Navy Training Course, NAVPERS 10099, 1960, (Unclassified).
7. —— *Research in CBR*, Committee on Science and Astronautics, U. S. House of

Representatives, 86th Congress, House Report No. 815, August 10, 1959, (Unclassified).

8. —— *Ordnance Proof Manual*, Volume I, *Vulnerability*, OPM 60–120, May 1959, (Unclassified).

9. —— *Tank Platoon and Tank Company*, Department of the Army Field Manual, FM17–32, March 1950, (Unclassified).

10. —— *Tank Battalion*, Department of the Army Field Manual, FM17–33, September 1949, (Unclassified).

11. E. J. Bryant, R. C. Wise and S. Wise, *Vulnerability of Tanks to Conventional and Nuclear Weapons*, BRL Technical Note No. 1087, BRL, Aberdeen Proving Ground, Maryland, October 1956, (Secret).

12. F. I. Hill, *Information for Tank Damage Assessors*, BRL Technical Note No. 236, BRL, Aberdeen Proving Ground, Maryland, June 1950, (Unclassified).

13. —— *The Vulnerability of Armored Vehicles to Ballistic Attack*, Armor Branch, Arms and Ammunition Division, D and PS, Aberdeen Proving Ground, Maryland, 21 March, 1950, (Confidential).

14. E. J. Bryant, et al, "Response of Drag-Type Equipment Targets in the Precursor Zone" (U), Operation Teapot, August 1956, (Secret–RD).

15. —— *Capabilities of Atomic Weapons*, Department of the Army Technical Manual, TM 23–200, 1957, (Confidential).

16. —— *Weapons Selection for Air Targets*, Physical Vulnerability Division, Department of the Air Force, PVTM 11, (Confidential).

17. N. B. Brooks and N. M. Newmark, *The Response of Simple Structures to Dynamic Loads*, University of Illinois Structural Research Series No. 51, 1953, (Unclassified).

18. C. W. Lampson and J. J. Meszaros, *Blast Instrumentation*, Ballistic Research Laboratories, Aberdeen Proving Ground, August 1957, (Unclassified).

19. J. J. Meszaros, *Target Response Instrumentation*, BRL, Aberdeen Proving Ground, Maryland, August 1957, (Unclassified).

20. A. Stein, *Optimum Caliber Program*, BRL Memorandum Report No. 437, BRL, Aberdeen Proving Ground, Maryland, July 1946, (Confidential).

21. H. K. Weiss and A. Stein, *Airplane Vulnerability and Overall Armament Effectiveness, BRL Memorandum Report No.* 462, BRL, Aberdeen Proving Ground, Maryland, May 1947, (Confidential).

22. A. Stein and H. Kostiak, *Methods for Obtaining the Terminal Ballistic Vulnerability of Aircraft to Impacting Projectiles, with Applications to Generic Jet Fighter, Generic Jet Bomber, F–47 Piston Fighter, and B–50 Piston Bomber*, BRL Report No. 768, BRL, Aberdeen Proving Ground, Maryland, June 1951, (Secret).

23. A. I. Kent and W. E. Parriott, *The Terminal Vulnerability of Aircraft to Nonnuclear Rounds: A Qualitative Review of Current Knowledge*, Rand Corporation, RM–1405, January 1955, (Secret).

24. H. K. Weiss, *The Vulnerability of Aircraft to Weapons*, BRL Technical Note No. 726, BRL, Aberdeen Proving Ground, Maryland, September 1952, (Confidential).

25. —— *Jane's All the World's Aircraft 1959-1960*, McGraw-Hill, (Unclassified).

26. —— *Vulnerability of Manned Aircraft to Guided Missiles*, British Joint Services Textbook of Guided Weapons, Part 19, August 1956, (Secret—Discreet).

3–18. BIBLIOGRAPHY

1. G. M. Gaydos and S. Stein, *Non-Nuclear Warhead Design Guide for FABMDS*, Tech Memo No. DW 329, Warhead and Special Projects Laboratory, Picatinny Arsenal, Dover, New Jersey. March 1961, (Secret).

Chapter 4 (S)

COLLECTION AND ANALYSIS OF DATA CONCERNING KILL MECHANISMS

Section I (S) —Blast

4–1. (U) INTRODUCTION

4–1.1. Scope of the Section

This section covers the collection and analysis of data involving blast waves as a kill mechanism. Separate paragraphs discuss both quantitatively and qualitatively the various parameters associated with air, surface, and subsurface blasts from conventional high explosives (chemical explosives) and nuclear explosions. In additional paragraphs are discussed the effects of mechanical factors on blast, and methods of blast instrumentation. In general, the bulk of the material will apply to blast waves produced by either conventional or nuclear explosions. In certain areas, however, the discussion will emphasize the particular features of the blast wave produced by nuclear explosions.

4–1.2. Comparison of Conventional and Nuclear Explosions

The primary differences between the conventional (HE) explosion and a nuclear explosion (setting aside from the present subject the radiation effects) is that the energy from nuclear explosions is developed in a much smaller space, and the temperatures developed are approximately 10,000 times higher. As a result, there is an almost instantaneous release of energy in the nuclear explosion. Consequently, the nuclear explosion may be considered more nearly a point source of energy, permitting simplified analytical solutions to the equations of motion.

Other differences between conventional and nuclear explosions concern blast pressures and energy yield. The pressure at small distances from ground zero is higher for nuclear than for conventional explosions; but at large distances the reverse is true. The much greater energy yield of a nuclear explosion makes a qualitative difference in the effects. For instance, the duration of the blast produced by an atomic bomb is longer than the characteristic vibration periods of most structures which can be destroyed. Therefore, the criterion for estimating the damage to structures by nuclear bombs is usually the peak overpressure or the peak drag pressure, rather than the impulse, which is the commonly used criterion for HE bombs.

4–1.3. Cross-Reference Information

The general discussion of the mechanisms of blast and ground shock in Ch. 2, Secs. IV and V, respectively, should be read for introductory purposes. In Ch. 3, each of the various sections includes information on the vulnerability of specific types of targets to blast phenomena. Reference should be made to each of the chapters of Part Two for information on the collection and analysis of blast data as applied to specific types of targets.

4–2. (S) AIR BURST

4–2.1. (U) Introduction

Most of the damage resulting from a high explosive or nuclear explosion air burst is due, either directly or indirectly, to the blast wave (shock wave) which accompanies the explosion. Most structures will suffer some degree of damage when subjected to pressures in excess of the standard atmospheric pressure (overpressure). The distance from the point of detonation to which damaging overpressures

will extend is dependent on the energy yield of the weapon and the height of burst. In considering the destructive effect of a blast wave, it is important to study, in some detail, the various phenomena associated with the passage of the wave through the atmosphere.

4–2.2. (U) Description of the Blast Wave

4–2.2.1. Overpressure

The expansion of the intensely hot gases at high pressure causes a blast wave to form and move outward at high velocity. The pressures in this wave are highest at the moving front and fall off toward the interior region of the explosion. In the very early stages of the blast wave movement, the pressure variation with distance from the point of detonation is somewhat as illustrated in Fig. 4–1.

As the blast wave travels in the air away from its source, the overpressure at the front steadily decreases, and the pressure behind the front falls off in a regular manner. After a short time, the pressure behind the front drops below the surrounding atmospheric pressure and the negative phase of the blast wave is formed. The variation of overpressure is shown in Fig. 4–2 for six successive instants of time, indicated by the numbers t_1, t_2, t_3, etc.

During the negative overpressure (rarefaction, or suction) phase, a partial vacuum is produced and the air is sucked in instead of being pushed away. This means that during the positive (compression) phase, the winds flow away from the explosion; but in the negative phase, the direction is reversed and the winds flow toward the explosion. However, the peak values of the negative overpressure are usually small compared to the overpressures generated during the positive phase. At the end of the negative phase, the pressure has essentially returned to ambient conditions (Ref. 1).

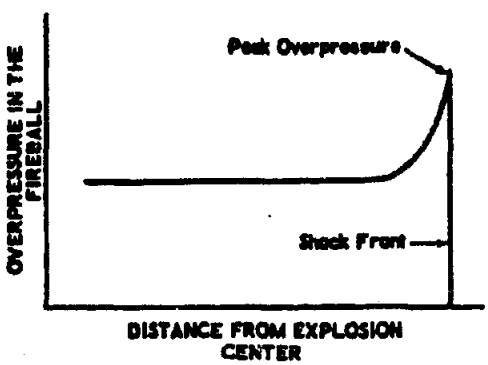

Figure 4–1. Overpressure vs Distance, Early Stages of Blast Wave

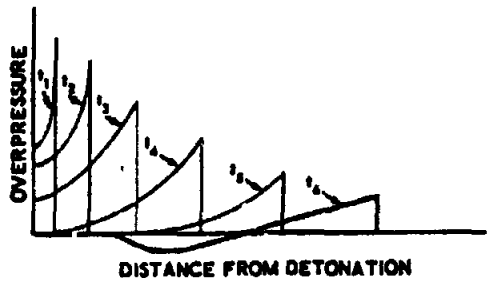

Figure 4–2. Variation of Overpressure With Time

Fig. 4–3 illustrates how overpressure varies with time at a given point. The corresponding general effects to be expected on a light structure, a tree, and a small animal are indicated. For a short interval after detonation there is no increase in pressure because the blast front (shock front) has not yet reached the target. When the shock front arrives, the pressure suddenly increases to a large maximum (the peak overpressure), and a strong wind commences to blow away from the explosion. The velocity of the wind decreases rapidly with time; therefore, it is generally referred to as a transient wind. Following the arrival of the shock front, the pressure falls rapidly, and shortly returns to the ambient condition. At this point, although the overpressure is zero, the wind still continues in the same direction for a short time. The interval from the arrival of the shock front to the return to ambient pressure is roughly one-half second to one second for a 20-kiloton (KT) explosion, and two to four seconds for a 1-megaton (MT) explosion. It is during this period that most of the destructive action of the air burst is experienced.

Official U. S. Army Photograph

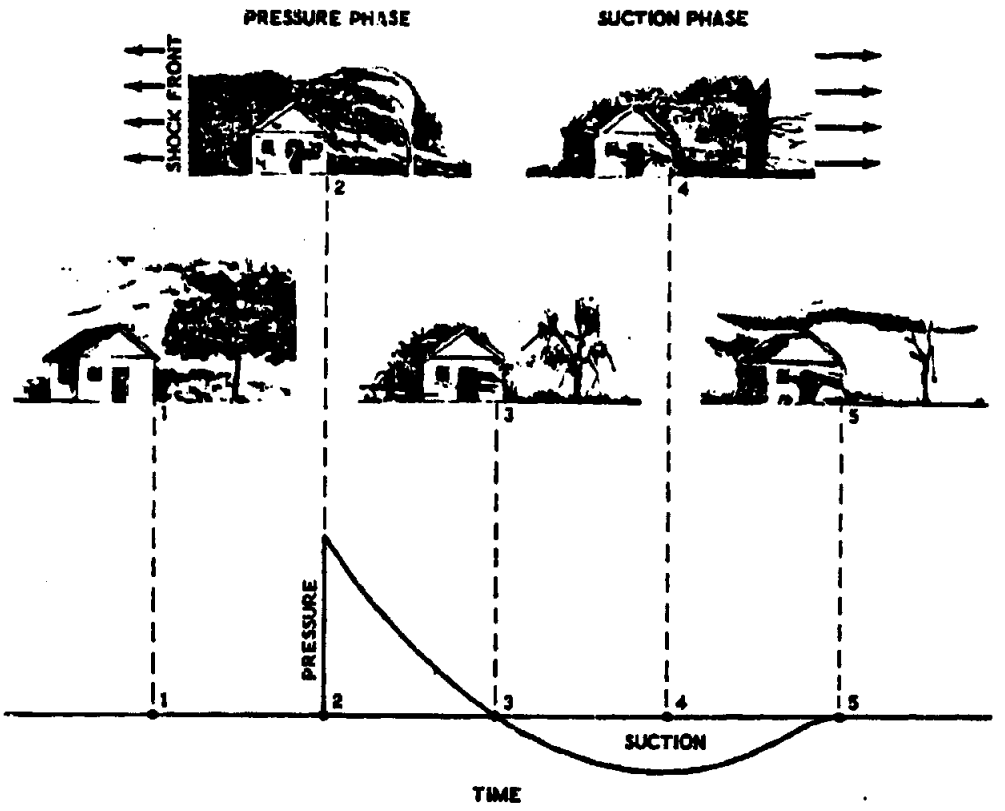

Figure 4–3. Variation of Blast Wave With Time, at a Given Point, and Corresponding Effect of Blast Wave Passing Over a Structure

As the pressure of the blast wave continues to decrease, it drops below ambient pressure, and the suction phase begins. This phase may last for several seconds, and for most of that time the transient winds blow inward toward the explosion. The damage during this phase is generally minor in nature because the peak negative overpressure is small in comparison with the maximum positive overpressure.

In striking opposing surfaces or structures, a process known as diffraction occurs, wherein overpressure is considered to be resolved into face-on (reflected) and side-on overpressures. A general discussion of these forces, and of the corresponding translational force, known as diffraction loading, is given in Ch. 2, Sec. IV.

4–2.2.2. *Dynamic Pressure*

Although the destructive effects of the blast wave are often related to values of the peak overpressure, the dynamic pressure may be of equal importance. As a function of the wind (particle) velocity and of the density of the air behind the shock front, dynamic pressure is expressed by the equation

$$q = \tfrac{1}{2}\rho u^2$$

where q represents the dynamic pressure, ρ the air density, and u the wind velocity. For very strong shocks, the peak dynamic pressure is larger than the overpressure, but below 69 psi overpressure at sea level, the dynamic pressure is smaller. The peak dynamic pressure, like

the peak overpressure, decreases with distance from ground zero, although at a different rate.

For a great variety of building types, the degree of blast damage depends largely on the drag force associated with the strong transient winds accompanying the passage of the blast wave. The drag force is influenced by certain characteristics of the structure, such as the shape and size, but is generally dependent upon the peak value of the dynamic pressure and its duration at a given location. (Ch. 2, Sec. IV).

At a given location, the dynamic pressure varies with time in a manner similar to the changes of overpressure, but the rate of decrease behind the shock front is different. Both overpressure and dynamic pressure increase sharply when the shock front reaches the given location, then they decrease. Fig. 4–4 indicates qualitatively how the two pressures vary in the course of the first seconds following the arrival of the shock front. The curves indicate that the overpressure and the dynamic pressure return to ambient (0) conditions at the same time. Actually, due to the inertia of the air, the wind velocity (and, therefore, the dynamic pressure) will drop to zero at a somewhat later time, but the difference is usually not significant for purposes of estimating damage. Table 4–1 gives some indication of the corresponding values of peak overpressures, and peak dynamic pressures, as related to the maximum blast wind velocities in air at sea level.

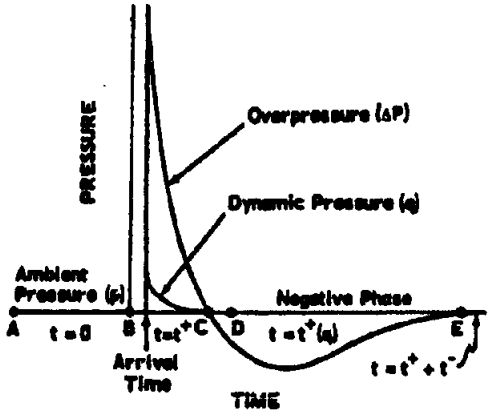

Figure 4–4. Comparison of Variations of Overpressure and Dynamic Pressure vs Time

TABLE 4–1. OVERPRESSURE AND DYNAMIC PRESSURE RELATED TO BLAST WIND VELOCITY IN AIR AT SEA LEVEL

Peak Over-Pressure (psi)	Peak Dynamic Pressure (psi)	Maximum Wind Velocity (mph)
72	80	1,170
50	40	940
30	16	670
20	8	470
10	2	290
5	0.7	160
2	0.1	70

4–2.2.3. *Arrival Time*

As previously stated, there is a finite time interval required for the blast wave to move out from the explosion center to any particular location. This time interval is dependent upon the yield of the explosion and the distance involved. Initially, the velocity of the shock front is quite high, many times the speed of sound, but as the blast wave moves outward its velocity decreases as the shock front weakens. Finally, at long ranges, the blast wave becomes essentially a sound wave and its velocity approaches ambient sound velocity.

4–2.2.4. *Duration*

The duration of the blast wave at a particular location also depends upon the energy of the explosion and the distance from ground zero. The duration of the positive overpressure phase is shortest at close ranges, increasing as the blast wave progresses outward. Because the transient wind velocity behind the shock front decays to zero, and then reverses itself at a time somewhat after the end of the positive overpressure phase, the dynamic pressures may endure longer than the overpressure. However, these elements of the dynamic pressures are so low they are not significant. Therefore, the effective duration of the dynamic pressures may be considered as being essentially the same as the positive phase of the overpressure.

4–2.2.5. *Overpressure and Dynamic Pressure Impulse*

Damage to targets is frequently dependent on duration of the loading as well as the peak

pressure. Parameters related to the duration are the impulses represented in Fig. 4–4, where the overpressure positive phase impulse is the area under the positive portion of the overpressure time curve, and the dynamic pressure impulse is the area under the positive portion of the dynamic pressure time curve.

The overpressure positive phase impulse is represented by the equation

$$I_p = \int_{t=0}^{t=t^+} \Delta P(t)\,dt \qquad (4\text{–}2)$$

in which: $t=0$ is the time of arrival of the shock front; $t=t^+$ is the end of the positive phase; and $\Delta P(t)$ is the overpressure as a function of time.

The positive phase pressure-time curve showing the decay of overpressure at a fixed point in space will vary, depending on the peak overpressure and duration for a given yield at that point. Where overpressures are less than 25 psi, the variation of overpressure with time may be expressed by the following semi-empirical relation:

$$\Delta P(t) = \Delta P\left(1-\frac{t}{t^+}\right)e^{-t/t^+} \qquad (4\text{–}3)$$

where: $\Delta P(t)$ is the overpressure at any time t; ΔP is the peak overpressure; and t^+ is the positive phase duration.

In a similar manner, the dynamic pressure impulse is represented by the area under the dynamic pressure-time curve, and may be represented by the integral

$$I_q = \int_{t=0}^{t=t_q^+} q(t)\,dt \qquad (4\text{–}4)$$

where: I_q is the dynamic pressure impulse; $q(t)$ the dynamic pressure as a function of time; and t_q^+ the duration of the dynamic pressure positive phase. As with overpressure, the rate of decay varies with peak pressure and duration. Where dynamic pressures are less than 12 psi, the variation of dynamic pressure with time may be represented by the approximate equation

$$q(t) = q(1-t/t^+)^2\, e^{-2t/t^+} \qquad (4\text{–}5)$$

where: $q(t)$ is the dynamic pressure at time t; q is the peak dynamic pressure at the shock front; and t^+ is the overpressure positive phase duration (Ref. 21).

4–2.2.6. Reflection

When the incident blast wave from an explosion in air strikes a more dense medium such as the earth's surface, either land or water, it is reflected. The formation of the reflected shock wave in these circumstances is represented in Fig. 4–5(A). This figure shows several stages in the outward motion of the spherical blast originating from an air burst bomb. In the first stage (t_1), the shock front has not reached the ground; the second stage (t_2) is somewhat later in time; and in the third stage (t_3), which is still later, a reflected wave, indicated by the dotted line, has been produced.

When such reflection occurs, an individual or object precisely at the surface will experience a single shock, because the reflected wave is formed instantaneously. Consequently, the value of the overpressure thus experienced at the surface is generally considered to be entirely a reflected pressure. In the region near ground zero, this total reflected overpressure will be more than twice the value of the peak overpressure of the incident blast wave. The exact value of the reflected pressure will depend on the strength of the incident wave and the angle at which it strikes the surface. The variation in overpressure with time, as observed at a point actually on the surface not too far from ground zero, such as point A in Fig. 4–5(A), will be as depicted in Fig. 4–5(B). The point A may be considered as lying within the region of regular reflection; i.e., where the incident (I) and reflected (R) waves do not merge above the surface.

At any location somewhat above the surface, but still within the region of regular reflection, two separate shocks will be felt. The first shock is due to the incident blast wave, and the second, which arrives a short time later, to the reflected wave. Fig. 4–5(C) depicts the variation of overpressure experienced at a location above

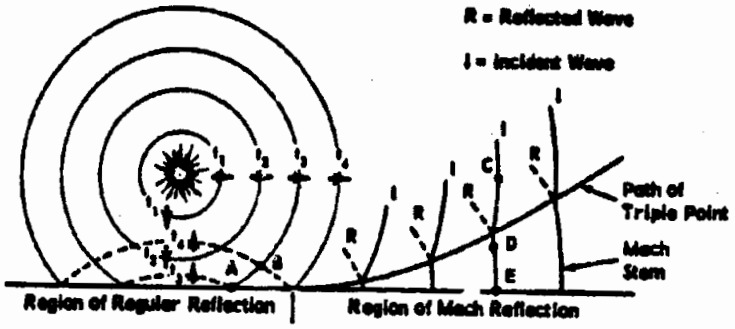

(A) REFLECTION CHARACTERISTICS OF BLAST WAVE NEAR SURFACE

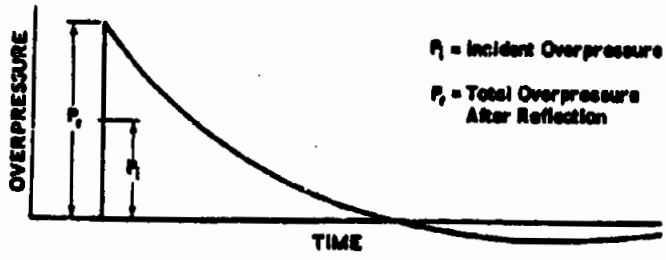

(B) OVERPRESSURE-TIME HISTORY AT POINT A

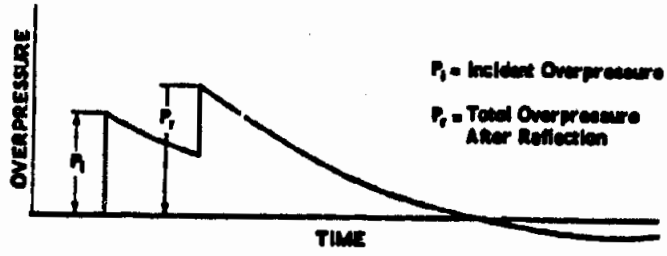

(C) OVERPRESSURE-TIME HISTORY AT POINTS B AND C

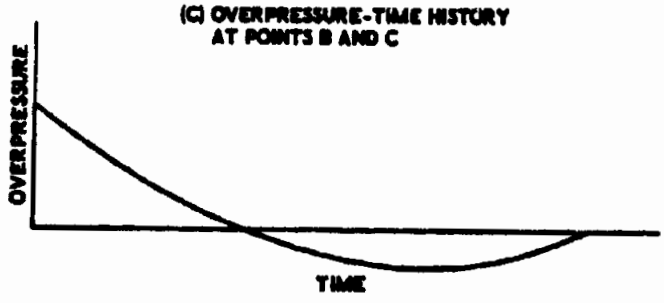

(D) OVERPRESSURE-TIME HISTORY AT POINTS [illegible] D E

Figure 4–5. Reflection of Air-Burst Blast Wave at Earth's Surface

the surface. In determining the effects of air blast on structures in the regular reflection region, allowance must be made for the magnitude and also the directions of motion of both the incident and reflected waves. After passage of the reflected wave, the transient winds near the surface becomes essentially horizontal.

In the early stages of propagation, when the shock front is not far from ground zero, it is reasonable to assume that both the incident and reflected waves travel with velocities that are approximately equal. The reflected wave, however, always travels through air that has been heated and compressed by the passage of the incident wave. As a result, the reflected shock wave moves faster than the incident wave and eventually overtakes it. The two waves then fuse to produce a single shock wave. This process of wave interaction is referred to as Mach or irregular reflection, and the region in which the two waves have merged is called the Mach region. The fusion of the incident and reflected blast waves is indicated schematically in Fig. 4–6, which illustrates a portion of the blast wave profile close to the surface. Fig. 4–6(A) represents a point close to ground zero. In Fig. 4–6(B), a later stage, farther from ground zero, the steeper front of the reflected wave shows that it is traveling faster than the incident wave. At the stage illustrated by Fig. 4–6(C), the reflected shock near the ground has overtaken and fused with the incident shock to form a single shock front, called the Mach stem. The point at which the incident shock, reflected shock, and Mach fronts meet is referred to as the triple point.

As the reflected wave continues to overtake the incident wave, the triple point rises and the height of the Mach stem increases as shown in Fig. 4–5(A). Any object, located either at or above the ground within the Mach region, will experience a single shock whose behavior will follow that of shock fronts in general (the overpressure at a particular location will decrease with time, and the positive phase will be followed by a suction phase). At points in the air above the triple point, a separate shock will be felt from the incident (I) and reflected (R) waves, also as shown in Fig. 4–5(A).

Two aspects of the reflection process are important with regard to the destructive action of the air blast. First, only a single shock is experienced in the region below the triple point (in the Mach region). Second, since the Mach stem is nearly vertical, the accompanying blast wave is traveling in a horizontal direction at the surface, and the transient winds are nearly parallel to the ground. In the Mach region, therefore, the blast forces are applied in a nearly horizontal fashion against above-ground structures and other objects, so that vertical surfaces are loaded more intensely than horizontal surfaces.

The distance from ground zero at which Mach fusion commences is dependent upon the yield of the weapon and the height of burst above the ground. This distance decreases with a decreasing height of burst. Conversely, if the air burst occurs at a sufficiently high altitude, only regular reflection takes place and no Mach stem will be formed (Ref. 1).

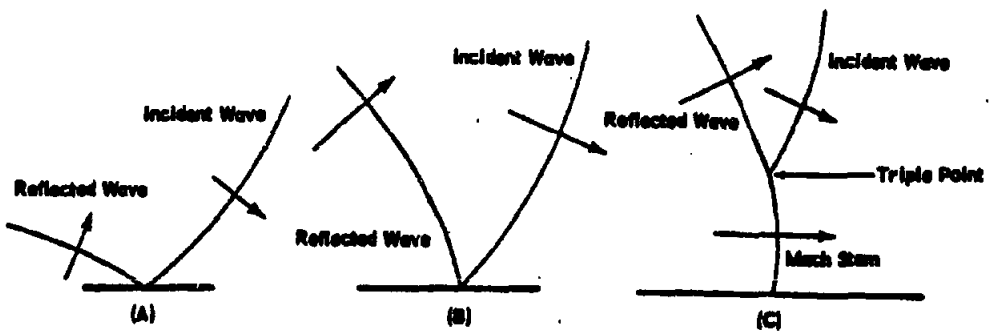

Figure 4–6. Fusion of Incident and Reflected Waves, and Formation of Mach Stem

The problem of reflection is treated more fully in the publications numbered 13 through 17 listed in the Bibliography for this chapter.

4–2.3. (U) Computation of Blast Wave Parameters

4–2.3.1. *General*

The following paragraphs summarize some pertinent aspects of blast wave theory and calculation. Much of the analysis which has been developed in the literature is applicable to either nuclear or high explosive blast. As previously indicated, however, there are certain physical differences which affect the validity of the solutions.

Compared with an ordinary high explosive blast, the energy density of a nuclear explosion is much greater and the corresponding temperatures developed are much higher, by a factor close to 10^4. An HE explosion generates temperatures near 5,000 C degrees; a nuclear explosion results in initial temperatures near 50 million degrees C. The tremendous difference in energy density has several consequences pertinent to the calculational aspects of the problem as well as the physical aspects.

The nuclear explosion can be considered more nearly a point source of energy, and solutions for the resulting blast wave are based on this concept. In an HE explosion the assumption of a finite size energy source is more appropriate, because it takes comparatively longer for the energy to be transferred to the surrounding air. Accordingly, immediately following the HE blast the shock wave pressure is actually less than that predicted from a point source solution. For this reason, much of the more recent literature has been directed toward finite source solutions.

4–2.3.2. *Basic Hydrodynamic Equations*

Before discussing some of the various approaches to the problems of blast wave computations, the basic hydrodynamic equations will be summarized for reference. This discussion is not concerned with equation derivation as such. Only sufficient analysis is given to provide a suitable background. The basic equations of hydrodynamics are equally valid for either a gas or liquid. The associated equations of state are, however, different in each case. The following discussion is based largely on Refs. 2 through 5.

The general problem of fluid flow is to describe what is happening to each region of the fluid as a result of certain outside influences. Frequently, the most significant parameters are the fluid velocity and the fluid pressure, described as functions of position and time. Fluid descriptions in hydrodynamics are based on the concept of a continuum. Roughly speaking, this corresponds to imagining an arbitrarily large number of particles distributed throughout the space of interest, such that each fluid property varies in a continuous manner from particle to particle. In order to adequately describe physical phenomena, however, it will be necessary to permit certain points, lines, or surfaces to exist upon which the fluid properties behave in a discontinuous manner.

The great difficulty of the subject is that, in terms of rigid body mechanics, a system of an infinite number of degrees of freedom has to be dealt with. Stated differently, because continuous variation in properties of the fluid is postulated, each property will be a function of both position and time. Correspondingly, the basic equations of hydrodynamics are partial, rather than ordinary, differential equations.

To make more explicit the above statements, a brief discussion of the two methods for describing fluid motion will be given. The first method, called the Lagrangian description, considers what happens to each individual fluid particle in the course of time. The other method, called the Eulerian description, considers what is happening at each point in space as a function of time. In the latter method, for example, the pressure at a point means the pressure associated with the particle that happens to be passing through that point at that instant. No attempt is made to follow the individual particle.

Consider first the Lagrangian description. Since the motion of each individual particle is to be followed, it will be necessary to identify each particle. This may be done by setting up a coordinate system at a fixed instant of time, say $t = 0$, and by assigning to each particle a set of numbers which may be taken as its co-

ordinate in space. Again for example, when limited to one-dimensional motion, the identifying tag associated with each particle is merely its position on the axis of motion at $t = 0$. As time proceeds, each particle moves, and its position will be a function of time. If x is its location at time t, then $x = x(t)$ for each particle. Let the term a be the initial position of a particle; then a will be different for each particle, and the entire "field" (that is, all particles at the same time) may be described by the single expression

$$x = x(a, t)$$

where, for each particle, a is a fixed number, and t is the time. Correspondingly, the velocity of each particle is given by

$$u = \frac{\partial x}{\partial t}(a, t)$$

where the partial derivative symbol is used to emphasize that a single particle is being considered. For brevity, it is conventional in hydrodynamic literature to write

$$\frac{\partial x}{\partial t}(a, t) = \dot{x}$$

so that

$$\dot{x} = u(a, t) \qquad (4\text{–}6)$$

In the Euler representation, consider a region of space which may be arbitrarily selected. Again using one-dimensional motion as an example, the location of this region is denoted by a position, x, relative to the coordinate system. Thus, x is an independent variable, and locates a point in space, not a particular particle. Through this space, however, particles pass, and each particle has certain properties associated with it at the instant of passing through the point x. These properties are velocity, acceleration, pressure, density, etc. Accordingly, for example, the velocity at (not of) any point in space is a function of time; for with time, different particles are passing the point. Let the variable which describes all the points in space be x, and let t be the time. Then, the velocity at the point, at that time may be written

$$u = u(x, t). \qquad (4\text{–}7)$$

At a given instant of time the particular particle passing through the point has this same velocity, by definition. Hence,

$$\dot{x} = u(x, t) \qquad (4\text{–}8)$$

and if u has been determined, the position with time of each particle may be determined by integrating Eq. 4–8. The solution will involve a constant of integration, which may be determined by the location of the particle at time $t = 0$. Accordingly, the solution will be expressed in terms of a, the Lagrangian coordinate, written after solution as,

$$x = f(a, t)$$

where f will now be a known functional form. This integration then forms the connection between the Eulerian and Lagrangian technique. It should not be inferred that the physical description just given is easily carried out. In fact, very few solutions are known even in the one-dimensional case.

Referring to Eq. 4–7, an important distinction is made. If each particle that passes the point x has the same characteristics in terms of speed, pressure, etc., as every other particle that passes through the point x, then u, given by Eq. 4–7 does not change with time.

In this case $u = u(x)$ and the flow is said to be steady. It should be noted that the flow, following each particle, may differ from point to point, and still be within this definition of steady. This simple fact illustrates the utility of the Euler description. If, on the other hand, particle properties are different for each succeeding particle that passes through x, then u, at x, is also a function of time, written

$$u = u(x, t).$$

In this case, the flow "field" is said to be *nonsteady*.

4–2.3.3. Basic One-Dimensional Flow Equations

On the basis of the simple introduction, given in the preceding paragraph, some of the basic equations of one-dimensional flow will be summarized. Once again, this discussion is explanatory in nature, and is not concerned with equation derivation as such.

The basic laws governing the behavior of the flow field are the same as those governing any other mechanical system. That is, Newton's laws of motion, conservation of energy, conservation of mass, and the laws of thermodynamics govern.

Consider first the conservation of mass. Using the Euler description, a region in space is selected through which the particles are passing. The rate at which mass leaves the region, minus the rate at which it enters, must equal the rate at which it decreases within the region. If ρ is the mass density, dx the length of the region of cross section A, and u is the entering speed, then ρAu is the mass per unit of time entering the region, and $\rho A\,dx$ is the mass within the region. Using subscripts to denote location,

$$[(\rho u)_{x+dx} - (\rho u)_x]A = -\frac{\partial}{\partial t}(\rho A\,dx)$$

or

$$\frac{(\rho u)_{x+dx} - (\rho u)_x}{dx} = -\frac{\partial \rho}{\partial t}$$

which, upon passing to the limit, gives the continuity equation for one-dimensional flow. (This assumes that A is a constant.)

Thus,

$$\frac{\partial(\rho u)}{\partial x} + \frac{\partial \rho}{\partial t} = 0 \qquad (4\text{–}9)$$

where $\rho = \rho(x, t)$ and $u = u(x, t)$ are the density and velocity of the particular particle that happens to be passing through the region located at x, at time t.

In a similar manner, by drawing a free body diagram of the region located at x, and by neglecting all forces except pressure, the momentum form of Newton's law is obtained,

$$\frac{\partial u}{\partial t} + u\frac{\partial u}{\partial x} = -\frac{1}{\rho}\frac{\partial P}{\partial x} \qquad (4\text{–}10)$$

where P is the static pressure between fluid particles.

Shearing forces are neglected because with such terms the practical problem of solving the blast equations, even in one dimension, is much too difficult; being even too difficult for solution on high speed computers. Fortunately, this assumption of frictionless flow does not invalidate the analysis. Instead, as will be presently discussed, there are regions of the flow in which the viscosity plays a very important part. These regions are the shock waves that show up, mathematically, as discontinuities in the flow. The discontinuities serve as boundaries across which the fluid properties undergo sharp, step changes. It has been found that if the flow field is assumed to be everywhere continuous, frictionless, and adiabatic, except at the discontinuities, a reasonable approximation to the real, physical system can be achieved. In fact, in the sense of a real fluid there are no discontinuities.

Fortunately, however, the rates of change of fluid properties are so great that shock waves may be treated as fluid discontinuities. This permits the neglect of viscosity and heat conduction elsewhere. Even with this simplification, however, straightforward solutions are very difficult, and it is only with the aid of approximation that solutions have been obtained for the one-dimensional, non-steady, blast problem.

The thermodynamic relations required express the first and second of Newton's laws. If E represents the internal energy per unit mass of fluid, which includes thermal and chemical, and $\frac{1}{2}mu^2$ represents the kinetic energy of a particle of mass m, then the first law states that the work done equals the change in total energy (neglecting heat transfer as stated above). Thus, for a particle of dimensions $A\,dx$, moving with the speed u, and having density ρ, and pressure P, there is the expression

$$[(Pu)_x - (Pu)_{x+dx}]\,dt \cdot A$$

which is the work done on the particle. Its change in energy is

$$dt A\,dx \rho \frac{d}{dt}\left[E + \frac{1}{2}u^2\right].$$

Upon passing to the limit, this gives

$$\rho\frac{d}{dt}\left[E + \frac{1}{2}u^2\right] = -\frac{\partial}{\partial x}(P, u)$$

which, by making use of the continuity equation, may be written,

$$\rho\frac{dE}{dt}=\frac{P}{\rho}\frac{d\rho}{dt} \qquad (4\text{–}11)$$

where $\frac{d}{dt}$ is the total derivative, following the particle. Since each particle is passing through a given location at each instant of time, its properties, ρ for example, may be written

$$\rho=\rho(x,t). \qquad (4\text{–}12)$$

Then, $\frac{d}{dt}$ of ρ means the total rate of change of ρ with time and position. Hence, using the chain rule of calculus, applied to Eq. 4–12

$$\frac{d\rho}{dt}=\frac{\partial\rho}{\partial t}+\frac{\partial\rho}{\partial x}\frac{dx}{dt}$$

but $\frac{dx}{dt}=u$, the speed, and hence the Lagrangian and Euler derivatives are connected by the relation

$$\frac{d\rho}{dt}=\frac{\partial\rho}{\partial t}+u\frac{\partial\rho}{\partial x} \qquad (4\text{–}13)$$

where the same expression may be applied to any one of the fluid properties; that is, for velocity itself,

$$\frac{du}{dt}=\frac{\partial u}{\partial t}+u\frac{\partial u}{\partial x} \qquad (4\text{–}14)$$

In these cases it is noted that $\frac{du}{dt}$ means the total rate of change, consisting of a part, $\frac{\partial u}{\partial t}$, caused by changing u at a given point, and of $u\frac{\partial u}{\partial x}$, caused by changing location at a given time.

If we assume there are no dissipating processes within the fluid, except at the discontinuities, then the thermodynamic condition of constant entropy may be applied to any region free of boundaries. This leads to the usual adiabatic relation that permits pressure to be expressed as a single-valued function of density alone. Note, however, that across discontinuities two different elements of fluid may have undergone different dissipative processes. Consequently, the adiabatic law may be different for the two particles.

In order to introduce the subject of shock waves in a manner most appropriate to the present discussion, it will be convenient to first discuss waves of small amplitude.

For reference, the continuity and momentum equations for one-dimensional flow are repeated:

$$\frac{\partial}{\partial x}(\rho u)+\frac{\partial\rho}{\partial t}=0 \qquad (4\text{–}9)$$

and

$$\frac{\partial u}{\partial t}+u\frac{\partial u}{\partial x}=-\frac{1}{\rho}\frac{\partial P}{\partial X} \qquad (4\text{–}10)$$

Assume that there exists an everywhere uniform and stationary fluid of (initial) density ρ_0. It is now desired to determine how the fluid reacts when a small pressure disturbance is created. This is the usual acoustic problem. It is instructive to see what assumptions must be made to arrive at the concept of a sound wave.

If the indicated differentiation is carried out in Eq. 4–9, the result is

$$\frac{\partial}{\partial x}(\rho u)=\frac{\partial\rho}{\partial x}u+\rho\frac{\partial u}{\partial x}.$$

If it is assumed that u, the particle velocity, is small, and that the density change at a point is small as a result of a small pressure pulse, the term $\frac{\partial\rho}{\partial x}u$ represents a quantity of second-order compared with $\rho\frac{\partial u}{\partial x}$. Accordingly, it may be neglected. Further, since P is presumed to be a function of ρ only,

$$\frac{\partial P}{\partial t}=\left(\frac{dP}{d\rho}\right)\frac{\partial\rho}{\partial x}.$$

Since $\left(\frac{dP}{d\rho}\right)$, evaluated for an adiabatic change is a slowly varying function of ρ, it will be treated within the framework of the present assumption as a constant, and be denoted by C_0^2. In the momentum equation, Eq. 4–10, the term $u\frac{\partial u}{\partial x}$ is also of second order and will be

neglected. Using these assumptions in Eqs. 4-9 and 4-10 leads to

$$\rho\frac{\partial u}{\partial x}+\frac{1}{C_o^2}\frac{\partial P}{\partial t}=0 \qquad (4\text{–}15)$$

and

$$\frac{1}{\rho}\frac{\partial P}{\partial x}+\frac{\partial u}{\partial t}=0. \qquad (4\text{-}16)$$

As a further assumption, consistent with those already made, $\rho\frac{\partial u}{\partial x}$ for example, may be written $(\rho_o+\Delta\rho)\frac{\partial u}{\partial x}$, and the term $\Delta\rho\frac{\partial u}{\partial x}$ is a second order quantity. Neglecting this term results in the pair of linear, partial, differential equations with constant coefficients,

$$\rho_o\frac{\partial u}{\partial x}+\frac{1}{C_o^2}\frac{\partial P}{\partial t}=o \qquad (4\text{–}17)$$

and

$$\frac{1}{\rho_o}\frac{\partial P}{\partial x}+\frac{\partial u}{\partial t}=o \qquad (4\text{–}18)$$

which may be combined into a single equation. Differentiating the first with respect to t, and the second with respect to x, and making use of the fact that

$$\frac{\partial}{\partial t}\left(\frac{\partial u}{\partial x}\right)=\frac{\partial}{\partial x}\left(\frac{\partial u}{\partial t}\right)$$

for continuous functions and derivatives, we combine the pair of equations to give the acoustic wave equation

$$\frac{\partial^2 P}{\partial x^2}=\frac{1}{C_o^2}\frac{\partial^2 P}{\partial t^2} \qquad (4\text{–}19)$$

A solution of this equation requires the substitution of some function that will reduce both sides to an identity. As may be seen by direct substitution, such a function is

$$P=f\ (t-x/C_o) \qquad (4\text{–}20)$$

where the argument of the function is the quantity $t-x/C_o$, and f is an arbitrary function. The exact form of f will depend on the boundary conditions; however, without considering that aspect considerable information can be obtained. In words, Eq. 4–20 states that the pressure in the fluid at any point x, and at any time t, is a function of the specific combination of x and t given by $(t-x/C_o)$, regardless of the functional form of f. To see the meaning of this, let

$$t-x/C_o=w.$$

Then

$$P=f(w)$$

and for all values of x and t which make w a constant, the pressure P is also a constant and equal to the same value, because a function of a constant is a constant. Let w be given a set of constant values, such as w_0, w_1, w_2, etc.; then,

$$x=C_o t+C_o w_i \qquad (4\text{–}21)$$

where w_i is one of the values of the series w_0, w_1, etc. If x is plotted against t for different values of w, the result is a set of straight lines, all having the same slope, as shown in Fig. 4–7.

Also note that because of $P=f\ (w_i)$, each line is also a line of constant pressure. The form of Eq. 4–21 shows that C_o is a speed factor, because (speed) × (time) gives distance. Consider then, the point a on line w_i. Let the pressure on this line (everywhere on the line) have the value P_i. This occurs at $x=x_a$, at time $t=t_a$, as shown. As other points are considered in the (x, t) flow field, it is seen that at point b, where $x=x_b$, and $t=t_b$, the pressure is still P_i. That is, the same pressure has been trans-

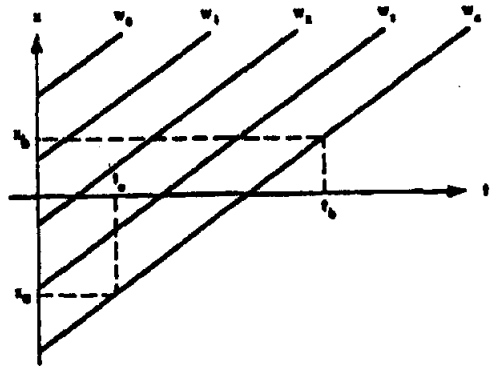

Figure 4–7. Plot of x Against t for Different Values of w

mitted from point a to point b. Since the speed of transmission is

$$\frac{x_b - x_a}{t_b - t_a}$$

using Eq. 4–21, the

$$\text{speed of transmission} = \frac{C_o(t_b - t_a)}{(t_b - t_a)} = C_o$$

showing that C_o is the speed of transmission of the pressure pulse. Since the lines given by $x = C_o t + C_o n$, are straight lines, it can be seen that C_o, called the speed of sound, is the same everywhere in the flow field. It is also seen that by holding x constant and varying the time, the pressure at a point changes with time. The pressure pulse may then be envisioned as being transmitted as shown in Fig. 4–8, where the pulse is moving to the right with the speed C_o. That is, energy is exchanged between particles to transmit the pressure; however, the movement of each particle need only be small. This is well illustrated by the familiar example of an ever-widening disturbance created on the surface of a still pool of water.

To examine the motion of each particle, consider Eq. 4–18. Then, with $P = f(t - x/C_o)$,

$$\frac{\partial u}{\partial t} = -\frac{1}{\rho_o}\frac{\partial P}{\partial x} = -\frac{1}{\rho_o} f'\left(t - x/C_o\right)\left(\frac{-1}{C_o}\right) \tag{4–22}$$

where $f'(t - x/C_o)$ is the derivative of f with regard to its argument $(t - x/C_o)$. In order to determine the variation in u at a point, we integrate this equation with respect to t, holding x fixed. This gives

$$u = \frac{1}{\rho_o C_o} f\left(t - x/C_o\right)\Big|_{P=P_o}^{P=P} \tag{4–23}$$

or

$$u = \frac{1}{\rho_o C_o}\left[P - P_o\right] \tag{4–24}$$

where the initial values of u and P are taken as zero and P_o, respectively.

To effect the integration of Eq 4–22 with respect to time, as above, write

$$t - x/C_o = z$$

then

$$\frac{\partial u}{\partial t} = \frac{1}{\rho_o C_o} f'(z)$$

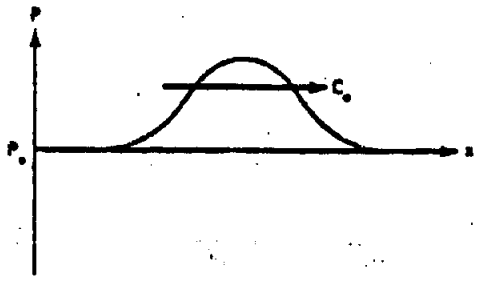

Figure 4–8. Transmission of Pressure Pulse in Point-Time Field

and

$$f'(z) = \frac{\partial f}{\partial t}\frac{\partial t}{\partial z} = \frac{\partial f}{dt}$$

since $\partial t/\partial z = 1$, and the result follows.

From Eq. 4–24 it is seen that u is small, compared with the speed of transmission, for small variations in P_o. To examine some numerical values recall that the sound speed C_o is given by

$$C_o = \sqrt{\frac{dP}{d\rho}}.$$

Using the adiabatic equations of state for air and water gives $C_o = 1{,}100$ ft/sec. for air and $C_o = 5{,}000$ ft/sec. for water, at near standard conditions. Since the densities of the two media are so different, Eq. 4–24 shows that the particle velocity is much less in water. If $\rho_o = 2.0 \times 10^{-3}$ slugs/cu ft for air, and $\rho_o = 2.0$ slugs/cu ft for water, the same pressure difference of (for example) one hundredth of an atmosphere = 20 lb/sq ft, produces particle velocities, induced by the passage of the pressure wave, equal to,

$$u_{water} = 2 \times 10^{-3} \text{ ft/sec.}$$

$$u_{air} = 10 \text{ ft/sec.}$$

4–2.3.4. *Basic Spherical Wave Equations*

Up to this point, the discussion has dealt with one-dimensional flow along a specified axis. Therefore, the waves produced have been plane waves, and the equations presented apply only to that case. [Observe that $P = f(t + z/C_o)$ is also a solution to the previous equation. This corresponds, physically, to a wave traveling in

the reverse direction.] Of even greater interest is the case of spherical waves. Fortunately, if it is assumed that the spherical waves are symmetrical and depend only on radius and time, the equations still depend on only one space variable. Let this variable be r, and by reasoning similar to that already employed, a set of equations may be derived that express the continuity and momentum relations. If these equations are linearized in the same way as the plane wave case, the following are obtained:

$$\frac{\partial u}{\partial t} = -\frac{1}{\rho_o}\frac{\partial P}{\partial r} \qquad (4\text{–}25)$$

and

$$\frac{1}{C_o^2}\frac{\partial P}{\partial t} = -\rho_o \frac{1}{r^2}\frac{\partial}{\partial r}\left(r^2 \frac{\partial u}{\partial r}\right) \qquad (4\text{–}26)$$

which, when combined, give,

$$\frac{1}{r^2}\frac{\partial}{\partial r}\left(r^2\frac{\partial P}{\partial r}\right) = \frac{1}{c_o^2}\cdot\frac{\partial^2 P}{\partial t^2} \qquad (4\text{–}27)$$

where u now means the radial speed, $u = \frac{\partial r}{\partial t}$, for a given particle. It may be verified by differentiation that a solution of Eq. 4–27 is

$$P = \frac{1}{r} f\,(t - r/C_o). \qquad (4\text{–}28)$$

Using exactly the same argument as before, it is seen that C_o is the speed of the spherical wave, but that now the amplitude decreases with radius because of the factor $(1/r)$. This is obviously caused, physically, by the greater area over which the advancing disturbance is spread. Integrating Eq. 4–25 with regard to t, and using the functional expression just found for P gives

$$u = \frac{P - P_o}{\rho_o C_o} + \frac{1}{\rho_o r}\int_o^t [P(r,t') - P_o]\,dt'$$

where t' is a variable of integration. Although integration cannot be performed explicitly, as in the plane case, it is seen that the velocity in the fluid u, at position r, is not only a function of the pressure difference at that time, but also a function of all previous pressures that reached the point prior to time $= t$. This is shown by the presence of the integral. That is, the velocity u, called the after flow, will exist even after the local pressure difference has fallen to zero. Further, u will equal zero only when P falls below P_o. This illustrates one significant effect of a spherical source. It also serves to show why the blast problem leads to mathematical difficulties, for a complete evaluation of pressures and flow at points behind (after the wave has passed) the wave front is clearly only possible by considering the properties of the source which generate the wave. Further, any source will be affected by the fluid surrounding it, and it is seen that a coupling exists between the cause and effect. In the blast computations to be considered later, this coupling will be seen to complicate, and determine, the boundary conditions.

In the blast problem, only weak sources produce acoustic waves. In the cases of interest, and in relation to an explosion, the pressure differences created by the passage of a wave front are too great to consider the linearized equations just discussed. In fact, the nonlinear character of the flow field, together with considerations of viscosity and heat transfer, lead to the formation of shock waves. To see, from a physical viewpoint, how this happens, consider the following argument.

In the linearized treatment, the sound speed $C(x,t)$ was replaced by a constant value, C_o, evaluated at the equilibrium state. In other words, the transmission speed was assumed to be independent of the pressure and the state of motion of the fluid. These assumptions lead to the conclusion that the $C = C_o$ was a constant in a fixed coordinate system. On the other hand, if C is permitted to vary and is measured with respect to a set of coordinates moving with the fluid at the point in question, matters become more complex. Since $P = P(\rho)$ is an adiabatic relationship, P is expected to increase at an increasing rate with ρ. That is, $\frac{dP}{d\rho}$ is positive and increases with increasing compression. Accordingly, the sound speed increases

with increasing compression. The great significance of this effect is shown in the following discussion, based on Ref. 4.

Consider subsequent spatial positions of the same wave, as shown in Fig. 4–9. Compression traveling to the right, as in position (1) will have the speed C_a, relative to the fluid, at point a. The absolute speed of compression at point a is, therefore, u_a+C_a, where u_a is the particle speed. Point b represents the pressure wave with speed of transmission u_b+C_b. Since point b is a point of higher compression than point a, u_b and C_b are both higher than at point a. Hence, as measured in absolute coordinates, the pressure pulse is being transmitted faster than at point a. Correspondingly, the sequence of events is shown in (2) and (3), where the crest of the wave has overtaken the valley. Here there is an exceedingly sharp wave front, across which quantities vary in an almost discontinuous fashion. The steepness of this wave front generates large gradients, from which it could be expected that heat conduction and viscosity would enter the picture. Because it is known that they do, to a significant extent, the elementary analysis just considered is not satisfactory for a complete evaluation of shock waves. However, it does point out the significant fact that strong compression waves lead to shock waves. Conversely, the argument also shows that rarefaction waves cannot produce shock waves. This aspect of the discussion is concluded by the observation that spherical waves, even though strongly initiated, will eventually approach sound waves because the energy density from a finite source is spread out over an ever expanding sphere.

4–2.3.5. *Various Approaches to the Blast Problem for Free Air Bursts*

a. General

The discussion of physical aspects in the preceding paragraph and the nonlinear character of the basic equations indicate that shock waves will develop. Further, it is clear that after the shock front has started to develop, the heat conduction effect and viscosity must become important because of the high gradients existing in pressure, temperature, etc., at the wave front. It would seem that an obvious solution would be to include the viscosity and conduction effects in the basic equations from the beginning, and to then solve the resulting partial differential equations. The resulting solutions would automatically account for the shock fronts and all aspects of the flow. Unfortunately, such an approach is far beyond the present applications of nonlinear differential equations. Even from a purely numerical viewpoint, the highest speed computers would be useless in a problem of this generality. Of necessity, then, approximations are made in obtaining solutions to the blast problem. Since the various methods are approximations, they are not unique, and differences in principal as well as in computational techniques would be expected.

It has already been indicated that none of the authoritative works in the field has attempted to solve the complete problem. Instead, the shock waves are treated as mathematical discontinuities, which serve as free boundaries between regions of assumed adiabatic flow fields. The term free boundary means that these discontinuities are not known

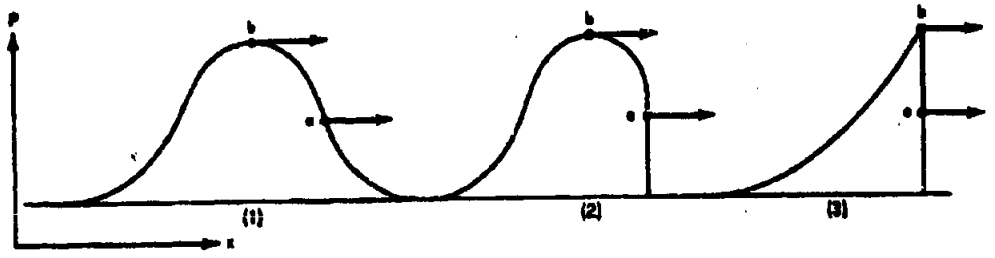

Figure 4–9. Compression Speed vs Transmission Speed

in advance, but must be determined as the solution proceeds. Indeed, this one fact accounts for some of the major difficulties encountered in problems of this type, both from a computational and theoretical viewpoint.

It should be pointed out here that von Neumann's scheme of fictitious viscosity is a departure from all former techniques. While this technique does not treat shocks as a mathematical discontinuity, neither does it attempt to solve the governing differential equations in all their generality. This fictitious viscosity method will be discussed in following subparagraphs. Since shock waves, treated as mathematical discontinuities, play such an important role in blast calculations, it is worthwhile to describe the conditions under which they exist. The physical basis for their formation has already been discussed. The analytical conditions existing at a shock front will now be examined. In order to discuss shock waves from an analytical viewpoint, it is necessary to develop the Rankine-Hugoniot equations. These are treated in many places (Ref. 3, for example) and will be repeated here only to the extent necessary to observe the physical implications behind them.

Consider, for illustration of the analytical conditions existing at a shock front, the case of a plane wave advancing into a region at rest. The side of the discontinuity facing the undisturbed flow is called the *front* of the shock wave. As this front passes, the particles of fluid have their properties changed. Hence, viewed from an absolute coordinate system, a condition of nonsteady flow exists. If it is assumed that the front advances at a uniform speed, U, with respect to fixed axes, then an observer traveling with the front would observe a condition of steady state. Let the subscript "o" refer to properties of the fluid in the undisturbed state, and let properties without a subscript refer to the condition after passage of the front. In Fig. 4–10, u represents the particle speed with respect to fixed coordinates, P the pressure, and ρ the density. E is the internal energy per unit mass. The shock-front is shown moving to the right into the undisturbed fluid, at speed U with respect to fixed coordinates.

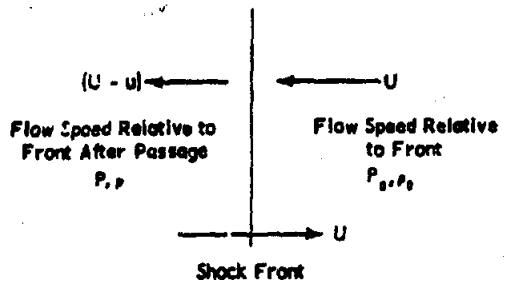

Figure 4–10. Movement of Shock Front in Undisturbed Fluid

The conservation of mass is expressed by the fact that the mass entering the front must leave the front. Therefore, for a unit area,

$$\rho\,(U-u)=\rho_o\,U. \qquad (4\text{–}29)$$

Newton's law may be expressed in the form: change of momentum equals impulse. In time dt, the mass crossing the boundary is

$$\rho\,(U-u)\,dt$$

and the momentum carried into the disturbed region in time dt is the product of the mass transported and the absolute speed of transport (because Newton's law is true with respect to absolute coordinates). The momentum transported out is, therefore,

$$\rho\,(U-u)\,u\,dt$$

and in a similar manner, the momentum transported into the boundary is

$$\rho_o\,U(o)\,dt=0$$

because the absolute speed before the shock is zero. The impulse in time dt is

$$[P-P_o]\,dt$$

and equating the two expressions gives

$$\rho\,(U-u)\,u=P-P_o$$

but from the continuity equation, Eq. 4–29, this may be written

$$\rho_o\,Uu=P-P_o. \qquad (4\text{–}30)$$

To establish the energy equation, we require that the work done on an element as it passes through the boundary is equal to the total change in energy. The work, in time dt, is

$$Pu\,dt$$

noting that the work of P_o is zero. The total change in energy in time dt is

$$\rho_o\,Udt[(E-E_o)+\tfrac{1}{2}u^2].$$

Equating the two expressions gives

$$Pu=\rho_o U(E-E_o)+\frac{1}{2}u^2$$

which, by elimination of u and U by use of Eqs. 4–29 and 4–30, may be written

$$E-E_o=\frac{1}{2}\left(P-P_o\right)\left(\frac{1}{\rho_o}-\frac{1}{\rho}\right). \qquad (4\text{–}31)$$

Eqs. 4–29, 4–30, and 4–31 show that a solution exists in the flow field for which the variables are not zero. That is, the basic laws of physics show that a discontinuous flow is possible. It is these equations that are needed as boundary conditions to relate the flow on one side of a discontinuity to the flow on the other, when solving the differential equations of fluid motion. Solving the first two explicitly for u and U gives,

$$U=\left[\left(\frac{\rho}{\rho_o}\right)\frac{P-P_o}{\rho-\rho_o}\right]^{1/2}$$

and

$$u=\frac{\rho-\rho_o}{\rho}U.$$

Thus, the shock and particle speeds may be determined in terms of the stated variables. This is what was meant by the term free boundaries. The speed, and hence position, of the boundaries are determined only after the flow variables are determined in the solution of the differential equations. Such solutions frequently require trial-and-error techniques which are, at best, very time consuming.

If it is assumed that adiabatic (but different adiabatic) conditions exist on either side of the shock wave, the energy terms may be expressed as

$$E=\frac{1}{\gamma-1}\frac{P}{\rho}$$

and

$$E_o=\frac{1}{\gamma-1}\frac{P_o}{\rho_o}$$

where γ is the ratio of specific heats. With these two relations and the Rankine-Hugoniot equations (Eqs. 4–29, 4–30, and 4–31), many useful relations may be developed. This is shown, for example, in Ref. 5. Some explicit expressions, taken from Ref. 6, are

$$\frac{\rho}{\rho_o}=\frac{1+6y}{6+y} \qquad (4\text{–}32)$$

$$\frac{U^2}{a_o^2}=\frac{1+6y}{7} \qquad (4\text{–}33)$$

$$\frac{u}{U}=\frac{5(y-1)}{1+6y} \qquad (4\text{–}34)$$

$$\frac{c^2}{a_o^2}=y\,\frac{6+y}{1+6y} \qquad (4\text{–}35)$$

where the equations give, respectively: the density ratio across the shock (4–32); the Mach number of the advancing front, referred to the speed of sound in the undisturbed fluid (4–33); the ratio of the particle velocity to the shock speed (4–34), and the ratio of the speed of sound behind the shock front to the speed of sound in the undisturbed fluid (4–35). In these equations, the terms not previously defined are:

a_o = speed of sound in the undisturbed flow. Under the present adiabatic assumptions, a_o may be expressed as

$$a_o=\left(\frac{\gamma P_o}{\rho_o}\right)^{1/2}.$$

c = speed of sound behind the shock front.

$$c=\left(\frac{\gamma P}{\rho}\right)^{1/2}.$$

y = ratio of the pressure after the shock to the pressure ahead of the shock, $y=P/P_o$.

γ = ratio of specific heats, taken equal to 7/5 for these expressions. It is a well-known fact that $\gamma=7/5=1.4$ is an adequate representation for air, provided the temperatures are not too high.

It is observed that these important flow parameters have all been expressed in terms of the pressure ratio across the shock wave.

Returning now to a discussion of possible types of solutions for the blast problem, we shall consider first the point source, strong blast solution of von Neumann, as discussed in Ref. 7.

b. *J. von Neumann's Solution of the Point Source, Strong Blast Case*

Some of the fundamental work performed on blast waves during World War II is represented by Ref. 7, which is readily accessible. The first topic of the report is the case under con-

sideration, introduced most effectively by quoting, in part, von Neumann's own words.

"The conventional picture of a blast wave is this: In a homogeneous atmosphere a certain sphere around the origin is suddenly replaced by homogeneous gas of much higher pressure. The high pressure area will immediately begin to expand against the surrounding low pressure atmosphere and send a pressure wave into it. As the high pressure area expands, its density decreases and with it the pressure; hence the effects it causes in the surrounding atmosphere weaken. As the pressure wave expands spherically through the atmosphere it is diluted over spherical shells of ever-increasing radii, and hence its intensity (the density of energy, and with it the over-pressure) decreases continuously also. This pressure wave is known (both theoretically and experimentally) to consist at all times of a discontinuous shock wave at the front, and to weaken gradually as one goes backward from that front.

"This description of the blast wave caused by an explosion is somewhat schematic, since the high pressure area caused by an explosion is not produced instantaneously, nor is its interior homogeneous, nor is it in general exactly spherical. Nevertheless, it seems to represent a reasonable approximation of reality.

"Mathematically, however, this approximate description offers very great difficulties. To determine the details of the history of the blast; that is, of its decay, the following things must be computed: (1) the trajectory of the shock wave; that is, of the front of the blast wave; and (2) the continuous flow of air behind the shock (ahead of the shock the air is unperturbed and at rest). This requires the solution of a partial differential equation bounded by the unknown trajectory (1). Along this trajectory the theory of shocks imposes more boundary conditions than are appropriate for a differential equation of the type (2), and this overdetermination produces a linkage between (1) and (2) which should permit one to determine the trajectory of (1) and to solve (2). To this extent the problem is a so-called "free boundary" partial differential equation problem. However, the situation is further complicated by the fact that at each point (2) the local entropy is determined by the entropy change the corresponding gas underwent when it crossed the shock (1); that is, by the shock strength at a certain point of (1). The latter depends on the shape of the trajectory (1), and the entropy in question influences the coefficients of the differential equation (2). Hence the differential equation (2) itself depends on the shape of the unknown trajectory (1). This dependence cannot be neglected as long as the entropy change caused by the shock is important; that is, as long as the shock is strong (in air a shock can be considered "strong" if the shock pressure exceeds 3 atm). Mathematically such problems are altogether inaccessible to our present analytical techniques. For this reason the general problem of the decay of blast has been treated only by approximate analytical methods, or numerically, or by combinations of these.

"For very violent explosions a further simplification suggests itself, which changes the mathematical situation very radically. For such an explosion it may be justified to treat the original, central, high pressure area as a point. Clearly, the blast coming from a point, or rather from a negligible volume, can have appreciable effects in the outside atmosphere only if the original pressure is very high. One will expect that, as the original high pressure sphere shrinks to a point, the original pressure will have to rise to infinity. It is easy to see, indeed, how these two are connected. One will want the energy of the original high pressure area to have a fixed value E_0, and as the original volume containing E_0 shrinks to zero, the pressure in it will have to rise to infinity. It is clear that of all known phenomena nuclear explosions come nearest to realizing these conditions."

The investigation presented in Ref. 7 concerning the decay of a blast wave due to a point explosion of energy E_0 was largely taken from the following sources: G. I. Taylor, Proc. Royal Soc., British Report RC–210, June 27, 1941; and John von Neumann, NDRC, Div. B, Report AM–9, June 30, 1941. Important simplifications (in particular, the use of the variable of Eq. 2.44) are due to G. Y. Kynch, British Report BM–82, MS–69, Sept. 18, 1943. The results

were generalized by J. H. van Vleck, NDRC, Div. B, Report AM-11, Sept. 15, 1942. Compare also the later work of G. I. Taylor, Proc. Royal Soc. (London), *A201*, 159 (1950).

One of the most significant aspects of the solution given by von Neumann is the use of dimensional similarity to reduce the complexity of the problem. Since he deals with a point source and considers very high pressures, the initial air pressure before burst, P_∞ is neglected. These assumptions permit a grouping of variables which leads to a set of ordinary, rather than partial equations. The report concludes with a set of formulae which may be used to compute the shock and flow parameters.

c. H. Bethe's Solution for Small $(\gamma-1)$

A method discussed by H. Bethe, in Ref. 7, is more general than von Neumann's solution. It is based on the fact that the term $(\gamma-1)$ may be considered small in many applications. Here, again, the best description of the method is afforded by the author's introductory remarks:

"The solution given in von Neumann Point Source Case is only valid for an exact point source explosion, for constant γ, for constant undisturbed density of the medium, and for very high shock pressures. It is very desirable to find a method which permits the treatment of somewhat more general shock wave problems and thereby comes closer to describing a real shock wave. The clue to such a method is found in the very peculiar nature of the point source solution of Taylor and von Neumann. It is characteristic for that solution that the density is extremely low in the inner regions and is high only in the immediate neighborhood of the shock front. Similarly, the pressure is almost exactly constant inside a radius of about 0.8 of the radius of the shock wave.

"It is particularly the first of these facts that is relevant for constructing a more general method. The physical situation is that the material behind the shock moves outward with a high velocity. Therefore, the material streams away from the center of the shock wave and creates a high vacuum near the center. The absence of any appreciable amount of material, together with the moderate size of the accelerations, immediately leads to the conclusion that the pressure must be very nearly constant in the region of low density. It is interesting to note that the pressure in that region is by no means zero, but is almost one-half of the pressure at the shock front.

"The concentration of material near the shock front and the corresponding evacuation of the region near the center is most pronounced for values of the specific heat ratio γ close to 1. It is well-known that the density at the shock increases by a factor

$$\frac{\rho_s}{\rho_\infty}=\frac{\gamma+1}{\gamma-1} \qquad (4\text{–}36)$$

This becomes infinite as γ approaches unity. Therefore, for γ near 1 the assumption that all material is concentrated near the shock front becomes more and more valid. The density near the center can be shown to behave as $(\gamma-1)/r^3$, where r is the radius.

"The idea of the method proposed here is to make repeated use of the fact that the material is concentrated near the shock front. As a consequence of this fact, the velocity of nearly all the material will be the same as the velocity of the material directly behind the front. Moreover, if γ is near 1, the material velocity behind the front is very nearly equal to the shock velocity itself; the two quantities differ only by a factor $2/(\gamma+1)$. The acceleration of almost all the material is then equal to the acceleration of the shock wave; knowing the acceleration one can calculate the pressure distribution in terms of the material coordinate; i.e., the amount of air inside a given radius. The calculation again is facilitated by the fact that nearly all the material is at the shock front and therefore has the same position in space (Eulerian coordinate).

"The procedure followed is then simply this: we start from the assumption that all material is concentrated at the shock front. We obtain the pressure distribution. From the relation between pressure and density along an adiabatic, we can obtain the density of each material element if we know its pressure at the present time as well as when it was first hit by the shock. By integration of the density we can then find a more accurate value for the

position of each mass element. This process could be repeated if required; it would then lead to a power series in powers of $\gamma - 1$.

"The method leads directly to a relation between the shock acceleration, the shock pressure, and the internal pressure near the center of the shock wave. In order to obtain a differential equation for the position of the shock as a function of time, we have to use two additional facts. One is the Hugoniot relation between shock pressure and shock velocity. The other is energy conservation in some form. In some applications such as that to the point source solution itself, we may use the conservation of the total energy which requires that the shock pressure decrease inversely as the cube of the shock radius (similarity law). On the other hand, if there is a central isothermal sphere no similarity law holds, but we may consider the adiabatic expansion of the isothermal sphere and thus determine the decrease of the central pressure as a function of the radius of the isothermal sphere. If we wish to apply the method to the case of variable γ without isothermal sphere, we may again use the conservation of total energy, but in this case the pressure will not be simply proportional to $1/Y^3$, where Y is the shock radius.

"As has already been indicated, the applications of the method are very numerous. The case of not very high shock pressures can also be included; in this case the density behind the shock wave does not have the limiting value of Eq. 4–36 but depends itself on the shock pressure. This does not prevent the application of our method as long as the density increase at the shock is still very large so that most of the material is still near the shock front.

"The only limitations of the method are its moderate accuracy and the possible complications of the numerical work. The accuracy seems satisfactory up to γ about 1.4. For the point source, a direct comparison with the exact solution is possible."

The most significant aspect of H. Bethe's solution is the fact that, although desired for conditions near $\gamma = 1$, it holds reasonably well for the case of $\gamma = 1.4$, the standard air value. The author shows that it agrees with von Neumann, if in von Neumann's solution γ is allowed to approach 1.

d. H. Bethe's, K. Fuchs' Solution for Small Blast Pressure

Ref. 7 is also the source of this theory. The purpose of the analysis was to provide an asymptotic solution that reduces to ordinary acoustic theory in the limit, as the radius of the blast sphere becomes large. Another reason given for the technique is that it may be used to indicate a suitable stopping point in a purely numerical computation. This point is reached when solution by machine has progressed sufficiently to make numerical techniques wasteful of machine time; because from this point, asymptotic, appropriate formulas are adequate. For further information, Ref. 7 should be consulted.

e. The Method of Kirkwood and Brinkley

Developed by the authors during World War II, this method differs in principle from those mentioned above, because the authors are specifically interested in the blast from high explosives rather than nuclear explosions. It is applicable to either air or water. The method is summarized in Ref. 5, and the original paper is listed herein as Ref. 8. The report is one in a long series on the same general subject by the same authors. Refs. 5 and 8 each give additional references.

The Kirkwood-Brinkley theory has become somewhat of a standard for high explosive work, and although experimental discrepancies have been reported, it still remains one of the best available means of approximating the physical occurrence of blast.

The theory is based upon nonviscous theory outside shock fronts, and uses the equations of motion and the equation of continuity in spherical coordinates. When these two equations are evaluated at the shock front, they represent two relations for the unknown radial velocity u and pressure P, and their derivatives. The Rankine-Hugoniot equation provides one more relationship, making three equations available. (It should be observed that the other Rankine-Hugoniot equations do not supply the needed information, for they introduce additional state variables.)

In developing the equations, the initial and boundary conditions are chosen to correspond to adiabatic explosion at constant volume. While these do not coincide exactly with real explosives, the inaccuracies introduced decrease with blast radius.

The fourth required relationship between the derivatives is achieved approximately by requiring that certain similarity conditions be satisfied. The authors point out in their basic report, Ref. 8, that it is futile to seek a fourth relation between the partial derivatives that does not involve a solution of the basic equations. They go on to show, however, that an approximate relationship can be achieved on physical grounds. The exact form of the relationship is discussed in detail in Ref. 3; physically, it amounts to choosing a functional form for the shape of the shock wave decay, and then determining unknown constants so that the basic equations are satisfied as nearly as possible. As the authors point out, such a procedure is similar to the Rayleigh method, in which an assumed solution is chosen, subject to the determination of constants.

The report concludes with a discussion of specific procedures for computing shock wave parameters. It should also be remarked that this theory is particularly suitable for extending measured data out to greater blast radii. This use, in fact, has become one of the major applications of the theory.

f. The Fictitious Viscosity Method of J. von Neumann and R. Richtmyer

In Ref. 9 von Neumann and Richtmyer introduce a significantly new concept for the calculation of flow fields bounded by, and containing, shock waves. A direct quotation from the introduction of this basic paper is appropriate

"In the investigation of phenomena arising in the flow of a compressible fluid, it is frequently desirable to solve the equations of fluid motion by stepwise numerical procedures, but the work is usually severely complicated by the presence of shocks. (10) The shocks manifest themselves mathematically as surfaces on which density, fluid velocity, temperature, entropy and the like have discontinuities; and clearly the partial differential equations governing the motion require boundary conditions connecting the values of these quantities on the two sides of each such surface. The necessary boundary conditions are, of course, supplied by the Rankine-Hugoniot equations, but their application is complicated because the shock surfaces are in motion relative to the network of points in space-time used for the numerical work, and the differential equations and boundary conditions are nonlinear. Furthermore, the motion of the surfaces is not known in advance but is governed by the differential equations and boundary conditions themselves. In consequence, the treatment of shocks requires lengthy computations (usually by trial and error) at each step, in time, of the calculation.

"We describe here a method for automatic treatment of shocks which avoids the necessity for application of any such boundary conditions. The approximations in it can be rendered as accurate as one wishes, by suitable choice of interval sizes and other parameters occurring in the method. It treats all shocks, correctly and automatically, whenever and wherever they may arise.

"The method utilizes the well-known effect on shocks of dissipative mechanisms, such as viscosity and heat conduction. (Lord Rayleigh (11) and G. I. Taylor (12) showed, on the basis of general thermodynamical considerations, that dissipation is necessarily present in shock waves. Later, R. Becker (13) gave a detailed discussion of the effects of heat conduction and viscosity. Recently, L. H. Thomas (14) has investigated these effects further in terms of the kinetic theory of gases.) When viscosity is taken into account, for example, the shocks are seen to be smeared out, so that the mathematical surfaces of discontinuity are replaced by thin layers in which pressure, density, temperature, etc., vary rapidly but continuously. Our idea is to introduce (artificial) dissipative terms into the equations so as to give the shocks a thickness comparable to (but preferably somewhat larger than) the spacing of the points of the network. Then the differential equations (more accurately, the

corresponding difference equations) may be used for the entire calculation, just as though there were no shocks at all. In the numerical results obtained, the shocks are immediately evident as near-discontinuities that move through the fluid with very nearly the correct speed and across which pressure, temperature, etc., have very nearly the correct jumps."

It should be noted that as useful as this concept is, it depends explicitly upon the numerical integration of the differential equations. The ability to carry out the numerical solutions has resulted from the great improvements in computers since World War II. Present day machines are not only much faster, but are more reliable.

It should be noted, too, that the present method is much more general than the other methods. Where the older methods assume the outward progress of the shock wave, they neglect the possibility (in most cases) of the formation of other, following shocks. In the present method, these additional shocks are automatically accounted for.

g. H. Brode's Application of the Fictitious Viscosity Method

H. Brode (Ref. 15) uses the fictitious viscosity method of Ref. 9 to carry through very complete solutions for the point source method. The author points out that solutions of the blast wave problem are available for point source-strong wave, and point source-weak wave. These are discussed in Ref. 7.

It will be recalled that mathematical difficulties lead to the need for simplifications in the early work. In particular, the shock problem of free boundaries presented an extremely difficult computational problem. With the disclosure of Ref. 9, complete new areas were opened for study and analysis. A detailed treatment of the point source case is given in Ref. 15. The paper outlines the approach and discusses the numerical integration scheme used. A very significant aspect of the paper is the presentation of a rather large number of numerical results. The presentation is given primarily in terms of nondimensional quantities from which detail calculations may be made. Following are some of the results presented in the report, either in the form of curves, explicit equations, or both.

1. Particle velocity at the shock front vs radius parameter.
2. Overpressure at the shock front vs radius parameter.
3. Dynamic pressure at the shock front vs radius parameter.
4. Pressure within the flow field as a function of time and distance, in terms of a time parameter and a radius parameter.
5. Particle velocity as a function of position and time.
6. Density as a function of position and time.
7. Positive and negative phase duration. That is, the times during which the overpressure is positive or negative.
8. Positive impulse.
9. Negative impulse.

In these presentations, nondimensional units for time and distance are normally used, so that the curves may be used for many cases of interest.

From both a theoretical and practical computational viewpoint, this paper is highly recommended as a working tool for blast computations. The paper concludes by examining the case of a finite-size source, and remarks on the basic differences in the mathematical models represented by the point and finite-size sources.

h. H. Brode's Application of the Fictitious Viscosity Method to a Finite-Size Charge of High Explosive

H. Brode's work on solutions of the point source method (Ref. 15) were extended to include the case of a finite-size sphere of high explosive as the initiating energy source (Ref. 16). The hydrodynamic equations were solved numerically, using the artificial viscosity concept. Results are presented graphically in most cases. The author also points out the significant fact that scaling laws are less appropriate in a blast computation based on a finite-size high explosive charge. This is true because the boundary conditions depend on the mass of the HE, and the effects, it has been found, extend out to low pressure levels. The

author presents as a working rule that usual scaling methods (Sachs) will be adequate only when the radius of the primary shock sphere is equal to or greater than that necessary to enclose a mass of air equal to ten times the initial mass of HE.

4-2.3.6. *Scaling and Damage Parameters*

The parameters of interest in blast computations, discussed in previous paragraphs (see also Ch. 2, Sec. IV) are listed and summarized at this point. The parameters of greatest interest are those which relate directly to damage. It has been found that these include peak pressure, positive duration, negative duration, positive impulse, negative impulse, peak negative pressure, and dynamic pressure. The peak pressure is most obvious. It corresponds to the value of the pressure given by the passage of the main shock wave. The other quantities are defined in the following way.

Consider a specified point in space. At this point, the pressure will vary with time after the passing of the initial shock wave. The time during which the pressure is positive relative to initial ambient pressure is called the duration of the positive phase, and is denoted by D^+_p. (Static pressure minus ambient static pressure is defined as excess pressure.) A similar definition is given for the time during which the excess pressure is negative. This time is called the duration of the negative phase, and it is denoted by D^-_p. Sometimes the terms, duration of the positive (or negative) phase for particle velocity, are used. They are frequently denoted by D^+_u and D^-_u, and are the times during which the particle velocity at a given point is either positive or negative.

The dynamic pressure (per unit mass is implied) is defined as $1/2\rho\, u^2$, where ρ is density and u is the particle velocity. It should be noted that these are both functions of time and position.

The impulse quantities are important in estimating damage; they are defined by the relations,

$$I^+_p = \int_0^{D^+_p} \Delta P\, dt = \text{Positive Impulse} \qquad (4\text{-}37)$$

where ΔP is the positive overpressure, and D^+_p has been defined. It is also of interest to define the integral of the dynamic pressure. It is given by

$$I^+_u = \tfrac{1}{2}\int_0^{D^+_u} \rho u^2 dt = \text{Dynamic Impulse.} \qquad (4\text{-}38)$$

The negative impulse is defined by

$$I^-_p = \int_0^{D^-_p} (\Delta P)\, dt. \qquad (4\text{-}39)$$

Brode, in Ref. 15, states that the negative impulse can be approximated to an accuracy of within 5 per cent by

$$I^-_p = \tfrac{1}{2}\,(\Delta P_-)\,(D^-_p) \qquad (4\text{-}40)$$

where (ΔP_-) is negative excess pressure as a function of time.

It should be emphasized that all of these quantities are functions of both position and time (except, ΔP maximum and minimum). Normally, they are evaluated at a fixed point in space as a function of time. The numerical values so determined will be different at different points of space.

The shock wave and flow field parameters may be calculated for any particular case by using the formulas and curves of Refs. 7, 15, and 16, for example. In particular, the graphical presentations given in the latter two references are quite complete. In using the curves and formulas, however, attention should be given to the stated range of applicability of the data.

4-2.4. (U) Scaling Laws

4-2.4.1. *Introduction*

Considering the difficulty, time, and expense of conducting explosive tests, it is highly desirable to have analytical techniques for predicting blast effects. In previous paragraphs some of the various techniques were outlined. An alternative approach which has proven very successful is the development of scaling laws. These laws depend on similarity considerations to provide formulas by which blast effects can be predicted for a given set of conditions if the

blast effects for some other set of conditions are known. The great utility of such formulas is obvious.

In these paragraphs the fundamental scaling laws of Ref. 17 will be deduced and briefly discussed. Although the results are the same, the method of derivation presented herein differs from that given in the reference. A relatively complete derivation is presented, because a discussion sufficiently elementary to satisfy the aims of the text does not appear to be available in the literature.*

The deduction of the scaling laws will be based on dimensional considerations. That is, the equation which determines the functional relationship between the blast parameters must be dimensionally homogeneous. An equation is said to be dimensionally homogeneous if the form of the equation does not depend on the units of measurement. Thus, taking a simple example from Ref. 18, the equation for the period of a pendulum,

$$T=2\pi\sqrt{L/g}$$

is true no matter what units are used to measure time and length. Time may be measured in days, seconds, years, etc., and lengths may be measured in feet, inches, centimeters, etc. However, if g of the equation is given the value 32.2, the equation is no longer dimensionally homogeneous, because the number 32.2 implies that length is measured in feet and time in seconds. Noting that the pendulum equation may be written

$$T/\sqrt{L/g}=2\pi$$

it is seen that $T/\sqrt{L/g}$ is a dimensionless grouping of the variables involved.

4-2.4.2. *Buckingham's Theorem*

From the discussion of the preceding paragraph it may be inferred that any dimensionally homogeneous equation can be reduced to a relationship between one or more dimensionless products. This is, in fact, the case. A somewhat stronger statement is the well-known Buckingham Theorem; the following formulation being taken directly from Ref. 18, where a proof of the theorem may be found.

Buckingham's Theorem states that if an equation is dimensionally homogeneous, it can be reduced to a relationship among a complete set of dimensionless products. In order to discuss this theorem, we note that any formula depends on certain variables. If these variables are grouped into a product such that the fundamental dimensions mass (M) length (L) and time (T) all cancel identically, then this grouping of variables is called a dimensionless product. In the pendulum example just given, the product $T/\sqrt{L/g}$ is a dimensionless product, because in terms of the fundamental dimensions of length (L) and time (T), we have

$$T/\sqrt{L/g}\sim\frac{T}{L^{1/2}\;\dfrac{1}{\left[\dfrac{L^{1/2}}{(T^2)^{1/2}}\right]}}=1$$

where the symbol "$\sim$" is used to mean, "the dimensions of."

A set of dimensionless products of given variables is said to be complete if each product in the set is independent of the others, and if every other dimensionless product involving the same variables can be formed by products or powers of members of the set.

At this point in the discussion it is postulated that every equation which describes a physical situation correctly must be dimensionally homogeneous. (In this connection, refer to the discussion in Ref. 18.)

4-2.4.3. *An Applied Example of Buckingham's Theorem*

In order to apply Buckingham's Theorem to a physical problem, it is first necessary to define the set of variables involved. This is usually not an easy task, because a complete knowledge of all variables involved would imply a thorough understanding of all the physical processes involved. In many cases the task is simplified, however, because experience will have shown that certain variables are important, but that others are relatively unimportant for the application contemplated and can be neglected.

* The basis of these paragraphs on scaling laws is an original treatment by Dr. Louis F. Doty, compiled expressly for inclusion in this publication.

To illustrate the point, consider the resistance to an object moving through the air. Both theory and experiment show that the resistance depends on the shape of the object, the air density, the velocity, the air viscosity, and the compressibility of the air. However, it is also known that if the speed is neither too high nor too low, the effects of viscosity and compressibility, as variables of the problem, can be neglected. Accordingly, for the degree of approximation considered, the equation

$$F = f(\rho, V, D)$$

may be written, where f is a general, unknown, functional relationship stating that the resistance F depends on the density ρ, the speed V, and a characteristic length D (for a set of geometrically similar objects). No indication of how ρ, V, and D are involved in the function is implied, as yet. One way of determining the functional relationship is to set up and solve the appropriate physical equations, based on the laws of mechanics, thermodynamics, etc. Since such solutions are frequently very difficult to obtain, it is worthwhile considering if any other information exists which will help formulate the functional relationship. It is a remarkable fact that the requirement of dimensional homogeneity, alone, is often sufficient to provide a partial solution to the problem.

As an example, consider again the functional form

$$F = f(\rho, V, D)$$

in which the variables have been previously defined. In order to satisfy the requirements of dimensional homogeneity, the variables will be grouped into dimensionless products as required by Buckingham's Theorem. To do this it will be sufficient to eliminate the dimensions of mass (M), length (L), and time (T) from both sides of the equation. This will be accomplished one step at a time, by dividing both sides of the equation by a variable or combination of variables which eliminates the dimension under consideration. First, note that the variables have the following dimensions,

F = force $\sim MLT^{-2}$
ρ = density $\sim ML^{-3}$
V = speed $\sim LT^{-1}$
D = length $\sim L$

where, as before, the symbol "$\sim$" denotes "has the dimensions of." Next, note that Newton's law,

force = mass × acceleration

or

$$F \sim M\left(\frac{L}{T^2}\right) = MLT^{-2}$$

has been used to relate force to the fundamental units of mass, length, and time. Inspection of the equation and the dimension of each variable shows that mass occurs to the first power in F and ρ. Hence, if both sides of the equation are divided by ρ, mass will be eliminated on the left side. Thus,

$$\frac{F}{\rho} = \frac{1}{\rho} f(\rho, V, D).$$

Since V and D do not contain mass, they will be unaffected. Further, because dimensional homogeneity is required, any mass terms must be removed from the right side as they were from the left. Accordingly, the mass term (density in this case) on the right side must cancel itself identically, because there cannot be a single mass term in the equation and still preserve homogeneity. Thus,

$$\frac{1}{\rho} f(\rho, V, D) = \psi(V, D)$$

where ψ is another arbitrary function. Since the functional form is arbitrary we may continue to use the symbol f for brevity, without fear of confusion. The equation with mass eliminated as an explicitly appearing variable now reads,

$$\frac{F}{\rho} = f(V, D)$$

in which it is observed that the dimensions of F/ρ are

$$\frac{F}{\rho} \quad \frac{MLT^{-2}}{ML^{-3}} = L^4T^{-2}.$$

Length will next be eliminated from the equation. On the right side, both V and D involve length. The length dimension may be eliminated by using either of these; for illus-

tration, D will be used. Dividing both sides by D^2, to eliminate length from F/ρ, gives

$$\frac{F}{\rho D^2}=\frac{1}{D^2}f(V,D)$$

but since V involves length to the first power, the equation is written as

$$f(V,D)=f\left(\frac{V}{D}\cdot D,D\right)$$

where V/D is now free of the length dimension, resulting in

$$\frac{F}{\rho D^2}=\frac{1}{D^2}f\left(\frac{V}{D}\cdot D,D\right)=\psi\left(\frac{V}{D},D\right).$$

Once again, the right side must be independent of D because it is the only length term in the equation. Therefore, the dimension length must cancel from the right side identically, giving

$$\frac{F}{\rho D^2}=f\left(\frac{V}{D}\right).$$

The next dimension of concern is time. Observing that the dimension of $\frac{F}{\rho D^2}$ is

$$\frac{F}{\rho D^2}\sim L^4 T^{-2}\frac{1}{L^4}=T^{-2}$$

and the dimension of V/D is

$$\frac{V}{D}\sim T^{-1}$$

the time dimension is eliminated by dividing by $(\frac{V}{D})^2$, resulting in

$$\frac{F}{\rho D^2\left(\frac{V^2}{D^2}\right)}=\frac{1}{\left(\frac{V}{D}\right)^2}f\left(\frac{V}{D}\right)=\psi\left(\frac{V}{D}\right)$$

Since the left side is now free of all dimensions, the right side must be also, and (V/D) must cancel identically. Writing $f(1)$ to denote a dimensionless quantity, the final result upon solving for F is

$$F=\rho D^2 V^2 f(1)$$

which gives the relationship that must be satisfied by the variables. (The technique of dimensional analysis which has been described herein is given in Ref. 19. Although it is a known, and particularly straightforward technique, it does not appear to be well-known in the engineering literature.) The constant $f(1)$ may be determined by experiment, and it is known that F depends upon the product $(\rho D^2 V^2)$, in the particular combination given, and is not dependent upon purely arbitrary values of ρ, D, or V. In other words, the result states that individual variations in ρ, V, or D do not affect the value of F, provided the product $\rho D^2 V^2$ remains the same.

This example serves to demonstrate the great power of dimensional homogeneity. It serves, also, to demonstrate the necessity of a prior knowledge of the physical variables involved. For example, suppose experiments were conducted on a set of geometrically similar objects acting at different speeds. If the speed range is one where compressibility and viscosity are unimportant, it is found that $F/\rho D^2 V^2$ remains a constant for different combinations of ρ, V, and D. Next, suppose that the test speeds are successively increased. A point will be reached at which

$$\frac{F}{\rho D^2 V^2}=f(1)$$

no longer is a constant, but becomes a function of something. Dimensional considerations, alone, will give no clue as to the identity of the unknown dependence. However, if the basic differential equations of compressible flow are inspected, it is seen that the speed of sound, a, is a measure of compressibility. With this understanding, the equation is written as

$$F=f(\rho, V, D, a)$$

where it is now assumed that the term a is an important parameter of the problem. If dimensionless products are formed, as illustrated above, it is found that

$$F=\rho D^2 V^2 f\left(\frac{V}{a}\right)$$

where the function f is now not a constant, but is a function of the ratio of the speed to the speed of sound. The quantity (V/a) is called the Mach number.

A set of experiments will now yield the result that f, although not a constant, depends only on the ratio (V/a), rather than on V or a alone. Furthermore, dimensional considerations have shown that f does not depend on ρ. It is now seen that dimensional considerations combined with a knowledge of the physics of the problem have produced a remarkably useful result. For an entire family of similar objects, $\frac{F}{\rho D^2 V^2}$ may be plotted against $\frac{V}{a}$ to provide a single curve (of the form shown in Fig. 4–11) which is valid for presenting resistance data over a wide range of speeds.

The simple example just described serves to introduce the technique of dimensional homogeneity. It also points up the need for caution in the use of the technique with blast scaling laws: these laws should be used only within the range of their demonstrated validity. Expressed in another fashion, if parameters not accounted for in the blast analysis become important under certain conditions, the analysis can not provide good results under these conditions.

4–2.4.4. *Deduction of Blast Scaling Laws*

The scaling technique in blast analysis is used to predict performance from the analyzed results of previous tests. The anayized data is used with general equations (scaling laws) which are established for each blast parameter of interest.

Suppose it is desired to develop a scaling law for the pressure in the fluid following the passage of a shock front caused by a blast. From a study of the differential equations of fluid flow, and with a knowledge of the physical phenomena involved, it is reasonable to assume that the pressure at any time and position, following the passage of a spherical shock front, depends upon the following variables:

P = pressure in the fluid $\sim \frac{MLT^{-2}}{L^2} = ML^{-1}T^{-2}$

P_o = ambient pressure of fluid before blast $\sim ML^{-1}T^{-2}$

E_o = internal energy of the explosive $\sim MLT^{-2}L = ML^2T^{-2}$

θ_o = ambient temperature of fluid before blast $\sim \frac{P}{\rho} \sim L^2T^{-2}$

R = distance from blast point $\sim L$

t = time after blast $\sim T$.

It is noted that temperature, θ_o, is not an independent dimension, but is related to density and pressure by an equation of state. The functional relationship may be written

$$P = f(P_o, E_o, \theta_o, R, t)$$

where all variables have been defined. Using the technique described in preceding paragraphs for forming dimensionless products, the dimensions, mass, length, and time, are eliminated, in that order, to give the following sequence of equations:

$$\frac{P}{P_o} = f\left(\frac{E_o}{P_o}, \theta_o, R, t\right)$$

$$\frac{P}{P_o} \sim 1, \qquad \frac{E_o}{P_o} \sim L^3$$

$$\frac{P}{P_o} = f\left(\frac{E_o}{R^3 P_o}, \frac{\theta_o}{R^2}, t\right)$$

$$\frac{E_o}{R^3 P_o} \sim 1, \frac{\theta_o}{R^2} \sim T^{-2}$$

$$\frac{P}{P_o} = f\left(\frac{E_o}{R^3 P_o}, \frac{\theta_o t^2}{R^2}\right)$$

$$\frac{\theta_o t^2}{R^2} \sim 1$$

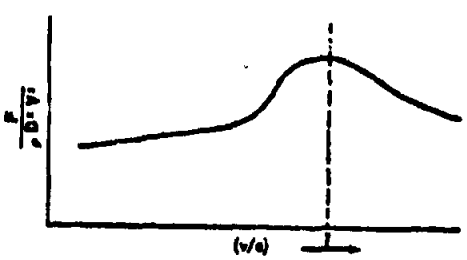

Figure 4–11. Resistance vs Mach Number

Note, that in applying the method of dimensional homogeneity, the equation

$$\frac{P}{P_o} = f\left(\frac{E_o}{R^3 P_o}, \frac{\theta_o}{R^2}, t\right)$$

was obtained by eliminating the dimension of length from the previous equation. The previously discussed argument was used, that R must cancel itself identically from the equation; otherwise, it would be the only term on either side of the equation containing the dimension length. This clearly would violate the requirement of dimensional homogeneity. In the same equation, the dimension of time occurs on the right side, but not on the left side. There is no violation of principle, however, since there is more than one term on the right side containing the dimension time, and the requirement of identical canceling does not exist. That is, identical canceling is required only when one term would otherwise remain in the entire equation.

It may be seen that the dimensionless products of the last equation are independent, because each contains a variable not contained in the others. Further, because the original six variables were combined by eliminating three dimensions, it is reasonable to expect three dimensionless products. For convenience, let these dimensionless products be called π to connote an absence of dimensions, and give them distinguishing subscripts. Thus, let

$$\pi_1 = \frac{P}{P_o}$$

$$\pi_2 = \frac{E_o}{R^3 P_o}$$

$$\pi_3 = \frac{\theta_o t^2}{R^2}$$

These π's satisfy the requirements of Buckingham's Theorem, but the theorem alone will give no further aid in determining the best form for presentation of results. That is, while π_1, π_2, π_3 are a complete set, they are not necessarily the most useful such set. *Different* complete sets may be derived by combining π_1, π_2, and π_3, and the most useful set can be selected only after a study of the physics of the problem.

The equations in this particular case are the equations of fluid flow. These are partial differential equations in which distances and time are each independent variables, and p is a dependent variable. Further, E_o, P_o, and θ_o are known conditions in any test. These comments imply a desirability of having, if possible, a complete set of π's, each of which contains only p, t, or R, together with the known variables. Note that π_1 and π_2 each satisfy this aim, but π_3 does not, because it contains both t and R. This may be remedied by solving π_2 for R and substituting that value in π_3. A more symetrical set is given by Sachs in Ref. 17. His groupings can be arrived at in the following way; let

$$\pi_4 = \left(\frac{1}{\pi_2}\right)^{1/3} = \left(\frac{P_o}{E_o}\right)^{1/3} R$$

$$\pi_5 = \pi_3^{1/2} = \left(\frac{t}{R}\right)\theta_o^{1/2}$$

$$\pi_6 = \pi_4 \pi_5 = \left(\frac{P_o}{E_o}\right)^{1/3} \theta^{1/2} t.$$

Then, taking π_1, π_4, and π_6 as the complete set, we have

$$\pi_1 = f(\pi_4, \pi_6)$$

or

$$\frac{P}{P_o} = f\left[\left(\frac{P_o}{E_o}\right)^{1/3} R, \left(\frac{P_o}{E_o}\right)^{1/3} \cdot \theta_o^{1/2} \cdot t\right]. \tag{4-41}$$

The last equation is the famous Sachs scaling law, given for the first time in Ref. 17. It is noted that Ref. 17 interprets E_o as the weight of explosive, W_o. This is an equivalent statement, for W_o is certainly proportional to E_o for a given class of explosives.

It is emphasized that the scaling laws were derived for free air bursts. They are applicable to bursts in the presence of ground reflections only by proper allowance for the reflection effect. For a discussion of these effects, Ref. 17, and the reports listed in the bibliography may be consulted.

In words, the scaling law, Eq. 4-41, states that the pressure measured in units of ambient pressure is the same for all conditions which make the functional relationship have the same numerical value. This will certainly be true

if each argument of the function has the same value for the set of conditions under consideration. Thus, P/P_o will have the same value for two different sets of conditions, provided $(P_o/E_o)^{1/3}\,\theta_o^{1/2}t$ have the same value in each condition. Specifically, suppose two successive tests are conducted, and let the two tests be designated by "a" and "b," respectively. Similarity then requires that the pressure ratio will be the same in each test, at corresponding positions and times given by

$$\frac{(P_o)_a^{1/3}}{(E_o)_a^{1/3}}R_a = \frac{(P_o)_b^{1/3}}{(E_o)_b^{1/3}}R_b \qquad (4\text{-}42)$$

$$(\theta_o)_a^{1/2}\frac{(P_o)_a^{1/3}}{(E_o)_a^{1/3}}t_a = (\theta_o)_b^{1/2}\frac{(P_o)_b^{1/3}}{(E_o)_b^{1/3}}t_b. \qquad (4\text{-}43)$$

Several conclusions may be inferred from these scaling laws. Dividing the first equation by the second gives

$$\frac{R_a}{(\theta_o)_a^{1/2}t_a} = \frac{R_b}{(\theta_o)_b^{1/2}t_b}.$$

Suppose, for example, that test "b" is conducted and that test "a" is then conducted under the same ambient temperature conditions; the scaling law reduces to

$$\frac{R_a}{t_a} = \frac{R_b}{t_b}$$

This equation states that if the pressure ratio P/P_o is observed at distance R_b from explosion "b" at time t_b, then the same pressure ratio would be observed at distance R_a from explosion "a" at time t_a. Since R is the distance the pressure wave travels in time t, R/t is the speed of the wave. Thus, waves from two different explosions travel at the same speed, provided the ambient temperature is the same in both cases. This would be expected from acoustic theory. If the ambient temperatures are different in the two tests, we have

$$V_a = \left(\frac{\theta_{o_a}}{\theta_{o_b}}\right)^{1/2} V_b \qquad (4\text{-}44)$$

where V has been written for R/t. This equation states that the speed of the wave varies directly as the square root of the absolute temperature. This is also in agreement with acoustic theory, which derives the fact that the speed of sound varies directly with the square root of the absolute temperature.

These considerations show that the scaling law, with respect to the speed of transmission, behaves correctly when the blast wave has moved sufficiently far from the source to be moving at a speed near the speed of sound. Conversely, the scaling law would be expected to be less reliable in the close vicinity of the explosion, where the blast wave is moving much faster than a sound wave.

Returning to Eqs. 4-42 and 4-43, the relationships are more clearly displayed by rewriting the equations in the form

$$\frac{R_a}{R_b} = \left(\frac{P_{o_b}}{P_{o_a}}\right)^{1/3}\left(\frac{E_{o_a}}{E_{o_b}}\right)^{1/3} \qquad (4\text{-}45)$$

$$\frac{t_a}{t_b} = \left(\frac{\theta_{o_b}}{\theta_{o_a}}\right)^{1/2}\left(\frac{P_{o_b}}{P_{o_a}}\right)^{1/3}\left(\frac{E_{o_a}}{E_{o_b}}\right)^{1/3} \qquad (4\text{-}46)$$

Considering a numerical example, suppose an explosion "b" occurs which is caused by a charge of energy (or weight) E_{o_b}, under the ambient condition $(P_o)_b$ and $(\theta_o)_b$; the pressure (P/P_o) of this explosion is observed to occur at distance R_b from the charge, at time t_b. Now, let an explosion "a" occur in which (as a numerical example) the charge is three times as great, the ambient pressure is one-half, and the ambient absolute temperature is eighty per cent of the value of test "b". Then the pressure ratio (P/P_o) will be numerically the same at the distance ratio

$$\left(\frac{R_a}{R_b}\right) = (2)^{1/3}(3)^{1/3} = 1.82$$

and at the time ratio

$$\left(\frac{t_a}{t_b}\right) = \left(\frac{1}{0.8}\right)^{1/2}(2)^{1/3}(3)^{1/3} = 2.04.$$

Thus (for example) if $(P_o)_b$ is 115 pounds per square inch and $(P)_b$ is 18 pounds per square inch, and if the ratio $\left(\frac{P}{P_o}\right)_b = \frac{18}{15} = 1.2$ is observed to occur at a distance $R_b = 6{,}000$ feet,

at time t_b = 5 seconds after the explosion: then the same pressure ratio will be observed in the "a" explosion at a distance of

$$R_a = 1.22\ (6{,}000) = 10{,}900 \text{ feet}$$

at a time after "a" explosion of

$$t_a = 2.04\ (5) = 10.2 \text{ seconds.}$$

In order that the pressure ratio be the same, the actual pressure in the "a" explosion observed at R_a, t_a, is

$$P_a = \left(\frac{P}{P_o}\right)_a \cdot P_{o_a} = \left(\frac{P}{P_o}\right)_b P_{o_a}.$$

In the statement of the problem, it was given that $P_{o_a} = \frac{1}{2} P_{o_b} = 7.5$ pounds per square inch. Expressed numerically, therefore, the result is

$$P_a = 1.2\ (7.5) = 9.0 \text{ pounds per square inch.}$$

To consider another example, let the ambient temperature be the same in both cases. This means that the speed of wave transmission is the same at the scaled distance, R_a, as it is at the reference distance, R_b. The direction of the positive (or negative) phase of pressure will, therefore, be the same in both explosions. In this case, the impulse computed at the scaled distance R_a is related to the impulse at the reference distance R_b, by the relation,

$$I_a = I_b \left(\frac{E_{o_a}}{E_{o_b}}\right)^{1/3}$$

for the same ambient temperature and pressure. (The impulse is the excess pressure integrated over the time interval of positive pressure duration.)

If both ambient pressure and temperature are different in the "a" and "b" explosions, an expression for I can be developed from the first principles. Since impulse is an integrated phenomenon, it does not explicitly depend on the time, and the functional relation may be written

$$I = f\ (P_o, E_o, \theta_o, R)$$

where all independent variables have been defined, and impulse is defined as the integral of pressure over a time interval. Its units are, therefore, given by, $ML^{-1}T^{-1}$. Proceeding in the manner previously discussed, dimensional homogeneity requires that

$$\frac{I}{P_o}\frac{(\theta_o)^{1/2}}{R} = f\left(\frac{E_o}{P_o R^3}\right)$$

and there are two non-dimensional groupings. A more useful set is obtained by using the cube root of the parameter $E_o/P_o R^3$, and by then eliminating R from the other parameter. The final result may be expressed as

$$\frac{I(\theta_o)^{1/2}}{P_o^{2/3} E_o^{1/3}} = f\left(\frac{P_o^{1/3}}{E_o^{1/3}} R\right)$$

in which it is seen that the parameter $\frac{P_o^{1/3}}{E_o^{1/3}} R$ is retained in the same form as in the previous formula. Impulse scaling, therefore, requires that

$$\frac{I_a}{I_b} = \left(\frac{P_{o_a}}{P_{o_b}}\right)^{1/3} \left(\frac{E_{o_a}}{E_{o_b}}\right)^{1/3} \left(\frac{\theta_o}{\theta_{o_a}}\right)^{1/2}$$

for a given value of $\frac{P_o^{1/3}}{E_o^{1/3}} R$. In this formula, as before, "a" and "b" denote two different explosions.

By virtue of the assumptions made in the derivation of the scaling laws, they should be equally applicable to nuclear explosions as well as to chemical explosions. Numerous experiments have verified that this is true, at least approximately. Further discussion of scaling of the type discussed herein is given in Refs. 1 and 20.

Information of a somewhat different nature may also be obtained from the scaling law, Eq. 4-41. For example, if the interest is in the peak pressure, time is not a parameter of the problem, and the scaling law reduces to

$$\frac{P_m}{P_o} = f\left[\left(\frac{P_o}{E_o}\right)^{1/3} R\right] \qquad (4\text{-}47)$$

where P_m is the peak pressure observed at a particular radius R.

The scaling law given in Ref. 17 states, that the pressure ratio (P_m/P_o) will be observed to have the same value for any explosion in which the dimensionless parameter, $\left(\frac{P_o}{E_o}\right)^{1/3} R$, has

the same value. Obviously, then, for a given ambient pressure and charge, P_m will vary with R. Dimensional considerations alone will not establish this functional relationship; however, dimensional considerations may be used to generalize an experiment in the following way.

Suppose that a charge is exploded and that the peak pressure is measured at a set of stations at varying distances from the charge. If an empirical equation is deduced from corresponding P_m and R data, dimensional homogeneity requires (P_m/P_o) and $\left(\frac{P_o}{E_o}\right)^{1/3} R$ to be the parameters of the problem. As an example, if an empirical law of the form

$$P_m = K/R^{3/2}$$

(where K is a known numerical constant) fits the data of the particular test, dimensional homogeneity permits the equation to be written,

$$\frac{P_m}{P_o} = \frac{K_1}{\left[\left(\frac{P_o}{E_o}\right)^{1/3} R\right]^{3/2}}$$

where K_1 is a non-dimensional constant to be determined. Evaluating P_o and E_o in this last equation for the conditions of the test, write

$$P_m = K_1 K_2/R^{3/2}$$

where K_2 is a known numerical value given by

$$K_2 = \left[\frac{P_o}{\left(\frac{P_o}{E_o}\right)^{1/3}}\right] \text{ test conditions}$$

Then, from the two equations for P_m

$$K = K_1 K_2.$$

From this is obtained

$$K_1 = K/K_2$$

in which K and K_2 are known. The generalized equation may then be written as

$$\frac{P_m}{P_o} = \frac{K_1}{\left(\frac{P_o}{E_o}\right)^{1/3} \cdot R^{3/2}}$$

where K_1 is now a known non-dimensional constant. This equation may now be used for various conditions of P_o and E_o, and it is seen that dimensional considerations have permitted a useful generalization of a single test.

In spite of the great utility of the Sachs scaling laws, it should not be inferred that all blast phenomena can be predicted from them. It has been shown that their derivation is based on simple assumptions that neglect the finite burning time of a finite size charge, the possibility of secondary shock waves (which are known to exist), and numerous other effects that are most pronounced in the vicinity of the charge. From these considerations, one would not expect perfect scaling in all cases. However, it is an established experimental fact that the laws are remarkably accurate for a great many practical predictions.

4–2.5. (U) Effects of Environment on Blast Wave Parameters for Nuclear Explosions

4–2.5.1. *Effects of Altitude*

The relations between overpressure, distance, and time that describe the propagation of a blast wave in air depend upon the ambient atmospheric conditions, which vary with altitude. In discussing the effects of altitude on blast phenomena, two cases will be considered: the point of burst and the target are at the same altitude; and the point of burst and the target are at different altitudes.

For a surface burst (the first case), the peak overpressures at a given distance from the explosion will depend on the ambient atmospheric pressure. This will vary with the height above sea level of the surface at the point of burst. With increasing altitude of both target and burst point, the overpressure at a given distance from ground zero will decrease. Correspondingly, an increase may be expected in the arrival time of the shock front and in the duration of the positive phase.

The effect when the burst and the target are at different altitudes is considerably more complex. Since the blast wave is influenced by any changes in air temperature and the pressure of the atmosphere through which it travels, variations occur in the pressure-distance relationship at the surface. Within the range of significant damaging overpressures, these variations are

small if the energy yield of the weapon is low. However, for large weapons, where the blast wave travels over appreciably longer distances, significant variations may be expected. In order to make precise calculations, a detailed knowledge of the atmosphere on the day of detonation would be necessary (Ref. 1). For a mathematical discussion of the effects of altitude, refer to Par. 1-2.1.

4–2.5.2. *Effects of Topography*

Hilly land masses tend to both increase and decrease air blast effects, dependent on the conditions. The increase or decrease of peak overpressure values seems to depend on the change in slope of the land mass from the horizontal. On the forward side of very steep slopes there may be a sharp increase of peak overpressure (up to a factor of two), for a short duration, as a result of the reflection process. A reduction in peak overpressure may be expected on the reverse side of very steep slopes. In general, the variation in peak overpressure at any point on a hill, from that expected if the hill were not present, depends on the size of the hill and its orientation with ground zero. The effects of terrain are not expected to be a significant factor in the damage caused to many types of structures, because the time interval in which the pressure increases or decreases is short compared with the duration of the positive pressure phase.

It is also important to emphasize that blast effects are not dependent upon line-of-sight considerations. The fact that the point of explosion cannot be seen from behind an obstruction by no means implies that the blast wave cannot be felt. Blast waves can easily diffract (bend) around apparent obstructions.

The departure from idealized or flat terrain presented by a city complex may be considered as an aspect of topography. It is to be expected that the presence of many closely grouped buildings will cause local changes in the blast wave and, in particular, the dynamic pressure. Although some shielding may result at certain points because of intervening objects and structures, in other areas multiple reflections between buildings, and channeling caused by streets, may tend to actually increase the overpressure and dynamic pressure. On the whole, it is expected that the local increases in damage will largely offset the local decreases in damage, and the resulting effect of structural protection will be relatively small (Ref. 1).

4–2.5.3. *Effects of Surface Conditions*

For a given height of burst and energy yield, variations in the blast wave characteristics will occur which are caused by the type of surface over which the weapon is detonated. A certain amount of energy loss will occur for low air or surface bursts where a shock wave is produced in the ground. For air bursts, the nature of the reflecting surface can affect the pressure-distance relationship and the development and growth of the Mach stem. These mechanical effects on the blast wave, however, are rather small, and have little influence on the damage-producing characteristics of the blast phenomena.

Particulate matter, such as rocks, boulders, etc., picked up and carried along by the blast front, may cause additional damage to the target. These objects do not necessarily affect the overpressures at the wave front, although in extremely dusty areas, enough foreign matter may be present to affect the dynamic pressure to a certain degree. The end effect on the target would, however, be of little consequence.

If the explosion occurs moderately near the surface, some of the energy is transferred into the ground. As a result, a minor oscillation of the surface is experienced and a mild ground-shock wave is produced. The pressure acting on the earth's surface is transmitted downward, with the principal stress in the soil being nearly vertical and approximately equal in magnitude to the air blast overpressure. For relatively high air bursts, where large blast pressures do not occur at ground zero, the effects of ground shock will be negligible. In the case of a surface burst where cratering occurs, the situation is quite different (Ref. 1). Cratering is discussed in Par. 4–3.3.1, following.

4–2.5.4. *Effects of Meteorological Conditions*

Moisture in the air and air temperatures are considered here in terms of their effects on blast. Although the presence of large amounts

of moisture in the atmosphere may affect the properties of a blast wave in the low overpressure regions, the probability of encountering proportions of water vapor significant enough to influence the amount of damage is considered to be quite small.

Differences in temperature of the atmospheric layers have been noted as causing some interesting blast effects. Window breakage, light structural damage, and noise have been experienced at distances great enough so that these effects were not expected, under suitable meteorological conditions. These phenomena are caused by the atmosphere bending the blast waves back to earth, in one of several ways.

If there is a decrease in air temperature at increasing distance from the ground, such as usually occurs in the daytime, combined with a wind whose velocity increases at a rate of more than three miles per hour for each 1,000-foot increase in altitude, the blast wave will be reflected back to the ground before it has risen more than a few thousand feet. When the conditions are such that several shock rays converge at one location, the blast energy concentrated at this position is greatly intensified. Under usual atmospheric conditions the direct striking focus is limited to a distance of about eight or ten miles from the explosion; but under these conditions, the blast energy may be refocused and cause damage at much greater distances.

A similar enhancement of pressure and noise has occurred at even greater distances from large explosions. This has been attributed to downward refraction and focusing of the shock rays by a layer of relatively warm air. The warm air layer is generally referred to as the ozonosphere, and is situated at a height of from 25 to 40 miles. Repeated reflection by the ground and refraction by the ozonosphere, causes the shock pattern to be repeated at intervals, thus greatly extending the effective radius of the shock wave (Ref. 1).

4–2.6. (S) Presentation of Nuclear Blast Data

4–2.6.1. (U) General

This paragraph provides representative examples of nuclear-blast, reference-data graphs, such as are used to estimate the damage which might be expected to occur at a particular range from a given explosion. From graphs and curves such as these, the values of blast wave properties at the surface can be calculated, and the results can be used to determine the loading and response of a certain target (Ref. 21).

The graphs (Figs. 4–12 through 4–15) present the properties of the blast wave for a one-kiloton nuclear explosion in free air, at standard atmospheric conditions, as a function of slant range. Instructions are provided for the use of each figure, and an example is given to illustrate their use.

Reference should be made to TM 23–200 (Ref. 21), which provides comprehensive, graphic coverage of the significant nuclear blast wave properties.

In addition, Par. 4–2.6.6., following, presents a discussion of scaling between high-explosive (Pentolite) and nuclear explosions.

4–2.6.2. (C) *Instructions for Using Fig. 4–12, Time of Arrival of Shock Front*

a. Scaling Procedure

To calculate the distance and time of shock arrival for a yield other than 1 KT, use the following scaling:

$$\frac{t_1}{t_2}=\frac{W_1^{1/3}}{W_2^{1/3}}=\frac{d_1}{d_2}$$

where t_1=time of arrival of shock front from explosion of yield W_2KT at range d_2, and t_1= time of arrival of shock front from explosion of W_1KT at range d_1.

b. Example

Given: A 100-KT burst in free air.

Find: The time of arrival of the shock front at 40,000 feet.

Solution: The corresponding distance for 1 KT is,

$$d_1=\frac{d_2\times W_1^{1/3}}{W_2^{1/3}}=\frac{40{,}000\times 1}{(100)^{1/3}}=8{,}600 \text{ feet.}$$

From Fig. 4–12, the time of arrival t_1 for a 1 KT burst at 8,600 feet is 7 seconds. Thus, the

time of arrival of the shock front from a 100 KT detonation at a distance of 40,000 feet is:

$$t_2 = \frac{W_2^{1/3} \times t_1}{W_1^{1/3}} = \frac{(100)^{1/3} \times 7}{1}$$

$$= 32.5\ (\pm 4.8) \text{ seconds.}$$

c. Reliability

Times of arrival obtained from this curve are considered to be reliable to ±15 per cent (0.1 KT to 100 MT).

4–2.6.3. (C) *Instructions for Using Fig. 4–13, Peak Overpressure*

a. Scaling Procedure

This curve may be used to predict incident pressures near the surface, from air bursts occurring at heights up to 40,000 feet. To calculate the distance to which a given overpressure extends for yields other than 1 KT, use the following scaling:

$$\frac{d_1}{d_2} = \frac{W_1^{1/3}}{W_2^{1/3}}$$

where d_1 = distance at which a given overpressure occurs from an explosion of yield W_1 KT, and d_2 = distance at which the same overpressure occurs for an explosion of yield W_2 KT. This scaling is often referred to as "cube root" scaling.

b. Example

Given: A 100-KT detonation in free air.

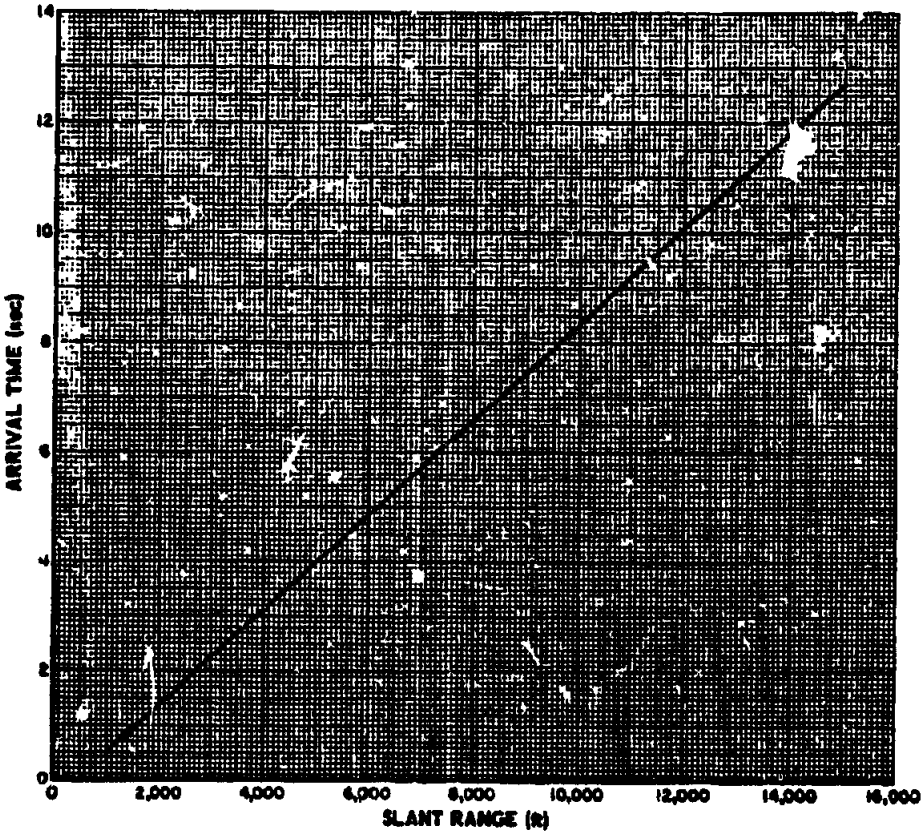

Figure 4–12 (C). Time of Arrival of Shock Front vs Slant Range, for a 1-KT Yield in a Homogeneous Sea Level Atmosphere (U)

Find: The distance to which 7 psi overpressure extends.

Solution: From Fig. 4–13, a 1 KT-burst produces 7 psi at a distance of 1,000 feet. Scaling to 100 KT:

$$\frac{1000}{d_2} = \frac{1}{(100)^{1/3}} \text{ or } d = \frac{1000 \times (100)^{1/3}}{1}$$

$$= 1000 \times 4.64 = 4{,}640 \text{ feet}$$

c. Reliability

For ranges less than 1,000 feet (overpressures greater than 7 psi) the values of peak overpressure obtained from the curve are considered reliable to ±5 per cent. This portion of the curve is based largely on analysis of data obtained by high-speed photography. For overpressures less than 7 psi, the curve is based on data obtained with pressure gages located near the ground. The reliability of this portion of the curve is estimated to be ±30 per cent.

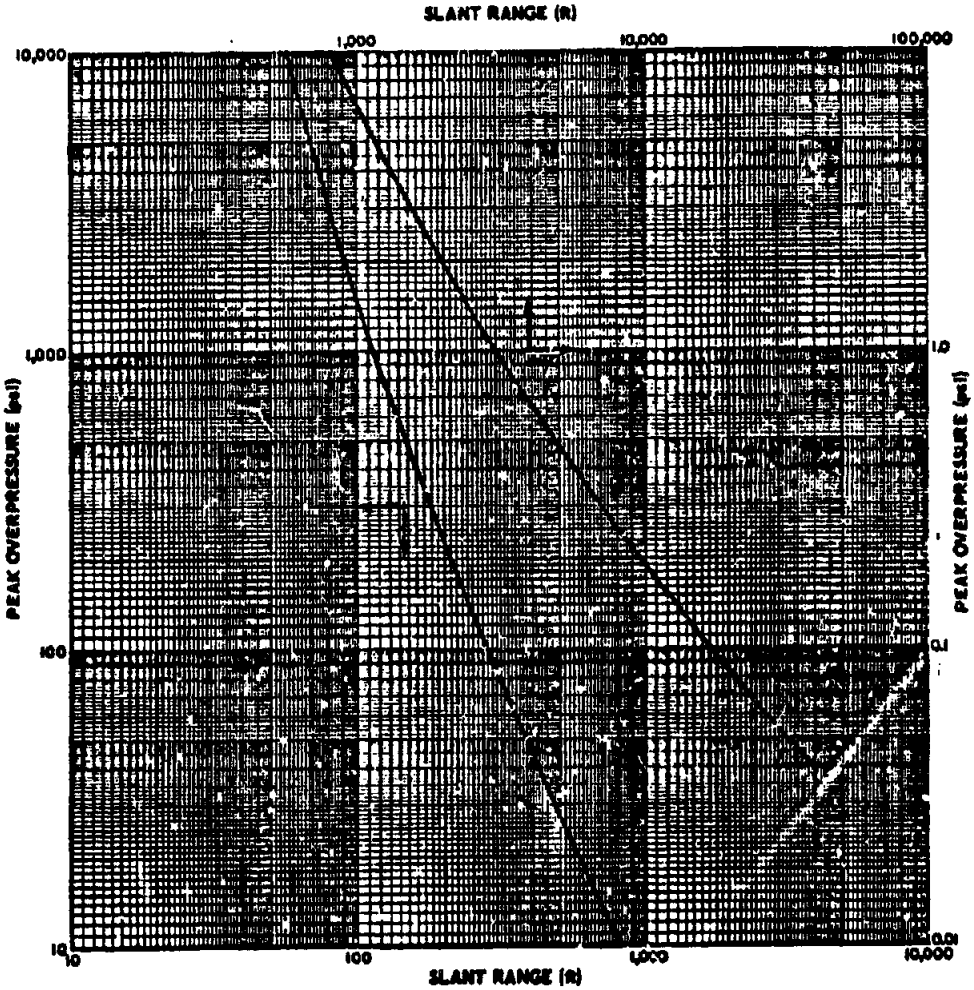

Figure 4–13 (C). Peak Overpressure vs Slant Range, for a 1-KT Yield in a Free Air Homogeneous Sea Level Atmosphere (U)

4–2.6.4. (C) *Instructions for Using Fig. 4–14, Duration of Positive Pressure Phase*

a. Scaling Procedure

To calculate the duration of a positive pressure phase, at any given distance, for a yield other than 1 KT, use the following scaling:

$$\frac{t_1^+}{t_2^+}=\frac{W_1^{1/3}}{W_2^{1/3}}=\frac{d_1}{d_2}$$

where t_1^+=duration of the positive phase for yield W_1 KT at distance d_1, and t_2^+=duration of the positive phase for yield W_2 KT at distance d_2.

b. Example

Given: A 160-KT detonation in free air.

Find: The positive phase duration at 27,000 feet.

Solution:

$$\therefore d_1=\frac{W_1^{1/3}\times d_2}{W_2^{1/3}}=\frac{1\times 27{,}000}{(160)^{1/3}}=5{,}000 \text{ feet}$$

which is the corresponding distance for 1 KT.

From Fig. 4–14, t_1^+, the duration of the positive phase for 1 KT at 5,000 feet is 0.35 second. For 160 KT the duration is:

$$t_2^+=\frac{t_1^+\times W_2^{1/3}}{W_1^{1/3}}=\frac{0.35\times(160)^{1/3}}{1}$$

$$=1.90\ (\pm 0.57) \text{ seconds.}$$

c. Reliability

Durations obtained from this curve are considered to be reliable to ±30 per cent (0.1 KT to 20 MT).

4–2.6.5. (C) *Instructions for Using Fig. 4–15, Peak Dynamic Pressure*

a. Scaling Procedure

To calculate the distance at which a given peak dynamic pressure extends for a yield other than 1 KT, use the following scaling:

$$\frac{d_1}{d_2}=\frac{W_1^{1/3}}{W_2^{1/3}}$$

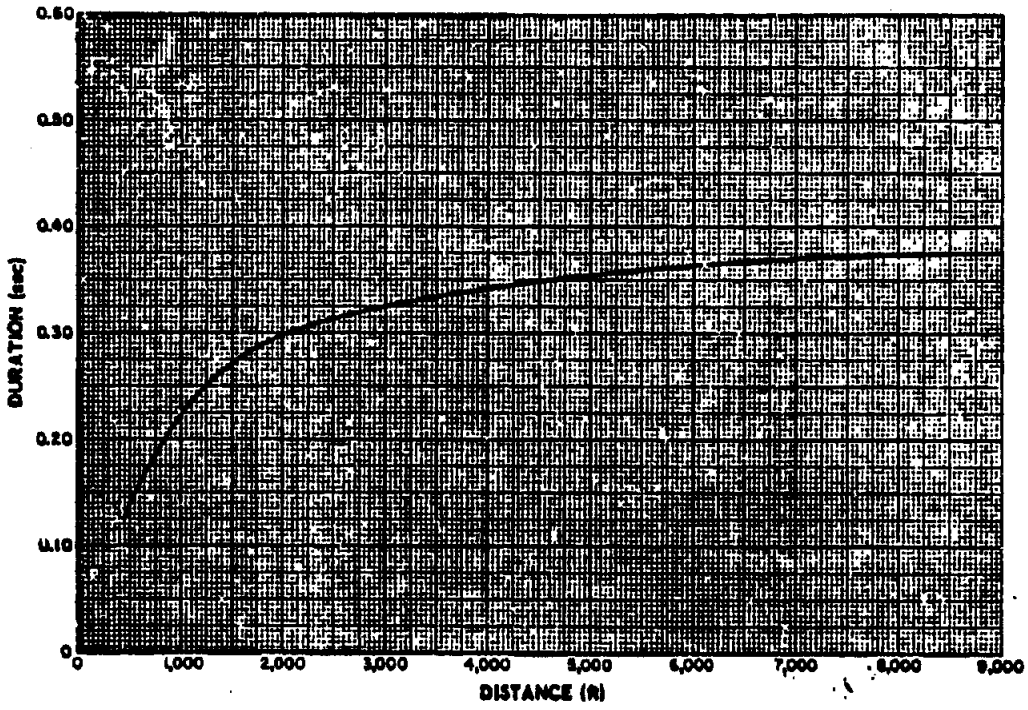

Figure 4–14 (C). Duration of Positive Pressure Phase vs Slant Range, for a 1–KT Yield in a Free Air Homogeneous Sea Level Atmosphere (U)

where d_1=distance to which a given dynamic pressure extends for yield W_1, and d_2=distance to which the same dynamic pressure extends for yield W_2.

b. Example

Given: A 100-KT detonation in free air.

Find: The distance to which 10 psi dynamic pressure extends.

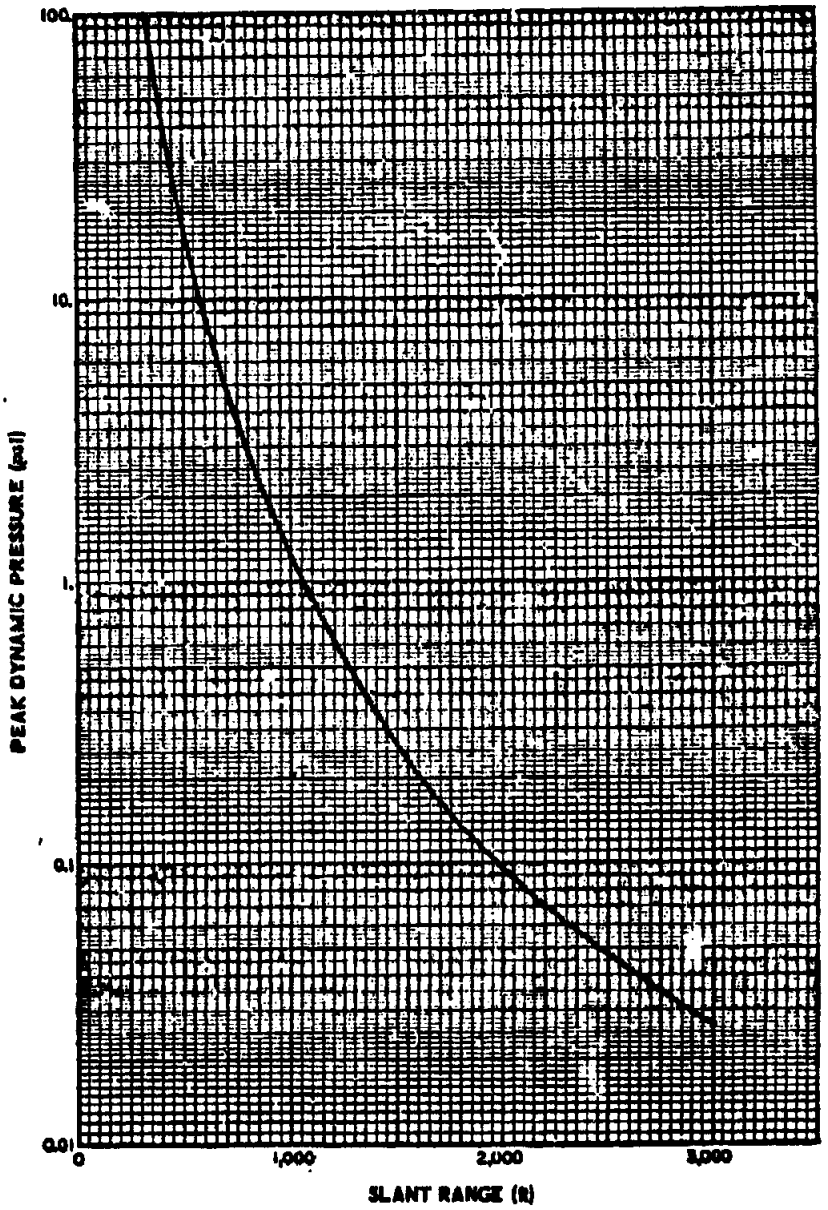

Figure 4–15 (C). Peak Dynamic Pressure vs Slant Range, for a 1-KT Yield in a Free Air Homogeneous Sea Level Atmosphere (U)

Solution: From Fig. 4–15, 1 KT produces 10 psi at a distance of 560 feet. Hence,

$$\frac{560}{d_2}=\frac{1}{(100)^{1/3}}, \text{ and}$$

$$d_2=560\times(100)^{1/3}=560\times(4.64)=2{,}590 \text{ feet.}$$

c. Reliability

Peak dynamic pressures obtained from this curve are considered to be reliable to ±5 per cent for pressures greater than 2 psi, and to ±10 per cent for pressures below 2 psi (0.1 KT to 100 MT).

4–2.6.6. (S) *Scaling Between Pentolite High Explosive and Nuclear Blast Yields* (Ref. 47)

a. Background to the Development of Conversion Factors for Pentolite and Nuclear Blasts

Because air blast phenomena associated with the detonation of chemical high explosives were comparatively well understood before the first nuclear explosion, it was convenient initially to compare blast data from nuclear explosions with those of conventional explosives, in particular with TNT. Accordingly, such comparisons were used to obtain estimates of the total energy yield for the first few nuclear explosions. By assuming a certain energy release upon detonation of a given weight of TNT, and scaling up existing TNT blast data to match the measured nuclear blast data, the nuclear yield was expressed in terms of the "equivalent weight" of TNT. This expression of the nuclear yield was not the total energy yield, but rather the blast energy yield. The comparisons of blast data were made at pressure levels less than 20 psi, where the rate of decay of peak overpressure with scaled distance is approximately the same for both TNT and nuclear explosions.

Subsequently, other methods were developed to determine the total energy yield of a nuclear explosion, but this total energy yield was still expressed as equivalent to the energy released upon detonation of a given weight (in kilotons or megatons) of TNT. Expression of the total yield in this manner is not for the purpose of predicting the total yield of the weapon (based on blast measurements), or even of predicting the blast effects for nuclear weapons (based on the TNT pressure-distance data), but is simply a convenient and easily understood way of expressing a very large amount of energy. Dependence on the pressure-distance relationship for TNT is no longer necessary, because blast measurements have now been made on a large number of nuclear explosions, and independent pressure-distance relationships have been determined for nuclear explosions. This does not, however, rule out the use of high-explosive data to predict blast parameters for new or unmeasured burst conditions.

Because the widely-used nuclear pressure-distance curves are based on the total energy yield, scaling of blast parameters from small Pentolite charges to obtain blast parameters expected from nuclear explosions, must take into account the fact that not all of the nuclear yield goes into the blast wave. A further complication results from the fact that Pentolite (the explosive used in the tests described in the referenced report) is a more powerful explosive than TNT, on an equal weight basis.

b. Comparison of Pressure-Distance Curves

Upon first examination of this scaling problem, it would appear that if the percentage of the total nuclear energy yield which appeared as blast were known, then a simple adjustment of the total yield would allow scaling between TNT and nuclear explosions. Furthermore, known relationships between TNT and Pentolite would permit the establishment of proper scaling factors for the latter explosive. However, embodied in such an analysis is the assumption that the decay of peak overpressure with scaled distance is identical with all three types (TNT, Pentolite, and nuclear explosions), providing only that linear adjustments in scale are made. To test the efficacy of this assumption, reference is made to Fig. 4–16, which is a plot of the peak overpressure versus scaled distance for a 1–KT nuclear device, and for 1–KT of Pentolite (50/50, PETN/TNT). The nuclear curve is the U.S. 1959 empirical free-air pressure-distance curve for 1 KT at sea level. The Pentolite curve is from compiled free-air blast data on bare spherical Pentolite.

Comparing the two curves on Fig. 4–16, sev-

eral things are to be noted. First, close to the burst, the peak overpressures from the nuclear explosion are higher than those from the Pentolite explosion. Second, in the same region, the rate of decay of the peak over-pressure with distance is greater for the nuclear explosion than for the Pentolite explosion. Third, at the larger distances, the overpressures from the nuclear explosion are less than those from the Pentolite explosion, but the rate of decay with distance is approximately the same.

Therefore, while it is possible to infer some conversion factor representing the weight of a given conventional explosive which will produce the same value of peak overpressure (or any other blast parameter) as that produced by a nuclear explosive at the same scaled distance, it is clear that this conversion factor must be a function of the peak overpressure, because the pressure-distance curves are not similar. The conversion factors required for scaling from Pentolite explosions to nuclear explosions have been calculated for peak overpressures between 5 lb/sq in. and 1,000 lb/sq in.

c. *Method of Determining Conversion Factors*

The procedure used to determine the HE-to-nuclear conversion factors makes use of the free-air, pressure-distance curves for Pentolite and nuclear explosions, and of the cube-root scaling laws. If a Pentolite charge of weight W_p is detonated, a given peak overpressure, P_s, will occur at a certain scaled distance, Z, where

$$Z = \frac{R_p}{(W_p)^{1/3}} \qquad (4\text{–}48)$$

and R_p is the actual distance from the center of the Pentolite charge. If a nuclear explosion

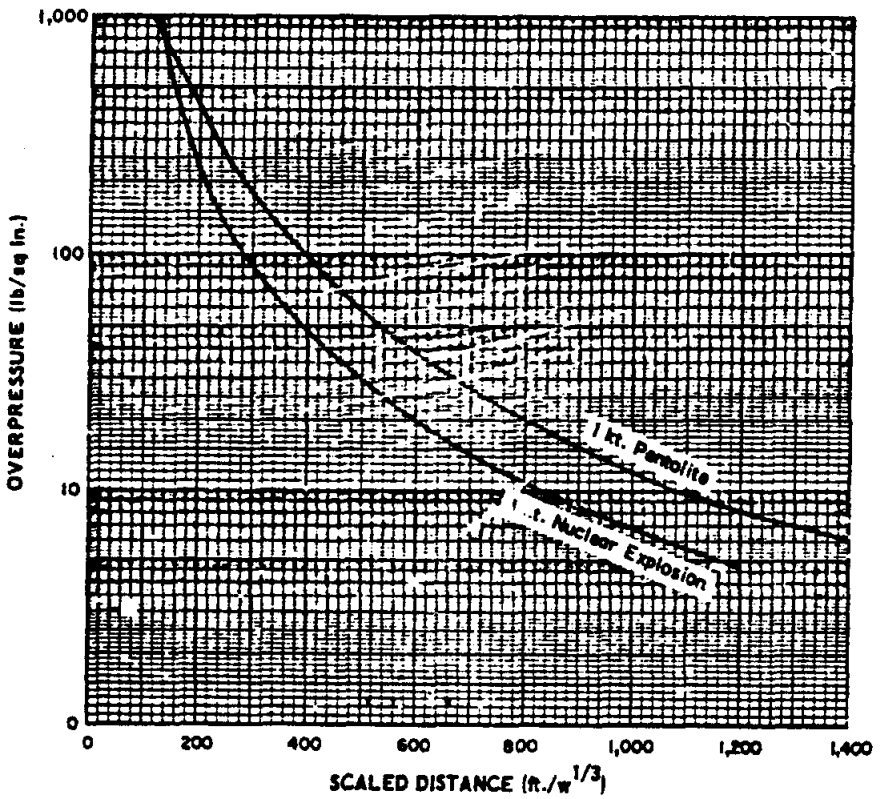

Figure 4–16 (C). Peak Overpressure vs Scaled Distance, For 1–KT (Total) Nuclear Yield and 1–KT of Pentolite, at Sea Level (U)

TABLE 4–2 (S). BLAST YIELD (IN EQUIVALENT POUNDS OF 50/50 PENTOLITE) OF A 1–KT NUCLEAR YIELD, AS A FUNCTION OF PEAK OVERPRESSURE (U)

Peak Overpressure Level (psi)	R_n (ft)	R_p (ft)	$\frac{W_n}{W_p}$	W_n (lb of Pentolite)
1000	120	117	1.085	2,170,000
500	155	179	0.655	1.310,000
250	200	262	0.445	890,000
100	283	398	0.357	714,000
30	493	662	0.414	828,000
10	848	1086	0.476	952,000
5	1180	1588	0.411	822,000

produces the same peak overpressure at distance R_n, then the effective blast yield, W_n, may be found by

$$Z=\frac{R_p}{(W_p)^{1/3}}=\frac{R_n}{(W_n)^{1/3}} \qquad (4\text{–}49)$$

or

$$\frac{W_n}{W_p}=\left[\frac{R_n}{R_p}\right]^3 \qquad (4\text{–}50)$$

Values of R_p for one kiloton of Pentolite, and of R_n for a one-kiloton total nuclear yield, are taken from Fig. 4–16, and are shown in Table 4–2, for overpressures between 5 lb/sq in. and 1,000 lb/sq in. The ratio of the effective blast yield to the 1 kiloton of Pentolite (W_n/W_p) is calculated by means of Eq. 4–50, and is shown in Table 4–2. Also shown is the value of W_n in pounds of Pentolite equivalent to the 1-kiloton nuclear yield. The relationship between the nuclear blast effectiveness (W_n/W_p) and the peak overpressure is shown graphically in Fig. 4–17. Over the pressure range of 10 to 300 lb/sq in., which is the region of interest in the referenced report, the nuclear blast effectiveness averages about 42 per cent.

4–3. (C) SURFACE AND SUBSURFACE BURSTS

4–3.1. (U) Surface Burst

For a considerable distance above the earth's surface, air burst effects are significantly modified by the earth's surface. As the height of burst is lowered in this zone, there is a gradual transition from the characteristics of an air burst to those of a surface burst.

A nuclear weapon burst at the earth's surface follows the same sequence of events as does an air burst, except that the fireball boundary and the shock front are hemispherical instead of spherical. For a contact surface burst there is no region of regular reflection; as a consequence, all objects on the ground are subjected to a blast similar to that in the Mach region below the triple point for an air burst (Par. 4–2.2.6). Therefore, for structures located near the ground, the shock front may be assumed to be essentially vertical and the transient winds approximately parallel with the ground. Both overpressure (Par. 4–2.2.1) and dynamic pressure (Par. 4–2.2.2) will decay in the same fashion as previously described for an air burst.

When a burst takes place at the surface of the earth, a portion of the energy is directly transmitted to the earth in the form of ground shock (Par. 4–3.3.2). In addition, the air blast induces a ground shock wave. At shallow depths, this ground shock wave has approximately the same magnitude as the air blast wave, for an equivalent distance. The directly transmitted ground shock, although initially of higher magnitude, attenuates faster than the air-blast induced ground shock.

In the vicinity of ground zero, tremendously large pressures are exerted on the earth's surface, causing a downward compression of the soil and displacing material to form a crater (Par. 4–3.3.1). In addition to the material thrown out by the blast, a considerable quantity of the soil is vaporized by the intense heat.

Methods of predicting and analyzing blast data from surface bursts are similar to those used for air bursts, in many respects. Reference is, therefore, made to Par. 4–2.6, where a number of representative reference-data graphs are presented and used as examples of the application of scaling laws for predicting blast data. In addition, reference should be made to TM 23–200 (Ref. 21) for a more comprehensive, graphic coverage.

4–3.2 (U) Underground Bursts from Conventional (Chemical) Explosions

4–3.2.1. *Introduction*

It was recognized during the early part of World War II that very little experimental and unified knowledge existed which could explain the general phenomena of underground explosions. Under the sponsorship of the Office of Scientific Research and Development, an experimental program was conducted in an attempt to understand the parameters of the problem and to lay the ground work for future analytical work. A very significant portion of the work was carried out under the general direction of Princeton University, with assistance from various Government and industrial organizations. The results of the research have been reported in a series of OSRD reports which have been, fortunately, summarized in a final report by Lampson (Ref. 22), an unclassified document which is readily available. Lampson's report presents an excellent description of the work that was performed, both theoretical and experimental, including fairly detailed information on the instrumentation that was used to obtain the measurements.

Because of the extreme variability of soils and their properties, and a general lack of

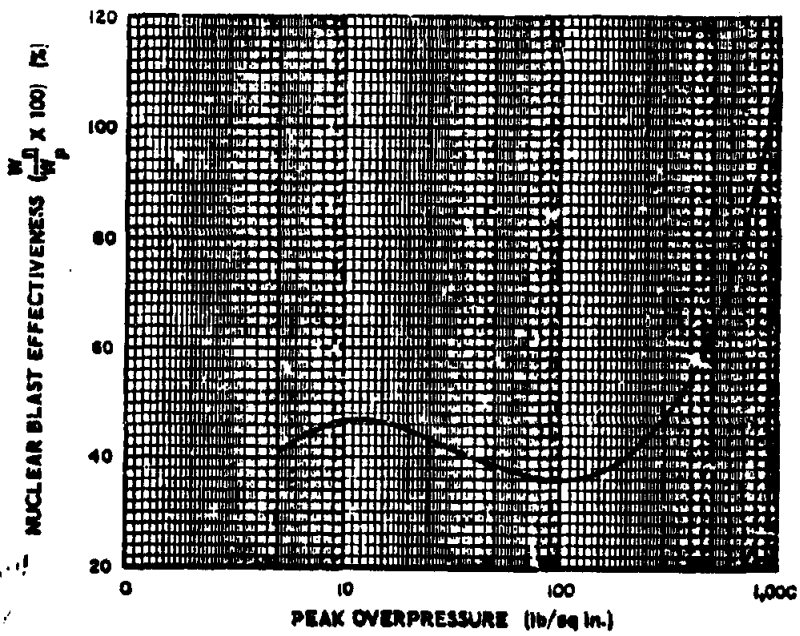

Figure 4–17 (S) Nuclear Explosion Blast Effectiveness vs Peak Overpressure (U)

understanding of the phenomena involved, no theoretical methods existed which were comparable to those available for hydrodynamic studies in air and water. In fact, so many unknown factors were involved that a straightforward dimensional analysis was not completely possible, because dimensional considerations require considerable knowledge of the physical phenomena involved. Accordingly, Ref. 22 is primarily an attempt to understand the parameters and processes involved by means of empirical studies of numerous experiments. It should be remarked, however, that dimensional considerations were used where possible.

For purposes of comparison it should be recognized that the present problem is much more difficult than such problems as the study of wave propagation in elastic structures. There, the basic parameters of the problem, such as stress modulus of elasticity, Poisson's ratio, strain, etc., are fairly well understood. In fact, the basic differential equations can be written for the latter problem, at least approximately. Such is not the case for underground explosions.

4–3.2.2 *Examination of Certain Analytical Techniques*

Certain features of Lampson's report, Ref. 22 will be examined in this paragraph, as representative of the significance of the work. Further information may be obtained from Ref. 22 and from the many original reports quoted as references therein.

It was recognized early in the work that a significant parameter was cube root scaling (Par. 4–2.6.3, above). That is, it was found that under identical conditions (except for charge weight) peak pressures were accurately given for scaled distances, scaled according to the relation

$$\frac{r_a}{r_b}=\left(\frac{W_a}{W_b}\right)^{1/3} \qquad (4\text{–}51)$$

where a and b represent two different explosions, and r and W are, respectively, the distance from the explosion and the weight of explosive.

The significance of this formula can be illustrated by an example. Thus, if a given weight of explosive W_b causes a peak pressure P to be observed at a distance of r_b from the explosion, then (for example) an explosion with a charge weight twenty-seven times as great would produce the same peak pressure P at a distance of $r_a=3\ r_b$; that is, at a distance three times as great. It is emphasized, however, that such conclusions are valid only if all other parameters of the problem, such as type of soil, moisture content, scaled distance below surface, etc., are held constant.

Further experimentation, described in Ref. 22, disclosed that certain other parameters were important in various different tests. A partial list of these parameters includes:

k = a soil constant which depends on the soil type, related to the modulus of elasticity of the soil,

W = charge weight,

E = explosive factor for pressure,

E' = explosive factor for impulse,

ρ = soil density,

V = speed of propagation of pressure waves,

F = a parameter which depends on the depth of burial of the charge,

and

B = an impulse parameter which depends on the soil type.

It was one of the aims of the study to fit empirical equations to the results of the tests in order to determine the responses to the independent parameters. The empirical analyses were highly successful, and formulas were derived for predicting the responses of interest, including:

P = peak pressure in free earth,

P_r = peak pressure against a target, including the effect of reflection,

I = impulse in free earth,

L_r = impulse against a target, including the effect of reflection,

u = maximum speed of displaced particles,

A = maximum acceleration of displaced particles,

d = maximum transient displacement,

dp = maximum permanent earth movement, and

Crater radius = surface radius of crater.

These results are presented in Ref. 22 in the form of equations and charts.

One of the most significant aspects of blast wave transmission in earth is the fact that shock waves (characterized as waves of steep slope approaching a pressure discontinuity) are impossible, because of the characteristics of the dynamic stress-strain curve for earth. (Rock, as distinguished from earth or soil, was not considered in Ref. 22.)

In connection with the formation of shock waves in air it was previously discussed (Par. 4–2.3, above) that a material which exhibits a linear stress-strain curve transmits its pressure waves unchanged in form. If the particle velocity is independent of pressure and is, therefore, constant as in acoustic theory, each element of the wave front travels at the same speed and the wave retains its form. In the nonlinear theory, the particle speed increases with increasing slope of the stress-strain curve. If the stress-strain curve is concave upward, then particle velocity increases with pressure and the particles at the crest of the wave (where the pressure is higher) move faster than the particles at the base. This causes a steepening of the front face of the wave, and a shock wave develops, as in explosions in air or water. In the case of soil, however, the stress-strain curve is concave downward during compression. This means that the particle velocity, since it depends directly on the curve slope, is lower at the wave crest where the pressure is greatest. This causes the crest to be retarded, and the entire wave spreads out as it is propagated through the soil. Further, since the unloading (decreasing stress) curve is concave upward, there is a considerable energy loss (hysteresis effect) associated with each compression and expansion. Accordingly, the pressure wave is less energetic than a shock wave, and it loses its energy faster than elastic theory predicts for a spherical wave. A typical stress-strain curve for soil is shown in Fig. 4–18.

Because the speed of wave transmission depends directly on the slope of the curve, it is seen to be a variable, as described above. The slope at a given point is the modulus of elasticity; hence, the speed of sound increases with modulus of elasticity. To compare an order of magnitude, a typical silty soil has a secant modulus (average value) of about 50,000 pounds per square inch, but steel (for example) has a modulus of about 30,000,000, or 600 times as great. For free soil explosions it was found that the peak pressure could be expressed quite adequately by an empirical formula of the form

$$P = K\left(\frac{r}{W^{1/3}}\right)^{-3} = K\frac{W}{r^3} \qquad (4\text{–}52)$$

where K is a soil parameter related to the modulus of elasticity of the soil. (Experimental values of K are given in Ref. 22.) In considering this, and other equations, it is helpful to recall that although dimensional considerations will show that P/K depends on $r/W^{1/3}$, the exact functional form can be determined only by experiment, or theory (if one exists for the problem under consideration). It should also be recalled that, in the discussion of scaling laws in the present text (Par. 4–2.4.4.), it was shown that a non-dimensional grouping was $\frac{P_o^{1/3}r}{E_o^{1/3}}$, where P_o is some ambient pressure and E_o is the energy of the explosive. In the present connection, however, if E_o is interpreted as weight (because weight of explosive is proportional to energy content, and P_o is considered

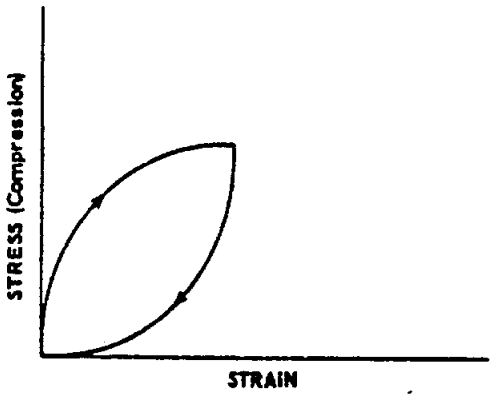

Figure 4–18. Typical Stress-Strain Curve for Soil

fixed), the dimensionless form reduces to $r/W^{1/3}$ for presentation of empirical data.

To consider the great variations that may occur in K, and hence in P, data included as part of Ref. 22 shows that K varies from several hundred to over one hundred thousand, a factor of more than one hundred. It is remarkable that the empirical formula fits all conditions so accurately. It is shown in Ref. 22 that K is related to the modulus of elasticity, as already mentioned. In fact, to within 25 per cent accuracy it was found that weak sound waves were transmitted at a speed given by

$$V = \sqrt{\frac{2K}{\rho}} \qquad (4\text{–}53)$$

where ρ is the density. With this expression it was possible to correlate the K value for a wide range of soils, thus giving an indication that the general shape of stress-strain curve is similar for a wide variety of soils.

4–3.3. (C) Underground Bursts from Nuclear Explosions

4–3.3.1. Cratering

a. Causes and Characteristics

Land craters are pits, depressions, or cavities formed in the surface of the earth by vaporizing, throwing, compressing, or scouring the soil in an outward direction from a nuclear detonation. Usually they are further characterized as to being apparent or true craters. The apparent crater is the visible crater remaining after a detonation; the true crater is the crater excluding fallback material. The true crater is bounded by a surface representing that limiting distance from the explosion at which the original material surrounding the apparent crater was completely disassociated from the underlying material. The ensuing discussion of craters resulting from underground bursts assumes weapons with no air space surrounding them, burst under a horizontal ground surface plane, in locations that have been completely backfilled and tamped. Fig. 4–19 shows schematically the dimensions used in describing a crater (Ref. 21).

The fallback zone is the zone between the true and apparent craters, as defined above. It contains both disassociated material that has fallen back into the crater, and disassociated material that received insufficient energy to be thrown out of the crater. There is usually insignificant fallback in craters from air or surface bursts, or bursts at depths less than 25 $W^{1/3}$ feet (where W is yield in KT). Consequently, there is little difference between apparent and true craters from such bursts.

The crater radius is the average crater radius as measured at the original ground surface. It scales as the cube root of the yield. The crater depth is the maximum depth of the crater as measured from the original ground surface. It scales as the fourth root of the yield. Estimated crater radii and depths are given in Figs. 4–20 and 4–21 as functions of burst height and depth for 1 KT. Figs. 4–22 through 4–25 are derived from Figs. 4–20 and 4–21, and present expected crater diameters and depths as functions of yield for specific burst conditions. All figures are directly applicable to dry soil or soft rock (rock that crumbles easily). For other types of soil or rock, crater dimensions may be estimated by multiplying the dimensions taken from Figs. 4–22 through 4–25 by the appropriate factors given in the instruction paragraphs for these figures.

The lip of the crater is formed both by fallback and by the rupture of the soil surrounding the crater. For a deep underground burst, the resulting crater lip is formed primarily from fallback. For a shallow underground or surface burst, the crater lip is formed primarily by the shearing of the ground nearest the burst and its subsequent piling up against the soil farther away from the crater. The approximate relative dimensions of the crater lip resulting from a surface burst are indicated in Fig. 4–19.

The rupture zone is characterized by extreme cracking. This zone surrounds the true crater, and at the ground surface extends outward approximately 1.5 times the apparent crater. However, for bursts at large-scale depths, the zone at the ground surface extends outward only slightly beyond the true crater. When an explosion occurs in rock, it disturbs the rock in the rupture zone by causing surface scabbing

of local areas, by opening pre-existing cracks, and by developing new fractures that tend to be radial from the point of burst. The rupture zone in sand may be difficult to define or may be nonexistent.

In the plastic zone the soil is permanently displaced, but is without visible rupture. This zone surrounds the rupture zone and may extend outward at the ground surface approximately three times the apparent crater radius. Even for bursts at large-scale depths, where there is an appreciable difference between the true and apparent crater dimensions, the plastic zone will extend considerably beyond the true crater at the surface. In rock, little or no plastic deformation occurs.

At a height of burst less than about 10 $W^{1/3}$ feet, the expanding gases from a nuclear detonation form a land crater primarily by vaporizing, and by throwing and compressing the soil in an outward direction from the detonation. As the height of burst decreases from about 10 $W^{1/3}$ feet, or the depth of burst increases, the crater radius continues to increase appreciably. This increase continues until a depth of burst of about 25 $W^{1/3}$ feet is reached. Below this depth, however, the apparent crater radius increases only slightly with increasing

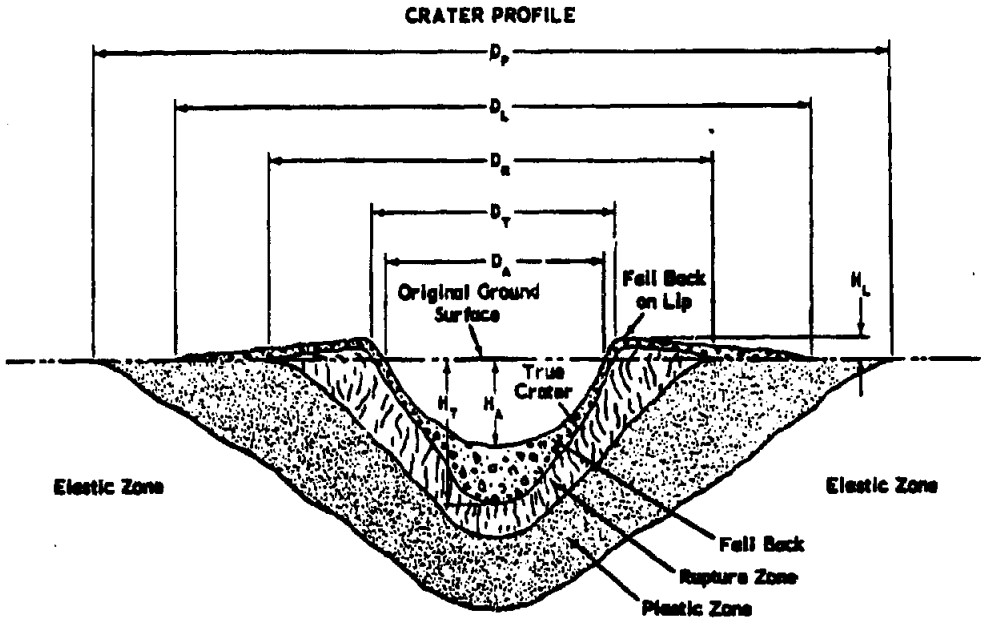

D_A = Diameter of Apparent Crater

H_A = Depth of Apparent Crater

D_T = Diameter of True Crater

H_T = Depth of True Crater

D_L = Depth of Lip = 2.0 D_A ±25%

H_L = Height of Lip = 0.25 H_A ±50%

D_R = Diameter of Rupture Zone = 1.5 D_A ±25%

D_P = Diameter of Plastic Zone = 3 D_A ±50%

V_C = Volume of Apparent Crater (Assumed Paraboloid) = $\frac{\pi D_A^2 H_A}{8}$

Figure 4–19 (C). Crater Dimensions (U)

depth of burst. Below a burst depth of approximately 70 $W^{1/3}$ feet, the apparent crater radius decreases with increasing depth of burst.

As the height of burst is lowered from about 10 $W^{1/3}$ feet, or the depth of burst is increased, the crater depth increases appreciably with increasing depth of burst, until a burst depth of approximately 60 $W^{1/3}$ feet is reached. Below this, the apparent crater depth increases but slightly with increasing depth of burst, until a depth of burst of about 90 $W^{1/3}$ feet is reached. Below this depth of burst, the fallback material may form a crater with an apparent depth less than the depth of burst. The true depth of the crater, however, remains greater than the depth of burst, by a constant value of approximately 57 $W^{1/3}$ feet, when the depth of burst is below about 60 $W^{1/3}$ feet.

For bursts at heights greater than about 10 $W^{1/3}$ feet, the mechanism of cratering is primarily compression and scouring of soil. As indicated in Fig. 4–20, the crater radius increases for burst heights above 20 $W^{1/3}$ feet, reaching a maximum at about 60 $W^{1/3}$ feet. This results in a crossover of the 50-, 100-, and 300-foot burst-height curves of Figs. 4–22 and 4–23. This increase in radius is not considered significant, however, because the crater depth decreases very rapidly, with increasing height of burst, to relatively small values in the range of crossover. For bursts at heights above about 60 $W^{1/3}$, the crater may be difficult to detect.

Crater dimensions are not expected to change materially with ground slope, except for very steep terrain. On very steep slopes, craters will be somewhat elliptical in shape, with the downhill lip considerably wider than the uphill lip. The crater depth, with respect to the surface plane of the terrain involved, is not expected to be appreciably different from that of a burst under horizontal terrain conditions.

b. *Instructions for Using Fig. 4–20, Crater Radius vs Burst Position*

(1) Description

Fig. 4–20 gives the estimated apparent and true crater radius as a function of burst position, for 1–KT bursts in dry soil or soft rock. For other soils, multiplication factors should be used as follows:

Soil Type	*Factor*
Hard rock (granite and sandstone)	0.8
Saturated soil (water slowly fills crater)	1.5
Saturated soil (water rapidly fills crater)*	2.0

*Only for apparent craters with sloughing or washing action on the crater sides.

(2) Scaling Procedure

The following relation can be used to estimate corresponding crater radii for a given burst yield and depth:

$$\frac{d_1}{d_2}=\frac{W_1^{1/3}}{W_2^{1/3}}=\frac{h_1}{h_2}$$

where d_1 = crater radius produced by a yield W_1 at burst height or depth h_1, and d_2 = crater radius produced by a yield W_2 at burst height or depth h_2.

(3) Example

Given: An 80–KT burst at a depth of 50 feet, in dry soil.

Find: The apparent crater radius.

Solution: The burst depth for 1 KT is:

$$h_1=\frac{50\times 1}{(80)^{1/3}}=12 \text{ feet.}$$

From Fig. 4–20 the apparent crater radius (and also the true crater radius) for 1 KT is 93 feet. Hence, the crater radius for 80 KT is:

$$d_2=\frac{93\times(80)^{1/3}}{1}=400\ (\pm 120) \text{ feet.}$$

(4) Reliability

The reliability of crater radii values obtained from Fig. 4–20 is estimated to be ±30 per cent, for burst heights of 5 $W^{1/3}$ feet to burst depths of 65 $W^{1/3}$ feet, for all yields above 1 KT. For other burst conditions the reliability is estimated to be ±40 per cent.

c. *Instructions for Using Fig. 4–21, Crater Depth vs Burst Position*

(1) Description

Fig. 4–21 gives the estimated apparent and true crater depth as a function of burst position

in dry soil or soft rock. Multiplication factors for other soils are as follows:

Soil Type	*Factor*
Hard rock (granite and sandstone)	0.8
Saturated soil (water slowly fills crater)	1.5
Saturated soil (water rapidly fills crater)*	0.7

*Only for apparent craters with sloughing or washing action on the crater sides.

(2) Scaling Procedure

For yields other than I KT, the following relations can be used to estimate corresponding crater depths for a given burst yield and depth:

$$\frac{h_1}{h_2}=\frac{W_1^{1/3}}{W_2^{1/3}} \text{ and } \frac{d_1}{d_2}=\frac{W_1^{1/4}}{W_2^{1/4}}$$

where d_1=crater depth produced by a yield W_1 at burst height or depth h_1, and d_2=crater depth produced by a yield W_2 at burst height or depth h_2.

(3) Example

Given: An 80-KT burst at a depth of 50 feet, in the wet sand of an ocean beach where water will rapidly fill the crater.

Find: Apparent crater depth.

Solution: Corresponding burst depth for 1 KT is:

$$h_1=\frac{50\times 1}{(80)^{1/3}}=12 \text{ feet.}$$

From Fig. 4-21 the crater depth for 1 KT at 12 feet=37 feet.

Crater depth (d_2) for 80 KT at 50 feet=

$$\frac{37\times (80)^{1/4}}{1}=111 \text{ feet.}$$

From the soil type table, above, the factor for relative crater depth in saturated soil (where

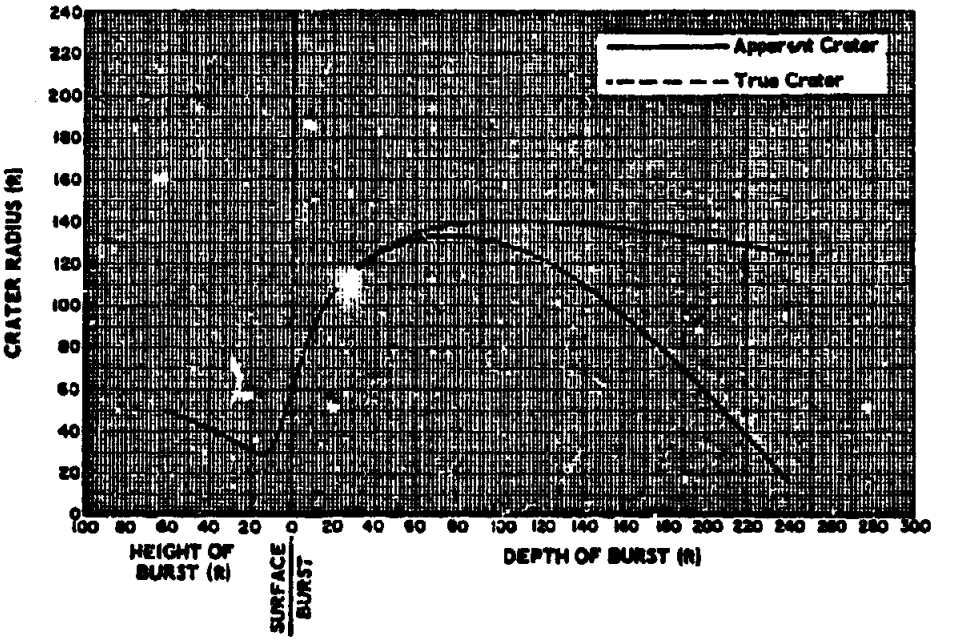

Figure 4-20 (C). Crater Radius vs Burst Position, in Dry Soil or Soft Rock, Scaled to 1-KT (U)

water rapidly fills crater) is 0.7. The crater depth is, therefore:

$$0.7 \times 111 = 78\ (\pm 39)\ \text{feet.}$$

(4) Reliability

The reliability of crater depths taken from Fig. 4–21 is estimated to be ±50 per cent for all yields and burst positions.

d. Instructions for Using Figs. 4–22 and 4–23, Apparent Crater Diameter vs Yield

(1) Description

Figs. 4–22 and 4–23 give values of apparent crater diameter vs yield for various depths and heights of burst, derived by scaling from Fig. 4–20. No interpolation of depth or height of burst should be made for this figure. For values other than those given, use Fig. 4–20. Since there is little difference between true and apparent crater diameters from bursts at depths less than 25 $W^{1/3}$ feet, or from above-ground bursts, these figures may be used also for true craters in that range. The assumed soil type is dry soil or soft rock (rock that will crumble or fall apart easily). For other soils, the diameter obtained from Figs. 4–22 or 4–23

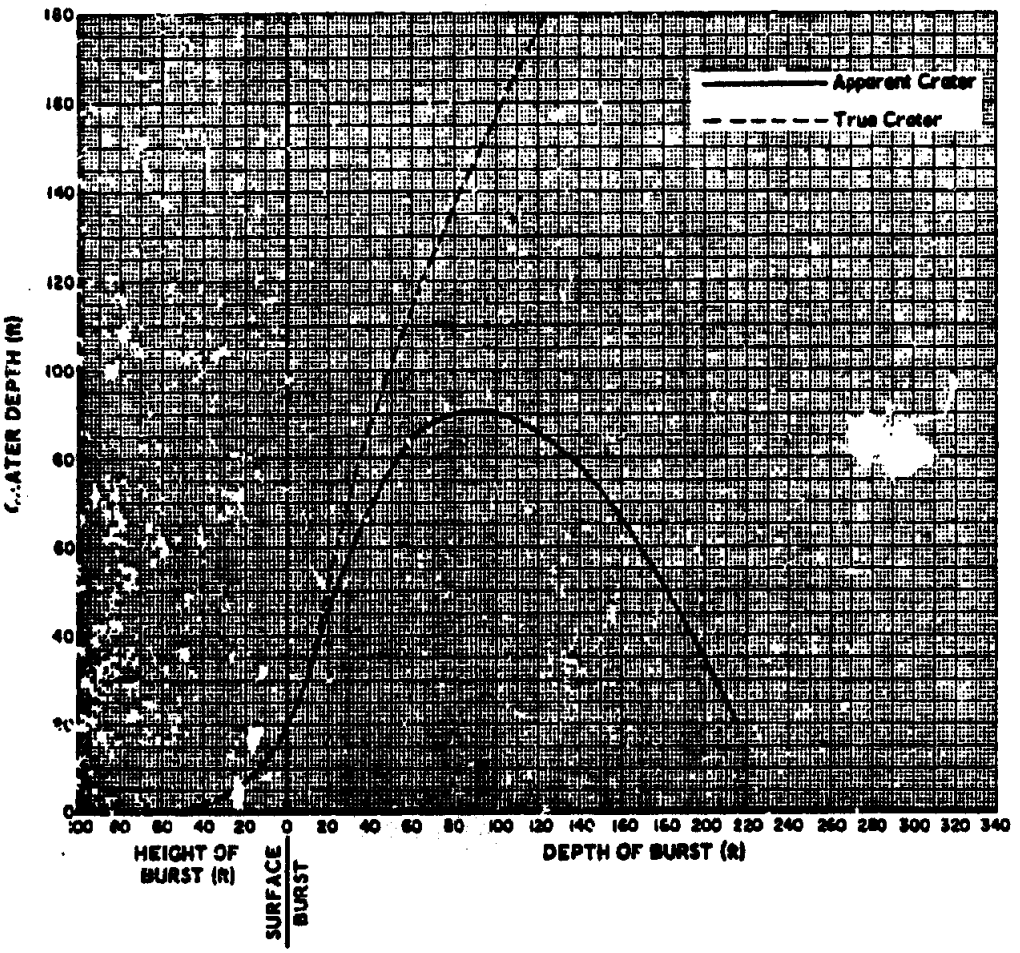

Figure 4–21 (C). Crater Depth vs Burst Position, in Dry Soil or Soft Rock, Scaled to 1–KT (U)

should be multiplied by the relative crater dimension factor, as follows:

Soil Type	*Factor*
Hard rock (granite and sandstone)	0.8
Saturated soil (water slowly fills crater)	1.5
Saturated soil (water rapidly fills crater)*	2.0

*Only for apparent craters with sloughing or washing action on the crater sides.

(2) Example

Given: A 30-KT burst at a depth of 100 feet, in dry clay.

Find: The apparent crater diameter.

Solution: The apparent diameter, taken directly from the 100-foot-depth-of-burst curve of Fig. 4–22 for 30 KT is 750 (±225) feet.

(3) Reliability

The reliability of crater diameters obtained from Figs. 4–22 and 4–23 for various yields is estimated to be ±30 per cent, for burst heights of 5 $W^{1/3}$ feet to burst depths of 65 $W^{1/3}$ feet, for all yields above 1 KT. For other burst conditions, the reliability is estimated to be ±40 per cent.

e. Instructions for Using Figs. 4–24 and 4–25, Apparent Crater Depth vs Yield

(1) Description

Figs. 4–24 and 4–25 give values for apparent crater depth vs yield for various depths and heights of burst, derived from Fig. 4–21 by scaling. No interpolation of depth or height of burst should be made from this figure. For values other than those given, use Fig. 4–21. Since there is little difference between true and apparent crater depths from bursts above ground or bursts at depths less than 10 $W^{1/3}$ feet, these figures may be used also for true craters in that range. The assumed soil type is dry soil or soft rock (rock that will crumble or pull apart easily). For other types of soil and rock, the depth obtained from Figs. 4–24 and 4–25 should be multiplied by the appropriate relative crater depth factor below:

Soil Type	*Factor*
Hard rock (granite and sandstone)	0.8
Saturated soil (water slowly fills crater)	1.5

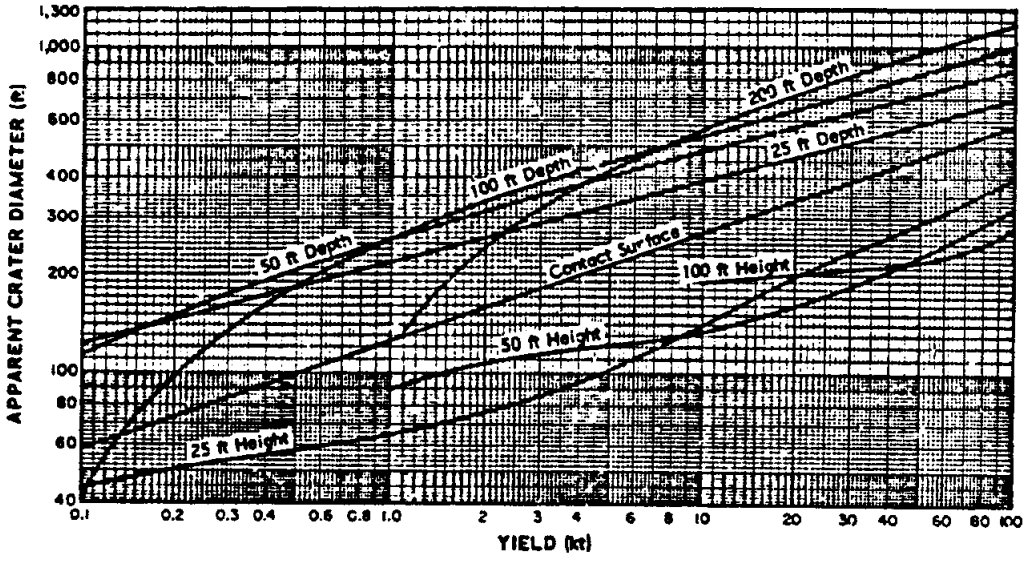

Figure 4–22 (C). Apparent Crater Diameter vs Yield, for Various Depths and Heights of Burst, in Dry Soil or Soft Rock, for 0.1–KT to 100–KT Yield (U)

Soil Type	*Factor*
Saturated soil (water rapidly fills crater)**	0.7

**Only for apparent craters with a sloughing or washing action on the crater sides.

(2) Example

Given: An 80–KT burst at a depth of 100 feet, in saturated clay containing water that will slowly fill the crater.

Find: The apparent crater depth.

Solution: From Fig. 4–24 the crater depth in dry soil is 158 feet. From the soil type table, above, the factor for relative crater depth in saturated soil (water slowly fills crater) is 1.5. The crater depth is

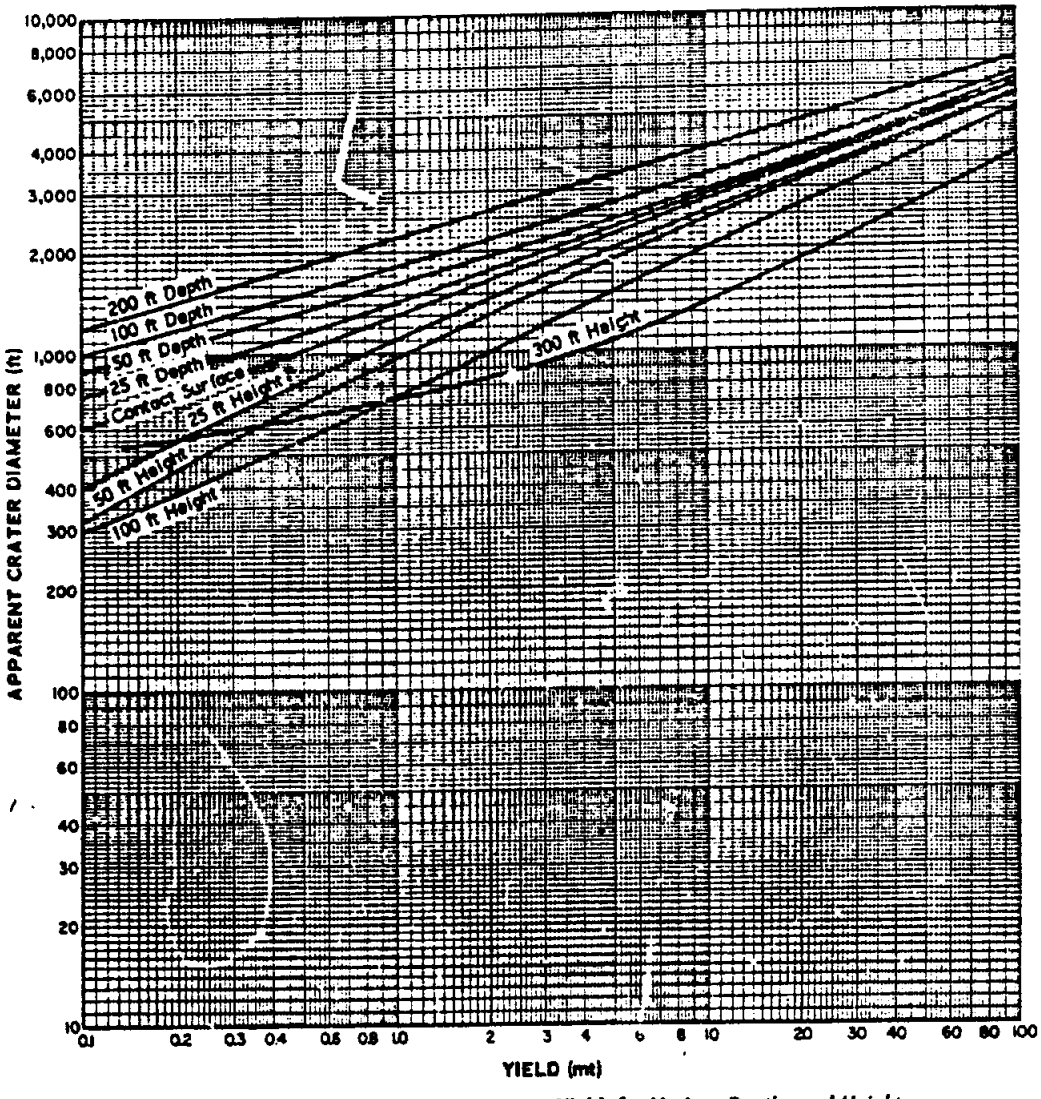

Figure 4–23 (C). Apparent Crater Diameter vs Yield, for Various Depths and Heights of Burst, in Dry Soil or Soft Rock, for 0.1–MT to 100–MT Yield (U)

therefore 1.5×158=237 (±119) feet.

(3) Reliability

The reliability of crater depths obtained from Figs. 4–24 and 4–25 for all yields and burst positions is estimated to be ±50 per cent.

4–3.3.2 Ground Shock

a. General

Two separate basic mechanisms are considered as producing ground shock. Direct ground shock is produced by the sudden expansion of the bubble of gas from an underground or surface explosion, which sets up a pulse or oscillation in the ground. Air-induced ground shock results from an air blast wave, from an explosion, that strikes and moves parallel to the ground.

Fig. 4–26(A) shows the relation of the direct ground shock wave to the air-induced ground

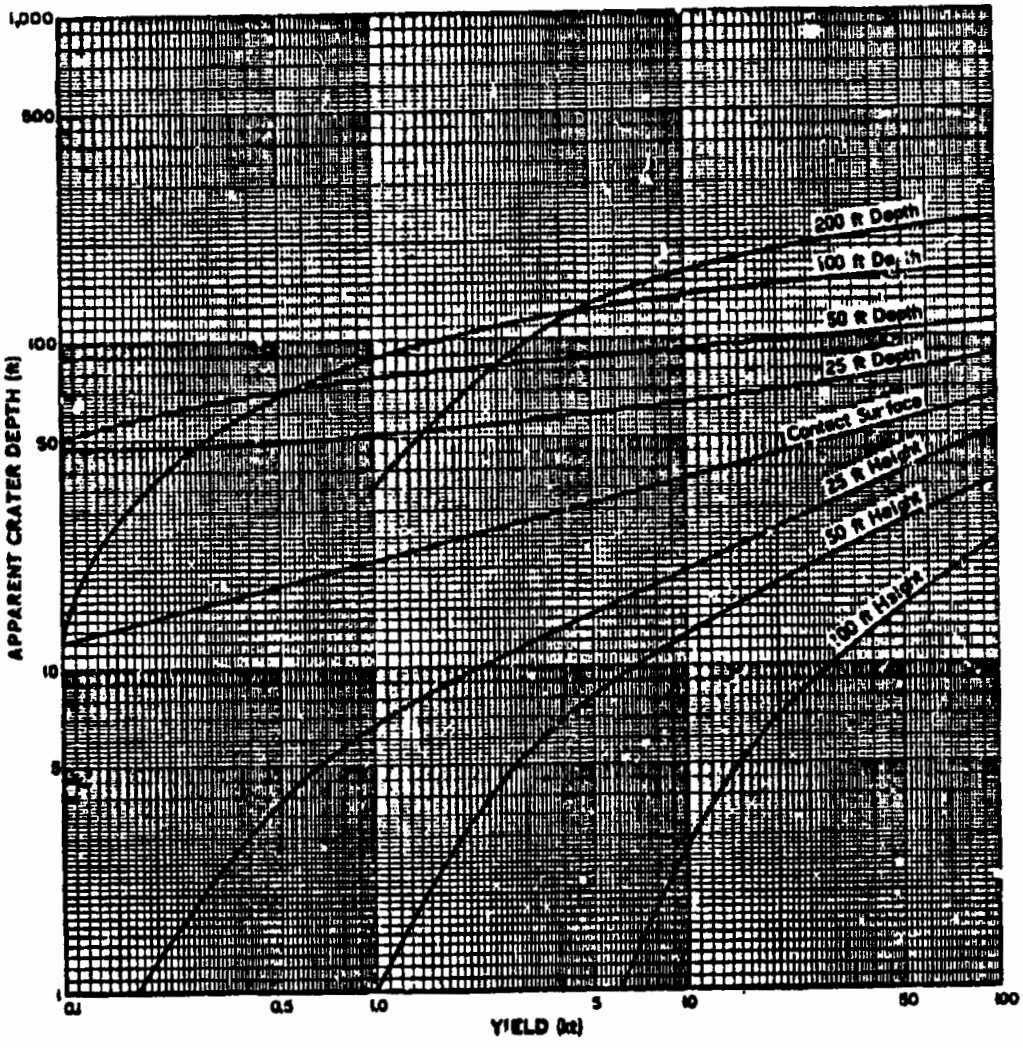

Figure 4–24 (C). Apparent Crater Depth vs Yield, for Various Depths and Heights of Burst, in Dry Soil or Soft Rock, for 0.1–KT to 100–KT Yield (U)

shock wave, in the case of the surface burst. Because sonic velocity is generally higher in the ground than in the air, the direct ground shock is indicated as moving faster than the air blast and, consequently, faster than the air-induced ground shock. Although the air blast of a surface or near-surface burst initially propagates faster than direct ground shock, the velocity of the air blast decreases more rapidly with distance than does the direct ground shock. Hence, the direct ground shock eventually moves ahead (Ref. 21).

Fig. 4–26(B) shows in idealized form the relation of the vertical acceleration of soil particles caused by the two different forms of ground shock. The direct vertical acceleration

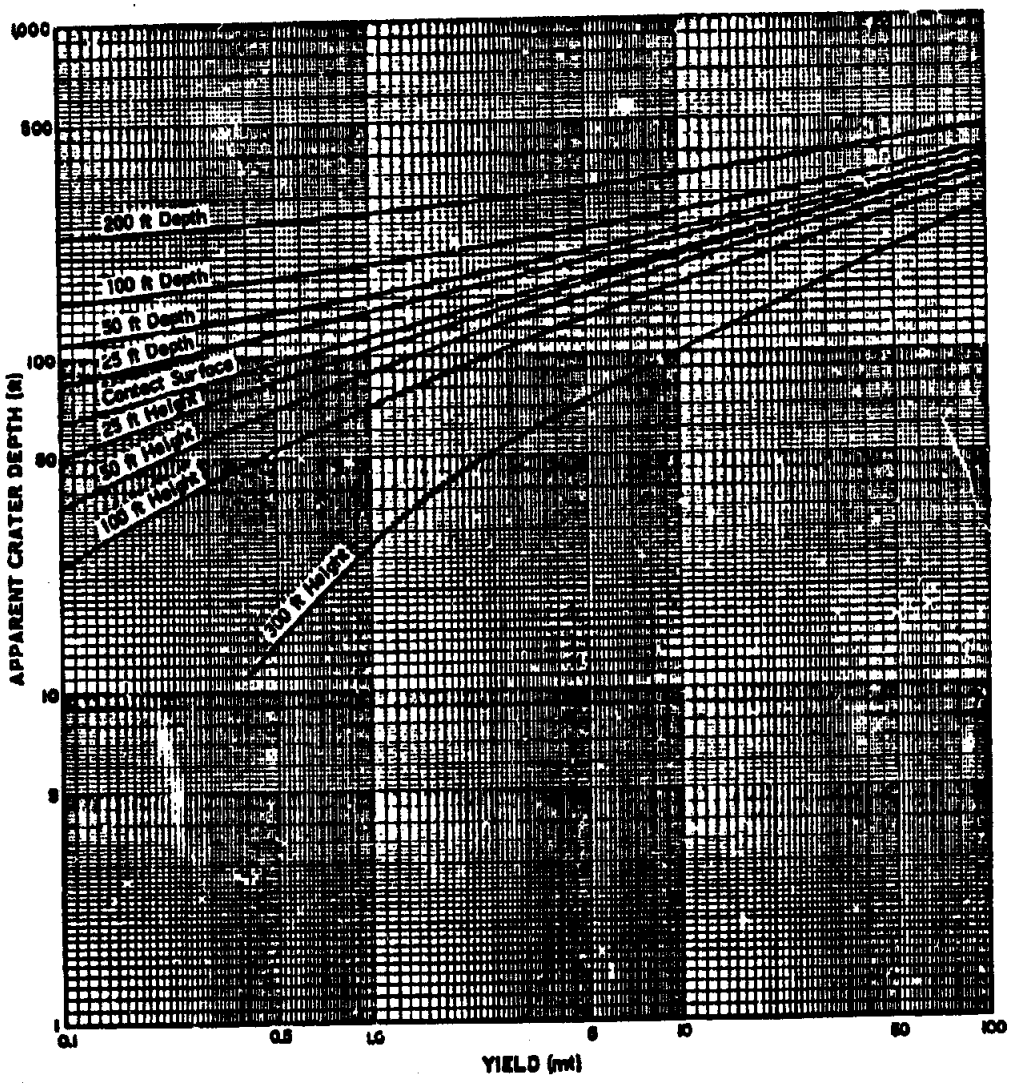

Figure 4–25 (C). Apparent Crater Depth vs Yield, for Various Depths and Heights of Burst, in Dry Soil or Soft Rock, for 0.1–MT to 100–MT Yield (U)

is initiated upon arrival of the direct ground shock. What is known as "air blast slap acceleration" (Par. 4–3.3.2.c.(3), following) is initiated upon the arrival of the air blast, which causes a sudden local increase in soil particle acceleration.

b. Direct Ground Shock

(1) Propagation

The direct ground shock wave produced by a surface or underground burst propagates radially outward from the burst point. For a 1–KT surface or shallow underground burst, in Nevada-type soil, propagation velocities on the ground surface are 4,600 ft/sec. approximately 300 feet from surface zero, and decrease to a more constant 3,500 ft/sec. approximately 2,500 feet from surface zero. The propagation velocity of ground shock at the surface may increase with distance from the burst, due to refraction and reflection from underlying higher velocity strata; and, as the shock reduces to an acoustic wave, the velocity will approach the normal acoustic velocity of the medium near the surface. In sound rock, and outside the zone of rupture, the propagation of shock obeys elastic formulae. In such a homogeneous medium (not generally characteristic of surface conditions), there is little attenuation due to internal friction of plastic defor-

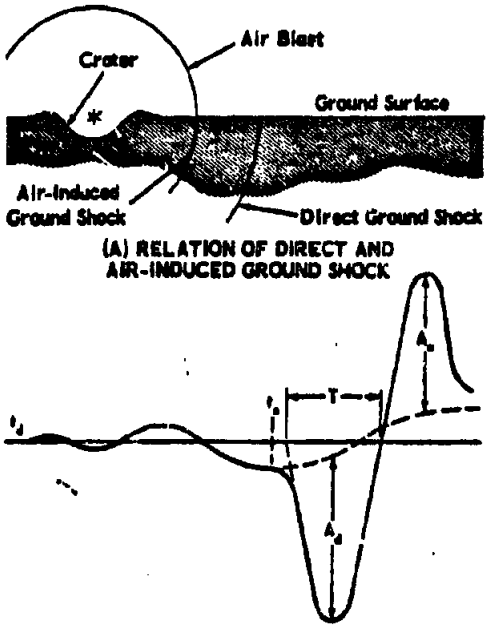

(A) RELATION OF DIRECT AND AIR-INDUCED GROUND SHOCK

t_d = Arrival Time Direct Acceleration
t_s = Arrival Time, Slap Acceleration
$\frac{1}{2T}$ = Slap Acceleration Frequency
A_d = Max. Downward Slap Acceleration
A_s = Max. Upward Slap Acceleration

(B) GROUND ACCELERATION AND SLAP ACCELERATION WAVEFORM

Figure 4–26 (C). Effects of direct and Air-Induced Ground Shock (U)

mation. Ground shock (compression type wave) in rock is reflected from an air-rock interface as a tensile wave. The intensity of this tensile wave is dependent on shock strength, wave shape, and angle of incidence of the direct shock with the free surface.

(2) Pressure (Stress)

At any given point air blast overpressures resulting from a nuclear detonation are equal in all directions, but ground pressures are not. Stress pulses appear as various combinations of direct ground and air-induced shock stresses, depending on arrival time and the range, depth and, direction of the measurement. Direct and air-induced ground shock stress pulses may coincide at close-in ranges outside the crater, as indicated above, but the pulses will gradually separate with increasing distance along the ground surface, until two separate pulses may be detected a few feet beneath the ground surface. The peak stresses from direct ground shock usually attenuate rapidly with distance; however, in highly saturated soils, the attenuation of these stresses is less, approaching the attenuation in water (approximately inversely as the range). The stress pulse from the direct ground shock is composed of vibrations of high and low frequencies, the period of which may vary from a few tenths-of-a-second to several seconds. Two hundred feet from a 1-KT underground burst in Nevada-type soil, the horizontal earth stress at a depth of 10 feet may be 125 psi; at 250 feet it may be 40 psi; while at 600 feet it may be only 3 psi. A rough comparison of peak stress intensities, for various yields at the same distances, may be made on the basis of relative crater size.

(3) Acceleration of Soil Particles

Acceleration of soil particles may be caused as a direct result of the explosion (direct acceleration), as a result of any shock reflection or refraction from underlying bedrock (indirect acceleration), or as a result of air blast (induced acceleration). Direct and indirect accelerations are generally indistinguishable, and together they are termed direct or fundamental acceleration. For acceleration values of 1 G or greater, measured beyond a range of two crater radii from ground zero, the frequency in soil will usually be less than 80 cps for all yields. For a 1-KT yield, the predominant frequencies will be from 3 to 15 cps. In rock, the amplitude of accelerations may be considerably greater, and the period may be less than in average soil.

(4) Displacement of Soil Particles

Displacement of soil particles is largely permanent within the plastic zone of a crater and transient beyond the plastic zone. For a small, near-surface burst, and at a range of three crater radii, the permanent displacement along the ground surface will probably be less than 0.0003 of a crater radius. The transient displacement will probably be less than 0.001 of a crater radius. A short distance beneath the ground surface, soil particle displacement is usually less than the displacement along the ground surface. Displacements are appreciably affected by soil types. In wet soils, for example, they may be of the order of ten times greater than the preceding values.

c. Air-Induced Ground Shock

(1) Propagation

Air-induced ground shock propagates outward from the burst with the air blast. The air blast loading may be considered as a moving, non-uniform load that generates a ground shock. The air-induced shock in soil quickly attains a velocity that may exceed the air blast velocity; however, the magnitude of any outrunning shock is small, and its effects may be ignored. Consequently, as the air blast wave proceeds, the air-induced ground shock propagates with a rather complex, underground, time-of-arrival contour, depending on underground shock velocities. In general, however, the ground-shock front slopes backward from the air-blast shock front, as shown in Fig. 4–26(A). Air-induced ground shock usually arrives with or after the direct ground shock.

(2) Pressure (Stress)

Air-induced ground stresses attenuate gradually with depth, and the rise time of the stress pulse increases. The pulse of the air-induced ground stress is composed of vibrations of high and low frequencies, the periods of which may vary from a few tenths-of-a-second to several seconds. Observations with 1-KT yields show

that, in general, air-induced ground stress is larger than direct ground stress at distances greater than two crater radii, for average soils, and for all heights and depths of burst down to about 75 feet.

(3) Acceleration of Soil Particles

Air-blast induced acceleration maintains its identity in the acceleration pattern, and it can be separated from the direct shock acceleration. When interactions with other accelerations from reflection and refraction occur, the magnitude is affected markedly, and separation is difficult. Upon its arrival, the air blast will cause a sudden local increase in soil particle acceleration termed "air-blast slap acceleration," as shown in Fig. 4–26B. For acceleration values of 1 G, or greater, measured away from ground zero, the predominant frequencies in soil of the air-blast induced acceleration are 20 to 120 cps. Peak vertical accelerations are larger than peak horizontal (radial) accelerations by an amount approximating 50 per cent. Peak accelerations attentuate with depth, are directly proportional to the overpressure, and are indirectly proportional to the rise time of the pressure pulse in the soil. See Fig. 4–27 for the relationship of peak accelerations to peak air-blast overpressures at a depth of ten feet.

(4) Displacement of Soil Particles

Air-induced ground shock causes little permanent horizontal displacement of ground particles beyond two crater radii. When the shock is reflected from vertical soil-air interfaces, local displacement (spalling) of ground particles may occur. Air-induced ground shock may cause a vertical displacement of soil particles. Dry Nevada-type soil subjected to a peak overpressure of 250 psi has sustained a permanent downward displacement of approximately 2 inches, and a transient downward displacement of approximately 8 inches.

d. Column and Base Surge

An effect of underground nuclear explosions is the large quantities of soil, rock, and debris thrown up in the form of a hollow column. As this material falls back to earth it will, in many instances, produce an expanding cloud of fine soil particles, known as a base surge (Ref. 1).

The maximum column diameter is generally two to three times the apparent crater diameter, and the maximum column height is roughly equal to 400 $W^{1/3}$. The characteristics of the base surge depend upon the depth and yield of burst. The shallowest burst depth at which an earth base surge has been observed is 16 $W^{1/3}$ feet. As the burst depth is increased, the extent of the base surge is expected to increase until a burst depth of about 125 $W^{1/3}$ feet is attained. No further increase in base surge extent is expected below this depth of burst. Figs. 4–28 and 4–29 show the rate of growth of the base surge, and maximum radii for various scaled depths of burst.

e. Instructions for Using Figs. 4–28 and 4–29, Base Surge Radius

(1) Description

Fig. 4–29 is based on extrapolation from the maximum base surge radii of the curves in Fig. 4–28. Radii obtained from the figures assume no wind, or are crosswind radii. To compute downwind base surge radii at a specific time after detonation, add the distance traversed by the wind, up to this time, to the base surge radius obtained from the figures; to obtain the upwind base surge radius, subtract.

(2) Scaling Procedure

Depth of burst, and the maximum radius of the base surge, scale as the cube root of yield between scaled depths of burst of 16 $W^{1/3}$ and 125 $W^{1/3}$ feet, using

$$\frac{h_1}{h_2}=\frac{r_1}{r_2}=\frac{W_1^{1/3}}{W_2^{1/3}}$$

where h_1 and r_1 are depth of burst and base surge radius for yield W_1, and h_2 and r_2 are the corresponding depth of burst and base surge radius for yield W_2; and using

$$\frac{t_1}{t_2}=\frac{W_1^{1/6}}{W_2^{1/6}}$$

where t_1=time to complete a given percentage of total radial growth for yield W_1, and t_2=corresponding time to complete the same percentage of total radial growth for yield W_2.

(3) Example

Given: A 64-KT detonation 65 feet underground.

Find: (a) The maximum base surge radius.

(b) The time at which the maximum radius occurs.

Solution: The corresponding depth of burst for 1 KT is

$$h_1 = \frac{w_1^{1/3} \times h_c}{w_c^{1/3}} = \frac{1 \times 65}{(64)^{1/3}} = 16 \text{ feet.}$$

From Fig. 4–28 the maximum radius for 1 KT at a 16 foot depth of burst is 2,010 feet, and it occurs at 180 seconds.

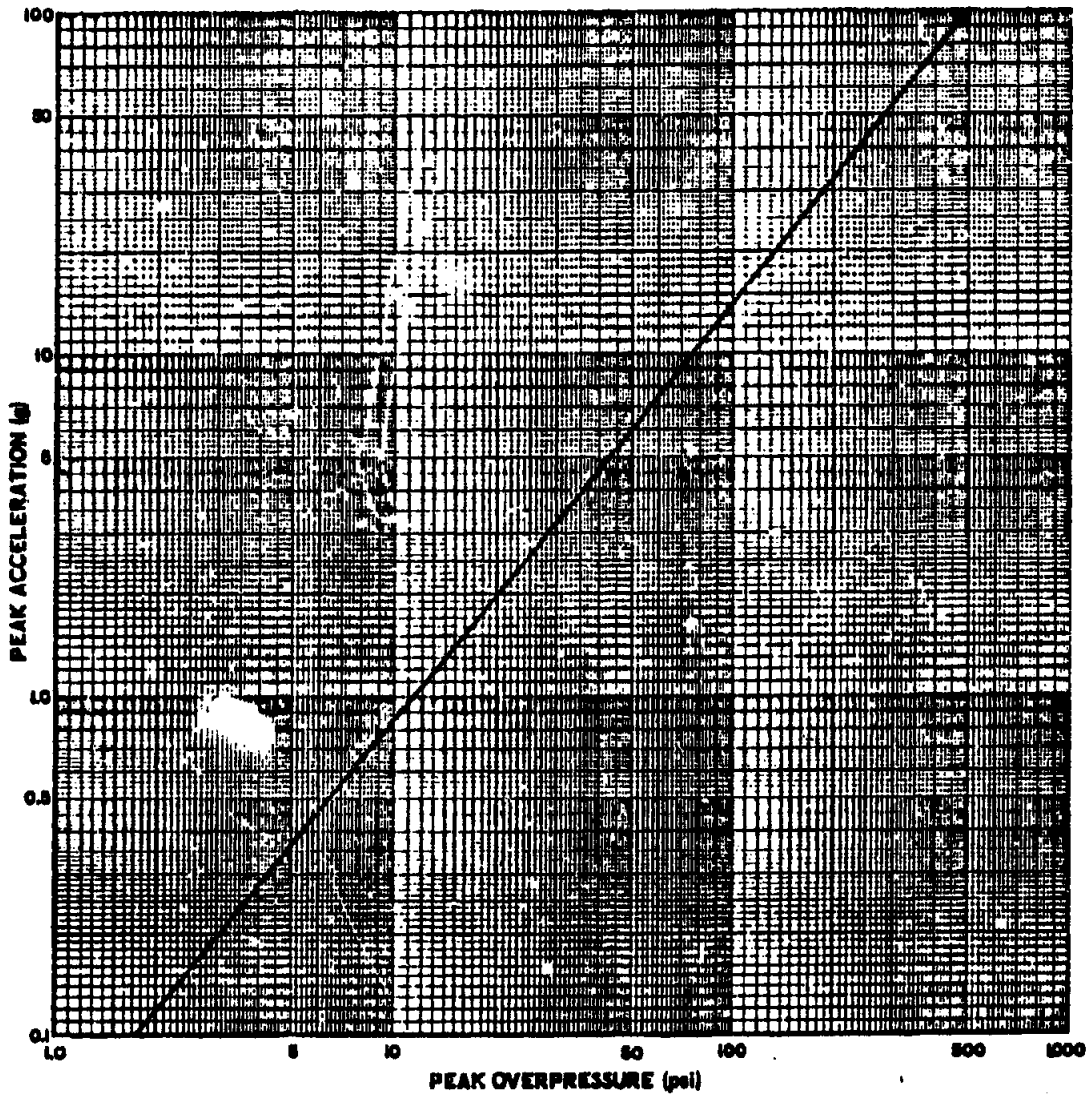

Figure 4–27 (C). Peak Air-Induced Ground Acceleration (Vertical Component) vs Peak Overpressure (U)

The corresponding radius for 64 KT is

$$r_2 = \frac{r_1 \times w_2^{1/3}}{w_1^{1/3}} = \frac{2{,}010 \times (64)^{1/3}}{1} = 8{,}040 \text{ feet.}$$

This may also be read directly from Fig. 4-29.

The time at which this maximum radius occurs is

$$t_2 = \frac{w_2^{1/6} \times t_1}{w_1^{1/6}} = \frac{(64)^{1/6} \times 180}{1} = 360 \text{ seconds.}$$

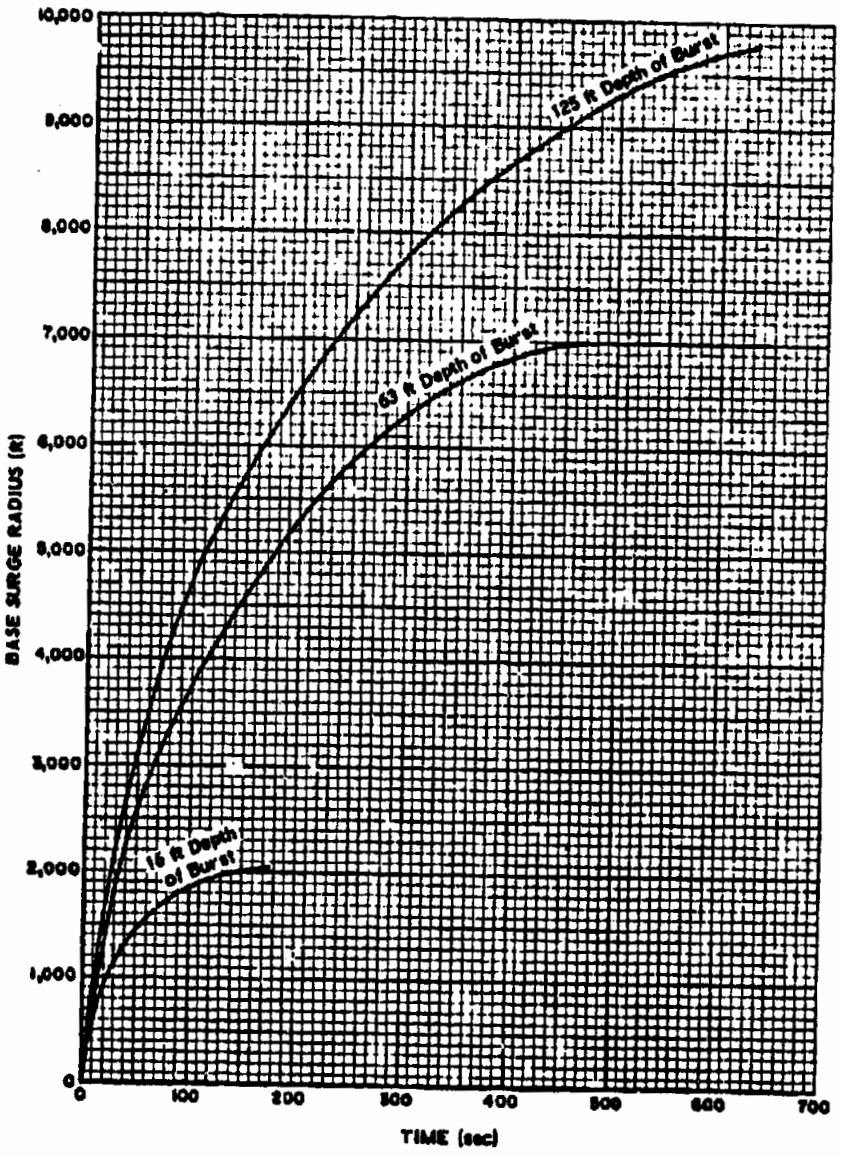

Figure 4-28 (C). Base Surge Radius vs Time, for 1-KT Underground Bursts at Various Depths (U)

(4) Reliability

The data presented in the figures are based on limited full-scale testing, and on extensive HE reduced-scale testing.

4–3.4. (U) Underwater Bursts from Conventional (Chemical) Explosions

4–3.4.1. *Introduction*

The subject of underwater explosions has been treated extensively, from both a theoretical and experimental point of view. An excellent presentation of all aspects of underwater, chemical explosions is given by Cole in Ref. 5. This reference is readily available in book form, and should be consulted for detailed information.

4–3.4.2. *Description*

When the charge is detonated, the resulting physical disturbance advances outward underwater through the solid material of the charge at a high rate of speed. In the case of a high explosive, as distinguished from a gun propellant, the resulting chemical reaction is also rapid. This reaction continues to reinforce the detonation wave, so that the entire process converts the solid explosive into a gas at high pressure, in an extremely short time. The initial sphere of high pressure and high temperature gas transmits this high pressure to the surrounding water. In this way, the boundary conditions for the wave phenomena in the water are generated. Once this happens, a shock wave forms and travels outward under the same hydrodynamic laws as those governing the motion of a blast wave in air. In fact, one of the theories most used, that of Kirkwood and Brinkley (Par. 4–2.3.5.*e*; and Refs. 3 and 5), can be used for predicting shock wave phenomena for either air or water.

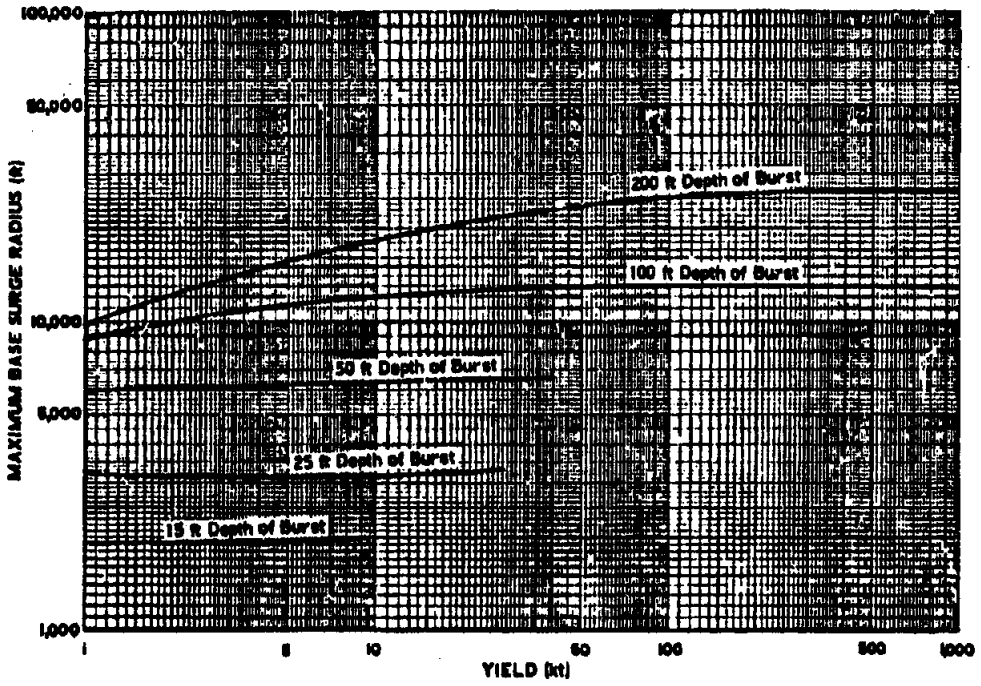

Figure 4–29 (C). Maximum Base Surge Radius vs Yield, for Underground Bursts at Various Depths (U)

The physical phenomena for the propagation of the shock wave is also similar. That is, following the initiation of the shock at the surface of the gas sphere, the wave travels outward at a speed greater than the speed of sound, and at a rate decay of pressure (being a spherical wave) somewhat greater than inversely with distance, as predicted by acoustic theory. As the radius increases, the disturbance approaches that predicted by acoustic theory, as one would expect.

A phenomenon associated with underwater explosions which is not present in air bursts, is the formation and subsequent motion of the gas sphere. Because the expanding gas causes outward flow of the surrounding water, the bubble continues to expand beyond its pressure equilibrium state; then, when outward motion stops, the external pressure in the water is higher than that of the gas in the bubble, and contraction occurs. Since the gas is a highly elastic system, bubble oscillation takes place. During this time, the bubble rises toward the surface because of its buoyancy. As stated in Ref. 5, other factors affect the motion, making analytical prediction of bubble behavior very difficult. Such factors would be the proximity of the bubble to the bottom, and to the free surface. Bubble pulsation has an important effect on the surrounding flow, however, since each pulsation becomes a possible source of secondary pressure waves. According to Ref. 5, the overpressure caused by the first bubble pulsation is only a fraction of the shock wave pressure. The duration of the overpressure is greater, however; therefore, the impulse imparted to the water is comparable in the two cases.

Returning to the shock wave formed in the water, and its effect, it is significant that scaling laws are applicable and give reliable results. For a given set of ambient conditions, the cube root scaling laws (Par. 4–2.6.3) are equally valid when comparing the effects of different size charges. That is, the same pressure ratio is observed for two different explosions at equal values of $\frac{R}{E_w^{1/3}}$ and $\frac{t}{E_w^{1/3}}$. For example, if a change of weight E_w produced a pressure ratio of P/P_o at a distance R, t seconds after explosion, then a charge of one-eighth the weight would produce the same pressure ratio at a distance $R/2$, $t/2$ seconds after detonation.

From an analytical viewpoint, the shock wave propagation problem is similar to the problem in air, as has been stated. It is remarked in Ref. 3, however, that the details are simpler in the case of underwater blast waves. This is because the relatively small entropy increment produced at the shock front permits the use of the approximation of adiabatic flow. Such approximations across a shock front are not permissible in air.

4–3.5. (C) Underwater Bursts from Nuclear Explosions

4–3.5.1. *Cratering*

An underwater crater is considered to be the crater existing in the bottom material at that time, shortly after the burst, when conditions are no longer changing rapidly. Subsequent hydraulic wash action by the current, tides, etc., will tend to erode away any crater lip, while making the crater wider and shallower. The degree of this effect depends on the depth of the water, type of bottom material, and current, wave, and tidal activity.

The size of the underwater crater is dependent upon weapon yield and burst depth, but also upon water depth and bottom composition. Figs. 4–30 through 4–35 are graphic illustrations of the data on crater diameter, depth, and lip height for both surface and bottom bursts in 25, 50, 100, and 200 feet of water. The figures show that the crater dimensions are greater for a bottom burst than for a surface burst. Also, as the depth of the water increases, the crater dimensions increase for a bottom burst, but decrease for a surface burst (Ref. 21).

4–3.5.2. *Water Shock*

a. Description and Analysis

The underwater detonation of a nuclear weapon at a distance from either the water surface or the bottom boundaries produces a shock wave early in the formation of the gas

bubble. This shock wave propagates spherically at the rate of roughly 5,000 ft/sec., and is characterized by an instantaneous rise in pressure followed by an exponential decay. In addition to this initial primary shock wave, several subsequent pressure pulses are produced within the water.

When the pressure wave is reflected from the water surface it is reflected as a rarefaction or tensile wave. This reflected rarefaction wave cuts off the tail of the primary compressional shock wave, thereby decreasing the duration of its positive phase. Fig. 4–36 shows qualitatively the effect of the reflection wave upon the pressure-time history. The effect of this cutoff decreases rapidly with increased depth of target

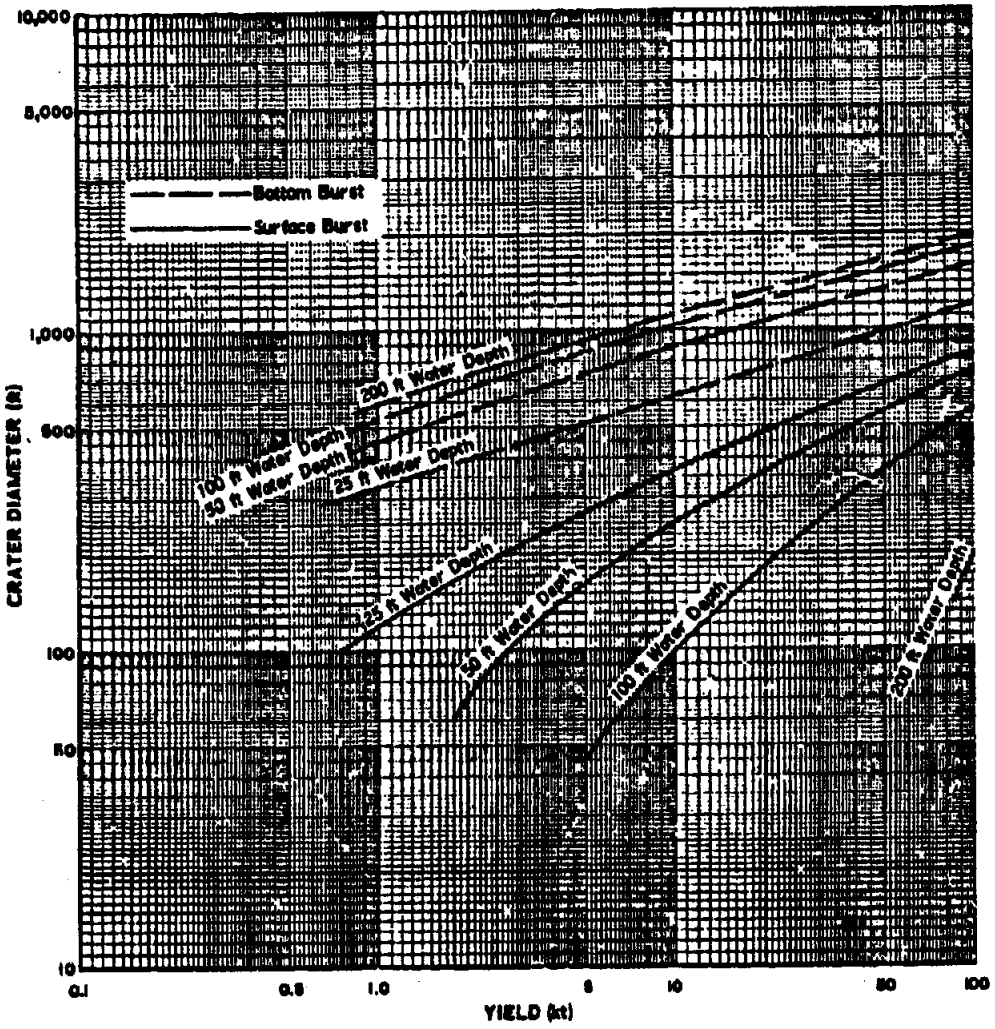

Figure 4–30 (C). Crater Diameter vs Yield, for Underwater Cratering for Various Water Depths with Sand, Sand and Gravel, or Soft Rock Bottoms, for 0.1-KT to 100-KT Yields (U)

in the water; that is, as the depth to the target increases, the less the effect of cutoff for a given depth of detonation. Conversely, as the depth of detonation increases, the less the effect of cutoff for a given target location.

The reflection of pressures from the bottom surface for an underwater burst, is similar to the reflection of pressures from the ground surface for an air burst. A crude approximation of the magnitude and shape of this reflected, water-shock wave can be obtained, if it is assumed that the wave is identical to an imaginary direct wave, this having traveled a distance equal to the path-distance of the reflected wave, i.e., that perfect reflection occurred. Estimated peak overpressures vs slant ranges, for vari-

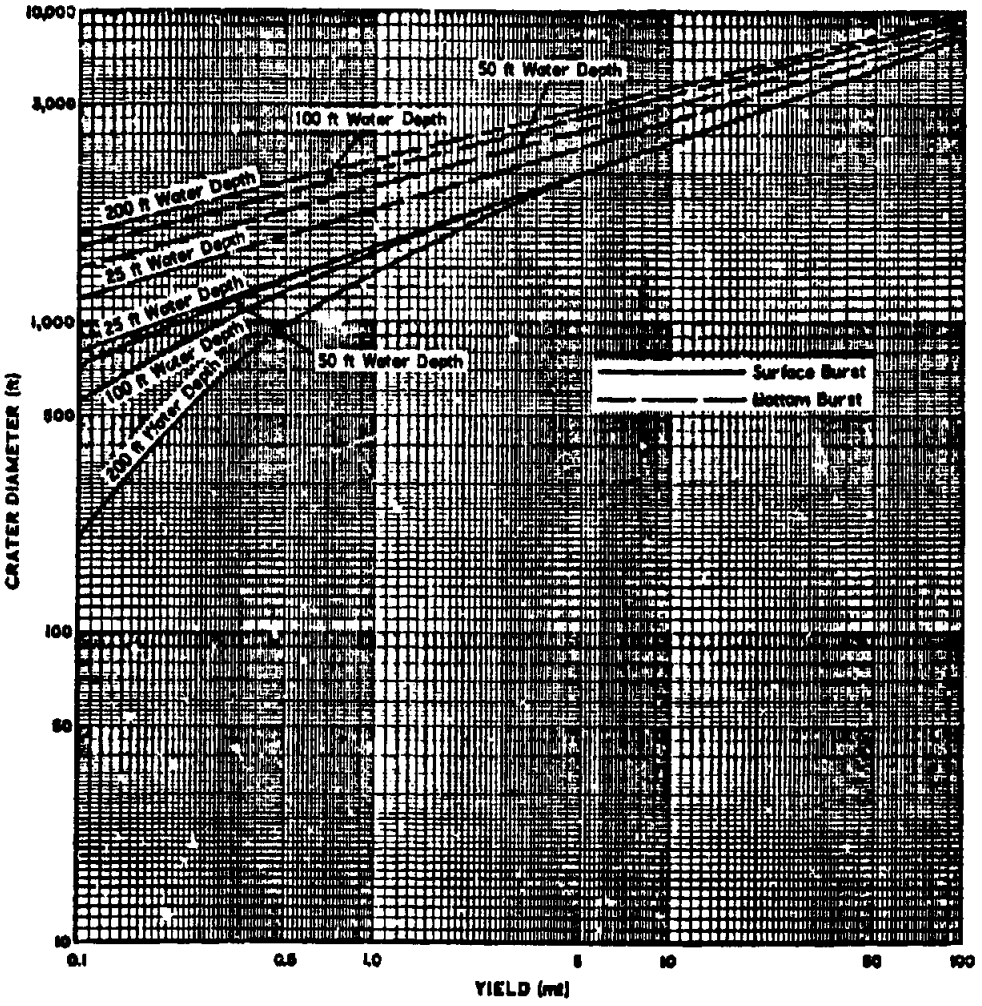

Figure 4–31 (C). Crater Diameter vs Yield, for Underwater Cratering for Various Water Depths with Sand, Sand and Gravel, or Soft Rock Bottoms, for 0.1-MT to 100-MT Yields (U)

ous yields, are shown in Fig. 4–39, where the order of magnitude of these pressures may be noted. However, the durations of these pressures are short, being measured in tens of milliseconds. They may be even shorter at points near the water surface, where the surface-reflected wave arrives at the point before the complete passage of the primary compressional wave.

If the nuclear weapon is set off at shallow depths in deep water, the peak overpressure estimates of Fig. 4–39 are excessive in terms of actual overpressures, for most regions of interest. For example, a 10-KT weapon set off

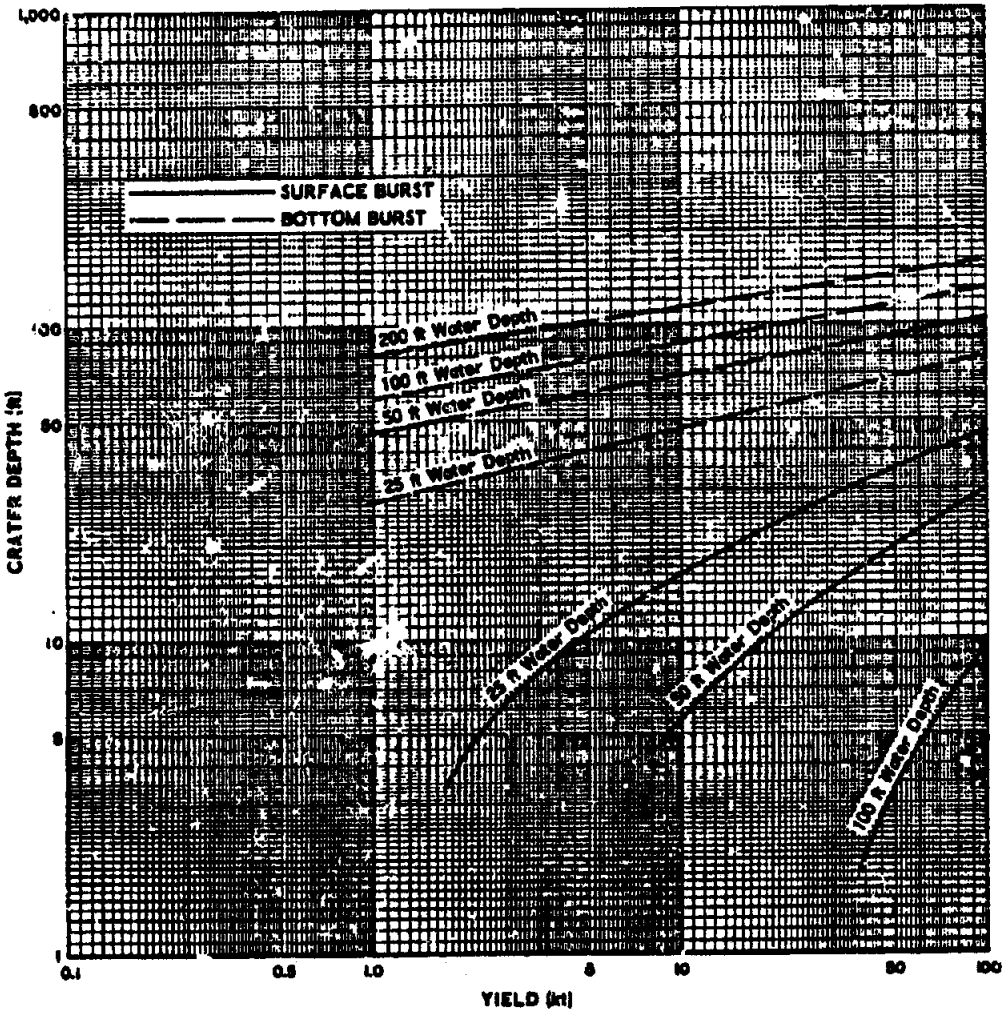

Figure 4–32 (C). Crater Depth vs Yield, for Underwater Cratering for Various Water Depths with Sand, Sand and Gravel, or Soft Rock Bottoms, for 0.1-KT to 100-KT Yields (U)

at a depth of 200 feet, in deep water, would actually develop a peak overpressure of approximately 350 psi at the range of 2,000 yards and the depth of 50 feet. This is in contrast to a pressure of 550 psi, as predicted by the figure. The actual overpressure is less than the predicted because the initial shock wave strikes the water surface at a high obliquity and reflects in an anomalous manner, and the sharp cutoff from the reflected pressure does not occur. Instead, the reflected tensile wave modifies the pressure-time history at early times, and forms a nearly triangular pulse (Fig. 4–37). The region wherein this anomalous reflection affects the pressure history is termed the nonlinear region.

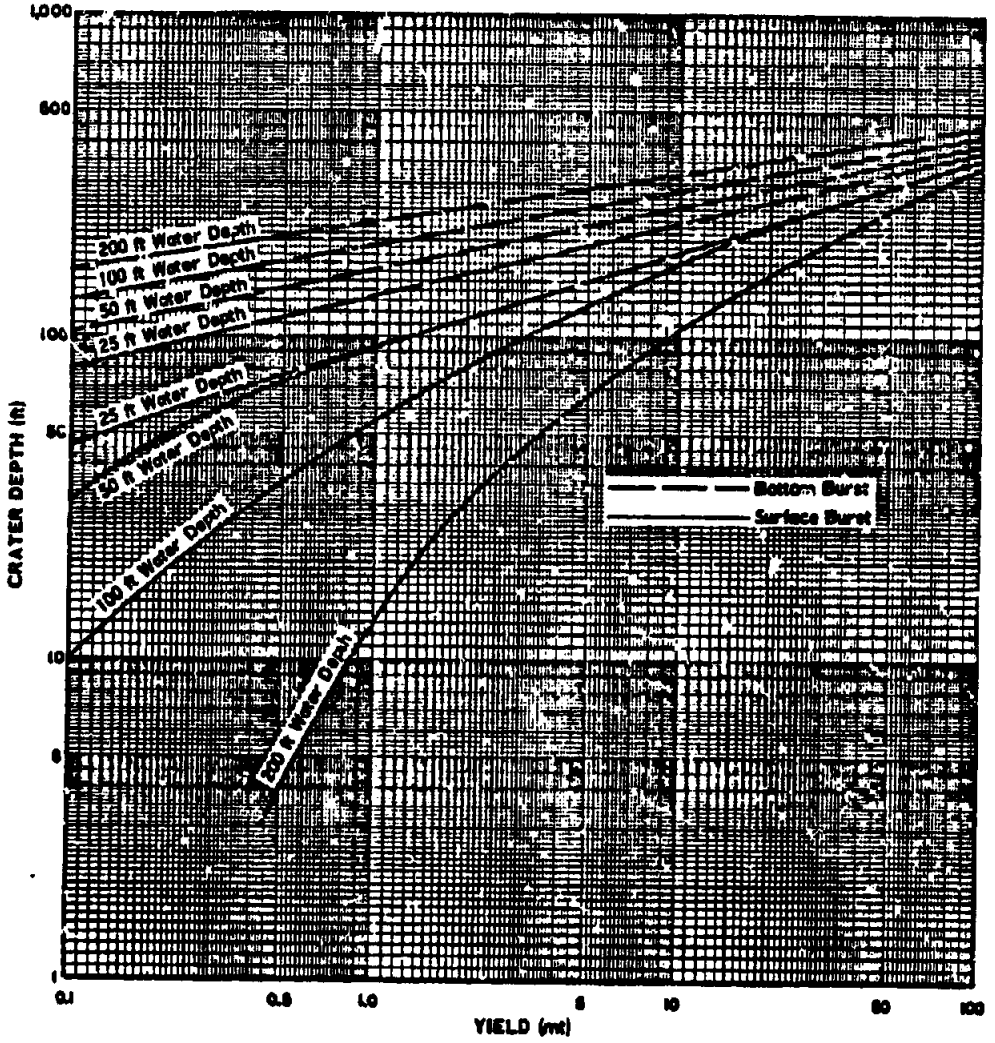

Figure 4–33 (C). *Crater Depth vs Yield, for Underwater Cratering for Various Water Depths with Sand, Sand and Gravel, or Soil Rock Bottoms, for 0.1-MT to 100-MT Yields (U)*

The nonlinear region is in the form of a wedge, increasing in depth as the range from the burst point increases. At the shallower depths in this region, the anomalous behavior is sufficient to reduce the magnitude of the initial peak overpressure. At greater depths, the effect shades off, until only at the later times of the pressure history is there any reduction of overpressure. As the depth of burst is decreased (or the yield increased) the nonlinear zone increases in scope and magnitude. Finally, for a surface burst, all points beneath the water surface (except those directly under the weapon) are in the nonlinear region. Be-

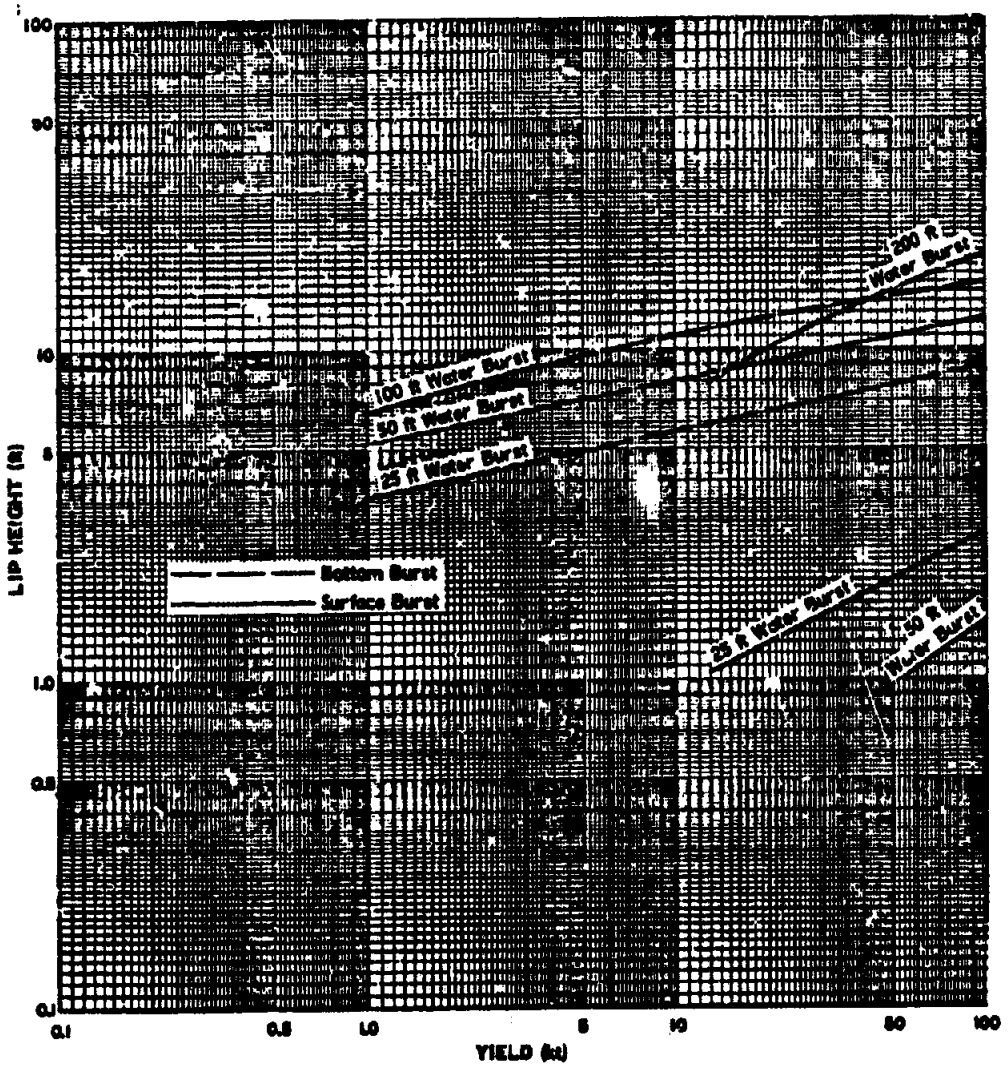

Figure 4–34 (C). Crater Lip Height vs Yield, for Underwater Cratering for Various Water Depths with Sand, Sand and Gravel, or Soft Rock Bottoms, for 0.1-KT to 100-KT Yields (U)

cause the peak pressure in the nonlinear region is a sensitive function of burst and target geometry, pressure-distance curves are not presented here, to account specifically for this effect.

When a nuclear weapon is detonated in shallow water, both the reflecting boundaries of the water surface, and the bottom, alter the peak pressure and duration of the primary underwater shock wave. In addition to the multiple reflections that occur, the shock wave is transmitted across these boundaries (i.e., propagated through the air and the bottom, and then coupled back into the water). Hence, at a

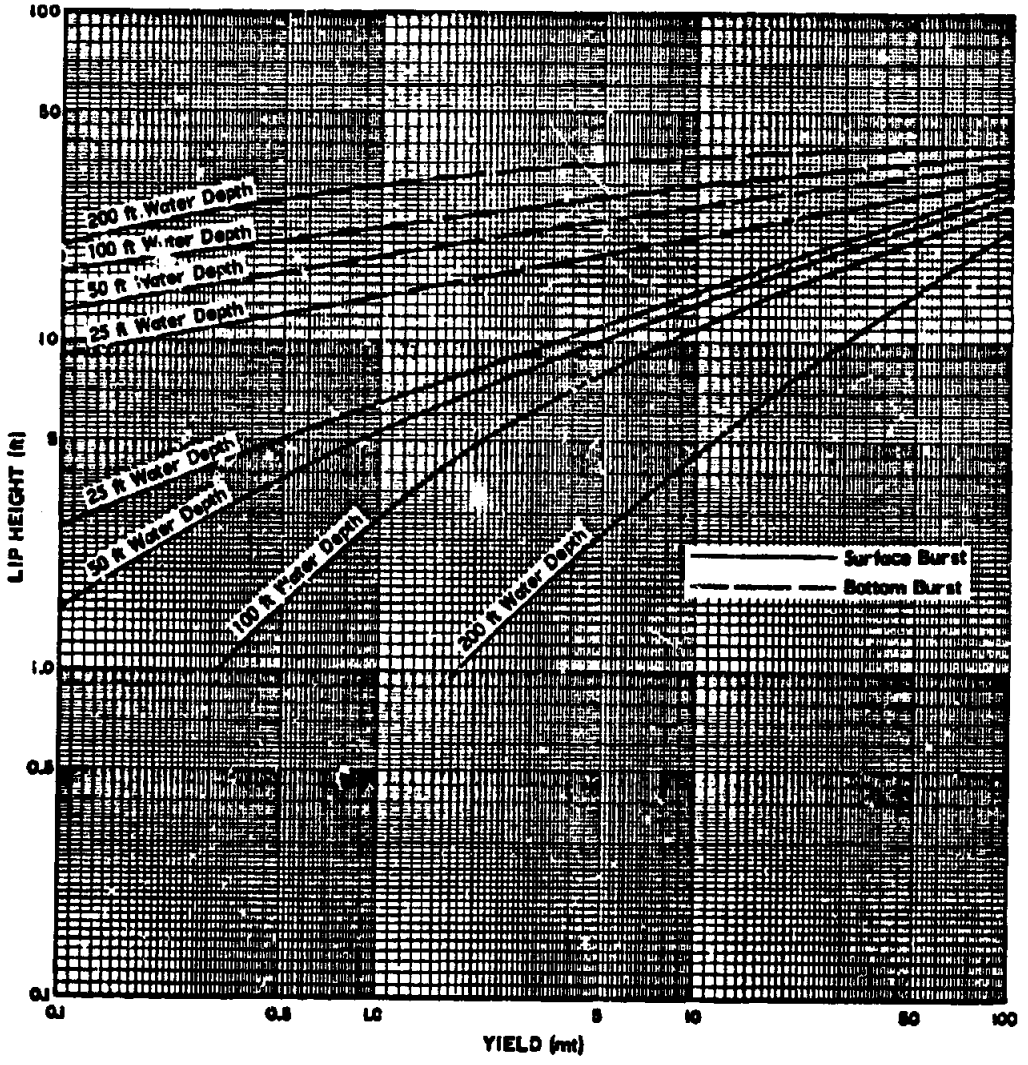

Figure 4–35 (C). Crater Lip Height vs Yield, for Underwater Craterng for Various Water Depths with Sand, Sand and Gravel, or Soft Rock Bottoms, for 0.1-MT to 100-MT Yields (U)

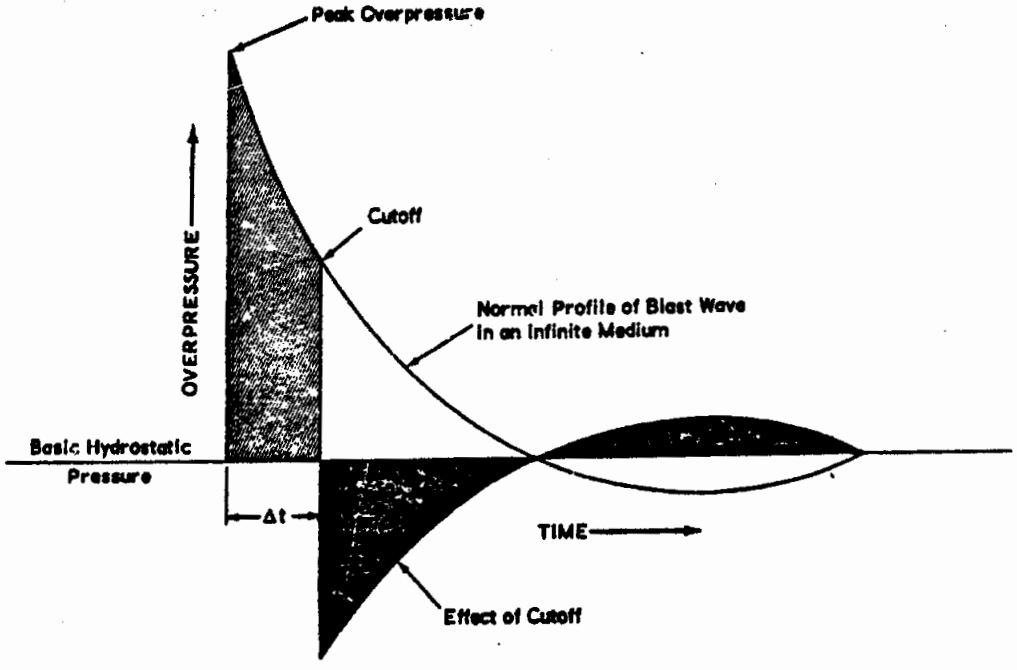

$$\Delta t \text{ in msec} = \frac{0.4 \times (\text{Bomb Depth in ft}) \times (\text{Target Depth in ft})}{\text{Slant Range in ft}}$$

Figure 4–36 (C). Effect of Cutoff on the Shape of the Positive Pulse (U)

point distant from the source, there will be a direct water shock, water shocks induced by ground and air shocks, and water shocks reflected from the surface and the bottom. The order of arrival will be: first, the ground induced shock; then, the direct shock with the

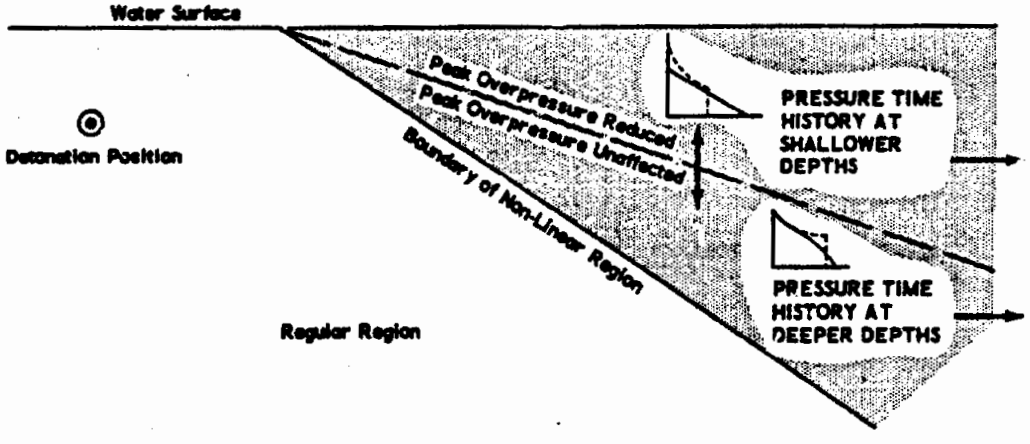

Figure 4–37 (C). Nonlinear Surface Reflection Effects (U)

reflections: and, finally, the air induced shocks (Fig. 4–38).

At most scaled depths, the direct water shock is the greatest. As the direct shock travels outward, the rate of attenuation with distance is determined primarily by the depth of water and the relative position of the weapon within that depth. The shallower the water and/or the closer the weapon to the water surface, the greater the rate of attenuation. This difference in attenuation can be attributed to the nonlinear surface reflection, and to the interference of multiple reflection waves with the direct shock wave. These effects far outweigh any apparent yield increase resulting from the weapon being detonated on the bottom, as contrasted with the yield increase that occurs in the case of the land surface burst.

Insufficient data exist for the preparation of water overpressure versus distance curves for detonations in shallow water, as is possible for deep water detonations. In the case of a 20-KT detonation at mid-depth in 180 feet of water, the peak overpressures at moderate ranges have been observed to be on the order of one-half those indicated for deep water. Pressures even less than these are expected for a mid-depth burst in more typical harbor conditions, because of the shallow depths of water and bottom irregularities. On the other hand, a burst on the bottom will result in slightly higher peak overpressures than one at mid-depth in shallow water.

Since water has no tensile strength, the rarefaction resulting from a reflection at the water-air interface causes the water surface to cavitate. Thus, a "spray dome" is formed. When this collapses, an additional shock is induced in the water by an effect similar to a water hammer. Little is known about the magnitude of the shock from this source; however, it is believed that it can generally be neglected.

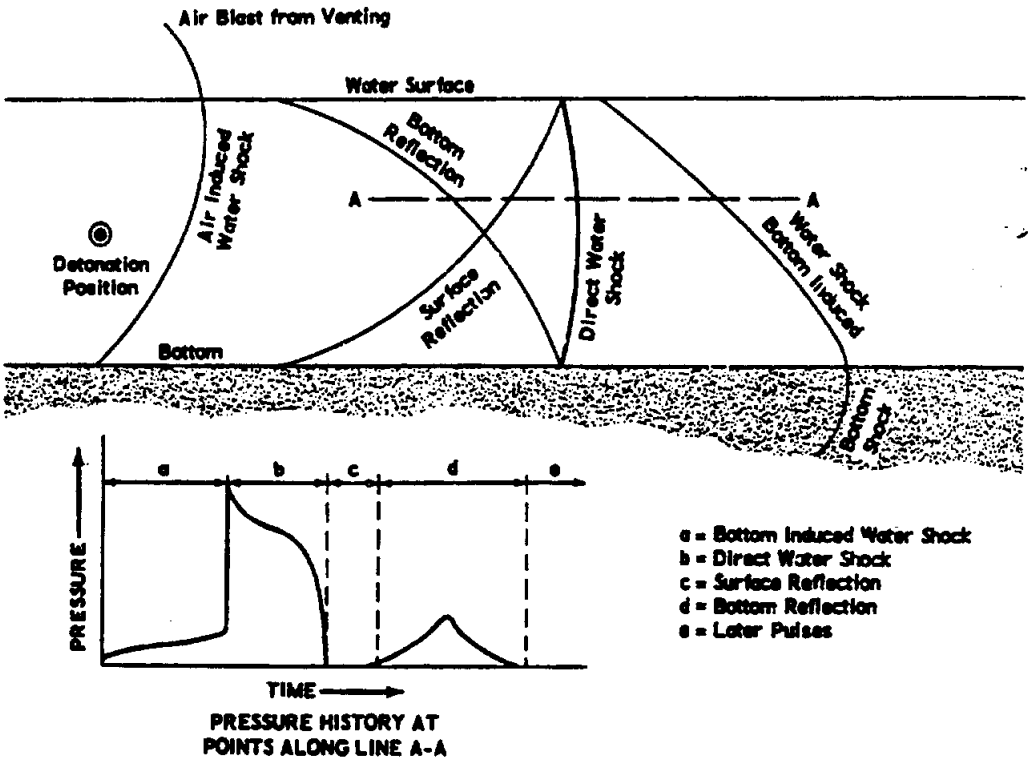

Figure 4–38 (C). Wave Front Propagation in Shallow Water (U)

The propagation of the underwater shock waves is distorted on passing through regions of sharp temperature changes within the water, with the result that the pressure wave form is affected. If the weapon is fired in close proximity to a region of temperature change, there is a shadow zone formed, wherein predictions based upon free water conditions overestimate the effectiveness of the shock wave. When the weapon is fired well above, or below, this temperature region, pressure histories at the normal ranges of interest are changed very little.

b. Instructions for Using Fig. 4–39, Peak Overpressure for Deep Underwater Bursts

(1) Description

Fig. 4–39 gives the expected values for peak water overpressure versus slant range for various yields burst deep in deep water, where the effects of a reflecting surface are absent.

(2) Scaling Procedure

Scaling for yields other than those shown may be done by linear interpolation between appropriate curves.

(3) Example

Given: A 40-KT weapon is burst at a depth of 1,000 feet in deep water.

Find: The peak water overpressure at a 1,000-foot depth 4,000 yards from the burst.

Solution: From Fig. 4–39, the peak water overpressure at a slant range of 4,000 yards, for a 40-KT weapon, can be read directly as 440 psi.

(4) Reliability

Slant ranges obtained from Fig. 4–39 are estimated to be reliable within ±20 per cent for the yield range shown.

4–3.5.3. *Wave Formation*

a. Surface Waves

Surface waves generated by underwater explosions are the result of the emergence and collapse of the gas bubble. The first wave is generally a well-defined breaking wave. (In the case of a deep burst in deep water, this wave was first observed at roughly 2,000 feet horizontal range.) The first wave is followed by a train of more stable oscillatory waves. As the disturbance moves outward, the number of waves in the wave train increases. At first, the initial wave of the group is the highest, but as the wave train progresses farther from the origin, the maximum wave height appears in successively later waves. It has been observed for a shallow water burst that, by the time the wave train had progressed out to 22,000 feet, the ninth wave was the highest of the group; but for a deep water burst at 10,000 feet, the seventh wave was observed to have the largest amplitude. For the shallow water burst, the maximum wave height one mile from the detonation was about 20 feet; for the deep burst, it was about 40 feet at the same distance, reflecting in this case the greater depth of water and burst depth.

Fig. 4–40 gives maximum wave heights as a function of range, under a number of stated conditions for a 1-KT underwater burst. These predictions are based upon the maximum wave passing the point of interest, without regard to its position in the train. Thus, the maximum crest-to-trough amplitude decreases linearly as the reciprocal of distance, while the amplitude change with distance for any individual wave varies in a more complex manner. In a given depth of water, a wave no higher than about 70 per cent of the water depth can propagate as a stable phenomenon. Higher waves are unstable, and they decrease in height until stability is attained.

The formation, propagation, and magnitude of surface waves generated by an underwater burst, in shallow water, vary rapidly with the scaled depth of water and the configuration of the bottom. For prediction purposes in water shallower than 80 $W^{1/3}$ feet, the burst position has little effect on the wave generation.

For the underwater burst in deep water, the size of the generated surface waves is dependent upon the position of the weapon relative to the surface. For practical purposes, as the depth of burst is lowered from the surface to

a depth of 180 W^1/3 feet, the maximum wave height can be considered to increase constantly. The scaled depth of 180 feet (two-thirds of the maximum bubble radius of a 1-KT burst) represents an optimum depth. With further increases in depth, the maximum height again drops off, approaching the scaled magnitude of waves observed from bursts at deep depths (scaled depth of burst of 850 W^1/3 feet).

Waves moving from deep into shallow water, or from open water into narrows, may be considerably increased in magnitude; however, this increase is unpredictable unless the exact geometry of the bottom is known. Waves break on arriving at water depths about equal to the wave height, momentarily increasing in height by approximately 30 per cent, then rapidly decreasing.

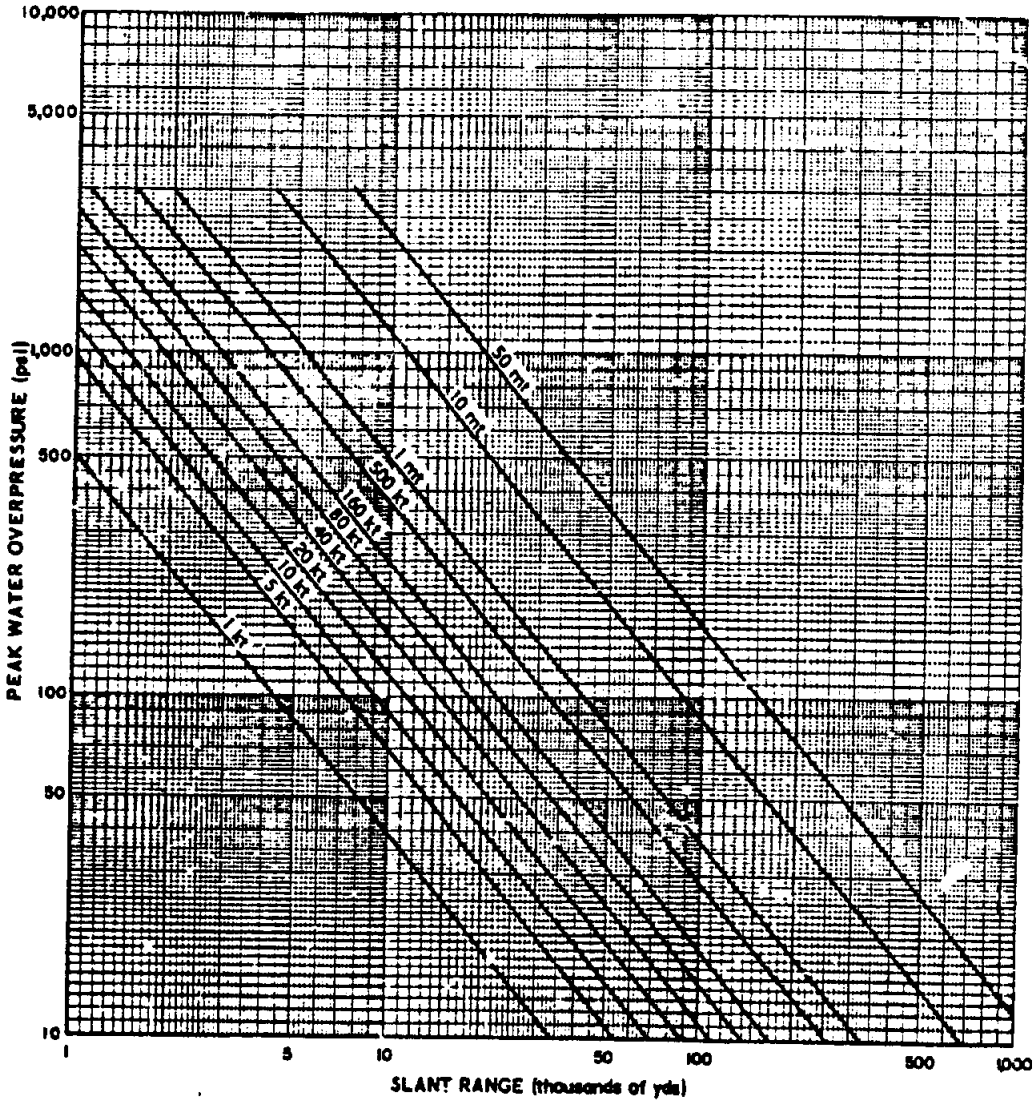

Figure 4–39 (C). Peak Water Overpressure vs Slant Range, for Deep Underwater Bursts (U)

b. Instructions for Using Fig. 4–40, Maximum Wave Height for Underwater Bursts

(1) Description

Figure 4–40 gives the approximate, maximum, crest-to-trough, wave heights (in terms of horizontal distance from surface zero) to be expected from surface and underwater bursts of 1-KT weapons. This data may be scaled to other yields, as explained below. For burst depths greater than 180 $W^{1/4}$ feet but less than 850 $W^{1/4}$ feet, a linear interpolation between the values from the above limiting cases will provide a satisfactory prediction. Below 850 $W^{1/4}$ feet, the wave height is expected to decrease almost inversely with increasing depth.

(2) Scaling Procedure

Use the following two relations: First,

$$\frac{W_1^{1/3}}{W_2^{1/3}} = \frac{h_1}{h_2}$$

where yield W_1 will give a wave height of h_1, and yield W_2 will give a corresponding wave height h_2, at the same scaled depth of burst. Secondly,

$$\frac{d_1}{d_2} = \frac{W_1^{1/4}}{W_2^{1/4}} = \frac{d'_1}{d'_2}$$

where yield W_1, burst at a depth d_1 in water of depth d'_1, is equivalent to a burst of yield W_2 at a depth d_2, in water of depth d'_2.

(3) Example

Given: A 40-KT detonation at 450 feet in 1,500 feet of water.

Find: The expected maximum wave height at 10,000 yards from surface zero.

Solution: The corresponding burst depth for 1 KT is:

$$d_1 = \frac{450}{(40)^{1/4}} = \frac{450}{2.5} = 180 \text{ feet.}$$

The corresponding water depth for 1 KT is:

$$d'_1 = \frac{1500}{(40)^{1/4}} = \frac{1500}{2.5} = 600 \text{ feet.}$$

Use the curve of Fig. 4–40 for burst depth of 180 feet and water depths of 450 feet or greater. From this curve, the maximum wave height at 10,000 yards for a 1-KT burst is 2.2 feet. Therefore, for a 40-KT burst, the wave height of 10,000 yards is:

$$h_2 = (2.2) \times (40)^{1/3} = (2.2) \times (6.3) = 14 \ (\pm 4) \text{ feet.}$$

(4) Reliability

The wave heights obtained from Fig. 4–40 are estimated to be reliable within ±30 per cent.

c. Base Surge

A significant phenomenon of underwater nuclear explosions is the base surge, a sizable cloud or wave of dense mist that moves outward from the water column. For depths of detonation less than 10 $W^{1/4}$ feet, the formation of a significant base surge is unlikely. When the detonation is at a greater depth, but one shallow enough for the gaseous explosion bubble to vent the surface while it is still expanding to its first maximum radius, an extensive column of water is thrown into the air. The collapse of this column forms the base surge.

As observed in one underwater explosion, a conical spray dome began to form about four milliseconds after the explosion. Its initial rate of rise was greater than 2,500 feet per second. A few milliseconds later, a hollow column began to form, rapidly overtaking the spray dome. The maximum height attained by the column of water was probably some 8,000 feet, and the greatest diameter was about 2,000 feet. The maximum thickness of the walls of the column was about 300 feet. Approximately 1,000,000 tons of water were thrown into the air. As the column fell back into the water, there developed on the surface, at the base of the column, a large doughnut-shaped cloud of dense mist. This cloud (the base surge), formed about ten seconds after detonation and traveled rapidly outward at an initial velocity greater than 100 feet per second, maintaining an ever-expanding doughnut-shaped form. In the first 100 seconds, the average velocity was 63 feet per second. In 180 seconds, the surge traveled 8,100 feet.

If the underwater detonation is at a depth such that the gas bubble goes through several

oscillations prior to venting, a bushy, ragged, plume-like mass of water is thrown into the air by the emerging bubble. The collapse of these plumes generates the base surge. In the observation of such a deep burst, the first visible surface phenomenon was a very flat spray dome some 7,000 feet in radius and 170 feet in height. Three seconds later a second spray dome emerged out of the first, sending spikes to a height of 900 feet. At ten seconds the plumes appeared, reaching a height of 1,450 feet and a diameter of 3,100 feet. As the plumes collapsed, a base surge spread out laterally to a cross-wind radius of 4,600 feet, at 90 seconds, and to approximately 7,000 feet at 15 minutes.

At intermediate depths of burst, such that the bubble vents after the first expansion is completed, but before several oscillations are

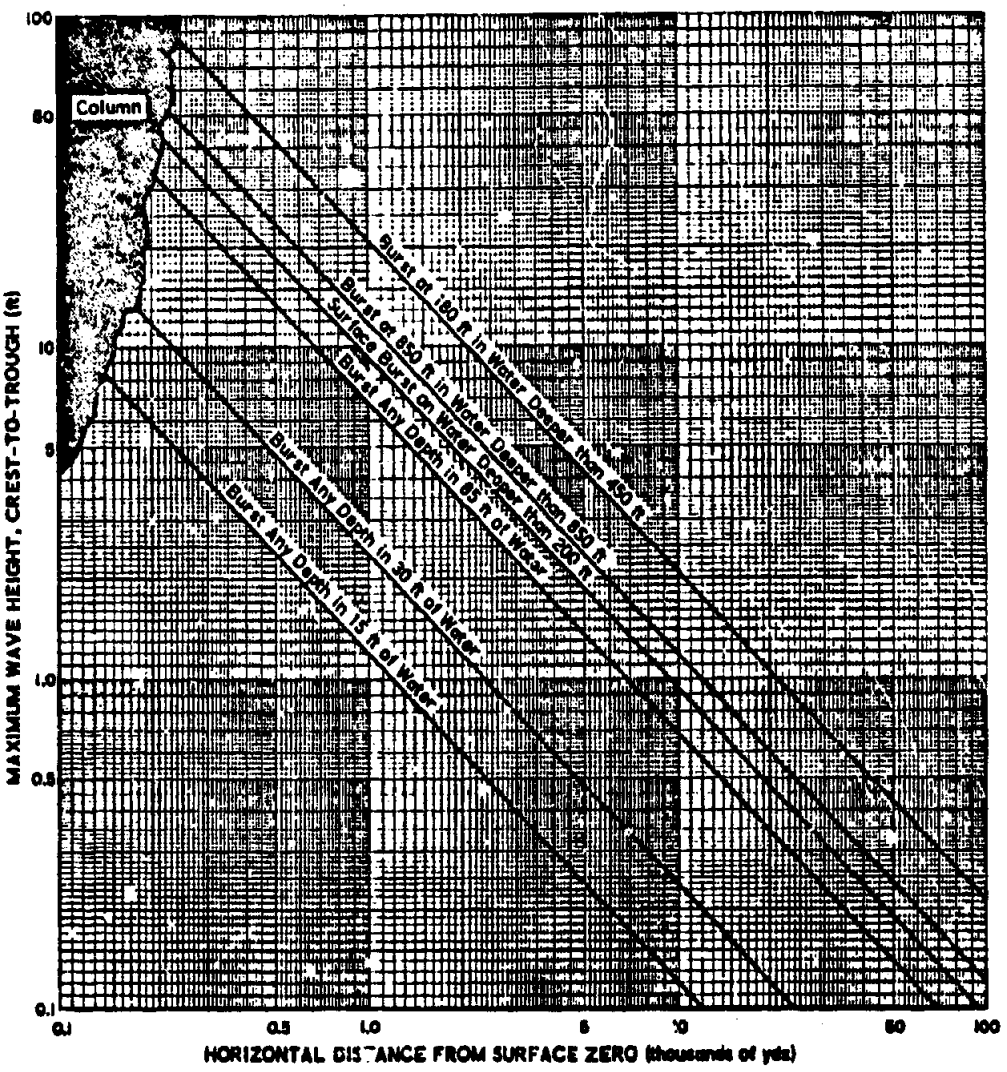

Figure 4–40 (C). Maximum Wave Height for 1-KT Underwater Bursts (U)

completed, the magnitude of the base surge varies in a manner dependent upon the phase of the bubble at venting. When the bubble vents in an expanding phase, the surge phenomenon is similar to that described for a shallow burst. When the bubble vents in a contracting stage, a tall spire of water is jetted into the air. The base surge resulting therefrom is less dense and of a smaller final radius. However, lack of knowledge of bubble behavior permits only a coarse prediction of the maximum size of base surge. Figs. 4–41 and 4–42 provide representative data on base surge radius, in terms of time and yield, respectively.

Winds cause the surge to travel faster in the direction in which the wind is blowing. Although relative humidity does not affect the initial formation of the base surge, it does influence its subsequent growth and duration. When the relative humidity is significantly less than 70 per cent, the extent and duration of the base surge are apt to be less than predicted. A significant increase in extent and duration of the base surge is expected when the relative humidity is appreciably greater than 70 per cent.

d. Instructions for Using Figs. 4–41 and 4–42, Base Surge Radius for Underwater Bursts

(1) Description

Fig. 4–41 gives the expected radial growth of the water base surge, as a function of time after detonation, for a 1-KT weapon at various depths of burst. Fig. 4–42 gives the expected maximum base surge radius as a function of yield, for several specific depth of burst conditions. The maximum base surge is developed from a weapon detonated at approximately the venting depth (250 $W^{1/4}$ feet).

Proximity of the bottom to the point of detonation has little effect upon the production of the base surge. For depths of burst between the limits to 10 $W^{1/3}$ and 250 $W^{1/4}$ feet, the diameter of the water column producing the base surge is approximately one-fourth of the resultant surge radius. With depths of burst below the venting depth of 250 $W^{1/4}$ feet, no such simple relation of the column or plume to the resultant surge exists. Little data or theory are available for base-surge predictions at deep depths. A prediction can be made, however, by linear interpolation between the base-surge radius of a burst at venting depth, and one at a deep scaled depth (650 $W^{1/3}$ feet). A prediction thus made represents the maximum base-surge which could be expected.

Radii obtained from Figs. 4–41 and 4–42 assume "no wind" conditions. To compute upwind or downward base-surge radii for a specific time after detonation, use the following procedure: to obtain the downwind base-surge radius, add the distance traveled by the wind up to this time to the "no-wind" base-surge radius: to obtain the upwind base surge radius, subtract.

(2) Scaling Procedure

Depth of burst, and the accompanying maximum radius of the base surge, scale as the cube root of yield for depths of burst between 25 $W^{1/3}$ and 250 $W^{1/4}$, or:

$$\frac{h_1}{h_2}=\frac{r_1}{r_2}=\frac{W_1^{1/3}}{W_2^{1/3}}$$

where h_1 and r_1 are depth of burst and base-surge radius for yield W_1, and h_2 and r_2 are the corresponding depth of burst and base-surge radius for yield W_2.

The time required to complete a given percentage of total radial growth of the base surge, scales as the one-sixth power of the yield for the same scaled depth of burst, or:

$$\frac{t_1}{t_2}=\frac{W_1^{1/6}}{W_2^{1/6}}$$

where t_1=time required to complete a given percentage of total radial growth for yield W_1, and t_2=the corresponding time required to complete the same percentage of total radial growth for yield W_2.

Time to maximum base-surge radius, from detonation at venting depth or less, may also be computed by:

$$t_{max}=2.25\ r^{1/3}$$

where t_{max}=time to the maximum base-surge radius in seconds, and r=maximum base-surge radius in feet.

(3) First Example

Given: A 10-KT detonation at a depth of 150 feet below the water surface.

Find: (a) The maximum base-surge radius.

(b) Time to maximum base-surge radius.

(c) The expected base-surge radius 1 minute after detonation.

Solution: (a) The maximum base-surge radius is read directly from Fig. 4–42 as 7,200 feet.

(b) The venting depth is 250 $W^{1/3}$ =440 feet. Since the depth of

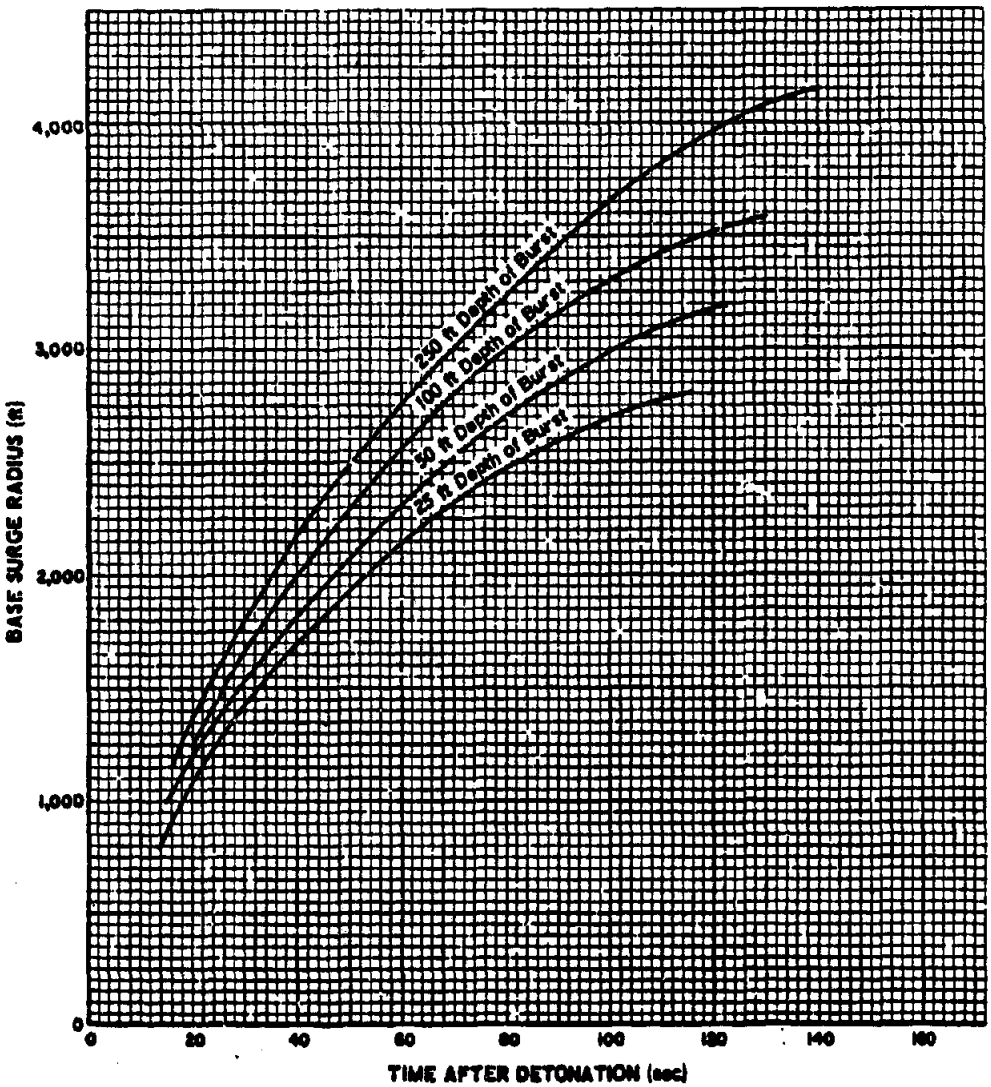

Figure 4–41 (C). *Base Surge Radius vs Time, for 1-KT Underwater Bursts at Various Depths (U)*

burst is less than venting, the simplified formula for time to maximum may be used. The time of maximum base-surge radius is

$t_{max} = 2.25\ (7{,}200)^{1/2} = 190$ seconds.

(c) A 10-KT detonation of 150 foot depth will complete the same percentage of its total radial growth in 60 seconds as a 1-KT detonation will complete a corresponding scaled time and depth. Using the scaling above, the corresponding depth of burst for 1 KT is

$$h_1 = \frac{W_1^{1/3} \times h_2}{W_2^{1/3}} = \frac{1 \times 150}{(10)^{1/3}} = 70 \text{ feet.}$$

The time that a 1-KT weapon burst at a depth of 70 feet will have completed the same percentage of its growth that a 10-KT burst will have completed in 60 seconds is:

$$t_1 = \frac{t_2 \times W_1^{1/4}}{W_2^{1/4}} = \frac{60 \times 1}{(10)^{1/4}} = 41 \text{ seconds.}$$

From Figure 4–41 the maximum surge for a 1-KT burst at 70 feet is 3,400 feet, and at 41 seconds the surge has a radius of 2,000 feet. Thus, it has completed 60 per cent of its growth. A 10-KT detonation at a depth of 150 feet will then complete, in one minute, 60 per cent of its maximum radial growth, or

$$0.60 \times 7{,}200 = 4{,}300 \text{ feet.}$$

(4) Second Example

Given: A 30-KT detonation at a depth of 1,000 feet below the water surface.

Find: The maximum base-surge radius.

Solution: The venting depth for a 30-KT detonation is approximately 250 $W^{1/4}$, or 600 feet. Few data are available upon which to

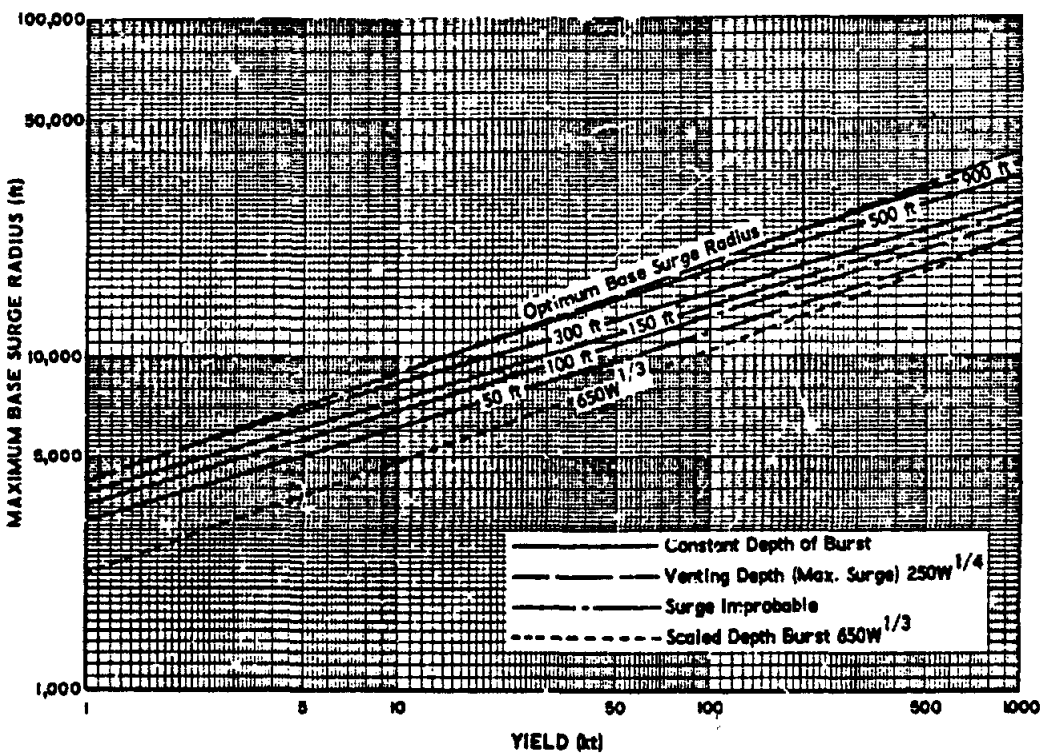

Figure 4–42 (C). Maximum Base Surge Radius vs Yield, for Underwater Bursts at Various Depths (U)

predict the maximum base-surge radius at depths exceeding this. Hence, a prediction must be made by linear interpolation between the venting depth, 600 feet, and a depth of 650 $W^{1/3}$=2,000 feet.

From Fig. 4–42 the maximum base-surge radius at venting depth is 12,000 feet. At 650 $W^{1/3}$ the maximum base-surge radius is 7,000 feet. By interpolation, the maximum base-surge radius for a 30–KT detonation at 1,000 feet is

$$12{,}000-\left(\frac{400}{1{,}400}\times 5{,}000\right)=10{,}600 \text{ feet.}$$

(S) Reliability

Figs. 4–41 and 4–42 are based upon limited full scale and extensive reduced scale testing.

4–4. (C) EFFECTS OF MECHANICAL FACTORS ON BLAST WAVE PARAMETERS

4–4.1. (C) *Effects of Charge Casing*

4–4.1.1. (U) General

It is common knowledge that the conventional projectile or warhead casing surrounding most explosive charges tends to reduce the blast damage effectiveness of the charge, because some portion of the explosive energy must be used in failing the casing and in accelerating the casing fragments. Estimates of the magnitude of this reduction have been considered both theoretically and experimentally. There is, however, no generalized method for accurately predicting this degradation.

An additional factor is that some explosives are difficult to detonate properly unless they are encased. Studies using certain casings of plastic-bonded powdered metals indicate that an explosive can be encased without reducing the effectiveness. In some instances, the damage capabilities of the explosive have been improved.

4–4.1.2. (C) *Fano-Gurney Prediction Methods*

The first attempt at accounting for the attenuation of air blast caused by the presence of a steel case was made by U. Fano and reported in Ref. 23. The reasoning used by Fano was an outgrowth of that developed by R. W. Gurney in Ref. 24. In this latter report Gurney concluded, by fitting experimental data to a simple theory concerning the partition of energy between fragments and blast wave, that 20 per cent of the total available energy from the explosive charge was still potential energy when the steel casing broke into fragments.

Considering a simplified model of the phenomenon, in which the HE charge is static and cased, the respective proportion of the explosive energy of the charge which the generated gases and the casing fragments possess at the instant of casing breakup is sought in the following manner:

If E=the total energy of the explosive charge material, per unit mass, and C=the mass of the charge; then, EC=the total energy of the explosive charge. Also, if M=the mass of the metal casing, and V_o=the initial velocity of the fragments, relative to the projectile, then $1/2\ MV_o^2 = KE$ (kinetic energy) of the fragments.

If it is now assumed that (at the instant of casing breakup) the velocity of the molecules of the generated gases varies linearly, from zero at the charge center, to V_o at the metal-charge interface, and that the density of the gases is constant throughout the charge volume, then: the KE of the generated gases=$1/4\ CV_o^2$ (cylindrical charge), or = $3/10\ CV_o^2$ (spherical charge). Considering no other factors:

$$EC=1/2\ MV_o^2+1/4\ CV_o^2 \qquad (4\text{–}54)$$

for the cylindrical charge, which is one form of the Gurney equation.

From this Fano reasoned that the total energy associated with the blast wave is equal to

$$\frac{1}{1+\frac{2M}{C}}$$

of the 80 per cent released at breakup, plus the 20 per cent potentially available at the instant of breakup. The concept of equivalent charge weight emerged as being the weight of bare charge with total available energy equal to the energy contributed to the blast wave by the cased charge. In Ref. 23 Fano computes the equivalent weight for a cylindrical cased charge as

$$w'=\left[0.2+\frac{0.8}{1+\frac{2M}{C}}\right]w \qquad (4\text{–}55)$$

where: w' = equivalent bare charge weight; and w = actual explosive weight for cased charge.

At the time Fano's report (Ref. 23) was written, all the bomb blast data collected in the period 1942-1945 at the Ballistic Research Laboratories (Ref. 25) were available. This data seemed sufficient to substantiate the equivalent weight theory. However, later results of experiments with cased charges cast some doubt on the expressed relationship between cased and equivalent bare charge weights (Ref. 26).

4-4.1.3. (C) U. S. Navy Prediction Method

In 1953 the Navy (Ref. 27) re-examined the data used by Fano, and upon comparison with the Kirkwood and Brinkley curves for bare charges (Ref. 28), proposed an improved equivalent charge relationship. This relationship was obtained by abandoning attempts at simple explanations for the behavior of cased charges; instead, the simple expedient was followed of choosing a relationship which best described the data. Two distinct formulas were specified, one of which was for positive impulse, as follows:

$$w' = \left[\frac{1 + M/C\ (1 - M')}{1 + M/C}\right] w \qquad (4\text{–}56)$$

with the condition that M' takes the value M/C for all values of M/C less than unity, but takes the value unity for all values of M/C greater than unity. For computing the peak pressure, w'/w is taken as 1.19 times that value used for computing positive impulse. However, results of additional experiments (Ref. 29) cast further doubt on the reliability of these relationships, and even on the whole concept of equivalent weight.

4-4.1.4. (C) Modified Fano Prediction Method

A modification of the formula due to Fano is in common use at the Ballistic Research Laboratories; this appears to provide a reasonable fit for experimental data (Refs. 30 and 31). An effective charge weight W'' is defined as $\frac{w' + w}{2}$, where w' is found from Eq. 4–55. The resulting expression for effective weight of the cylindrical cased charge is

$$w'' = \left[0.6 + \frac{0.4}{1 + \frac{2M}{C}}\right] w \qquad (4\text{–}57)$$

or for the spherical cased charge

$$w'' = \left[0.6 + \frac{0.4}{1 + \frac{5M}{3C}}\right] w. \qquad (4\text{–}58)$$

The effect of altitude and charge composition is often factored into these expressions and defined as the effective equivalent static bare charge weight w^*, used in the formula

$$w^* = \frac{w''(1 + n)}{n_h} \qquad (4\text{–}59)$$

where: n = effectiveness increasing (or decreasing) factor for a different explosive; and n_h = altitude degrading factor.

4-4.2. (C) Effects of Charge Shape and Composition

4-4.2.1. (U) Charge Shape

Experimental studies have been made comparing air blasts resulting from differently shaped explosive charges, in order to provide basic data for the terminal ballistic design of explosive charges to be used in guided missiles developed for the Air Force (Refs. 32 and 33). From these studies it has been determined that the peak pressures and positive impulses from the detonation of explosive charges of different shapes do not differ significantly at large scaled distances ($Z = R/W^{1/3} \geq 9$ ft/lb$^{1/3}$), when averaged in all directions with respect to charge orientation. However, scaled distances of this order are too great to cause lethal damage to most targets, unless the explosive weights considered are of the order of 4,000 pounds or more.

The peak pressures and positive impulses associated with particular directions about explosive charges of non-spherical configuration can be as much as 50 per cent higher than those from an equivalent spherical charge (Ref. 32), especially if the charge configuration is cylindrical. Double shock waves are often observed from the non-spherical charges. In measurements off the sides of cylinders, these secondary shocks are small relative to the primary wave, and usually occur in or beyond the rarefaction phase. In measurements off the ends of cylinders or blocks, however, the second peaks can

be large; because these occur well within the initial positive phase, they contribute to the resulting impulse.

Fig. 4–43 illustrates how pressure and impulse vary at angles about a cylindrical charge (taken in the plane of the axis) as compared to those about a spherical charge. In the figure, $\theta = 0°$ refers to measurements taken off the cylinder ends. From the illustration, it is evident that orientation of a conventional blast-type missile with respect to the target may be important.

4–4.2.2. (C) Charge Composition

(U) Numerous studies have been conducted to rank explosives of different compositions according to their effectiveness. The basis for this ranking has usually been either free-air blast measurements or evaluation of target damage. Ranking according to free-air blast effects is of interest here (Refs. 33, 34, and 35). The relative damage capabilities of various explosives based on target tests is presented in Ch. 8, Par. 8–18 in the discussion of aircraft targets.

(U) To rank explosives according to their effectiveness usually implies the comparison of the resulting shock wave intensity, namely, pressure and impulse. Peak pressure and positive impulse in shock waves from different bare explosives detonated in free air may be compared in a multitude of ways; the two most common methods of comparison are:

1. On the basis of the same volume, congruent shape, and orientation.
2. On the basis of the same weight, congruent shape, and orientation.

These two methods would be equivalent if the densities of the various charges were equal. Since variation in densities between the different types of high explosives commonly used is not large, either method of comparison is satisfactory for military applications.

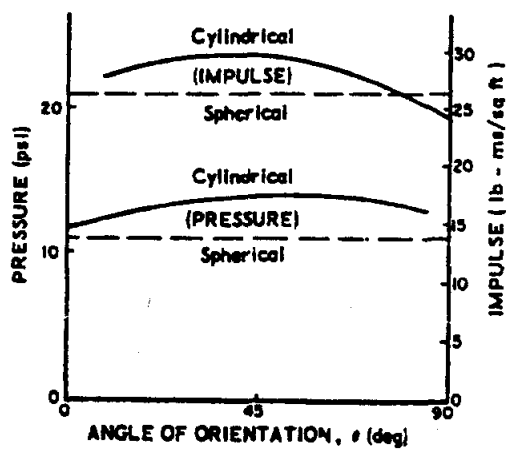

Figure 4–43. Comparison of Variation of Blast Parameters, Spherical and Cylindrical Charges

(C) Table 4–3 lists the composition of certain service-type explosives, in the general order of decreasing effectiveness. Some of these service-type explosives, TNT or Pentolite, for example, can be cast. Others, like MOX–2B, must be pressed. An infinite variety of explosive compositions can be obtained by taking combinations of explosives in various proportions and mixing them homogeneously. A present trend in mixing explosives is to add metallic powders, such as aluminum, to an optimum amount. The large amount of heat released in reactions with metals seems to enhance blast intensities, particularly the impulse. Small amounts of desensitizing agents, usually wax, are also frequently added to explosives to increase safety in handling and firing. Such agents tend to decrease the blast effectiveness slightly.

(C) Data has been compiled by W. D. Kennedy (Ref. 34) on the order of effectiveness of explosives based on air blast measurements, as conducted in the United States and Great Britain. This comprehensive report lists the side-on peak pressures and impulses of various explosives as ratios in terms of Composition B. These figures are based on blast tests using a wide range of charge weights (bare charges of about one pound up to bombs of several thousand pounds). Table 4–4 provides a general idea of the relative, quantitative effectiveness of several service type explosives. Certain qualifications are in order. It is to be noted that the differences in relative intensities are small, as is generally the case for all the common service explosives. Torpex–2 is usually

TABLE 4–3 (C). COMPOSITION OF CERTAIN SERVICE TYPE EXPLOSIVES (U)

Explosive	Composition: Per Cent by Weight	Composition: Components	Typical Specific Gravity
Torpex–2	42/40/18	RDX/TNT/Al	1.76
Mox–2B	54/36/4/6	$Al/NH_4ClO_4/TNT/\frac{97}{3}\frac{RDX}{TNT}$	2.05
H–6	47/31/22	RDX/TNT/Al	1.76
HBX–1	40/38/17/5	RDX/TNT/Al/Wax	1.68
Tritonal	80/20	TNT/Al	1.70
Composition B	60/40	RDX/TNT	1.65
Pentolite	50/50	TNT/PETN	1.61
TNT	100	TNT	1.60

considered the most effective. Later explosive combinations such as Mox–2B, H–6, and HBX–1 are considered as effective as, but not superior to, Torpex–2. Although explosive combinations exist which are several times more powerful, they are too sensitive for practical military applications. It should also be noted that the ranking of the explosives depends on scaled distances. Curves derived from excess peak-pressure ratio and scaled positive impulse versus scaled distance, for various charge compositions found in Ref. 33 often intersect at one or more distances. Consequently, there is no single ranking or effectiveness ratio that can be indicative for all cases. However the small relative difference between the blast wave intensities of the commonly used high explosives is again demonstrated.

TABLE 4–4 (C). PEAK PRESSURE AND POSITIVE IMPULSE, RELATIVE TO COMPOSITION B, FOR VARIOUS SERVICE TYPE EXPLOSIVES (EQUAL-VOLUME BASIS) (U)

Explosive	Relative Peak Pressure	Relative Positive Impulse
Torpex–2	1.13	1.16
Tritonal	1.04	1.08
Composition B	1.00	1.00
Pentolite	0.98	0.97
TNT	0.92	0.94

4–4.3. (C) Effects of Charge Motion

4–4.3.1. *General*

The effect of charge motion (often referred to as the velocity effect) on blast parameters was first noted during the many aircraft vulnerability tests conducted after World War II. Since most projectiles are in motion when blast occurs, the study of the effects of this motion on the various parameters of the associated blast wave attracted considerable interest. Tests indicated an appreciable amount of pressure increase in the direction of motion, and a corresponding decrease in the opposite direction. Although various theories were advanced concerning the velocity effect, proper evaluation of these explanations required the formulation of considerable amounts of quantitative data. Accordingly, in 1952, experiments were instituted at the Ballistic Research

Laboratories for the purpose of providing such data.

4–4.3.2. BRL Test Procedures

Early experiments at BRL (Ref. 36) were successful in establishing the basic experimental procedure since used in subsequent moving charge tests. Unfortunately, however, the instrumentation used was suitable only for providing qualitative results. In 1954, using minor modification in the procedure, data of a more quantitative nature was obtained. This still was not sufficiently accurate to establish a rigorous theory (Ref. 37). Further experiments (Ref. 38), however, have provided enough information to substantiate, at least in part, a theory explaining the behavior of the shock wave produced by a charge in motion.

The first step in the development of the moving charge experiments was to select the type and size of charge, and to determine some means of propelling the charge at high velocity. Because even a light casing will produce sufficient fragmentation to interfere with the measurements of free air blast, a bare charge of spherical shape was used. The spherical shape was chosen since charges of this configuration produce roughly symmetrical shock waves. For the projection device, a 57-mm gun with the rifling bored out to a diameter of 2.293 inches was eventually selected. Use of this gun fixed the charge weight at 3/8 of a pound. The original experiments used a bare charge of Composition B (Par. 4–4.2.2, preceding) traveling at a velocity between 1,700 and 1,900 ft/sec. In about 40 per cent of these shots, the charge broke up prior to detonation, thus spoiling the test. Based on the work of B. F. Armendt (Ref. 39), to eliminate this problem a Fiberglas-reinforced Pentolite charge was substituted for Composition B. Pentolite charges have been used in all recent experiments.

Fig. 4–44 is a diagram of the charge construction and gun loading method. The charge is cast in a spherical form with a cylindrical well. A small quantity of Composition C–3 and a Tetryl booster is placed in the bottom of the well to insure high-order detonation. An electric detonator with a small, iron-core, copper coil across its back is placed in the well. Any remaining voids are then carefully packed with Composition C–3 to prevent the firing forces from dislodging any of the components.

The charges fuzed in this manner are fired through a screen woven from number 40 copper wire, which is placed just in front of a stationary coil of heavy copper (Fig. 4–45). As the charge breaks through the screen, an electronic circuit is broken, discharging a large condenser into the coil. The resulting, pulsed, magnetic field induces a current in the small coil inside the charge. This activates the electric detonator and detonates the explosive.

If the measured data are to be sufficiently accurate, the point of detonation must be determined with fair accuracy. The errors involved when using the smoothbore gun system and the magnetic detonating system allow considerable variation in the point of detonation. To establish an accurate fix on this point, two cameras equipped with 1-ms electronic shutters and activated by a photocell are placed 90 degrees apart and 10 feet from the desired point of detonation. By triangulation, the position of the charge at the instant of detonation can be located to about 1/4 of an inch.

The velocity at which the charge is traveling is measured by two velocity screens placed about eight feet apart. Breakage of the first screen activates an electronic counter chronograph which stops when the second screen is broken, thus measuring the time necessary to traverse this interval. From this measurement, the average velocity over the interval can be calculated.

The peak pressure and positive impulse are measured by twelve side-on pressure gages, each spanned by a pair of face-on velocity gages. The gages are placed at a distance of 2.71 feet from the desired point of detonation, and at angles of 15°, 45°, 75°, 105°, 135°, and 165° to the direction of motion of the charge, as shown in Fig. 4–45. When the charge detonates, the same photocell that triggers the cameras activates twelve counter chronographs, one at each angular position. When the shock wave reaches the first velocity gage at one of the twelve positions, the chronograph corresponding to that position is stopped, giving a

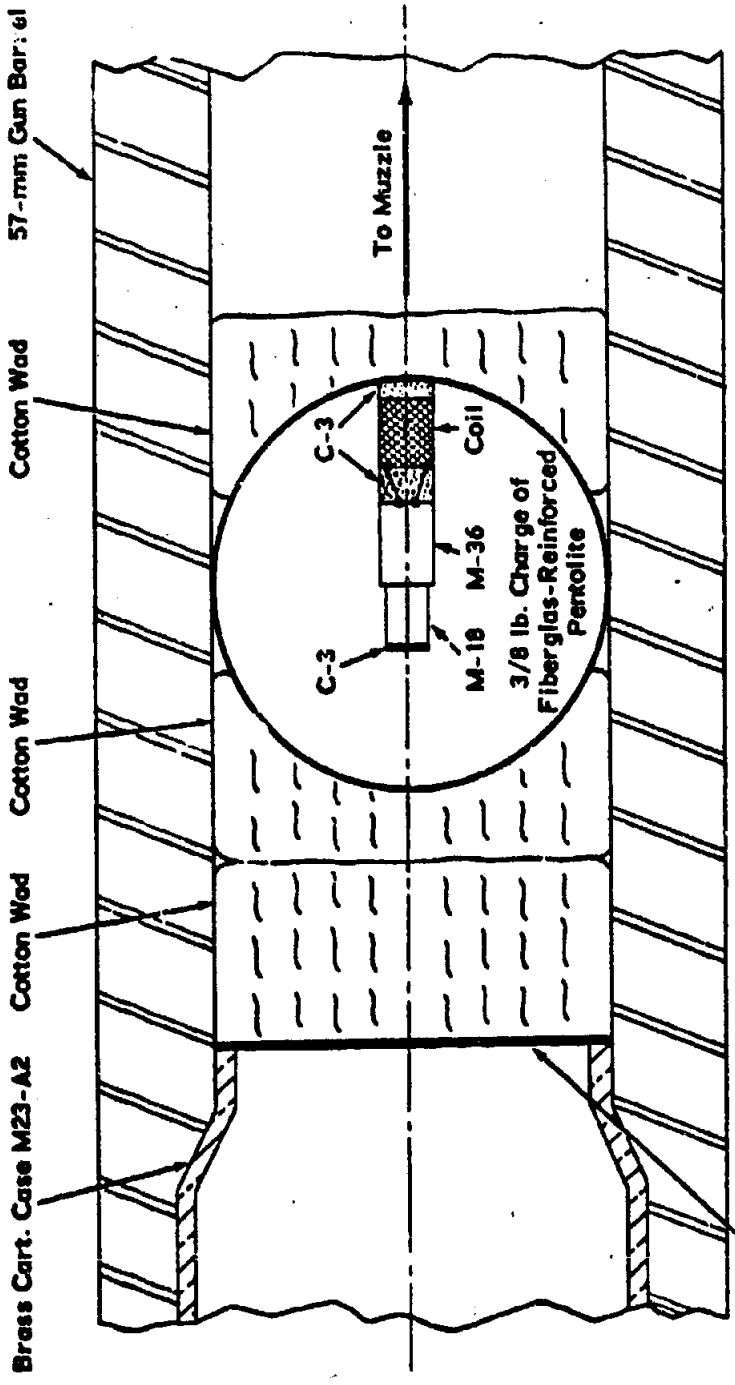

Figure 4-44 (C). Sectional View of Fuzed Charge Loaded in 57-mm Smoothbore Gun, Velocity Effect Program (U)

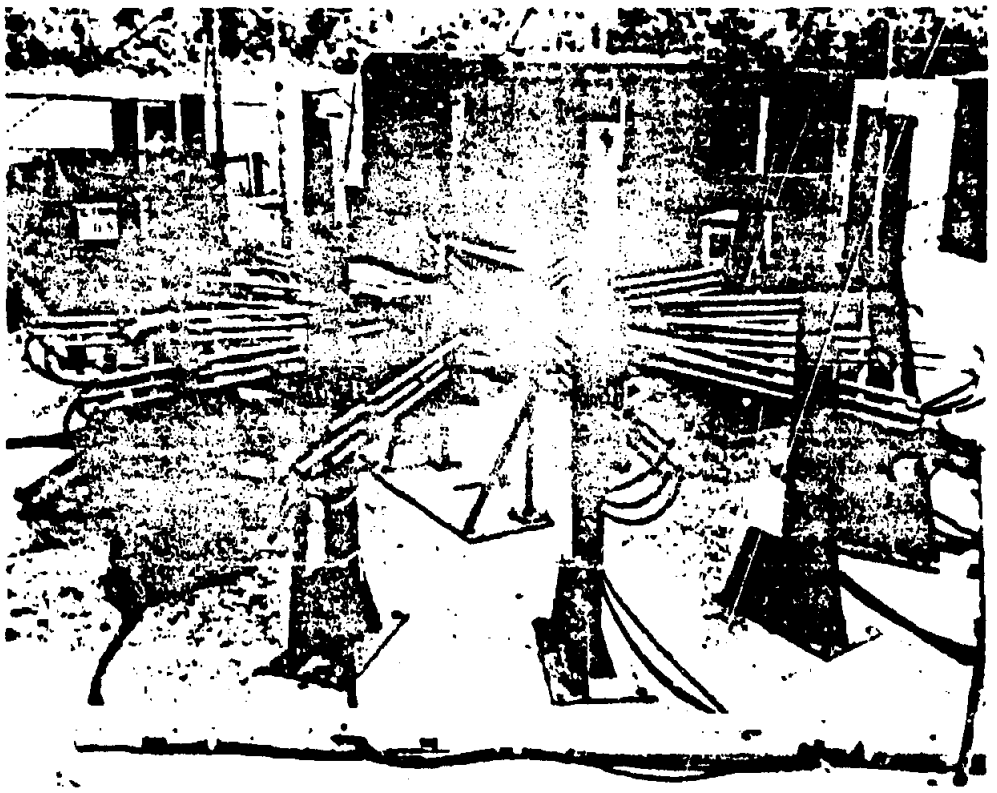

Figure 4–45 (C). Test Setup, Velocity Effect Program (U)

measure of the time of arrival, and a second counter is initiated. This second counter is stopped when the shock reaches the rear velocity gage, thus measuring the time the shock has taken to traverse the interval between the gages. From this measurement, the average velocity can be calculated, and the peak pressure at the center of the interval can be found from the Rankine-Hugoniot relation:

$$\frac{P_s}{P_o} = \frac{2\gamma}{\gamma+1}\left(\frac{V^2}{C_o^2} - 1\right) \qquad (4\text{–}60)$$

where P_s is the peak excess pressure, P_o is the atmospheric pressure, γ is the ratio of specific heats for air, V is the shock velocity and C_o is the speed of sound (Ref. 38).

Thus, the system of chronographs, velocity gages, cameras, and the photocell can measure shock arrival time, shock velocity, and peak overpressure at twelve locations around the detonating charge. Alternate tests with moving and stationary charges provide a basis for comparison, from which the effects of motion on the shock wave may be determined.

4–4.3.3. Computation Methods

The data resulting from these experiments seem to agree fairly well with results calculated by the theory advanced by C. K. Thornhill and R. Hetherington (Ref. 40). Thornhill and Hetherington predicted that, close to the surface of a moving charge, the shock velocity could be approximated by vectorial addition of the shock velocity of the stationary charge and the terminal velocity of the moving charge. The experimental time-of-arrival data indicate that

the same rule could be applied to the expanded shock wave, if the velocity of the center of the shock wave resulting from the detonation of the moving charge is substituted for the terminal velocity of the charge (Ref. 38).

The velocity of the center of the shock wave, at any given time, can be predicted by the application of the principle of the conservation of linear momentum. Thus, the momentum of the charge prior to detonation is established as equal to the momentum of the explosion gases and air contained by the spherical shock. Then, assuming the average velocity of all the gases and air contained in the spherical shock is at the same velocity as the center of the sphere,

$$w_e V_e = (w_e + w_a) V_s \qquad (4\text{–}61)$$

where w_e = weight of explosive (lbs.), V_e = terminal velocity of the explosive (ft sec.), w_a = weight of air contained by the spherical shock (lbs.), and V_s = the velocity of the center of the shock wave (ft/sec.).

Then, letting ρ_a equal the density of the air (lbs/cu. ft.) and d the diameter of the shock sphere (ft.), and neglecting the mass of air displaced by the explosive charge, the result is

$$w_e V_e = \left(w_e + \frac{4}{3}\pi\rho_a d^3 \right) V_s$$

or

$$V_s = \frac{w_e V_e}{w_e + \frac{4}{3}\pi\rho_a d^3} \qquad (4\text{–}62)$$

Substituting $w_e = \frac{4}{3}\pi\rho_e a^3$, where ρ_e is the density of the explosive and a the original charge radius, into Eq. 4–62, the result is

$$V_s = \frac{\frac{4}{3}\pi\rho_e a^3 V_e}{\frac{4}{3}\pi\rho_e a^3 + \frac{4}{3}\pi\rho_a d^3} = \frac{\rho_e a^3 V_e}{\rho_e a^3 + \rho_a d^3}$$

and dividing through by $\rho_e a^3$

$$V_s = \frac{V_e}{1 + \frac{\rho_a d^3}{\rho_e a^3}}$$

Lettering $r = \frac{d}{a}$ = radius of spherical shock wave in increments of charge radii, then

$$V_s = \frac{V_e}{1 + \frac{\rho_a}{\rho_e} r^3} \qquad (4\text{–}63)$$

Eq. 4–63 for a known r will then give the value of the velocity of the center of the shock wave. The distance, r_s, that the center has traveled in the direction of the original motion at a time t, is then given by the expression

$$r_s = \int_0^t V_s \, dt. \qquad (4\text{–}64)$$

When viewed from a stationary reference frame, the shock velocity on the surface of the spherical shock wave produced by the moving charge becomes

$$\vec{U}_m = \vec{U}_s + \vec{V}_s \qquad (4\text{–}65)$$

where $\vec{U}_m$ is the shock velocity at the distance r and the angle ψ from the original line of motion, and $\vec{U}_s$ is the shock velocity at a distance r. Once $\vec{U}_m$ is known, the peak pressure can be found. These quantities are illustrated in Fig. 4–46.

Fig. 4–47 shows the relationship the point of detonation and the center of the spherical shock wave.

Ordinarily, because the measurements are made from the point of detonation, only the distance R and the angle θ are known. By integration, r_s may also be found. The distance r and the angle ψ can then be found by use of the following geometric relations:

$$R = r_s \cos\theta + (r^2 - r_s^2 \sin^2\theta)^{1/2} \qquad (4\text{–}66)$$

and

$$\sin\psi = \frac{R}{r}\sin\theta. \qquad (4\text{–}67)$$

Up to the present, no simple scheme has been devised to allow scaling of the various parameters of altitude, charge weight, charge velocity, etc. Therefore, separate computation is necessary for each case. Table 4–5 (Ref. 38) presents a set of calculations made for a given

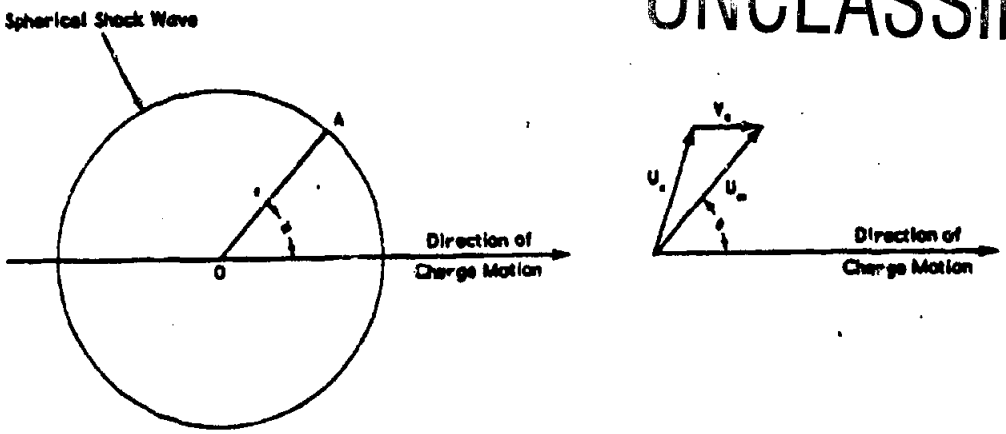

Figure 4–46 (C). Relationship Between Shock Velocities at Center and Surface of Spherical Wave (U)

set of conditions as compared to the actual experimental results.

4–5. (C) BLAST INSTRUMENTATION

4–5.1. General

This section is a summary description of the types of instrumentation used in the measurement of blast parameters. Generalized descriptions of various types of significant instruments and methods are given. Where applicable, discussions are included of the techniques of reducing the data obtained to a more usable form. For more complete details on the instruments, operational reports and manufacturers' manuals are available for further study.

The many field tests conducted during the past decade have contributed significantly to the evolution of blast instruments in their present form. Sandia Corporation, Stanford Research Institute, the Naval Ordnance Laboratory, and the Ballistic Research Laboratories have been outstanding in this respect, and should be considered as additional sources of detailed information (Refs. 41 and 42).

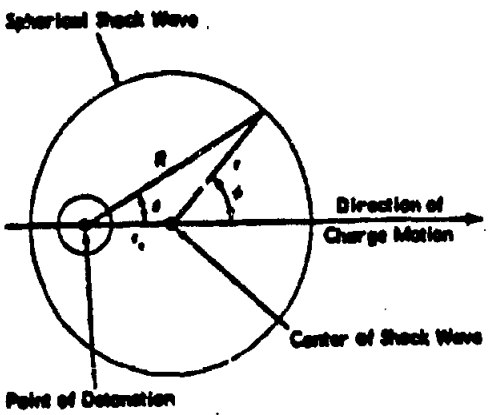

Figure 4–47 (C). Relationship Between Point of Detonation and Center of Spherical Shock Wave (U)

4–5.2. The BRL Face-on and Shock-Velocity Gages

The face-on gage, as developed by Mr. A. J. Hoffman and Mr. S. N. Mills, Jr. of the Ballistic Research Laboratories, consists of a pair of tourmaline discs assembled in a shallow cavity in the face of a solid brass housing (Fig. 4–48). The crystal stack is glued into place and then immobilized in the cavity by a thermosetting plastic. The gage is designed to be massive enough for its acceleration sensitivity to be quite low, but short enough for its lowest natural frequency to be well above the 200-KC limit of the associated recording equipment.

The shock-velocity gage, shown in Fig. 4–49, employs the same active element as the face-on gage in a lightweight, shock-mounted housing (Ref. 43).

TABLE 4-8 (C). CALCULATED AND EXPERIMENTAL DATA FOR MOVING CHARGES (U)

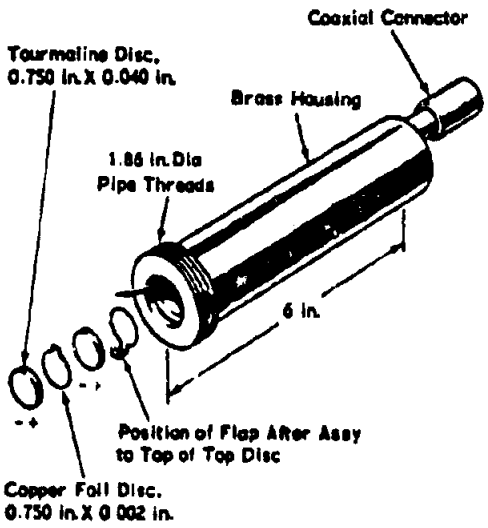

Figure 4–48. BRL Face-On Gage

4–5.3. The BRL Stressed-Diaphragm Gage

This gage is a piezoelectric blast gage for recording the side-on pressure-time history associated with blast waves. Originally developed by Mr. Roy Sampson of BRL, the gage has been used with a great deal of success in small charge ($\frac{1}{8}$ pound to 64 pound) air blast experiments.

The sensitive element of the BRL stressed-diaphragm gage is a stack of four wafer-shaped crystals (made of tourmaline or a synthetic piezoelectric material), approximately 0.050 inches thick, with silver foil electrodes between crystals to collect the charge. The crystals are usually one inch or one-half inch in diameter, but gages have been built in which the diameter of the crystals was as small as one-eighth inch.

The design principle which is believed to be most directly responsible for the success of this gage is the preloading of the crystal stack by brass diaphragms approximately 0.020 inch thick. Interference between the crystal stack and the cavity in the gage housing, of 0.005 to 0.002 inch, has been found to give the best results. Silicon grease applied between the faces of the stack and the brass diaphragms, as well as in the clearance around the stack, is helpful in damping spurious oscillations.

The quality of the workmanship in machining the housing, grinding and polishing the tourmaline crystals, and assembling the crystals into the housing has been found to be of the utmost importance in producing gages which give records of high fidelity. A schematic drawing of this gage is shown in Fig. 4–50.

Calibration of piezoelectric gages is achieved by paralleling known voltages across accurately known capacitors. The gage circuit is shown in Fig. 4–51, with a list of significant circuit elements.

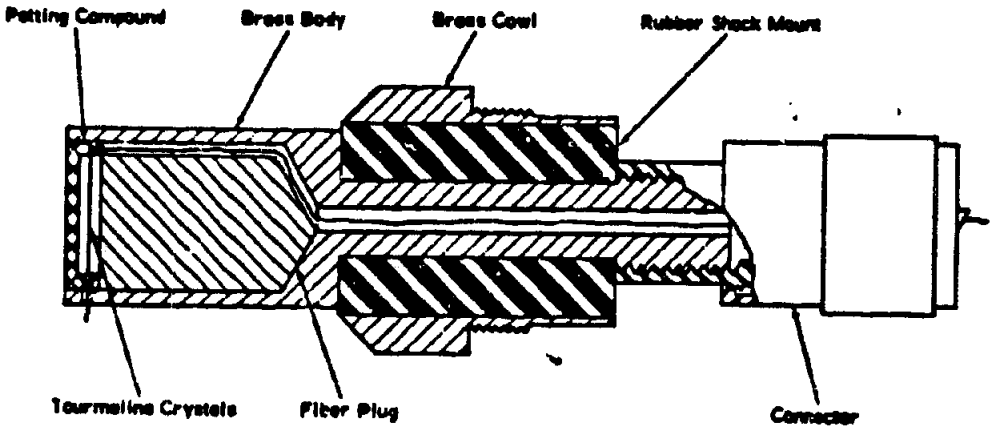

Figure 4–49. BRL Shock-Velocity Gage

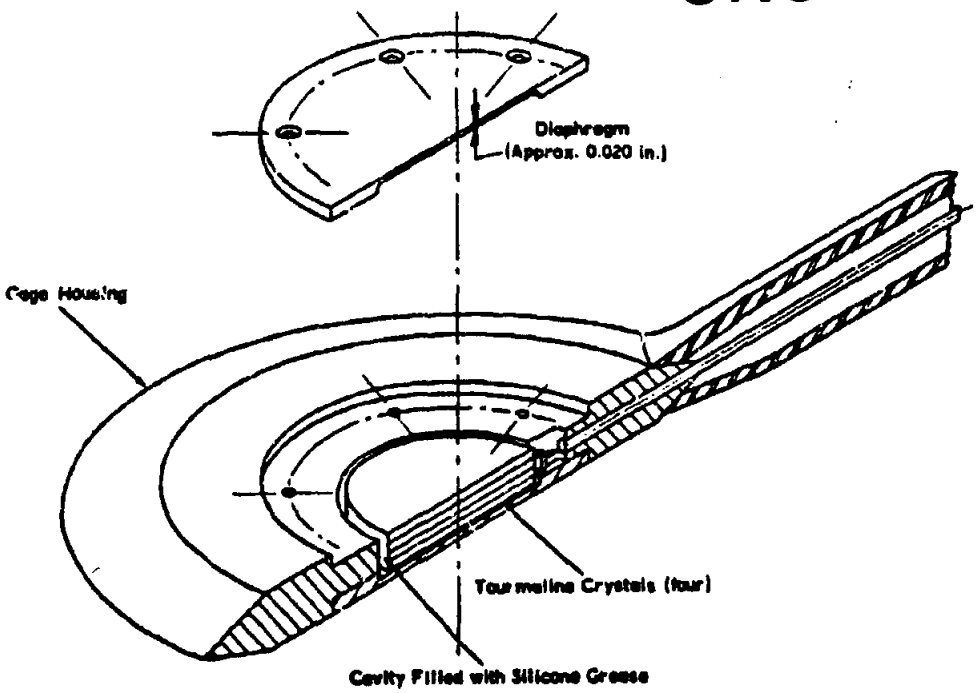

Figure 4–50. The Stressed-Diaphragm Gage

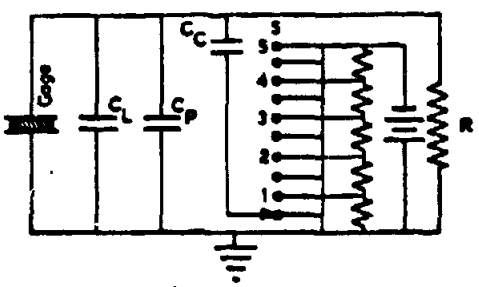

C_g = gage capacitance.
C_L = coaxial cable capacitance.
C_P = padding capacitance (used to adjust signal level).
C_c = calibration capacitance.
R = input resistance of d.c. amplifier (100 megohms).
KA = sensitivity of gage (in micro micro-coulombs/psi).
P = peak excess pressure acting on gage (in psi).

Figure 4–51. Wiring Diagram, BRL Gage Calibration Circuit

For recording, the switch S grounds the calibration condenser C_c. In this condition, the peak voltage V_1 across R becomes:

$$V_1 = \frac{P \times KA}{C_g + C_L + C_P + C_c}. \qquad (4\text{–}68)$$

Calibration is performed by switching S through the five positions and back to ground. When the switch is in position 3, for example, the voltage V_3 across R is:

$$V_3 = \frac{C_c}{C_g + C_L + C_P + C_c} E_3, \qquad (4\text{–}69)$$

where E_3 is the voltage at step 3 of the switch. The voltages V_1 and V_3 are proportional to the maximum deflection recorded on the film for the pressure-time history, and to the third calibration step, respectively. Therefore, the ratio of the height of the maximum pressure, h, to the height of the third calibration step, g_3, becomes:

$$\frac{h}{g_s}=\frac{V_1}{V_2}=\frac{\dfrac{P\times KA}{C_a+C_L+C_r+C_c}}{\dfrac{C_cE_s}{C_a+C_L+C_r+C_c}}=\frac{P\times KA}{C_c\times E_s} \qquad (4\text{–}70)$$

and

$$P=\frac{h\times C_c\times E_s}{g_s\times KA}. \qquad (4\text{–}71)$$

The calibration capacitance can be measured to sufficient accuracy on a capacitance bridge. The voltages appearing at the various steps on switch, S, are adjusted by comparison with a standard cell. As previously mentioned, the sensitivity of the gage, KA, must be known.

4–5.4. Photographic Measurements of Peak Pressures

Measurements can be made of peak air blast pressures by photographing the passage of the shock wave against an interrupted background, such as a fence. This technique is dependent upon the principle of refraction. Light waves passing obliquely from one medium to another, in this case from undisturbed air to the compressed region immediately behind the shock wave (Refs. 44 and 45), undergo an abrupt change in direction. The bending of the light rays by the shock wave causes an apparent displacement of the background against which the shock wave is viewed. By projecting high-speed photographs of the event at a much reduced rate, the phenomenon can be observed. The arrival of the shock front at the line of sight, from the camera to each fence pole, is evidenced on the film records by apparent distortion or deletion of successive poles. The shock velocity can be determined by counting frames between shock arrival at successive poles, and measuring time of travel by timing marks on the film.

For the referenced tests, Fastax cameras were used. Each fence was approximately 250 feet in length, and consisted of 21 pairs of poles approximately 12 feet apart. The distance between the two poles in each pair was 1.5 feet. The cameras were placed with the line of sight perpendicular to the fence at the midpoint of the fence.

Peak overpressures were inferred from the shock velocities, which were computed from the fence data by use of the Rankine-Hugoniot equation (expressing pressure as a function of shock velocity), as follows:

$$P=\frac{2\gamma}{\gamma+1}\left[M^2-1\right]P_o \qquad (4\text{–}72)$$

where

P = side-on peak pressure, in psi,

γ = ratio of specific heats (1.4 for air),

M = ratio of shock velocity in still air to velocity in air ahead of shock,

and

P_o = ambient atmospheric pressure, in psi.

Fig. 4–52 illustrates the geometry for the fence technique computation. The distances a, b, c, d, and h are not scaled, as the figure is intended only as a guide for following the velocity computations. Furthermore, R_i is the pole distance from R_1, or r_i the radius of the shock wave at t_i; and t_i is the arrival time of the shock wave at r_i. Referring to Fig. 4–52,

$$\theta=\tan^{-1}\left(\frac{b+c}{a}\right)$$

$$\theta_i=\tan^{-1}\left(\frac{b-R_i}{a+d}\right), \text{ for } i\leqq 22$$

$$\theta_i=\tan^{-1}\left(\frac{R_i-b}{a+d}\right), \text{ for } i\geqq 23$$

$$r_i=h\sin(\theta-\theta_i), \text{ for } i\leqq 22$$

$$r_i=h\sin(\theta+\theta_i), \text{ for } i\geqq 23$$

$$V_i=\frac{\Delta r_i}{\Delta t_i}=\frac{r_i-r_{(i-1)}}{t_i-t_{(i-1)}},$$

where V_i = average velocity

and

$$r'_i=\frac{r_i+r_{(i-1)}}{2},$$

where r'_i = radius of shock at V_i.

Before application of the velocity measurement data to the Rankine-Hugoniot equations, the velocity components of the prevailing wind parallel to the fences at the time of the test were eliminated. This was necessary as the wind effectively increases or decreases the velocity of the shock front, depending upon the direction of the wind vector in relation to shock wave propagation. A wind vector that is tan-

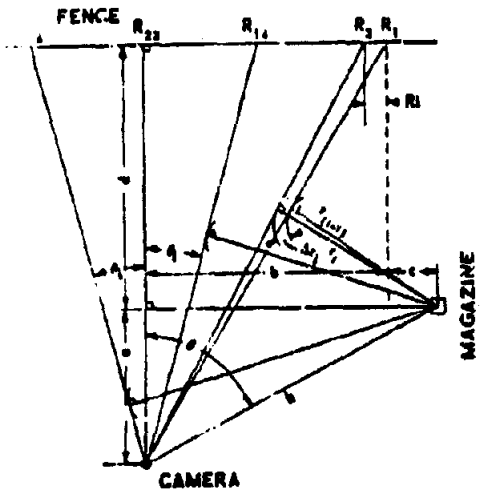

Figure 4–52. Field Setup, Fence Technique Computation

gent to the shock front will have no effect on shock velocity measurements.

4–5.5. The BRL Pressure-Time Gage

The BRL mechanical self-recording, pressure-time gage is used for the measurement of overpressure and positive impulse resulting from the detonation of nuclear devices and large high-explosive charges. It is completely self contained. When used on nuclear tests, it is self-initiated, but it can also be initiated by a voltage transmitted by wire. Interchangeable sensing elements are available to cover pressure ranges from 0-1 2 psi to 0-1,00 psi with a number of intermediate ranges.

The pressure sensing capsule of the gage (Fig. 4–53) consists of two concentrically convoluted diaphragms, silver soldered or welded together around their periphery, and also silver soldered to a mounting base. A spring stylus with an osmium-tipped phonograph needle is soldered to a mounting post at the center of the movable diaphragm. Pressure entering through a small inlet on the mounting base of the capsule causes the diaphragm to expand, causing attached needle to scratch the recording medium. The displacement of the recorded scratch is proportional to the applied gage pressure (Refs. 45 and 46).

An aluminized glass disc, 3½ inches in diameter and 1/16 inch thick, is rotated under the stylus and records its motion. The resulting scratch record can be read with a microscope of 50 power or more.

The turntable holding the glass recording disc is driven at constant angular velocity by a chronometrically governed d.c. motor. A switch operated by a star-gear cam controls the number of revolutions of the turntable.

The components of the gage are mounted on an H-channel welded to the center of a circular steel plate. A sheet-metal can housing the initiating relay and battery is mounted on the free end of the H-frame. An interconnecting plug provides for electrical coupling between the can and the gage mechanism. The entire unit is inclosed in a case made of steel pipe and plate. Pressure-tight sealing is accomplished with a neoprene gasket. Fig. 4–54 shows the gage construction, and Fig. 4–55 shows the gage ready for use. The overall dimensions of the gage are about 5 inches in diameter by 10 inches long, with the flange top being about 8 inches in diameter. In normal operation, the gage top is mounted flush with the ground surface.

The standard initiation system of the gage is a cadmium-sulfide cell backed by a thermal-sensi[illegible] spring-loaded link. In tests of chemi-

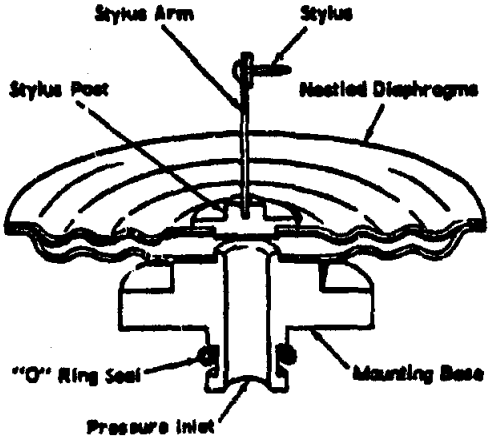

Figure 4–53. Pressure Sensing Capsule, BRL Self-Recording Pressure-Time Gage

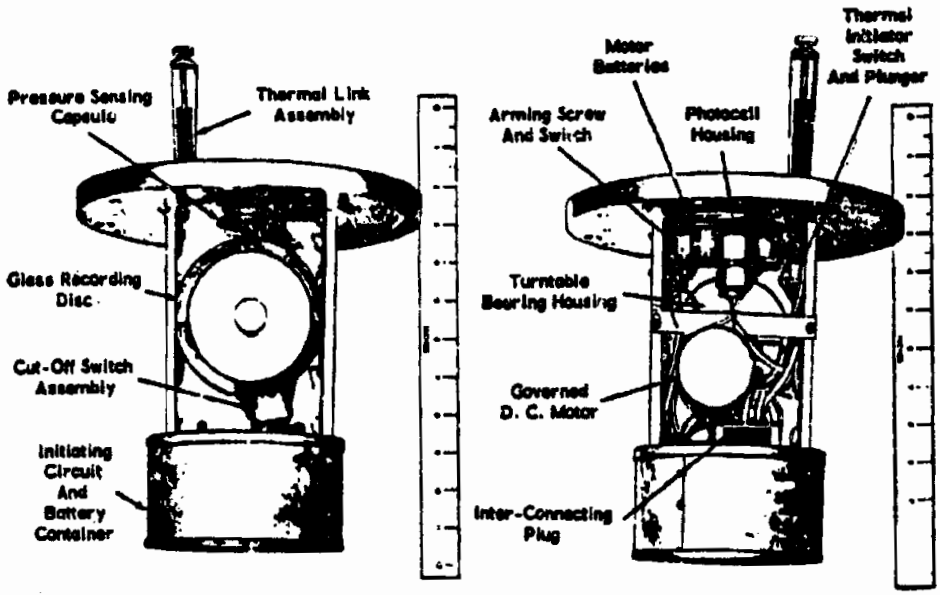

Figure 4–54. BRL Self-Recording Pressure-Time Gage, Construction

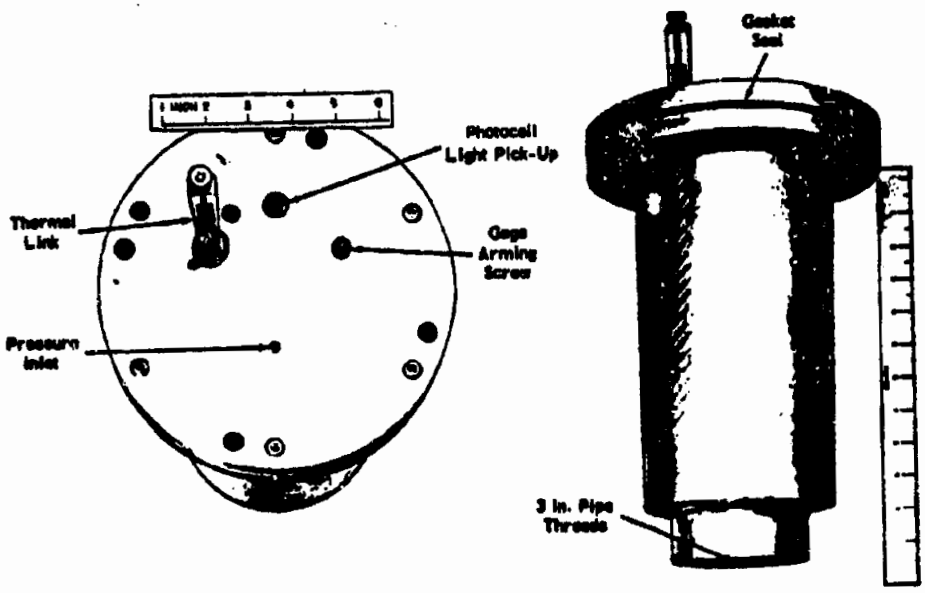

Figure 4–55. BRL Self-Recording Pressure-Time Gage, Setup

cal explosives, a wire signal line can be used to replace the photocell, with the starting signal occurring at zero time minus 2 seconds.

The records appearing on the glass disc of the self-recording gages are in the form of a pressure-time history in polar coordinates. The time axis is calibrated by knowing the angular velocity of the glass disc, which is determined by the motor and battery used. The pressure axis calibration is a function of the sensing capsule used, and is determined by subjecting the capsule to accurately known static pressures and measuring the stylus deflections. Thus, for any measured deflection, the pressure can be computed from the static calibration curve for the particular sensing capsule used.

A Gaertner Toolmaker's microscope is an effective instrument for reading the ordinates, h, of the record at small intervals, Δd, of the abscissa (Fig. 4–56), because the digital readout heads on the microscope put the readings simultaneously into Telecordex and IBM summary punch equipment. A computer, such as the EDVAC (Electronic Digital Variable Automatic Computer) can then be used to linearize

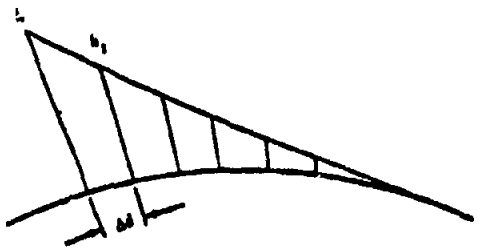

Figure 4–56. Illustration of Static Calibration Curve from PRL Self-Recording Pressure-Time Gage

the time and pressure values, and to compute peak pressure and positive impulse.

4–5.4. The Atlantic Research Air-Blast Gage

This gage, illustrated in Fig. 4–57, is manufactured by the Atlantic Research Corporation, Alexandria, Virginia. It consists of a cylindrical piezoelectric crystal mounted on a stainless steel housing, with leads connecting the crystal to a suitable connector. The sensitivity of this type of gage ranges from 500 to 1,000 micro-micro coulombs per psi, depending upon the individual gage.

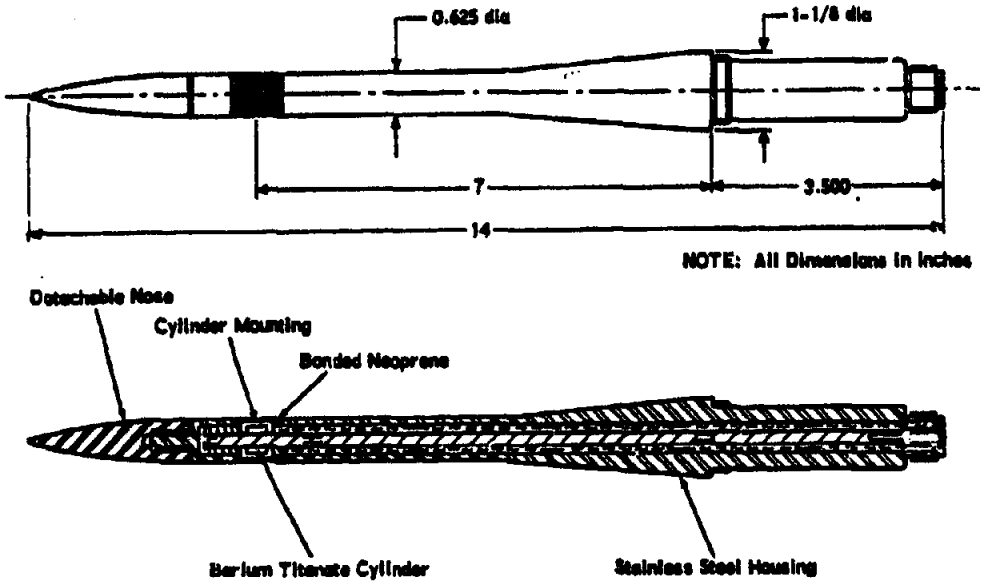

Figure 4–57. Atlantic Research Air-Blast Gage

4–5.7. The Cantilever-Beam Gage

The cantilever-beam gage consists of an aluminum strip of predetermined size held rigid at one end and placed face-on to the blast. The strip may have SR–4 strain gages mounted on it, to measure bending strain, or it may be uninstrumented. If strain gages are used, their output is recorded on recording equipment of low frequency response, and the maximum bending strain due to blast is measured.

The beam gages can be made of 61ST aluminum strips one inch wide and twelve inches long. Each gage position can consist of two beams, one 0.091 inch thick and one 0.051 inch thick. All beams can employ strain gages except those 100 feet or more from the blast. The beams, mounts, and strain gages of a typical installation are shown in Fig. 4–58. The strain gages are arranged to measure longitudinal strain at a station one inch above the beam clamp. Selected gages are mounted on each side of the beam, so that when a transverse load is applied, one gage is in tension, and the other is in compression. As a result the resistance of one is increased, and the other is decreased by the same amount. The two resistances are connected in a bridge circuit using two dummy resistors. Using two strain gages in this manner doubles the sensitivity and cancels out temperature effects and unwanted axial strains. The change of resistance of the gages is amplified and recorded by a commercial magnetic oscillograph.

The beam gages are calibrated by firing bare charges of known weights and measuring the maximum strain or permanent deformation. By varying the distance and charge weights, maximum strain can be measured in terms of distance from the charge, for given charge weights. The beams that deform plastically are calibrated in a similar manner, except that permanent deflection is measured and plotted versus distance from the charge. To determine the equivalent charge weight, a calibration curve is entered at the distance the gage is from the charge. Then, by applying the maximum measured strain, the equivalent charge weight can be read or interpolated from the curve.

Section II (C)—Thermal and Nuclear Radiation

4–6. (U) INTRODUCTION

4–6.1. Scope of the Section

This section discusses the general phenomena accompanying the detonation of a nuclear weapon, with the exception of blast effects (Ch. 4, Sec. I). The two major subjects covered are thermal radiation and nuclear radiation. The thermal radiation paragraph presents data concerning the measurement of thermal radiation, the thermal scaling laws, slant range versus exposure data, and the mathematical techniques for computing radiant exposure. The nuclear radiation paragraph discusses in detail the units of nuclear radiation, the techniques of measuring such radiations, data for both initial and residual dosages, and the problems associated with nuclear shielding.

4–6.2. Cross-Reference Information

As mentioned above, the blast effects of nuclear explosions are presented in Ch. 4, Sec. I. General information concerning thermal radiation and nuclear radiation as kill mechanisms is located in Ch. 2, Secs. XI and XII, respectively. This material should be read prior to the present section. In addition, various chapters and sections of Part Two present the information necessary to apply the data discussed here to targets of a specific nature. Cross-references are made, as necessary, to these various, related bodies of information.

4–7. (C) THERMAL RADIATION

4–7.1. (U) Introduction

The extremely high temperatures in the fireball of a nuclear explosion result in a large emission of thermal radiation. The relatively large fraction of the total energy of a nuclear explosion which is emitted as thermal radiation is one of its most striking characteristics. This radiant energy amounts to approximately one-third of the total energy of an air-burst weapon

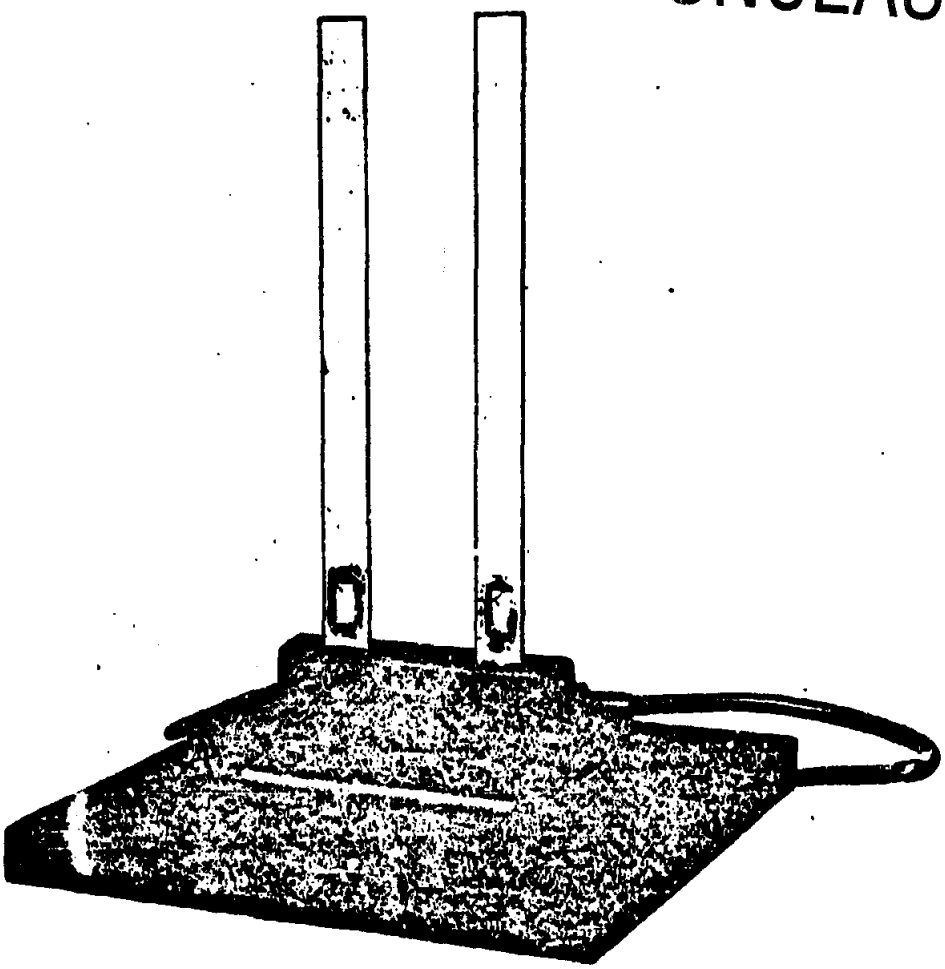

Figure 4–58. The Cantilever-Beam Gage

yield; it is sufficient to cause serious burns to exposed personnel at considerable distances. The duration of the thermal emission depends upon the weapon yield, being longer for the larger yields (Ref. 1).

For a surface burst having the same yield as an air burst, the presence of the earth's surface results in a reduced thermal radiation emission and a cooler fireball. This is due primarily to heat transfer to the soil or water, the distortion of the fireball by the reflected shock wave, and the partial obscuration of the fireball by dirt and dust (or water) thrown up by the blast wave.

In underground bursts, the fireball is obscured by the earth column; therefore, thermal radiation effects are negligible. Nearly all of the energy of thermal radiation is absorbed in fusing and vaporizing the earth.

The energy of thermal radiation from an underwater detonation is absorbed increasingly in vaporization and dissociation of the sur-

rounding medium as the depth of burst is increased. Its direct effects are insignificant for most practical purposes; e.g., for a 20-KT burst in ninety feet of water, thermal effects are negligible.

If it is assumed that the fireball in a nuclear explosion behaves in the same manner as the sun, as a perfect radiator (black body), then the thermal radiation energy can be related to the surface temperature of the fireball by Planck's radiation equation. If $E_\lambda\, d\lambda$ denotes the energy density (energy per unit volume) in the wave length interval λ to $\lambda + d\lambda$, then:

$$E_\lambda = \frac{2\pi hc^2}{\lambda^5} \cdot \frac{1}{e^{hc/\lambda kT} - 1} \qquad (1\text{–}73)$$

where c is the velocity of light, h is Planck's quantum of action, k is the Boltzmann constant (the gas constant per molecule), and T is the absolute temperature.

From the Planck equation it is possible to calculate the energy density of the thermal radiation over a range of wave lengths for any specified temperature. Results obtained for several temperatures are presented in Fig. 4–59. It may be noted that for temperatures exceeding 8,000° K (this is the case during most of the first radiation pulse), most of the thermal radiation lies in the short wave length (ultraviolet) region of the spectrum.

As the temperature of the fireball decreases, the wave length at which the energy density is a maximum increases. By differentiating Eq. 4–73 with respect to λ, and equating the derivative to zero, an expression for the wave length for maximum energy density, λ_m, can be obtained. This expression is:

$$\frac{dE_\lambda}{d\lambda} = 0$$

$$\frac{C_2}{\lambda_m T} = 5\left(1 - e^{-C_2/\lambda_m T}\right)$$

where $$C_2 = \frac{hc}{k} = 1.439 \text{ cm-}^\circ K$$

then, by trial,

$$\frac{C_2}{\lambda_m T} \cong 4.9651$$

$$\lambda_m = \frac{C_2}{4.9651} \frac{1}{T} = \frac{A}{T} \qquad (4\text{–}74)$$

where

$$A = \frac{C_2}{4.9651} = \frac{1.439}{4.9651} = 0.2898 \text{ cm-degree } K.$$

The wave length for maximum energy density is, therefore, inversely proportional to the absolute temperature.

Since A is a known value, it can then be calculated that the maximum energy density of thermal radiation falls just into the visible region of the spectrum at a temperature of about 7,600° K. This value is very close to the maximum surface temperature during the second pulse, and it is considerably higher than the average temperature during that period. It is evident, therefore, that most of the radiant energy emitted during the second pulse consists of visible and infrared rays, with very little of the energy falling in the ultraviolet region of the spectrum.

The intensity of radiant energy is defined as the amount of energy passing through one square centimeter of surface of a black body per second. By integrating Eq. 4–73, it is seen that the flux (intensity) of radiant energy, ϕ, is related to the absolute temperature by the expression

$$\phi = \int_0^\infty E_\lambda d\lambda \qquad (4\text{–}75)$$

$$\phi = \sigma T^4 \qquad (4\text{–}76)$$

where σ is a constant equal to

$$\frac{\pi^4}{15} \frac{C_1}{C_2^4} = 5.6685 \times 10^{-5} \text{ erg/cm}^2 K^4\text{sec}.$$

The total radiant energy intensity from the fireball then can be calculated for any required temperature.

As shown in Eq. 4–76, the intensity of the radiation emitted from the fireball is proportional to the fourth power of the absolute fireball temperature. Because the surface temperatures are very high during the primary pulse, the rate of energy emission per unit area will also be high. However, because of the short duration of the initial pulse, the total quantity

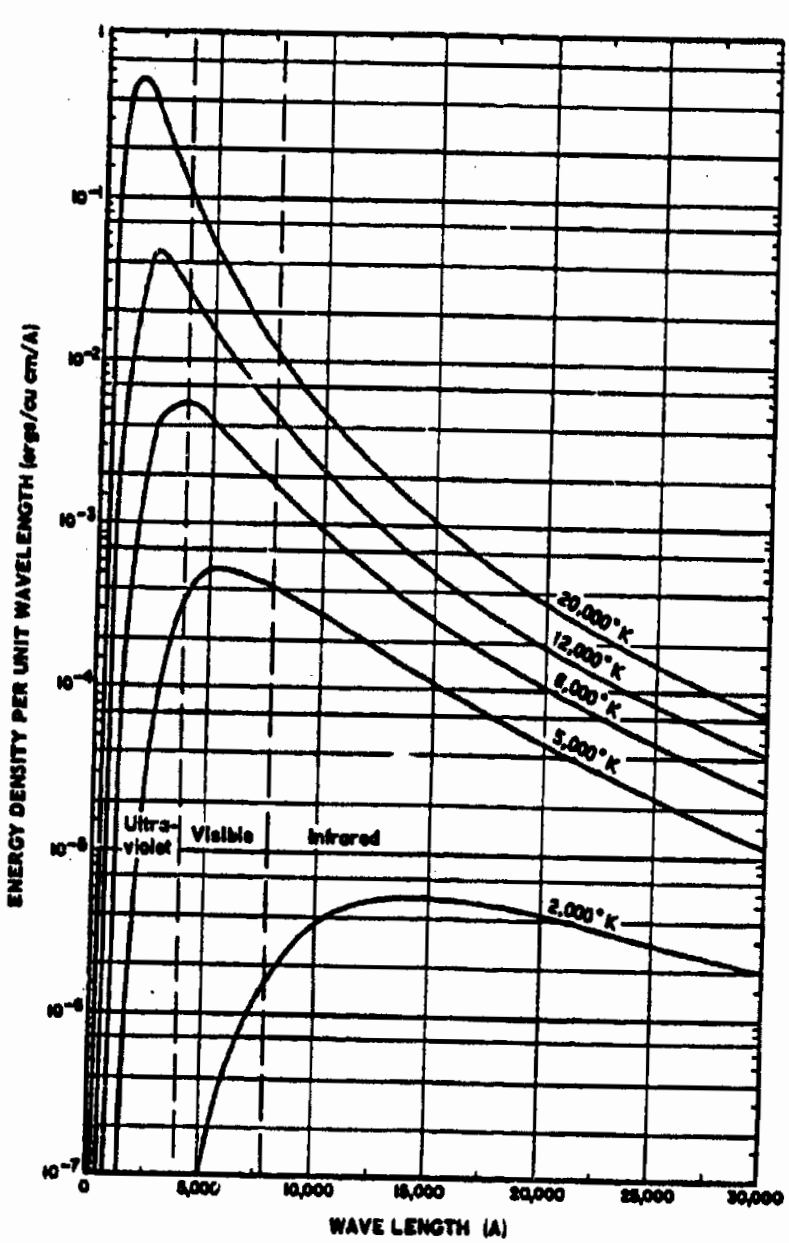

Figure 4–59. Energy Density Per Unit Wave Length of Radiations of Various Wave Lengths

of radiation emitted is relatively small when compared with the quantity emitted during the second pulse.

The total rate of emission of radiant energy can be obtained by multiplying Eq. 4–76 by the surface area of the fireball. If the radius of the fireball is represented by the symbol R, then the area of the fireball is $4\pi R^2$, and the total rate of thermal energy emission is $\sigma T^4 \times 4\pi R^2$. Because power is defined as the rate of production or expenditure of energy, this is the same as the thermal power. Then, representing the thermal power by the symbol P,

$$P = 4\pi\sigma T^4 R^2 \qquad (4\text{–}77)$$

$$P = 7.13 \times 10^{-4}\, T^4 R^2 \text{ ergs per second}$$

where T is in degrees K and R is in cm.

However, due to a number of factors, the fireball does not act as a perfect radiator. This has been proved conclusively by the results of a number of tests. During the first radiation pulse the surface temperature is modified by the disturbed air immediately around the fireball. At later stages, the temperature is not that of the surface, but the result of radiation some distance inside the fireball. In addition, the radius of the fireball during the second pulse becomes extremely difficult to determine, because the surface of the fireball becomes very diffuse. Because the fireball radius and surface temperature will depend on yield, a different curve will be obtained for every value of energy yield. By means of scaling laws it is possible to generalize the results, however, so that a curve applicable to the second pulse can be obtained for all energy yields, from a single set of calculations. The thermal scaling laws will be discussed in detail in Par. 4–7.4, following.

4–7.2. (U) Measurement Techniques

4–7.2.1. *Units of Measurement*

Because radiant flux is a flow of energy, its value may be expressed in any of the units of power (the amount of energy per unit time). For example, the solar constant (intensity of radiation from the sun) is usually expressed as the energy in calories that falls in one minute upon a square centimeter, at the earth's mean distance, and normal to the sun's rays. Ergs, joules, calories, or BTU/second, watts, or even horsepower (all per some unit area) may be used. Most physicists, however, prefer calories-per-square-centimeter.

When measuring spectral radiant energy, the unit of wave length must also be defined. The four most common sets of units, with their symbols and values are presented in Table 4–6.

Whichever units are used, care must be taken when absolute measurements are to be made, because the numerical constants (for example, the constants of the Planck equation) are given for a definite unit of wave length. If the c.g.s. units for the constants are used, the wave length must be expressed in centimeters.

4–7.2.2. *Calibration of Instruments*

Radiant energy measurement divides itself into two classes: the measurement of the total radiant energy, or flux, for all wave lengths; and the measurement of the thermal flux for various wavelength intervals. The first measurement is the easier of the two, as a single measurement may suffice. However, for accurate results, the receiver must have the same radiant energy absorption characteristics for all wave lengths present.

For spectral-radiant-energy measurements, the absorption characteristics of the receiver may be included in the instrument calibration for any particular wave length. There are two problems involved in measuring spectral radiant energy: the separation of the energy into different wavelength intervals; and the measurement of the energy within these intervals. In addition, the radiant energy must be separated into intervals permitting energy meas-

TABLE 4–6. UNITS OF WAVE LENGTH MEASUREMENT

Unit	Symbol	Value
Micron	μ	$1\,\mu = 10^{-3}$ mm
Millimicron	$m\mu$	$1\,m\mu = 10^{-6}$ mm
Angstrom	Å	1 Å $= 10^{-7}$ mm
X-Unit	XU	1 XU $= 10^{-10}$ mm

urement without too great an error due to stray radiation.

When measuring total or spectral radiation, either comparative or absolute values may be desired. If absolute values are necessary, the instruments must be calibrated. The calibration of an energy-measuring device consists of finding the response of the instrument when a known amount of radiation falls upon it. The best method of achieving this is to expose the measuring device to the radiation from a standard radiator (black body) at a definite temperature, and to then compare the reading with the known amount of energy incident upon it. If the surface temperature of the black body is known, and the distance to the device is measured, by making use of the inverse square law (Ch. 2, Sec. XI) the radiation incident upon the device can be calculated and compared with the reading.

In practice, however, use of a black body for calibration purposes is a tedious and expensive operation. Therefore, incandescent lamps calibrated in terms of a specified amount of radiation per square centimeter at a definite distance and direction from the lamp, may be used. These lamps can be obtained from the National Bureau of Standards. To obtain a calibration for spectral measurements, relative intensities within the visible spectrum for a lamp or other source of known luminous intensity may be measured, and a summation taken of the product of this relative energy and the relative luminosity, wave length by wave length. The calibration constant is then given by the candlepower of the lamp, or other source, divided by this sum.

4–7.2.3. *Basic Considerations*

For the general case, the amount of radiation that passes from the source to the measuring device is geometrically dependent upon the distance between the two surfaces, the size of the two surfaces, and their respective orientation with respect to the line joining them. This constitutes five geometric parameters. In actual practice, the receiver is generally mounted perpendicular to the line joining the two surfaces, and is calibrated to record the incident energy per unit time and unit area. This eliminates the measurement factors of size and orientation of the receiver, and reduces the variables to three. In addition, for a nuclear detonation the orientation of the source is not a variable, because the source radiates in all directions. Thus, for field measurements of a nuclear detonation, the amount of radiation is geometrically dependent upon two factors: the distance between the source and the measuring device; and the size of the fireball.

The field of radiant-energy measurements includes not only the free-field measurements described above, but the study of the alterations produced in the characteristics of bodies upon which the energy falls or through which it passes (i.e., the reflection, absorption, and transmissivity of material bodies. Because these values are ratios, only relative calibration of the measuring devices is required. For objects more than a few wave lengths thick, the reflection depends only on the surface characteristics, while the absorption and transmissivity vary with thickness.

4–7.2.4. *Instrumentation*

a. Calorimetry

Calorimetry is the measurement of quantities of heat. In general, the quantities of heat are measured indirectly by observing the effects of the heat on various substances. Heat effects most frequently used for measurement are: the rise in temperature of a mass of known heat capacity; the change of state of a substance of known latent heat; and the transformation of energy. In order to execute heat measurements, a system of units must be obtained.

For instance, if the quantity of heat required to melt one pound of ice is known, the measurement of any unknown quantity of heat can be reduced to the simple act of determining how many pounds of ice can be melted by that unknown quantity. Such is the principal of the calorimeter. Another and more familiar measurement unit is the quantity of heat required to change the temperature of one kilogram of water one degree centigrade (from 15° C to 16° C). This unit is defined as the calorie.

b. Radiometer

The radiometer is an instrument designed to measure the quantity of radiant energy by de-

termining its mechanical effect. It consists of crossed arms of very fine glass which have vanes of thin mica at their extreme ends. These vanes are blackened on one side with all blackened sides facing in the same direction around the axis of rotation. The instrument is suspended by a quartz fibre in an evacuated glass vessel. When the vanes are exposed to rays of light or heat they rotate with a speed proportional to the strength of the thermal rays to which they are exposed. In principal, heat is absorbed by the blackened side of the vanes and is then transmitted to such rarefied gas particles as remain in the vessel. The energized particles thrust against the vanes and effect a torsional moment. Modern radiometers are extremely efficient and accurate even when only a single reading is taken.

c. Spectroscope

The spectroscope is an optical device which uses prisms, diffraction gratings, or interferometers to separate radiant energy into its constituent wave lengths to produce a spectrum. This spectrum may then be observed visually, recorded photographically, or detected by radiometric means. Among the more important uses of the spectroscope is the study of the emission and absorption of radiant energy by matter. Wave lengths may be found to an accuracy of 0.001 with a small prism spectroscope, $\frac{1}{2{,}000{,}000}$ by using a large diffraction grating device, and within $\frac{1}{50{,}000{,}000}$ if a Fabry-Perot interferometer is utilized.

d. Summary

The radiant energy measuring devices described are general classes of instruments. No attempt has been made to present detailed information pertaining to specific instruments with the general class. The problems involved in modern quantitative measurement of thermal radiation necessitate the use of many specially designed measuring devices. These instruments, although in general adhering to the basic principles of calorimetry, radiometry, and spectography, are much more elaborate than the simple devices discussed. Detailed information concerning the specific types of radiant energy measuring equipment can be found in Refs. 48 and 50.

4–7.3. (C) Energy Partition

Energy partition is defined as the distribution of the total energy released by a nuclear detonation among nuclear radiation, thermal radiation, and blast. Energy partition depends primarily upon environmental conditions; i.e., whether the detonation takes place in air, under ground, or under water. Furthermore, energy partition has meaning only when related to a particular time after detonation. For example, if evaluated within the first minute, the energy partition of a nuclear detonation in free air, under ambient conditions varying from a homogenous sea level atmosphere to the conditions existing at 50,000 feet altitude, is in the proportion of about 50 per cent blast, 35 per cent thermal, and 15 per cent nuclear (5 per cent initial radiations, 10 per cent from fission products). The energy partition of an underground burst, on the other hand, is entirely different. There is a reduction of thermal radiation received at a distance due to the amount of heat used in vaporizing the surrounding soil, and a reduction of air blast due to the amount of blast energy used to produce cratering and ground shock.

4–7.4. (C) Thermal Scaling

4–7.4.1. General

The fireball has been described (Ch. 2, Sec. XI) as emitting thermal radiation in a pulse characterized by a rapid rise to a first maximum, a decline to a minimum, another rise to a second maximum, and a subsequent final decline. The first phase of this pulse occurs so very rapidly that less than 1 per cent of the total thermal radiation is emitted. Consequently, it is the second phase of the pulse which is of interest in weapons-effects considerations at altitudes in the lower troposphere.

Throughout, the fireball may be considered to radiate essentially, though not ideally, as a black body, for which the radiant power is proportional to the radiating area and the fourth power of the temperature. (See Par. 4–7.1.

preceding). After the radiant power minimum, the radiating area and radius increase relatively slowly, so that the radiant power is predominantly determined by the temperature cycle of the fireball. An illustration of the apparent temperature (and fireball radius) versus time, for a 20-KT airburst, is shown in Fig. 4-60. It should be emphasized, however, that the actual radiating area may vary substantially from that of the luminous fireball. Very little quantitative information is available concerning the rate of growth of the fireball following the time at which the shock front breaks away from the fireball (approximately 0.015 seconds for the 20-KT burst shown in Fig. 4-60). Up to the time of break away, however, the radius increases approximately as the 0.4 power of the time after detonation (Ref. 21).

4-7.4.2. *Thermal Pulse*

a. General

The shape of the pulse after the radiant power minimum (t_{min}) is sufficiently similar for nuclear detonations, permitting a single curve to be used to represent the time distribution of radiant power emitted (Fig. 4-61). This curve has been developed by using ratios. The ratio $\frac{P}{P_{max}}$ is plotted against ratio $\frac{t}{t_{max}}$, where $\frac{P}{P_{max}}$ is the ratio of the radiant power at a given time to the maximum radiant power, and $\frac{t}{t_{max}}$ is the ratio of time after detonation to the time to the second thermal maximum for that detonation.

The per cent of the total thermal radiation emitted versus the ratio $\frac{t}{t_{max}}$ is also shown on Fig. 4-61. From this figure it is seen that approximately 20 per cent of the total emission occurs up to the time of the second power maximum, whereas 82 per cent is emitted prior to ten-times-the-time to the second power maximum. By this time, the rate of delivery has dropped to such a low value that the remaining energy is no longer of significance in damage production (Ref. 21).

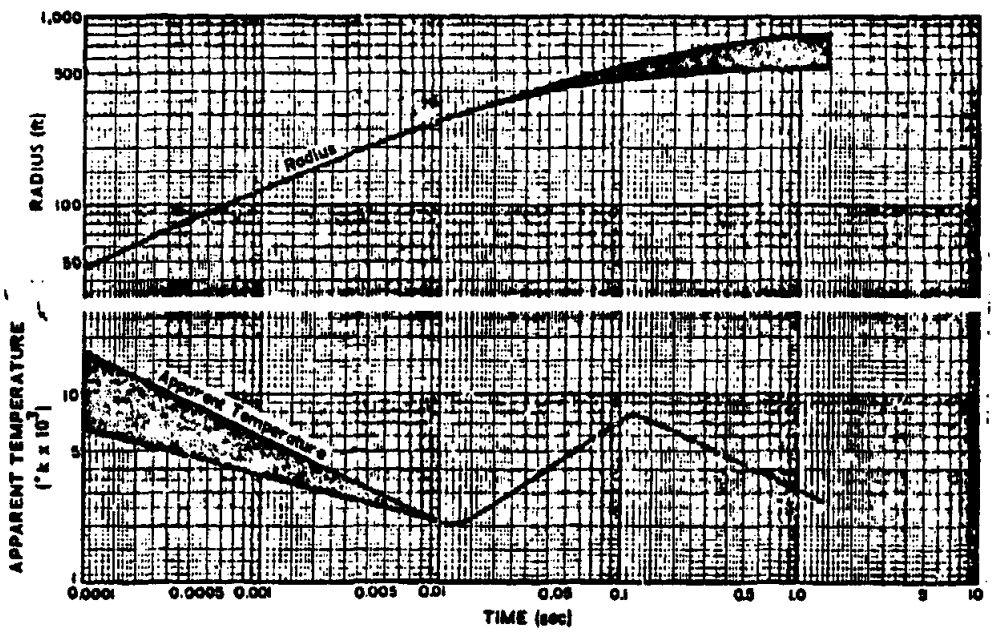

Figure 4-60. Radius and Apparent Temperature of Fireball vs Time, for a 20-KT Air Burst

b. Instructions for Using Fig. 4–61, Generalized Thermal Pulse

(1) Description

Fig. 4–61 shows the scaled radiant power relative to the second maximum, and the per cent of total thermal radiation emitted, as functions of time-after-burst relative to the time of the second maximum. The figure applies to weapons burst at altitudes between 50,000 feet and the surface. Only the second phase (second maximum) of the pulse is shown, since the first phase includes less than one per cent of the emitted thermal energy and is usually neglected in effects considerations.

(2) Scaling Procedure

The second radiant power maximum and the time to this peak both scale as the square root of the yield. To determine for a weapon of yield "W" KT any instantaneous level of radiant power, and the corresponding time of this level after detonation, the values obtained from Fig. 4–61 are multiplied by P_{max} and t_{max}, respectively. The latter are determined by:

$$P_{max} = 4\ W^{1/3}\ \text{KT/sec.} = 4\times10^{12}\ W^{1/3}\ \text{cal/sec.} \quad (4\text{–}78)$$

$$t_{max} = 0.032\ W^{1/3}\ \text{sec.} \quad (4\text{–}79)$$

(3) Example

Given: A 90–KT air burst.

Find: The radiant power at 2 seconds, and the per cent thermal radiation emitted up to 2 seconds.

Solution: From the scaling above,

$$t_{max} = 0.032\times(90)^{1/3} = 0.304 \text{ second.}$$

For a 90–KT air burst, when $t = 2.0$ seconds,

$$\frac{t}{t_{max}} = \frac{2.0}{0.304} = 6.6$$

Reading from Fig. 4–61, for a value of $\frac{t}{t_{max}} = 6.6$, the value obtained for $\frac{P}{P_{max}} = 0.06$.

From the scaling above, $P_{max} = 4\times(90)^{1/3}$ KT/sec. = 38.0 KT/sec.

For a 90–KT air burst, when $t = 2.0$ seconds,

$P = P_{max}\times0.06 = 38.0\times0.06 = 2.28\ (\pm0.68)$ KT/sec.

Reading from the per cent emitted curve, when $\frac{t}{t_{max}} = 6.6$, gives the value of 76 per cent.

(4) Reliability

The radiant power values obtained from Fig. 4–61 are reliable to within ±30 per cent for air burst yields between 6 and 100 KT. The reliability decreases for air burst weapon yields lower than, or above, this range. Times are reliable to ±15 per cent for air burst weapons in the range 6 KT to 100 MT. For air burst weapon yields lower than 6 KT, the times may be as much as 30 per cent higher than those obtained from the above scaling relationship.

For other types of burst, the reliability of the scaling of radiant power is expected to be lower than that shown for air bursts; the reliability cannot be estimated accurately, however on the basis of available data (Ref. 21).

4–7.4.3. *Time Scaling*

a. General

It has been found that both the time to the radiant power minimum and the time to the second maximum are proportional to the square root of the weapon yield. Thus, for air bursts at altitudes below approximately 50,000 feet, the time to minimum (t_{min}) is 0.0027 $W^{1/3}$ second. The time to the second maximum (t_{max}) is 0.032 $W^{1/3}$ second. (See Figs. 4–62 and 4–63. These figures may also be used for surface bursts.) It should be noted that for weapon yields lower than six kilotons the actual values of t_{max} may be as much as 30 per cent higher than those given by Fig. 4–62. This is caused by the higher mass-to-yield ratio characteristics of the low yield weapons. These relations indicate that a one megaton weapon delivers its thermal radiation over a period 32 times as great as does a one kiloton weapon. This can be expected to result in variations in the total thermal energy required for a given effect. The significance of the dependence of delivery rate on weapon yields is discussed in the sections

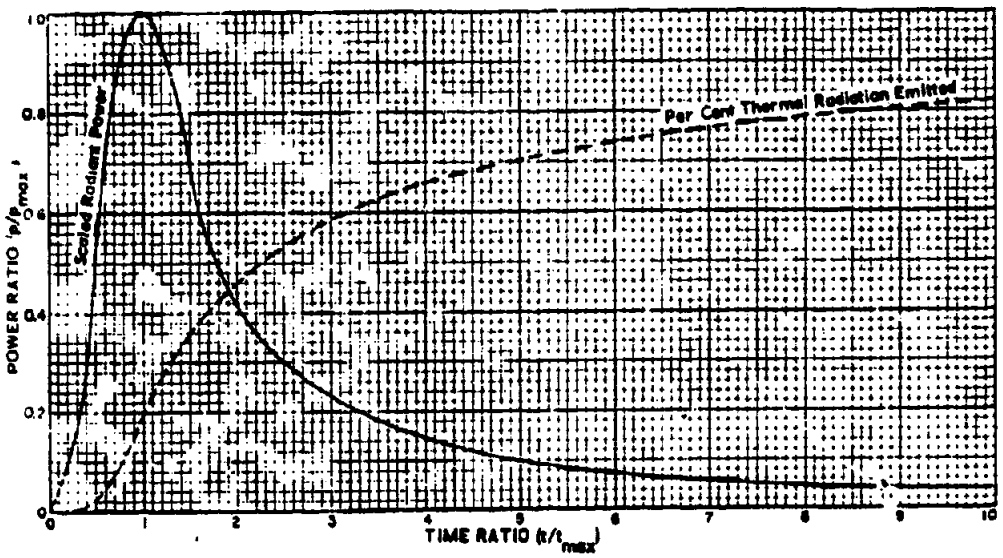

Figure 4–61. Plot of Generalized Thermal Pulse

dealing with thermal injury and damage (Ref. 21).

b. Instructions for Using Figs. 4–62 and 4–63, Time to Second Radiant Power Maximum and Time to Minimum, vs Yield

(1) Description

Figs. 4–62 and 4–63 give the time to the second radiant power maximum (t_{max}), and the time to the radiant power minimum (t_{min}), both as a function of weapon yield for air burst weapons at altitudes below 50,000 feet. The figures may also be used for surface bursts.

(2) Example

Given: The air burst of a 1-MT weapon.

Find: The time to the radiant power minimum, and the time to the second radiant power maximum.

Solution: Find 1 MT on the abscissa of Fig. 4–63, and read from the two time curves $t_{min}=0.085$ (± 0.009) second, and $t_{max}=1.1$ (± 0.2) second.

(3) Reliability

The times read from the t_{min} curve of Figs. 4–62 and 4–63 are reliable to ± 10 per cent. The times read from the t_{max} curves of Fig. 4–62 and 4–63, in the range 6 KT to 100 MT, are reliable to ± 15 per cent. For weapon yields lower than 6 KT, the values of t_{max} may be as much as 30 per cent higher than those given by Fig. 4–62. (Ref. 21).

4–7.4.4. Thermal Yield

a. General

Measurements of the total thermal energy emitted for air burst weapons of low yield indicate that this thermal energy is proportional to weapon yield and is about one-third of the total yield. From this and Fig. 4–61, a scaling procedure for maximum radiant power may be derived. Thus

$$P_{max}=4\ W^{1/2}\ \text{KT/sec. or } 4\times 10^{12}\ W^{1/2}\ \text{cal/sec.} \quad (4\text{–}80)$$

Measurements from the ground of the total thermal energy from surface bursts, although not as extensive as those for air bursts, indicate that the thermal yield is a little less than half that from equivalent air bursts. For a surface burst, thermal yield is assumed to be one-seventh of the total yield. For surface bursts, the

scaling of the second radiant power maximum (P_{max}) cannot be determined on the basis of available data. Similarly, there are no data which show what the thermal radiation phenomenology may be for detonation altitudes in excess of 50,000 feet. It is expected that the thermal energy may increase with altitude of burst. Fig. 4-64 gives a purely theoretical estimate of this increase (Ref. 21).

b. Instructions for Use Fig. 4-64, Relative Thermal Yield vs Burst Altitude

(1) Description

Fig. 4-64 gives an estimate of the relative thermal yield for various burst altitudes. The values of atmospheric transmissivity at very high altitudes are not known with any certainty, but are believed to be only slightly less than unity.

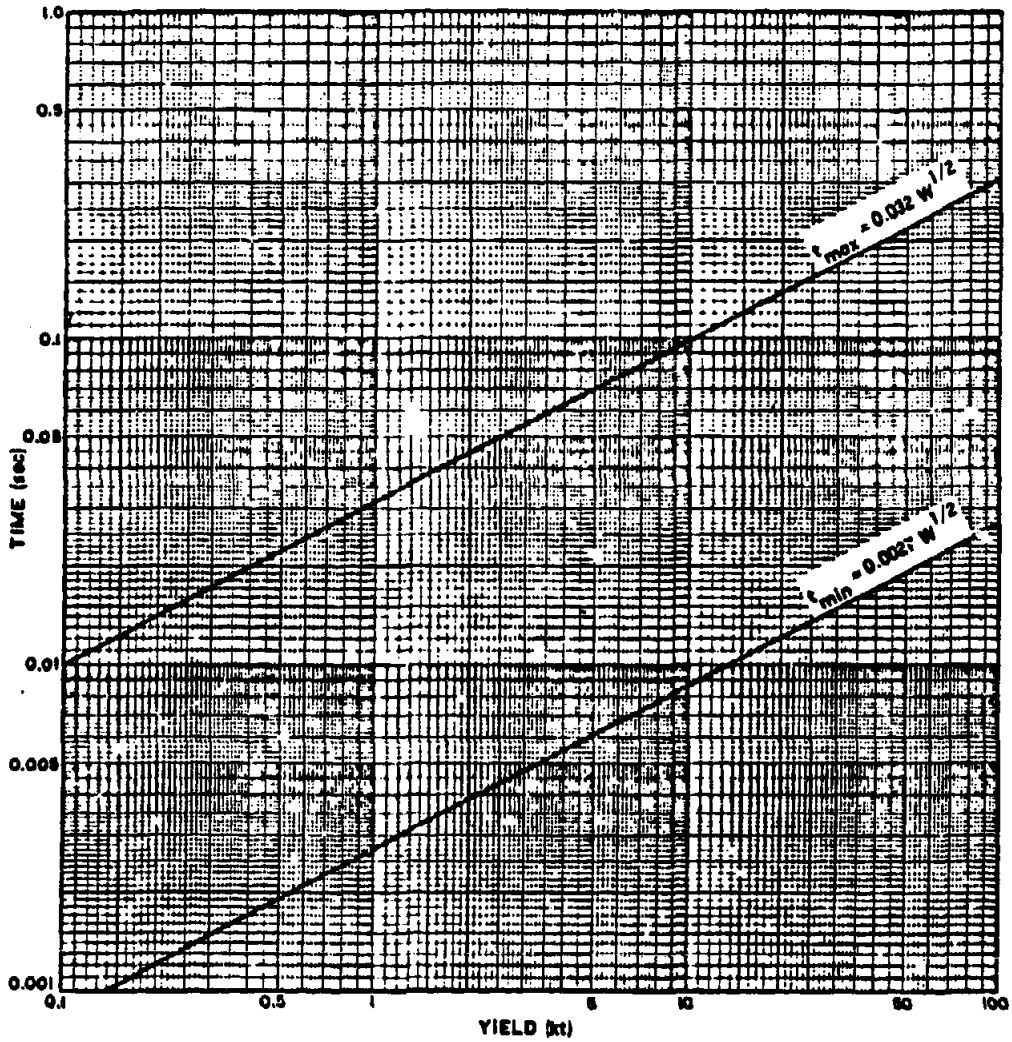

Figure 4-62 (C). Time to Second Radiant Power Maximum (t_{max}) and Time to Minimum (t_{min}), vs Weapon Yield, 0.1 KT to 100 KT (U)

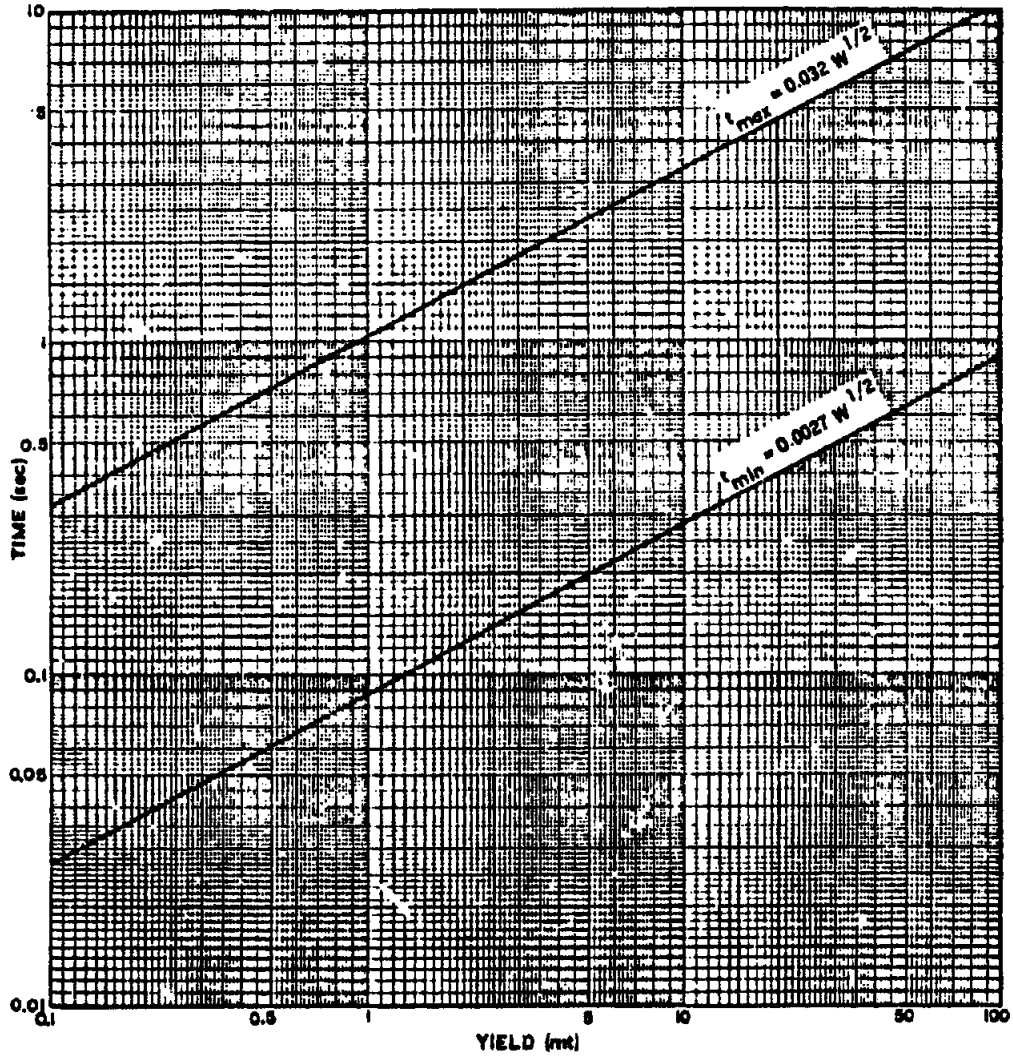

Figure 4–63 (C). Time to Second Radiant Power Maximum (t_{max}) and Time to Minimum (t_{min}), vs Weapon Yield, 0.1 MT to 100 MT (U)

(2) Procedure

To calculate for a high altitude burst the radiant exposure, Q, at a given slant range, use the following equation:

$$Q = \frac{3.16 \times 10^6\ WF}{D^2} \text{ cal/sq cm} \qquad (4\text{–}81)$$

where

W = weapon yield (in KT),

F = relative thermal yield (from Fig. 4–64), and

D = slant range from detonation (yards).

(3) Example

Given: A 10–KT burst at 50,000 feet.

Find: Radiant exposure at 1,000 yards from the detonation.

Solution: From Fig. 4–64 the relative thermal yield, F, at 50,000 feet is 1.02. Therefore,

$$Q=\frac{3.16\times10^6\ (10)\ (1.02)}{(1000)^2}=32.2\ (\pm4.8)$$

cal/sq cm.

(4) Reliability

The values given for the relative thermal yield are subject to errors of ±15 per cent at 50,000 feet and to increasingly larger errors at greater altitudes.

4–7.5. (C) Radiant Exposure Versus Slant Range

4–7.5.1. *Spectral Characteristics*

At distances of operational interest, the spectral (wave length) distribution of the incident thermal radiation, integrated with respect to time, resembles very closely the spectral distribution of sunlight. For each, slightly less than one-half of the radiation occurs in the visible range of the spectrum, approximately one-half occurs in the infrared region, and a very small fraction (rarely greater than 10 per cent) lies in the ultraviolet region of the spectrum. (See Fig. 4–59 for energy densities of various wave lengths.) The color temperature of the sun and an air burst are both about 6,000° K. A surface burst, as viewed by a ground observer, contains a higher proportion of infrared radiation and a smaller proportion of visible radiation than the air burst, with almost no radiation in the ultraviolet region. The color temperature for a surface burst is about 3,000° K. However, a surface burst viewed from the air may exhibit a spectrum more nearly like that of an air burst.

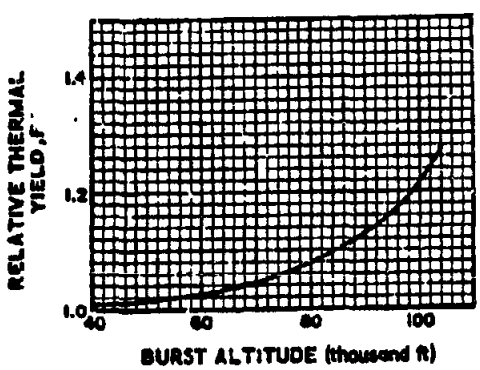

Figure 4–64 (C). Relative Thermal Yield vs Burst Altitude (U)

4–7.5.2. *Atmospheric Transmissivity*

a. General

The atmospheric transmissivity, T, is defined as the fraction of the radiant exposure received at a given distance, after passage through the atmosphere, relative to that which would have been received at the same distance if no atmosphere were present. Atmospheric transmissivity depends upon several factors; among these are water vapor and carbon dioxide absorption of infrared radiation, ozone absorption of ultraviolet radiation, and multiple scattering of all radiation. All of these factors vary with distance and with the composition of the atmosphere.

Scattering is produced by the reflection and refraction of light rays by certain atmospheric constituents, such as dust, smoke, and fog. Interactions (such as scattering) which divert the rays from their original path result in a diffuse, rather than a direct, transmission of the radiation. As a result, a receiver which has a large field of view (i.e., most military targets) receives radiations which have been scattered toward it from many angles, as well as the directly transmitted radiation. Since the mechanisms of absorption and scattering are dependent on wave length, the atmospheric transmissivity depends not only upon the atmospheric conditions, but also upon the spectral distribution of the weapon radiation.

In Fig. 4–65, the atmospheric transmissivity is plotted as a function of the slant range, for air and surface bursts. For each type of burst three sets of atmospheric conditions are assumed. It is believed that these conditions represent the average and the extremes normally encountered in natural atmospheres. These conditions correspond to the following: a visibility of 50 miles and a water vapor concentration of 5 gm/cu m; 10 miles visibility and 10 gm/cu m water vapor concentration; and 2 miles visibility and 25 gm/cu m water vapor concentration.

The curves of Fig. 4–65 are plotted to slant ranges equal to one-half the visibility of each of the three visibility conditions. The reason for this is that the transmissivity values have not been verified for higher visibility conditions. As a result, the curves cannot be extrapolated to represent greater slant-range distances with any confidence. If the curves are extended beyond one-half the visibility range, there is reason to believe that the values of transmissivity would be too high. Where cloud cover is appreciable, or the air contains large quantities of fog or industrial haze, knowledge of the interactions with the radiation is too limited to provide estimates of atmospheric transmissivity.

b. Instructions for Using Fig. 4–65, Atmospheric Transmissivity

(1) Description

Fig. 4–65 gives the atmospheric transmissivity versus slant range for three sets of atmospheric conditions, for both air and surface burst weapons. These curves are presented only for illustrative purposes, as they were used to derive the radiant exposure versus slant range curves of Fig. 4–66.

The differences between the air burst and surface burst curves are caused by the difference in apparent radiating temperatures (when viewed from the ground), and by the difference in geometrical configuration of the two types of burst. The three sets of atmospheric conditions represented are:

1. 50 mile visibility and 5 gm/cu m water vapor.
2. 10 mile visibility and 10 gm/cu m water vapor.
3. 2 mile visibility and 25 gm/cu m water vapor.

It is believed that these conditions pertain to the naturally occurring average and extreme atmospheric conditions.

Reference can be made to the atmospheric water vapor concentration curves in Fig. 4–71 to ascertain under what conditions of relative humidity and ambient temperature a particular water vapor concentration will occur.

(2) Reliability

The curves of Fig. 4–65 have not been verified at ranges beyond one-half the visibility. As a result, they are subject to considerably reduced reliability beyond these ranges (Ref. 21).

4–7.5.3. Reflection

If a weapon is burst in the air below a large cloud, the thermal radiation is diffusely deflected downward from the cloud, resulting in greater radiant exposures at a given distance than would be received if no cloud were present. If a weapon is burst near the earth's surface, the radiant exposure received at some altitude above the earth (as in the case of an aircraft flying above the detonation) will be greater, because of the reflected radiation, than that which is received on the ground at the same distance. If the receiver is directly over the burst and the terrain has a high albedo, the reflected radiation from the terrain may be as much as twice the direct radiation. If a reflect-

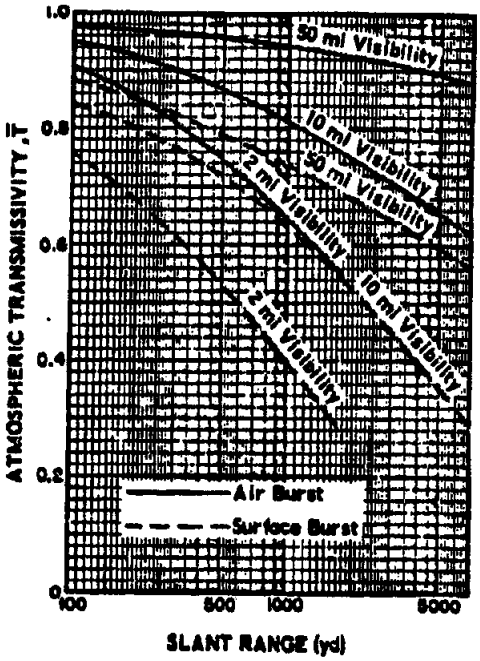

Figure 4–65 (C). Atmospheric Transmissivity vs Slant Range, for Air and Surface Bursts at 100 to 7,000 Yards (U)

ing or scattering layer such as a cloud, however, is between the detonation and the target, the radiant exposure received will be reduced considerably.

4–7.5.4. *Calculation of Radiant Exposure*

a. General

The radiant exposures at various slant ranges from air and surface bursts can be calculated from the following expressions:

$$Q=\frac{3.16\times10^{6}\,W\,(T)}{D^{2}} \quad \text{(air burst)} \qquad (4\text{–}82)$$

and

$$Q=\frac{1.35\times10^{6}\,W\,(T)}{D^{2}} \quad \text{(surface burst)} \qquad (4\text{–}83)$$

where

Q = radiant exposure (cal/sq cm),

T = atmospheric transmissivity,

W = weapon yield (kiloton),

and

D = slant range (yards).

The values of T for both air and surface bursts are obtained from the appropriate curves in Fig. 4–65. Curves showing the radiant exposure (Q) as a function of slant range (D) for three atmospheric conditions, for both air and surface bursts, are shown in Fig. 4–66. These curves are plotted for ranges up to one-half the visibility, for the reasons mentioned in the Par. 4–7.5.2.*a*, preceding. The surface burst curves differ from the air burst curves for two reasons: the apparent thermal yield from a surface burst, when viewed from the surface, is lower than that for an air burst; and the spectral distribution of the surface burst is sufficiently different from that of an air burst to warrant the use of different atmospheric transmissivity curves. Radiant exposure for a burst in the transition zone may be estimated by interpolation between these curves, as explained in Par. *b*, following. It should be emphasized that these surface burst curves apply to the radiant exposure of ground targets. When the surface burst is viewed from the air (as from aircraft) the apparent radiating temperature and the thermal yield will be greater than when viewed from the ground. All of the curves plotted in Fig. 4–66 are for a total weapon yield of one kiloton. For weapon yields greater or less than one kiloton, these radiant exposures should be multiplied by the yield of the weapon in question.

b. Instructions for Using Fig. 4–66, Radiant Exposure from Air and Surface Bursts

(1) Description

Fig. 4–66 presents the radiant exposure (i.e., incident radiant energy per unit area) versus slant range curves for 1–KT air and surface bursts. The solid curves are for the air burst, those above 180 $W^{0.4}$ feet. For bursts at heights between 180 $W^{0.4}$ feet and the surface, the radiant exposure will lie between the corresponding solid and dashed curves. Until further data are obtained, a linear interpolation between the two curves should be made for bursts in the transition zone (Example 2). For each type of burst shown, three curves are presented: 50 mile visibility and 5 gm/cu m water vapor; 10 mile visibility and 10 gm/cu m water vapor; and 2 mile visibility and 25 gm/cu m water vapor. Fig. 4–66 is based on the air and surface burst thermal yields and the atmospheric transmissivity curves of Fig. 4–65.

(2) Scaling Procedure

For a given slant range, the radiant exposure, Q, is proportional to the weapon yield, W:

$$\frac{Q_1}{Q_2}=\frac{W_1}{W_2}.$$

In Fig. 4–66, Q_1 is given for $W_1=1$ KT.

(3) Example 1

Given: A 40–KT detonation at a burst height of 3,000 feet and a 10-mile visibility.

Find: The slant range at which the radiant exposure is 10 cal/sq cm.

Solution: The scaled burst height is $\frac{3000}{(40)^{0.4}}$ = 685 feet; therefore, the air burst curve should be used. Then,

$$Q_1=10\,\frac{1}{40}=0.25 \text{ cal/sq cm.}$$

From Fig. 4–66, the slant range at which 0.25

cal/sq cm would be received from an air burst (visibility=10 miles) is 3,000 yards.

(4) Example 2

Given: A 500–KT detonation at a burst height of 1,200 feet, and a 50-mile visibility.

Find: The slant range at which the radiant exposure is 25 cal/sq cm.

Solution: The scaled burst height is $\frac{1200}{(500)^{0.4}}$ =100 feet; therefore, for this transition burst, the range sought will lie $\frac{100}{180}$ of the distance between the surface and air burst values. Then,

$Q_t = 25 \frac{1}{500} = 0.05$ cal/sq cm.

From Fig. 4–66, the ranges at which 0.05 cal/sq cm would occur for surface and air bursts

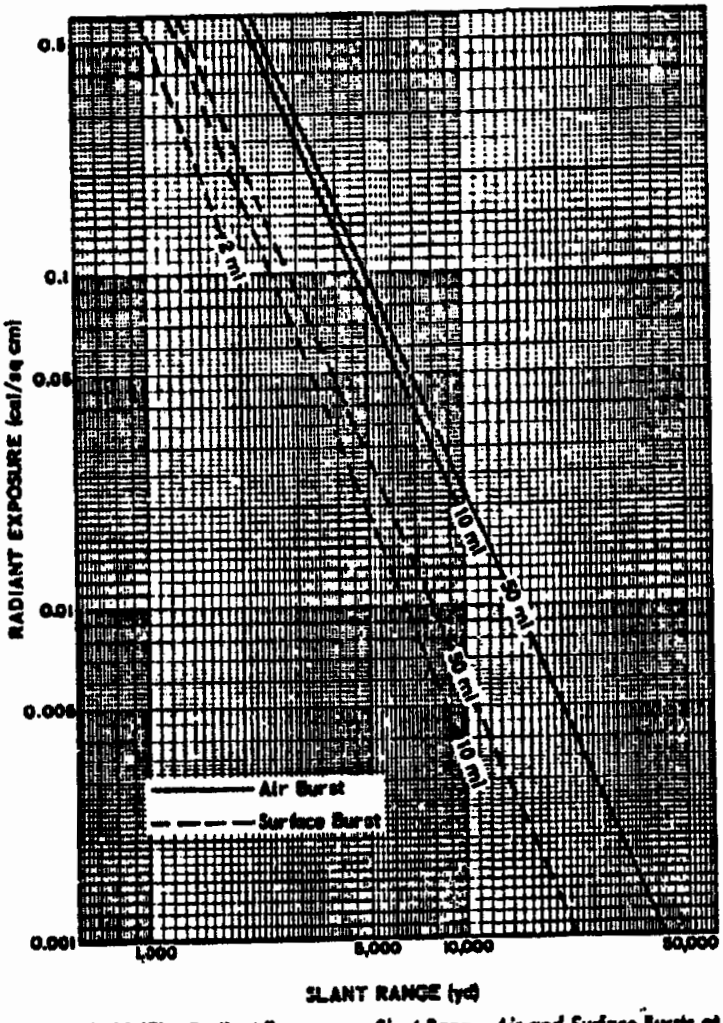

Figure 4–66 (C). Radiant Exposure vs Slant Range, Air and Surface Bursts at 2-, 10-, and 50-Mile Visibilities, 1–KT Burst (0.001 to 0.6 cal/sq cm) (U)

(visibility=50 miles) are 4,100 and 7,000 yards, respectively. The answer is then:

$$4{,}100+\frac{100}{180}(7{,}000-4{,}100)=5{,}700 \text{ yards.}$$

(5) Reliability

Factors limiting the applicability of Fig. 4–66 are discussed in Par. a, preceding. In addition, the reliability is expected to decrease as the weapon yield is increased above 100 KT, and as the slant range is increased beyond one-half the visibility, as noted in Fig. 4–65.

4–7.4. (C) Other Influences on Thermal Radiation Propagation

4–7.4.1. *Topography and Clouds*

Propagation of thermal radiation from a nuclear detonation, like that from the sun, is affected by topography and by the atmosphere. At close ranges, however, where the fireball subtends a relatively large angle, the shadowing effects of intervening objects such as hills or trees are less than are experienced with the sun. As discussed earlier, (Ch. 2, Sec. V), clouds in the atmosphere significantly affect the propagation of radiation through the atmosphere.

4–7.4.2. *Fog and Smoke*

Where the burst is in the air above a fog covering the ground, a significant fraction of the thermal radiation incident on the fog layer is reflected upward. That radiation which penetrates the fog is scattered. These two effects result in substantial reductions in thermal energies incident on ground targets covered by fog. White smoke screens act like fog in the attenuation of thermal radiation. Reductions as large as 90 per cent of incident thermal energies are realized by dense fogs or smoke screens (Ch. 2, Sec. XI).

4–8. (C) NUCLEAR RADIATION

4–8.1. (U) Introduction

The detonation of a nuclear or thermonuclear weapon has associated with it certain phenomena not typical of conventional high explosive bombs. Perhaps the unique phenomenon is the emission of nuclear radiation. The nuclear radiations consist of several types of emission: gamma rays, neutrons, beta particles, and alpha particles. The majority of the neutrons and a considerable portion of the gamma rays are emitted simultaneously with the explosion. The remainder of the gamma rays and the beta particles are produced by radioactive decay of the fissionable materials. Not all of the uranium or plutonium is consumed by the explosion, and the material remaining emits a portion of the alpha rays as a result of natural radioactive decay. Other alpha particles are produced by hydrogen fusion reactions.

The nature of the radiations, either by immediate emission or by radioactive decay, makes it convenient for practical purposes to consider them as either initial or residual radiations.

The initial nuclear radiation is usually defined as that emitted within a time span of one minute after the explosion. The time period of one minute is somewhat arbitrary, and was originally based on the following data from a twenty-kiloton weapon. As a consequence of attenuation by the atmosphere, the effective range of the radiation is roughly two miles. Therefore, as far as effect at the earth's surface is concerned, rays originating from a source at an altitude of over two miles may be ignored. The rate of rise of the atomic cloud, from which the nuclear radiations emanate, is such that it takes approximately one minute for the cloud to reach this altitude.

For a bomb of energy yield greater than twenty kilotons, the distance over which the radiations are effective will be correspondingly larger than two miles. However, there is also an increase in the rate of rise of the atomic cloud. Because one factor compensates for the other, it is sufficiently accurate to consider the effective period of the initial radiation as one minute. Similarly for a bomb of lower energy, the effective distance is less, but so also is the rate of ascent of the cloud.

The above considerations are largely relative to air burst type detonations. For underground and underwater explosions, the line of demarcation between initial and residual radiation is less sharply defined, and it is, therefore, less meaningful to make the differentiation.

4–8.2. (U) Nuclear Radiation Units

4–8.2.1. General

In order to express the nuclear radiation exposures, and to correlate measurement techniques to energy distributions and physiological effects, it is necessary to establish suitable units of measurement for the various radiations. The unit used to measure the exposure to gamma rays at any particular point is referred to as the roentgen.

Radiation measuring instruments do not measure the number of roentgens directly. However, by suitable design, the phenomena observed (e.g., electrical pulses, scintillation, or film fogging) can provide a practical recording of the exposure in roentgens. The various radiation measuring devices (Par. 4–8.3, following) are thus calibrated with a standard gamma ray source. For this purpose, a known quantity of radioactive cobalt or radium is generally used. The gamma-radiation exposure in roentgens from such a source can be measured accurately with special laboratory equipment, and the measurements then used to calibrate field instruments.

It is generally believed that the harmful consequences of nuclear radiations to living organisms are largely due to the chemical decomposition of the molecules present in animal or vegetable cells. Fundamentally, it is the ionization and excitation caused by nuclear radiations that is responsible for this action. Therefore, the amount of ionization or the number of ion pairs provide a basis for measurement.

4–8.2.2. The Roentgen Unit

The roentgen is defined as the amount of gamma radiations or X-rays which will form 1.61×10^{12} ion pairs when absorbed in one gram of air. The absorption of one roentgen is equivalent to the absorption of 87 ergs of energy per gram of air, at conditions of standard pressure and temperature. The roentgen, as a unit of radiation dosage, is defined with respect to gamma or X-rays, and applies only to these radiations. Further, it is a measure of the strength of the radiation field at a given location, not of the radiation absorbed by an individual at that location. The radiation dose in roentgens is thus referred to as an "exposure" dose.

4–8.2.3. Roentgen Equivalent Physical (Rep) Unit

Originally the roentgen equivalent physical (rep) was established to meet the need for an "absorbed" dose unit. As previously stated, a gamma ray exposure dose of one roentgen is equivalent to the absorption of 87 ergs of energy per gram of air. Accordingly, the rep was originally defined as the dose of any type of nuclear radiation that results in the absorption of 97 ergs of energy per gram of animal tissue. However, it was later found that the exposure of one gram of soft tissue to one roentgen of gamma radiation was accompanied by the absorption of 93 ergs of energy by the tissue. The definition of the rep was therefore revised, to denote the dose that would produce, in a unit volume of soft tissue, the same energy absorption as that produced by one roentgen of gamma or X-rays, 93 ergs per gram.

4–8.2.4. The Rad Unit

As a unit of measurement, the rep, based on the roentgen, is somewhat unsatisfactory for several reasons. First, because the number of ergs absorbed is based on the amount of energy required to produce an ion pair. This quantity is relatively uncertain, and as new experimental information becomes available, the number of ergs in the definition must change. Second, the quantity of energy absorbed varies with the material irradiated. To compensate for these drawbacks, another unit, the "rad" has been introduced. The rad is defined as the absorbed dose of any nuclear radiation which is accompanied by the liberation of 100 ergs of energy per gram of absorbing material. For soft tissue the difference between the rep and the rad (93 ergs to 100 ergs) is insignificant, and numerical values of absorbed dose formerly expressed as reps may be considered essentially unchanged when converted to rads.

4–8.2.5. The Relative Biological Effectiveness (RBE) Unit

Although all ionizing radiations are capable of producing similar biological effects, the absorbed dose which will produce a certain effect may vary appreciably from one type of radiation to another. In other words, different radiations, even though producing the same energy absorption per unit volume, have different effectiveness in producing biological injury. In order to evaluate the probable effects of an absorbed dose of combined radiations (neutrons plus gamma radiations) it is necessary to take the relative biological effectiveness (RBE) into account. If, for example, a rep (or rad) of neutrons is found to cause 30 per cent more damage than a rep of gamma rays, it is said that such neutrons have an RBE of 1.3. The unit of measurement is based on assigning an RBE of 1.0 to X-rays or gamma rays having a 250 KVP (kilo-volt peak). The hazard of other radiations is measured in terms of effectiveness relative to rays of this nature.

The value of the RBE for a particular type of nuclear radiation depends upon several factors: the energy of the radiation, the nature and degree of the biological damage, and the organism or tissue under consideration. As far as weapons are concerned, the RBE's are estimated in terms of disabling sickness and death as consequences of a nuclear explosion.

4–8.2.6. The Roentgen Equivalent Mammal (Rem) Unit

Along with the concept of the RBE, it became advantageous to introduce a unit of biological dose called the "rem" (roentgen-equivalent-mammal). This is defined by the equation

$$\text{Dose in rem} = \text{Dose in rad} \times \text{RBE} \qquad (4\text{–}84)$$

or, for soft tissue

$$\text{Dose in rem} = \text{Dose in rep} \times \text{RBE}. \qquad (4\text{–}85)$$

4–8.2.7. Total Dosage

Because the criterion for RBE evaluation is based on the gamma ray RBE being unity, the biological dose in rem, for other radiations, may be related directly to the gamma dose in rep or roentgens. Most tables of biological effects for nuclear radiations are established in terms of the total dosage expressed in roentgens. Therefore, to use these tables for combined radiation results, the gamma dose in roentgens is simply added to the other radiation dosages in rem, to determine the total dosage.

4–8.2.8. The Curie

The curie is that quantity of radioactive material which provides 3.7×10^{10} disintegrating atoms per second (Ref. 49). One gram of radium decays at such a rate. The total amount of gamma fission products at one hour after the detonation of a 20-KT bomb is 6×10^6 curies. One megacurie (10^6 curies) of fission products per square mile, distributed uniformly over an ideal, flat surface, produces a gamma radiation dose rate of approximately 4 roentgens/hour, at 3 feet above the surface, at the 1 hour reference time.

4–8.2.9. Damage Significance of the Rem

The biological effects of various radiation doses are described in general in Ch. 3, Sec. I, and are considered in detail in Ch. 5, Par. 5–16. However, in order to provide some indication of the significance of the units, it may be stated that a single whole-body dose of 25 rem will produce no detectable clinical results. Larger doses have increasingly more serious consequences, and a single exposure of 400 to 500 rem may be expected to prove fatal to about 50 per cent of those exposed. Exposures of 1,000 or more rem over the whole body can be expected to produce 100 per cent fatality.

4–8.3. (U) Measurement Techniques

4–8.3.1. Radiation-Matter Reactions Used for Measurement

The human senses do not respond to nuclear radiation except at very high intensities, under which conditions of itching and tingling of the skin are experienced. Therefore, special instrumental methods have been developed for the detection and measurement of the various types of nuclear radiations, based primarily on the interaction of the radiations with matter.

There are three important types of gamma ray interaction with matter, as a result of

which the rays are scattered or absorbed. The first of these is generally referred to as the photoelectric effect. A gamma ray photon possessing a kinetic energy greater than the energy which binds the electron to the atom transfers all its energy to the electron, which is consequently ejected from the atom. Since the photon involved in the photoelectric effect has lost all its energy, it ceases to exist. The atom, after losing the negatively charged electron, now has a positive charge. This process is referred to as ionization. The magnitude of the photoelectric effect, like that of the Compton effect, increases with the atomic number of the atom and decreases rapidly with increasing energy of the photon.

The second type of interaction of gamma rays and matter is by the Compton effect. In this interaction, when the gamma ray photon collides with one of the atomic electrons some of the energy of the photon is transferred to the electron. The photon, with its energy decreased, then usually moves off at some angle to its original direction of motion. The electron, having acquired an additional amount of energy, is converted into an excited (high energy) state. This phenomenon is known as excitation. The extent of the Compton scattering effect is proportional to the number of electrons in the atom (i.e., to the atomic number). It is greater per atom for an element of high atomic number than for one of low atomic number. However, irrespective of the atomic weight of the atom, the Compton scattering effect decreases rapidly with an increase in the energy of the gamma ray photon.

Gamma radiation can interact with matter in a third manner, that of pair production. When a gamma ray photon with energy in excess of 1.02 million electron volts (Mev) passes near the nucleus of an atom, the photon may be converted into matter, with the formation of a pair of particles: a positive and a negative electron. As in the case of the photoelectric effect, pair production results in the disappearance of the photon. However, the positive electron eventually interacts with a negative electron to form two photons of 0.51 Mev energy. The occurrence of pair production per atom, as with the other interactions, increases with the atomic number of the material. However, it also increases with the energy of the photon in excess of 1.02 Mev.

Neutrons, being electrically neutral particles, do not produce ionization or excitation directly in their passage through matter. They can, however, cause ionization to occur indirectly, as a result of their interaction with certain light nuclei. For instance, when a fast neutron collides with the nucleus of a hydrogen atom, enough energy is transferred to the nucleus to free it from its associated electron, and the nucleus moves off as a positively charged, high-energy proton. Such a proton is capable of producing a considerable number of ion pairs.

Neutrons in the slow and moderate speed ranges can produce indirect ionization in other ways. When such neutrons are captured by the lighter isotope of boron (boron-10) two electrically charged particles of high energy are formed—a helium nucleus (alpha particle) and a lithium nucleus. Both of these particles are capable of producing ion pairs.

Indirect ionization can also result from the fission of plutonium or uranium isotopes. The fission fragments are electrically charged nuclei of high energy which leave considerable ionization in their path (Ref. 1).

All of the processes previously described can be utilized to measure and detect the presence and intensity of nuclear radiations.

4–8.3.2. *Radiation Measurement Instruments*

Two types of instruments, the Geiger Counter and the pocket chamber (dosimeter), are based on the formation of electrically charged ion pairs in a gas and on the consequent ability of the gas to conduct electricity. Normally, a gas does not conduct electricity to any great extent, but as a result of the passage of nuclear radiations, and the subsequent forming of ion pairs, the gas becomes a reasonably good conductor (Ref. 50).

The operation of scintillation counters depends upon excitation. When an atom or molecule becomes excited it will generally give off the excess energy within about one millionth of a second. Certain materials, usually in the solid or liquid state, are able to lose their excitation energy in the form of visible flashes of

light. These flashes, or scintillations, can be counted by means of a photomultiplier tube and associated electronic devices.

In addition to the direct effects of ionization and excitation, there are some indirect consequences, notably chemical changes. One example is the blackening or fogging of photographic film, which appears after the film is developed. Film badges for the measurement of nuclear radiation usually contain two or three pieces of film wrapped in paper which is opaque to light, but is readily penetrated by gamma rays. The degree of fogging observed on the developed films is a measure of the gamma ray exposure. In addition, self-indicating chemical dosimeters are in an advanced state of development. With these devices, the nuclear radiation exposure can be determined directly, by observation of the color changes accompanying certain chemical reactions induced by radiation.

The instruments employed to detect and measure neutron intensities, such as boron counters and fission chambers, are similar in general principle to the Geiger counter.

Tissue-equivalent chambers have been developed. In these, the ionization produced indirectly by neutrons is related to the energy which would be taken up from the neutrons by animal tissue.

In addition to the methods described above, foil-activation methods have been extensively applied to the detection and measurement of nuetrons in various velocity ranges. Certain elements are converted into radioactive isotopes as a result of the capture of neutrons. The amount of induced radioactivity, as determined from the ionization produced by the emitted beta particles or gamma rays, is the basis of the activation process. The detector is generally used in the form of a thin sheet (or foil), so that its effect on the neutron field is not significant.

A fission-foil method makes use of fission reactions. A thin layer of a fissionable material, such as an isotope of uranium or plutonium, is exposed to neutrons. The fission products formed are highly radioactive, emitting beta particles and gamma rays. By measuring the radioactivity produced in this manner, the amount of fission, hence the neutron flux, can be determined.

4–8.3.3. *Applications of the Foil Method*

The neutron dose (in rads) absorbed at a particular location, can be determined by applying certain calculations to the measurements of foil activation. Instruments based on ionization measurements are usually calibrated by means of foil activation data; thus, they can also be used to indicate the dose in rads of neutrons of various energy intervals. Methods are, therefore, available for determining neutron absorption doses in rads.

To determine the biological dose in rems, once the absorbed dose in rads has been measured, the RBE for neutrons must be known. The value of this quantity for neutrons associated with a nuclear explosion has been in doubt. Observations made on mice suggest that the RBE of bomb neutrons, at distances where casualties due to neutron absorption may be expected, is about 1.3. Some confirmation of the applicability of a similar value to man has been obtained, from an analysis of the data on radiation injury and death collected after the nuclear explosions in Japan. It should be noted that the RBE is an experience factor, and as such is constantly subject to change.

The energies of the neutrons received at some distance from a nuclear explosion cover a very wide range, from several million electron volts down to a fraction of an electron volt. The determination of the complete energy spectrum has been calculated by Monte Carlo Code at the Los Alamos Scientific Laboratory (Ref. 51). It is possible, however, to obtain a general idea of the spectrum by measurement of the neutron intensities within a few specified ranges.

Measurements of this kind are made by the use of "threshold" detectors of the activated foil or fission foil type. For example, the element sulphur acquires induced radioactivity as the result of the capture of neutrons having energies greater than 2.5 Mev. Hence, the extent of activation of a sulphur foil is a measure of the intensity of neutrons with energy in

excess of 2.5 Mev. Similarly, the appreciable fission of uranium-238 requires neutrons having an energy of 1.5 Mev or more. The difference between the two results gives the neutron intensity in the energy range of 1.5 to 2.5 Mev. Other foil materials which are used in the same manner are: neptunium-237, with a fission threshold of 0.7 Mev; plutonium-239 (shielded with boron), with a fission threshold of 100 Mev; and gold, which is activated by the very slow neutrons.

The results of a series of measurements, made at various distances from a nuclear test explosion, are presented in Fig. 4-67, in which ND^2 on a vertical logarithmic scale is plotted against D on a horizontal linear scale. N represents the number of neutrons per square centimeter which produce fission, or activation of the foils of the indicated material, at a distance D from the explosion. Since the actual values of ND^2 are not necessary to this discussion, relative values are given in the figure.

It will be observed from Fig. 4-67 that the various lines slope downward to the right, as is to be expected, indicating a steady decrease in the intensities of the neutrons at all energy ranges, with increasing distance from the explosion. However, the really significant fact is that the lines are all approximately parallel. Hence, although the total number of neutrons received per square centimeter decreases with increasing distance, the proportions in the various energy ranges remain essentially the same throughout. This is the so-called equilibrium spectrum. Thus, one set of foil measurement should be sufficient to indicate the total neutron dose at any given location.

The conversion from the measured neutron flux to neutron dose may be accomplished with the following formula (Ref. 52):

$$D_R = [0.029N_t + 1.0(N_{Pu} - N_{NP}) + 2.5(N_{NP} - N_u) + 3.2(N_u - N_s) + 3.9(N_s)] \times 10^{-9} \quad (4\text{-}86)$$

where D_R = the tissue dose in rads; N_t = the thermal neutron flux; N_{Pu}, N_{NP}, N_u, and N_s = the number of neutrons per sq cm above the threshold for plutonium, neptunium, uranium, and sulphur, respectively.

Occasionally, there is no N_{NP} data available. If such is the case, the following formula should be used to compute the neutron dose:

$$D_R = [0.029N_t + 1.8(N_{Pu} - N_u) + 3.2(N_u - N_s) + 3.9(N_s)] \times 10^{-9}. \quad (4\text{-}87)$$

For many uses, the contribution of the thermal neutrons to the dose is negligible, compared with the fast neutron components, and can therefore be excluded from the calculation (Ref. 53). The basic conversion formula is then:

$$D_R = [1.0(N_{Pu} - N_{NP}) + 2.5(N_{NP} - N_u) + 3.2(N_u - N_s) + 3.9(N_s)] \times 10^{-9}. \quad (4\text{-}88)$$

Since a statistical error is involved in taking the difference of two large numbers, Eq. 4-86 is often written in the following form:

$$D_R = [0.029N_t + 1.0N_{Pu} + 1.5N_{NP} + 0.7(N_u + N_s)] \times 10^{-9}. \quad (4\text{-}89)$$

By combining terms, Eqs. 4-87 and 4-88 may be written in similar form.

4-8.4. (C) Initial Nuclear Radiation

4-8.4.1. (U) General

The ranges of the alpha and beta particles produced by a nuclear explosion are comparatively short and, even when the fireball touches the ground, these particles may be regarded as insignificant. The initial nuclear radiation may, therefore, be considered as consisting of only the neutrons and gamma rays emitted during the first minute after detonation. Both of these nuclear radiations, although different in character, can penetrate considerable distances through the air. Further, both gamma rays and neutrons are capable of producing harmful effects in living organisms. It is the injurious nature of these nuclear radiations, combined with their long range, that makes them such a significant hazard.

At distances not too close to ground zero, shielding from thermal radiation is a relatively simple matter. This is not true for the initial nuclear radiation. For example, at a distance of one mile from the point of burst of a one megaton bomb, the initial nuclear radiation would probably prove fatal to approximately fifty per cent of all humans, even if sheltered

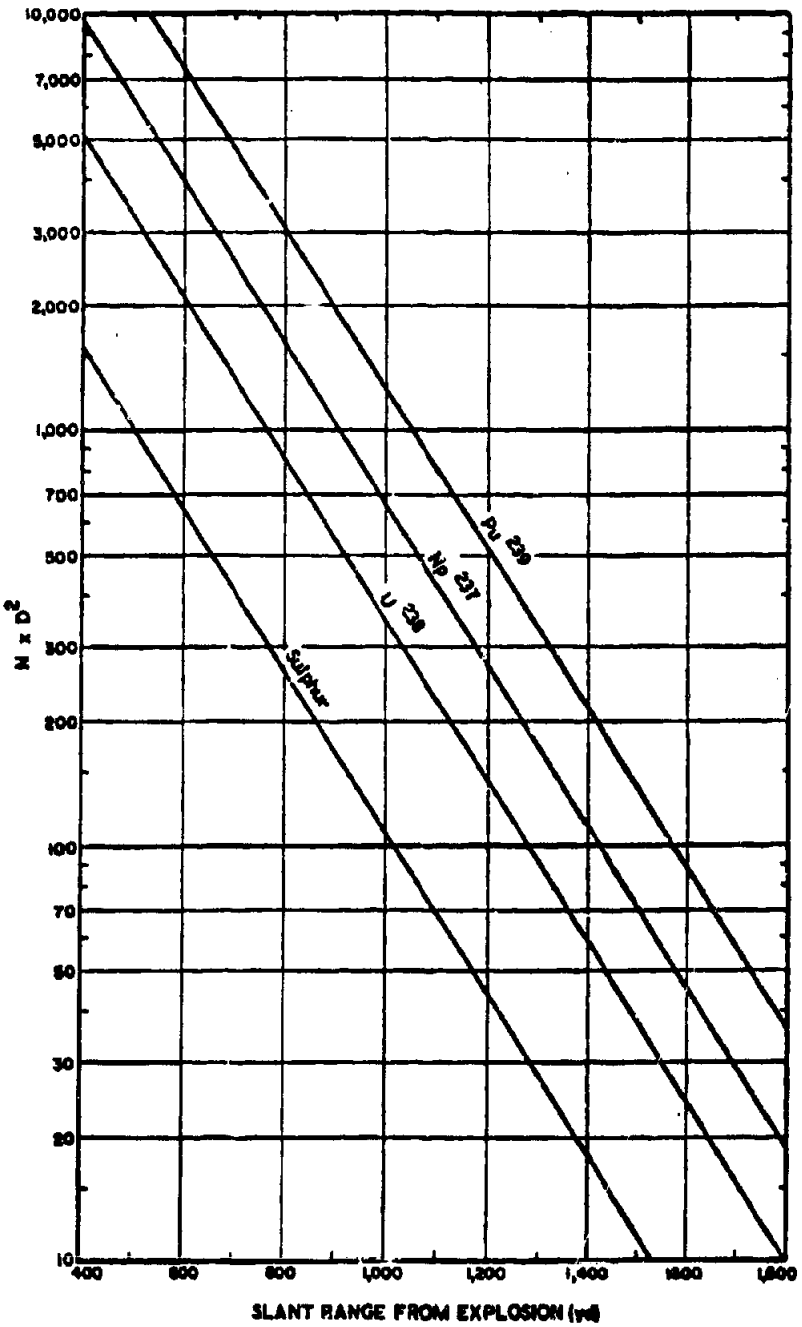

Figure 4–67. Typical Threshold Detector Results for Fast Neutrons in Air

by 24 inches of concrete. In contrast, a much lighter shield would provide complete protection against thermal radiation at the same distance.

The effective injury ranges of thermal and nuclear radiations may vary widely. For explosions of moderate and large energy yields, thermal radiation can have harmful consequences at appreciably greater distances than can the initial nuclear radiation. However, when the energy of the explosion is relatively small, such as a kiloton or less, the nuclear radiation has the greater effective range.

In discussing the characteristics of the initial nuclear radiation, it is preferable to consider the neutrons and gamma rays separately. Although their ultimate effects on living matter are much the same, the two kinds of nuclear radiations differ in many respects.

4-8.4.2. (U) Gamma Rays

In addition to the gamma rays which accompany the fission process, additional gamma rays are contributed to the initial nuclear radiation by other sources. A large proportion of the neutrons produced in the fission reaction are captured by nuclei of nonfissionable material. As a result of neutron capture, the nuclei are converted into a new species known as compound nuclei, which are in an excited (high energy) state. The excess energy is emitted almost instantaneously, as gamma radiation. This radiation is referred to as capture gamma rays, and the process is referred to as radiative capture.

The neutrons produced in the fission reaction can undergo radiative capture with the nuclei of atmospheric nitrogen, as well as with the nuclei of the materials present in the bomb. The interaction with nitrogen nuclei is of particular importance, because the gamma rays emitted from this reaction have very high energies and are, therefore, much less easily attenuated.

In addition to radiative capture by nonfissionable nuclei, radiative capture may occur with nuclei of radioactive nature, thereby providing a further source of gamma radiation. All the gamma rays produced by fission and by radiative capture with the bomb materials appear in less than a second after the instant of detonation. For this reason, the radiations are known as the prompt or instantaneous gamma rays.

The fission fragments, and many of their decay products, are radioactive isotopes which emit gamma radiations, the half-lives of which range from less than a millionth of a second to many years. Because the decay commences at the instant of fission, and because the rate of decay is greatest at the beginning, these radioisotopes make a significant contribution to the initial radiation. The gamma rays liberated by this means are referred to as delayed gamma rays.

The prompt gamma rays, and the portion of the delayed gamma rays which comprises the initial nuclear radiation, are nearly equal in quantity, but they are by no means equal portions of the initial radiation transmitted from the exploding bomb. The prompt gamma rays are produced almost entirely before the bomb has disintegrated. Therefore, they are largely absorbed by the dense bomb materials, and only a small portion are actually transmitted to the atmosphere. On the other hand, the delayed gamma rays are generated mostly after the bomb materials have vaporized and expanded into a tenuous gas. Thus these rays suffer little or no attenuation before emerging into the atmosphere. With respect to the total initial radiation received at a point some distance from ground zero, the delayed gamma rays and those rays produced by radiative capture with atmospheric nitrogen contribute about a hundred times as much radiation as do the prompt rays.

Still another possible source of gamma rays may be mentioned. If the nuclear explosion occurs near the earth's surface, the emitted neutrons can cause what is referred to as induced radioactivity in the materials present in the earth. This may be accompanied by radiations which will be part of the delayed gamma rays. Since induced radioactivity is primarily an aspect of residual nuclear radiation, it will be discussed more fully in the section under that heading (Par. 4-8.5.3.).

As is to be expected, the gamma ray exposure dose resulting from a nuclear explosion becomes less with increasing distances from the point of burst. The relationship of the radiation dose to the distance is dependent upon the same factors as those which influence the thermal radiation: first, the general decrease due to the dispersal of radiation over an increasingly larger area as it moves away from ground zero; and, second, to an attenuation factor due to absorption and scattering by the intervening atmosphere.

4–8.4.3. (U) *Neutrons*

Gamma rays are electromagnetic and similar to X-rays in character, while neutrons are nuclear particles of considerable mass. Both, however, affect the human body in the same manner. Only extremely large doses of these radiations can possibly be detected by the human senses. Even though neutron radiation represents only about 0.025 per cent of the total explosion energy, the long range penetration characteristics of the neutrons make them a significant hazard.

Essentially, all the neutrons accompanying the detonation of a nuclear weapon are released in the fission (or fusion) process. All the neutrons from a fusion reaction, and approximately 99 per cent of those from a fission reaction are produced within a millionth of a second of the initiation of the explosion. These are referred to as the prompt neutrons.

In addition, somewhat less than the remaining one per cent of the fission neutrons, called the delayed neutrons, are emitted subsequently. Even the delayed neutrons are produced in the first minute, therefore, they constitute part of the initial nuclear radiation. Some neutrons also result from the action of high energy gamma rays on the nuclear bomb materials. However, neutrons from this source make such a minor contribution that they can be readily ignored.

The prompt neutrons, although released in a very short time span, are somewhat delayed in escaping the environment of the exploding bomb. This delay is caused by numerous collisions of the neutrons with the nuclei present in the bomb residue, resulting in a complex, zig-zag path before the neutrons finally emerge. The delay in the escape of the prompt neutrons is, however, no more than a hundredth of a second.

Although neutrons travel at speeds less than that of light, they still travel at such speeds that at those distances from the explosion at which they represent a hazard nearly all of the neutrons are received by the target during the first second. Consequently, any evasive action initiated at the instant of detonation would have little effect in reducing the total neutron dose received.

The neutrons produced in the fission process are virtually all high kinetic-energy particles. These high energy neutrons are generally referred to as fast neutrons. The scattering collisions between the fast neutrons and the atomic nuclei result in a slowing down of the neutrons, and in a corresponding transfer of energy to the atomic nuclei. Therefore, the neutrons actually emerging from the bomb may have speeds ranging from very fast to very slow.

After these neutrons leave the environment of the bomb, they undergo more scattering collisions with the nuclei of elements present in the atmosphere. Because of the lower pressure and density, these collisions are less frequent in the atmosphere than in the bomb, but their effect is important. On the average, the fractional decrease in neutron energy is greater for relatively light nuclei (such as those of oxygen and nitrogen) than for the heavier nuclei. This results in an appreciable slowing of the neutrons during their passage through the atmosphere. Further, in some collisions, particularly with nitrogen nuclei, the neutrons can be captured and become non-effective. The probability of capture is greater with the slower neutrons.

It is important, in connection with the measurement of neutron radiation, to know something of the manner in which the distribution of neutron energies (speeds) varies with distance from ground zero. From a series of measurements made at the nuclear test explosions in Nevada in 1955, for each particular device tested it would appear that the energy

spectrum remains the same over the ranges which are of biological interest. This condition is referred to as an equilibrium spectrum. The total number of neutrons per unit area received at a given distance from ground zero decreases with increasing distance, but the proportion of neutrons of any particular energy range appears to be essentially the same, at all distances which are biologically of interest (Par. 4-8.3., preceding).

4-8.4.4. (C) *Effects of Altitude and Type of Burst*

a. Gamma Radiation

Air density is the controlling factor affecting attenuation of gamma radiation in the atmosphere; consequently, gamma radiation dose varies with air density. Fig. 4-68 illustrates gamma radiation dose, for different yields, in air density of 1.0 atmospheres. Relative air density is the ratio of the density under a given condition to the density at a temperature of 0° C and a pressure of 1,013 millibars (mb). (Standard pressure = 1 atmosphere = 1,013 mb = 14.7 psi = 29.9 inches of mercury.) Typical relative air densities at various altitudes are listed in Table 4-7, and information for obtaining relative air density in various situations is given in Figs. 4-70 and 4-71. The contribution of relative humidity to the atmospheric density is negligible as compared with those changes which are due to temperature and pressure. Therefo s effect is not included in the gamma dose igures.

A considerable fluctuation of air density occurs after the shock front from a nuclear detonation has passed a given point. The reduced air density in the negative phase allows a heavy dose of gamma rays to arrive at the point before the air density returns to its ambient value. This hydrodynamic enhancement varies with weapon yield, range, and height of burst. The enhancement factor increases with increasing yield and distance, within the ranges of interest. From a burst close to the surface of the earth, there will be both a direct shock wave and a reflected shock wave. As a result, the shock enhancement of the dose is greater for bursts on or near the surface than it is for higher altitude bursts, where the magnitude of the reflected shock wave is small. The height of burst above which the enhancement due to the reflected shock wave becomes negligible is taken as the lower limit of an air burst, for the initial gamma radiation effect. Although a precise determination of this height is difficult, or impossible, with existing data, a scaled height-of-burst of 1,500 $W^{1/3}$ feet has been estimated as the point at which the changeover occurs.

TABLE 4-7 (C). TYPICAL RELATIVE AIR DENSITIES (R), PRESSURE (P), AND TEMPERATURES (t), AT VARIOUS ALTITUDES (Ref. 21) (U)

Altitude (ft)	P (mb)	t (° C)	t (° F)	R
0	1,013	15	59	0.95
2,000	940	10	50	0.90
6,000	810	0	32	0.80
10,000	690	−5	23	0.70
14,000	580	−15	5	0.60
20,000	460	−25	−13	0.50
26,000	350	−35	−31	0.40
34,000	250	−52	−62	0.30
43,000	160	−55	−67	0.20
56,000	80	−55	−67	0.10

b. Surface Burst

Fig. 4-68 presents the initial gamma radiation dose in roentgens, versus slant range, for various yields of nuclear weapons detonated on the surface of the earth. These curves are presented for the relative air density of 1.0. Instructions for interpolating for values of relative air density other than that presented in Fig. 4-68 are given in Par. *e*, following.

The curves of Fig. 4-68 are strictly applicable only to a receiver in close proximity to the earth's surface, such as a man standing on the ground. The received gamma ray dose does not all arrive directly as a line-of-sight propogation from the source, owing to scatter by the atmosphere, and elevation of the man to significant distances away from the surface

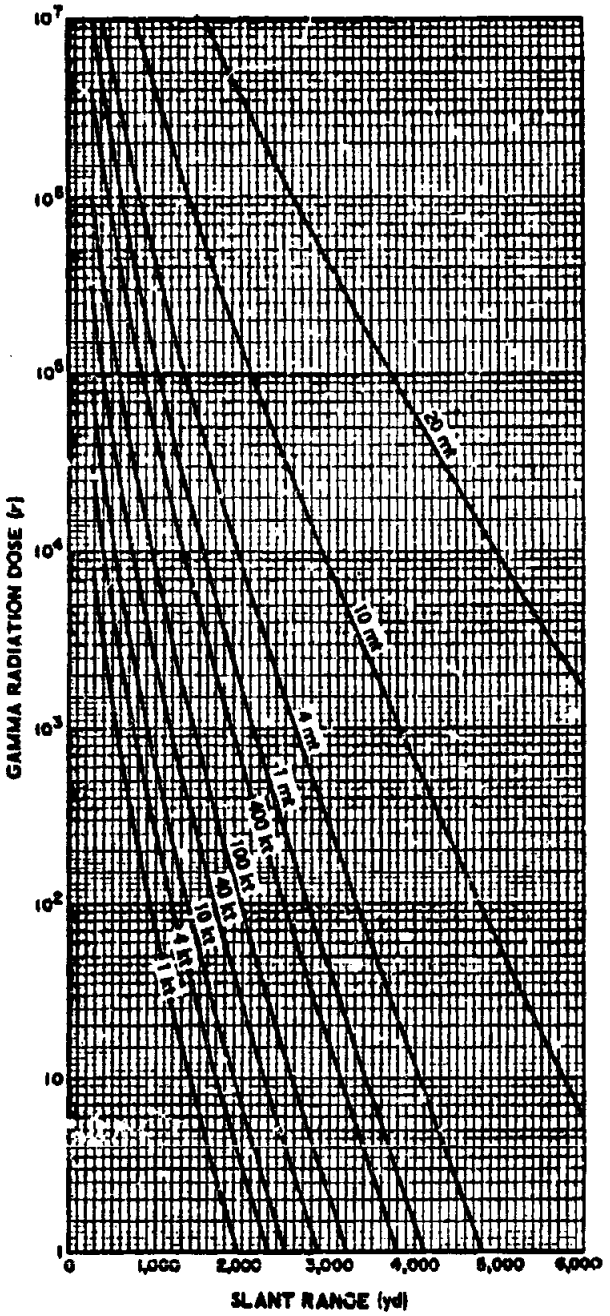

Figure 4–68 (C). Initial Gamma Radiation Dose vs Slant Range, Surface Burst and Surface Target, Relative Air Density 1.0, for 1–KT to 20–MT Yields (U)

permits a larger amount of radiation to reach him from all directions. correct for this effect, the dose shown in Fig. 4–68 should be multiplied by 1.3 when the receiver is three hundred feet or more above the surface, as would be the case for personnel in aircraft.

c. Burst in the Transition Zone

The shock enhancement of the gamma radiation dose from weapons detonated near the surface will be about the same as that for a surface burst. This condition holds through most of the transition zone, but changes rapidly to the air burst condition near the top of the zone. For this reason, the dose from weapons detonated in the transition zone should be obtained from the surface burst curves (Fig. 4–68) in the manner described.

d. Air Burst

As used in this paragraph, the term air burst refers to a burst above 1,500 $W^{1/3}$ feet. The shock enhancement factor of the initial gamma radiation from an air burst is about equal to that from a surface burst of half the yield. Thus, to find the initial gamma radiation dose received by a surface target from a particular air burst, the dose delivered during the surface burst of a weapon of half that yield must be found (which will have the same enhancement factor as the weapon of interest). Because the gamma flux emitted is proportional to yield, the dose delivered during the surface burst of the smaller weapon must then be doubled to obtain the dose delivered by the weapon of interest in air (Fig. 4–68). If the target is more than 300 feet above the surface of the earth, the dose thus calculated should once again be multiplied by 1.3.

e. Instructions for Using Figs. 4–68 and 4–69, Initial Gamma Radiation Dose for Surface Bursts, and Air Density Interpolation Sheet

(1) Description

The curves of Fig. 4–68 present the initial gamma radiation dose as a function of range for various yields. From these curves can be determined the slant range at which a weapon of given yield will produce a specified dose, or, conversely, the yield required to produce a given dose at a desired range.

The figure is directly applicable to bursts on the surface or in the transition zone (heights of burst up to 1,500 $W^{1/3}$ feet), surface targets, and conditions of standard relative air density. The relative air density to be used is an average between burst point and receiver. Methods for obtaining the proper value are detailed in Figs. 4–70 and 4–71, and for ready reference, atmospheric properties are listed in Tables 4–8 and 4–9.

Interpolation to obtain the initial gamma radiation dose for conditions of relative air density other than those presented in Fig. 4–68 may be accomplished in the following manner. Obtain the dose for the burst height and target location of interest, and for the two values of relative air density closest to the value of interest. Plot the doses, so obtained, opposite their respective relative air densities on the accompanying interpolation sheet (Fig. 4–69), and connect two points with a straight line. The desired dose is then read opposite the in-

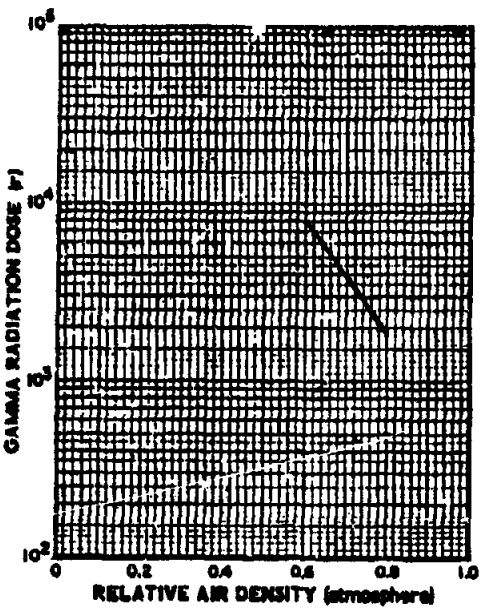

Figure 4–69 (C). Relative Air Density Interpolation Sheet (U)

tersection of this line with the value of relative air density in question. When applying this method of interpolation, it must be borne in mind that the doses must be obtained for the same condition of burst height and target location.

(2) Example 1

Given: A 10-MT surface burst, with relative air density $R=1.0$.

Find: The dose at a point on the ground 3,400 yards from the burst.

Solution: From the 10-MT curve of Fig. 4–68, the dose at 3,400 yards is 4,000 r.

(3) Example 2

Given: A gamma radiation dose of 1,900 r, when relative air density $R=0.8$; and a dose of 3,000 r, when $R=0.6$.

Find: The gamma radiation dose for relative air density $R=0.7$.

Solution: Plot the given doses on the relative air density interpolation sheet (Fig. 3–11), opposite $R=0.8$ and $R=0.6$, respectively. Connect these points by a straight line. At the intersection of this line, with the line representing $R=0.7$, the dose is read as 3,800 r.

(4) Reliability

The curves of Fig. 4–68 apply to surface burst weapons in the range of 1 KT to 20 MT.

TABLE 4–8. STANDARD ATMOSPHERIC CONDITIONS

Geometric Altitude (meters)	Temp. (° C.)	Pressure (millibars)	Density (kg/cu m)	Sound Velocity (cm/sec.)
0	15.0	1013.25	1.2250	34,029.1
304.79	13.02	977.17	1.1895	33,911.7
609.57	11.04	942.13	1.1549	33,794.4
914.36	9.05	908.13	1.1210	33,676.4
1,219.14	7.08	875.13	1.0879	33,557.9
1,523.9	5.09	843.11	1.0556	33,439.3
3,047.9	− 4.80	696.94	0.90474	32,839.2
4,571.8	−14.69	572.06	0.77103	32,228.0
6,095.7	−24.59	466.00	0.65310	31,605.3
7,619.6	−34.47	376.50	0.54951	30,970.7
9,143.6	−44.35	301.48	0.45903	30,322.7
10,667.5	−54.22	239.09	0.38044	29,661.3
12,191.4	−54.49	188.23	0.30266	29,506.8
13,715.3	−56.49	148.16	0.23823	29,506.8
15,239.3	−56.49	116.64	0.18755	29,506.8
18,287.1	−56.49	72.31	0.11627	29,506.8

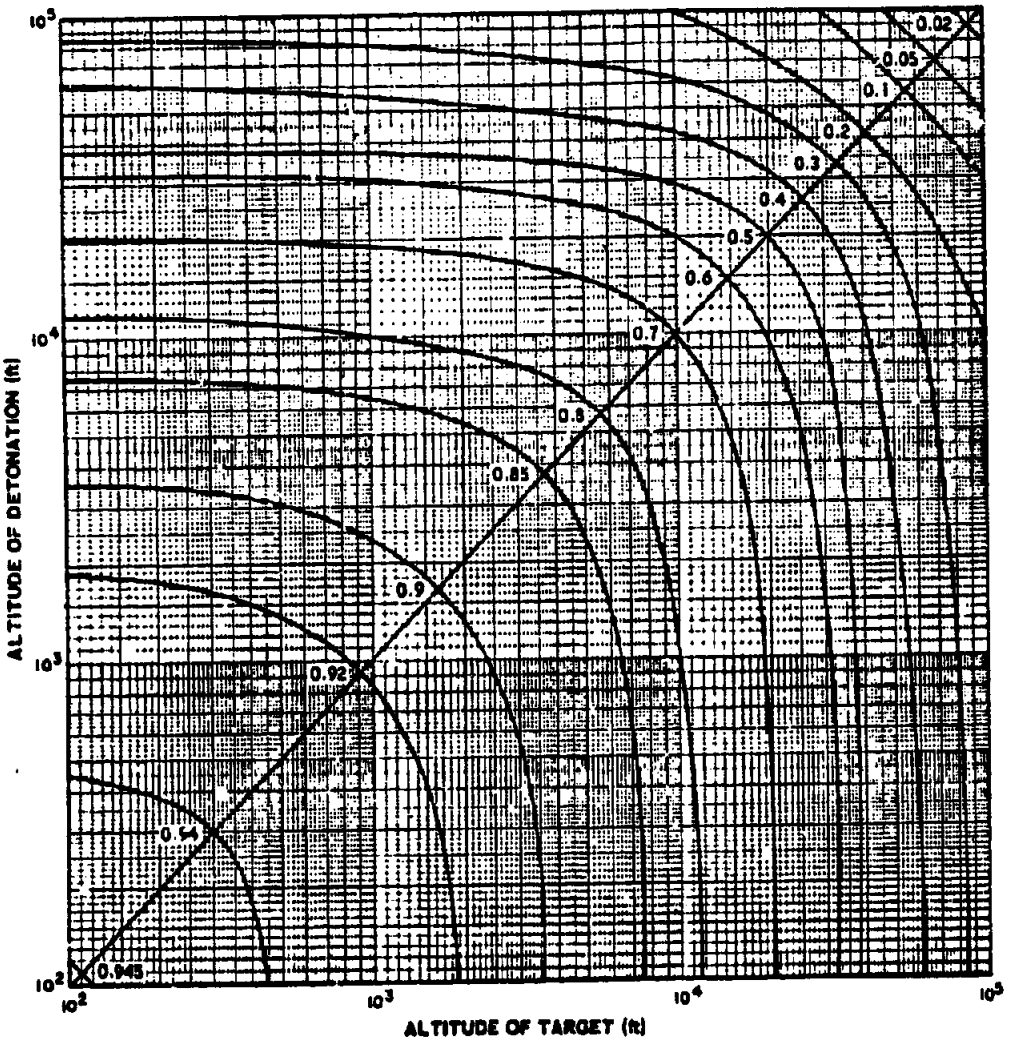

Figure 4–70 (C). Relative Air Density (Standard Atmosphere) (U)

For yields from 1 KT to 100 KT the doses obtained are reliable within a factor of 2. For yields greater than 100 KT and less than 1 MT, the doses obtained are reliable within a factor of 5. For yields above 1 MT the doses obtained are reliable within a factor of 10. Extrapolation to yields greater than 20 MT for surface bursts is not recommended. The range obtained for a given dose will be reliable to within 10 per cent for yields from 1 KT to 100 KT, 20 per cent for yields greater than 100 KT and less than 1 MT, and 30 per cent for yields greater than 1 MT.

j. Underground Burst

The initial gamma radiation dose from an underground nuclear explosion at a depth of 17 feet is given in Fig. 4–72 for a 1–KT detonation. For yields between 0.2 and 7.5 KT, and depths between 12 and 22 feet, the dose is proportional to the yield. Extrapolation to

higher yields is unreliable. For detonations at greater depths, the initial gamma dose is less than that indicated in Fig. 4–72. The magnitude of this reduction with increased depth is not known. The gamma radiation from an underwater burst is believed to be similar to that from an underground shot, though it may well be somewhat greater. The underground detonation curves of Fig. 4–72 may be used to estimate initial gamma radiation dose as a function of distance, for underwater bursts.

g. Instructions for Using Fig. 4–72, Initial Gamma Radiation Dose for an Underground Burst

(1) Description

The curves of Fig. 4–72 present the initial gamma radiation dose as a function of distance for several air densities, for a 1–KT detonation 17 feet underground. These curves may also be used for underwater bursts.

(2) Scaling Procedure

For other yields, at about the same depth and the same relative air density, the dose at a given range is proportional to weapon yield. For relative air density see Fig. 4–70.

(3) Example

Given: A 5–KT burst 15 feet underground, with relative air density $R=0.9$.

Find: The distance at which 450 r initial gamma dose is received.

Solution: The quotient $\frac{450}{5}=90$ r dose for 1 KT.

From the curve for $R=0.9$, the range at which 90 r is received is 1,100 yards.

(4) Reliability

The curves of Fig. 4–72 apply to weapons in the yield range from 0.2 KT to 7.5 KT, and for actual depths of burst from 12 to 22 feet. Used within the prescribed limits, results are good within a factor of two, provided the soil at the point of burst is not too different from the soil at the Nevada Test Site. The error that would be introduced by a very different soil type is similar in origin, but not necessarily in magnitude, to the error that would be expected from a distinctly different burial depth. At the present time, the effect of soil type cannot be estimated. Extrapolation to other yields is unreliable.

h. Neutron Radiation

The neutron radiation dose delivered as a result of a nuclear detonation varies widely with different weapon configurations. Fig. 4–73 presents the neutron radiation dose versus slant range in various air densities for a 1–KT detonation. Fig. 4–74 presents the prompt neutron dose versus slant range, for three different weapon yields, for surface bursts in relative air density of 1.1. The curves of Figs. 4–73 and 4–74 may be considered as representative of fission weapons. From these curves the slant

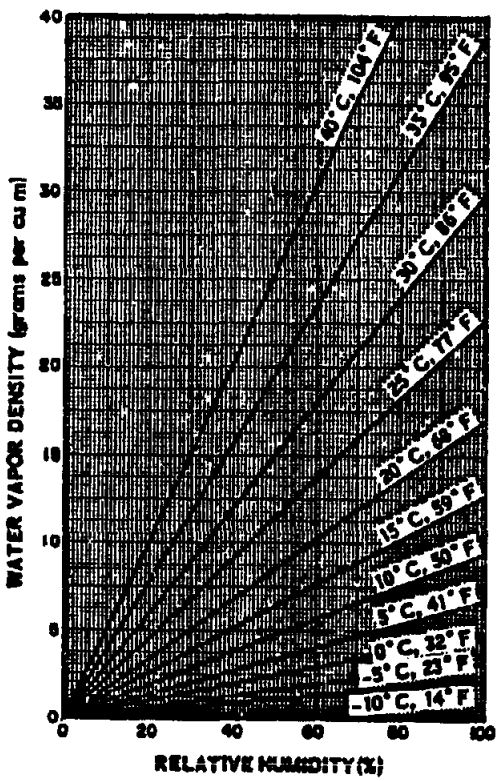

Figure 4–71. Atmospheric Water Vapor Density vs Relative Humidity for Various Air Temperatures

TABLE 4–9. AVERAGE ATMOSPHERE

Geometric Altitude (meters)	Temp. (° C.)	Pressure (millibars)	Density (kg/cu m)	Sound Velocity (m/sec.)	Mean Free Path (m)
0	+ 15.0	1013.25	1.2250	340.29	6.6317×10^{-8}
10,000	− 49.90	265.00	4.135×10^{-1}	299.53	1.9646×10^{-7}
20,000	− 56.49	55.293	8.891×10^{-2}	295.07	9.1374×10^{-7}
30,000	− 41.92	11.855	1.786×10^{-2}	304.83	4.5484×10^{-6}
40,000	− 12.25	2.9977	4.003×10^{-3}	323.80	2.0296×10^{-5}
50,000	+ 9.50	8.786×10^{-4}	1.082×10^{-3}	337.03	7.5023×10^{-5}
60,000	− 19.94	2.531×10^{-4}	3.492×10^{-4}	321.71	2.3266×10^{-4}
70,000	− 53.82	6.321×10^{-5}	1.004×10^{-4}	296.88	8.0912×10^{-4}
80,000	− 76.29	1.224×10^{-5}	2.165×10^{-5}	281.26	3.752×10^{-3}
90,000	− 76.29	2.253×10^{-6}	3.995×10^{-6}	281.26	2.033×10^{-2}
100,000	− 66.15	4.629×10^{-7}	7.123×10^{-7}	281.26	1.043×10^{-1}
110,000	− 45.06	1.187×10^{-7}	1.589×10^{-7}	281.26	4.481×10^{-1}
120,000	− 40.46	3.610×10^{-8}	1.216×10^{-7}	281.26	1.629
130,000	+ 11.74	1.256×10^{-8}	1.299×10^{-8}	281.26	5.291
140,000	+ 89.53	5.336×10^{-9}	4.296×10^{-9}	281.26	1.585×10^{-1}
150,000	+ 166.82	2.698×10^{-9}	1.799×10^{-9}	281.26	3.803×10^{-1}
160,000	+ 243.61	1.531×10^{-9}	8.554×10^{-10}	281.26	7.872×10^{-1}
225,000	+ 494.59	1.308×10^{-9}	4.308×10^{-11}	281.26	1.368×10^{-3}
500,000	+1120.73	8.541×10^{-10}	1.197×10^{-13}	281.26	3.807×10^{-4}

range can be determined at which a weapon of given yield will produce a specific dose. Conversely, the yield required to produce a given dose at a given range also can be found. The doses predicted from Fig. 4–73 might be high by a factor of ten for weapons containing large quantities of neutron attenuating material. A better estimate of neutron dose for many specific weapons may be obtained from the Nuclear Radiation Handbook (AFSWP–1100), published under a SECRET classification (Ref. 55).

Fig. 4–75 presents the neutron radiation dose versus slant range in various air densities for a 1–MT detonation of a thermonuclear weapon, and may be considered as representative of fusion weapons. The curves of Figs. 4–73 and 4–75 may be applied to all bursts except subsurface. Neutron radiation is not expected to be significant for subsurface bursts.

Adjustment factors for a receiver not on a land surface are as follows. For a receiver at water surface (or within ten feet), use the factor of 0.9 with the land surface value. For an airborne receiver, 300 feet or more above land surface, use the factor of 1.5.

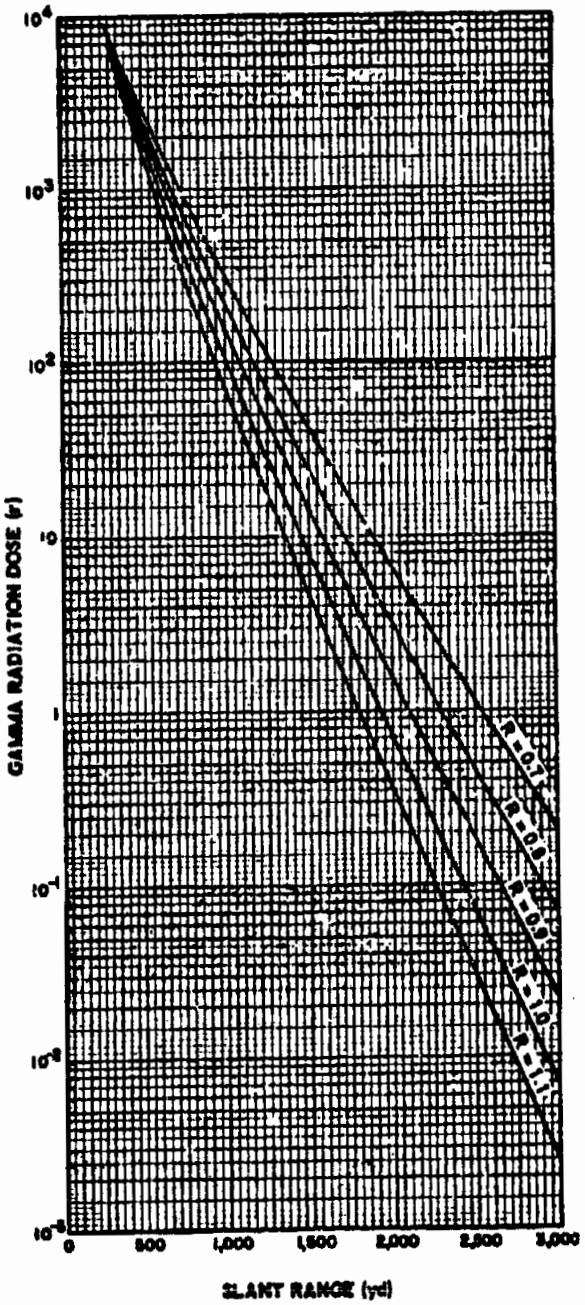

Figure 4–72 (C). Initial Gamma Radiation Dose vs Slant Range, 1–KT Underground Burst, Depth 17 Feet, for Various Relative Air Densities (U)

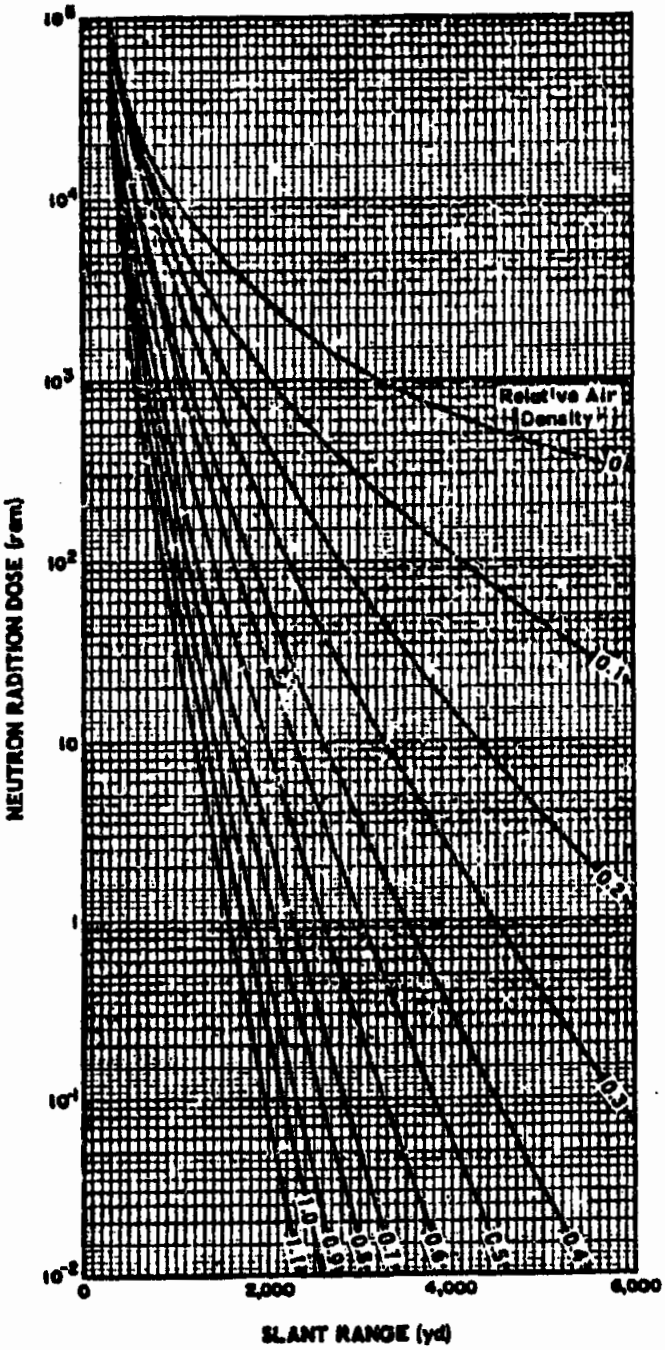

Figure 4–73 (C). Neutron Radiation Dose vs Slant Range for Various Relative Air Densities, 1–KT Air or Surface Bursts (Fission Weapons) (U)

i. Instructions for Using Figs. 4–73 and 4–74, Neutron Radiation Dose from Fission Weapons

(1) Scaling Procedure

At a given range and relative air density, the neutron dose is proportional to weapon yield. For relative air density, see Fig. 4–70.

(2) Example

Given: A 50-KT burst at 2,000 feet above the surface, where the pressure at the burst point is 935 mb, the pressure at the surface is 1013 mb.

Find: The maximum dose at a slant range of 1,750 yards.

Solution: From Fig. 4–70, the relative air density is 0.77. From Fig. 4–73, for $R=0.8$, the dose for 1 KT at 1,750 yards is 6 rem. Therefore the maximum dose for 50 KT at 1,750 yards and $R=0.8$ is $6\times50=300$ rem.

(3) Reliability

Depending upon weapon design, the dose values in Figs. 4–73 and 4–74 are estimated to be low by as much as a factor of 4, for certain experimental devices, and can be high by a factor of 10 for other weapons.

j. Instructions for Using Fig. 4–75, Neutron Radiation Dose from Fusion Weapons

(1) Scaling Procedure

At a given range and relative air density the neutron dose is proportional to the yield of the weapon. See Fig. 4–70 for determination of relative air density.

(2) Example

Given: A 2-MT burst at an altitude of 2,000 feet above the surface, where the pressure at the burst point is 800 mb, and the pressure at the surface is 860 mb.

Find: The slant range at which a minimum neutron dose of 500 rem would be received by a surface target.

Solution: From Fig. 4–70 the relative air density is 0.77. The corresponding

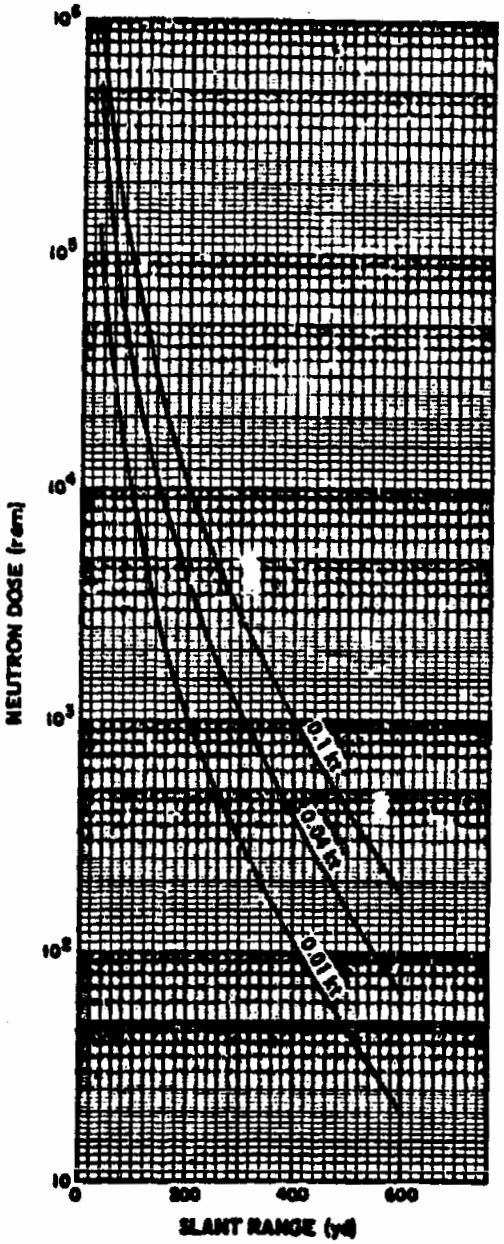

Figure 4–74 (C). Prompt Neutron Dose vs Slant Range, Surface Burst and Surface Target, Relative Air Density 1.1 (U)

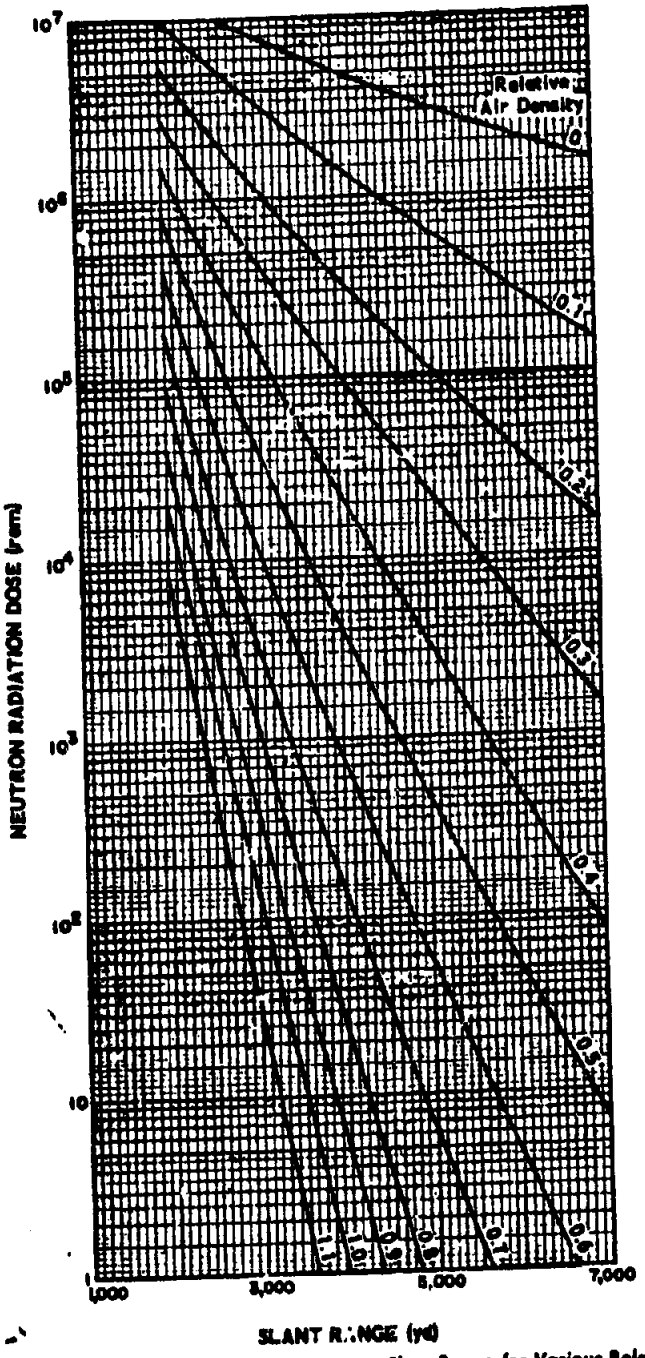

Figure 4–75 (C). Neutron Radiation Dose vs Slant Range for Various Relative Air Densities, Air or Surface Burst (Fusion Weapons) (U)

With respect to the rate of speed of neutron travel, any evasive action taken after the instant of detonation would have little effect. For, while it is true that neutrons travel with speeds less than that of light, at such distances from the explosion that they represent a hazard, nearly all of the neutrons are received within a tenth of a second. This rapid rate of delivery exists for neutron radiation regardless of yield.

4-8.4.6. (U) Shielding

a. General

The basic data necessary for accurate consideration of shielding problems include: the variation of dose with distance from the point of detonation; the angular distribution of neutrons and gamma radiation; and quantitative information concerning the spectral distribution of fast neutrons. Empirical data and formulae have been collected and presented in the preceding sections of this chapter to supply dose-distance relationships. The problem of providing sufficient information concerning the angular distribution and radiation spectrum is a more difficult one.

Until very recently, quantitative information in these areas are practically non-existant. In January 1960, the Los Alamos Scientific Laboratory published the results of a Monte Carlo calculation of the distribution of neutrons, which give neutron fluxes and spectra as a function of distance and time (Ref. 52). The Nuclear Products Division of the Lockheed Aircraft Corporation, in conjunction with the Aberdeen Proving Grounds Ballistic Research Laboratories, is currently engaged in a study of nuclear weapons radiation doses in armored vehicles, utilizing the Monte Carlo technique (Ref. 54).

Richie and Hurst (Ref. 53) have contributed much information on the angular distribution of nuclear radiation, and have applied this data to studies of light buildings such as those present at Hiroshima and Nagasaki.

The utilization of these techniques involves elaborate computer programs, and a specialized knowledge of the subject. Therefore, the discussion of shielding which follows will make certain basic assumptions, which will allow the development of approximate methods of computation on a more general level. Detail information on the more advanced techniques may be found in Refs. 52, 53, and 54.

b. Gamma Ray Shielding

(1) General Considerations

Gamma rays are attenuated to some extent in the course of their passage through any material. As an approximation rule, it may be said that the decrease in the radiation intensity is dependent upon the mass of material that intervenes between the source of the rays and the point of observation. Therefore, it would require a greater thickness of low density material than of high density material to provide equivalent attenuation. Actually, it is not possible to attenuate gamma rays completely, but if a sufficient thickness of matter is interposed between the radiation source and the target, the exposure dose can be reduced to negligible proportions.

In a vacuum, gamma rays travel in a straight line with the speed of light. However, in atmosphere, gamma radiation is scattered, particularly by oxygen and nitrogen particles. As a result, the gamma rays arrive at the target from all directions. Most of the dose received will come from the direction of the explosion, but a considerable amount of scattered radiation will arrive from other directions. A person taking shelter behind an embankment or a hill will be partially shielded from the direct radiation, but will still be exposed to scattered gamma rays. Adequate protection can be obtained only if the shelter completely surrounds the individual, so that both direct and scattered radiations can be attenuated.

The shielding effectiveness of a given material in decreasing the radiation intensity can be conveniently represented by a quantity referred to as the half-value layer thickness. This is the thickness of the particular material which absorbs half the gamma radiation falling upon it. Each succeeding half-value layer thickness decreases the radiation dose by half, as follows: one half-value layer thickness decreases the radiation dose to half of its original value; two half-value layers reduce it to one-quarter; three to one-eighth; four to one-sixteenth, and so on.

dose for 1 MT is $\frac{500}{2}$=250 rem.

From Fig. 4–75 for R=0.8 and a dose of 250 rem, read slant range =3,400 yards.

(3) Reliability

Reliability is very poor, due to almost complete lack of data and sensitivity of neutron flux to weapon design. Actual dose may be within a factor of 10 of dose computed using Fig. 4–75. Extrapolation of curves to slant ranges less than 2,000 yards is not recommended.

4–8.4.5. (C) *Delivery Rate*

In order to determine the amount of radiation which could be avoided by taking shelter within a second or two of observing the luminous flash of the explosion, it is necessary to know the rate at which the radiations are delivered. This differs for the gamma rays and the neutrons.

The rate of delivery of the initial gamma rays is dependent upon a number of factors, the most significant of which are the energy yield of the explosion and the distance from the point of burst. The percentage of the total dose received at various times for two different cases is shown in Fig. 4–76. One curve represents the rate of delivery at a distance of 1,000 yards from a 20–KT air burst, and the other at 2,500 yards from a 5–MT explosion. As shown in the figure, about 65 per cent of the total initial gamma radiation dose is delivered in the first second, in the first case, and about 4 per cent in the second case.

It is conceivable, therefore, that if some shelter could be obtained within the first second (e.g., by *falling prone behind* a substantial object) in certain circumstances it might make the difference between life and death. The curves in Fig. 4–76 also show that for a bomb of high energy the gamma radiation may be emitted more slowly than for one of relatively low yield. Avoidance of part of the initial gamma ray dose would appear to be more practical for explosions of higher energy yields.

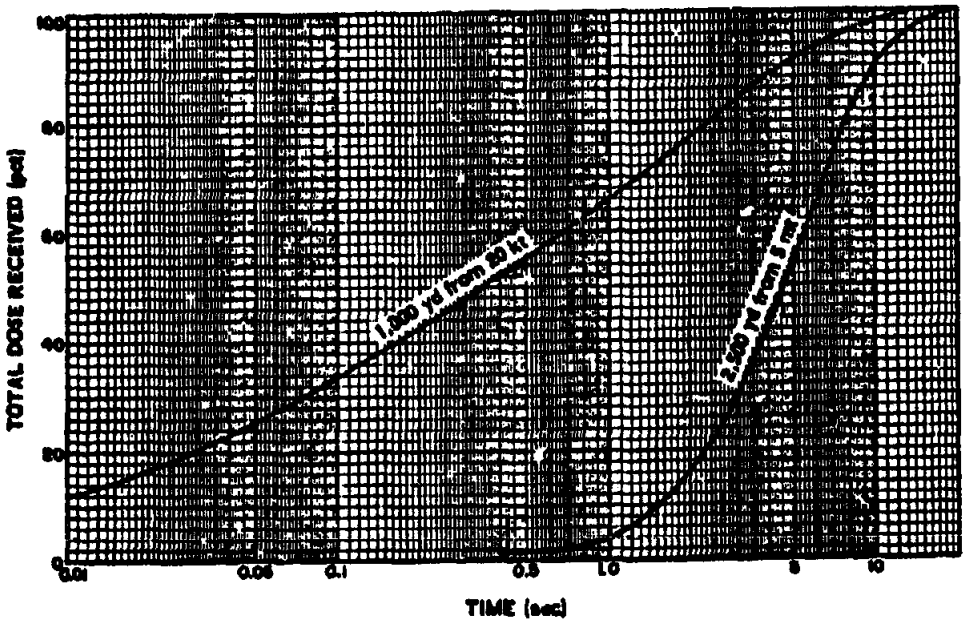

Figure 4–76 (C). Percentage of Total Dose of Initial Gamma Radiation vs Time After Detonation (U)

The same general rule can be applied to any specified fraction. For example, a one-tenth value layer would reduce the radiation by a factor of 10; two one-tenth value layers by a factor of 10^2 (100), etc.

Strictly speaking, the half-value layer thickness concept should be applied only to shielding against gamma radiation meeting the following conditions: all of the radiation must be of the same energy range, because different energy gamma rays are attenuated at different rates; and the radiation must be mono-directional, or the shielding material must be relatively thin. Although none of these conditions actually apply in shielding against gamma rays from a nuclear explosion (the rays cover wide energy ranges, are spread out over a considerable area, and thick shields are necessary), adjusted half-value layer thicknesses can serve a useful, practical purpose, by providing a rough approximation of the degree of attenuation that can be achieved by means of a particular amount of shielding.

The chief materials likely to be available for shielding against the initial gamma radiations are steel, concrete, earth, water, and wood. The approximate half-value layer thicknesses for these substances are given in Table 4–10. With fair accuracy, the data in the table are applicable to thick shields, and to the energy ranges that are most significant in the initial gamma radiation. In general, as previously stated, the more dense the material, the more effective an attenuating substance it makes.

TABLE 4–10. APPROXIMATE HALF-VALUE LAYER THICKNESSES OF MATERIALS FOR INITIAL GAMMA RADIATION

Material	Density (lb/cu ft)	Half-Value Thickness (in.)	Product
Steel	490	1.82	892
Concrete	144	6.0	864
Earth	100	7.5	750
Water	62.4	13	811
Wood	34	23	782

From the results in the last column of Table 4–10, it is seen that the product of the density and the half-value thickness for the five materials is roughly the same. Consequently, if the half-value thickness of a substance is not known, but the density is, a fair estimate can be made of its effectiveness. This is accomplished by assuming that the product of the half-value layer thickness, and the density in pounds per cubic feet, is about 800 $\frac{\text{pound inches}}{\text{cu ft}}$.

The attenuation factor of a given shield can be readily calculated from the number of half-value thicknesses, together with the data in Table 4–10. For example, a 30-inch thick shield of earth will contain $\frac{30 \text{ inches}}{7\frac{1}{2} \text{ inches}} = 4.0$ half-value thicknesses. The attenuation factor is then $2^4 = 16$, so that the gamma radiation dose will have been decreased to 1/16th of that which would have been received without the shield.

The calculations may be simplified by the use of Fig. 4–77, in which the attenuation factors are plotted for various thicknesses of lead, iron, concrete, earth, water, and wood. Suppose that at a given location, the gamma ray exposure without shielding is 500 roentgens. The thickness of a material required to reduce the dose to 10 roentgens would be found as follows: The required attenuation factor is $\frac{500}{10} = 50$. If the material chosen is concrete, it can be seen from Fig. 4–77, that the attenuation factor of 50 can be obtained with 29 inches of concrete.

The foregoing discussion of initial gamma radiation shielding has been somewhat general in nature. Enough information has been provided to enable the user to make reasonable approximations of the various materials and thicknesses required to successfully attenuate the initial gamma radiations. The following paragraph will deal with some of the more technical aspects of gamma radiation and absorption.

(2) Theoretical Considerations

If a narrow (collimated) beam of gamma rays of a specific energy having an intensity of I_o falls upon a thickness, x, of a given material,

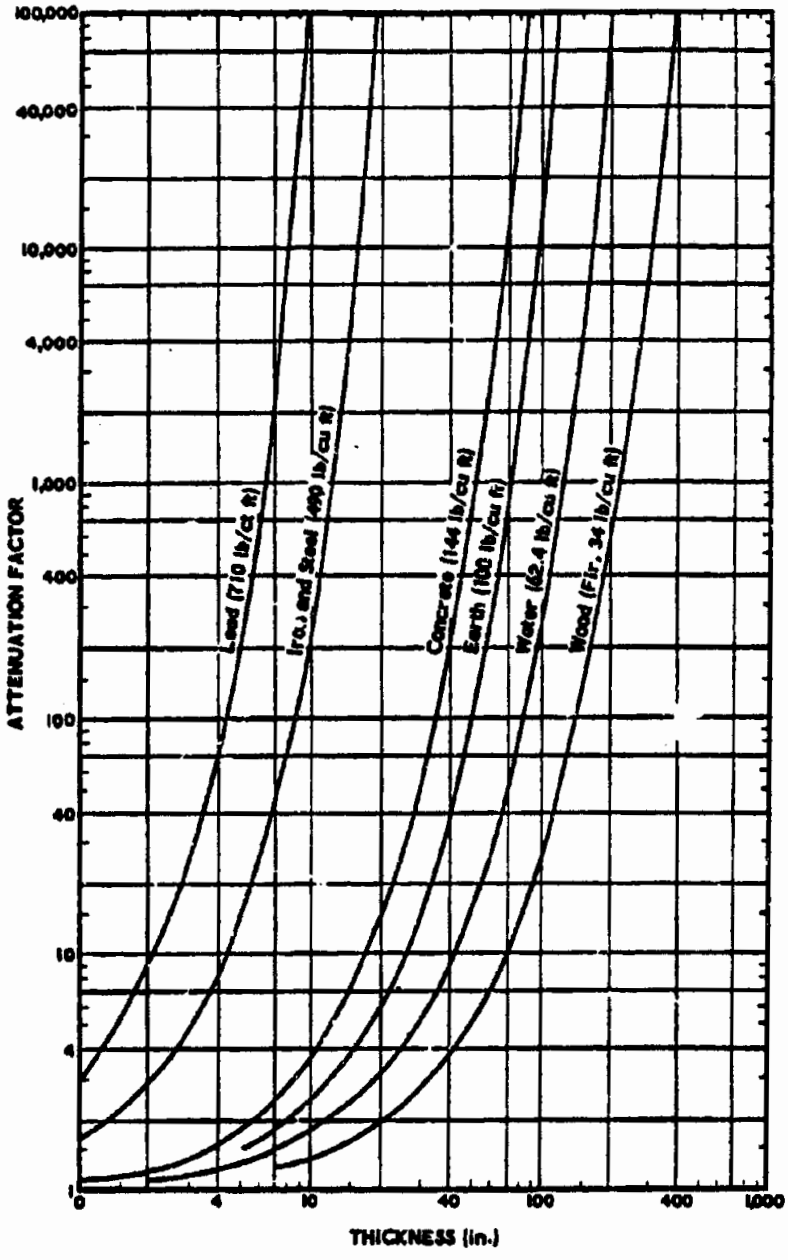

Figure 4–77. Attenuation of Initial Gamma Radiation

the intensity, I, of the rays which emerge can be represented by the equation,

$$I = I_0 e^{-\mu_a x} \qquad (4\text{–}90)$$

where μ_a is referred to as the linear absorption coefficient. The distance, x, is usually expressed in centimeters, so that the corresponding unit for μ_a is the reciprocal centimeter (cm^{-1}). The radiation intensity is defined as the rate at which the energy flows past a unit area at a given location. It is essentially proportional to the exposure dose rate. The value of μ_a, for any material and for gamma rays of a specific energy, is proportional to the sum of the Compton, photoelectric, and pair production effects (Par. 4–8.3.1, preceding). It can be seen from Eq. 4–90 that, for a given thickness, x, of material, the intensity, I, of the emerging gamma rays will be less the larger the value of μ_a. In other words, the linear absorption coefficient is a measure of the shielding ability of a definite thickness of any material.

The value of μ_a under any given conditions can be obtained with the aid of Eq. 4–90, by determining the gamma ray intensity before and after passage through a known thickness of a material. Some of the data obtained in this manner, for gamma rays ranging in energy from 0.5 Mev to 10 Mev, are recorded in Table 4–11. The values given for concrete apply to the common mixture having a density of 144 pounds per cubic foot. For special, heavy concretes, containing iron, iron oxide, or barytes, the coefficients are increased roughly in proportion to the density.

By suitable measurements and theoretical calculations, it is possible to determine the separate contributions of the Compton Effect (μ_c), of the photoelectric effect (μ_{pe}), and of pair production (μ_{pp}) to the total linear absorption coefficient. The results for lead, a typical heavy element, are presented in Fig. 4–78, and those for air, a mixture of light elements, in Fig. 4–79. It is seen that for low gamma-ray energies, the linear absorption coefficient decreases with increasing energy. This phenomenon is due to the Compton and photoelectric effects (Par. 4–8.3.1, preceding). At energies in excess of 1.02 Mev, pair production begins to make an increasingly significant contribution. Therefore, at sufficiently high energies, the absorption coefficient begins to increase after first passing through a minimum. This is apparent in Fig. 4–78. For elements of lower atomic weight, the increase does not commence until exceptionally high energies are obtained; e.g., about 17 Mev for concrete and 50 Mev for water.

The fact that the absorption decreases as the gamma ray energy increases, and may pass through a minimum, has an important bearing on the shielding problem. For example, a shield designed to attenuate gamma rays of 1 Mev energy will be much less effective for

TABLE 4–11. LINEAR ABSORPTION COEFFICIENTS FOR GAMMA RAYS

Gamma Ray Energy (Mev)	Linear Absorption Coefficient (μ_a) in cm^{-1}				
	Air	Water	Concrete	Iron	Lead
0.5	1.11×10^{-4}	0.097	0.22	0.63	1.7
1.0	0.81×10^{-4}	0.071	0.15	0.47	0.80
2.0	0.57×10^{-4}	0.049	0.11	0.33	0.52
3.0	0.46×10^{-4}	0.040	0.088	0.28	0.47
4.0	0.41×10^{-4}	0.034	0.078	0.26	0.47
5.0	0.35×10^{-4}	0.030	0.071	0.25	0.50
10	0.26×10^{-4}	0.022	0.060	0.23	0.61

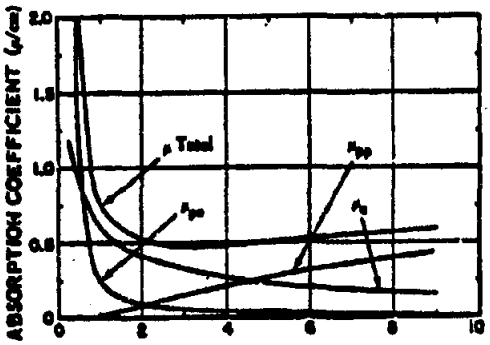

Figure 4–78. Absorption Coefficient of Lead for Gamma Radiation

radiations of 10 Mev energy, because of the decrease in the value of the absorption coefficient. This is true regardless of the material of which the shield is composed.

The initial gamma rays from a nuclear explosion cover a wide range of energies, up to 10 Mev or more. For the purpose of making approximate shielding estimates, an empirical value of 4.5 Mev appears to give satisfactory results. The half-value layer thicknesses presented in Table 4–10 are based on gamma radiation of this energy.

As a rough approximation, the linear absorption coefficient for gamma rays of a particular energy has been found to be proportional to the density of the shield material; i.e., the linear absorption coefficient divided by the density is approximately the same for all substances in any specified energy range. This quotient is generally referred to as the mass absorption coefficient. This is especially true for elements of low and medium atomic weights, where the Compton effect makes the major contribution to the absorption coefficient. For the initial gamma rays, the effective mass absorption coefficient has a value close to 0.021 for water, wood, concrete, earth, and iron; the densities being expressed in grams per cubic centimeter. The value 0.021 has included in it an adjustment to allow for the conditions applying to thick shields, discussed subsequently.

Using the symbol ρ for the density of the shield material, Eq. 4–90 can then be rewritten in the form

$$\frac{I_0}{I} = e^{\mu x \rho} = e^{(\mu/\rho)\rho x} \qquad (4\text{–}91)$$

when $\frac{I_0}{I}$, as previously defined, is the attenuation factor of the shield of thickness x cm and density ρ gm per cubic cm. The factor μ_a/ρ is, also by definition, the mass absorption factor and, for initial gamma rays, is taken to be 0.021. Then:

$$\text{Attenuation Factor} = e^{0.021\rho x} \qquad (4\text{–}92)$$

and the attenuation factor of a thickness of x cm of any material of known density can be calculated to a good approximation, provided the material consists of elements of low or moderate atomic weight.

A half-value layer, as previously defined, is the thickness of any material which will attenuate specified-energy gamma radiation by a factor of 2. Thus setting $\frac{I_0}{I}$ in Eq. 4–91 equal to 2, it follows that

$$2 = e^{\mu_a x_{1/2}} \qquad (4\text{–}93)$$

where $x_{1/2}$ is the half-value layer thickness in centimeters. From this equation, it is readily shown

$$\mu_a x_{1/2} = \text{Log}_e 2 = 0.693$$

and

$$x_{1/2} = \frac{0.693}{\mu_a}. \qquad (4\text{–}94)$$

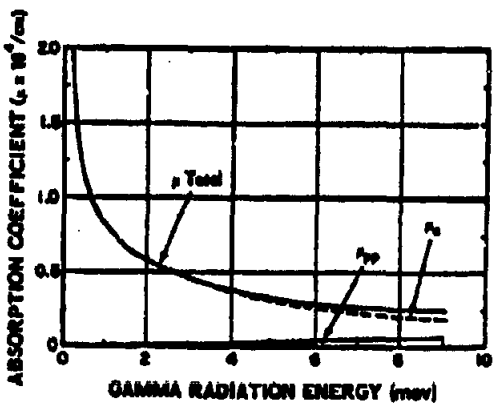

Figure 4–79. Absorption Coefficient of Air for Gamma Radiation

The half-value thickness is, therefore, inversely proportional to the linear absorption coefficient of the given material and the specified-energy rays, and is independent of the radiation intensity or dose.

If the mass absorption coefficient μ_a/ρ is taken to be a constant (0.021) for gamma rays in the initial nuclear radiation, then from Eq. 4–94.

$$x_{1/2}=\frac{0.693}{\mu_a(\rho/\rho)}\quad\frac{0.693}{0.021\rho}=\frac{33}{\rho}\text{ cm.}\qquad(4\text{–}95)$$

For a tenth-value layer thickness,

$$10=e^{\mu_a x_{1/10}}$$

$$\mu_a x_{1/10}=\text{Log}_e\,10$$

$$x_{1/10}=\frac{2.30}{\mu_a}=\frac{2.30}{\mu_a(\rho/\rho)}=\frac{2.30}{0.021\rho}$$

and

$$x_{1/10}=\frac{110}{\rho}\text{ cm.}\qquad(4\text{–}96)$$

Eq. 4–90 is strictly applicable only to cases in which the photons scattered in Compton interactions may be regarded as essentially removed from the gamma ray beam. This situation holds fairly well for narrow beams, or for shields of moderate thickness, but it fails for beams with a wide field or for thick shields. In the latter case, the photon may be scattered several times before emerging from the shield. For broad radiation beams and thick shields, such as are of interest with regard to shielding from nuclear explosions, the intensity, I, of the emerging radiation is larger than that given by Eq. 4–90. Allowance for the multiple scattering of the radiation is made by the inclusion of a build-up factor. This factor is represented by the symbol $B(x)$, and the value of $B(x)$ depends upon the thickness of the shield. Eq. 4–90 is now written as

$$I=I_0B(x)e^{-\mu_a x}\qquad(4\text{–}97)$$

The magnitude of the build-up factor has been calculated for a number of elements, from theoretical considerations of the scattering of photons by electrons. The build-up factors for monoenergetic gamma rays having energies of 4 Mev and 1 Mev, respectively, are given in Figs. 4–80 and 4–81 as functions of the atomic number of the absorbing material, for shields of various thicknesses, expressed in terms of x. The build-up factors in Fig. 4–80 can be applied to the absorption of the initial nuclear radiation, and those in Fig. 4–81 to the residual nuclear radiation (Par. 4–8.5., following).

From the preceding discussion, it can be seen that the half-value and tenth-value layer concepts apply only to monoenergetic radiations and thin shields, for which the build-up factor is unity. However, as already discussed, by taking the mass absorption coefficient for the initial gamma radiation to be 0.021, an approximate empirical correction has been made for both the polyenergetic nature of the gamma-rays and the build-up factors due to multiple scattering of the photons. Consequently, Eqs. 4–95 and 4–96 are reasonably accurate when used to calculate the initial gamma attenuation. It may be noted that the attenuation factors in Fig. 4–78 also include allowances for multiple scattering in thick shields. Figs. 4–81 and 4–82 may be used in conjunction with Eq. 4–97 if more accurate results are desired.

c. Neutron Shielding

Neutron shielding is a completely different problem than shielding against gamma rays. As far as gamma rays are concerned, shielding is a matter of interposing sufficient matter between the radiation source and the target. Such is not the case with neutron shielding. An iron shield, for example, will attentuate bomb neutrons to an extent, but it is far less effective

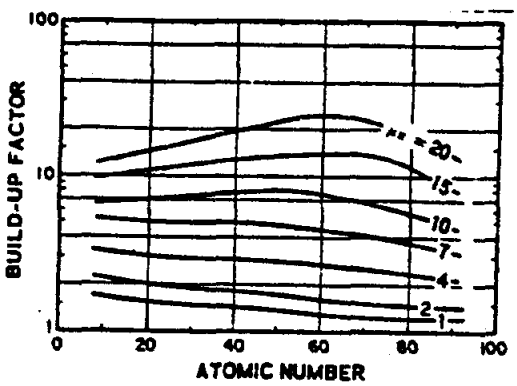

Figure 4–80. Build-Up Factor as a Function of Atomic Number for Gamma Rays in Initial Nuclear Radiation (4.0 Mev)

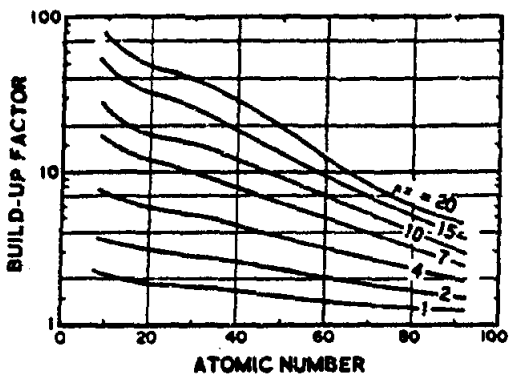

Figure 4–81. Build-Up Factor as a Function of Atomic Number for Gamma Rays in Residual Nuclear Radiation (1.0 Mev)

than the shields which will be discussed in the following paragraphs.

The attenuation of neutrons from a nuclear explosion involves several different phenomena. First, the very fast neutrons must be slowed down into the moderately fast range; this requires an inelastic scattering material such as barium or iron. Next, the moderately fast neutrons must be decelerated into the slow range by means of elements of low atomic weight. Water is very satisfactory in this respect. Then, the slow neutrons must be absorbed. This is not a difficult matter, as the hydrogen in water will do the job nicely. Unfortunately, most neutron captures are accompanied by the emission of gamma rays. Therefore, as a final consideration, sufficient gamma attenuating material must be included to minimize the escape of capture gamma rays.

In general, concrete or damp earth would represent a fair compromise for neutron as well as gamma-ray shielding. Although these materials do not normally contain elements of high density, they do have a fairly large proportion of hydrogen to slow down and capture neutrons, and a considerable portion of calcium, silicon, and oxygen to absorb the gamma radiations. A thickness of 10 inches of concrete will decrease the neutron dose by a factor of approximately 10, and 20 inches by a factor of roughly 100. The initial gamma radiation would be attenuated to a lesser extent, but if a sufficient thickness were employed, concrete could be used to provide adequate protection from neutron and gamma radiation. Damp earth may be expected to act in a somewhat similar manner.

An increase in the attenuation factor may be achieved by using a "heavy" concrete, made by adding a good proportion of an iron oxide ore. The presence of a heavy element improves both the neutron and the gamma-ray attenuation characteristics of the material. The attenuation of the neutron dose by a factor of 10 requires about 7 inches of this heavy mix.

The presence of boron, or a boron compound, in neutron shields offers certain advantages. The lighter (boron –10) isotope of the element captures slow neutrons very readily, the reaction being accompanied by the emission of moderate energy gamma rays (0.48 Mev) that are more easily attenuated. The mineral colemanite, which contains a large proportion of boron, can be easly incorporated into concrete.

Neutrons, like gamma-rays, suffer considerable scattering from the atmosphere. However, at longer ranges from the point of detonation, the atmospheric scattering has so attenuated the neutrons that they do not make a large contribution to the total dose. At shorter ranges, as in the case of gamma rays, adequate protection can be secured only from a shelter which is shielded in all directions.

The attenuation of a narrow beam of neutrons by a shield can be represented by an equation similar to that applied for gamma rays:

$$N = N_o e^{-\Sigma x}. \qquad (4\text{–}98)$$

Where N_o is the neutron dose that would be received without the shield, and N is the dose penetrating the shield of x cm thickness. The symbol Σ represents the macroscopic cross section, which is similar to the linear absorption coefficient for gamma rays. Actually, there is a specific value of Σ for every neutron energy, and for each type of reaction the neutron can participate in. However, for shielding calculations, an empirical value based on actual measurements is used. This experimental Σ is a complex average for all the possible neutron interactions over the range of energies in-

TABLE 4–12. EMPIRICAL MACROSCOPIC CROSS SECTIONS FOR ATTENUATION OF FAST NEUTRONS

Material	$\Sigma(cm^{-1})$
Water	0.1
Concrete	0.09
Iron concrete	0 16

volved. Some rough values of Σ for fast neutrons are contained in Table 4–12; these include an adjustment for broad neutron beams and thick shields.

(U) When a substance possesses a relatively large macroscopic cross section, this means that a smaller thickness of the material will be as effective as a greater thickness of a substance with a smaller macroscopic cross section. Thus, concrete containing iron is more effective than ordinary concrete. There is no simple correlation, however, between the density of the material and attenuation, as is true in the case of gamma rays. In conclusion, it should be emphasized that a good neutron shield must do more than attenuate fast neutrons; it must be able to capture the retarded neutrons and to absorb any gamma radiation accompanying the capture process.

4–8.5. (C) Residual Radiation and Fallout

4–8.5.1. (C) *General*

Although most of the damage accompanying a nuclear explosion occurs within a few seconds after the instant of detonation, there is a further hazard which extends over long periods of time. This hazard, residual nuclear radioactivity, is most intense when the weapon is exploded at such an altitude that surface particles are drawn into the fireball. The intense heat of the fireball changes the physical characteristics of the particles, causing them to become efficient scavengers of the finely divided radioactive remains of the weapon. Under the action of gravity, these particles then fall and are deposited over an area which may cover thousands of square miles. The size and pattern of the fallout are determined by such factors as particle size, cloud height, and wind velocity and direction.

For an air burst, particularly when the fireball is well above the earth's surface, a fairly sharp distinction can be made between the initial and the residual radiation. After the first minute, essentially all of the radioactive residue has risen to such a height that the nuclear radiations which reach the ground are no longer significant. The particles are finely dispersed in the atmosphere and descend to earth very slowly. For energy yields less than 100 KT, the height of burst at which fallout ceases to be significant is approximately 100 $W^{1/3}$ feet. For yields in excess of 100 KT, although not well substantiated, this height may be conservatively taken to be 180 $W^{0.4}$ feet.

With surface and, especially, subsurface explosions, the demarcation between initial and residual radiation is not as definite. Since some of the radiations from the bomb residues will be within range of the earth's surface at all times, the initial and residual radiation categories will merge continuously with each other. For very deep underwater and underground bursts, the initial radiation may be ignored. The only radiations of significance are those arising from the bomb residues, and these can be treated exclusively as residual nuclear radiation.

4–8.5.2. (U) *Fission Products*

a. General

The fission products constitute a very complex mixture of some 200 different isotopes of 35 elements. Most of these isotopes are radioactive, decaying by the emission of beta particles and gamma radiation. Approximately 0.11 pounds of fission products are formed for each kiloton of fission energy yield. Initially, the total radioactivity of the fission products is extremely large, but the radioactivity falls off at a fairly rapid rate.

At one minute after a nuclear detonation, the radioactivity from a one-kiloton weapon (0.11 pounds of fission products) is comparable to that of a hundred thousand tons of radium. Thus, it can be seen that the radioactivity produced by megaton explosions is enormous. In-

deed, the radiation intensity at the end of the first day is still large, even though it has decreased by a factor of about 6,000 from the concentration present one minute after detonation.

An indication of the rate at which the fission-product radioactivity decreases with time may be obtained from the following approximate rule: for every seven-fold increase in time after the explosion, the activity decreases by a factor of ten. For example, using the radiation intensity at 1 hour after detonation as a reference point, at seven hours after the explosion the intensity will be $\frac{\text{Intensity at 1 hr}}{10}$ at 7^2 hours it will be $\frac{\text{Intensity at 1 hr}}{10^2}$ at 7^3 hours it will be $\frac{\text{Intensity at 1 hr}}{10^3}$, etc. This rule is roughly applicable for about 200 days after the explosion, after which time the radiation intensity decays at a more rapid rate.

b. Radiation Dose Rate

Fig. 4–82 presents data concerning the decrease of activity of the fission products, by plotting the time after the explosion against the ratio of the exposure-dose-rate to the one-hour-reference-dose-rate. It is to be noted that at great distances from the ground zero of high yield explosions, the fission products may not arrive until several hours have elapsed. Nevertheless, the hypothetical dose rate at one hour is still used as a reference in making calculations. In such a case, the reference value is defined to be what the dose rate would have been one hour after the explosion, if the fallout had been complete at that time.

For example, at a given location the fallout commences at five hours after detonation. At 15 hours the fallout is complete, and the observed dose rate is 3.9 roentgens per hour. Entering Fig. 4–82 at 15 hours, on the lower scale, and reading the scale at the left opposite the intersection of the curve and the 15-hour line, it is found that $\frac{\text{1 hr ref. dose rate } (r/\text{hr})}{\text{dose rate } (r/\text{hr})} = 0.039$. From this the 1 hour reference dose rate $= \frac{3.9}{0.039} = 100$ roentgens per hour.

By means of this reference dose rate and the curve, it is possible to determine the dose rate at any time after detonation. Thus, if the dose rate at 24 hours is desired, Fig. 4–82 is entered at the point representing 24 hours on the horizontal scale. Moving vertically until the plotted curve is intersected, it is seen that the required dose rate is 0.02 times the 1-hour reference dose rate, or $0.02 \times 100 = 2$ roentgens per hour (r/hr).

If the dose rate at any time is known, the rate at any other time can be determined by comparing the ratios to the 1-hour reference for the two given times. For example, if the dose rate at 3 hours is known to be 50 roentgens, the value at 18 hours is $50 \times \frac{0.031}{0.27} = 5.7$ r/hr, where 0.031 and 0.27 are obtained from Fig. 4–82.

The results in Fig. 4–82 also may be represented in an alternate form, as in Table 4–13. This is a more convenient, although less complete presentation of data. The 1-hour reference dose rate is taken as 1,000 (any radiation units desired). The dose rates at a number of subsequent times are given in the table. If the dose rate at any time after the explosion is known, the dose rate at any other time, within the limits of the table, can be determined by simple proportion.

TABLE 4–13. RELATIVE DOSE RATES AT VARIOUS TIMES AFTER A NUCLEAR EXPLOSION

Time (hours)	Relative Dose Rate	Time (hours)	Relative Dose Rate
1	1,000	30	17
1½	610	40	12
2	440	60	7.3
3	270	100	4.0
5	150	200	1.7
7	97	400	0.75
10	63	600	0.46
15	39	800	0.33
20	27	1,000	0.25

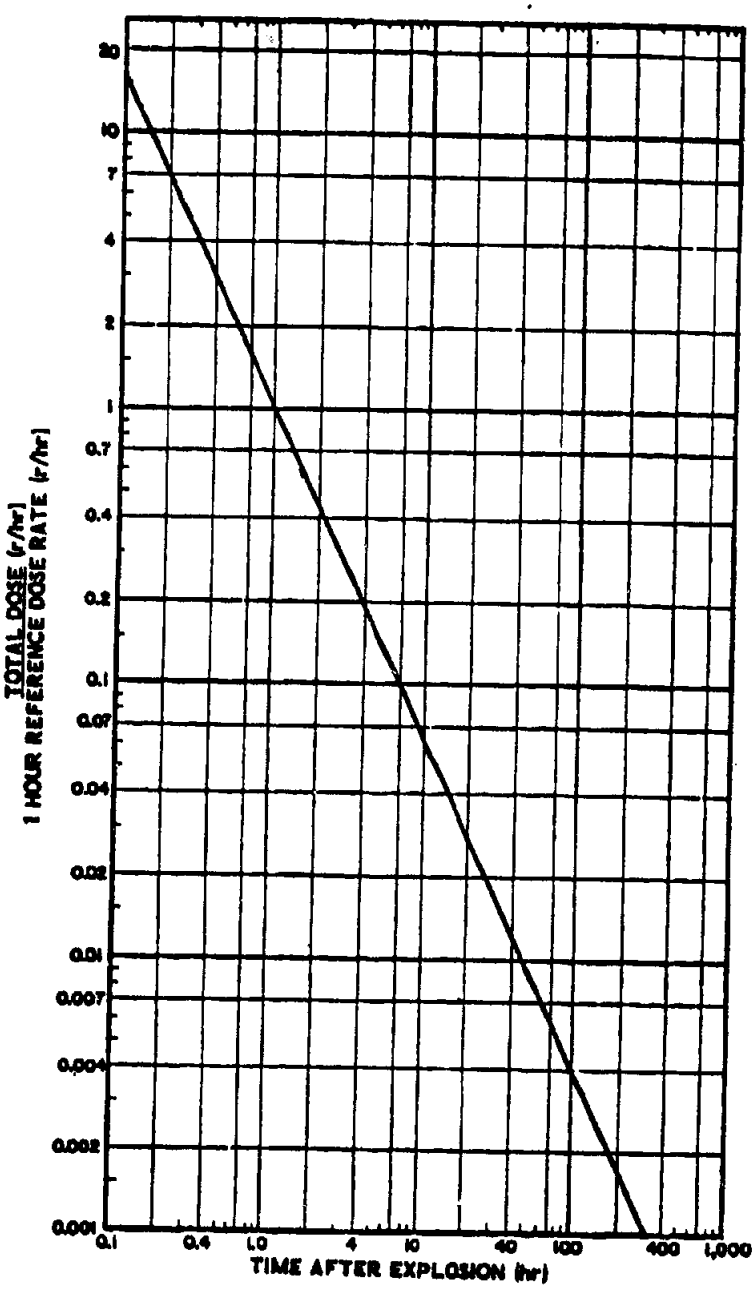

Figure 4–82. Decrease of Dose Rate From Fission Products With Time

c. Actual or Total Radiation Dose

Fig. 4–82 and Table 4–13 are used only for the calculations of dose rates. In order to determine the actual or total radiation dose received it is necessary to multiply the dose rate by exposure time, taking into account the decay of the fission products with time.

The mixture of radioisotopes constituting the fission products is so complex that a mathematical representation of the rate of decay in terms of individual half lives is impractical. However, from experimental data it has been determined that, for the period of several minutes to several years after detonation, the overall rate of radioactive decay can be expressed by the relatively simple equation

$$\text{Rate of disintegration} = A_1 t^{-1.2} \qquad (4\text{–}99)$$

where t is the time after the explosion, and A_1 is a constant factor (defined as the rate of disintegration at unit time) that is dependent on the quantity of fission products. With appropriate values of A_1, this equation can also be used to give the rates of emission of beta particles or gamma rays. A beta particle is emitted with each disintegration, but gamma ray photons are liberated only in approximately half the disintegrations. The exact fraction varies with the time after the explosion.

In considering the dose rate due to fission products, the gamma rays, because of their long range and penetrating power, are of much greater significance than the beta particles. (This is not true if the beta particles are on the skin or within the body.) Therefore, for most cases the beta particle radiation can be neglected when estimating the dose rate variation with time. Since the gamma rays in the early stages of fission-product decay have higher energies than those emitted later, the dose rate cannot be directly related to the rate of emission of gamma rays. However, for the period of practical interest, the mean energy of the gamma ray photons may be approximated as a constant 0.7 Mev. Although the fraction of gamma ray emissions varies slightly with time, a fair approximation is then,

$$\text{Gamma Radiation Dose Rate} = r_1 t^{-1.2} \qquad (4\text{–}100)$$

where r_1 is a constant, equivalent to the reference dose rate at a unit time. Usually the time, t, is expressed in hours, and r_1 is, therefore, the reference dose rate at one hour after the explosion. If r_t represents the dose rate from a certain quantity of fission products at t hours after the explosion, then, from Eq. 4–99,

$$\frac{r_t}{r_1} = t^{-1.2} \qquad (4\text{–}101)$$

taking logarithms

$$\text{Log}\,\frac{r_t}{r_1} = -1.2\,\text{Log}\,t. \qquad (4\text{–}102)$$

Using Eq. 4–102, a log-log plot of $\frac{r_t}{r_1}$ against t should give a straight line of slope -1.2. When $t=1$, $r_t=r_1$ and $\frac{r_t}{r_1}=1$. This is the basic reference point through which the line of slope -1.2 is drawn in Fig. 4–82.

If the time, t, is in hours, the radiation exposure dose rates r_t and r_1 are expressed in roentgens per hour. The total dose in roentgens can be readily determined by direct integration of Eq. 4–100. For the interval from t_1 to t_2 hours after detonation

$$\text{total dose} = r_1 \int_{t_1}^{t_2} t^{-1.2}\,dt$$

$$\text{total dose} = \frac{r_1 t^{-0.2}}{-0.2}\Bigg]_{t_1}^{t_2}$$

$$\text{total dose} = \frac{r_1}{0.2}\left(\frac{1}{t_1^{0.2}} - \frac{1}{t_2^{0.2}}\right) = 5r_1\left(t_1^{-0.2} - t_2^{-0.2}\right). \qquad (4\text{–}103)$$

Hence, if the reference dose rate r_1 (roentgens per hour) is known, the total dose (roentgens) may be calculated for any period. The curve in Fig. 4–83 is derived from Eq. 4–103 with t_1 taken as 0.0167 hour (1 minute), the time at which the residual nuclear radiation is postulated as beginning.

Another application of Eq. 4–103 is the determination of the length of time an individual can stay within an area contaminated by fission products, without receiving more than a speci-

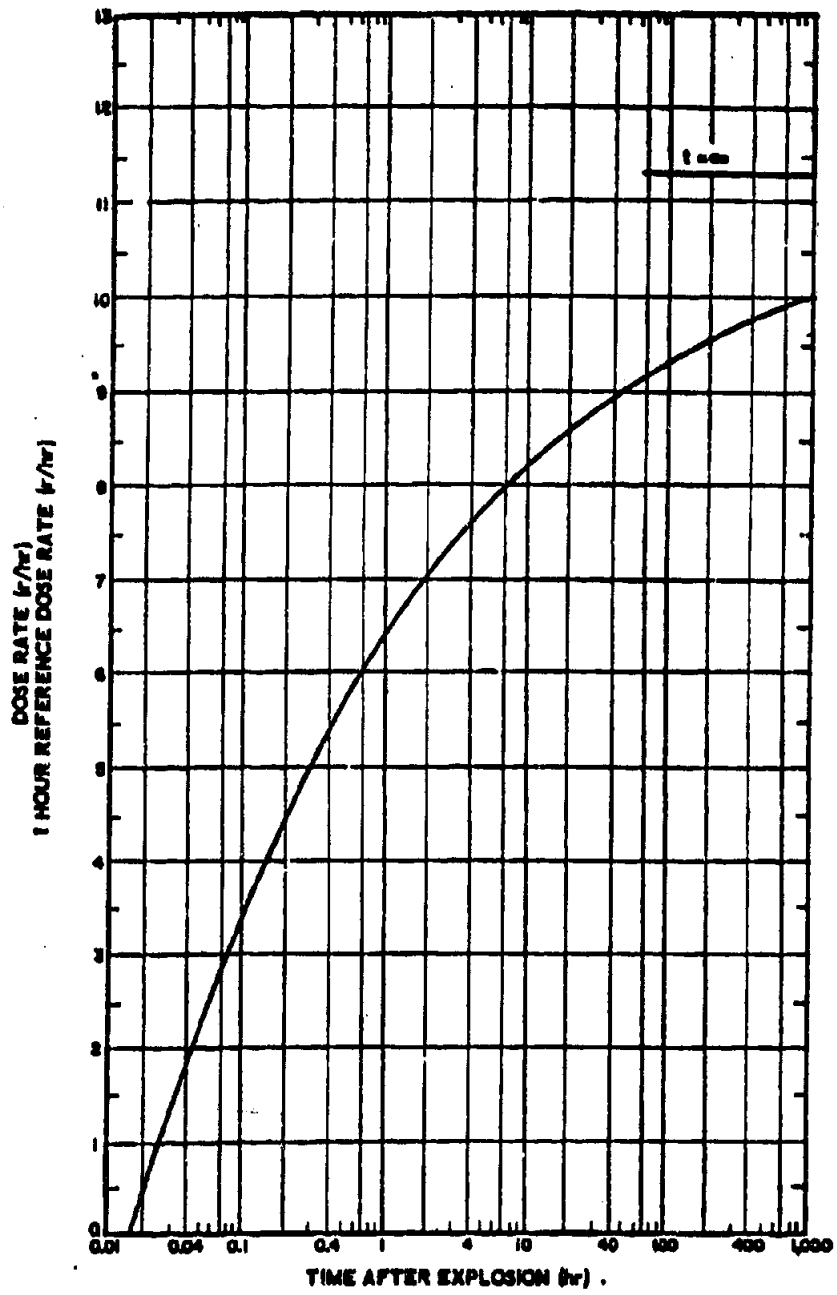

Figure 4–93. Accumulated Total Dose of Residual Radiation from Fission Products, from One Minute After the Explosion

fied dose of radiation. In this case, the total dose is specified; t_1 is the known time of entry into the region; and t_2 is the time at which the exposed individual must leave. The reference dose rate, r_1, must be known before the equation can be solved for various values of t_2 (Ref. 1).

4-8.5.3. (C) Neutron-Induced Activity

a. Air Burst

The neutron-induced gamma activity from an air burst will depend on soil type as well as weapon type and yield. It is therefore impractical to attempt to define a height of burst above which this effect ceases to have military significance.

b. Burst in the Transition Zone

(1) General

Even if a nuclear weapon is detonated at a height of burst above that at which fallout is expected to be a hazard, the radioactivity which is induced in the soil by neutrons still can give rise to dose rates of military importance in the vicinity of ground zero. The type, intensity, and energy distribution of the residual activity produced will depend on which isotopes are produced and in what quantity. This, in turn, depends on the number and energy distribution of the incident neutrons, and on the chemical composition of the soil. Induced contamination contours are independent of wind effects, except for some wind redistribution of the surface contaminant, and can be expected to be roughly circular.

Four soils have been chosen to illustrate the extent of the hazard which may be expected from neutron-induced activity. The soils were selected to illustrate wide variations in predicted dose rates; the activity from most other soils should fall within the range of activities presented for these soils. The chemical composition of the selected soils is shown in Table 4-14 (Ref. 21).

The elements which may be expected to contribute most of the induced activity are sodium, manganese, and aluminum. Small changes in the quantities of these materials can change the activity markedly; however, other elements which capture neutrons can also influence the magnitude of the activity. The elements are listed in Table 4-14 in the order of their probable importance as far as induced activity is concerned.

Fig. 4-84 indicates the manner in which the induced activity is expected to vary with slant range and weapon type. H + 1 hour dose rates for the four soils may be obtained by multiplying the dose rate obtained from Fig. 4-84 by the multiplying factor for that soil, as given in the instructions for use of the figure (Par. 2, following).

In order to calculate the dose rates at times other than one hour after the detonation, decay factors may be taken from Fig. 4-85, which represents the decay characteristics of the four soils. The decay factors are constants, and are multiplied by the value of the dose rate at one hour, to give the rate at any other time.

Fig. 4-86 is presented to facilitate computation of total dose. Multiplying factors may be obtained from this figure which, when applied to the one-hour dose rate for the particular soil (Type I), will give the dose accumulated over any of several periods of time, for various times of entry into the contaminated area.

When applying the data presented to soils other than those used for illustrative purposes, the activity should be estimated by using the data for the illustrative soil which most closely resembles the soil in question in chemical composition. If none of the illustrative soils resembles the soil in question very closely, the following remarks should be kept in mind. For times less than H + 1/2 hour, aluminum is the most important contributor. For times between H + 1/2 hour and H + 5 hours, manganese is generally the most important element. In the absence of manganese, the sodium content will probably govern the activity for this period. Between H + 5 hours and H + 10 hours, sodium and manganese content are both important. After H + 10 hours, sodium will generally be the only large contributor. In the absence of sodium, manganese, and aluminum, the activity will probably be low, and will generally be governed by the silicon content. Soil type IV is an example of this latter type. Thus, the time (of interest) after H time is of sig-

TABLE 4–14. CHEMICAL COMPOSITION OF SELECTED SOILS

Element	Percentage (by weight)			
	Soil Type I Liberia, Africa	Soil Type II Nevada Desert	Soil Type III Lava Clay, Hawaii	Soil Type IV Beach Sand Pensacola, Fla.
Sodium		1.30	0.16	0.001
Manganese	0.008	0.04	2.94	....
Aluminum	7.89	6.90	18.79	0.006
Iron	3.75	2.20	10.64	0.005
Silicon	33.10	32.00	10.23	46.65
Titanium	0.30	0.27	1.26	0.004
Calcium	0.08	2.40	0.45	....
Potassium	...	2.70	0.88	....
Hydrogen	0.39	0.70	0.94	0.001
Boron	...	...	...	0.001
Nitrogen	0.065	...	0.26	....
Sulphur	0.07	0.03	0.26	....
Magnesium	0.05	0.60	0.34	....
Chromium	...	....	0.04	....
Phosphorus	0.008	0.04	0.13	....
Carbon	3.87	...	9.36	....
Oxygen	50.33	50.82	43.32	53.332

nificance in the choice of the most representative soil type.

If a weapon is burst at such a height as to be in the transition zone (from the fallout standpoint), the neutron-induced activity can generally be neglected if the burst height is in the lower three quarters of the fallout transition zone. For weapons burst in the upper quarter of the fallout transition zone, the neutron-induced activity may be significant when compared to fallout. For the cases where fallout dose-rate contour parameters, are much smaller than those for a burst on the surface, an idea of the magnitude of induced activity may be obtained from Figs. 4–84 through 4–86. The overall contour values may then be obtained by combining the induced activity and fallout activity. For these cases, it must be remembered that fission products and induced activity will decay at different rates. This necessitates a determination of the magnitude of each type of activity for each time of interest.

(2) Instructions for Using Fig. 4–84, Neutron-Induced Gamma Activity

(a) Description

Given the weapon type and the slant range from the point of burst to the point of interest,

the induced gamma dose rates can be estimated using Fig. 4–84. These rates are for the vicinity of ground zero at H + 1 hour, for bursts over soils similar in composition to the four soils listed in Table 4–14. To estimate the dose rate, enter the slant range axis with the slant distance in yards, read the dose rate for the appropriate weapon type, and multiply this dose rate by the appropriate factor for the soil type of interest. Soil types I, II, III, and IV are multiplied, respectively, by the factors of 0.11, 1.0, 12.0, and 0.0026.

(b) Scaling Procedure

For yields other than 1 KT, multiply the dose rate read from the curve by the yield in KT.

(c) Example

Given: An average neutron-flux 50-KT weapon burst at a height of 900 feet above soil of Type III.

Find: The H + 1 hour dose rate at ground zero, and at 600 yards from ground zero.

Solution: From the average neutron flux weapon curve of Fig. 4–84, the dose rate at H + 1 hour at ground zero (300-yard slant range) is 9 r/hour, per KT of weapon yield. The multiplying factor for soil type III is 12. Therefore, the dose rate at ground zero one hour after detonation of a 50-KT weapon over soil type III is:

$$50 \times 12 \times 9 = 5{,}400 \ r/\text{hour}.$$

At 600 yards from ground zero the slant range is 670 yards. From the curve, the induced gamma intensity is 0.35 r/hour per KT of weapon yield at this distance. Therefore, the dose rate 600 yards from ground zero, one hour after detonation of a 50-KT weapon over soil type III is:

$$50 \times 12 \times 0.35 = 210 \ r/\text{hour}.$$

(d) Reliability

Dose-rate values taken from the curves for the soils presented are correct to within a factor of 5, for the conditions indicated. For other soils, the data will merely furnish an estimate of the magnitude of the hazard (Ref. 21).

(3) Instructions for Using Fig. 4–85, Decay Factors for Neutron-Induced Gamma Activity

(a) Description

From the dose rate at H+1 hour, the dose rate at any other time is obtained by computing the product of the appropriate decay factor from Fig. 4–85 and the 1-hour dose rate (see Example 1). The decay curves may also be used to determine the value of the dose rate at H+1 hour, by means of the dose rate at a later time. In this case, the measured dose rate is divided by the appropriate decay factor (see Example 2).

(b) Example 1

Given: The dose rate, at a given point on soil type I, is 30 r/hour at H+1 hour.

Find: The dose rate at that point at H+½ hour, and at H+10 hours.

Solution: From Fig. 4–85, the decay factors for soil type I for ½ hour and 10 hours are 3.0 and 0.083 respectively. The dose rate at ½ hour is

$$30 \times 3.0 = 90 \ r/\text{hour},$$

and the dose rate at 10 hours is

$$30 \times 0.083 = 2.5 \ r/\text{hour}.$$

(c) Example 2

Given: The dose rate at a given point on soil type II, 20 hours after detonation, is 100 r/hour.

Find: The dose rate at the same point 1 hour after the detonation.

Solution: From Fig. 4–85, the decay factor at 20 hours is 0.24. Therefore, the dose rate at 1 hour is

$$\frac{100}{0.24} = 417 \ r/\text{hour}.$$

(d) Reliability

The reliability is the same as for Figs. 4–84 and 4–85.

(4) Instructions for Using Fig. 4–86, Total Neutron-Induced Gamma Dose for Soil Type I

(a) Description

From Fig. 4–86 can be obtained the total

dose that will be received by a person entering a contaminated area of soil type I, in terms of the time-of-entry and time-of-stay. The vertical axes give the accumulated dose for each unit of dose rate (r/hr), at one hour after a detonation over that soil. The various curves represent times-of-stay in the contaminated area. To determine the accumulated dose, a

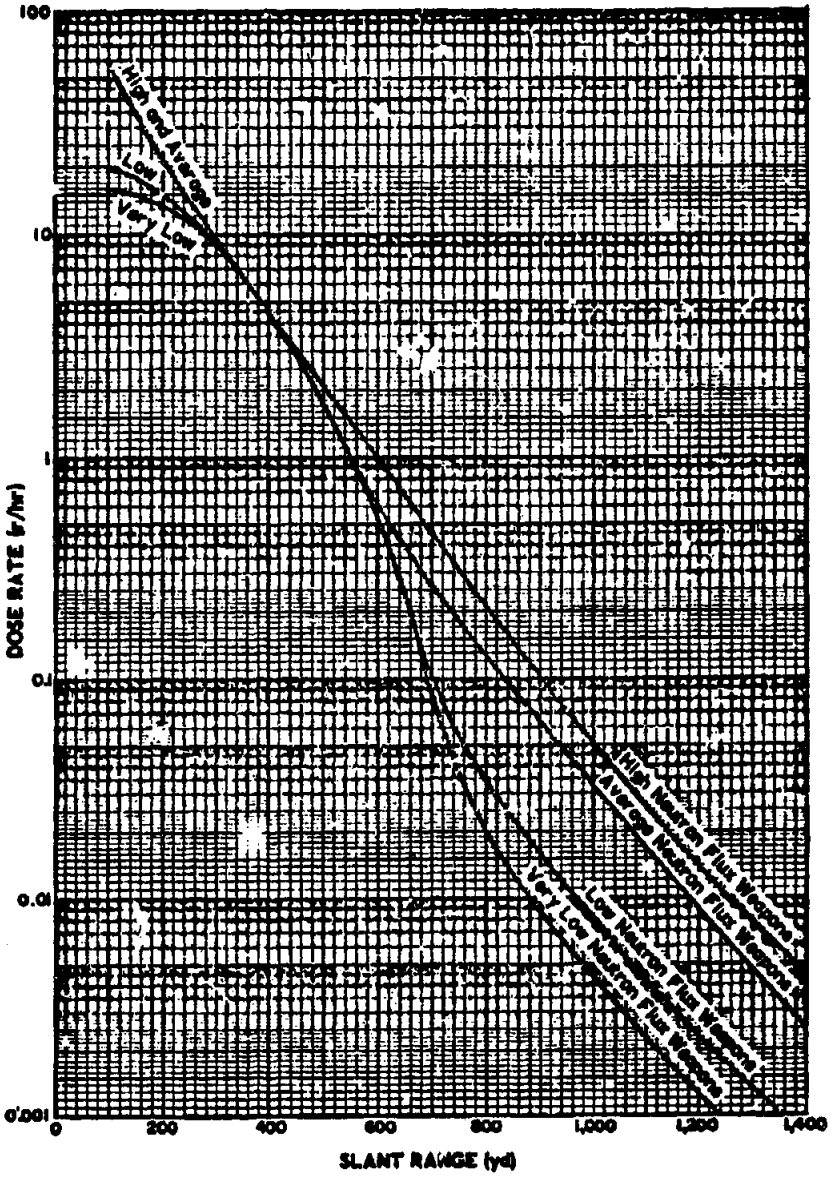

Figure 4–84 (C). Neutron-Induced Gamma Activity vs Slant Range (0 to 1,400 Yards), at a Reference Time of One Hour After Burst, for a 1-KT Yield (U)

multiplication factor is taken from the vertical axis, corresponding to the intersection of the time-of-stay curve and the time of entry. The product of this multiplication factor and the dose rate at one hour gives the accumulated dose.

(c) Example

Given: The dose rate in a given area over soil type I at one hour after detonation is 300 r/hour.

Find: The total dose received by a man who enters the area 5 hours after detonation and remains 0.3 hours.

Solution: From Fig. 4–86, the intersection of the line for time-of-entry of 5 hours after detonation with the 0.3-hour time-of-stay gives a factor of 0.09. Therefore, the accumulated dose is:

$$300 \times 0.09 = 27 \text{ r}.$$

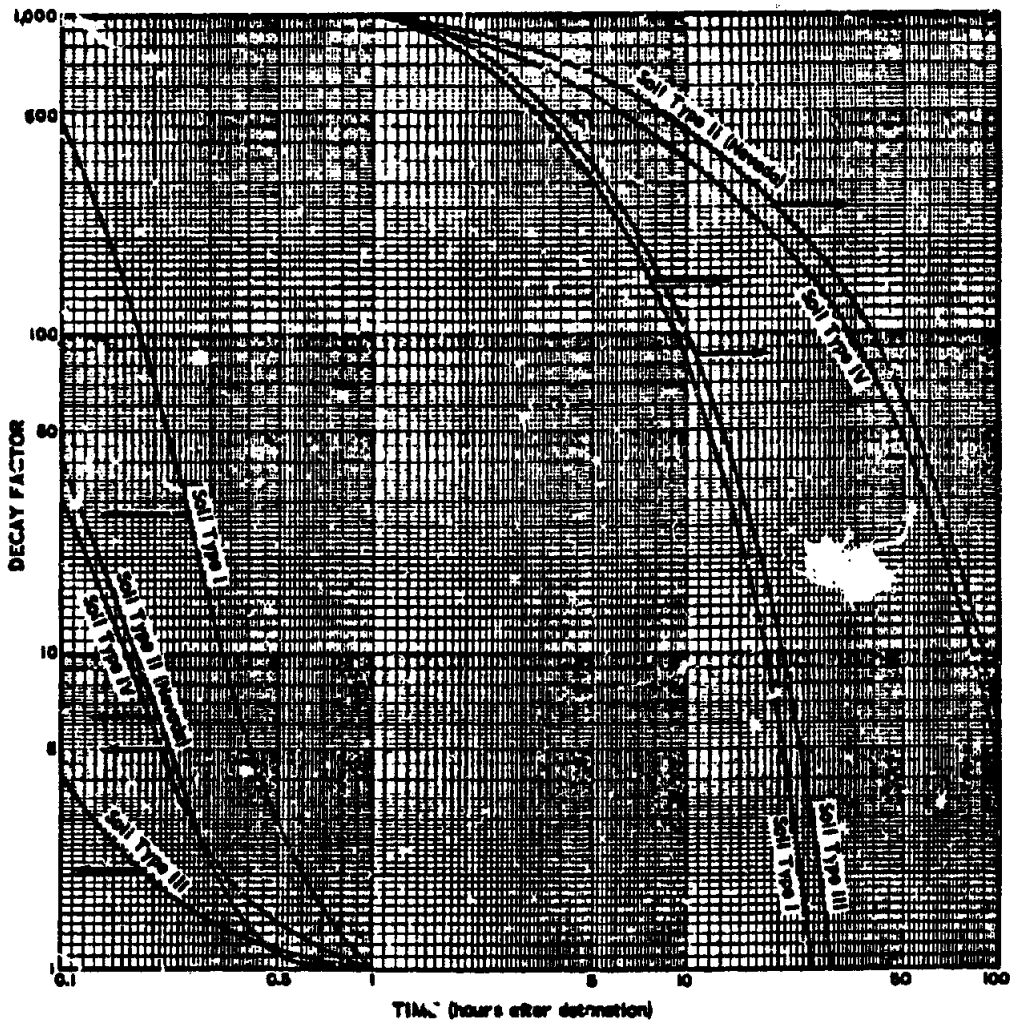

Figure 4–85 (C). Decay Factors for Neutron-Induced Gamma Activity (U)

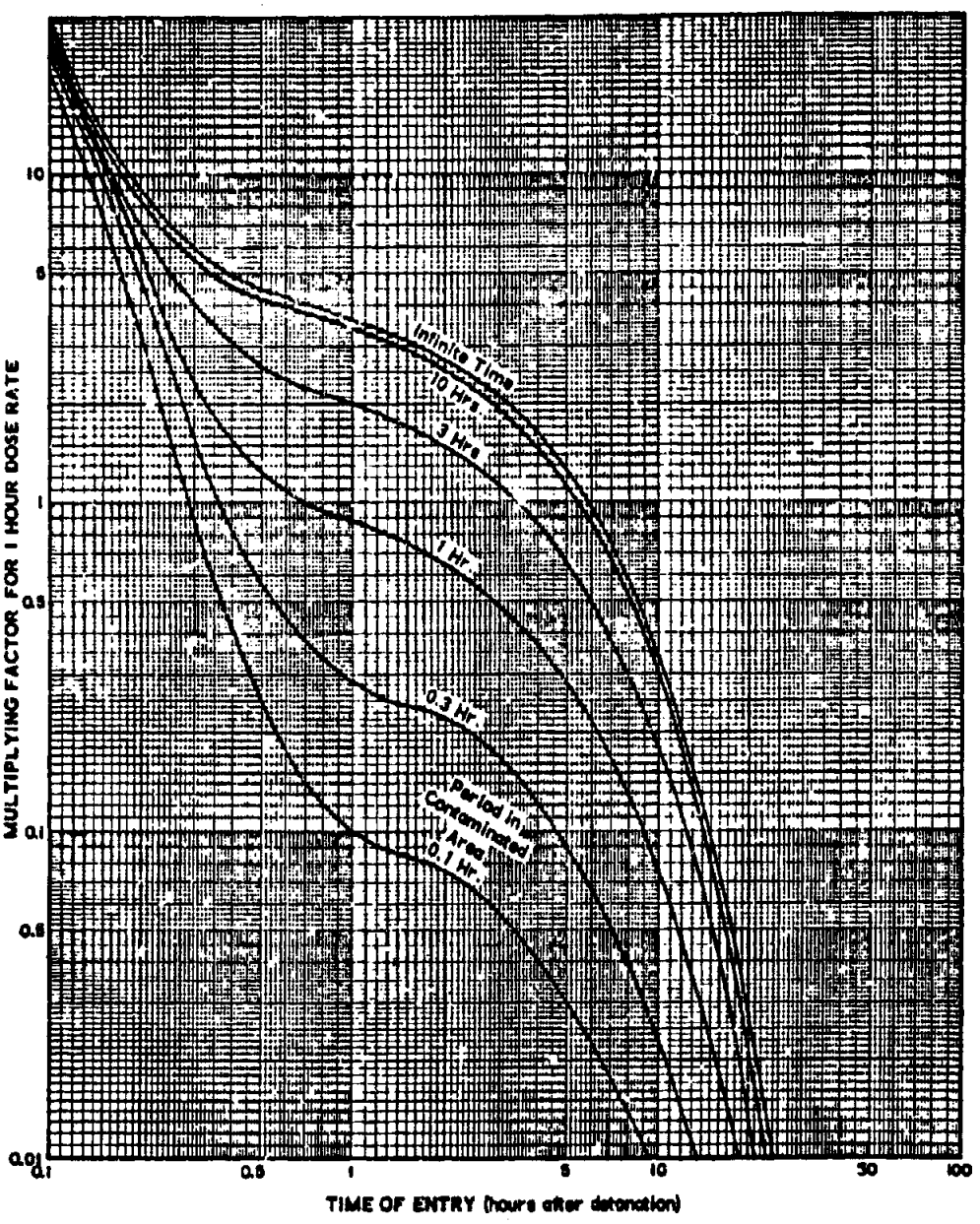

Figure 4–86 (C). Total Radiation Dose Received in an Area Contaminated by Neutron-Induced Gamma Activity, Soil Type I (U)

c. Surface and Subsurface Bursts

For surface and subsurface bursts, the residual radioactive contamination from fission products is vastly greater than the neutron-induced activity. As a result, neutron-induced activity can generally be neglected for surface and subsurface bursts.

d. Cloud Contamination

(1) General

Much of the radioactive material of the nuclear explosion is airborne. This nuclear cloud may constitute a great radiation hazard for some time for personnel in aircraft flying through it. The cloud size and rate of rise vary with the yield of the bomb and the prevailing meteorological conditions. In fair-weather detonations, except where meteorological conditions such as high wind velocities are involved, the top and bottom of the mushroom head of the cloud have been observed to stabilize in altitude at a time approximately 6 to 10 minutes after detonation, independent of yield. The altitude above burst point of this portion of the cloud increases with weapon yield, when other factors remain the same. Fig. 4–87 illustrates this for yields between 0.1 KT and 100 MT.

The height of a nuclear cloud is influenced by atmospheric conditions, which include the temperature gradient, winds, relative humidity, and the height of the tropopause. Because these atmospheric effects are very complex, and also because it would be most difficult to consider all possible weather variations, a quantitative treatment of the effect of atmospheric conditions on cloud heights is not included in this publication. The percentage of maximum cloud height reached by the cloud, at any time after a detonation, and before stabilization, is relatively independent of the yield. The diameter of the cloud increases rapidly at times earlier than 1 minute after a detonation. After about 1 minute, the width of the cloud increases more slowly, until the cloud reaches its maximum altitude. This is true for all yields except those that are extremely large. If the yield is large enough for the cloud to reach the tropopause, the cloud rises more slowly upon reaching this level and increases in lateral dimension more rapidly, as though flattening out against a ceiling. The rate of lateral growth of the cloud during this time is about three times the rate before reaching the tropopause. After reaching maximum altitude, the diameter slowly increases as the cloud drifts downwind.

(2) Instructions for Using Fig. 4–87, Stabilized Cloud Altitudes

(a) *Example*

Given: An 80-KT burst at 3,000 feet above terrain.

Find: The altitude above terrain of the top and bottom of the stabilized cloud.

Solution: From Fig. 4–87, a cloud from an 80-KT burst stabilizes above the burst point at:

top = 52,000 feet

and

bottom = 38,000 feet.

Therefore, the altitude above terrain is:

top = 52,000 + 3,000 = 55,000 feet

and

bottom = 38,000 + 3,000 = 41,000 feet.

(b) *Reliability*

It is expected that clouds will not rise above the burst point more than 20 per cent higher than indicated. However, extremes in meteorological conditions, such as winds of 50 knots or greater, can cause clouds from weapon yields less than 100 KT to rise only half as high as indicated. For yields greater than 100 KT, under almost all conditions, meteorological conditions are less important in limiting the altitudes given.

4–3.5.4. (C) *Radioactive Contamination and Fallout Patterns*

a. Air Burst

The surface contamination effects of fallout from an air-burst weapon are militarily insignificant in most cases, because the bomb cloud carries practically all the radioactive bomb debris to high altitudes. In general, by the time this material can fall back to earth, dilution and radioactive decay will have decreased the activity to levels which are no longer important. An exception may occur in the case of a small-

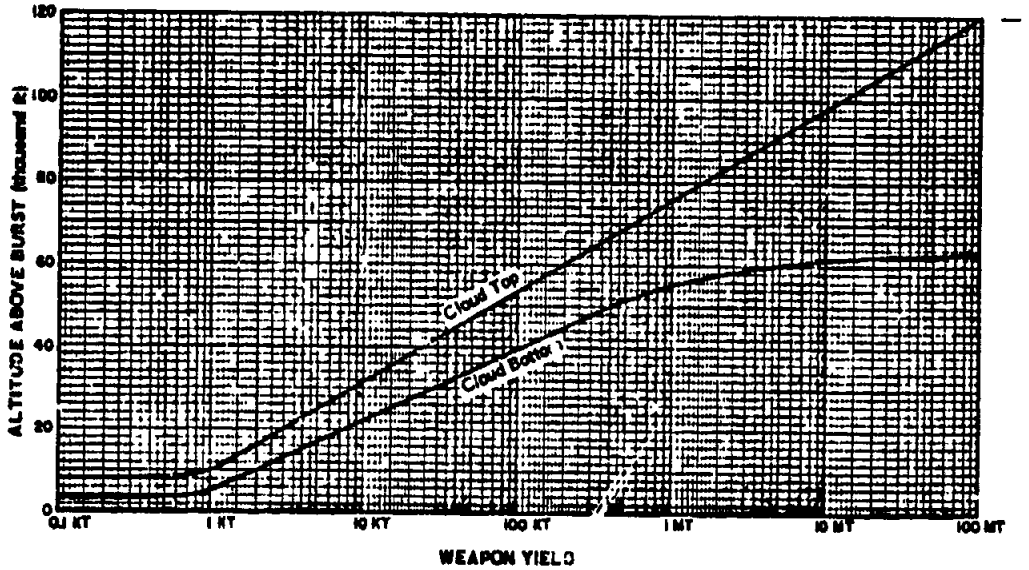

Figure 4–87 (C). Altitude Above Burst Point of Top and Bottom of Stabilized Nuclear Cloud vs Weapon Yield (U)

yield weapon burst in the rain. In this case, the scavenging effect of the precipitation may cause a rain-out of radioactive material, creating a hazard to personnel located downwind and downhill, although outside the hazard area of initial radiation and other nuclear effects.

The range of weapon yields for which rain-out may become hazardous is not large, but quantitative treatment of the problem is difficult. The contamination pattern on the ground depends upon two major dynamic processes, each of which is extremely sensitive to several factors. The major processes are: the scavenging effect of precipitation on suspended fission products in the atmosphere; and the flow and ground absorption of rain water after reaching the ground. Some of the factors which influence the scavenging effect are the height and extent of the rain cloud, the raindrop size and distribution, the rate of rainfall, and the duration of precipitation. Other factors of significance are the position of the nuclear cloud relative to the precipitation, the hygroscopic character of the fission products, the solubility of the fission products, and the size of the fission fragments. The flow and ground absorption of the rain water will, in turn, depend upon such factors as the soil porosity, drainage features, including rate of drainage, and the degree of soil saturation.

Even in extreme cases, the rainout from an air burst should not be a serious military problem for yields in excess of 20 KT, and for the average case, it should not be a serious problem for yields in excess of 8 KT. Although the weapons of greater yield produce more radioactive material, the updrafts carry the bulk of the material up through the weather to an altitude above the level of precipitation.

Where a rain-out problem does exist, it must be evaluated with respect to local conditions. Ditches, puddles, and low ground where water collects should be avoided by personnel unless survey indicates these areas are safe. Caution should be exercised for a considerable distance downwind and downhill from the burst. However, as long as drainage is taking place, the rate of decrease in intensity is likely to be greater than decay laws predict.

In addition to rain-out, another contamination mechanism assumes some importance in the case of a low air burst. This is the formation of radioactive elements in the soil by action

of the neutrons emitted by the weapon. Activity induced in this manner is treated in Par. 4–8.5.3, preceding.

b. Surface Burst

(1) Land-Surface Burst

The radiation activity available from weapon components, at a reference time of one hour after the detonation, is approximately that corresponding to 300 megacuries per kiloton of bomb yield. For a burst exactly at the earth's surface, roughly fifty per cent of the activity available is deposited in the general vicinity of the detonation, while the remainder is carried hundreds, or perhaps thousands, of miles from the point of detonation by the winds of the upper atmosphere.

In a complete calm, the fall-out contamination forms a roughly circular pattern around the point of detonation. The existence of a wind leads to an elongated area, the exact nature of which depends upon the velocity and direction of the wind, from the ground surface up to the altitude of the top of the stabilized cloud. If the direction of the wind does not vary excessively from the surface up to the top of the cloud, the ground fall-out contours may be characterized by a circular pattern around ground zero, and by an elliptical pattern extending downwind from ground zero. The circular pattern is formed by the rapid settling of the heavier particulate matter in the stem, while the downwind elliptical pattern is formed by fall-out of smaller and lighter particles from the cloud.

The existence of complicated wind patterns (wind shear), as well as variations of the wind pattern in time and space, may cause extreme departures from a simple elliptical pattern. In addition, the measured dose-rate contours have frequently been observed to occur in patterns best described as a series of islands of relatively high activity surrounded by areas of lower activity. The most common pattern of this type has been one in which the higher dose-rate contours appear around two major areas and one or more smaller areas. One of the larger areas is in the immediate vicinity of ground zero while the other is in the general downwind direction from ground zero. The locations of the smaller areas of high activity have not demonstrated patterns which can be described simply in terms of the wind structure.

The dose rates observed within these high activity areas have been of comparable magnitude when extrapolated back to some early time after detonation, such as H+1 hour. However, due to the earlier arrival of the contaminant, the activities actually observed near ground zero have been higher than in the areas away from ground zero. It should be noted that these islands of relatively high activity generally cover areas considerably larger than those of the "hot spots," caused by local meteorological conditions discussed elsewhere. A quantitative treatment of such complicated deposition patterns would be possible only through use of a complex computational model, together with time-consuming calculations. The simplified method for obtaining deposition patterns, which is presented below, will not predict these islands of relatively high activity.

The area covered, and the degree of localization of the contamination, depend also upon the character of the soil at the burst point. For example, a surface detonation over dry soil with small particle sizes results in a larger than average area enclosed by low dose rate contours, and in a smaller than average area enclosed by high dose rate contours. A similar detonation over water-covered, finely divided soil, such as clay, probably results in relatively high dose contours over larger areas close to the detonation, with a corresponding reduction in the areas of the lower dose-rate contours farther out.

In discussions of the areas affected by residual contamination from fall-out, it is convenient to set up a system of contamination dose-rate contours which, although simplified and idealized, fit actual contours measured in the field as closely as possible. Fig. 4–88 illustrates such a contour system. The idealized contour shown consists necessarily of two parts: the ground zero circle, and an elliptical approximation to the downwind component of the fallout. The ground zero circle is formed quite soon after the detonation, largely from heavy particulate matter, throw-out, and soil made active

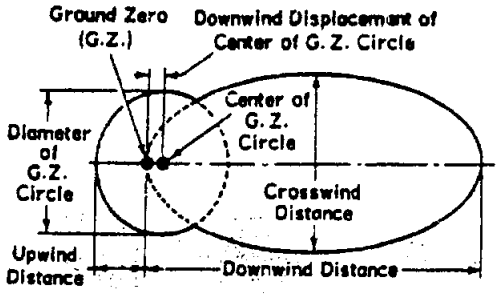

Figure 4–88. Generalized Local Contours for Residual Radiation

by neutron-capture reactions. The parameters which define it are its diameter and the downwind displacement of its center from ground zero.

The idealized downwind component, consisting of the fall-out proper, is elliptical in shape. The parameters which define it are its major and minor axes (the downwind and crosswind extent, respectively). One end of the ellipse is at ground zero. To define the downwind axis, the simplifying assumption is made that the downwind direction and extent are determined by a single wind of constant velocity, the so-called scaling wind. To obtain the scaling wind, it is first necessary to obtain the resultant wind vector for each of an arbitrary number of equally spaced altitude zones located between the top and bottom of the stabilized cloud. Each resultant wind vector is the vector average, of all wind vectors for equally spaced altitude intervals, from the altitude zone in question down to the surface. The scaling wind is, then, the vector average of all the resultant wind vectors for the various altitude zones within the cloud.

As a rule, wide discrepancy from the idealized elliptical pattern results if there are large directional shears in the resultant winds computed for the altitudes of the stabilized bomb cloud. Such shears can give rise to serious distortion of the idealized elliptical pattern, so that in practice radical distortions of these idealized patterns can be expected. However, contour areas will remain substantially unchanged. In such a case, the close-in portions of the fall-out pattern, in general, follow the direction of the resultant winds from the lower cloud altitudes, while the more distant downwind portions of the pattern tend to lie in the direction of the resultant winds from the upper cloud altitudes. The idealized contours described herein have a more general application.

It is important to recognize that H + 1 hour is used as the reference time in the preparation of these contours, and that only the contours from low yield weapons are complete one hour after burst time. For very high yield weapons, fall-out over some parts of the vast areas indicated does not commence until many hours after the burst. In order to calculate the dose rates at times other than 1 hour after the detonation, decay factors may be taken from Fig. 4–82, which is a representation of the decay law. The factors are constants, which are multiplied by the value of the dose rate at 1 hour to give the rate at any other time. (These decay factors apply only to fission product contamination, such as predominates on the ground after a surface burst, and must not be used to estimate the decay of neutron-induced, ground contamination resulting from an air burst.) The $t^{-1.2}$ law, which approximates the decay of the mixture of fission products, holds reasonably well for actual contamination over long periods of time, but not as well over short periods of time, because of the presence of weapon contaminants other than fission products.

Families of curves (Figs. 4–89 through 4–94) are given from which data may be obtained to draw idealized dose-rate contours, for land-surface bursts of weapons with yields between 0.1 MT and 100 MT. A 15-knot scaling wind has been used in the preparation of the curves. This rate is near the average of the scaling wind values most commonly encountered under field test conditions; it is probably a good average value for general application. Fig. 4–94 provides height-of-burst adjustment factor data.

Contour areas are substantially constant over the range of scaling winds likely to be experienced, but the linear contour dimensions, except for the diameter of the ground zero circle, must be scaled. Directions for scaling are given in

Par. (2), following. Use of a true ellipse as the idealized contour results in areas larger than those actually observed. The downwind contours observed in field tests, in general, cover slightly less area than true ellipses. For this reason, true contour areas should be read directly from the area curves, rather than computed from the contour dimensions obtained.

(2) Instructions for Using Fig. 4–89 through 4–94, Dose-Rate Contour Parameters

(a) Description

The basic data presented in these figures is for weapons for which all of the yield is due to fission. However, as described below, the data can also be used to obtain fallout contours for weapons for which the fission yield is only a fraction of the total yield, provided that essentially all of the contamination produced (90 per cent or more) is due to fission products.

The dose rate values are given for a reference time of H+1 hour. It must be recognized that the more distant portions of the larger contours do not exist at H+1 hour, because the fallout which eventually reaches some of these more distant areas is still airborne at that time. The dose rate contours do exist at later times, when fallout is complete, but with contour dose-rate values reduced according to the appropriate decay factor from Fig. 4–82. Visual interpolation may be employed for dose-rate contour values between those for which curves are given. Extrapolation to higher or to lower dose-rate contour values than those covered by the families of curves cannot be done accurately, and should not be attempted.

To obtain dose rate values for times other than H+1 hour, decay factors from Fig. 4–82 should be used. To obtain contour values for scaling winds other than 15 knots, multiply downwind distance and downwind displacement of the ground-zero circle by the appropriate factor given in Table 4–15, and divide crosswind distance by the same factor. Numerical values of contour areas and ground-zero circle diameters are essentially wind-independent.

TABLE 4–15 (C). ADJUSTMENT FACTORS FOR CONTOUR PARAMETERS FOR VARIOUS SCALING WINDS (U)

Scaling Wind Vel (knots)	Adjustment Factor
5	0.7
10	0.9
15	1.0
20	1.1
25	1.2
30	1.3
40	1.4
50	1.5

For the special (and unusual) case of a zero scaling wind velocity, contours would be circular and centered at the burst point, with radii determined from the area curves by the formula:

$$\text{Contour Radius} = \left(\frac{\text{Contour Area}}{\pi}\right)^{1/2}.$$

For a burst in the transition zone, a rough estimate of the resulting fallout contamination patterns may be made by multiplying the dose-rate contour values, for a contact surface-burst weapon of the same yield, by an adjustment factor obtained from Fig. 4–94 for the appropriate yield and height of burst.

Note that the contribution made by neutron-induced activity may be significant, compared to the fallout activity in the area near ground zero for weapons burst in the upper quarter of the fallout transition zone. For guidance, a rough estimate of this contribution may be obtained by using Figs. 4–84 through 4–86, together with the discussion in Par. 4–8.5.3, preceding.

It should be recognized that contour shapes and sizes are a function of the total yield of the weapon, whereas the dose-rate contour values are determined by the amount of contaminant available; i.e., the fission yield. Thus, if only a fraction of the total yield of the weapon is due to fission, and this fraction is known, Figs. 4–89 through 4–93 may be used

to estimate fallout contours resulting from the detonation of such a weapon. The dose rate for the dimension of interest, read from the figures opposite the total yield, must be multiplied by the ratio of fission-yield to total-yield to obtain the true dose-rate value for that dimension. Similarly, to obtain contour dimensions for a particular dose rate, the value of the desired dose rate must be divided by the ratio of fission to total yield, and the dimension of the resultant dose rate read from the figures opposite the total yield.

(b) Example 1

Given: A weapon with a total yield of 600 KT, of which 200 KT is due to fission, is detonated on a land surface under 10-knot scaling wind conditions.

Find: Contour parameters for a dose rate of 100 r/hr at a $H+1$ hour reference time.

Solution: The 100 r/hr contour for a fission-yield to total-yield ratio of 200/600 is the same as the contour for $100 \div \frac{200}{600} = 300$ r/hr, for a weapon for which the total yield is fission yield. Figs. 4–89 through 4–93 can, therefore, be applied together with wind factors from Table 4–15; i.e., the 300 r/hr contour values read from Figs. 4–89 through 4–93 (for fission yield = total yield = 600 KT) are also those for the 100 r/hr contour of the weapon described in the example. The problem solution is indicated in Table 4–16.

(c) Example 2

Given: Same conditions as in Example 1.

Find: If the weapon were burst at a height of 1,950 feet above the surface, what fallout contour would be represented by the 100 r/hr surface-burst contour solved for in Example 1?

Solution: From Fig. 4–94, the adjustment factor for a 600-KT burst at a height of 1,950 feet is about 0.04, and the contour solved for in Example 1 corresponds for this burst condition to $0.04 \times 100 = 4$ r/hr at $H+1$ hour.

(d) Reliability

The sensitive wind-dependence of the fallout distribution mechanism, and the degree to

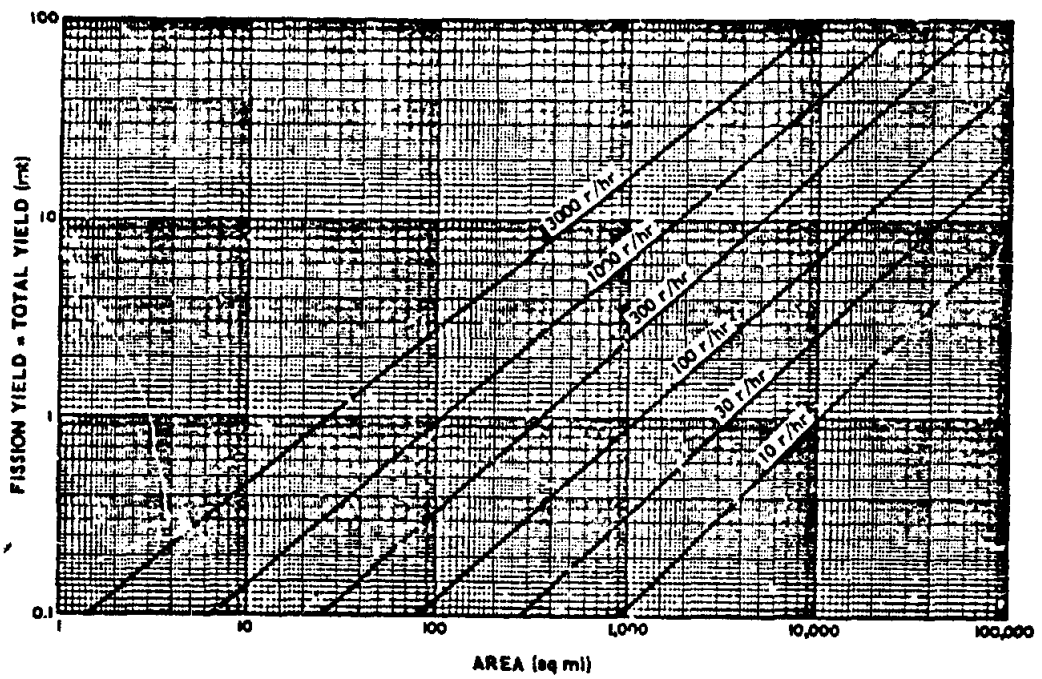

Figure 4–89 (C). Land-Surface Burst Dose-Rate Contour Areas at a Reference Time of One Hour After Burst, Megaton Yields (U)

TABLE 4–16 (C). CONTOUR PARAMETERS FOR DOSE RATE OF 100 R/H (U)

Parameter	Source Figure	Basic Value	Wind Factor	Parameter Value for 10-Knot Wind
Area	4–89	190 sq mi	1.0	190 sq mi
Downwind distance	4–90	38 mi	0.9	34 mi
Crosswind distance	4–91	6.7 mi	1/0.9	7.4 mi
Diameter of ground zero circle	4–92	4.5 mi	1.0	4.5 mi
Downwind displacement of ground zero circle	4–93	0.8 mi	0.9	0.7 mi

which wind and other meteorological conditions affect these contour parameters, cannot be over-emphasized. The contours presented in these curves have been idealized in order to make it possible to present average, representative values for planning purposes. Recognizing these limitations, for average fair-weather conditions, the curves can be considered reliable within ±50 per cent.

(3) *Water Surface Burst*

Although detailed experimental confirmation is lacking, it is expected that there will be some difference in the character and distribution of residual radioactive contamination between a water-surface and a land-surface detonation. For a surface burst over water deep enough that particulate matter from the bottom is not carried aloft in the nuclear cloud and stem, it is expected that the contaminant is distributed as a very fine mist. As a result, the lower dose-rate contours are expected to be larger and the higher dose-rate contours smaller than for a corresponding burst over a land surface. There is also a somewhat greater probability that local meteorological conditions may cause condensation and rain-out of portions of this mist, resulting in localized hot spots, the prediction of which would be a nearly impossible task. However, the total activity available for a given weapon burst under the two conditions is the same, and there are indications from limited test experience that the extent of the contaminated areas will be about the same as for land-surface bursts. The contour parameters given in Figs. 4–89 through 4–94 for land-surface bursts may also be used for water-surface bursts, to obtain dose rates over adjacent land masses.

For the case of a burst over water so shallow that a significant portion of the contaminant is entrained in mud and particulate matter from the bottom, and is carried aloft, localization of the fallout may be expected to be greater than for the deep water case, with high dose-rate contours of increased size close to the burst point, and low dose-rate contours of somewhat smaller size farther out. Quantitative estimates of contour parameters may be obtained from the land-surface burst curves (Figs. 4–89 through 4–94), with the reservation that the values for contours of 300 *r*/hour or greater, at $H+1$ hour, should be thought of as minimum values, while the values for contours of 100 *r*/hour or less, at $H+1$ hour, should be thought of as maximum values.

c. Burst in the Transition Zone

The deposition patterns and decay rate of the contamination from weapons detonated very close to the surface will be similar to those for a weapon of the same yield burst detonated on the surface. However, a smaller quantity of the available radiation activity will be deposited locally, resulting in lower dose-rate values along contours derived for surface-burst conditions. As the height of burst is increased, the activity deposited as local fall-out decreases, but the residual contamination due to neutron-

induced activity becomes an increasingly more important part of the total contamination.

The exact scaling of the fallout dose-rate contour values with height of burst is uncertain. Residual contamination from tests at heights of burst immediately above, or below, 100 $W^{1/3}$ feet has been small enough to permit approach to ground zero within the first 24 to 48 hours after detonation, without exceeding reasonable dosages. In these tests, the mass of the tower, special shielding, and other test equipment are considered to have contributed a considerable portion of the fallout actually experienced, and neutron-induced activity in the soil has furnished an added contribution to the total contamination.

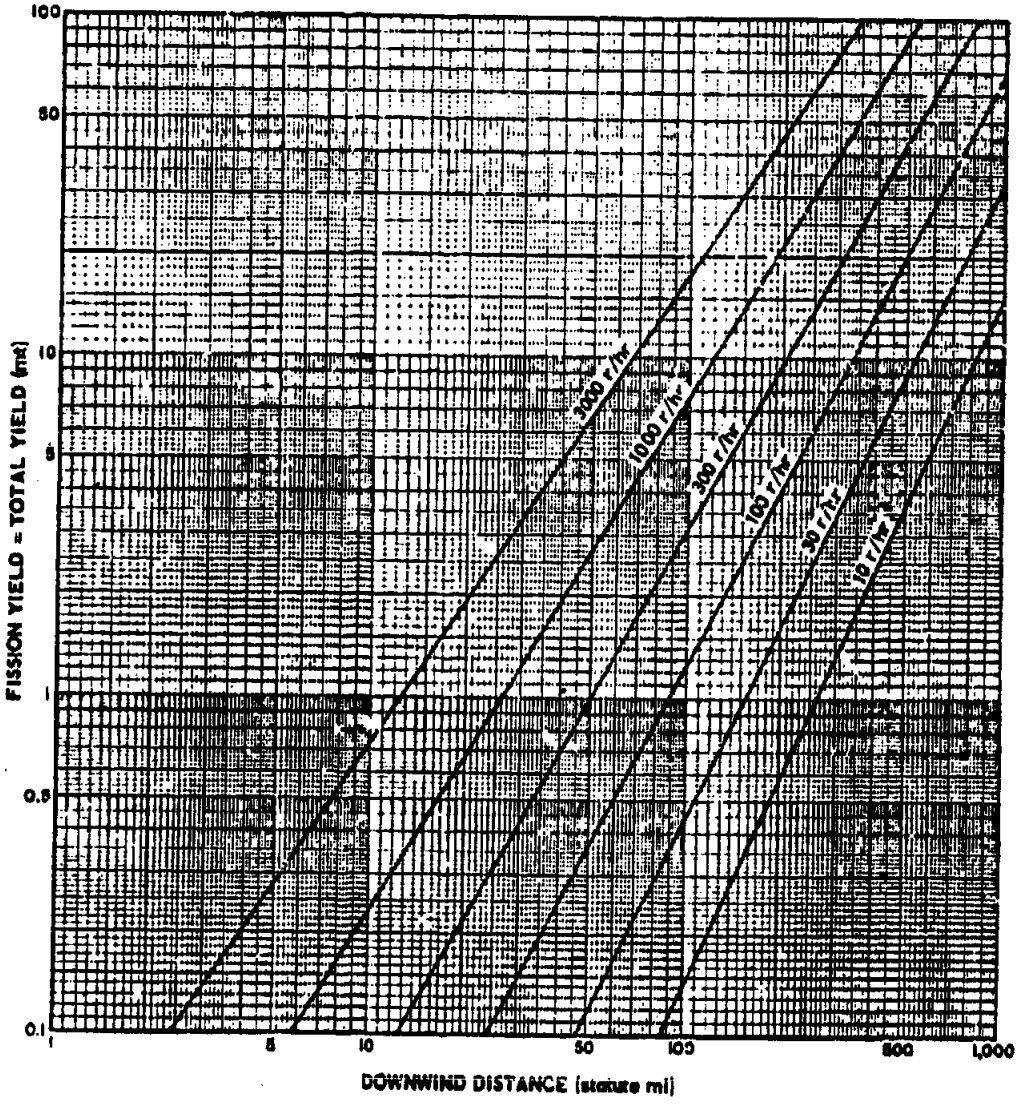

Figure 4–90 (C). Land-Surface Burst Dose-Rate Contour Downwind Distance, One-Hour Reference Time, 15-Knot Scaling Wind, Megaton Yields (U)

Thus, for yields less than 100 KT, and for heights of burst of 100 $W^{1/3}$ feet or greater, it is considered that fallout contamination will not be sufficiently extensive to affect military operations materially. This is not to say that there will never be a residual radiation problem under such conditions. The neutron-induced gamma activity can be very intense in a relatively small area around ground zero.

Due to the uncertainties in the scaling, it is unsafe to extrapolate the above conclusions to weapons having yields greater than 100 KT. In the absence of data, a conservative estimate may be obtained by using a height of burst of 180 $W^{0.4}$ feet as the point above which fallout ceases to be militarily significant. It should be noted again that the neutron-induced gamma

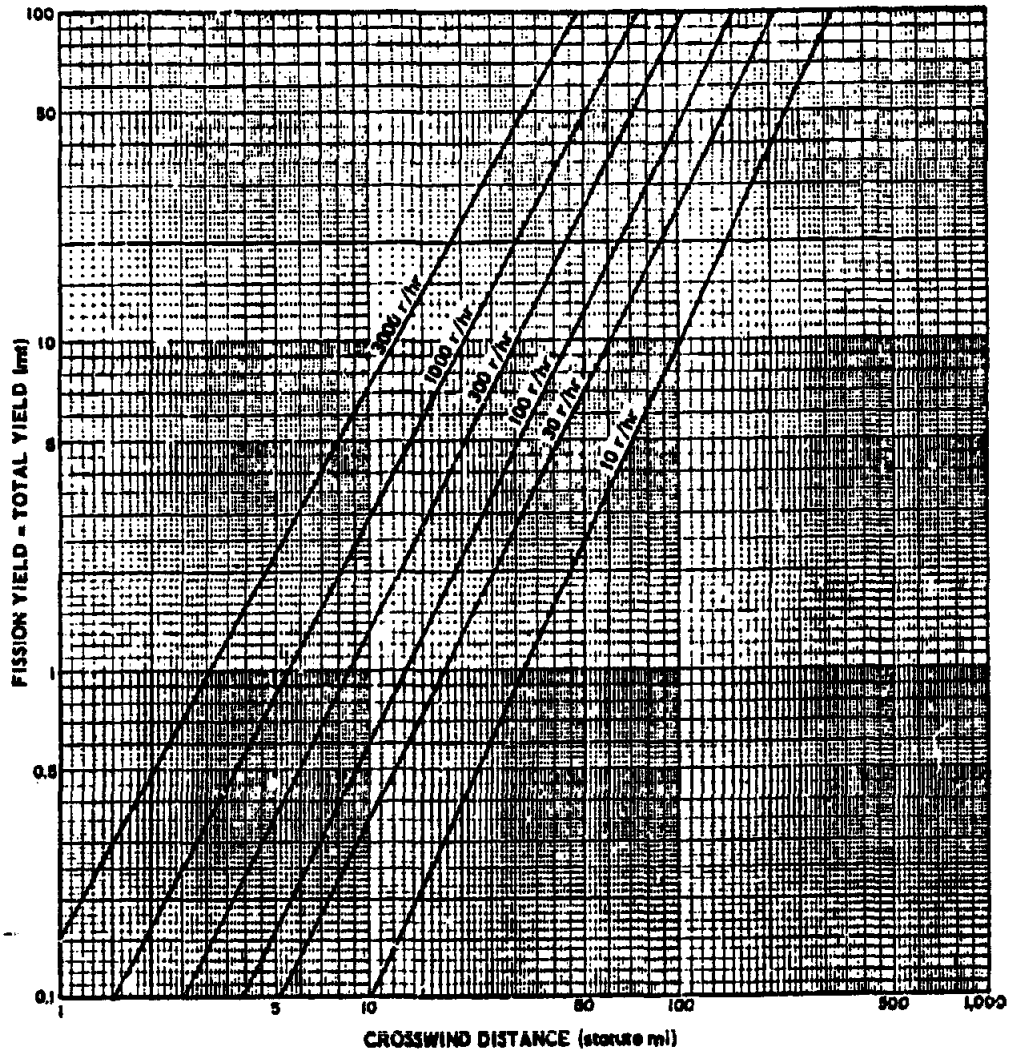

Figure 4–91 (C). Land-Surface Burst Dose-Rate Contour Crosswind Distance, One-Hour Reference Time, 15-Knot Scaling Wind, Megaton Yields (U)

activity may be intense for bursts above or below this height.

A rough estimate of the dose-rate contour values for bursts in the transition zone may be obtained by applying an adjustment factor from Fig. 4–76 to the dose-rate contour values obtained from Figs. 4–89 through 4–94. For bursts in the upper quarter of the fallout transition zone, neutron-induced activity must also be considered. For bursts in the lower three quarters of the transition zone, the neutron-induced gamma activity can generally be neglected when compared to the fallout activity.

d. Subsurface Burst

(1) Underground Burst

A large amount of residual contamination is

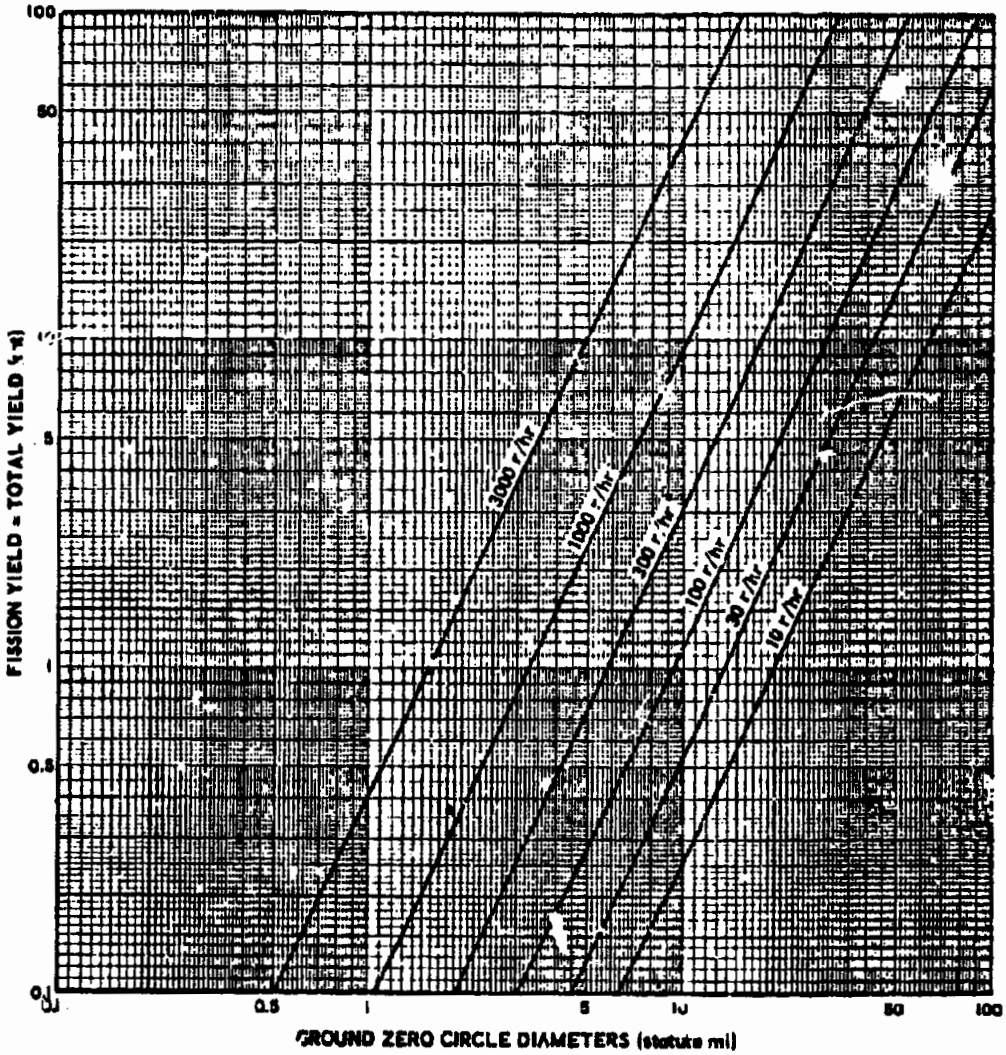

Figure 4–92 (C). Land-Surface Burst Dose-Rate Contour Ground-Zero Circle Diameters, One-Hour Reference Time, Megaton Yields (U)

deposited in the immediate vicinity of the burst point after an underground detonation, because the major portion of the radioactive material falls quickly from the column and cloud to the surface. A very shallow underground burst conforms rather closely to the contamination mechanisms and patterns outlined previously for land-surface bursts. As depth of burst is increased, however, a greater percentage of the total available contaminant is deposited as local fallout, until for the case of no surface venting, all of the contamination is contained in the volume of ruptured earth surrounding the point of detonation.

Families of curves exist for different ranges of weapon yield, depths of burst, reference

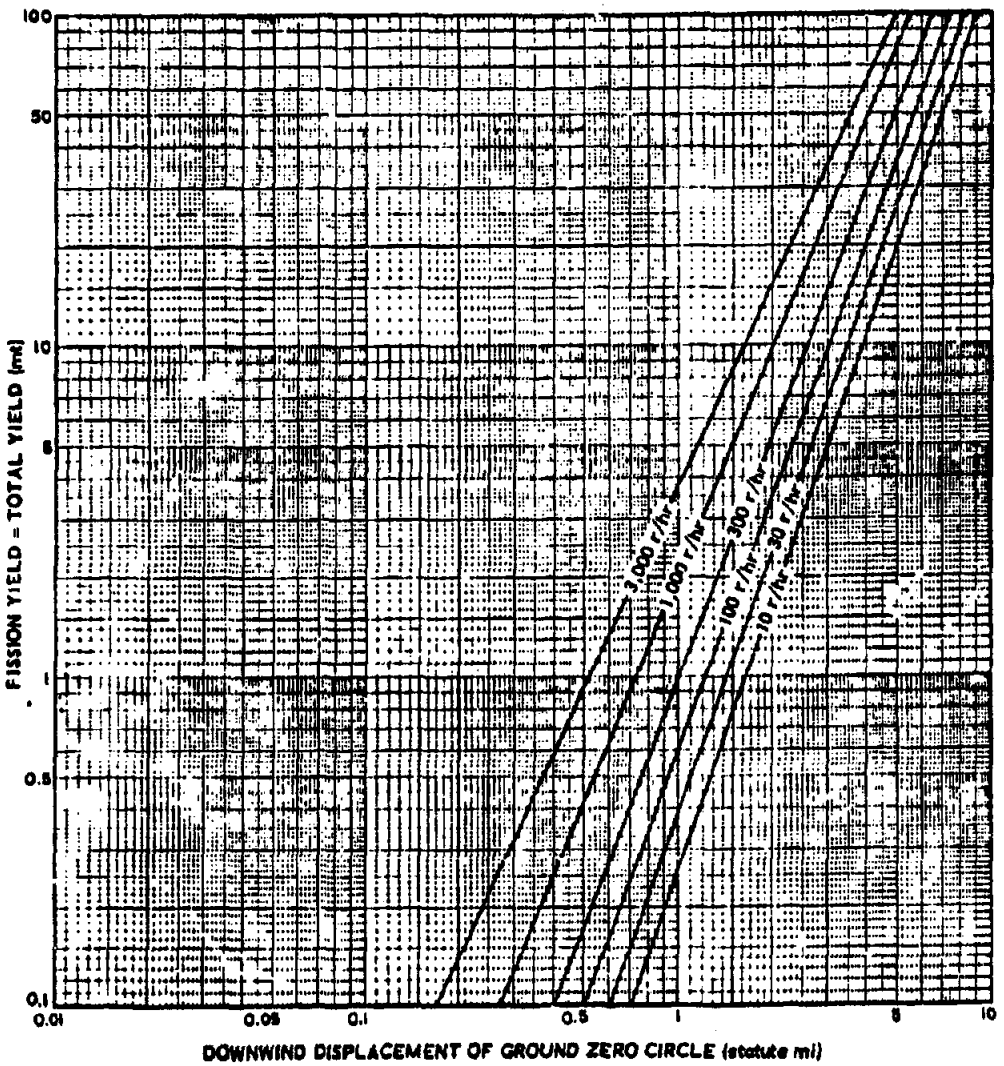

Figure 4–93 (C). Land-Surface Burst Downwind Displacement of Ground-Zero Circle for 15-Knot Scaling Wind, One-Hour Reference Time, Megaton Yields (U)

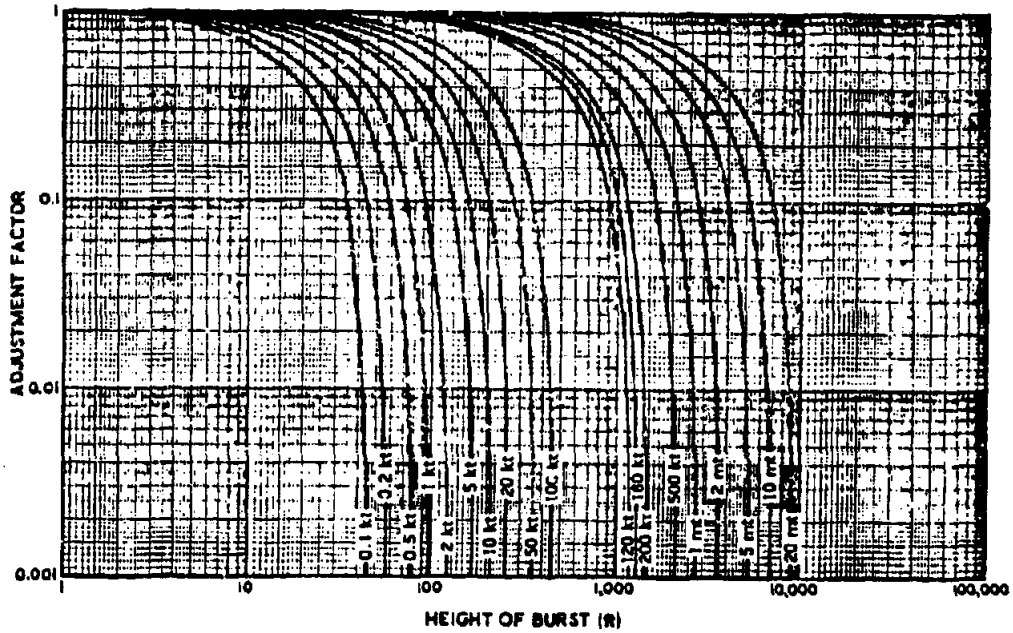

Figure 4–94 (C) Height-of-Burst Adjustment Factor for Dose-Rate Contour Values (U)

times, and wind conditions, by means of which idealized dose-rate contours can be drawn for underground weapon bursts. These curves are similar to those presented as representative of land-surface dose-rate contour parameters (Figs. 4–89 through 4–94).

As the depth of burst becomes greater, the contour shapes depart from the idealized pattern, and, particularly in the case of the higher dose-rate contours, tend to become more nearly circular. For depths of burst greater than 70 $W^{1/3}$ feet, virtually all of the available contamination comes down in the vicinity of the burst point. As burst depth is increased, contours can be expected to decrease in size, with increase in dose-rate values in and near the crater.

(2) Underwater Burst

One test at mid-depth in 150 feet of water provided some information on the residual radiation from an underwater detonation. The rather specialized burst conditions make application of the results to specific cases of interest of doubtful validity; however, certain guidelines were established, which are applicable and useful in the general case. It was shown that on a ship subjected to fallout radiation, much of the contaminated fallout material drained off the ship into the water, and rapidly became relatively ineffective because of the diluting effect of the water.

For land areas adjacent to the explosion, and at the same relative position as the ship, residual radiation dose rates about four times as great as on board ship are expected soon after completion of fallout, because dilution and runoff do not occur. For adjacent land areas, the decrease in dose rate with time can be calculated from Fig. 4–82; however, this cannot be done for ships. As in the case of other types of contaminating bursts, the area of contamination varies considerably with meteorological conditions, particularly with wind.

In the case of a nuclear explosion in a comparatively shallow harbor, as in the hold of a ship, more than half of the available radioactivity associated with the device is deposited as local fallout, and large, localized, high dose-rate

contours are expected on the adjacent land masses. Although it does not appear feasible on the basis of available information to attempt a detailed delineation of contour shapes for a harbor burst, magnitudes of expected contour areas can be given with some confidence. Fig. 4–95 indicates expected harbor burst contour areas on adjacent land masses for yields from 1 KT to 1 MT. For yields in the megaton range, contour areas should be estimated from the surface burst curves already presented (Fig. 4–89). To estimate dose rates on the weather decks of anchored ships in a harbor divide the given land-mass values by four; and for ships alongside a wharf, divide the land-mass values by two.

(3) Instructions for Using Fig. 4–95, Harbor Burst Dose-Rate Contour Areas

(a) Description

Fig. 4–95 presents dose-rate contour areas to be expected over adjacent land masses at 1 hour after burst time, resulting from residual radiation from shallow-harbor bursts of nuclear weapons with yields from 1 KT to 1 MT Assumptions for this purpose are a harbor depth of 30 to 80 feet of water, a mud bottom, and burst depth a few feet below the water surface, such as in the hold of a ship. The areas given may be assumed to be independent of wind, although specific location of the contaminated areas with respect to the burst point is a sensitive function of wind and other meteorological conditions, as with other types of contaminating bursts. Area magnitudes may be read directly from the curves for those dose-rate values for which curves are provided. Extrapolation to higher or lower dose-rate contour values than covered by the curves cannot be done accurately, and should not be attempted. To obtain dose-rate values for times other than $H+1$ hour, multiplying factors from Fig. 4–82 should be used.

(b) Example

Given: A 30-KT harbor burst.

Find: The area of effect for dose rates of 1,000 r/hr, or greater, at $H+1$ hour.

Solution: Reading directly from Fig. 4–95, the area for a dose rate of 1,000 r/hr or more at $H+1$ hour, for a 30-KT harbor burst, is 3.4 ($\pm$1.7) square miles.

(c) Reliability

Area magnitudes obtained from these curves for a specific yield are considered reliable within $\pm$50 per cent, for the burst conditions indicated.

e. Ground Zero Dose Rates

The residual dose rate curves presented herein make no provision for contours delineating dose rates greater than 3,000 roentgens per hour, except in the case of harbor bursts. Such dose rates occur in hot spots, rather than over significant areas. The maximum, residual-radiation, dose rates observed on the ground in such hot spots at a reference time of $H+1$ hour, regardless of weapon yield, have been more than 3,000 r/hour and less than 10,000 r/hour for surface burst nuclear weapons. The burst conditions for most of these shots were not truly representative of land shots; hence, there is a large degree of uncertainty regarding the maximum dose rates which may be expected at ground zero under true land-surface burst conditions. Higher dose rates may be expected only under certain special circumstances, such as deep underground bursts and bursts in shallow harbors, and are not normally expected for land-surface bursts.

f. Total Radiation Dose Received

(1) General

To estimate the dose actually received at a point within an area contaminated by fallout, the time of arrival of fallout at that point is estimated (using the scaling wind velocity and the distance from the burst point), and the curve of the dose rate is integrated as a function of time over the period the individual is within the area. The same procedure is used for the case of a person entering a contaminated area at some time after completion of fallout. Fig. 4–96 is presented to facilitate this computation, and can be used to estimate total radiation dose received while in a contaminated area. If, at the time of the explosion, the individual is within the radius of effect of the initial radiation, the acute dose so received must be added to the cumulative residual radiation

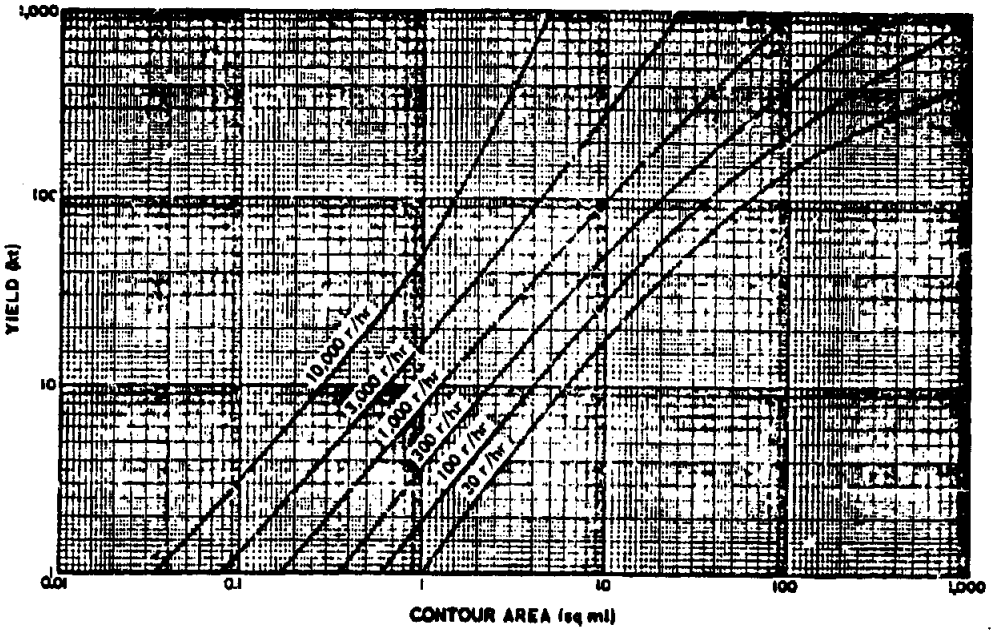

Figure 4–95 (C). Harbor Burst Dose-Rate Contour Areas, Assuming Shallow Water (30 to 50 Feet) Over Clay Bottom, at One-Hour Reference Time (U)

dose, thus giving the total dose received. If the individual is sheltered, the free field value so obtained should be multiplied by a reduction factor, estimated from the degree of shielding involved, as described in Par. 4–8.5.5, following.

(2) Instructions for Using Fig. 4–96, Total Radiation Dose Received in a Contaminated Area

(a) Description

From Fig. 4–96 can be obtained the total dose received by personnel entering a given contaminated area, at a specified time, and remaining for a specified interval of time. The vertical axis gives the accumulated dose for each unit (*r*/hr) of dose rate, at one hour after the detonation. The various curves represent times-of-stay in the contaminated area. To determine the accumulated dose, a factor corresponding to the time of entry and the time of stay is taken from the vertical axis. The product of this factor and the dose rate at one hour gives the accumulated dose.

(b) Example

Given: The dose rate in a given area at one hour after detonation is 500 *r*/hr.

Find: The total dose received by a man entering the area two hours after detonation and remaining 4 hours.

Solution: From Fig. 4–96, the intersection of the line for a time of entry of two hours after detonation with the 4-hour curve gives a factor of 0.80. Therefore, the accumulated dose is

$$500 \times 0.80 = 400 \text{ } r.$$

g. Dose Contours

(1) General

Approximate total dose contours, for accumulated doses received during the 48 hours immediately following burst time, can be estimated using the appropriate 1-hour, dose-rate contour curves in conjunction with a scaling factor obtained from Fig. 4–97. The scaling factor averages the time of arrival effect for 500-roentgen, total-dose contours using a 15-

knot scaling wind, and gives results sufficiently accurate for planning purposes over a range of doses from 100 *r* to 1,000 *r*. This method may be used with somewhat less accuracy for accumulated doses outside this range. It should be recognized that dose contours and dose-rate contours do not have the same shape, although the shapes are sufficiently alike to make this approximate method useful.

(2) Instructions for Using Fig. 4–97, 48-Hour Dose Scaling Factor

(a) Description

Fig. 4–97 gives scaling factors for weapon yields from 0.1 KT to 100 MT, by means of which approximate contours can be obtained for residual gamma-radiation doses accumulated during the 40 hours immediately following burst time. Given a 1-hour dose-rate contour, the dose-rate value is multiplied by the appropriate scaling factor from this curve. This gives the approximate total-dose value received, over the 48-hour period following the burst, by personnel in the open within that contour. If a particular 48-hour dose contour is to be constructed, the desired 48-hour dose value should be divided by the scaling factor obtained from Fig. 4–97, to obtain a preliminary dose-rate value.

For a surface burst, this value may be used with Figs. 4–89 through 4–93, to obtain the desired contour dimensions for the 1-hour dose rate resulting in the desired 48-hour dose value. For a burst in the transition zone, divide the preliminary dose-rate value by the appropriate height-of-burst adjustment factor obtained from Fig. 4–94 before using Figs. 4–89 through 4–93 to obtain the desired contour parameters for the necessary 1-hour dose rate.

If the fission yield is less than the total yield, the values (for each burst condition) that would have been used with Figs. 4–89 through 4–93 are not used as such, but are further divided by the fission-yield to total-yield ratio. This will give the actual value to be used with the appropriate figure.

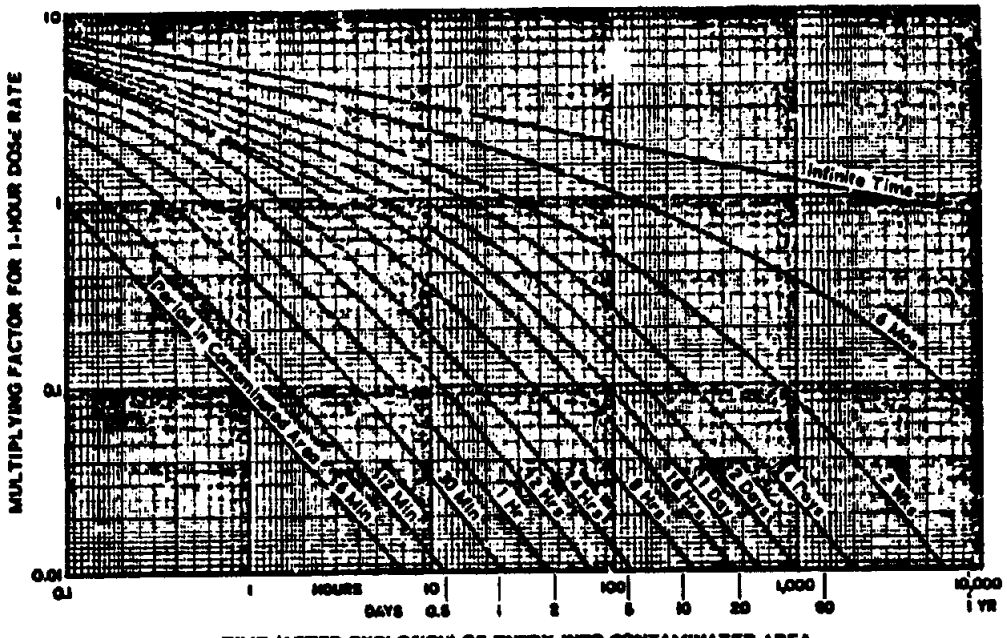

TIME (AFTER EXPLOSION) OF ENTRY INTO CONTAMINATED AREA

Figure 4–96 (C). Total Radiation Dose Received in Contaminated Area (U)

(b) Example

Given: A 400-KT surface burst under 15-knot scaling wind conditions.

Find: Approximate contour parameters for a total dose of 500 roentgens, accumulated up to 48 hours after burst time.

Solution: From Fig. 4–97, the scaling factor for a 400-KT weapon is 2.0. Hence, the dose-rate contour at $H+1$ hour is $\frac{500}{2.0}=250$ r/hr. This approximates the 48-hour total-dose contour for 500 r, and it is used with Figs. 4–89 through 4–93. The approximate total-dose contour parameters for 500 roentgens accumulated

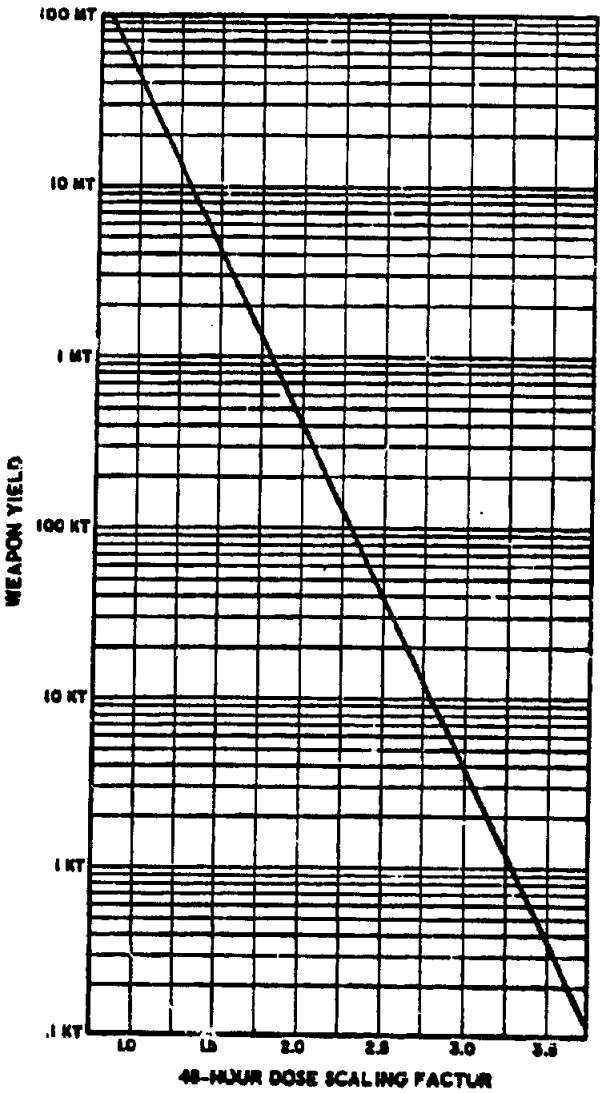

Figure 4–97 (C). 48-Hour Dose Scaling Factor vs Weapon Yield (U)

TABLE 4–17 (C). APPROXIMATE CONTOUR PARAMETERS FOR 48-HR TOTAL DOSE OF 500 R (U)

Parameter	Source Figure	Parameter Value
Area	4–89	160 sq mi
Downwind distance	4–90	34 mi
Crosswind distance	4–91	6 mi
Diameter of ground zero circle	4–92	4 mi
Downwind displacement of ground zero circle	4–93	0.7 mi

during the 48 hours following the burst are given in Table 4–17.

(c) Reliability

Recognizing the idealized nature of the basic contours, total-dose contours obtained in the manner described above are considered reliable within a factor of two, for doses between 100 *r* and 1,000 *r* and for scaling winds up to about 15 knots. The method may be applied for other dose conditions with somewhat less confidence in the results, but should not be applied for scaling wind conditions significantly greater than 15 knots.

4–8.5.5. (C) *Shielding from Residual Radiation*

(U) In their passage through matter, alpha particles produce a considerable amount of ionization, and in doing so rapidly lose their own energy. An alpha particle is identical with the nucleus of a helium atom. After traveling a certain distance (range) the particle, which has then lost most of its energy, captures two electrons and reverts to a harmless helium atom. The range of an alpha particle depends upon the initial energy, but even those particles of relatively high energy have an average range in air of just over 1-1/2 inches. In more dense media, such as water, the range is about one-thousandth of the range in air. Consequently, alpha particles are unable to penetrate even the outer layer of the skin. Therefore, as far as attenuation is concerned, they do not constitute a radiation problem.

(U) Beta particles, like alpha particles, cause direct ionization. The beta particles dissipate their energy much more slowly, however, and correspondingly have a much greater range. Although beta particles traverse an average distance of 10 feet in air, due to constant deflections their effective range is considerably less. In more dense media, the range is still shorter, approximately one-thousandth of that in air. Even clothing provides substantial protection from beta radiation. Consequently, unless the particles are deposited directly on the skin, beta radiation provides little radiation hazard.

(U) The residual gamma radiations present a different situation. These gamma rays, like those which form part of the initial nuclear radiation, can penetrate a considerable distance through air and into the body. If injury is to be minimized, definite action must be taken to provide adequate shielding from residual gamma radiations. As a matter of consequence, any method used to decrease the gamma radiation will provide almost complete protection from alpha and beta particles.

(U) The absorption of residual gamma radiation is based upon exactly the same principles as those discussed in connection with the initial gamma radiation (Par. 4–8.4.2., preceding). However, except for the earliest stages of decay, the residual gamma rays have much less kinetic energy than those emitted in the first minute after the explosion (0.7 Mev for residual compared to 4.5 Mev initial average energies). Therefore, as compared with the initial radiation shielding requirements, a smaller thickness of a given material will produce the same degree of attenuation.

(U) The approximate half-value layer thicknesses of some common shielding materials for residual gamma radiation are presented in Table 4–18. As in the case of the initial gamma radiation, the product of the density and the half-value thickness is approximately the same in all cases. However, since the half-value thickness is smaller for residual gamma radiation, the product is lower also.

TABLE 4–18. APPROXIMATE HALF-VALUE LAYER THICKNESSES OF MATERIALS FOR SHIELDING AGAINST GAMMA RAYS FROM FISSION PRODUCTS

Material	Density (lb/cu ft)	Half-Value Thickness (in.)	Product
Steel	400	0.7	343
Concrete	144	2.2	317
Earth	100	3.3	330
Water	62.4	4.8	300
Wood	34	8.8	300

(U) For additional illustration of attenuation factors, Fig. 4–98 and Table 4–19 are provided. The attenuation factors for steel, concrete, soil, earth, wood, and lead are presented in Fig. 4–98 as a function of various thicknesses of these materials. From the practical standpoint, it is of interest to record the transmission factors (attenuation factor $^{-1}$) offered by various structures and mechanisms. Approximate values for these are given in Table 4–19. These have been estimated partly from calculations and partly on the basis of actual field measurements.

TABLE 4–19 (C). DOSE TRANSMISSION FACTORS (INTERIOR DOSE/EXTERIOR DOSE) (U)

Item	Gamma Rays		Neutrons
	Initial	Residual	
Foxhole	0.05 –0.10	0.02 –0.10	0.3
Underground position (3 feet)	0.04 –0.05	0.0002	0.002–0.01
Built-up city area (in open)		0.7	
Frame house	0.9	0.3 –0.6	0.9 –1.0
Basement	0.05 –0.5	0.05 –0.10	0.1 –0.3
Multistory building:			
Upper portion	0.9	0.01	0.9 –1.0
Lower portion	0.3 –0.6	0.1	0.9 –1.0
Blockhouse walls:			
9 in. thick	0.1	0.05	0.3 –0.5
12 in. thick	0.05 –0.09	0.01 –0.02	0.2 –0.4
24 in. thick	0.01 –0.03	0.001 –0.002	0.1 –0.2
Factory, 200 x 200 feet		0.10 –0.20	
Shelter, partly above grade:			
With earth cover (2 ft)	0.02 –0.04	0.005 –0.02	0.02 –0.08
With earth cover (3 ft)	0.01 –0.02	0.001 –0.005	0.01 –0.05
Rough terrain		0.6	
Grader, road, motorized, D12	1.0	0.50	1.0

TABLE 4-19 (C). (cont)

Item	Gamma Rays		Neutrons
	Initial	Residual	
Tanks M-24, M-41; Tank recov. vehicles M-51, M-74	0.1 -0.2	0.06	0.1 -0.3
Tanks M-26, M-47, M-48, T-43E1; Eng. armd. vehicle T-39E2	0.05	0.02	0.55
Tractor, crawler, D8 w/blade	1.0	0.40	1.0
1/4-ton truck	1.0	0.75	1.0
3/4-ton truck	1.0	0.65	1.0
2-1/2-ton truck	1.0	0.5 -0.6	1.0
Personnel carrier, T18E1		0.1 -0.26	1.0
Armd. inf. vehicle M-59, M-75 and SP Twin 40-mm gun M-42	0.2 -0.5	0.1	0.2 -0.5
SP 105-mm howitzer M-37	0.4 -0.6	0.1	0.8 -1.0
Multiple cal. .50 mg motor carriage M-16	0.8 -1.0	0.6	0.9 -1.0
LVT (landing vehicle tracked)	0.5 -0.9		1.0
Battleships and large carriers:			
15% of crew	1.0	1.0	0.8 -1.0
25% of crew	0.2	0.1	0.2 -0.8
10% of crew	0.05	0.03	0.05 -0.2
50% of crew	0.0005-0.005	0.0003-0.003	0.001-0.05
Cruisers and carriers:			
10% of crew	1.0	1.0	0.8 -1.0
20% of crew	0.5	0.3	0.4 -0.8
30% of crew	0.1 -0.3	0.1	0.1 -0.4
40% of crew	0.005 -0.1	0.003 -0.05	0.01 -0.1
Aircraft	1.0		1.0
Destroyers, transports, and escort carriers:			
10% of crew	1.0	1.0	0.8 -1.0
20% of crew	0.7	0.5	0.6 -0.8
30% of crew	0.4	0.2	0.3 -0.6
40% of crew	0.1 -0.4	0.1	0.1 -0.3

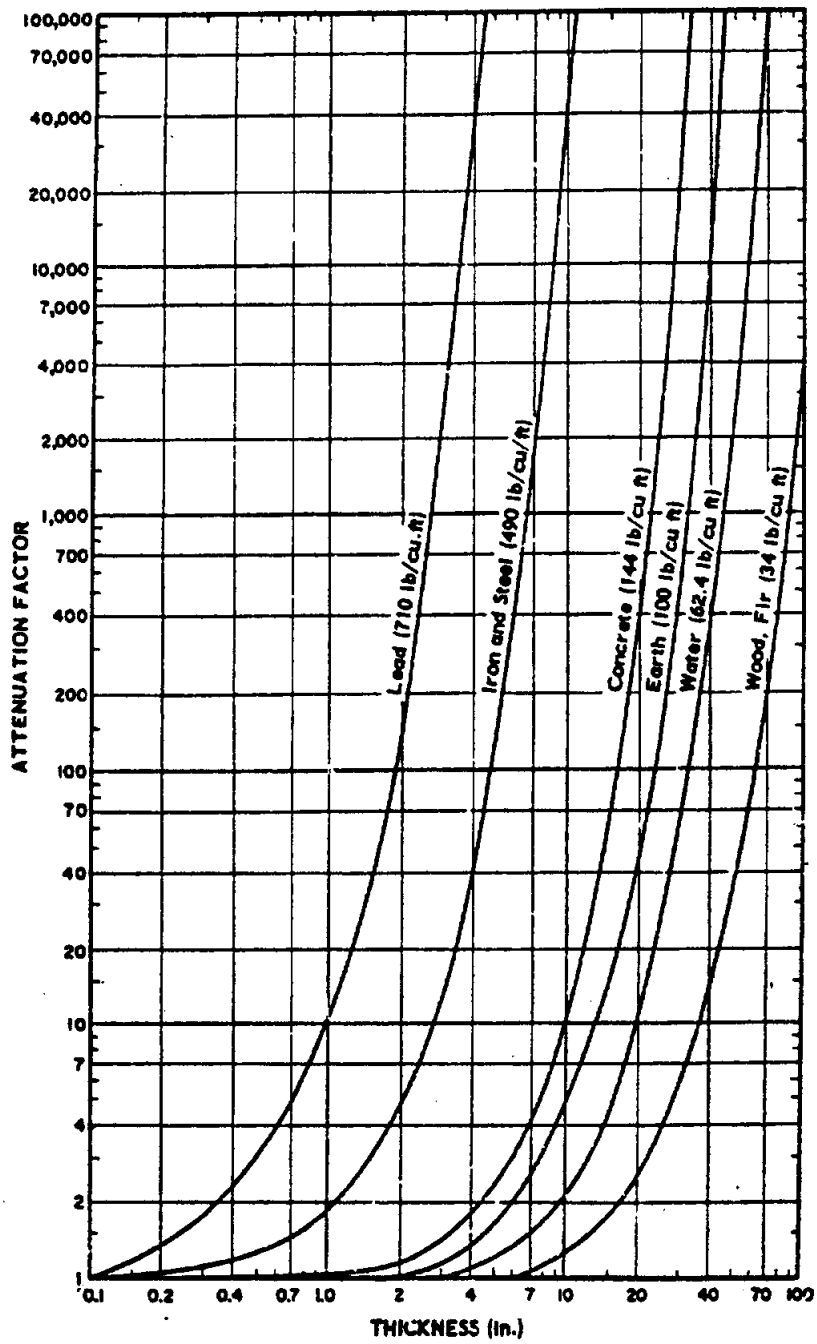

Figure 4–98. Attenuation of Residual Fission Product Radiation

Section III (S)—Basic Fragmentation and Penetration Data

4–9. (U) INTRODUCTION

4–9.1. Scope of the Section

This section presents the analytical and experimental techniques for obtaining terminal ballistic data concerning the physical processes of fragmentation and the mechanisms of penetration and perforation. Included in the section are a description of fragment density and mass distribution, a discussion of the techniques for analyzing and/or measuring the fragment initial velocity and velocity decay, a description of mechanisms of penetration and perforation by single fragments, and a discussion of the theoretical and experimental aspects of fragment performance in the hypervelocity speed regime.

The literature of this subject is somewhat inconsistent with respect to the symbols and units of measurement used by the various authors. No attempt has been made to standardize these items; quoted reference material is presented in the notation and units of the particular author.

4–9.2. Description of Fragmentation

Fragmentation is an important phenomenon associated with artillery shells, warheads, aerial bombs, mortar shells, grenades, etc. The shell or bomb is basically a high explosive charge contained within a metal casing. The forces released by the detonation of the high explosive break up the casing into fragments. It is desirable to be able to predict the mass distribution, spatial distribution, and velocity characteristics of these fragments so that the effect can be optimized for the intended target. When no provisions are made to control the size of the fragments, irregular shapes and various sizes are obtained.

The problem of uncontrolled fragmentation is to predict the mass distribution of the fragments. This is treated in Par. 4–10.2, following. There are several methods of controlling the size and shape of fragments into which a casing will break. The problem, here, is to select the best method of control. Controlled fragmentation is treated in Par. 4–10.3, following. Methods of predicting other fragment characteristics, such as velocity and direction of projection, hold for natural or controlled fragmentation, and may be treated independently.

4–9.3. Cross-Reference Information

The general discussion of the mechanisms of fragmentation is presented in Ch. 2, Sec. I. Comparable information on solid projectiles and shaped charges is given in Ch. 2, Secs. II and III, respectively. These sections should be read for introductory purposes. In Ch. 3 each of the various sections includes appropriate information on the vulnerability of specific types of targets to fragmentation and penetration. Reference should also be made to Part Two for information on the collection and analysis of fragmentation and penetration data as applied to specific types of targets.

4–10. (C) FRAGMENT MASS AND SPATIAL DISTRIBUTION

4–10.1. (U) Introduction

This paragraph presents the general laws of natural (uncontrolled) fragmentation and the usual methods for controlled fragmentation. A discussion is presented relating the dynamic fragment distribution to the static distribution and the procedure for obtaining desired results. Experimental techniques for the measurement and reduction of data are given in considerable detail.

4–10.2. (C) Mass Distribution, Natural Fragmentation

4–10.2.1. (C) General

(U) Natural fragmentation of a bomb or shell casing results when no special design features are incorporated to control the fragment size. Some predetermination of the fragment mass distribution can, however, be made by selection of charge-to-metal ratio, casing material, and thickness of casing. Thin casings fragment in two dimensions, whereas thick casings fragment in both two and three dimensions.

(U) The damage that will be produced by a fragment, impacting with a given velocity, depends on the mass and presented area of the fragment. In order to compare the fragmentation efficiencies of different projectiles, it is therefore necessary to know, for each projectile, the approximate mass and area distribution of all the fragments large enough to produce damage.

(C) Mott and Linfoot (Ref. 56) present a theory on the mass and mass distribution of fragments from an exploding warhead. The theory given is applicable only to casings which expand plastically before rupture.

(C) At the moment of rupture, the kinetic energy of the casing per unit length, referred to the axis moving with the casing, is

$$KE = \frac{1}{24} t_r V^2 \rho \frac{a^3}{r^2} \qquad (4\text{–}104)$$

where

ρ = mass density of the material, in slugs/cu in.,

a = distance between cracks, in inches,

r = radius of the shell casing at rupture, in inches,

KE = kinetic energy, in ft-lb/in. fragment length,

t_r = thickness at rupture, in inches,

and

V = outward velocity at rupture, in ft/sec.

(C) If W is the energy per unit area required to form a crack, the energy required per unit length will be Wt_r. Thus, no fragment will be formed with a width a greater than that given by equating Wt_r to KE, as defined by Eq. 4–104, or

$$a = \left[\frac{24 r^2 W}{\rho V^2}\right]^{1/3}. \qquad (4\text{–}105)$$

(C) W is known from the results of impact tests; it ranges from 70 to 800 foot-pounds per square inch. The lower value, 70 foot-pounds per square inch, is normally used. In a later report (Ref. 57), Mott concluded that the ratio of length-to-breadth of fragments is constant, and is approximately 3.5/1 for steel.

(C) For a bomb which is roughly spherical at the moment of rupture, the mean mass of a fragment is

$$\rho^{1/3} r^{4/3} W^{2/3} V^{-4/3} t_r.$$

(C) If r_e and t_e refer to the bomb before expansion, and if r, the radius at the moment of burst, is equal to er_e, then $t_r = t_e/e^3$, so that the mean fragment mass is proportional to

$$\frac{r_e^{4/3} \rho^{1/3} t_e W^{2/3}}{V^{4/3} e^{2/3}}.$$

(C) If the charge is kept constant and the thickness t_e is varied, V^2 will be proportional to $1/t_e$ for heavy casings; thus, the average mass of fragment is proportional to $t_e^{5/3}$ if t_r is constant. Theoretically, a scaling law can be applied from one test to another to predict the average fragment mass, by varying t_e and keeping the other parameters the same. Actually, however, thick-walled shells expand further than thin ones before breaking up, and a less rapid variation with t_e is expected.

(C) For the two-dimensional breakup of a shell, Mott (Ref. 56) postulates that the mass distribution of fragments can be stated as:

$$N(m) = Ce^{-\left(\frac{m}{\mu}\right)^{1/2}} \qquad (4\text{–}106)$$

where

$$\mu^{1/2} = Kt_e^{\frac{5}{6}} d_i^{1/2} \left(1 + \frac{t_e}{d_i}\right) \qquad (4\text{–}107)$$

in which $N(m)$ = total number of fragments of mass greater than m,

μ = related to average fragment mass, in grams,

C = constant,

K = constant dependent on explosive, for example: K = 0.30 (TNT); K = 0.325 (Amatol 50/50). Units of K are grams$^{1/2}$/inch$^{5/6}$,

In addition, t_e = casing thickness, in inches (initial),

and d_i = internal diameter of casing, in inches.

(C) If it is assured that two-dimensional

breakup holds down to the finest fragment, then

$$N(m) = \frac{M}{2\mu} e^{-\left(\frac{m}{\mu}\right)^{1/2}} \qquad (4\text{–}108)$$

where M = total mass of shell,

and 2μ = arithmetic average fragment mass.

(C) Noting that $M/2\mu$ represents the total number of fragments, N, Eq. 4–108, may be written

$$N(m) = N e^{-\left(\frac{m}{\mu}\right)^{1/2}}. \qquad (4\text{–}109)$$

(C) In the case of thick-walled shells, a three-dimensional analysis is required, due to the reduced effect of the casing thickness.

Then,

$$N(m) = N e^{-\left(\frac{m}{\mu'}\right)^{1/3}} \qquad (4\text{–}110)$$

and

$$\mu' = \mu t. \qquad (4\text{–}111)$$

(C) Figs. 4–99 and 4–100 show examples of the distribution of Eqs. 4–109 and 4–110 as a function of $m^{1/2}$ and $m^{1/3}$.

(C) Another expression for $\mu^{1/3}$ is given by Gurney and Sarmousakis (Ref. 59) for thin-walled shells, as

$$\mu^{1/3} = A \frac{t_c(d_i + t_c)}{d_i} \sqrt{1 + 1/2\left(\frac{C}{M}\right)} \qquad (4\text{–}112)$$

where t_c = casing thickness, in inches (initial),

d_i = internal diameter of casing, in inches,

and $\frac{C}{M}$ = mass of explosive charge and metal casing in the same units.

(C) The factor A will have a different value for each explosive filling. Values of the factor A are given in Table 4–20 for several shell and bomb explosive loadings. Additional values of factor A, as determined by the Naval Ordnance Laboratory (Ref. 60), are listed for cast and pressed explosives in Table 4–21.

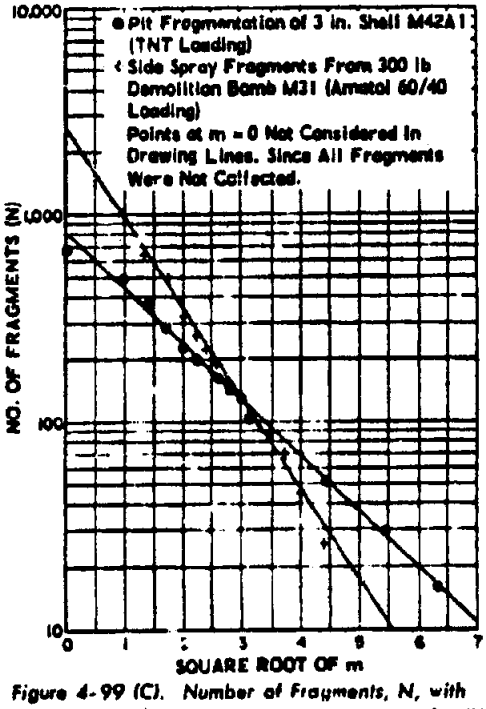

Figure 4-99 (C). Number of Fragments, N, with Masses Greater than m Grams vs Square Root of m (U)

4–10.2.2. (U) *Steel Casings*

In general, the average weight of fragments produced from a steel casing decreases as the

TABLE 4–20 (C). VALUES OF "A" FOR VARIOUS EXPLOSIVE LOADINGS (U)

Projectile	Loading	A (gm/cu in.)$^{1/3}$
Shell	TNT	1.7
Shell	Ednatol, Pentolite Tetrytol, RDX, Composition B	1.8
Bomb sidespray	Amatol (50/50 and 60/40)	0.9
Bomb sidespray	Ednatol, Torpex, RDX	0.6

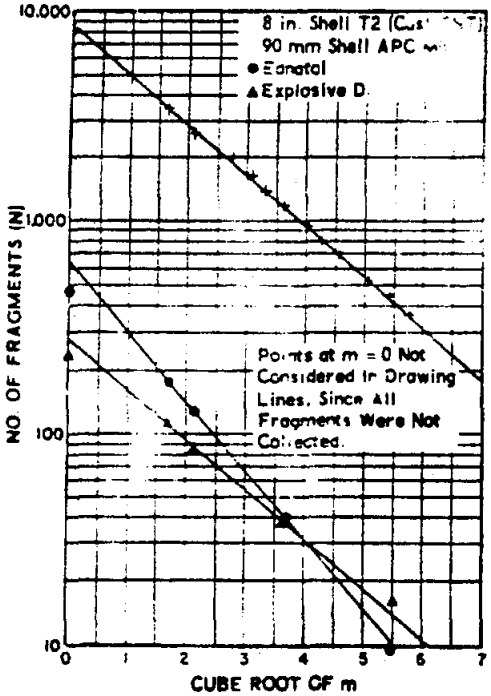

Figure 4–100 (C) Number of Fragments, N, with Masses Greater than m Grams vs Cube Root of m (U)

tensile strength of the steel is increased and the ductility is decreased (Ref. 61). This has been shown to be true in tests on carbon steels varying from 0.05 per cent to 1.06 per cent carbon. At 1.06 per cent carbon, it is believed that the different microstructure caused the test results to vary from the theory. Shapiro, et. al. (Ref. 60), lists scaling law constants for the Mott parameters derived from the mass distribution study of steel casings.

4–10.2.3. (C) *Ductile Cast Iron Casings*

From investigations on ductile cast iron casings (Ref. 62), it was found that the half weight (the particular fragment weight which divides the individual fragments into two groups, each containing half the total weight of fragments) appears to be on the order of 1/4 that of steel casings for ring type fragmentation, and on the order of 1/16 for cylindrical type fragmentation. Three grades of ductile cast iron were used in experiments. These showed little or no difference in fragmentation, notwithstanding a substantial difference in strength and ductility.

4–10.3. (C) Mass Distribution, Controlled Fragmentation

4–10.3.1. (U) *General*

The effectiveness of a fragmentation warhead against any target or targets for which

TABLE 4–21 (C). VALUES OF "A" FOR VARIOUS CAST AND PRESSED EXPLOSIVES (U)

Explosive (cast)	A (gm/cu in.)$^{1/3}$	Explosive (pressed)	A (gm/cu in.)$^{1/3}$
Baratol	2.55	BTNEN/Wax (90/10)	0.92
Comp B	2.14	BRNEU/Wax (90/10)	1.10
Cyclotol (75/25)	1.01	Comp A–3	1.13
H–6	1.34	MOX–2B	2.79
HBX–1	1.30	Pentolite (50/50)	1.27
HBX–3	1.65	RDX/Wax (95/5)	1.09
Pentolite (50/50)	1.27	RDX/Wax (85/15)	1.23
PTX–1	1.14	Tetryl	1.41
PTX–2	1.17	TNT	2.10
TNT	1.61		

it is used is largely determined by the size, number, and velocity of the fragments it produces. A warhead which will produce a predetermined number of fragments, of a predetermined weight and velocity, will be more effective against the target for which it is designed than will a naturally fragmented warhead.

Controlled fragmentation refers to control of the size, and consequently the weight, of each fragment. The size and weight of fragments produced by a controlled fragmentation warhead are determined by a combination of design factors within the basic method selected for producing the fragment. None of the methods employed in controlling fragments are completely successful; that is, they do not achieve 100 per cent fragmentatior control. Varying degrees of success have been achieved by the methods described in following paragraphs.

Considerations in the selection of the basic design approach include ease of manufacture, cost, size of warhead, size of fragment, and the intended use of the warhead.

4–10.3.2. (C) *Preformed Fragments*

(U) Preformed fragments are those which are molded, machined, or otherwise formed to the desired size, prior to detonation of the warhead in which they are used. Preformed fragments achieve nearly 100 per cent fragmentation control, because breakage upon expulsion, adhesion between fragments, and adhesion of fragments to other warhead parts are usually negligible.

(U) The principal objection to preformed fragments is the need for additional structure to support the fragments. The structure adds weight which contributes little to the effectiveness of the warhead. This additional weight decreases the number of fragments and/or the amount of explosive which can be placed in the warhead. However, in applications where the acceleration of the exploding device is low, such as in missile warheads or grenades, the supporting structure is light and preformed fragmentation is widely employed. In the artillery shell, which must withstand large accelerations in the gun, preformed fragmentation has never been used.

(U) One type of preformed fragment which has been investigated is the flechette, an arrow-shaped fragment (Ref. 63). The advantages of this type of fragment are its aerodynamic characteristics, which are far superior to those of cubes, spheres, or irregular fragments. The fin-stabilized fragment has greater range, higher remaining velocity (if it does not tumble), and greater penetrating power than its "chunky" counterparts at velocities under 3,000 fps. At velocities greater than 3,000 fps, however, the fin-stabilized fragment has greater cavitational effect. The difficulty in explosively launching fin-stabilized fragments from a warhead surface, without causing excessive damage to the fins of the individual projectiles, is the major problem encountered with this type of fragment.

(C) An additional problem is in finding a suitable method of holding the fragments in position prior to detonation, without hindering the launching and flight of the fragment. Experiments have been conducted with small scale warheads in which the fragments were launched from both the fin-forward and the fin-backward positions. A projectile pack which was tried in a limited experimental program is shown in Figure 4–101. The fragments were imbedded in a polyester resin matrix and backed up with an aluminum plate and a rubber buffer. Composition D explosive was used. These limited experimental results indicate that the fragments may be launched most effectively from a point forward position, and that they can be launched at velocities of 1,800 fps without damage.

(C) One widely used type of preformed fragment warhead is loaded with cubical steel fragments. Tests have been conducted on a warhead of this type (Ref. 64) in which the fragments were bonded to a thin steel shell which surrounded an annular-shaped explosive charge. The major problem was to obtain a method of bonding the fragments to the shell that provided individual launching of the fragments and 100 per cent controlled fragmentation. The tests indicated that soldering was the

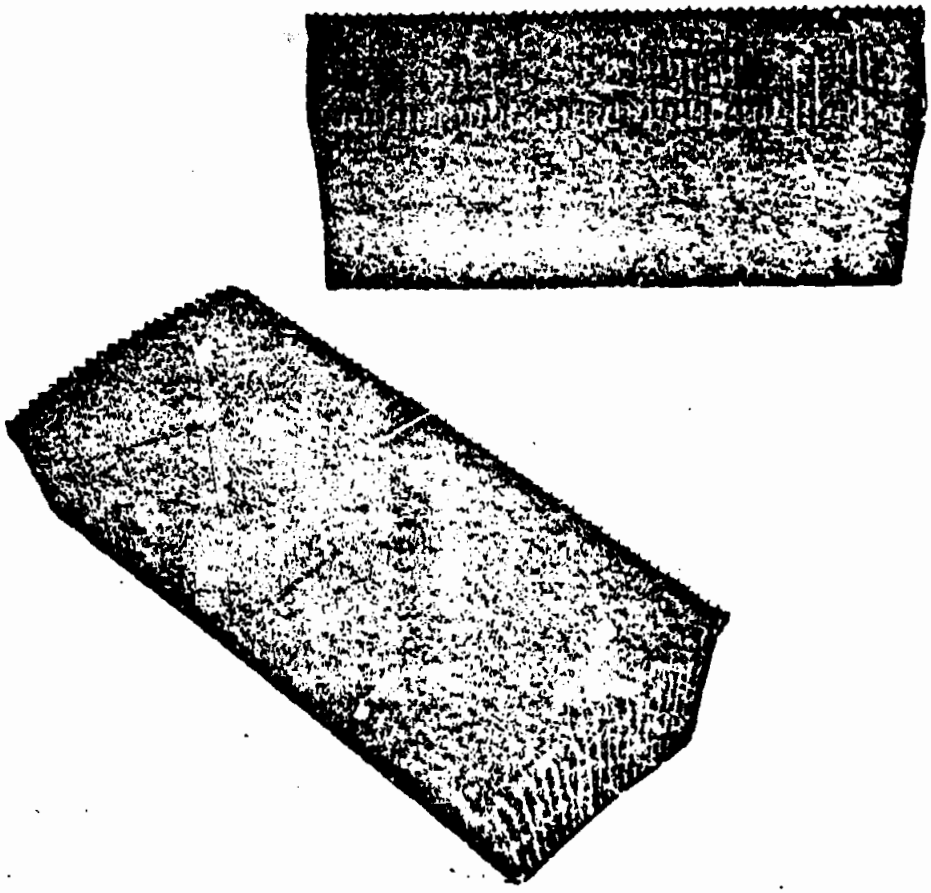

Figure 4-101 (C). Flechette Projectile Pack for Model Warhead (U)

most effective method for eliminating fragment break-up and for achieving fragment separation.

(U) The principle disadvantage in producing a warhead of the preformed fragment type is the high cost encountered in manufacturing and assembly.

4-16.3.3. (C) *Notched Rings*

This method of forming fragments consists of assembling a series of notched (grooved) rings so that each ring forms a section of the warhead casing, perpendicular to the axis of symmetry. The thickness and width of the rings provide control of two dimensions of the fragments, while notches along the circumference of the ring provide lines of least resistance, where breakage in the third plane occurs. Tests have been conducted on various size warheads with different weights of fragments, materials, and numbers of grooves (Ref. 65). A typical warhead of this type is shown in Fig. 4-102. The conclusions reached in these tests were that satisfactory uniformity of fragment weights can be secured, using the following principles:

1. The width and thickness of the ring should be equal.

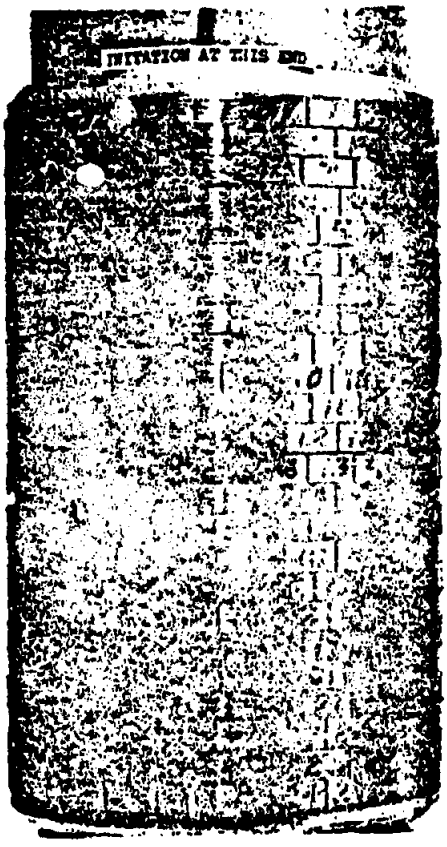

Figure 4–102. Notched Ring Warhead

2. The number of notches per ring for ductile steel should be determined by the formula $G = 456\ V/S$, where V = fragment velocity (ft/sec.), and S = tensile strength of the steel (psi).
3. The length-to-diameter ratio of the warhead should not be less than 1.25.
4. Medium carbon, low sulphur steel, Rockwell hardness B95 is desirable.
5. The notches should have sharp bottoms with a depth of 5 to 10 per cent of the ring thickness.
6. The ring should have a smooth finish.
7. A thin liner should be used. (Five per cent of the radius has been found satisfactory for phenolic.)

When these principles are adhered to, the following results may be expected:

1. The average weight of the majority of fragments should lie within the range of 80 to 95 per cent of the design weight.
2. The average fragment velocity should be within 10 per cent of the velocity computed by Gurney's formula, Eq. 4–120.

The fragments recovered during the tests reported in Ref. 65 indicated that small slivers, triangular in cross section, were produced as is shown in Fig. 4–103.

In general, the fracture is a tensile break along a radial line. Near the inner surface, the tensile break changes to two 45-degree shears, making the sliver. This characteristic is explained as follows. With increasing values of acceleration, the tangential or tensile stress decreases rapidly, and may become zero for sufficiently high acceleration. The shearing stress decreases also, but at a much slower rate than tangential stress. For sufficiently high acceleration, shearing stress may equal or exceed the tensile stress. It is concluded that if the

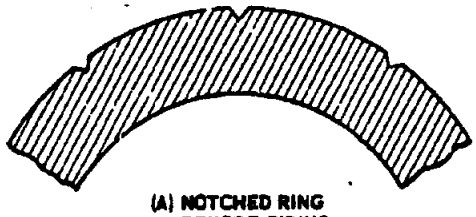

(A) NOTCHED RING BEFORE FIRING

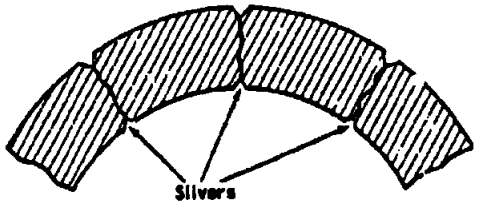

(B) NOTCHED RING FRAGMENT PATTERN

Figure 4–103 (C). Notched Ring Fragmentation Characteristics, Cross-Section Views (U)

acceleration is high, at the inner surface the ratio of shearing stress to tensile stress will exceed the ratio of shearing strength to tensile strength, for the metal, and any failure starting at the inner surface will be one of shear.

It was found (Ref. 66) that the addition of wood or cork cushions placed between the charge and case resulted in elimination of the slivers. The reason given for this is that the cushion reduces the acceleration and velocity of the case, thereby reducing the shearing stress without reducing the tensile stress. However, the cushion reduces the fragment velocity by reducing the amount of charge weight available for conversion into kinetic energy.

4–10.3.4. (C) *Notched Wire*

(U) The notched-wire wrapped warhead is similar in design and theory to the notched ring type. The wire is actually a long bar, with two of its dimensions equal to those desired for the fragments. The bar is notched at intervals along its length and wound in a helix to the shape of the warhead casing.

(C) Reasonably good fragment control has been obtained using notched wire wound on a cylindrical warhead, in that approximately 80 per cent of the design number of fragments were produced (Refs. 67 and 68).

4–10.3.5. (C) *Notched Solid Casings*

(U) Instead of notching in one direction and having actual discontinuities in the other direction, such as in the notched ring or wire method, casings with a two dimensional network of notches (grooves) may be used. The notches may either be machined or integrally cast on the inside or outside surface of a casing.

(C) Tests conducted on a machined warhead (Ref. 69) of this type were very successful, in that approximately 89 per cent of the design number of fragments were produced. The warhead was made by milling a pattern of longitudinal and circumferential grooves on the inside of a cylindrical tube. The tube was then swaged into the modified ogive shape of the warhead section.

(C) Tests were also conducted on three cast-steel warheads with internal slots designed to give controlled fragmentation (Ref. 70). Additional heat treatment after casting was applied to warheads 1 and 2, but warhead 3 was tested in the as-cast condition. The design weights of fragments were 9.37 grams in warhead 1, 9.13 grams in warhead 2, and 8.83 grams in warhead 3. The results of the tests, considered to be good, are shown in Table 4–22. The initial velocity was the same for all three warheads. A greater number of partial fragments was produced by the non-treated casing than for the heat-treated ones.

TABLE 4–22 (C). FRAGMENTATION RESULTS OF INTERNALLY SLOTTED WARHEADS (U)

Warhead No.	Weight of Fragments (grams)	Per Cent of Designed Number of Fragments Produced
1	6.5 to 9.5	79.5
2	5.5 to 8.5	83.9
3	5.5 to 8.5	79.5

4–10.3.6. (C) *Fluted Liners*

(U) Instead of using irregularities or weak areas in the casing of a warhead for controlling fragmentation, a method of shaping or grooving the charge may be used. The explosive charge is shaped so that irregularities of the detonation will break up the casing in the desired pattern. The charge is shaped by means of a liner constructed of plastic, cardboard, balsa wood, or similar material which is inserted between the warhead casing and the explosive. When the warhead is detonated, the flutes or grooves in the explosive give a shaped charge effect which tends to cut the metal casing in the pattern formed by the flutes.

(C) The casing used with fluted liner warheads may be solid (Ref. 71) or partially preformed by means of rings or wire (Ref. 67). Tests on warheads using fluted liners indicate that fragment control can be as successful as with the notched casing or notched wire wrapped types. The fragment velocities from lined warheads are lower, due to the reduced ratio of explosive to casing weight. Use of the fluted liner introduces voids between the casing and

explosive, with the result that some loss of weight and space for explosive occurs. The fluted liner technique is practical for thin casings where the flute size and explosive weight loss is small. Test results with identical casings produced 14 per cent lower fragment velocities with the fluted liner than with the notched wire wound type of warhead.

4–10.3.7. (C) *Multi-Wall Casings*

A method for producing a greater number of fragments from a naturally fragmented warhead has been devised through the use of a multi-walled casing (Ref. 72). Tests were conducted on straight walled cylindrical warheads consisting of one to five press-fitted cylinders. The inside and outside diameters were the same for all warheads. The total shell thickness was divided equally by the number of walls being tested. Different charge-to-metal ratios were used to determine their effect on the performance.

It was discovered that the number of fragments produced is directly proportional to the number of walls. In this respect, Mott's Equation for natural fragmentation,

$$N(m) = C \cdot e^{-\left(\frac{m}{\mu_0}\right)^{1/2}}$$

in which $N(m)$ = number of fragments of mass greater than m,

C = a constant dependent on the weight of the casing,

m = mass of the fragment,

and μ_0 = a measure of the mean fragment mass

takes the form

$$N(m) = WC \cdot e^{-\left(\frac{m}{\mu_0/W}\right)^{1/2}} \qquad (4\text{–}113)$$

for a warhead having W walls.

The spatial distribution of the fragments from multi-walled warheads was satisfactory, in the sense that adjacent fragments from each cylinder were separate in space and showed no evidence of being fused together. However, it was shown that the fragments deteriorate into flaky shapes as the number of walls is increased.

4–10.4. (C) Spatial Distribution

4–10.4.1. General

If detonation started at all points simultaneously throughout the explosive, each fragment would be projected normal to the element of casing from which it originated. The fact that detonation starts at a finite number of points, usually one or two, results in a deviation of the direction of projection of each fragment from the normal direction. How to determine the angle of deviation from the normal is the main topic of this section.

In the case of a fragmentation warhead, it is usually assumed that the fragmentation pattern is symmetrical about the missile axis. For truly symmetric warheads, the available evidence does not contradict this hypothesis of symmetry of the fragment pattern, although there is limited experimental evidence on this point. Efforts have been concentrated to a greater degree on the determination of the variation in asymmetric warheads, as discussed in the next paragraph.

Warheads with asymmetric staggering of notches in the casing, casings made in more than one part, or asymmetric location of the point where the detonation is initiated, give some indications of asymmetry in the fragment pattern. However, the only example in which the problem appears serious is that of a very asymmetric detonation point, especially if the warhead is annular in shape (i.e., has a large hollow space along the axis). In this example, the detonation wave may strike the casing at substantially different angles on the near and far sides and produce correspondingly different fragmentation patterns; moreover, in the zone where detonation waves traveling around opposite sides of the annulus meet, fragment shatter and alteration of velocities are to be expected.

Returning to the usual example of axial symmetry, fragment density as a function of angle of emission (measured from the forward direction of the warhead axis) remains to be

considered. Of interest are two different versions of this pattern, usually termed static and dynamic. The static pattern is the one produced if the warhead is detonated while motionless, while the dynamic pattern is the one obtained if the warhead is in flight.

4–10.4.2. *Prediction of Static Fragment Pattern*

The basic idea for the prediction of static pattern fragments is given in Taylor's theory. Applications have been made by Shapiro (Ref. 18) and by Gibson and Wall. In the Shapiro method, the shell or warhead is assumed to be arranged in successive rings (Fig. 4–102), the part of the shell or warhead casing of interest being composed of many such rings stacked one on another, each with its center on the axis of symmetry. Although this may not be the actual mode of fabrication of the casing, the Shapiro method is probably a sufficiently accurate approximation for initial design purposes.

In order to establish the beam spray angles for each ring, the following formula by Shapiro can be used. This equation gives the direction of fragment throw-off from the warhead casing. According to Shapiro, the detonation wave emanates as a spherical front from all points on the surface of the booster or auxiliary detonator, which is assumed to be a point D, as shown on Fig. 4–104. The normal to the warhead casing makes an angle ϕ_1 with the axis of symmetry, and the normal of the detonation wave at a point on the casing makes an angle ϕ_2 with the axis. The deflection θ of the fragment velocity vector from the normal to the casing is given by Shapiro's formula

$$\tan\theta = \frac{V_o}{2V_D}\cos\left(\frac{\pi}{2}+\phi_2-\phi_1\right) \quad (4\text{–}114)$$

where

V_o = initial fragment velocity,

and

V_D = detonation velocity of the explosive.

Allowance may also be made for the dispersion about the predicted direction of throw.

Some representative detonation velocities for several common explosives are listed in Table 4–23.

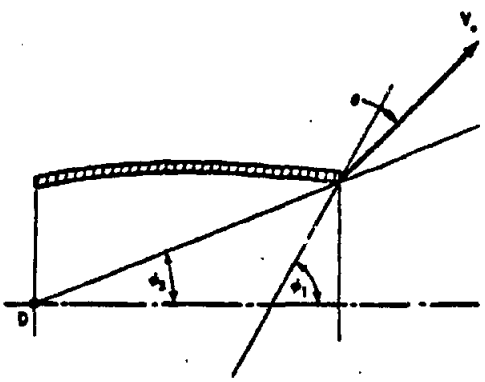

Figure 4–104 (C). Factors Used in Estimation of Fragment Beam Angle (U)

TABLE 4–23 (C). DETONATION VELOCITIES OF SELECTED EXPLOSIVES (U)

Explosive	Velocity (m/sec.)
TNT (Cast)	6640
Comp B	7840
H–6	7600
75/25 Octol	8400

4–10.4.3. *Prediction of Dynamic Fragment Pattern*

From the static fragment pattern, the fragment density for the dynamic condition is derived. If the warhead is moving through space, the vector velocities of the fragment (static condition) and warhead are added to find the actual direction in which the fragment proceeds outward.

The dynamic density $D(\theta_d)$ for a given direction, θ_d, is obtainable from the static density $D(\theta_s)$ for the corresponding direction, θ_s, by the equations:

$$\operatorname{ctn}\theta_d = \operatorname{ctn}\theta_s + \frac{V_m}{V_f}\csc\theta_s \quad (4\text{–}115)$$

and

$$D(\theta_d) = D(\theta_s)\left(\frac{\sin\theta_s}{\sin\theta_d}\right)^3 \frac{1}{1+\frac{V_m}{V_f}\cos\theta_s} \quad (4\text{–}116)$$

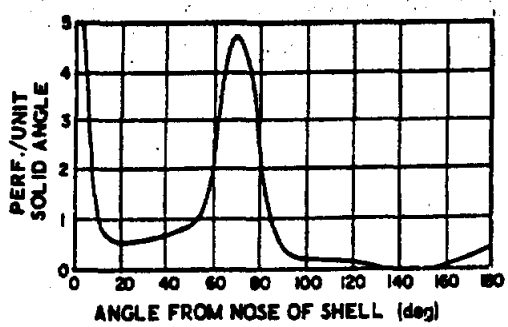

Figure 4–105. Typical Angular Fragment Distribution

where

V_f = static fragment velocity in direction of θ, in ft/sec.,

and

V_m = relative velocity of missile and target in ft/sec.

Angular distributions of fragments from high explosive shells and bombs are experimentally determined at the Aberdeen Proving Ground by detonating static projectiles. For these tests, screens are placed around the projectile at various distances, and the number of fragment hits on each unit area of the screens is determined. A typical distribution found by this type of test is shown in Fig. 4–105.

Results of statically detonated shells having various degrees of end confinement and shell lengths indicate that the spatial distribution is not affected by the type of end confinement, but that it is affected by the shell length, for lengths less than about 1-1/4 calibers (Ref. 74). This is caused by the escape of detonation products at the ends of the cylinder, thereby releasing and diverting energy that could be used more uniformly, as is apparent from spatial distributions of projectiles several calibers in length.

4–10.5. (C) Techniques for Measurement and Reduction of Data (Refs. 67 and 75)

(U) The techniques employed in measuring mass and spatial distributions of fragments from both uncontrolled and controlled fragmentation warheads are identical. The techniques which follow are basic; later improved and standardized techniques are available (Ref. 88). Fragment recovery by a means that provides known orientation with respect to the warhead is the logical and most frequently used technique in fragment distribution tests and experiments.

(U) For fragment recovery, it is assumed that the fragments produced will be equally distributed around the warhead. Fragments are recovered in a sector, usually 180°, and are considered as being representative of the total distribution. The warheads are normally supported with their longitudinal axes horizontal, in an arena which contains appropriately placed recovery boxes, velocity panels, velocity-recovery boxes for velocity mass correlations, and ricochet stops. Warheads are supported at a height that will place their axes in the same horizontal plane as the centers of their recovery boxes. In other words, the axes of the warheads will be four feet higher than the bases of the normally eight-foot high boxes. Warheads must be supported exactly horizontal, as determined by the use of spirit levels or quadrants. They may be supported in one of two ways:

1. When the total weight to be supported is less than 35 pounds, the warhead should be suspended from a cord running from the tops of opposite recovery boxes, or from poles placed outside of the arena.
2. When the total weight is greater than 35 pounds, the warhead should be supported in a wooden cradle, cut to the contour of the under side of the warhead, and mounted upon an upright wooden pole or poles.

(U) A ricochet stop is used to prevent fragments from ricocheting from the ground into the recovery boxes. Ricochet stops may be constructed in one of the following ways: a ridge of dirt, with or without a retaining wall on one side, having a plateau two-feet wide; steel plates resting against a ridge of dirt or mounted on a frame; or parallel wooden walls enclosing a two-foot thickness of tamped earth. Ricochet stops are normally required only where there is a possibility of fragments strik-

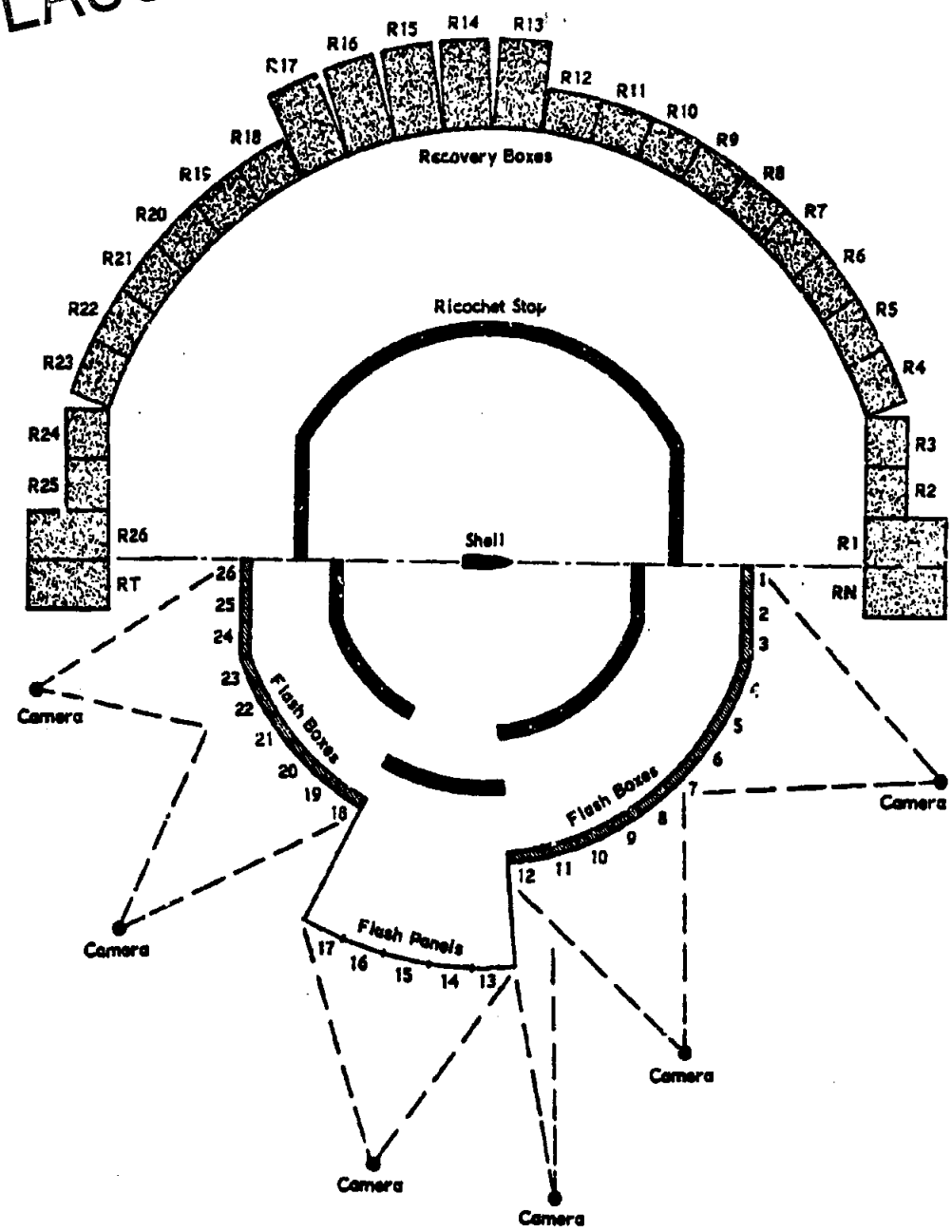

Figure 4–106. Fragmentation Test Arena

ing the ground at angles of less than 15 degrees.

(U) Recovery boxes are used to entrap undamaged samples of the warhead fragments, which are used to determine both spatial distribution and the weights of fragments. Recovery boxes are fabricated of wood and are large enough to house four-by-eight foot sheets of half-inch composition wallboard (celotex), or other suitable recovery media, to a depth of three to six feet. The boxes are placed on end, with one open side exposing the wallboard to the warhead. The depth of a box depends upon the size and velocity of the fragments expected to strike that box. To determine the spatial distribution, the recovered fragments must be oriented with respect to the warhead location. The areas of the recovery boxes are subdivided to permit fragment recovery in terms of zones, lunes, squares, or other suitable geometric configurations. A representative fragmentation test arena is shown in Fig. 4–106.

(U) After detonation of the warhead, the fragments in the wallboard are located with an electronic metal detector. Each fragment is removed from the wallboard, cleaned of all residue, and weighed to a maximum error of 1 per cent. As the fragments are recovered, their location in the recovery box is recorded for determination of spatial distribution. The mass distribution is then determined by separating the fragments into weight groups. Results of a typical mass distribution test are shown graphically in Fig. 4–107. These results indicate the ability of a warhead to produce fragments which will be lethal or damaging against the target for which it is designed.

(U) Spatial distribution is a measure of the density of fragments in space. The number of fragments in any area around the warhead can be determined from the locations of fragments in the recovery boxes, and a relationship similar to that shown in Fig. 4–108 can be plotted. From this curve, the fragment spray can be determined by noting the size of sector in which effective fragments were projected. In the case illustrated, the fragment spray was approximately ±24 degrees from the equatorial plane.

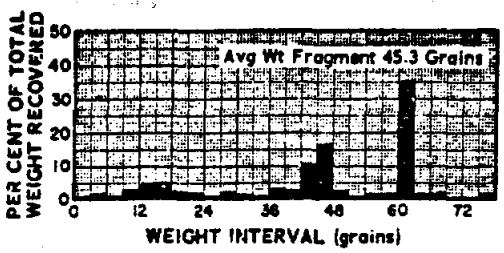

(A) PER CENT WEIGHT OF FRAGMENTS RECOVERED IN WEIGHT INTERVALS

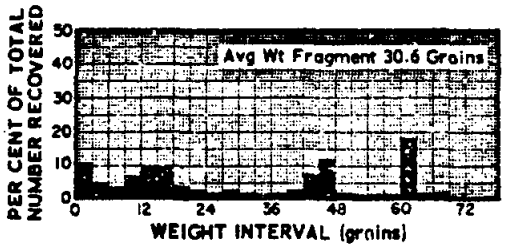

(B) PER CENT NUMBER OF FRAGMENTS RECOVERED IN WEIGHT INTERVALS

Figure 4–107 (C). Histogram of Fragment Mass Distribution (U)

(U) Strawboard is often used by the British when recovering fragments. The density of strawboard is approximately twice that of the Celotex used in this country. The density of the material used sometimes affects the results, because secondary fragment break-up may occur in the higher density materials, and a true measure of the mass distribution may not be

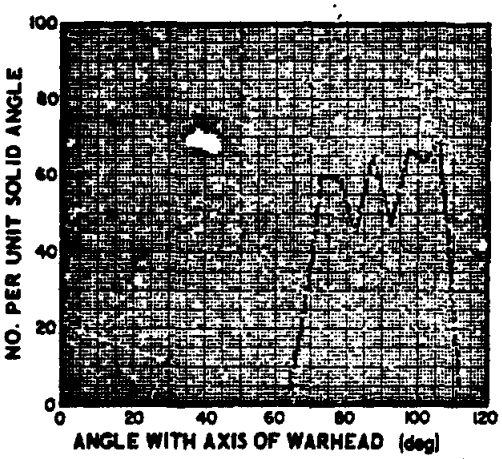

Figure 4–108 (C). Spatial Distribution Graph (U)

obtained. During the fragment recovery operation, careful observation as to fragment location and size should be employed, in order to detect any fragment break-up after impact with the recovery material.

(U) Closed sand pits were previously used to recover fragments; however, due to fragment break-up upon impact with the sand, and the inability to orient the fragments to the warhead location, this method is now considered inadequate and obsolete.

4–11. (C) FRAGMENT VELOCITY

4–11.1. (U) Introduction

This paragraph discusses the theoretical aspects and experimental techniques for obtaining the initial and downrange (decayed) fragment velocities. The experimental methods include various explosive shapes, types of explosives, inert materials included as cushions, and detailed photographic instrumentation.

4–11.2. (C) Initial Velocity

4–11.2.1. (C) Theory

a. (U) *General*

The theoretical expression for initial velocities has been well predicted by kinetic energy considerations, and most laws and formulas have been derived from the basic kinetic energy expressions as presented here.

b. (C) *Cylinders and Spheres*

(U) The detonation of a long cylinder of explosive, encased by a cylindrical shell of metal, is considered in the following manner (Ref. 24). If M is the mass of metal and C the mass of the charge, and if during the expansion the velocity of the gas increases uniformly from zero on the axis to the fragment velocity, V, at the internal surface of the expanding cylinder of metal, then the local kinetic energy is

$$T=\frac{MV^2}{2}+\frac{CV^2}{4} \qquad (4\text{–}117)$$

at any instant. If E is the energy per unit mass (specific energy) of the explosive that can be converted into mechanical work, then it follows that, at the time when all this energy has been converted, the fragment velocity (usually called the initial fragment velocity) is given by

$$V=\sqrt{2E}\sqrt{\frac{C/M}{1+C/2M}}\,. \qquad (4\text{–}118)$$

The velocities predicted by Eq. 4–118 were found by Gurney to be in good agreement with the experiment, when the quantity $\sqrt{2E}$ was given a value of 8,000 fps for TNT.

(C) Picatinny Arsenal (Ref. 76) gives the value of $\sqrt{2E}$ as 8,800 fps for Composition B and $C3$ explosives.

(U) Gurney's formula for spheres, obtained in a similar manner, is

$$V=\sqrt{2E}\sqrt{\frac{C/M}{1+3C/5M}}\,. \qquad (4\text{–}119)$$

(C) For the initial fragment velocity of a cored cylinder, where a_r is the ratio of the core radius to internal cylinder radius, at rupture, the initial fragment velocity (Ref. 77) is

$$V=\sqrt{2E}\sqrt{\frac{C/M}{1+C(3+a_r)/(1+a_r)\,6M}}\,. \qquad (4\text{–}120)$$

For steel, $a_r\approx\frac{a}{1.6}$, where a is the initial ratio of the core radius to the internal cylinder radius.

(C) Sterne (Ref. 78) gives fragment velocity of a spherical shell containing an inert core as

$$V=\sqrt{2E}\sqrt{\frac{C/M}{1+3/5\,C/M\,f(a)}} \qquad (4\text{–}121)$$

where

$$f(a)=\frac{1+3a_r+6a_r^2+5a_r^3}{(1+a_r+a_r^2)^2}\,.$$

Again, a_r denotes the radius of the core divided by the radius of the spherical shell, and may be taken as the original a divided by 1.6.

c. (C) *Flat Charges*

(1) Sterne's Flat Plate Formula

Considering the velocity of fragments from a flat slab of metal in contact with a flat slab of high explosive, all in free space, Sterne (Ref. 77) writes the momentum balance as

$$C\frac{U-V}{2}=MV$$

where M = the mass of metal per unit area,
C = the mass of charge per unit area,
V = the velocity of the metal at any instant of expansion,
and U = the gas velocity at the free boundary.

Assuming uniform gas velocity variation from U to V, the kinetic energy of the gas is

$$T = \frac{C}{6}(V^2+U^2-UV). \quad (4\text{–}122)$$

Assuming that the internal energy of the explosive, EC, is converted into kinetic energy of metal and gas, by application of the Sterne flat plate formula:

$$V = \sqrt{2E}\sqrt{\frac{C^2+3CM}{C^2+3M^2+4MC}}. \quad (4\text{–}123)$$

(2) Flat Sandwich Charges

In the case of two slabs of metal with mass per unit area of M_1 and M_2, separated by a slab of high explosive sandwich charge of mass per unit area, C, the fragment velocity is

$$V = \sqrt{2E}\sqrt{\frac{C}{M_1+M_2y^2+\frac{C}{3}(1-y+y^2)}} \quad (4\text{–}124)$$

where

$$y = \frac{M_1+C/2}{M_2+C/2}$$

For the symmetric case $M_1 = M_2$,

$$V = \sqrt{2E}\sqrt{\frac{C/2M_1}{1+C/6M_1}}. \quad (4\text{–}125)$$

d.* (C) *Projection from the End of High Explosive

(U) Hauver and Taylor (Ref. 79) present a method of projecting a thin plate, intact, with minimum deformation. Sterne's equation

$$V = \sqrt{\frac{6\phi^2E}{(\phi+1)(\phi+4)}}, \quad \phi = \frac{\rho_e t_e}{\rho_p t_p} \quad (4\text{–}126)$$

was found to apply, in which

ρ = density, in slugs/cu in.,
t = thickness, in inches,
E = specific energy of explosive, in ft-lb/slug,
e = explosive,
and
p = plate.

(C) The Misznay-Schardin effect (projecting plates from the end of high explosives), described by Pugh (Ref. 80), states that the axial fragment velocity is well represented by Sterne's equation.

(C) Experiments have produced velocities up to 5.4 km/sec. for a pellet projected from a cavity at the end of a cylinder of explosive.

e.* (C) *Effect of Type of Explosive on Velocity

Experimental results from Grabarek (Ref. 81) list the relative fragment velocity of thin and thick walled warheads. Taking Composition B as 1.00, the relative fragment velocities of HBX and Tritonal, for both thin and thick walled warheads, are found to be 0.92 and 0.82, respectively. Statistical tests applied to the data showed that these differences are significant.

By ratioing Gurney's Constant, E, the Naval Ordnance Laboratory gives the following, partial list for several explosives: Composition B=1.00; PTX-2=1.01; HBX-3=0.83; and Baratol=0.59.

Sheperd and Torry (Ref. 82) measured the average speed of fragments from the No. 70 Mk II grenade for various explosive fillings, and list the following velocities: Amatol (80/20)=2,000 ft/sec.; Baratol (20/80)=2,705 ft/sec.; TNT=3,730 ft/sec.; and RDX/TNT (50/50)=4,245 ft/sec.

f.* (U) *Effect of HE Confinement on Velocity

The United States Naval Proving Ground (Refs. 83 and 84) lists the fragment velocities found from open and closed ends of cylindrical warheads. Small length/diameter ratios were used as shown in the results listed in Table 4–24.

In another report, cylindrical warheads with axial cavities were detonated for fragment velocity measurements. Under the conditions of the test, the removal of an axial core of explosive results in the reduction of fragment velocities as indicated by Table 4–25.

TABLE 4-24. COMPARISON OF FRAGMENT VELOCITIES FROM OPEN- AND CLOSED-END 6" CYLINDERS

Measurement Location	l/d Ratio = ½		l/d Ratio = 1	
	(Open End)	(Closed End)	(Open End)	(Closed End)
Fuze End	4,360 ft/sec.	5,090 ft/sec.	4,480 ft/sec.	3,260 ft/sec.
Side Spray	3,420 ft/sec.	4,110 ft/sec.	4,570 ft/sec.	4,960 ft/sec.

Gurney (Ref. 85) considers the hypothetical case of a cylinder which expands indefinitely without cracking. At any moment during this expansion, when the radius has reached a value r, let the velocity of the metal be V. As the value of r tends to infinity, V tends to a limiting final velocity V_f. The value of $\frac{1}{2} MV_f^2$ is less than E, the difference being the kinetic energy retained by the explosion gases. The expression for the kinetic energy of the metal is

$$\frac{MV^2}{2} = AE\left[1-\left(\frac{r_o}{r}\right)^{2(\gamma-1)}\right] \quad (4\text{-}127)$$

where

$$A = \frac{(2\gamma-1)\left[(1+C/M)^{\frac{\gamma-1}{\gamma}} - 1\right]}{(\gamma-1)\left[(1+C/M)^{\frac{2\gamma-1}{\gamma}} - 1\right]} \quad (4\text{-}128)$$

M = mass of metal per unit length,

C = mass of explosive per unit length,

and

E = energy per unit length liberated from explosive by the passage of the detonation wave.

The value of A is less than unity, unless C/M is negligible in comparison to unity, in which case A is unity. From Eq. 4-127, for $A=1$, $E=1/2MV_f^2$, and

$$\frac{V}{V_f} = \left[1-\left(\frac{r_o}{r}\right)^{2(\gamma-1)}\right]^{1/2} \quad (4\text{-}129)$$

where

r_o = initial internal radius of metal cylinder,

and

γ = ratio of specific heats of propellant gases.

While 1.26 for γ is usual, Thomas (Ref. 86) used 2.75, which is some average value between γ of a gas and γ of a fluid.

Finally, for the per cent of the total charge lost through cracking, Gurney (Ref. 85) gives

$$\phi(\%) = \frac{K}{r_o}\left(\frac{2M}{\pi\rho}\right)^{1/2}\left(\frac{r-r_o}{r_o}\right)^{1/2} \quad (4\text{-}130)$$

where

$K < 1/2 \cos\theta$,

θ = angle between cracks made with elements of the cylinder,

ρ = propellant density,

and

M = mass of metal per unit length.

Using average numerical values, Gurney shows only small amounts of gas will escape.

g. (U) *Effect of Warhead Length/Diameter Ratio on Initial Fragment Velocity*

None of the theories used for predicting initial fragment velocity (Gurney, Sterne, etc.) takes into account the effects of warhead length or of the end plates of the warhead on the development of the detonation wave, nor is

TABLE 4-25. EFFECT OF AXIAL CAVITIES ON FRAGMENT VELOCITIES

Percentage of Explosive Removed	Charge-Mass Ratio	Mean Velocity (ft/sec.)
0	0.9218	6,070
14.1	0.7913	5,560
31.8	0.6281	4,840
55.6	0.3997	3,700

there much information available on this subject. It has been shown, however, that when the length of the warhead is not effectively infinite, and particularly when the warhead length/diameter ratio is less than 2, the velocities predicted by the various theories are not achieved. Correction (γ) to the initial velocity of side-spray fragments from a cylindrical warhead, due to variation in the length/diameter ratio, is shown in Fig. 4–109 (Ref. 87).

4–11.2.2. (C) *Measurement Techniques*

a. (U) *General*

The initial velocities of fragments produced by the explosion of a warhead or shell are determined experimentally by several methods. Each method employs some means for recording the time of flight of the fragment over a measured distance. The average velocity of the fragment is then calculated, using this time and the known distance. In most cases, the fragments are recovered and identified, so that an analysis of velocity versus mass may be made. In addition, the distribution of the fragments is determined for use in the analysis of the effectiveness of the warhead. The following paragraphs describe some of the common methods of measuring the velocity of fragments.

b. (U) *Flash Photographic Method*

The rapidity and broad scope of improvements being made in the flash photographic method of measuring fragment velocity render it infeasible to describe such a method in a publication of this type. Ref. 88 describes the latest method in use at the time of this writing.

c. (U) *Shadow Image Method* (Ref. 90)

This method consists of recording, with a rotating drum camera, the shadow images of the fragments passing in front of three illuminated slits. The slits are equally spaced, and when illuminated they produce three bands on the moving film. The slits are illuminated for a time slightly less than that required for one rotation of the film drum. Fragments passing between the slit box and camera produce shadow images on these bands. The velocity of a fragment, with suitable correction for deviation of its trajectory from horizontal, is inversely proportional to the relative displacement along the film of the three image spots. The three image spots produced by each of a number of fragments passing in front of the camera, at about the same time, are easily identified because they lie on a straight line.

The fragment velocities measured by this method are actually average velocities measured over the distance between the slits. Since this distance is usually small, the calculated velocity may be considered as being the instantaneous velocity of the fragment at a distance s, which is the average distance from the point of initiation to the slits. The initial velocity may then be calculated by using the aerodynamic drag principle, as described in Par. 4–11.3.1.

d. (U) *Multiple Break-Wire Screen Method* (Refs. 91 and 92)

This method uses a wire screen, located at a known distance from the warhead, for measuring the fragment velocity. The screen includes a bank of identical resistors in parallel. The resistors are mounted on a terminal board, with one end of each resistor tied to a common bus. The other end of each resistor is terminated at another common bus by the individual wires making up the screen. A typical screen is shown in Fig. 4–110.

The fragments travel a measured distance to the screen and break a number of the wires. The breaking of each wire produces a voltage change in the screen circuit. After shaping and amplification, the voltage deflects the electron beam of a cathode ray indicator. A high-speed streak image camera views the face of the scope and records the action of the intensified electron beam.

Light from the explosion triggers a photo tube which is used to trigger the scope to indicate the start of the explosion. Simultaneous recording on the film of a known time base completes the data necessary to determine the time of flight of each fragment to the screen.

A modification of this method utilizes a predetermined, single-frame raster or pattern of scanning lines displayed on an oscilloscope screen. The raster is triggered at the instant of warhead detonation. Spikes impressed on the

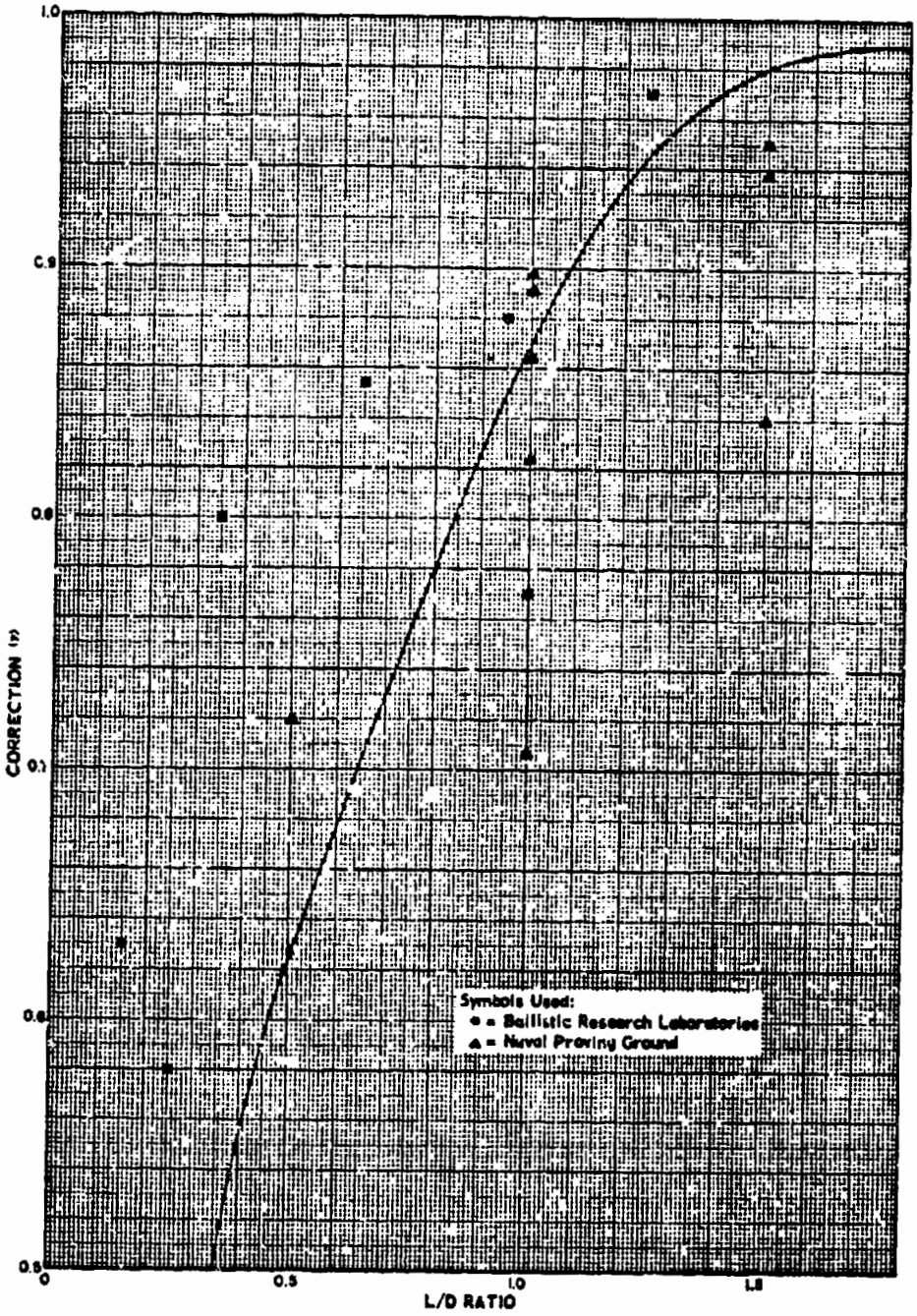

Figure 4–109. Correction (γ) to the Initial Velocity (V_o) of Fragments from a Cylindrical Warhead, Due to Variation in the Length/Diameter (L/D) Ratio

Official U. S Army Photograph

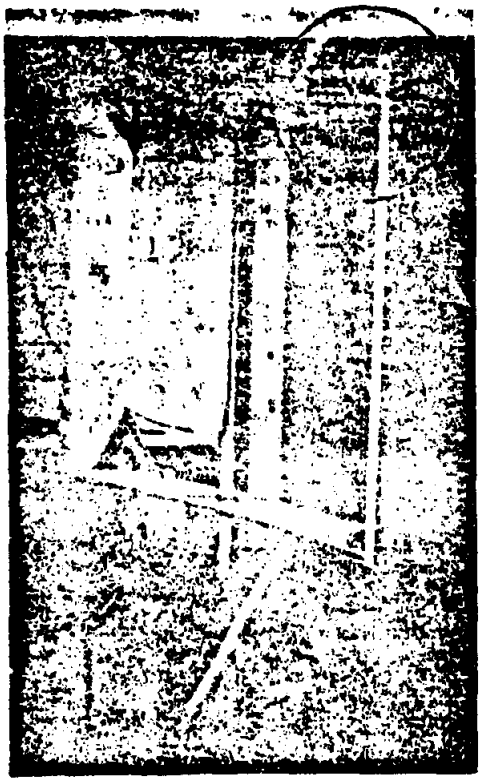

Figure 4–110. Multiple Break-Wire Screen

raster indicate the arrival time of the fragments at the wire screen, and a developing camera records the event. A photograph showing raster calibration and a typical firing record is shown in Fig. 4–111.

Without any sacrifice of accuracy, this modified method can be used to obtain either subsonic or supersonic velocities of fragments, regardless of the time of detonation. Much less film is used in this method than in the method employing the high speed camera. In addition, the record is available for reading within a few minutes after firing.

The velocity obtained by dividing the known distance from the warhead to the wire screen, x, by the time of flight of the fragment as measured from the film, t, is the average velocity of the fragment over the distance x. The initial velocity of the fragment may be determined by applying the aerodynamic drag principle described in Par. 4-11.3.1.

e. (C) ***Flash Radiographic Method*** **(Ref. 89)**

This method utilizes two flash radiographs for determining the distance traveled by the fragments during a known time interval. Be-

Official U. S. Army Photograph

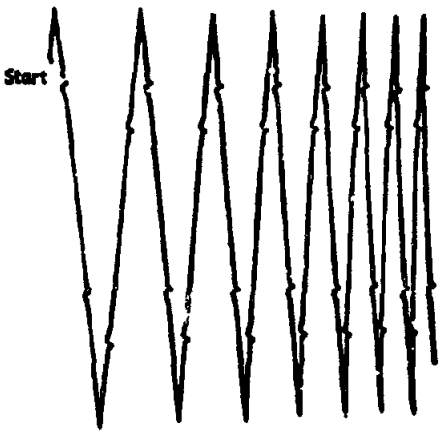

(A) CALIBRATION

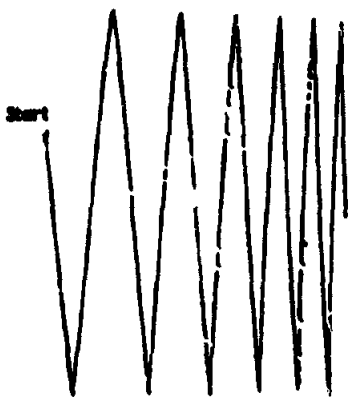

(B) RECORD

Figure 4–111. Typical Raster Calibration and Firing Record

cause the amount of explosive used with this method is limited to approximately one pound, a scaling problem can exist. Therefore, the flash radiograph method is more often used for qualitative than for quantitative results.

The warhead is set up in firing position and a static picture is taken. A "primacord clock" consisting of pin electrodes is initiated simultaneously with the warhead. When the primacord detonates to the pin electrodes, which have been placed at a calculated distance from the point of initiation for the desired time interval, the hot gases ionize the gap between them and trigger the X-ray unit. By this means, another picture is taken after detonation.

Fragment velocity is then determined by superimposing the two negatives and measuring the expansion in the following three zones: 2 cm from the top; at the center; and 2 cm from the bottom. The size of the static picture, s, subtracted from the total expansion, x, and divided by twice the magnification factor, μ, gives the actual distance traveled, d, or

$$d=\frac{x-s}{2\mu}.$$

The average velocity, V, for each zone is then calculated by dividing the distance d by the time t, or

$$V=\frac{d}{t}$$

where t is determined by the length of the primacord.

Figs. 4–112 and 4–113 are contact prints from radiographs of a steel cylinder filled with RDX Composition C–3, before detonation and 25.19 microseconds after detonation, respectively. Other radiographs were taken at 60 and 67 microseconds after initiation. For all three of the post-detonation radiographs, the measurements indicated that, the velocity of the fragments was 1,338 meters per second. This proves that the times and distances involved in this method of velocity measurement are such that no velocity decay takes place. Therefore, the velocities of the fragments, as measured, may be considered equal to or nearly equal to the initial velocity of the fragments, without the need for applying correction factors for drag during this short time interval.

4–11.3. (C) Velocity Decay

4–11.3.1. (U) Theory

This paragraph presents the theory and experimental techniques for determining the decay of fragment velocity from some initial velocity. It is assumed that a quadratic law of resistance applies to the motion of the fragments; an assumption well substantiated by experiment.

The ability of a fragment, projectile, or flechette to penetrate a target is dependent upon its velocity at the instant of impact. This velocity, referred to as striking velocity, will be less than the initial fragment velocity because of the decrease due to air drag.

In the movement of a body through a fluid medium such as air, the body encounters a certain amount of resistance, tending to retard its motion (Ref. 93). The major source of resistance lies in the unbalanced pressure distribution over the surface of the moving body. Reasoning that a body of cross-sectional area A, normal to the direction of flight, and moving with velocity V, will impart its own speed to a

Official U. S. Army Photograph

Figure 4–112 (C). Radiograph of Steel Cylinder before Detonation (U)

Official U. S. Army Photograph

Figure 4–113 (C). Radiograph of Steel Cylinder 25.19 Microseconds After Detonation (U)

mass of fluid of mass density ρ, and that the force necessary to do this is proportional to the rate of change of momentum, the resistance or drag, D, offered by the air is found to be

$$D=\frac{1}{2}C_D\rho A V^2. \qquad (4\text{–}131)$$

While the mechanism of resistance is much more complex than indicated, this quadratic law of resistance applies in a great variety of cases, provided the aerodynamic drag coefficient, C_D, is properly evaluated. The value of C_D depends principally upon the size and shape of a body and its velocity. In the case of a projectile the resistance is sometimes written

$$D=K_D\rho d^2V^2 \qquad (4\text{–}132)$$

where d=the projectile diameter,
and K_D=ballistic coefficient of resistance.

Note that

$$K_D=\frac{1}{2}C_D\frac{A}{d^2}$$

and that for projectiles, $\frac{A}{d^2}=\frac{\pi}{4}$.

The value of the drag coefficient is usually obtained from wind tunnel experiments where the resisting force, R, is measured for a given air velocity. Then the drag coefficient, C_D, is computed, based on some presented area, A. Hence, the scaling laws can be applied for similar shapes and various velocities, provided the area upon which the drag coefficient was computed is given. A typical curve from a bullet of C_D versus the Mach number M is shown in Fig. 4–114.

Note that there is a large change in the drag coefficient for the region around Mach 1, passing from subsonic to supersonic velocities.

In general, then, the equation of motion for a body in flight of relatively flat trajectory (the effect of gravity is neglected) is written

$$D=mV\frac{dV}{dx} \qquad (4\text{–}133)$$

where m is the mass of the body. Applying the quadratic law of resistance, and integrating

$$\int_{V_o}^{V_x}\frac{dV}{C_DV}=\int_0^x\frac{\rho A}{2m}dx \qquad (4\text{–}134)$$

where V_x is the down range velocity at distance x, and V_o is the initial velocity. In most cases, where the initial and the decayed velocities remain above the sonic value, an average value of C_D is assumed and the integration yields the downrange velocity as

$$V_x=V_oe^{-\frac{1}{2}\frac{C_D\rho A}{m}x}. \qquad (4\text{–}135)$$

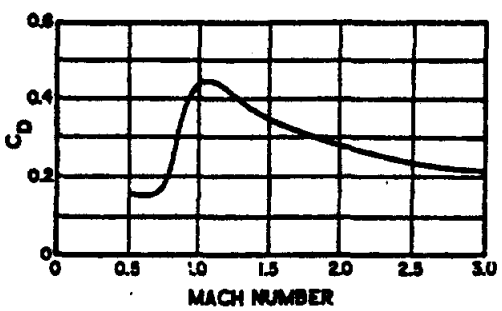

Figure 4–114. Graph of C_D vs Mach Number

If one is given the drag coefficient, C_D, of a fragment and the necessary striking velocity (in this case V_s) at the downrange position, the necessary initial velocity can be computed from Eq. 4–135.

The drag coefficient for fragments is usually determined by measuring the times of flight of a projected fragment over known distances x_1 and x_2 (Ref. 94). Eq. 4–133 is left in a finite difference form and C_D is defined by the equation

$$D = C_D A \rho V^2$$

Substituting in Eq. 4–133 gives:

$$-\frac{\Delta V}{C_D V} = \frac{\rho A}{m} \Delta x$$

and

$$C_D = \frac{\dfrac{-\Delta V}{\Delta x}}{\dfrac{\rho V A}{m}} \qquad (4\text{–}136)$$

Referring to Fig. 4–115, the term ΔV is the difference in the average velocity over a measured distance, where the times t_1 and t_2 are obtained from three velocity screens.

From Fig. 4–115, $V_1 = \dfrac{x_1}{t_1}$

$$V_2 = \frac{x_2}{t_2}$$

and

$$V_2 - V_1 = \Delta V = \frac{x_2}{t_2} - \frac{x_1}{t_1}$$

V_1 and V_2 are taken as the velocities at the mid points of the distances x_1 and x_2, so that

$$\Delta x = \frac{1}{2}(x_1 + x_2)$$

and

$$\bar{V} = \frac{1}{2}(V_1 + V_2) = \frac{1}{2}\left(\frac{x_2}{t_2} + \frac{x_1}{t_1}\right).$$

Having accurately measured the distances x_1 and x_2, and the times t_1 and t_2, the drag coefficient C_D is obtained from Eq. 4–136. As previously stated, the drag coefficient must be based upon some given fragment presented area. A mean presented area is determined as discussed in the Par. 4–11.3.2, following. Results of tests conducted on various fragments are shown in Fig. 4–116. It can be seen from the curves how C_D varies with respect to fragment shape and velocity.

4–11.3.2. (C) Measurement Techniques

a. (C) General

The variables which must be determined for each different fragment are the drag coefficient, C_D, and the presented area, A. The equation by which C_D is obtained was derived in Par. 4–11.3.1, preceding, and is repeated here:

$$C_D = \frac{\dfrac{-\Delta V}{\Delta x}}{\dfrac{\rho V A}{m}} \qquad (4\text{–}136)$$

In order to determine ΔV and V, of the equation, the velocities of a fragment must be measured at several points along its trajectory. These velocities may be measured by either the wire screen (Par. 4–11.2.2.d.), shadow image (Par. 4–11.2.2.c.), or flash photograph (Par. 4–11.2.2.b.) methods, or by other suitable methods. The fragments for these tests may be projected either singly from a gun, or in groups from a warhead. In the former method, the fragment is placed in a cup-shaped container, called a sabot, which lags behind the fragment after it emerges from the gun.

b. (C) Wire Screen Method

When the fragment is to be fired singly from a smooth-bore gun, the wire screen measurement method is normally employed. For these measurements, three wire screens are deployed as shown schematically in Fig. 4–117. As the fragment in its flight breaks a wire in each screen, a sharp voltage pulse is produced which starts or stops an electronic chronograph. One

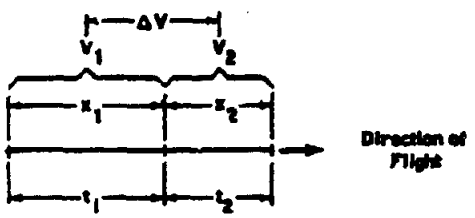

Figure 4–115. ΔV Relationship

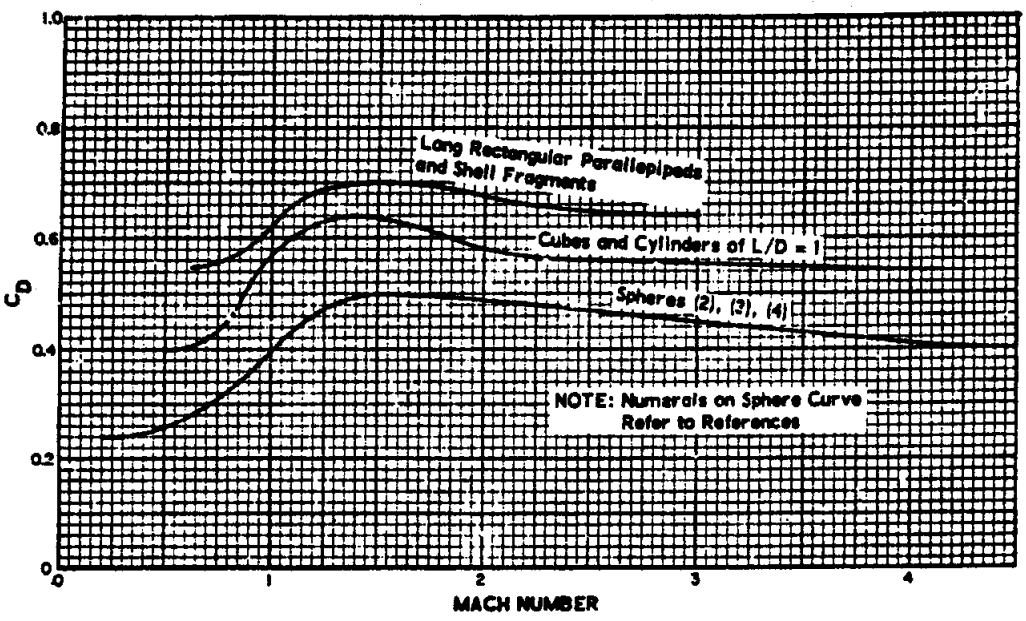

Figure 4–116 (C). Summary of C_D vs Mach Number for Various Unstabilized Fragments in Air (U)

set of chronographs is started by the pulse from the first screen and stopped by the pulse from the second screen. This measures the time t_1 over the distance x_1, from the first to the second screen. Another set of chronographs similarly measures the time t_2 over the distance x_2, from the second to the third screen. The average velocity over x_1 is $V_1=\frac{x_1}{t_1}$ and the average velocity over x_2 is $V_2=\frac{x_2}{t_2}$. It is assumed that these are the velocities at the mid-points between the screens.

c. (U) ***Shadow Image Method***

The velocities of fragments projected from a shell or warhead may be measured by either the shadow image or flash photograph methods (Ref. 97). The shadow image apparatus measures the velocities of the same fragments at three locations which are of known distances x_1 and x_2 apart. Only a small portion of the total number of fragments produced is allowed to pass in front of the slit boxes for velocity measurements. Normally, controlled fragmentation warheads are used in these tests, so that representative velocities of the fragments which are lethal are obtained. Only major, or design size, fragments are considered, because the velocities of the small fragments and slivers may be greater for short distances and smaller for large distances, thereby affecting the value of C_D.

d. (U) ***Flash Photographic Method***

The flash photograph method of velocity measurement (Ref. 95), employs flash targets located at various distances from the initiation point. Since the velocities of the fragments would be considerably reduced in passing through the target used in this method, it is necessary to measure a different set of fragments for each target. A schematic picture of a typical test setup, with targets for measuring five velocities at different distances, is shown in Fig. 4–118. To eliminate the velocities of the small fragments and slivers, recovery screens are placed behind the targets and all of the fragments are recovered. Only those velocities which are definitely correlated with major fragments are retained.

e. (U) ***Determination of Fragment Presented Area***

Determination of the presented area of a fragment is difficult, since orientations of the fragment vary during time of flight. The assumption is made that fragments are tumbling when projected from a warhead, and that the uniform orientation theory is applicable. Based on this theory, the mean presented area of a fragment is used. The mean presented area of a regularly shaped fragment is taken to be one-quarter of the fragment's total surface area. An Electro-Optic-Icosahedron Gage (Ref. 76) is used to measure the mean presented area of irregular fragments. A schematic diagram of the gage appears in Fig. 4–119. In general, the oscillator delivers a modulator signal through the driver unit to the light source. After collimation, the modulated light is directed on the gimbal system, on which is mounted the fragment whose area is to be determined. After the light beam passes through the condenser lens, it is focused on the photo tube. Minute, electrical signals originate here that are proportional to the total light flux permitted to pass the gimbal system. These signals are amplified, rectified, and then metered. The meter reading is used to determine the presented area.

To determine the mean presented area of a fragment, the presented area is measured with the fragment in 16 different orientations. The 16 orientations correspond to the normal, the ten essentially different mid-points of the faces, and the five essentially different vertices of an icosahedron. The remotely controlled mechanical gimbal system automatically orients, to the desired angles, the fragments whose areas are to be measured, and communicates these positions to the operator through indicating lights. Fig. 4–120 illustrates the gimbal system with a mounted fragment. The gimbal system is capable of orientation about the following two axes:

1. The horizontal axis coinciding with the ring gear diameter, motion about which is defined as "tilt."
2. An axis perpendicular to the horizontal axis at the ring gear center, about which the gear may rotate in its own plane of

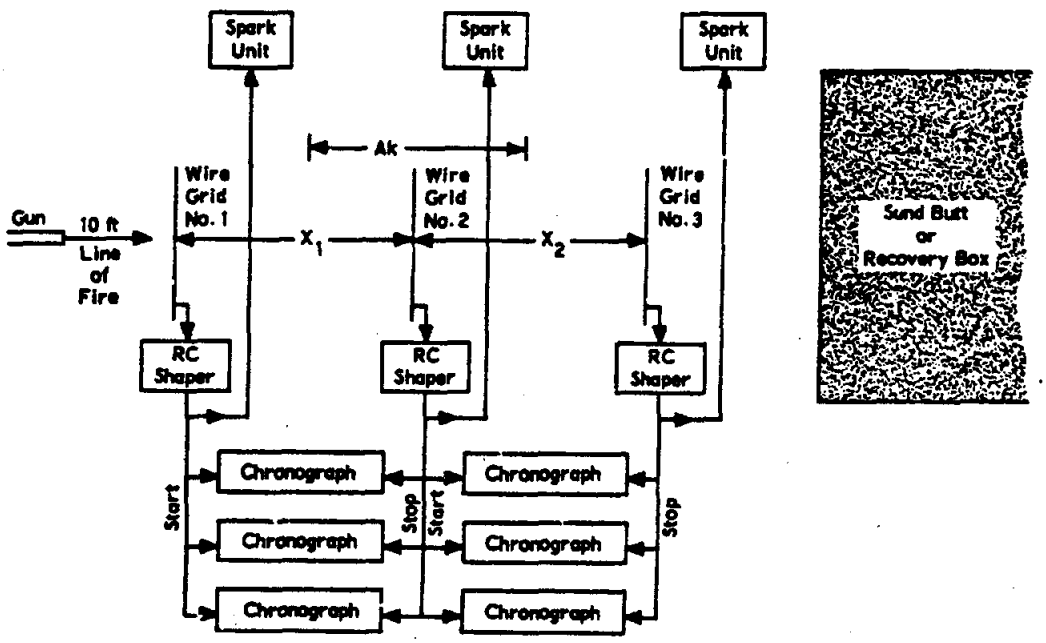

Figure 4–117 (C). Wire Screen Method Setup for Velocity Decay Measurements, Schematic Diagram (U)

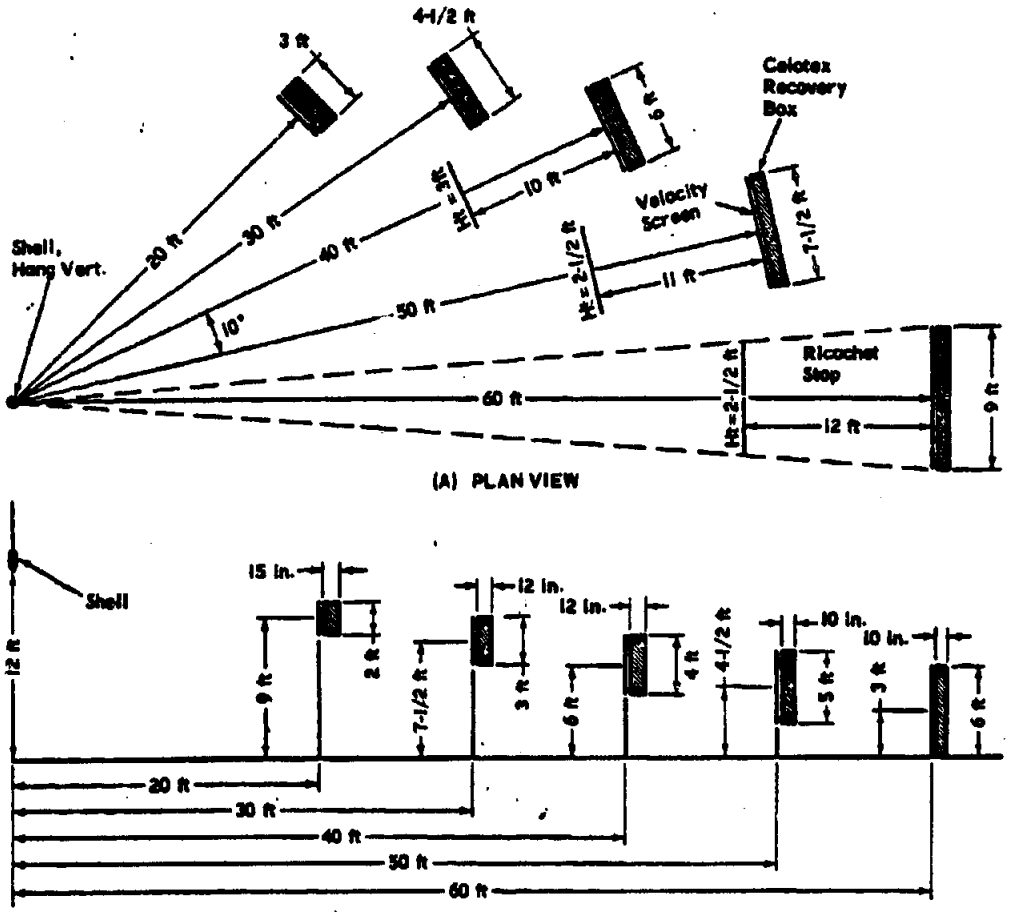

Figure 4–118. Flash Target Method Setup for Velocity Decay Measurement, Schematic Diagrams

motion. This motion is defined as "rotation."

The 16 different orientations which are employed are shown in Table 4–26. The mean value of the areas measured, with the fragment oriented in the poistions shown, is used as the mean presented area of the fragment for determining the drag coefficient.

4–12. (S) MECHANISMS OF PENETRATION AND PERFORATION BY SINGLE FRAGMENTS AND PROJECTILES

4–12.1. (U) Introduction

This paragraph presents the theory of penetration and perforation, as generally used for projectiles against various targets. Certain ex-

amples of experimental data are also included to illustrate the application of the theory.

4-12.2. (S) Theory

4-12.2.1. (S) General

(U) The theory of penetration is usually some form of the Poncelet Resistance Law; it is based on projectile motion through a target being similar to a projectile's motion through air or water.

(S) To determine the relation between the penetration power and perforation power of projectiles, and the physical properties of targets, the target resistance R to the projectile is assumed as

$$R = [B + 12\gamma\rho(V - V_s)^2]A \qquad (4\text{-}137)$$

where R = resisting force, in lb,
V = instantaneous projectile velocity, in in./sec.,
ρ = target density, in lb-sec^2/in.^{4},
B = maximum stress that can be maintained in the material of the target

TABLE 4-24. ORIENTATION ANGLES USED WITH GIMBAL SYSTEM

Tilt	Rotation
0°	0°
37° 23′	0°
37° 23′	72°
37° 23′	144°
37° 23′	216°
37° 23′	288°
63° 26′	36°
63° 26′	108°
63° 26′	180°
63° 26′	252°
63° 26′	324°
79° 11′	0°
79° 11′	72°
79° 11′	144°
79° 11′	216°
79° 11′	288°

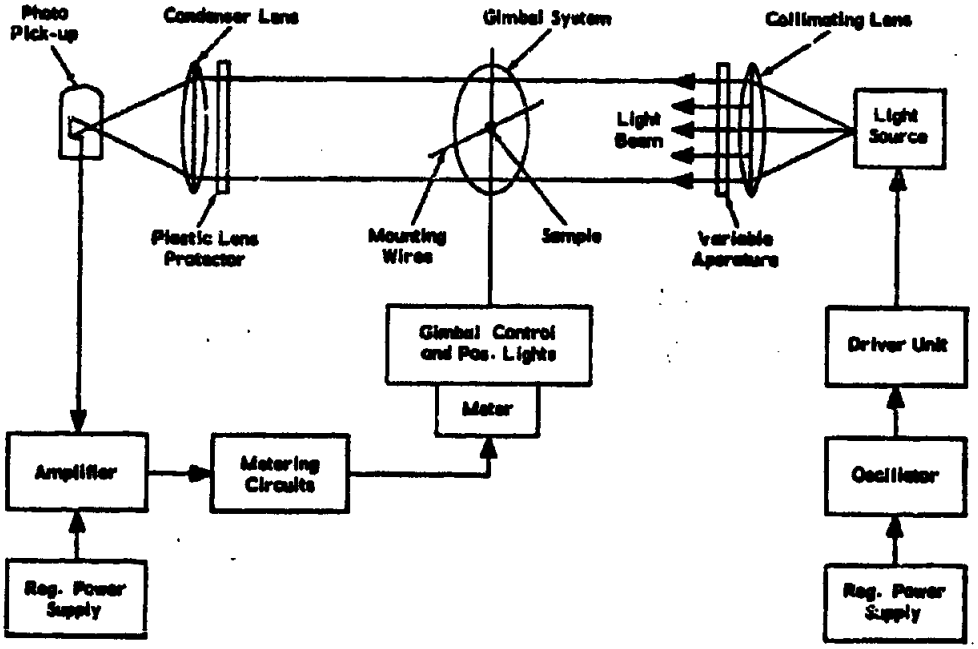

Figure 4-119. Electro-Optic-Icosahedron Gage, Schematic Diagram

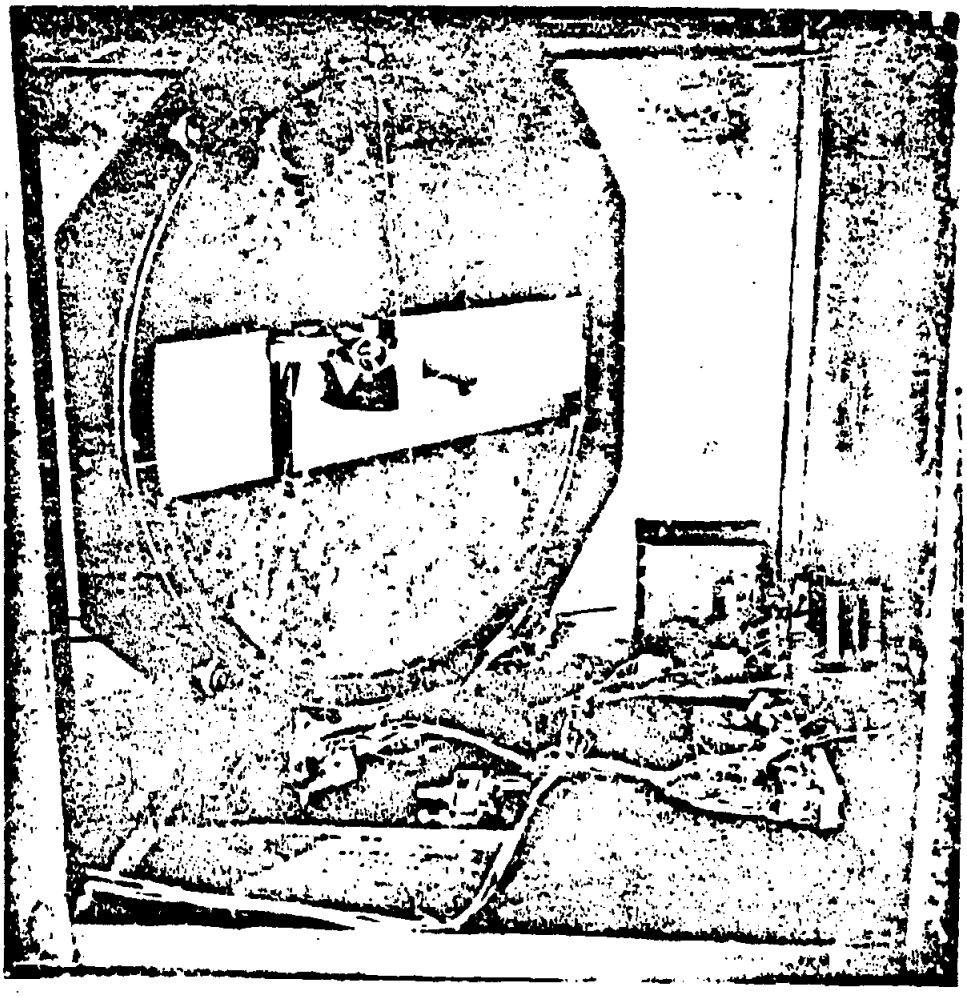

Figure 4–120. Gimbal System with Mounted Fragment

without rupture occurring, in lb/sq in.,

V_s = particle velocity in the rupture front, in in./sec.,

A = the projection of the area of contact between the projectile and the target, on a plane perpendicular to the line of flight, in square inches,

and γ = target resistance coefficient (analogous to a drag coefficient).

(S) The velocity, V_s, depends on the form of the stress-strain curve of the material of the target, and it is analogous to the rupture velocity in a semi-infinite wire where it is snatched at one end. This velocity is generally small; it is neglected, here, to give

$$R = (B + 12\gamma\rho V^2)A \qquad (4\text{–}138)$$

which is the Poncelet Resistance Law. The Poncelet Resistance Law attempts to account for the two most important components of re-

sistance: the strength of the target material; and the inertia of the target material. Values obtained for B from experimental data are reasonable, in that B is large for strong materials, such as rolled homogeneous armor, and is small for weak materials, such as gelatin and sand. In the latter case, the inertia term is predominant. However, the resistance to penetration is much more complicated than the Poncelet Resistance Law implies. Thus, the value of B will change with the shape of projectile and the target thickness. Nevertheless, the Poncelet Resistance Law is useful for analytical purposes, because it can be made to fit experimental data over a limited range. It should not be extrapolated, however.

(S) When a target material has considerable strength, such as steel, the inertia term usually is neglected. The Poncelet equation then implies that the target resistance is BA, a constant times the presented area. Bethe, in a detailed treatment of the resistance during penetration, found the resistance to radial motion of the target material to be of this form for very thin or very thick plates. In practice, longitudinal resistance is not negligible, so that $R=BA$ does not hold. For instance, if $R=BA$

$$t \sim V^2$$

where t is the thickness that can just be perforated at the striking velocity V, but it is found that

$$t \sim V^n$$

with n usually lying between 1 and 2. Hence, for strong target materials, a more general approach based on dimensional analysis is used. Putting

$$t = f(M, A, V, C, \theta)$$

where M is the mass of projectile, θ is the obliquity, and C is a strength parameter; then

$$\frac{1}{2}\frac{MV^2}{A^{1/2}} = Cf\left(\frac{t}{\sqrt{A}}, \theta\right) \qquad (4\text{–}139)$$

should hold for homologous projectiles. An equation similar to the last equation is used by the Navy. This involves an F coefficient defined by

$$\frac{W^{1/3}V\cos\theta}{t^{3/2}d} = F_f\left(\frac{t}{d}, \theta\right). \qquad (4\text{–}140)$$

When Eq. 4–139 is tested experimentally, it is found to account for scaling reasonably well, although large projectiles are found to perforate at velocities somewhat lower than is predicted from small projectile data.

(S) Examples of penetration formulas are given below. It will be noted that most formulas are variations of the Poncelet equation, or of the equation obtained from dimensional analysis. Most of the laws imply that the thickness perforated is proportional to $\frac{M}{A}$, a prediction in good agreement, except for large changes, with experimental data. For normal attack by irregular fragments, if ρ_m is the density of the material of the fragment, ρ is the density of the target, and if the dimensionless quantity, k (shape factor), is defined by

$$k = \text{average}\frac{(\text{volum})^{2/3}}{\text{presented area}},$$

then the mean depth of penetration of fragments of mass m is

$$x = K\frac{\rho_m^{2/3}m^{1/3}}{2\rho}\text{Log}\left(1+\frac{\rho}{B}V_s^2\right). \qquad (4\text{–}141)$$

4–12.2.2. (S) *Armor Plate (Striking Velocity < 10,000 FPS)*

The perforation of armor plate of thickness T, at an angle of obliquity θ, by an ogival-headed bomb is given by Walters' and Rosenhead's expression (Ref. 44).

$$\text{Log}\left(1+\frac{\rho}{B}V_s^2\right) = \frac{\rho\pi d^2 T}{2m}\sec\theta \qquad (4\text{–}142)$$

in which d is the bomb diameter and the other terms are as previously defined. The value of $\frac{B}{\rho}$ has been experimentally deduced as 2.01×10^6 (ft/sec.)^2. The corresponding value of B is 95 tons per square inch, but the ultimate tensile strength at low rates of strain varies between 65 and 80 tons per square inch. Typical test results for attack of homogeneous plates by 6-pounder shot are shown in Table 4–27.

TABLE 4-27 (S). PENETRATION DATA, HOMOGENEOUS PLATES VS SIX-POUNDER SHOT (U)

d (in.)	m (lb)	V_s (ft/sec.)	θ (deg)	T (mm)	B/ρ (ft/sec.)^2
2.25	6.25	1,783	30	60	1.91×10^6
2.25	6.25	2,090	30	70	2.04 "
2.25	6.28	2,250	30	70	2.37 "
2.25	6.28	2,640	30	80	2.61 "
2.25	6.31	1,920	30	60	2.25 "
2.25	7.25	1,665	30	60	2.09 "

4-12.2.3. (S) *Mild Steel*

Road Research Laboratory (Ref. 98, es the following partial list (Table 4-28) for the penetration of mild steel plates by spherical balls. V_s is the velocity necessary for perforation, T the plate thickness, and D the diameter of the spherical projectile. From this list i 3 deduced that $B=44$ tons per square inch.

From dimensional analysis, for fragments of similar shape the relation for steel fragments attacking mild steel is of the form given by Eq. 4-139.

$$\frac{\frac{1}{2}MV^2}{A^{3/2}}=Cf\left(\frac{t}{\sqrt{A}},\theta\right) .$$

The unknown function $f\left(\frac{t}{\sqrt{A}},\theta\right)$ is obtained approximately from experimental data (Ref. 101):

For normal obliquity

$$t=\sqrt{A}\left[\frac{MV^2}{2CA^{3/2}}\right]^{4/3} \qquad (4\text{-}143)$$

where $C=0.51\times10^6$ pounds per square inch in the British Gravitational System.

Experimental data presented by Dunne show good agreement with the above scaling for both irregular fragments and rectangular parallelepipeds.

Figs. 4-121, 4-122 and 4-123 plot $t/\sqrt{A}$ versus $\frac{1}{2}\frac{MV^2}{A^{3/2}}$ for angles of obliquity of 0 degrees, 30 degrees, and 60 degrees, respectively. The graphs give reasonable values when com-

TABLE 4-28 (S). PENETRATION DATA, MILD STEEL PLATES VS SPHERICAL BALLS (U)

T (in.)	D (in.)	V_s (ft/sec.)^2	B/ρ (ft^2/sec.)^2	V (calc. ft/sec.)
.040	0.25	600	0.60×10^6	780
.040	0.125	1,150	0.82 "	1,220
.070	0.125	2,200	1.11 "	2,160
.070	0.0938	2,650	0.84 "	2,850
.099	0.125	3,200	1.05 "	3,050
.099	0.0938	4,200	0.79 "	4,500

paring fixed parameters of projectile shape and obliquity, and projectile and target materials.

As a result of experimental firings of general purpose bomb fragments against mild steel, the following empirical formula has been obtained for thickness, t, perforated at normal impact (Ref. 102).

$$t = 0.112\, M^{1/2} \left(\frac{V}{1000}\right)^{4/3} \qquad (4\text{–}144)$$

Here t is in inches, M is the weight of the fragment in ounces, and V the striking velocity in ft/sec. The ballistic limit on which this formula is based ranges from 1,690 ft/sec. to 3,775 ft/sec., and the weights of the fragments vary from 0.197 ounces to 0.130 ounces. Note that the numbers 0.012 and 1,000 must be dimensioned constants for this equation to be correct.

Welch (Ref. 102) reproduced the following list (Table 4–29) of the required critical values of a parameter for penetration versus angle of obliquity. The values listed are for the expression

TABLE 4–29 (S). CRITICAL VALUES OF PENETRATION PARAMETER VS ANGLE OF OBLIQUITY (U)

Angle of Obliquity $\theta°$	Penetration $\frac{m^{1/3}V_s}{1{,}000\,t}$
0	7.3
20	6.3
40	6.7
60	8.8
70	17.5
80	25

$$\frac{m^{1/3}V_s}{1{,}000\,t}$$

where m = fragment weight in ounces,
t = plate thickness in inches,
and V_s = velocity for perforation in ft/sec.

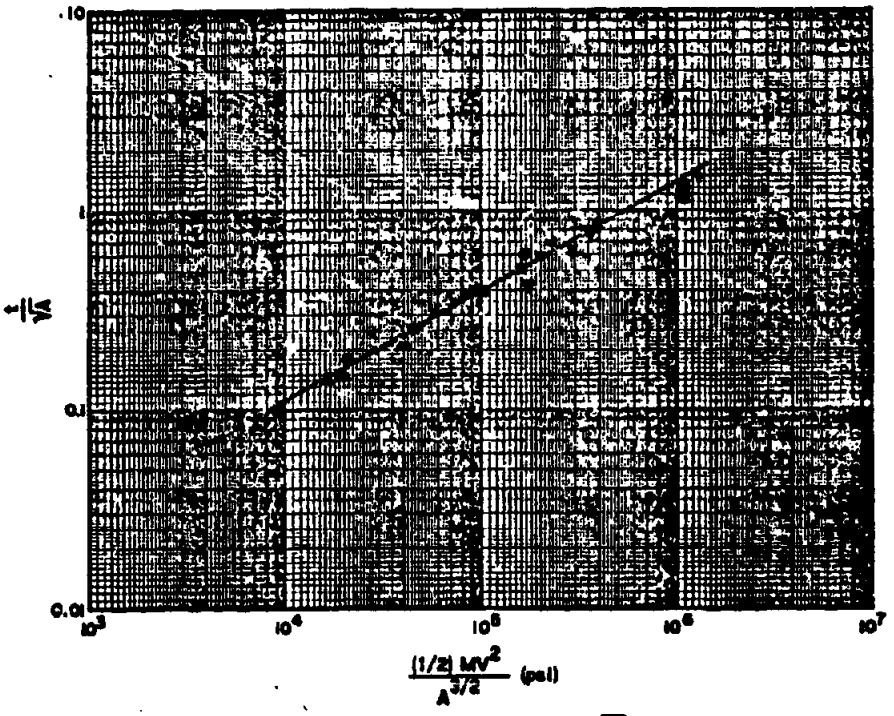

Figure 4–121 (S). Graph of $1/2MV^2/A^{3/2}$ vs $t/\sqrt{A}$, for 0 Degrees (U)

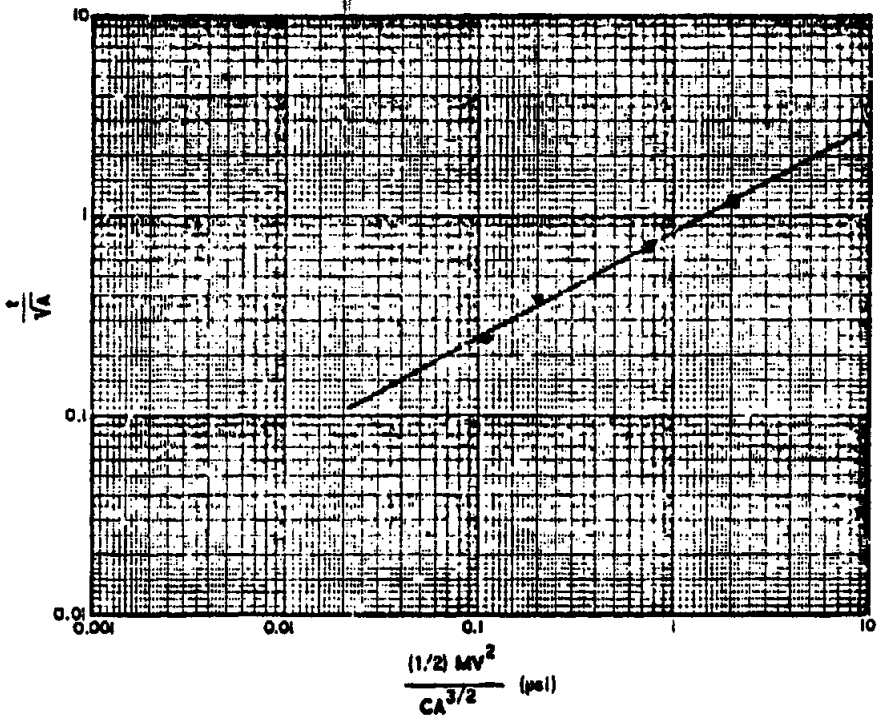

Figure 4–122 (S). Graph of $1/2MV^2/CA^{3/2}$ vs $t/\sqrt{A}$, for 30 Degrees (U)

4–12.2.4. (C) *Aluminum Alloys*

Taylor (Ref. 103) found experimentally that penetration of duralumin plates by steel spheres at velocities of up to 4,000 ft/sec. can be described by a Poncelet equation:

$$1+\frac{\alpha\rho_t V^n}{\beta}=e^{\frac{2\alpha\rho_t x}{m}} \qquad (4\text{–}145)$$

where α = a dimensionless constant corresponding to a drag coefficient,

β = a constant that relates to the resistance of the target material, in lb/sq. in.

ρ_t = target mass density,

A = area of hole,

V = velocity corresponding to 50% probability of perforation,

x = depth of penetration,

and m = mass of pellet.

For best general results, Taylor uses $V^{1.5n}$ instead of V^2, $\alpha=0.40$, and $\beta=3.49\times10^5$ lb/sq. in. There is evidence that a different value of β should be used for velocities below 1,000 ft/sec.

4–12.2.5. (U) *Titanium Alloys*

The considerable experimental data obtained for penetration of titanium alloys is too detailed to be presented here. Perhaps the most extensive data is presented in reports by Midwest Research Institute (Ref. 100), describing the depth of penetration, ballistic limits, and the various parameters used for comparison.

4–12.2.6. (C) *Soft Targets*

Repeated experiments (Ref. 104) with steel spheres of various sizes showed consistently that a critical striking velocity of $V_c=5{,}200$ cm/sec. is required to break the skin of goats, which is considered to be compatible with

human tissue. The experimental data were all consistent with

$$V_r = (V_s - V_r)\, e^{-1.32\, s/d} \qquad (4\text{–}146)$$

where V_r is the remaining velocity after emergence, V_s the striking velocity greater than V_c, s the skin thickness in centimeters, and d the sphere diameter in inches. Sterne (Ref. 105) rewrites the equation, to account for an (A/m) factor, as

$$V_r = (V_s - V_c)\, e^{-1.32 s \left(\frac{A}{m}\right)}. \qquad (4\text{–}147)$$

where A is the missile cross-sectional area, and m is the mass of the missile.

For fragments striking the skin, and for average skin thickness of $s = 0.176$ cm

$$V_s = 5200 + V_r\, e^{0.0332\, A/m}. \qquad (4\text{–}148)$$

For penetration through soft tissues with steel balls

$$V_s = V_r\, e^{1.32 s/m} \qquad (4\text{–}149)$$

For penetration, P, through bone, with steel spheres of radius r

$$P = 2.31 \times 10^{-6}\, r^3\, V_s^2 \qquad (4\text{–}150)$$

with P in millimeters, r in inches, V_s in ft/sec.

For complete penetration of non-spherical fragments through bone

$$V_s = V_r \left(1 + \frac{8.06 \times 10^{-5}\, PA^{1/2}}{mV_r^2}\right)^{1/2} \qquad (4\text{–}151)$$

in cgs. units.

For penetration into gelatin tissue models, the dynamics of a sphere above the critical velocity are described by the following equation (Ref. 52). The constants of this equation have the values listed in Table 4–30.

$$-\frac{dV}{dt} = aV^2 + BV + \gamma \qquad (4\text{–}152)$$

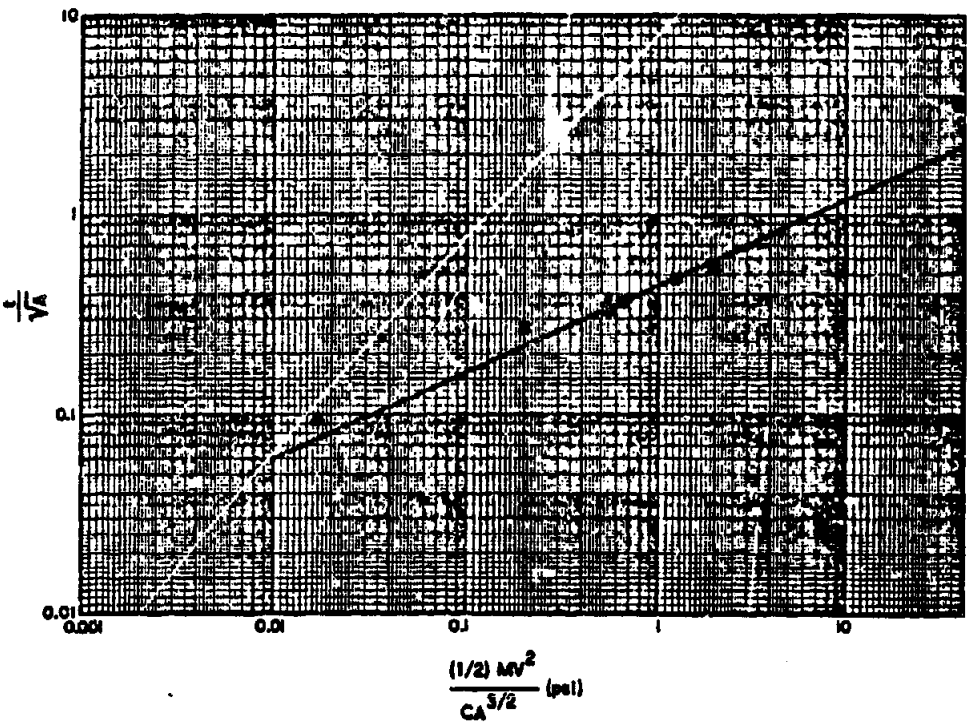

Figure 4–123 (S). Graph of $1/2MV^2/CA^{3/2}$ vs $t/\sqrt{A}$, for 60 Degrees (U)

where V = velocity in m/sec.,
and t = time in seconds.

When the velocity of the sphere is below the critical velocity

$$-\frac{dV}{dt}=\frac{aV_c+BV_c+\gamma}{V_c}V \qquad (4\text{–}153)$$

where V_c = critical velocity.

The general equations of penetration into gelatin are

$$-\left(\frac{m}{A}\right)^{1.21}\frac{dV}{dt}=a_1V^2+B_1V+\gamma_1$$

(above critical velocity) (4–154)

and

$$-\left(\frac{m}{A}\right)^{1.21}\frac{dV}{dt}=\frac{a_1V_c+B_1V_c+\gamma_1}{V_c}$$

(below critical velocity) (4–155)

where

a_1 = 20.207,
B_1 = 1,925,
γ_1 = 333,000,
A = cross-sectional area of sphere, in square meters,
and
M = weight of sphere, in kilograms.

By the proper integration of the above equations, the velocity, time, and distance of penetration at any point in the gelatin target can be calculated, if the striking velocity and the size and weight of the sphere are known.

4–12.3. (C) Residual Velocity Data

4–12.3.1. General

It is necessary when considering penetration by fragments to remember that there is no one velocity limit above which perforation (for a given set of parameters) will occur, and below which perforation will not occur. There is rather, a range of velocities over which perforation may or may not occur; the probability of perforation being close to zero at the lower end of the range and closer to 1 at the higher end. Furthermore, the velocity differential at which perforation may occur is wider in the, say, 9,000 fps regime, than it is in the 1,000 fps regime. This means that the "ballistic limit" (see Ch. 6, Par. 6–13.2.) is less meaningful at higher velocities. The upper and lower ends of the range are of more interest than the ballistic limit. Also, perforation alone is not the sole criterion for defeat of the target material. The target material, itself, is usually an intermediate target (the armor of a tank, the hood of a truck) which protects the primary target (tank crew and combustibles, an engine block). What is of interest is whether or not the perforating fragment has enough residual velocity and residual mass to damage the primary target, and if so, how badly.

These questions would not be important if it were possible to estimate the residual weight and velocity of fragments, after impact, under a variety of conditions (Ref. 115). The residual velocity estimate could then be associated with an estimate of residual fragment weight, so that a better decision could be rendered with respect to the primary target. The criterion for success is no longer, therefore, whether or not perforation occurs, but is based on behind-the-plate damage.

4–12.3.2. The Residual Velocity Concept

It has been recommended that the ballistic limit be replaced by two other values of strik-

TABLE 4–30 (C). VALUES OF CONSTANTS FOR EQ. 4–152 (U)

Sphere	Critical Velocity	a	B	γ
3/16 in.	30 m/sec.	5.85	925	97,000
1/4 in.	20 m/sec.	4.42	544	75,070
3/8 in.	15 m/sec.	8.00	250	50,000
7/16 in.	10 m/sec.	2.90	120	46,000

ing velocity (Ref. 115). The first, called the protection velocity, V_p, is used to identify the highest striking velocity below the ballistic limit at which the fragment never perforates the plate. The second, called the guarantee velocity, V_g, will identify the lowest striking velocity for which the fragment is assured of success in perforating the armor.

Experimental residual velocity data have been collected with respect to mild steel, Dural, bullet-resistant glass, and Plexiglas (Ref. 115). From these data, an empirical relationship for predicting fragment residual velocities for each material has been derived:

$$V_r = V_s - K(eA)^{\alpha} m^{\beta} (\sec\theta)^{\gamma} V_s^{\lambda} \qquad (4\text{–}156)$$

where

V_r = the fragment residual velocity, in fps,

V_s = the fragment striking velocity, in fps,

e = the plate thickness, in inches,

A = the average impact area of the fragment, in square inches,

m = the weight of the fragment, in grains,

θ = the angle of obliquity between the trajectory of the fragment and the normal to the plate, and K, α, β, γ, and λ are constants that are determined separately for each material.

The basic formula is converted into the associated logarithmic form:

$$\log(V_s - V_r) = \log K + \alpha \log(eA) + \beta \log m + \gamma \log \sec\theta + \lambda \log V_s. \qquad (4\text{–}157)$$

With this linear form, the method of least squares is employed to determine a satisfactory set of values for K, α, β, γ, and λ for each material. This concept is developed in much more detail in Ref. 115, and cannot be fully treated here.

A typical set of results of these studies is illustrated in Fig. 4–124, where the ratio of residual velocity to striking velocity, $\frac{V_r}{V_s}$, is plotted against striking velocity for eight different thicknesses of mild steel. It can be seen that a 30-grain fragment impacting a mild steel plate 0.05" thick, at a striking velocity of 2,000 fps, will have a residual velocity between 1,000 and 2,000 fps. By interpolation, a residual velocity of approximately 1,220 fps is indicated. The same fragment impacting a plate 0.10" thick (other parameters unchanged), will have a residual velocity of only 500 fps.

The results of the above ballistics studies emphasized the need of a companion effort to analyze data on the residual weight of steel fragments, after impact under a variety of conditions. A documentation of this effort is found in Ref. 116, a summary of which is found in the following paragraph.

4–12.3.3. *Loss in Fragment Weight During Perforation*

With low striking velocities, the loss in weight of a fragment during perforation is small, and is usually ignored (Ref. 116). With the advent of high striking velocities, the break-up of the fragment is inevitable and spectacular, and can no longer be disregarded. The residual weight of the fragment, as well as the residual velocity, must be known to the vulnerability analyst. Only then can a reasonable estimate be made of the continuing potentiality of the fragment to create damage.

In most cases, the weight of the largest piece of fragment approximates the total weight of fragment recovered. The ability of the fragment to damage a primary target beyond an initial barrier can be conservatively approximated, by considering the residual velocity of only the largest piece of fragment which successfully perforates the barrier.

An empirical approach, similar to that which has been used and described for obtaining an equation relating loss in velocity to impact parameters (Eq. 4–157) has been attempted for estimating loss in fragment weight. The form of the equation fitted to the data is:

$$m_r = m_s = 10^{c}(eA)^{\alpha} m^{\beta} (\sec\theta)^{\gamma} V_s^{\lambda}, \qquad (4\text{–}158)$$

where

m_s = the initial fragment weight, in grains,

m_r = the residual weight, in grains, of the largest piece of fragment which passes through the target, and c, α, β, γ, and λ

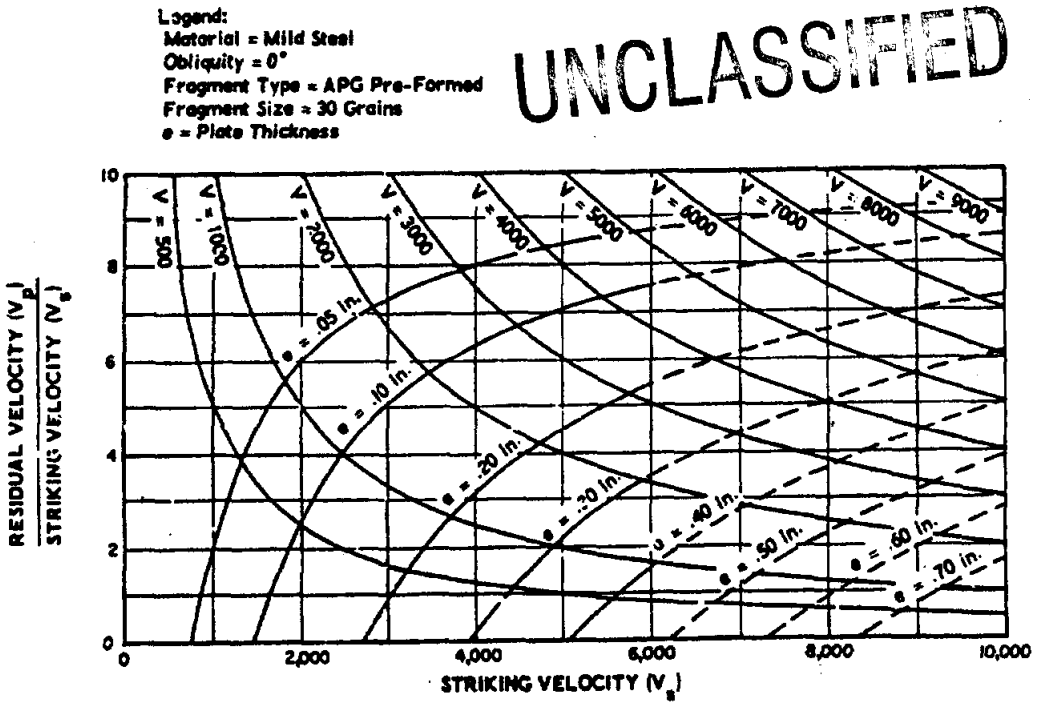

Figure 4–124 (C). V_r/V_s vs V_s for Selected Plate Thicknesses (U)

are constants determined separately for each target material.

All constants are determined by the application of the method of least squares to the linear equation relating the Briggs' logarithms:

$$\log (m_s - m_r) = c + \alpha \log (eA) + \beta \log m + \gamma \log \sec \theta + \lambda \log V_s. \qquad (4\text{–}159)$$

To accommodate this logarithmic treatment, a fragment which emerges intact is assumed to have lost one grain in weight.

This concept also is more fully treated in the original document (Ref. 116). Fig. 4–125 is an illustration of the type of data obtained. As in Fig. 4–124, $\frac{V_r}{V_s}$ is plotted against V_s. However, the abscissa on the right plots the ratios of residual mass to striking mass, $\frac{m_r}{m_s}$, against striking velocity for selected plate thickness. A graph of this type permits the vulnerability analyst to estimate the residual mass and velocity (for the material tested) of an impacting fragment of known velocity and mass.

For a more detailed understanding of the concept of residual velocity and residual mass, the reader is referred to Refs. 115 through 117.

4–12.4. (U) Experimental Techniques

In experiments concerning penetration and perforation by single fragments, a means of controlled fragmentation is usually employed to eliminate approximations of fragment size, weight, and impact area in the empirical equation of penetration. Regular shapes such as spheres, cubes, prisms, and cylinders are used, and in line with current thought, they are normally in the weight range of 1/4 to 1/25 ounces.

The fragments may be launched one at a time from a smoothbore gun, or they may be projected by a controlled fragmentation type explosive bomb or warhead. By either launching method, it is possible to produce fragment ve-

locities up to about 16,000 ft/sec. The velocities of explosively launched fragments may be measured by one of the methods described in Par. 4–11.2.2, such as: break-wire (Ref. 91), tin-foil "make" screens (Ref. 107), light interrupting screens, spark photography (Ref. 91), or Faraday shutters (Ref. 107). Kerr cells and X-ray photography are used with gun-launched projectiles.

The attitude of fragments is indicated by the pattern they make in passing through the velocity screens.

One technique is the use of target plates located at various distances from the bomb (approximately 16 feet, depending on bomb size) and arranged in a semi-circular pattern. The plates are positioned at predetermined angles to the line of fragment flight, so that penetration data as a function of angle of obliquity can be obtained.

Jameson and Williams (Ref. 107) discuss a method of obtaining projectile velocities before and after the target plate. The projectile velocity above the plate is found by using make screens, of photographic mounting tissue sandwiched between aluminum foil 0.0007 inch thick, and Potter chronograph counters, model 450. Projectile orientation is determined by using the plates, themselves, as yaw cards.

Make screens, however, can not be used below the plates, because it becomes impossible to determine what velocity is being measured. A photographic technique, which is a variation of the usual shadowgraph method, proves adequate for this purpose. This method employs two one-half microsecond Rapatronic shutters (Edgerton, Germeshausen, and Grier) and a half-silvered mirror. The projectile is backlighted by slightly convergent light from a double spark source. The time between exposures is controlled by a preset interval generator, and is recorded on 1.6 megacycle, model 450 Potter chronograph counters. The preset interval generator is triggered by the pulse

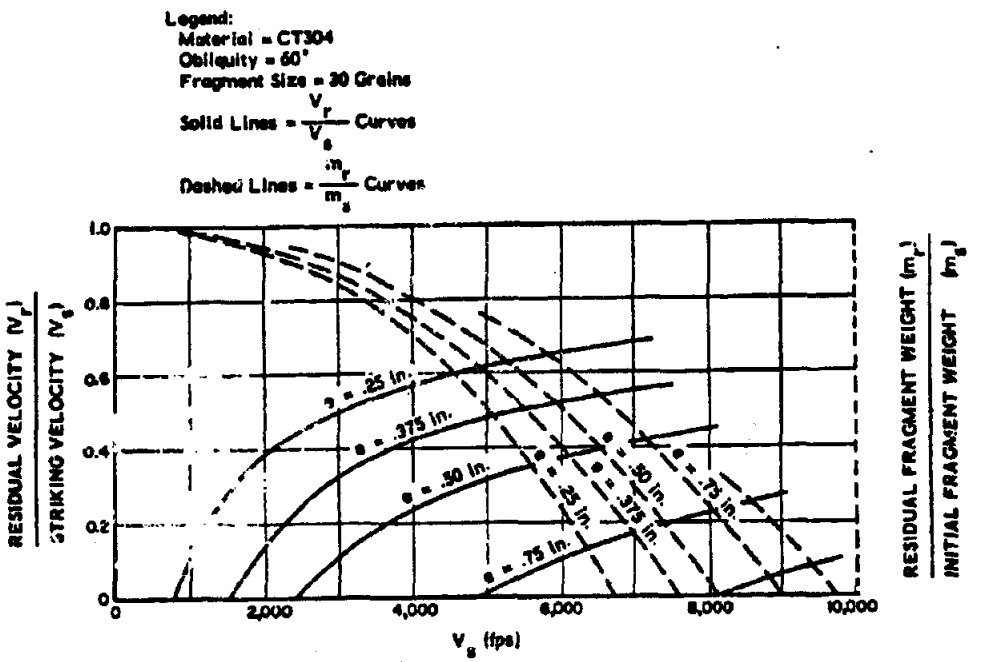

Figure 4–125 (C). V_r/V_s and M_r/M_s vs V_s for Selected Plate Thicknesses (U)

from the second screen of the pair of screens used to determine projectile velocity above the plate. Fragment and projectile shapes are determined both from pictures and by recovery of samples for comparison.

4–13. (U) HYPERVELOCITY FRAGMENTS

4–13.1. Introduction

The theoretical and experimental aspects of fragment impact in the hypervelocity regime are presented in this paragraph, which also includes a discussion of the state-of-the-art. A general description is also given in Ch. 2, Sec. I.

4–13.2. Theory

4–13.2.1. General

The superficial differences between the process of penetration at moderate velocities and the effects of hypervelocity impact are illustrated by Fig. 4–126, which shows craters produced in lead targets by steel spheres impacting at a variety of velocities (Ref. 108). At relatively low velocities (top-left view), the projectile penetrates the target without being deformed and forms a deep, roughly conical cavity. If the velocity is increased by a modest amount, as shown in the second view (top-right), the amount of cavitation produced increases considerably but the cavity does not become significantly deeper. In this velocity range. the pellet begins to be deformed but not destroyed. Increase in impact velocity to approximately 1 km/sec. results in complete destruction of the pellet and in the formation of a crater which is considerable greater in diameter, but still not significantly deeper. (Note that gun velocities are given in the nomenclature of that phase of the science, i.e., ft/sec., but that pellet velocities from explosive devices are given in m/sec.) Further increases in velocity to 1.7 km/sec., 1.9 km/sec. and, finally, to 3.1 km/sec., result in successive increases in the dimensions of the crater, and a closer approximation to a hemispherical shape. The hemispherical shape of the crater is considered a necessary, although not a sufficient, indication for hypervelocity impact.

The transition from the narrow, deep cavity to the hemispherical cavity can be produced at

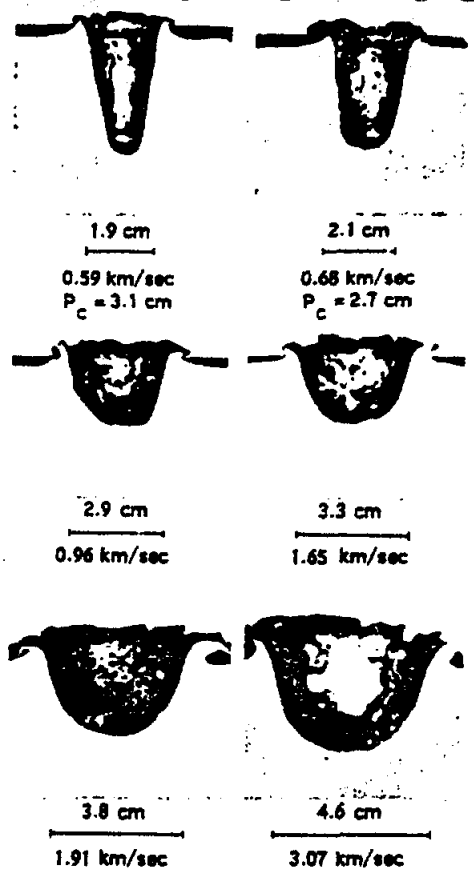

Figure 4–126. Steel Pellet Penetration Into Lead Targets, at Various Pellet Velocities

lower velocities in soft target materials, by using soft projectiles. Therefore, the condition is not simply one of velocity, but also depends upon the strength characteristics of the materials. Higher velocities are required with either harder target materials or harder projectiles. At the higher velocities, the pellet is not only deformed and destroyed, but it is found plated over the surface of the resulting crater

Another, more critical, criterion for hypervelocity impact depends upon the behavior at oblique incidence. At lower velocities, as illustrated in Fig. 4–127, the crater produced at high angles of obliquity is very asymmetric and

considerably shallower than that produced at low angles of obliquity or at normal incidence. However, if the velocity of impact is increased, even at very high angles of obliquity, a completely symmetrical and hemispherical crater will be formed. In the case of a steel pellet fired into a lead target, a velocity of 3.2 km/sec. is sufficient to produce a hemispherical crater even at 60 degrees obliquity. The volume of the crater, however, is considerably smaller than would be obtained with the same projectile traveling at the same velocity but impacting at normal incidence. It has been found, empirically, that to assure a symmetrical, hemispherical crater, the impact velocity must be so high that the components normal to the target surface exceed the shock velocity in the target corresponding to the impact pressure. This condition can be used as another criterion for hypervelocity.

The above-mentioned criteria depend upon only superficial aspects of crater formation. The really fundamental criterion depends upon the velocities of propagation of disturbances in the target material, and the impacting projectile, and upon the equations of state of the two materials. By definition, true hypervelocity impact occurs when the velocity of penetration is greater than the usual propagation velocity of stress waves (sound or dilatational velocity). This insures that deformation of both pellet and target will occur immediately at the interface between pellet and target, with an intense stress front (probably a shock wave) preceding the interface at supersonic velocity. Because pressures produced under typical conditions of hypervelocity impact will be in the megabar range, the velocities of propagation concerned will, in general, be considerably different from the velocity of sound in the material.

All the energy of the system is confined to a small volume, etc., because under the velocity conditions it cannot escape. The explanation of the crater form lies in the answer to such fundamental questions.

One means of obtaining dependable predictions is the establishment of a really satisfactory theory of the phenomenon, with verification by use of such materials as can be subjected to hypervelocity conditions. Considerable effort has been put into theoretical investigations, but thus far with little real success. The most acceptable theoretical treatment carried out thus far is that by Bjork, however, the results appear to be in essential disagreement with experimental observations. With present knowledge, in order to make qualitative predictions of what would be expected to occur in structural materials at much higher impact velocities, reliance must be placed on experimental observations, using such available materials that can be subjected to hypervelocity conditions, and on a physical model of the phenomena that take place.

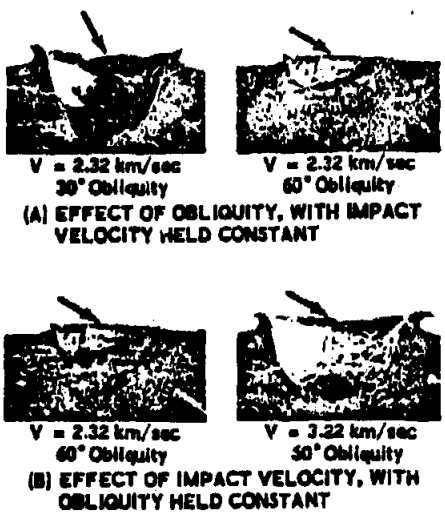

Figure 4–127. Hypervelocity Crater Formation Under Oblique Impact, Steel Pellets into Lead Targets

4–13.2.2. *High Speed Photography, and Electronic Detectors*

One approach to the problem is represented by the photographs in Fig. 4–128. For transparent target materials, high speed framing camera observations can be made before and during the formation of the crater, and the propagation of shock waves can be observed in a quantitative manner. In the pictures shown, which progress in time from upper left to lower right, the pellet can be seen approaching the

target in the third, fourth, and fifth frames. The pellet is a thin disc; the elongated, luminous trail behind it is due to ionization of the air. In the sixth frame, impact occurred, and in the seventh and eighth, the resulting crater can be seen expanding. During these early stages of crater expansion, no detached shock wave is visible. This condition would be anticipated, because in this experiment the impact velocity is much greater than the velocity of propagation of waves in the plastic material

Figure 4–128. High Speed Camera Observations of Projectile Penetration into Transparent Target

used; and even the most stringent conditions specified earlier for hypervelocity impact have been achieved. In the ninth frame, a shock wave can be seen to detach itself from the surface of the crater. In succeeding frames, the shock wave is seen to propagate at a velocity somewhat in excess of the velocity of expansion of the crater, although the crater continues to increase in size. After approximately the twelfth frame, crater expansion is no longer observed, although the shock wave continues to expand and to dissipate its energy throughout the body of the target material.

Quantitative measurements of propagation rates, using such pictures, are being combined with known equations-of-state for the target material, in an attempt to determine the pressures and particle velocities within the material. It is intended that these quantities will then be correlated with the rates of expansion of the crater, in an attempt to test a hydrodynamic model of crater formation.

Similar data are being obtained for opaque target materials, including metals, by inserting electronic detectors at various positions in the target, by means of which the velocities of propagation of stress waves can be measured.

4–13.2.3. The Crater Formation Model

As a result of the described observations, and of other experimental and theoretical investigations, a model has been developed of the phenomenon of crater formation under hypervelocity impact conditions. The model is illustrated by the sketches shown in Fig. 4–129. The relative time required for the crater formation process to reach the stage shown in each view is shown as $\frac{t}{T}$, where T is the total time required to form the crater.

During the initial stages of the process, a mutual deformation of the target and the impacting projectile takes place, in accordance with hydrodynamic concepts. Since the pressure at the boundary during this period is in the megabar range, it cannot be satisfactorily approximated by the use of Bernoulli's equation because of the extreme compression of the material. The velocity of motion of the crater wall exceeds the speed of propagation of stress

waves at the pressures produced, so that all of the energy of the system is contained in a very small volume in a thin layer near the interface.

The crater expands, and the projectile continues to deform until it has been completely deformed and plated over the surface of the crater. The energy of the system is then all contained in a thin layer of target material, and the pressure is to some extent relieved. The rate of expansion of the crater decreases and the wave thereafter propagates at a greater rate than the crater wall, with the volume of material in which the energy is confined increasing rapidly. During all of this period, the combination of radial and shear flow of material in the vicinity of the crater wall results in an ejection of considerable amounts of material at appreciable velocities. Eventually, the expansion of the shock wave and the dissipation of energy result in a reduction in the local pressure below the value required to overcome the intrinsic strength of the material, and the expansion of the crater ceases. The shock wave continues to propagate, and to dissipate energy in the form of heat and local changes in structure of the material which are irrelevant to the process of crater formation. At this stage, that projectile material which has not been ejected remains plated over the surface of the crater wall.

In soft target materials, the expansion of the crater may proceed to such an extent that the plated projectile material is separated into fragments, distributed at random over the surface of the crater. In ductile target materials, the ejection of material terminates in the for-

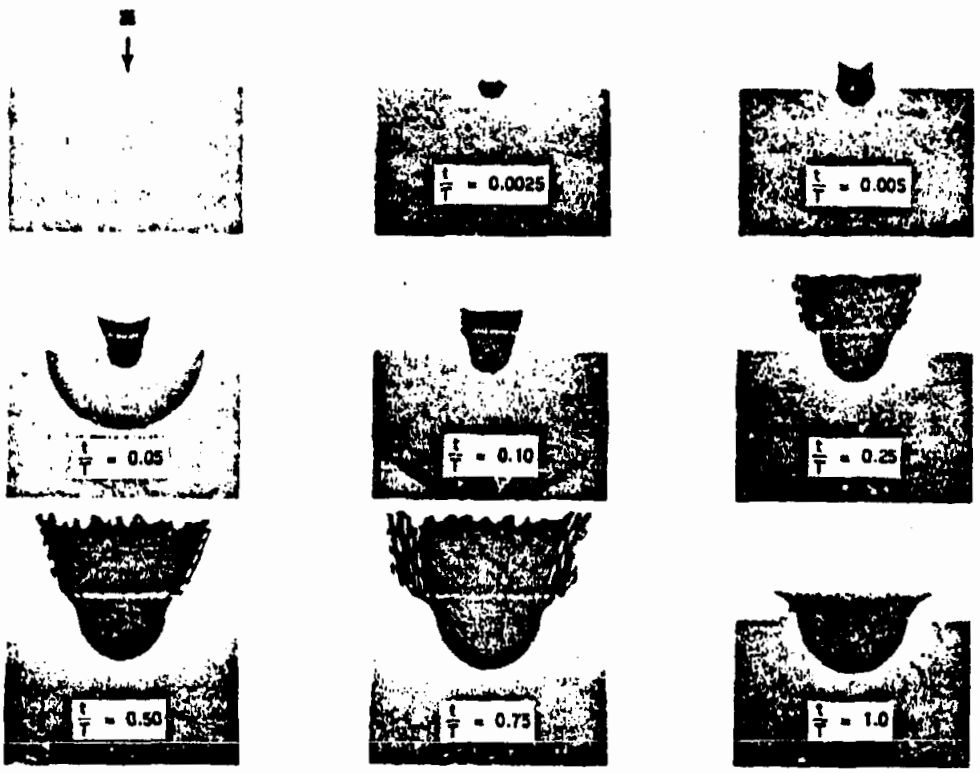

Figure 4–129. Sketch of Crater Formation Phenomenon

mation of an extensive lip at the edge of the crater. In brittle target materials, the propagation of a tension wave from the free surface results in fracture and removal of the lip. In the case of very frangible target materials, extensive shattering may occur and actually obscure the original form of the crater.

It will be noted that at no point in the model is the possibility of "explosion" or fusion of the material suggested. In the early stage of the process, when the energy densities far exceed those required for fusion and vaporization, the material is subjected to such great pressure that its density may be more than double the normal value. Therefore, questions concerning its state are purely academic. Later, after the prssure is somewhat relieved, the energy retained within the material is too low to cause vaporization.

The initial stage of the process, during which the projectile maintains its integrity, but is deforming, continues for only a very short time. If projectile and target material have approximately the same density, the duration of this part of the process can be approximated by $t=\frac{2l}{v}$, where l is the length of the impacting projectile, and v is the impact velocity. Thus, a projectile 1 cm long, striking at a velocity of 20 km/sec., will have completely disappeared as a causative factor after one microsecond, and the crater at that time would have a depth equal to the initial length of the projectile. The second stage of the process, cavitation, may continue for a period of the order of hundreds of microseconds, resulting in a final crater having dimensions many times greater than those of the projectile.

The densities and compressibilities of the projectile and the target material are important in determining the pressures produced, the duration of the initial stage of crater formation, and, consequently, the intensity and shape of the stress wave that produces the later cavitation. The dynamic strength properties of the target material, in addition to density and compressibility, determines the extent of cavitation and the ultimate dimensions of the crater.

From the model that has been developed, several inferences can be drawn that have significance for possible applications. In the first place, plates of thicknesses many times the dimensions of a projectile can be perforated under hypervelocity conditions, but it cannot be expected that any significant portion of the impacting projectile will be found behind a target whose thickness is greater than the dimensions of the pellet. Consequently, behind even moderately thick plates, the only damage that can be anticipated is that produced by fragments of the target spalled off by the stress wave. These particles will be fairly large and will be spread over a considerable area, but will be traveling at relatively low velocities, therefore, their damaging capacity will be determined primarily by the type of internal component being considered ("hard" or "soft"), and not by the mass and velocity of the spall fragment.

4–13.2.4. *Macro-Particle and Micro-Particle Projection and Observation*

A sketch of a typical crater by macro-particle impact (0.1 to 10 grams) in a comparatively ductile material is shown in Fig. 4–130. In the sketch, P_c is the depth of the crater below the level of the undisturbed surface, D_c is the diameter of the crater at that level, and PH is the height of the crater lip or petal above the surface. Fig. 4–131 shows quantitatively how penetration, P_c, into lead targets varies with impact velocity, for projectiles of different materials, as determined by various agencies involved in this work. In order to include data

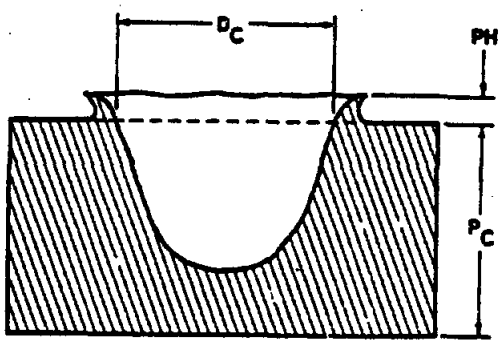

Figure 4–130. Typical Crater Formed by Macro-Particle Impact

for a range of pellet masses, the ordinates have been normalized by dividing penetration depths by the cube root of the pellet mass, in accordance with scaling laws.

It can be seen from the figure that initially, penetration increases very rapidly, and approximately linearly with impact velocity. The slope of this portion of the curve is quite sensitive to the hardness of the projectile. At about 0.6 km/sec., the projectiles tend to fracture, and the penetration falls off rather sharply. For a comparatively hard projectile, a velocity is reached where fracture occurs shortly after impact, and penetration is continued by each of the individual pieces. Because in aggregate these present a larger area in the direction of motion, and because at low velocities penetration is inversely proportional to the presented area of the projectile, the penetration falls off rapidly. As the impact velocity is increased still further, the penetration again starts to increase.

Referring to the figure, the significant point should be made that, when the impact occurs in the hypervelocity range, penetration relations obtained at low velocities cannot be used, because penetration is being produced by an entirely different mechanism. At low velocities, the projectile maintains its integrity and pushes aside the target material that is ahead of it; thus, during the entire penetration process, the pellet is present as a causative force. At hypervelocities, the pellet acts as a point source of energy on the free surface of the target. Whereby, the projectile acts like an extremely short shaped-charge jet, and is used up within a few microseconds after impact, while the crater continues to increase in size for a considerable time afterward.

Equipment and techniques are described in Ref. 109 for the projection of hypervelocity micro-particles and in the evaluation of their terminal ballistic effectiveness. Velocities of 12.0 km/sec. have been achieved by these techniques for clusters of micro-particles in the size range of 1 to 100 microns. Higher velocities are expected with suitable refinement and modification of the means of projection.

It is not possible to associate a particular measurable microcrater with a unique deter-

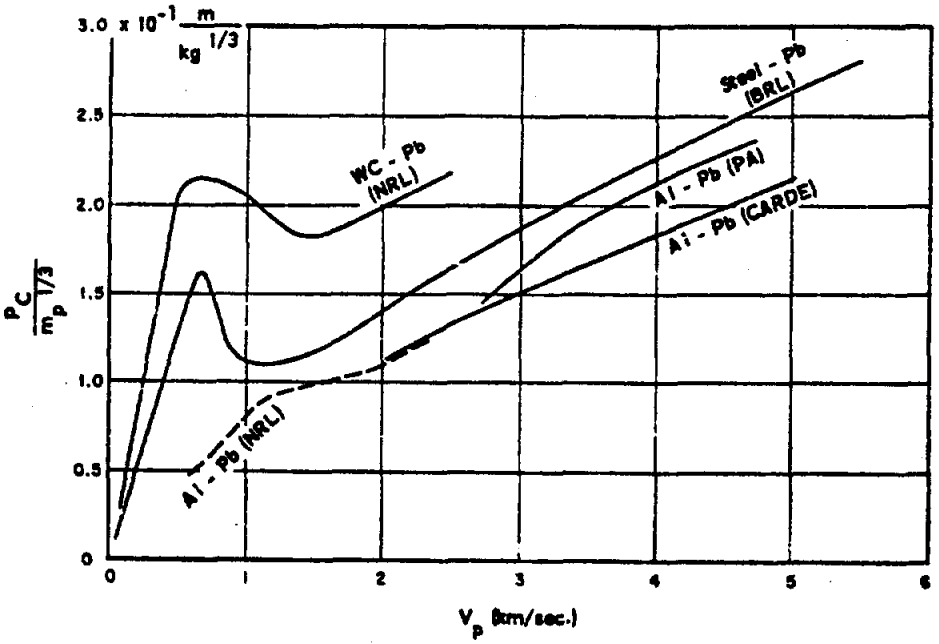

Figure 4–131. Quantitative Presentation of Projectile Penetration Into Lead Targets, at Various Impact Velocities

minable particle mass, for quantitative analysis of velocity-energy cratering relationships. Therefore, it is necessary to treat the crater measurements statistically for relating to corresponding particle size and, hence, to mass.

For several materials, targets exhibiting several hundred measurable craters have been subjected to crater size distribution counts and analysis. It was found that a 100-micron particle forms a crater approximately 730 microns in diameter in a copper target. Converting the particle size to mass gives a value of 4.5 cm/grams$^{1/3}$ for comparison with macro observations at lower velocities. Fig. 4–132 shows this comparison plotted together with some data of Kineke's which is previously unpublished (Ref. 110). The solid line represents the data for the macro pellets, for which detailed analysis is still incomplete. Similarly, the 100-micron particle corresponds to a 1,150-micron diameter crater in lead, and the normalized value computes to 7.0 cm/gram$^{1/3}$ for comparison with the micro pellet lead data of Fig. 4–132. The double-circled point with an arrow, indicating the value reported at the Third Hypervelocity Symposium, is plotted to show the effect of refinements in technique.

The statistical distribution method of treating the particle size versus crater size correlation has resulted in the determination of the size of crater, formed by a given mass particle, at an impact velocity of 10 km/sec. in lead and copper targets. These techniques are presently undergoing further necessary refinements, in order to extend the observations to higher velocities, in excess of 12 km/sec, and other target materials. Results of these experiments, together with the macro pellet data, indicate that scaling laws hold for the range of particle mass from 10^{-4} to 10.0 grams.

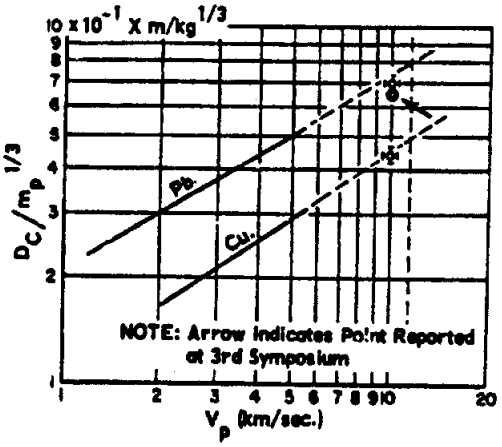

Figure 4–132. Comparison of Observations of Micro-Particles at 10 km/sec. with Micro Data at Lower Velocities, for Two Target Materials; Diameter vs Velocity

Figs. 4–133 and 4–134 show penetration, P_c, of various projectiles into aluminum and copper targets. It is evident that the penetration depends upon such physical and mechanical properties as density, hardness, and yield strength of both the target and projectile materials.

4–13.3. (U) Experimental Techniques

4–13.3.1. *General*

The acceleration of projectiles for the study of hypervelocity phenomena is accomplished by three general classes of projectile accelerators. They are light gas guns, high-explosive devices, and electrostatic and electromagnetic accelerators. Light gas guns include both the expendable and non-expendable types, while explosive devices include both single pellet projectors and devices that produce a number of particles.

4–13.3.2. *Light-Gas Guns*

Fig. 4–135 is a schematic diagram of the operation of a typical light gas gun. In the first stage of the gun, a conventional gun-cartridge case containing propellant accelerates the piston and, thereby, compresses the light gas. After about three milliseconds of compression, the light-gas pressure increases from an initial value of approximately 600 psi to approximately 100,000 psi, and a temperature of 3,600 degrees Fahrenheit. At about this time, the shear disc ruptures, and the projectile begins its movement down the bore of the second stage of the gun. Because of the large mass of the piston, its inertia causes it to continue the compression stage and push the light gas down the bore of the second stage, behind the projectile.

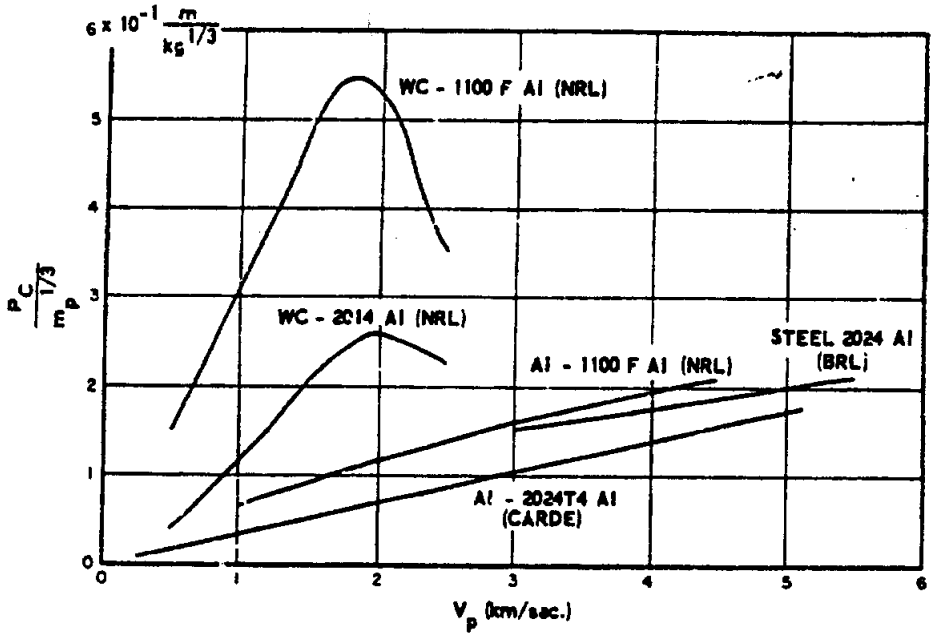

Figure 4–133. Quantitative Presentation of Projectile Penetration Into Aluminum Targets, at Various Impact Velocities

Limitations to the maximum velocity of conventional light-gas guns are:

1. A shock is propagated down the barrel ahead of the projectile, which causes the projectile to break up when the gun is operated near its maximum conditions.
2. The maximum pressure within the chamber is limited by the strength of the chamber material.
3. The available kinetic energy is divided between the driving gas and the projectile; therefore, a large fraction of the

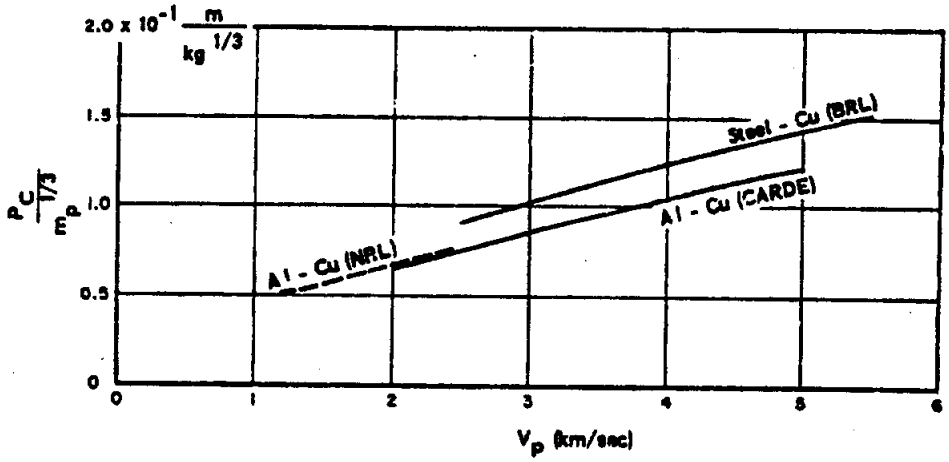

Figure 4–134. Quantitative Presentation of Projectile Penetration Into Copper Targets, at Various Impact Velocities

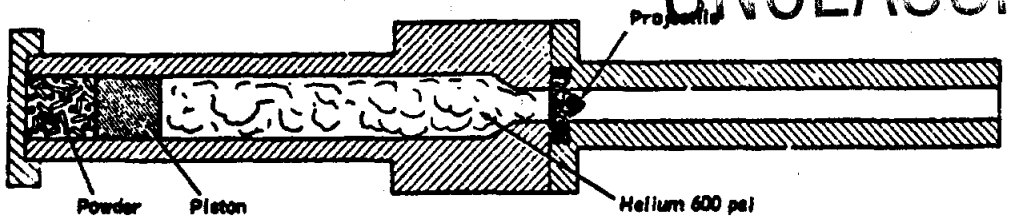

(A) BEFORE FIRING

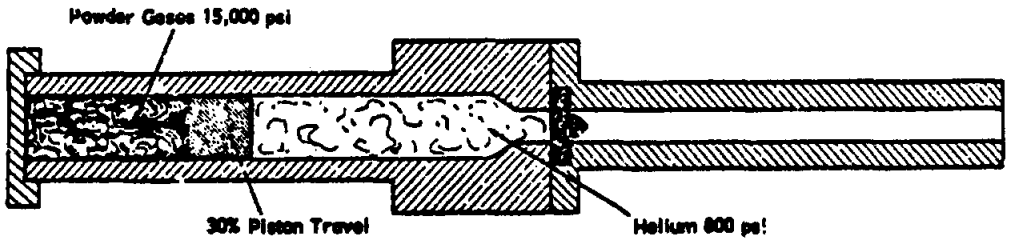

(B) 2 MILLISECONDS AFTER FIRING

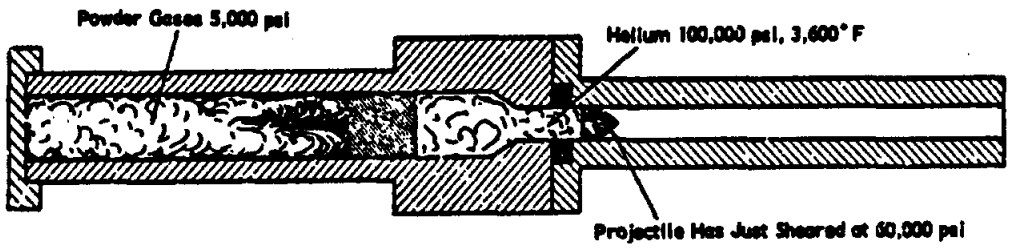

(C) 3 MILLISECONDS AFTER FIRING

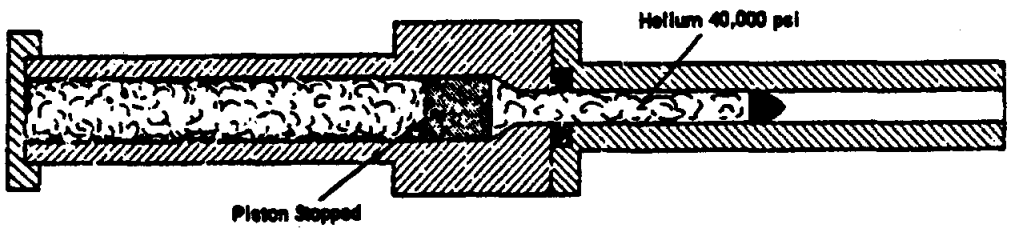

(D) 3.1 MILLISECONDS AFTER FIRING

Figure 4–135. Typical Light-Gas Gun Operation, Schematic Diagram

available energy is used in moving the gas, even when a light gas like hydrogen or helium is used.

Shocks in the barrel of the gun can be prevented to some extent by evacuating the bore. Most of the research efforts to date have concentrated on raising the maximum chamber pressure, by operating near the limits of the strength of the material, and on reducing projectile fracture by varying the thickness and strength of the projectile.

The maximum velocity obtainable with exist-

ing light-gas guns is about equivalent to that obtainable with explosive devices. Reproducibility of data with light-gas guns is not as satisfactory as with explosive devices. In addition, the initial cost of existing guns is very high, and they are also very expensive to operate on a per-shot cost basis. For these reasons, only a limited amount of usable data has been obtained by this method.

4–13.3.3. *Expendable Guns*

In view of the high cost and the limitations of the more conventional light-gas guns, several investigations have been made into the use of expendable gun systems. Since explosives represent a cheap and compact energy source, they have been used to obtain the necessary high pressures within the gun chamber. This brute-force technique has the disadvantage, however, of an extremely rapid rise in pressure, which tends to cause pellet breakup in the barrel of the expendable gun system.

The techniques used in this instance are illustrated in Fig. 4–136 wherein a conventional gun design, if it may be considered as such, has the chamber of the gun surrounded with high explosive (Ref. 111). At an appropriate time, after the first detonator has released the helium, the HE is exploded by means of its detonator, thus collapsing the chamber to essentially zero volume, compressing the light gas, and accelerating the projectile. A second design for an expendable gun is that shown in Fig. 4–137. The explosive is placed within and at the rear of the gun chamber. Upon detonation, the pressure rise is attenuated through the air chamber, so that pellet breakup is inhibited.

Each of these guns is capable of projecting an intact pellet at 12 000 fps, or a broken pellet at 18,000 fps. Tests are being conducted with the goal of obtaining velocities in the order of 18,000 fps with an intact pellet, by varying the attenuation of the pressure pulse rise, or by varying the chamber wall thickness, or by varying the pellet strength, in such a manner that the high explosive does not cause the breakup of the pellet.

4–13.3.4. *Repeated Pulse and Traveling Charge Guns*

The repeated pulse gun acts on the principle of firing a pellet through a hole along the axis of an explosive cylinder. As the pellet emerges from the front end of the explosive cylinder, the explosive is detonated. In principle, the explosion will accelerate the projectile by a finite amount. By using one, two, or many stages of high explosives, and by detonating each charge of explosive at the appropriate time, it should be possible to realize a small increase in velocity with each stage of the gun. Ideally, it should be possible to achieve almost any velocity, up to the escape velocity of the detonation products, given controlled explosion timing and controlled pressure pulse shape, provided the projectile maintains its straight course along the axis of the explosive charges.

The traveling charge gun is based on the principle of Langweiler (Ref. 112), which requires a propellant, with a high linear burning rate, affixed to the base of the projectile in a more or less conventional gun system. Because the propellant is traveling along with the projectile, it is not necessary to maintain an extremely high pressure nor an extremely high

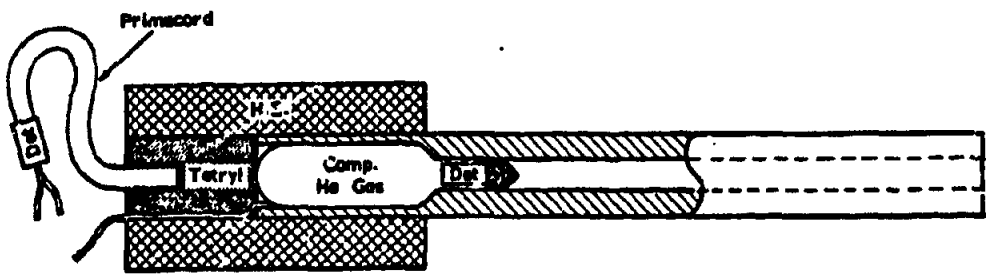

Figure 4–136. Representative Expendable Gun, Using External Explosive

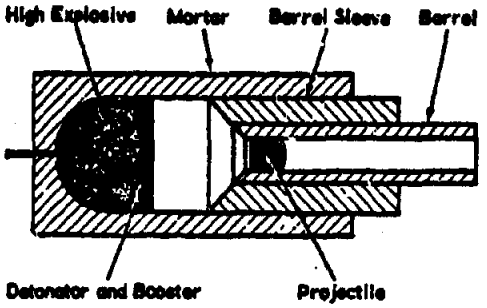

Figure 4–137. Representative Expendable Gun, Using Internal Explosive

sonic velocity in the propellant gas. If the propellant can be controlled to such an extent that it burns uniformly, and imparts a suitable fraction of its energy to the base of the projectile, it should be possible to realize an extremely high projectile velocity. Attempts to date to build a traveling charge gun have provided only a ten per cent improvement upon the normal velocity of a conventional gun system, primarily because it has not been possible to control the burning of the propellants that were used.

4–13.3.5. *High-Explosive Devices*

Three explosive charge designs used to obtain hypervelocity pellets are shown in Fig. 4–138 (Ref. 113). In the first type, a pellet is placed on the end of a simple explosive charge and confined with a "surround," which is usually made of a material such as lead, that will be vaporized by the detonation. The second type is the air cavity charge, in which a pellet is embedded in an air cavity in the case of an explosive charge. The third type is the self-forging fragment (Ref. 80).

Charge designs (A) and (C) of Fig. 4–138 have been made to accelerate masses at velocities approaching 7,000 m/sec.; however, the mass of the projected pellet has not been reproducible. Consequently, these designs have not been used extensively to obtain terminal ballistic data.

The most promising of the three designs is that using an air cavity (B), which reduces the pressure on the pellet and alleviates breakup (Ref. 113). By varying the dimensions of the air cavity and the thickness of the pellet, intact masses having a known velocity and mass have been projected at velocities of from 2,000 m/sec. to 7,000 m/sec. In every instance, the pellet lost some mass around its periphery, the quantity depending upon the particular charge design used. In general, it has been found that as the depth of the air cavity behind the pellet is increased to a limit, the velocity of the pellet is increased: beyond this point the pellet breaks up. As the velocity of the pellet increases, however, the mass lost is reproducible for a given pellet and charge design. The final mass of a given pellet is reproducible to less than 3 per cent of probable error.

4–13.3.6. *Shaped-Charge Accelerator of Micro-Particles*

Micro-particles can be fired in a cloud from a low-angle, conical-cavity charge. These small masses (10^{-11} to 10^{-4} grams) have been fired at velocities of up to 15 km/sec. A statistical technique is used to obtain data on single impacts. Two kinds of charge that have been used effectively to accelerate micro-particles are described below (Ref. 114). A 20-degree cone having a very thin wall (0.010 inch or less) has provided particle velocities of up to 10,000 m/sec. and a cylinder has been used to project particles up to 12,000 m/sec. The designs and properties of the materials are such that a conventional jet is not obtained from this type of shaped charge. Instead, a cluster of particles having a preferred particle size, depending upon the grain size of the original liner ma-

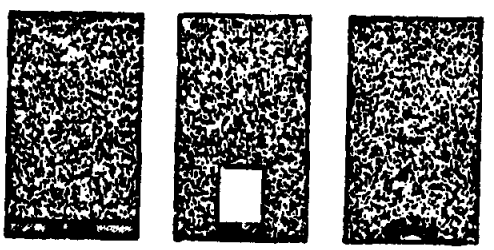

Figure 4–138. Representative Explosive Charge Designs for Hypervelocity Projectile Tests

terial, is projected at high velocity. This small cluster of particles is quite compact and has very little gradient in velocity. Trailing the high-velocity cluster of particles will be the slug and residue material, which are natural consequences when using shaped charges. This massive material, however, is moving at a velocity low enough so that it can be eliminated with an explosive shutter.

As described and illustrated in Ch. 2, Sec. III, when the metal liner of a shaped charge collapses on charge detonation, a ductile jet is formed which is continuous in nature and has a velocity gradient from its tip to its tail (Ref. 110, J. E. Feldman, Jr., "Volume-Energy Relation from Shaped Charge Jet Penetrations"). The jet ultimately breaks off from the liner slug and, when it has reached its maximum elongation, begins to break up into discrete particles. In principle, it should be possible to consider each element of the jet as a separate entity, and to determine the volume of crater in the target due to each increment of jet length. Ideally, from a single shaped charge firing, one can obtain the volume of crater produced in the target per-unit-energy of the impacting material for a complete spectrum of velocities, due to the velocity gradient of the jet. It should be possible, therefore, to obtain data from a conventional, copper-lined, shaped charge at velocities ranging from 8,000 m/sec. at the tip to approximately 2,000 m/sec. at the tail of the jet.

Another shaped charge used to obtain high velocity crater data is the charge with a cylindrical liner. Normally, cylindrical liners do not produce a jet-like configuration, but rather a dispersed scatter of fragments. This is true when the liner material approaches the stagnation point, at a velocity in excess of the elastic wave velocity of the liner material. However, if an explosive is used that has a detonation rate such that the liner approaches the stagnation point at less than the elastic wave velocity, a true jet can be formed. By using Baratol explosive (detonation rate, 4,900 m/sec.) and a cylindrical aluminum liner (elastic wave velocity, 5,100 m/sec.), a well-defined jet is obtained having the velocity of 9,800 m/sec. The length of the jet was approximately one-half the length of the original liner and, in flash radiographs, appeared to have little or no velocity gradient.

Using beryllium liners (elastic wave velocity, 12,000 m/sec.) and explosives having a detonation rate in excess of 9,000 m/sec., appreciably large, yet well-defined, masses of material have been projected at velocities as high as 21,000 m/sec. Use of wave-shaping techniques should even permit velocities up to 50,000 m/sec. with the same materials.

4–13.3.7. *Electromagnetic and Electrostatic Accelerators*

The techniques of electromagnetic and electrostatic acceleration of particles have been investigated for some time. Electromagnetic accelerators are dependent upon the characteristics of the power supply. A number of power supply types, including capacitors, inductors, rotating machines, and batteries have been used; none, however, have shown great success. Direct current rail guns have been successful in accelerating 10 gms to 3,300 ft/sec., and 45 gms to 2,000 ft/sec., velocities not high enough for hypervelocity particle work. It can be concluded, therefore, that a successful electromagnetic accelerator has not yet been built.

Electrostatic acceleration of small particles is even less feasible than electromagnetic acceleration, since the charge is only on the surface of the body and is limited by the field strength of the air. It is, therefore, necessary to make the particles as small as possible in order to increase the charge to mass ratio, so that greater velocities may be possible. Macroscopic particles cannot be accelerated practically to high velocities by electrostatic means; it has been calculated that an acceleration potential of 1 million volts is required to accelerate a 2 micron copper sphere to 20 km/sec. Furthermore, the actual surface charge density will be less than calculated, due to surface irregularities and charging difficulties, so that the required accelerating potential is actually greater than calculated.

It has been concluded that neither electromagnetic or electrostatic accelerating tech-

niques are practical. With great cost and effort, an electromagnetic system could possibly be coupled with a non-electromagnetic first stage used to overcome the original inertia of the projectile. Electrostatic accelerators could possibly be used to accelerate particles less than 1 micron in diameter.

4–13.3.8. Summary

Each of the techniques available to the experimeter, by which hypervelocity projectiles can be obtained, has been briefly described. It has been seen that, with conventional light-gas guns, velocities up to approximately 23,000 ft/sec. have been obtained. Future efforts, specifically along the lines of a combination light-gas electric-discharge gun, could in the future lead to velocities as high as 35,000 ft/sec. Expendable guns have given velocities as high as 18,000 ft/sec.; if pellet breakup can be overcome, possibly this present limit could be extended. Light-gas guns are expensive, particularly at velocities much above 12,000 ft/sec. They are flexible in being able to project a variety of pellet shapes, masses, and materials, although the effect of saboting, and the loss in velocity when pellet density is increased must be carefully considered.

The high-explosive techniques described (particularly the air cavity charge) have led to the capability of projecting fragments to velocities of 7,000 m/sec. No estimate of a limiting velocity for the air cavity charge is available. Explosive techniques are most promising for two reasons: first, they provide reproducible pellet masses and velocities; and, secondly, they are cheap and easy to use. A terminal ballistic program requiring many shots can be accomplished with relative ease and little expense.

The conventional shaped charge technique of projecting a stream of large particles having a spectrum of velocities shows promise, but remains to be proven. The most significant advance in this area is in the technique described for producing short jets with little velocity gradient, thereby projecting tangible masses to velocities in excess of twice detonation velocity (18,000 m/sec.).

Small shaped charges using a cast iron liner for projecting micro-particles have been used with marked success. Unfortunately, there is always a question as to the mass of a discrete particle which caused a particular crater in the target. Attempts to obtain an accurate correlation between crater dimensions and mass have been based on a statistical treatment. However, it is possible to project microscopic particles up to velocities of at least 12,000 m/sec. This velocity represents the highest obtained by actual experiment.

Section IV (U)—Detonation Physics

4–14. INTRODUCTION

4–14.1. Scope of the Section

This section is concerned with the collection and analysis of data covering the physics of explosive detonation. The mathematical theory covering the detonation processes, including the usual equations of hydrodynamics, is outlined, and the implications of the theory with regard to propagating shock and detonation waves in explosives are discussed.

Experimental techniques for the study of detonation waves are also discussed. These include such methods as the pin technique, streak photography, X-ray, and optical techniques, and a discussion of recent developments in the use of high-speed cameras. In addition, empirical data such as detonation velocities, equations of state, and thermochemical properties of different materials are presented.

4–14.2. Cross-Reference Information

The subject of detonation physics is by its very nature primarily theoretical knowledge, rather than knowledge applied to specific kill mechanisms or targets. Review of earlier parts of the publication, prior to the study of this subject, is not required, therefore; and there will be a minimum of references to the other parts.

4–15. EXPERIMENTAL TECHNIQUES

4–15.1. Introduction

Probably the most important and the most significant parameter associated with explosive detonation is the resulting detonation pressure. However, due to its transient nature, high magnitude, and short duration, direct measurement of the pressure has not been practicable. Various theories have been postulated which analytically relate detonation pressure to detonation wave velocity, and several experimental techniques are presently used to measure the detonation wave velocity. Recent investigations at Aberdeen Proving Ground indicate a procedure for the direct measurement of detonation pressures by use of sulphur transducers. In addition, investigations are continuing on direct temperature measurements, but to date limited success has been achieved.

4–15.2. Measurement of Detonation Velocity

4–15.2.1. *Pin Method*

Prior to 1955, most of the measurements of detonation rates were made by using either streak cameras, the method of Dautriche, or the Mettegang recorder (Ref. 118). The pin method, an electronic technique which measures detonation velocity with extreme precision, offers several advantages over other available methods. Among these advantages are very high time resolution, and the ability to indicate whether the detonation wave is in an advanced state of decay or is still comparatively strong. The pin method also provides a means of directly observing the progress of the wave in the interior of an irregularly shaped piece of explosive.

A brief description of the pin method follows. The electronic circuit consists basically of three parts: the explosive, into which is inserted either ionization-operated or shock-operated pin switches; a signal mixer circuit and transmission line; and a cathode-ray chronograph. The pin switches are placed at very accurately measured distances along the explosive. After closure of the switches, the cathode-ray chronograph records the time between pulses of the pin switches, as received through the mixer circuit and transmission line.

The pin method of measuring detonation velocities has a standard error of observation that is less than 0.1 per cent of the detonation rate, for charges only a few inches in length. Expressed in terms of time, the error is less than 3×10^{-8} seconds for most experiments. Fig. 4–139 is a schematic of the test apparatus.

Distortion of the detonation wave at the charge boundaries is not detrimental, nor does confinement of the charge in metal or other opaque materials hamper the measurement of detonation rate. However, if full advantage is to be taken of the precision afforded by the pin technique, great care must be taken in preparing each charge and in controlling the firing conditions.

4–15.2.2. *Microwave Technique*

The microwave technique is used primarily in place of the pin method to measure nonsteady detonation velocities. This technique is based on the reflection of microwaves from the ionized detonation front, and it yields a sequence of detonation velocities which are averages over equal and adjacent intervals along the length of the explosive being studied. The circuits for generating and detecting the microwaves, and for the display and reduction of the resultant signal, are given in Ref. 119.

Simply described, the apparatus is a piston (representing the detonation front) generating a periodic signal that is recorded by a probe

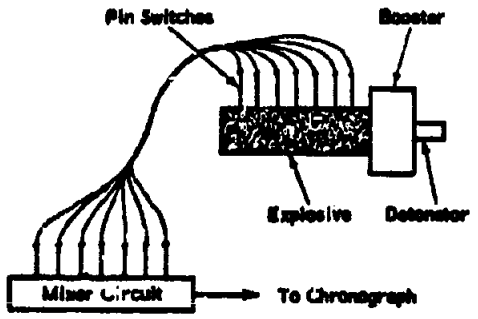

Figure 4–139. Pin-Method Test Apparatus, Schematic Diagram

and detector (Fig. 4–140). An attenuator is inserted between the movable piston and the oscillator, to isolate the oscillator from any load changes caused by the piston movement. One recorded cycle of the signal corresponds to a piston displacement of one-half the wavelength in the guide. If the guide wavelength and the initial position of the piston are known, the position of the piston as a function of time can be determined. This gives, in turn, the detonation velocity.

The microwave technique is more complicated than the pin method, has an accuracy on the order of one or two per cent, and is limited to use with explosives which have good dielectric properties.

4–15.2.3. *High Speed Photography*

There are various high-speed photographic methods employed for measuring detonation velocity. Brixner has developed a high-speed framing camera with a maximum rate of 3,500,000 frames/second (Ref. 120). This camera uses the general principle of a rotating mirror relaying the image to the film by a series of lenses, but adds a two-faced rotating mirror to divide the optical system, so as to appreciably reduce the blind time.

Sultanoff presents an extensive survey of streak, single-exposure, and high-speed successive framing cameras employed in the study of explosive mechanisms (Ref. 121). The highest frame-rate camera is a grid framing camera by Sultanoff, having a rate of 10^8 frames/second (Ref. 122). Among the other more popular cameras listed by Sultanoff are the low-cost, Bowen RC–3, rotating-mirror, streak-type camera (Ref. 123), with a writing speed of 3.1 mm/μsec, and the Rapatronic Faraday single-exposure type camera (Ref. 124), with exposure time of 1 μsec. These three types are discussed in more detail in Ref. 121, and photographic results typical of each type are presented. Several other rotating-mirror cameras of interest are described in Ref. 125.

The streak cameras produce photographs of distance as a function of time, for studies of detonation and shock rates. The Rapatronic Faraday camera takes a single exposure at any preset time interval after the first burst of light. Sultanoff's grid-framing camera exposes 100 independent frames at the rate of 10^7 frames per second, allowing the entire film to be exposed in 1 μsec. Because the luminosity prevails longer than 1 μsec, multiple exposures are made, permitting a direct measure of the velocity at 100-frame intervals.

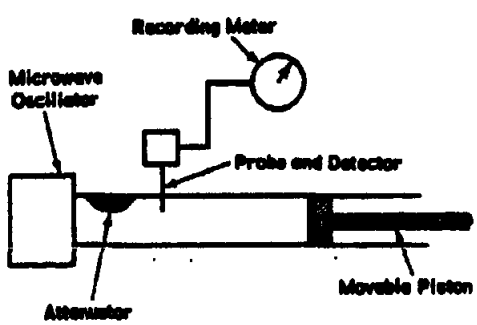

Figure 4–140. Microwave Technique Test Apparatus, Schematic Diagram

4–15.3. *Measurement of Detonation Pressure*

4–15.3.1. *General*

Due to the very transient nature and high magnitude of explosive pressures, only limited work has been reported on the direct measurement of detonation pressures. Two such methods are presented here, with some initial graphical results.

4–15.3.2. *Gehring and Dewey Method*

Gehring and Dewey describe the following method of determining the detonation pressure (Ref. 126). Consider a detonation front traveling into a metal surface. At normal incidence, reflection occurs with a large increase in pressure. With the front perpendicular to the metal surface, the compression of the surface produces a rarefaction in the explosion products, resulting in a decrease in pressure below the detonation pressure. At some small angle between the surface and direction of flow, the flow into the metal just compensates for the effect of compression of the metal. The pressure on the metal surface is then the detonation pressure. The desired condition is clearly that

at which the flow behind the front is along the compressed surface.

Fig. 4–141 is a diagram of such a flow, the detonation front making an angle α_s with the perpendicular to the original surface of the metal, such that the flow immediately behind the front is parallel to the depressed surface. This surface is then a streamline, and the normal component of stress on it is the detonation pressure. The material flow has a component $D \tan \alpha_s$ in the detonation front. Because this component is unchanged by the passage of the detonation front,

$$D \tan \alpha_s = (D - U_d) \tan (\alpha_s + \delta), \tag{4–160}$$

where D is obtained from optical measurements. Thus, determination of α_s and δ determines U_d, and the detonation pressure can be computed from

$$p_d = \frac{\rho_0 D^2 \sin \delta}{\cos \alpha_s \sin (\alpha_s + \delta)} \tag{4–161}$$

where p_d, ρ_0, and D^2 are expressed in consistent units.

Direct observation from densitometric measurements on radiographs of the angle α_s, at which no rarefaction occurs, is subject to the same difficulties as is the observation of the density. However, α_s can be determined another way. A compression shock propagates with a velocity monotonically increasing as α. At larger values of α, beyond α_s, flow behind the detonation front is unstable. A graphical plot of U_d versus α will then determine α_s at the abrupt change in the monotonic function.

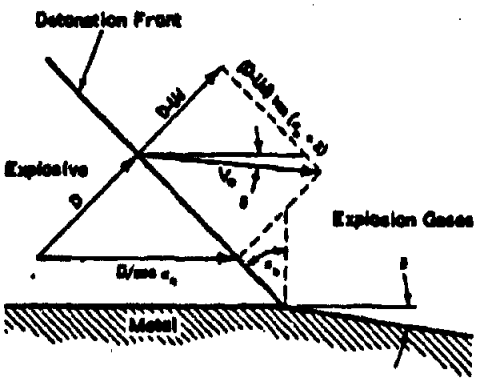

Figure 4–141. Detonation Pressure, Flow Diagram

4–15.3.3. Hauver's Method

Perhaps the most direct and recent method of obtaining detonation pressure is that of Hauver at Aberdeen Proving Ground (Ref. 127). In this method, the dependence of the electrical conductivity of sulphur upon pressure is used to measure a pressure-time profile for detonating Baratol. The measurements indicate an initial pressure spike, and lend further confirmation to the hydrodynamic theory proposed by von Neumann and others.

Fig. 4–142 shows an experimental arrangement of Jaigneau and Thouvenin (Ref. 11), and Fig. 4–143 shows the modified system used by Hauver in obtaining pressure-time data. Appropriate resistance-capacitance (RC) circuits are used for the measurements. They consist of a known resistor in series with the sulphur transducer element. A constant voltage is maintained across the combination, and the potential drop across the resistor is recorded with an oscilloscope. From this measurement the resistance of the sulphur transducer is determined, and is related to pressure by using a sulphur resistance versus pressure calibration curve.

Fig. 4–144 is a schematic diagram of the test setup used to measure the transient pressure pulse imposed by the impact plate. Here, a 24ST aluminum plate is driven by an explosive to produce plane impact on a 24ST aluminum target that is in contact with the transducer assembly. In the tests, 1/16-inch and 1/8-inch

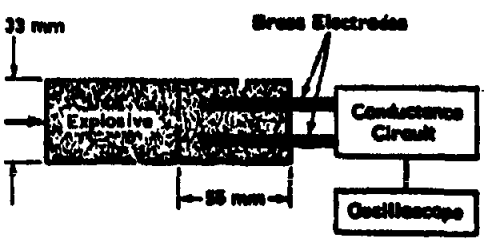

Figure 4–142. Jaigneau and Thouvenin Experimental Arrangement for Determining Pressure-Time Data, Schematic Diagram

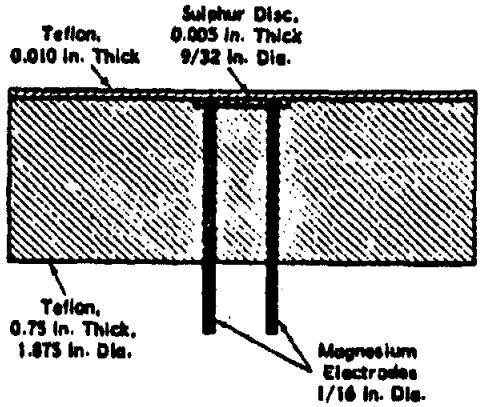

Figure 4–143. Hauver Experimental Arrangement for Determining Pressure-Time Data, Schematic Diagram

thick driven-plates were used, and target plate thickness was varied.

Fig. 4–145 shows the oscilloscope resistance-time records, together with the corresponding pressure-time profiles. For both 1/16" and 1/8" thick driven plates, flat-topped, pressure-time curves are obtained with a 1/16" thick target over the transducer. Small pressure variations along the top are attributed to impedance mismatch still present in the transducer system. As the target thickness is increased, the pressure pulse is reduced to a spike. The spike pressure is reduced by further increase in target thickness.

The flat-topped pulses are not as wide as predicted by the theory if the hydrodynamic sound velocity is used. Also, the pulse is reduced to a spike sooner than expected. Reduction of the driven-plate thickness by vaporization at the explosive-metal interface was considered, but was rejected, because a reduced thickness could not account for both the observed pulse width and the short travel required for the rarefaction to reduce the pulse to a spike. However, by assuming that the pressure relief wave travels with a velocity of approximately ten millimeters per microsecond, the observed pressure-time curves are explained. In a recent paper, Morland has predicted that a velocity higher than the hydrodynamic sound velocity should be associated with pressure relief (Ref. 129). The plate impact tests are interpreted to show that the sulphur transducer follows pressure changes with good accuracy.

A pressure profile for detonating Baratol was calculated from the first portion of the interface pressure-time curve, which is the portion interpreted to represent the reaction zone. The following interface equation (Ref. 130)

$$P_x = \frac{P_i\,(\rho_0 D_0 + \rho_x D_x)}{2\,\rho_x D_x} \qquad (4\text{–}162)$$

was used. In this equation, P, ρ, and D are pressure, density, and shock (detonation) velocity, respectively, in consistent units. Subscripts x

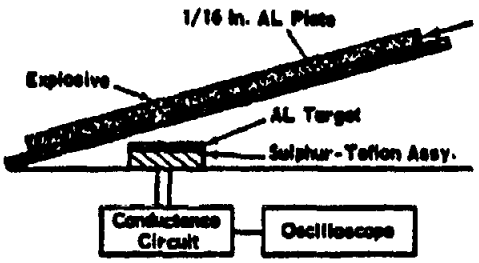

Figure 4–144. Transient Pressure Pulse Setup, Schematic Diagram

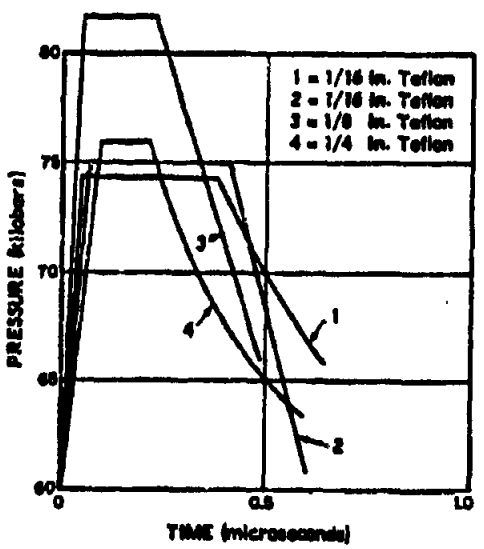

Figure 4–145. Oscilloscope Resistance-Time Records with Corresponding Pressure-Time Profiles

and *s* refer to the explosive and sulphur. Fig. 4–146 is a plot of the pressure-time curve.

The pressure-time curve indicates the von Neumann spike followed by the Taylor wave. The indicated pressure of 190 kilobars is not the actual maximum. This initial pressure is limited by the rise time of the conductance circuit, and by attentuation during passage through the thickness of Teflon between the explosive and the sulphur. For measuring the initial portion of the pressure-time curve, 0.005-inch thick Teflon insulation was used. A 5-mil Teflon front has consistently indicated a pressure from 5 to 10 kilobars higher than that measured with a 10-mil front. The curve indicates a Chapman-Jouguet pressure of approximately 150 kilobars, although this point is not sharply defined. The accuracy of these pressure values depends upon the accuracy with which the interface pressure was estimated when the sulphur was calibrated. The aluminum pressure as determined by free surface measurements and the equation of state is not in doubt, but at present there is some doubt as to the exact position of the Hugoniots for the materials in the sulphur-Teflon system.

The use of sulphur as a pressure transducer is not in a state of perfection, but the elimination of spurious contributions to the conductance signal, better impedance match throughout the system, and modified configurations for use at higher pressures should achieve greater accuracy and usefulness.

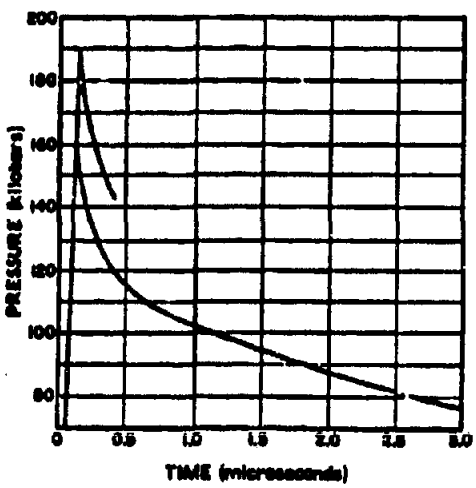

Figure 4–146. Pressure-Time Curve for Baratol Detonation

4–15.4. Measurement of Detonation Temperature

Suitable methods for the determination of the temperature in the detonation front is one of the most urgent needs in the field of solid explosives. Although the measurement of this parameter has been of active interest for some time, the experimental determination of definitive temperatures has not been very successful.

One method under examination (Ref. 131), although it introduces a foreign material into the explosive powder, provides an interval of time conductive to sampling by one-megacycle circuitry and views the detonation radiation at the core of the charge in solid explosives.

The novel feature of this method for sampling the radiation, which is to be evaluated for quality, is the use of a transparent plastic rod imbedded axially in the explosive charge during fabrication of the test pellet. The plastic rod (methyl methacrylate) protrudes from the end of the cylinder opposite to the end that is to be initiated. In this way the radiation is transmitted along the plastic rod. During the detonation time (3 μsec., or more) luminosity-time records are made of the imbedded plastic rod. From these records, the radiation wavelengths are determined, in order to compute the temperature.

To date, most of the work on this method has been devoted to recognition of the idiosyncrasies and deficiencies of the system; hence, only preliminary data have been obtained.

4–15.5. Flash Radiography of Shaped Charge Effects

Flash radiography is generally accepted as being the best means of obtaining direct pictorial presentation of the dynamic performance of shaped charges. Optical methods (although useful in other studies of detonations) are not altogether suitable, due both to the luminescence of the object and to the obscuring of the

view by the material given off by the jet. In addition, optical pictures often required interpretation; but flash radiographs give a direct picture of the material in front of the film. The low-voltage, X-ray method (24 kv, compared to 100 kv) that has been developed produces softer X-rays (Ref. 132). The system consists of a simplified low-voltage, X-ray, pulse-generator circuit, and a method of protecting the X-ray tube and film.

Particular advantages accrue from the use of low voltage. Of prime importance is the ability to get greater detail from objects of small size or low density. The breakup of a jet, for instance, taken with high-voltage X-rays, may be lacking in detail due to the transparency of the smaller particles of the jet to the X-rays. Likewise, materials of low atomic number such as aluminum, which would be almost transparent to high voltage X-rays, show up quite well when the voltage is reduced. The low-voltage, flash, X-ray equipment is lightweight and relatively simple.

The low-voltage, flash radiography was originally developed to investigate the jets from 105-mm, steel-cased rounds. To reduce the penumbra effect (to form a sharp image and improve definition) the film-to-jet distance must be made as small as possible. Making the tube-to-jet distance large will also improve definition, but the X-ray intensity will fall off as the inverse square of the distance. In practice, the film-to-jet distance is of the order of 6 inches, and the tube-to-jet distance is of the order of 74 inches.

4–16. INITIATION AND DETONATION

4–16.1. Introduction

In preceding paragraphs, detonation has been discussed without defining the phenomenon. It consists of a self-sustaining, very-rapid chemical reaction which, on proper initiation, propogates through an explosive, converting it to largely gaseous products and liberating a considerable amount of energy. The process of initiation of detonation is of considerable interest, since most explosives can react to external stimulus in other ways than by detonating, i.e., they can deflagrate or burn, with these processes occurring at much lower rates than detonation. Detonation of a military explosive cannot be normally caused by merely lighting it with a match, while detonation can be caused by a sufficiently intense shock. A somewhat more technical discussion of initiation and detonation follows.

A detonation wave, as it passes through an explosive, must initiate the explosive reaction in every layer of unexploded material that it traverses (Ref. 133). Several theories have been set forth as to the method of initiation of the reaction. These include hypotheses such as the deformation of molecular groupings, high pressures, and direct action by the reaction products which move along with the gas stream velocity.

The most widely accepted view is that initiation of the reaction at the shock front is mainly due to heating. In degassified liquids and homogeneous solids which detonate at velocities which are higher than the local speed of sound, the shock front, no doubt, produces a thermal rise at the detonation front sufficient to sustain detonation.

Work has also been performed on the origin and propagation of explosions initiated by mechanical means in small quantities of material (Ref. 133). These studies have demonstrated that initiation is caused by the formation of hot spots of finite size in the explosive material. Effective hot spots may be produced either by boundary friction between solids of high melting point, whether the solids are explosive or contaminant, or by adiabatic compression of minute gas or gas vapor pockets trapped in the explosive during manufacture. Extremely high temperatures can be achieved in the gas pockets by such compression.

4–16.2. Thermal Considerations (Ref. 136)

The conditions for initiation of detonation must cause detonation when it is wanted and prevent it when it is not wanted. Many methods have been designed for the study of these conditions. Among them are tests of sensitivity to impact, friction, heat, spark, and other forms of electrical discharge, boosters of various types, sympathetic detonation through condensed media and air, and shock

and heat sensitivity as a function of impurity content, grit, etc.

The initiation of detonation is a complex heat balance problem, although for simplicity it may be expressed as the equation:

$$F+G=H \qquad (4\text{–}163)$$

where F accounts for heat loss, G for accumulation of heat in the explosive mixture, and H for chemical energy generated by decomposition of the explosive.

Even this approximate equation can only be solved for the degenerate cases; i.e., isothermal and adiabatic decomposition. Although these cases are treated in considerable detail in Ref. 136, their interest lies chiefly in their difference from high order initiation, therefore, they will not be further discussed here.

4–16.3. Detonation Theory

The following analysis of detonation theory is based on a one-dimensional, detonation wave, to gain a clear insight to the mechanisms of detonation, and to predict the pressure, specific volume, mass flow rate, and detonation velocity. (Ref. 137).

It is assumed that the detonation wave moves across the explosive in the direction of the negative X axis. The explosive is confined by some cylindrical boundary which is assumed to be absolutely unyielding. (This may even be applicable to an unconfined stick of explosive, because the great velocity of the detonation wave, i.e., the brevity of the available time interval, makes the inertia of the solid explosive itself act as a confinement.)

Assuming the detonation wave has reached the stage of constant velocity D, the origin of the X coordinate at every moment is taken at the detonation front.

The detonation wave is assumed to be at rest, in this example. This means that the intact explosive has the velocity D with respect to, and directed toward, the fixed detonation front. Therefore, for

$$X<0$$

the velocity of matter is D, and for

$$X>0$$

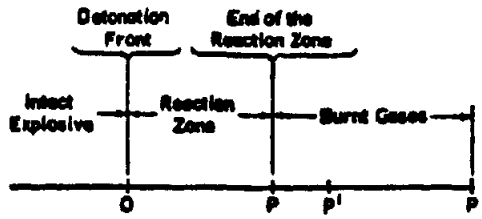

Figure 4–147. General State of Explosive Reaction

the velocity of matter is $u=u(X)$. The fraction expressing to what extent the chemical reaction has taken place at $X>0$ is $n=n(X)$; $1\geq n(X)>0$. (At $X>0$, a unit mass contains n parts of burnt gas and $1-n$ parts of intact explosive.) During the time dt, the matter in this region moves by $dX=u\,dt$. So if the reaction velocity is $\alpha=\alpha(X)$,

$$\frac{dn}{dX}=\frac{(1-n)\alpha}{u}. \qquad (4\text{–}164)$$

Finally, at every point $X<0$, the same physical conditions exist, for example, pressure p_o and specific volume V_o. These describe the intact explosive. At every point $X>0$, there exists a pressure $p=p(X)$ and a specific volume $V=V(X)$.

The nature of the chemical reaction is expressed by a functional relationship

$$\alpha=A(n,p,V) \qquad (4\text{–}165)$$

where $A(n,p,V)$ is assumed to be a known function. The stability of the intact explosive requires that

$$A(0,p,V)=0. \qquad (4\text{–}166)$$

The nature of the explosive and its mixtures with the burnt gas will be expressed by its caloric equation for each n; $0\leq n\leq 1$. The functional relationship determining its internal energy per unit mass is

$$e=E(n,p,V) \qquad (4\text{–}167)$$

where $E(n,p,V)$ is assumed to be a known function.

From the laws of conservation, then, for mass,

$$D=\rho V_o,\ u=\rho V \qquad (4\text{–}168)$$

for momentum,

$$\mu(D-u)=p-p_o \qquad (4\text{–}169)$$

and for energy,

$$\mu[1/2D^2+E(O,p_o,V_o)-1/2u^2-E(n,p,V)] = up-Dp_o \qquad (4\text{–}170)$$

Eqs. 4–168, 4–169, and 4–170, together with Eqs. 4–164 and 4–165, determine all of the parameters, where u is the amount of matter crossing the detonation front per second (i.e., the amount of matter detonating per second). Eqs. 4–168, 4–169, and 4–170 are transformed into

$$\frac{p-p_o}{V_o-V}=\mu^2 \qquad (4\text{–}171)$$

$$1/2(p_o+p)(V_o-V)=E(O,p_o,V_o)-E(n,p,V). \qquad (4\text{–}172)$$

Plotting Eq. 4–171 for some n, results in the Rankine-Hugoniot curve shown in Fig. 4–148, together with the point p_oV_o.

The Rankine-Hugoniot curve is drawn with the tangent from the point p_oV_o to determine the p,V, conditions at the n^{th} stage of the chemical reaction. This also gives

$$\mu=\sqrt{\frac{p-p_o}{V_o-V}} \qquad (4\text{–}173)$$

and

$$D=V_o\sqrt{\frac{p-p_o}{V_o-V}} \qquad (4\text{–}174)$$

$$u=V\sqrt{\frac{p-p_o}{V_o-V}} \qquad (4\text{–}175)$$

This is also valid for the case $n=0$, in which case the equations describe a condition under which a discontinuity can exist in the substance, without making use of any chemical reaction at all. This phenomenon is particularly important in gases and in liquids. It is known as a shock wave, and is an essential component in the theory of a detonation wave.

With the tangent drawn as shown in Fig. 4–148, ($p>p_o, V<V_o$, hence $u<D$), the burnt gases are carried along with the detonation wave,

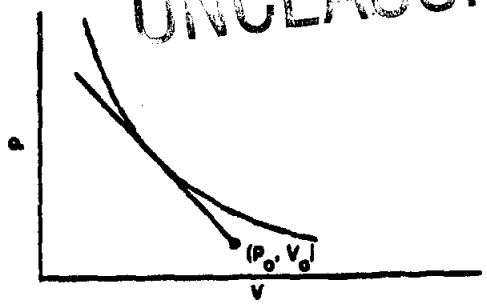

Figure 4–148. Rankine-Hugoniot Curve

and their density and pressure are higher than those in the explosive. This is detonation proper.

For the tangent drawn in the other quadrant, where

$$p<p_o, V>V_o, \text{ hence } u>D$$

the burnt gases are streaming out of the explosive; their density and pressure are lower than those in the explosive. This is the process commonly known as burning.

The classical theory of detonation is based on the Chapman-Jouguet hypothesis,

$$D=u+a. \qquad (4\text{–}176)$$

This is equivalent to drawing a tangent to the Rankine-Hugoniot curve, $n=1$.

For certain forms, as shown in Fig. 4–149, of

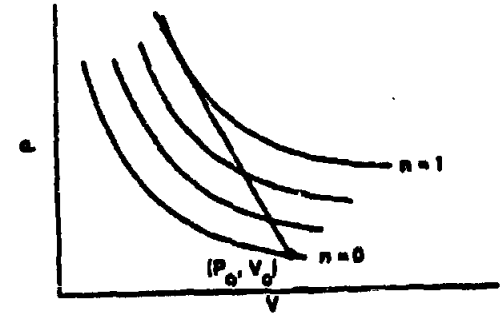

Figure 4–149. Hugoniot Curves, Parallel Characteristics

the family of curves n; $0 \leq n \leq 1$, the Chapman-Jouguet hypothesis is true.

However, for families of curves of n; $0 \leq n \leq 1$, as shown in Fig. 4–150, the tangent from (p_o, V_o), must be drawn to the envelope instead of the curve $n=1$.

Further discussion, with more detail, on the understanding of the elementary theory of the steady plane detonation wave is given by Taylor (Ref. 133). More rigorous analyses are given by Courant and Friedrichs (Ref. 138).

4–17. WAVE SHAPING

4–17.1. Introduction

Wave shaping is of great importance in many modern explosive-actuated devices, as well as in fundamental studies of explosive phenomena and impulse loading (Ref. 139). Shaping the front of the detonation wave to impact the target in a predetermined way is one important problem for successful wave shaping. A factor of at least as great importance, because wave shaping is used principally in the impulse loading of targets, is that of regulating and controlling the integrated pressure-time pulse or total impulse loading upon the target, at each element of its surface.

The shape of the wave front can be easily observed by streak photography or pin techniques, but the determination of the nature of the pressure-time pulse is a far more difficult problem. The experimental method for its study, at present, is the direct observation of the rate of acceleration and the terminal velocity of each element of the target (and the compressions and tensions set up in the target, if they can be determined). For example, see Hauver's method, Par. 4–15.3.3, preceding.

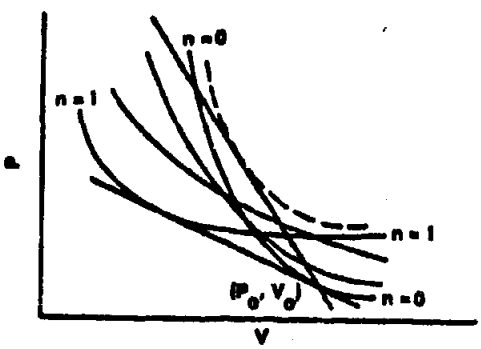

Figure 4–150. Hugoniot Curves, Nonparallel Characteristics

4–17.2. Shaping of the Wave Front

The shape of the wave front may be regulated by a variety of means, including the application of one or more combinations of the following:

1. Wave interrupters, which require the wave to go around the interrupter. In general, these are inert fillers of such thickness that the shock wave emerging from the filler is too low in intensity to reform the detonation wave.
2. Two explosives of appreciably different detonation velocities.
3. Low order detonation.
4. Density and composition variations in the explosive.
5. Transfer lenses.
6. Air and/or inert fillers of such thickness as to merely delay the wave, but not completely destroy it. (Actually, this type will also act as a wave interrupter most of the time, but the shock wave emerging from the inert medium is of such intensity as to cause eventual reformation of the detonation wave, after a time lag.)

Perhaps the most satisfactory and useful method of wave shaping is the last type described. This type (Ref. 140) has been used in a "cylindrical-wave" initiator (Fig. 4–151). The initiator consists of a double-tapered steel core, loaded with cast 50/50 Pentolite, and fitted with an M36 detonator, an air gap, and a cylindrical 61ST aluminum sleeve. A 1/2 inch layer of Tetryl surrounds the sleeve. This initiator has been used with satisfactory results, producing cylindrical detonation waves, in testing both shaped-charge and continuous-rod warheads.

4–17.3. Geometric Optics

The shaping of detonation waves by slow explosives, shocked media, and transfer plates can be analyzed by the use of geometric optics (Ref.

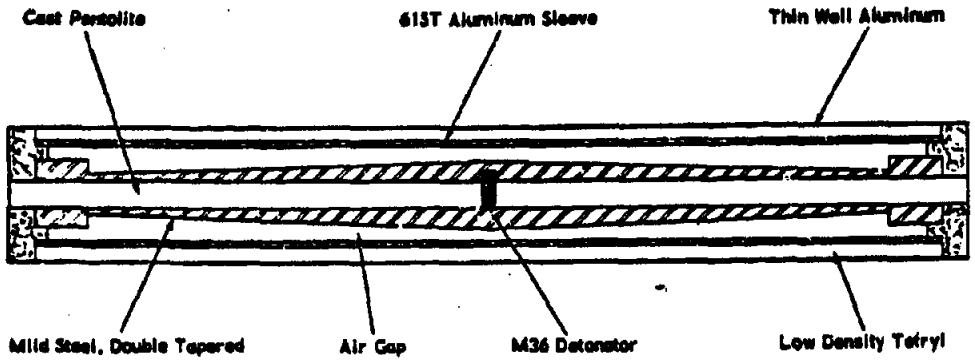

Figure 4–151. Cylindrical Wave Initiator, Schematic Diagram

141). The simplest analogy would be that of an optic lens. A detonation in a fast explosive could pass, after some distance of travel, across a plano-convex or double-convex lens made of slow explosive, and could then pass back to the high velocity explosive to give a wave which is plane, convergent, or divergent (Fig. 4–152). All lens laws would apply as long as the proper index of refraction is used. In using a lens for shaping detonation waves, it is desirable that a minimum amount of explosive be used in the unshaped region. This is the same as saying that lenses of very small *f* numbers are most desired (*f* numbers, as in optics, can be defined as the focal length divided by the diameter). The amount of explosive in the unshaped region can be minimized by reducing the boundary from a spherical surface to a conical surface. The center of initiation then must be the apex of the cone (Fig. 4–153).

If it is desired that the center of initiation be removed a small distance from the boundary, the interface becomes a hyperbola. A possible variation is to place the plane surface of the slow explosive at the detonator side, and to shape a second boundary where the detonation passes back from the slow explosive to the fast explosive, as shown in Fig. 4–154.

The shape indicated by Fig. 4–153 has a lower height of slow explosive than the shape shown by Fig. 4–154; therefore, it is more efficient. In the cone model, the height of slow explosive is given by

$$h = r/\tan\alpha \qquad (4\text{–}177)$$

where $$\tan\alpha = \sqrt{n^2-1};\ n = V_f/V_s, \qquad (4\text{–}178)$$

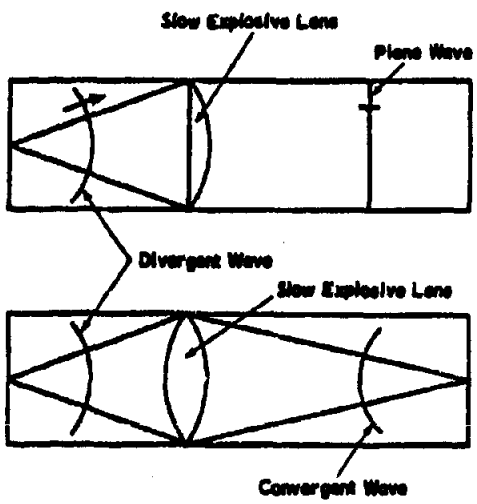

Figure 4–152. Optic Analogy of Shaped Detonation Wave

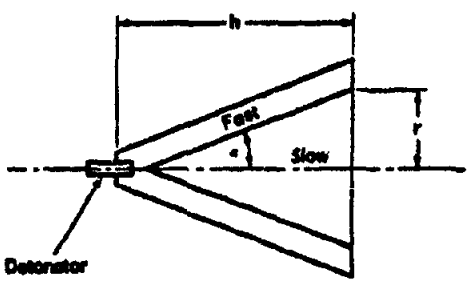

Figure 4–153. Apex Detonation

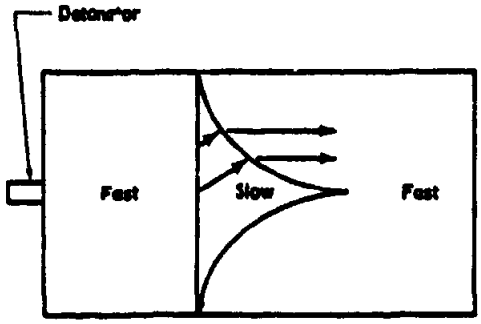

Figure 4–154. Hyperbolic Wave Shaping

V_s = the propagation velocity in the slow medium,

V_f = the propagation velocity in the fast medium,

and n = the index of refraction.

In the transfer or air lens, the equivalent of the single line boundary can be approximated as a flat metal plate of constant thickness. If the metal plate is flat, like the first boundary of Fig. 4–154, and the detonator is removed a small distance from the boundary, the second surface becomes approximately parabolic. If the second surface is flat, as in Fig. 4–153, the transfer plate of constant thickness approximates a hyperbola. In the limit for very large n, the height, h, approaches r/n. The ratio h/r for a Baratol Composition B lens is about 0.8, whereas the ratio for a satisfactory NOL type booster is about 0.12, a sizeable reduction.

4–18. ELECTRICAL PROPERTIES

4–18.1. Introduction

Combustion flames and gaseous detonations contain ions and free electrons capable of influencing the propagation of the detonation waves through external magnetic and electrical fields. Experiments have shown, for instance, that spinning detonation waves traversing longitudinal magnetic fields can be significantly reduced and even completely quenched (Refs. 136 and 142). Transverse fields, on the other hand, have little or no influence on the propagation of the detonation wave.

The pitch of the spinning detonation can be increased slightly by passing from positive to negative in a magnetic field. However, in going from negative to positive, the spin can be completely interrupted, causing the wave speed to drop abruptly, but to rise again beyond the positive terminal of the electrical field. Inasmuch as a flame in a uniform electrical field always bends toward the negative electrode (Ref. 143), it can be concluded that the particle motion, W, is accelerated toward the negative electrode and away from the positive electrode.

These definite experimental results occurred with explosives at the detonation threshold, where small influences are believed to have an appreciable effect. If the detonating gas system is not a threshold one, the external applied fields have little influence on the detonation velocity.

4–18.2. General Theory

Significant investigations of the mechanism of electrical conductivity in gases ionized by explosions have been performed by Birk, et al (Ref. 144), who started with general principles and later, by checking the results, decided which factors were important and which assumptions were justifiable.

To begin with, the current flowing between two electrodes in an ionized medium is

$$I = j \cdot s \qquad (4\text{–}179)$$

where, in a consistent set of units,

j = the current density,

s = the cross sectional area,

and

$j \cdot s$ = the scalar product.

The current density vector, j, is given in its general form as

$$j = \Sigma n_s e_s \bar{c}_s \qquad (4\text{–}180)$$

where

n_s = the number of charge carriers of type s, per unit volume,

e_s = the carrier charge,

and

$\bar{c}_s$ = the carrier velocity.

The factor e_s is equal to the charge of the electron, because at the temperatures involved, the possibility of double ionization is small. The state of the gas determines the number of charge carriers, n_s. Assuming a state of equi-

librium, with equipartition of energy for the various particles such as ions, molecules, and electrons, the number of charge carriers may be calculated by

$$\alpha_i^2/(1-\alpha_i^2) = [(kT)^{5/2}/p][(2\pi m/h^2)^{3/2}]\rho^{-U_i/kT} \quad (4\text{–}181)$$

where, in a consistent set of units,

α_i = the ratio of ionized particles to the total number of particles,
k = Boltzmann's constant,
T = the absolute temperature,
p = the pressure,
m = the mass of the electron,
h = Planck's constant,

and

U_i = the ionization energy.

The values of p and T can be calculated from the measured velocities of detonation and of shock waves.

Using Saenger's theory (Ref. 144), the energy from the detonation wave is at first transferred to the undisturbed gas as a uniform translational energy. Within the first ten molecular collisions, the average molecular velocity is equal to the translational velocity. The molecules with a kinetic energy equal to or higher than their ionization energy become ionized, and their number is given by the expression:

$$\frac{n_i}{n_m} = \sqrt{\frac{6}{\pi}}\left(\frac{c_i}{c_t}\right) e^{\frac{-3c_i^2}{2\overline{c_t}^2}} + \frac{2}{\sqrt{\pi}}\left(\sqrt{3/2}\cdot\frac{c_i}{c_t}\right) \int_{\sqrt{3/2}\cdot\frac{c_i}{c_t}}^{\infty} e^{-x^2}dx \quad (4\text{–}182)$$

where

n_i = the number of ions per cu cm,
n_m = the number of molecules per cu cm,
c_i = the average velocity corresponding to the energy of ionization,

and

c_t = the average translational velocity.

It is most difficult to estimate $\overline{c}_e$, which is the average velocity of the charge carriers. The factor $\overline{c}_e$ depends on numerous quantities, such as the mass velocity of the gas, the field strength, the mass of the particles, and the gradients of pressure, temperature, and concentration. This velocity may be divided into two components, the mean mass velocity of the gas, c_m, and the mean velocity of the charge carriers relative to the gas, $\overline{c}_e$. Neglecting gradients of pressure, temperature, and concentration for simplification,

$$\overline{c}_e = K_e E \quad (4\text{–}183)$$

where

K_e = the mobility of the charge carriers,

and

E = the field strength.

Neglecting the effect of mass flow, Eq. 4–180 may be written

$$j = n_e e K_e E \quad (4\text{–}184)$$

where

K_e = the mobility of electrons,
n_e = the number of electrons per cu cm,

and

e = the electron charge.

The mobility of the electrons is given by the expression

$$K_e = 0.921\,\lambda\varepsilon/\sqrt{m}[kT + [k\cdot T^2 + (\lambda^2 M X^2 e^2/1.33m)]^{1/2}]^{1/2} \quad (4\text{–}185)$$

where

λ = the mean free path of the electron,
M = the mass of the gas molecule,

and

X = the field strength.

Eq. 4–185 gives the mobility of the electron in the detonation zone of the order of 10^{-4} cm/sec per V/cm. In air, the mobility increases from 10^2 to 10^3 cm/sec per V/cm by increasing the distance from the charge from 3 to 15 cm.

For small degrees of ionization the electrical conductivity of the gas is approximately given (Ref. 145) by the expression

$$\sigma = \text{constant}\; x\; \frac{T^{1/4}}{\rho 1/2}\, e^{-q_1/2kT}, \quad (4\text{–}186)$$

where

ρ = the density of gas,

and

q_1 = the first ionization potential of the gas.

Probe experiments indicate that at a given initial density the indicated conductivity, σ, varied exponentially with temperature for small degrees of ionization. However, the indicated conductivity has been measured as low as 1/1,000 of theoretical value.

Theories of electrical conductivity in gases have been developed for two extreme cases. One case is concerned with a very slightly ionized gas, where the close encounters between the electrons and the neutral atoms decide the electron mobility. (Refer to Par. 4–18.3, following.) The other case is concerned with a completely ionized gas, where the distant encounters between the ions predominate. (Refer to Par. 4–18.4, following.)

For an intermediate case, the following approximation is used,

$$\frac{1}{\delta}=\frac{1}{\delta_e}+\frac{1}{\delta_d}. \qquad (4\text{–}187)$$

In Eq. 4–187, $1/\delta_e$ denotes the electrical resistivity entirely due to close encounters between electrons and the gas molecules and positive ions; $1/\delta_d$ denotes the resistivity due to distant encounters between electrons and positive ions; and δ denotes the resultant conductivity of the gas.

Electrical resistivities (i.e., the reciprocal of conductivity) are given for several explosives in Table 4–31.

4–18.3. Theory for Slightly Ionized Gas

The electrical conductivity of a slightly ionized gas assuming rigid elastic spherical molecules is

$$\delta=0.532\,\frac{\alpha e^2}{(m_e kT)^{1/2}}\,\frac{1}{Q_e} \qquad (4\text{–}188)$$

where, in a consistent set of units,

$\alpha=n_i/n_m$, which is the degree of ionization,

e = the electronic charge,

m_e = the mass of an electron,

and

Q_e = the electron-atom collision cross section.

For a slightly ionized monatomic gas, the degree of ionization α at equilibrium is

$$\alpha=G\,\frac{T^{3/4}}{(\rho)^{1/2}}\,e^{-\epsilon_i/2kT}. \qquad (4\text{–}189)$$

Eqs. 4–188 and 4–189 show that, when the degree of ionization is low, the electrical conductivity varies exponentially with temperature, while its dependence on pressure (or density) is small. The conductivity is very sensitive to those impurities which have lower ionization potential than the gas.

4–18.4. Theory for Completely Ionized Gas

The electrical conductivity of a completely singly ionized gas (i.e., each gas atom has been ionized once) is given by

$$\delta=\frac{0.591\,(kT)^{3/2}}{m_e^{1/2}e^2\ln(h/b_e)} \qquad (4\text{–}190)$$

where, h is the Debye shielding distance in the plasma, and is given by

$$h^2=\frac{kT}{8\pi n_e e^2} \qquad (4\text{–}191)$$

while, b_e, the impact parameter at which a posi-

TABLE 4–31. RESISTIVITY OF SEVERAL EXPLOSIVES (Ref. 146)

Explosive	Density (g/cc)	Average Grain Diameter (cm)	Resistivity (ohm-cm)
PETN	0.91	0.036	1.13
RDX	1.0	0.05	1.26
Tetryl	1.0	0.07	1.10
EDNA	0.98	0.036	2.40
Fine TNT	0.90	0.042	2.03
Coarse TNT	1.03	0.23	2.73
80/20 AN–TNT	1.0	0.041 (AN)	28.5
Cast TNT	1.57	—	2.93
Composition B	1.69	—	2.56

tive ion deflects a mean-energy electron by 90 degrees, is defined as $e^{2/3}\,kT$.

The above theories show that for a completely ionized gas, the electrical conductivity is approximately proportional to the 3/2 power of the temperature, and that it changes very slowly with ion concentration density (through the logarithmic term). Moreover, it is independent of the nature of the gas.

4–19. RAREFACTION WAVES

4–19.1. Introduction

A rarefaction wave is defined as a simple wave in which the pressure and density decrease upon crossing the wave; if the pressure and density increase, the wave is called a compression or condensation wave (Ref. 138). In the following discussion, the analogy of a piston moving in a gas which is initially at rest is used to describe the rarefaction wave.

If the specified piston either recedes from or advances into the gas, not all parts of the gas are affected instantaneously. A "wave" proceeds from the piston into the gas, and only the particles which have been reached by the wave front are disturbed from their initial state of rest. If this wave represents a continuous motion, as is always the case if the piston recedes from the gas, the wave front progresses with the speed of sound, c, of the undisturbed gas. If the piston moves into the gas, the situation may become more complicated through the emergence of a supersonic discontinuous shock wave. In this discussion the concern is with continuous wave motion produced by a piston; such a wave motion is always a simple wave (Fig. 4–155).

Distinguishing between expansive (rarefaction) and compressive (condensation) motion, consideration is first given to the expansive action of a receding piston, assuming that the medium is a gas originally at rest with constant density ρ_0 and sound speed c_0. Furthermore, it is assumed that the piston, originally at rest, is withdrawn with increasing speed, until ultimately the constant particle velocity

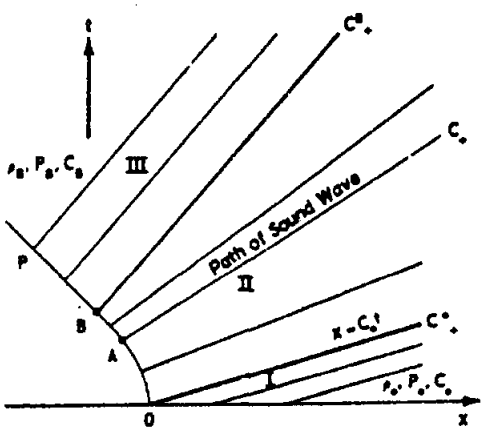

Symbols
ρ = Density
P = Pressure
C = Sound Speed

Subscripts
B = Burnt Gas
0 = Undisturbed Gas
+ = Forward Wave
− = Backward Wave

Figure 4–155. Simple Wave Region (III), Connecting Two Regions (I and III) of Constant State ($-U_B<l_0$), $l_0=\frac{2}{\gamma-1}C_0$

$U_B<0$ is attained. Then the "path" P in the (x, t)-plane, which represents the piston motion, bends backward from the origin O to a point B, where the slope U_B with respect to the t axis is reached, and then continues as a straight line in the same direction as shown in Figs. 4–155, 4–156, and 4–157.

4–19.2. Escape Speed, Complete and Incomplete Rarefaction Waves

The above construction is to be modified if the final piston speed exceeds a certain limit. The reason is that the law of rarefaction expressed by $u=l-l_0$ becomes meaningless as soon as $|U_B|<l_0$, because $l\geq 0$. The quantity l_0 is, therefore, called the escape speed of the gas originally at rest. For polytropic gases

$$l_0=\frac{2}{\gamma-1}C_0, \qquad (4\text{–}192)$$

where γ is the ratio of specific heats.

If $-u_p$ reaches the escape speed, the rarefaction thins the gas down to density zero; pressure and sound speed are likewise de-

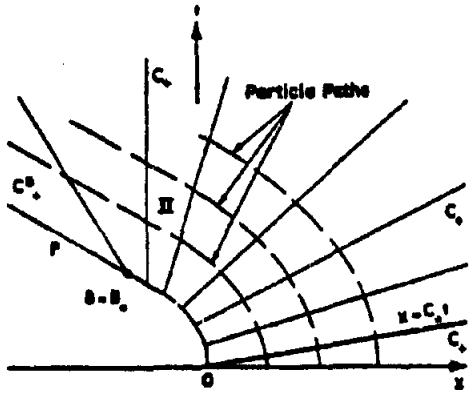

Figure 4–156. Rarefaction Wave Just Ending in a Zone of Cavitation ($l_- U_p > l_0$)

creased to zero. If a rarefaction wave extends to this stage it is called a complete rarefaction wave because it ends in a vacuum.

Generally, a piston receding at constant speed from a gas at rest causes a rarefaction wave of particles moving toward the piston at the head of the wave. This rarefaction wave moves into the gas at sound speed; the velocity of the gas is zero. Through the wave, the gas is accelerated. If the piston speed, $-U_p$, is below the escape speed, l_0, the gas expands until it has reached the speed $-U_p$ of the piston, and then continues with constant velocity, density, and pressure. If, however, the piston speed exceeds the escape speed, the expansion is complete and the wave ends in a zone of cavitation between the tail of the wave and the piston. In any case, the wave moves into the undisturbed gas, while the gas particles move at increasing speed from the wave head to the tail; i.e., from zones of higher pressure and density to zones of lower pressure and density.

The disturbance in the gas resulting from the motion of the piston is propagated into the undisturbed gas with sound velocity, c_0, corresponding to the state (ρ_0, p_0) of the undisturbed gas. This follows from the fundamental fact that the domain of dependence of the zone $x > c_0 t$ is the positive part $x > 0$ of the x axis, so that there the initial state of rest implies a constant state of rest. (The domain of dependence for a point of this region is obtained by drawing the characteristics $C+$ and $C-$ through it, to their intersection with the x axis). The flow resulting from the motion of the piston is thus confined to the region $x \leq c_0 t$. Because this region is adjacent to a region of constancy, the flow in it is a simple wave. Evidently, it is a forward facing wave, because the gas enters this region from the right. In this region, therefore, $u - l = -l_0$ is constant.

Along the path $x = X(t)$, the gas velocity agrees with the piston velocity $x = X(t) = U_p(t)$; therefore, the density ρ, and hence pressure, p, and sound speed, c, are determined from $l = l_0 + U_p(t)$, because $dl/d\rho > 0$ and $dp/d\rho > 0$. The slope $u + c$ of the straight characteristics issuing from the piston path is likewise determined; hence, the simple wave is determined as a whole. Because the piston was assumed to be withdrawn and its velocity U_p decreases, density and pressure also decrease across the wave. Thus, the wave is a rarefaction wave. Also, the velocity $dx/dt = u + c$ of the forward sound waves changes in the same sense as the gas velocity u. Therefore, because the velocity u and, hence, $u + c$ decrease, the straight characteristics issuing from the piston curve fan out.

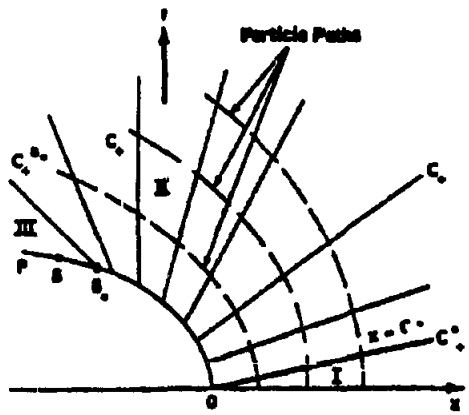

Figure 4–157. Rarefaction Wave Ending in a Zone (III) of Cavitation ($l_- U_p > l_0$)

4-19.3. Centered Rarefaction Waves

4-19.3.1. General

Of particular interest is the case in which the acceleration of the piston from rest to a constant terminal velocity U_s takes place in an infinitely small time interval; i.e., instantaneously. Under these conditions, the family of characteristics $C+$ forming the simple wave degenerate into a pencil of lines through the origin O: $x=o$, $t=o$ (Fig. 4-158). In other words, the simple wave has degenerated into a centered simple wave. It is clear that such a centered simple wave is a rarefaction wave, for u decreases on crossing the wave, if it is forward-facing, and increases if it is backward-facing. In both cases ρ and p decrease across the wave; therefore, it is a rarefaction wave.

At the center O, the quantities u, ρ, p as a function of x and t are discontinuous, but this discontinuity is immediately smoothed out in the subsequent motion.

4-19.3.2. *Explicit Formulas for Centered Rarefaction Waves*

A centered simple wave may be described by the equation

$$x=(u+c)\,t \qquad (4\text{-}193)$$

in which

$$u=l-l_o \qquad (4\text{-}194)$$

may be considered a given function of c. Inversely, u and c may be expressed in terms of $u+c$, and thus in terms of x/t. For a polytropic gas, the relations

$$c=\mu^2\frac{x}{t}+(1-\mu^2)C_o \qquad (4\text{-}195)$$

and

$$U=(1-\mu^2)\left(\frac{x}{t}-C_o\right) \qquad (4\text{-}196)$$

where

$$\mu^2=\frac{\gamma-1}{\gamma+1} \qquad (4\text{-}197)$$

give the distributions of U and c in a centered simple wave explicitly.

The solutions of the differential equations given in Courant and Friedrichs (Ref. 138) are,

$$x=-(\mu^{-4}-1)c_o t+\mu^{-2}c_o t_o\left(\frac{t}{t_o}\right)^{1-\mu^2} \qquad (4\text{-}198)$$

for the particle paths, and

$$x=-(\mu^{-4}-1)c_o t+\mu^{-2}c_o t_o\left(\frac{t}{t_o}\right)^{1-\mu^2} \qquad (4\text{-}199)$$

for the cross-characteristics, where t_o is the time at which the particle path or the cross-characteristic begins at the line $x=c_o t$.

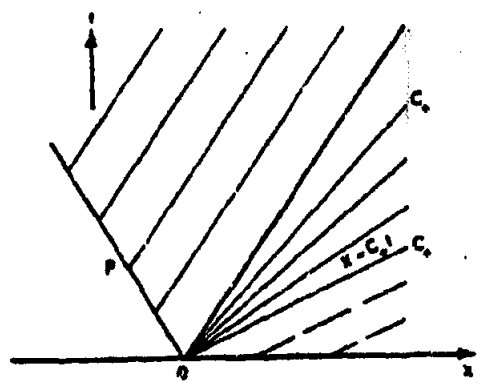

Figure 4-158. Centered Rarefaction Wave ($-U_s<l_o$)

4-20. INTERACTION WITH THIN INERT MATERIALS

4-20.1. Introduction

The dynamics of interaction at a metal-explosive interface have been discussed theoretically in considerable detail in Ref. 147, where statically obtained compressibility data is extrapolated and the pressure at the interface, as viewed from within a steel plate, is determined to be about 280,000 atmospheres. The initial velocity of the surface of a steel plate would be about 2,300 ft/sec. Comparable figures for lead are 270,000 atmospheres and 2,600 ft/sec. It is apparent from these data that the effect of explosions may be equivalent in certain respects to that of physical impacts in the order of 2,000 to 3,000 ft/sec. (Ref. 148).

The reaction of the metal to the explosion may be summarized as follows. First, near its surface, the meta. is initially severely com-

pressed under the action of the high pressure of the explosive. This compression may be as much as 30 per cent. Second, on the sudden release of the pressure the surface will, of course, eventually return to a stress-free condition. The metal, however, may have suffered severe permanent deformation. Third, a disturbance will be set up in the body. The duration of the disturbance will be a few microseconds, so that the length of the pulses in the common metals will be a few inches. The disturbance of the metal will appear as a sharp-fronted, transient wave whose propagation can be described approximately by known laws. Experimental work is described in the following paragraph.

4-20.2. Experiments

Plane-wave explosive systems are employed to determine the equations-of-state of various homogeneous metals at higher pressures. An explosive is detonated at one end of a metal specimen, and the shock wave is transmitted through the specimen to a plate at the other end, giving the plate some initial velocity. A photographic method is used to measure the velocities associated with the shock wave in each specimen.

Pressure and specific volume data can be obtained by the equations of conservation from the measured velocities. From the experimental curves, a more complete high pressure equation of state can be computed. The Mie-Gruneisen theory and the thermodynamic variable

$$\gamma = V\left(\frac{\partial P}{\partial E}\right)_V \qquad (4\text{-}200)$$

are used in extending the equation of state by solving the Dugdale-MacDonald relation (Ref. 149).

A typical shot assembly used by McQueen and Marsh (Ref. 149*) to determine the equations of state of the metallic elements is shown in Fig. 4-159. In such a setup, small test specimens are mounted on the free surface of the brass target plate, and the shock wave velocity for each specimen and the shock strength in the brass are measured. These data determine the (P, V, E) state behind the shock wave in each specimen.

To avoid errors caused by rarefaction waves originating at the explosive-driven interface, the maximum ratio, R, of target thickness (including the specimen) to drive plate thickness is expressed as

$$R = \left[U_s^{-1} + \left(\frac{\rho_0}{\rho c}\right)\right]_d \Big/ \left[U_s^{-1} - \left(\frac{\rho_0}{\rho c}\right)\right]_t \qquad (4\text{-}201)$$

where, in a consistent set of units,

c = the sound velocity behind the shock wave,

$\frac{\rho_0}{\rho}$ = the ratio of densities across the shock front,

and

U_s = the shock wave velocity.

The subscripts, d, and t, refer to the driver and target plates, respectively.

The transformation of measured velocities to pressure-compression points is accomplished by

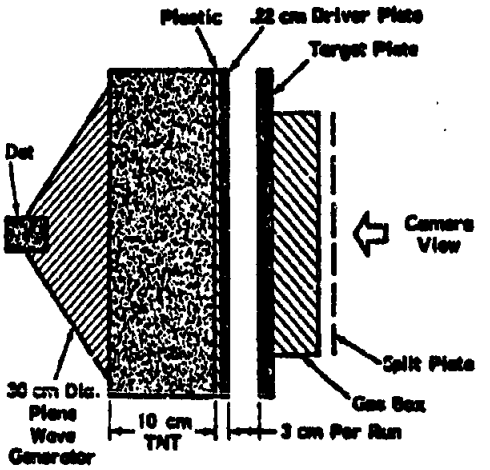

Figure 4-159. Profile of a Typical Shot Assembly

* As indicated by the reference, material has been excerpted from the work of R. G. McQueen and S. P. March, "Equation of State for Nineteen Metallic Elements from Shock Wave Measurement to Two Megabars," *Journal of Applied Physics*, Vol. 31, No. 7, July 1960.

methods using the Rankine-Hugoniot relations for the conservations of mass and momentum across a shock front.

$$V/V_{oH}=(U_s-U_p)/U_s \qquad (4\text{–}202)$$

and

$$P_H=\rho_o U_s U_p+P_{oH} \qquad (4\text{–}203)$$

where

P_{oH} = pressure of undisturbed state ahead of the shock front,

V_{oH} = specific volume of undisturbed state ahead of the shock front,

P_H = pressure for the state behind the shock front,

V = specific volume for the state behind the shock front,

and

U_p = is the shock particle velocity.

One transformation method reasons that

$$U_{fs}=U_p+U_r \qquad (4\text{–}204)$$

and approximates

$$U_p=U_{fs}/2 \qquad (4\text{–}205)$$

where

U_{fs} = the free surface velocity,

and

U_r = the particle velocity, due to the centered rarefaction wave relieving the pressure.

Eqs. 4–204 and 4–205 are combined with Eqs. 4–202 and 4–203, and measured values of U_s and U_{fs} then determine the pressure-volume points of the Hugoniot curve. The experimental data is plotted and fitted by the equation

$$U_s=C+S\,U_p \qquad (4\text{–}206)$$

The experimental results transformed by the Rankine-Hugoniot become

$$P_H=C^2(V_o-V)/[V_o-S(V_o-V)]^2 \qquad (4\text{–}207)$$

and

$$E_H=E_o+\frac{1}{2}\left\{C(V_o-V)/[V_o-S(V_o-V)]\right\}^2 \qquad (4\text{–}208)$$

where P_H and E_H are, respectively, the pressure and internal energy on the Hugoniot, and C and S are constants. The Gruneisen ratio γ is

$$\gamma=V(P_H-P_I)/(E_H-E_I) \qquad (4\text{–}209)$$

where the subscript I pertains to the properties on an isentrope, and is obtained by using the Dugdale-MacDonald relationship

$$\gamma_H(V)=-\frac{V}{2}\frac{d^2(PV^{2/3})/dV^2}{d(PV^{2/3})/dV}-\frac{1}{3}. \qquad (4\text{–}210)$$

From known specific heat and thermal expansion data, a complete (P, V, E) equation of state can be obtained with γ (V) and Eq. 4–209. McQueen and Marsh (Ref. 149) list experimental data of values of C and S for nineteen metallic elements, from which equations of state of the elements can be calculated. Walsh, et al (Ref. 33), reproduce similar experimental data for 27 metals by analytical fit of the form

$$P_H=A\mu+B\mu^2+C\mu^3 \qquad (4\text{–}211)$$

where

$$\mu=\rho/\rho_o-1=(V_{oH}/V)-1. \qquad (4\text{–}212)$$

The constants A, B, and C are listed in tabular form, and from the conservation of energy

$$E_H-E_{oH}=\frac{1}{2}(P_H+P_o)(V_{oH}-V)$$

$$E_H-E_{oH}=(A\mu^2+B\mu^3+C\mu^4)/2\rho_o(\mu+1). \qquad (4\text{–}213)$$

Here, Eqs. 4–211, 4–212, and 4–213, with the tables, provide all the thermodynamic data obtainable by the shock wave measurements.

Section V (U)—List of Symbols, References, and Bibliography

4–21. LIST OF SYMBOLS

a	fragment dimension between planes of rupture	(in.)
c	velocity	
d	diameter of shell casing	(in.)
d	horizontal range; depth	(ft, yd)
e_c	carrier charge	
f	order function	

h	Planck's constant	
h	height of burst	(ft)
j	current density	
k	Boltzmann's constant	
m	mass	
λ, μ	wave length	(millimicrons)
n	exponent	
n	index of refraction	
n_e	number of electrons per cu cm	
n_i	number of ions per cu cm	
n_m	number of molecules per cu cm	
n_s	number of charge carriers of type s per unit volume	
n_Θ	number of fragments per given interval of Θ	
p	pressure	
p_o	ambient fluid pressure before blast	(psi)
q	heat of explosion retained by the gases after the work process	
q_i	first ionization potential of the gas	
r	roentgen	
r	radius	(ft)
s	cross sectional area	
t	time	(sec.)
t	thickness	(in.)
u	velocity	(ft/sec.)
w	weight of explosive	(lb, ton, KT, MT)
x	thickness	(noted)
x	distance	(ft)
x	velocity	(ft/sec.)
A	constant	(as noted)
A	cross sectional area	(sq in., sq ft)
A	Arrhenius constants	
A	wave length	(Angstroms)
B	maximum material stress before rupture	(lb/sq in.)
$B(x)$	radiation build-up factor	
C	heat capacity	
C	mass of explosive charge	(slugs)
C_1	constant	(as noted)
C_d	drag coefficient	
C_o	speed of sound	(ft/sec.)
D	slant range	(noted)
D	drag	(lb)
D	velocity of detonation wave	(ft/sec.)
D_A	diameter of apparent crater	(ft)
D_L	diameter of crater lip	(ft)
D_p	diameter of plastic zone	(ft)
D_p^+	duration of positive phase	(sec., min)
D_p^-	duration of negative phase	(sec., min)
D_R	diameter of rupture zone	(ft)
D_R	tissue dose	(Rads)
D_T	diameter of true crater	(ft)
$D(\theta_s)$	static fragment density, number of fragments per steradian	
E	internal energy per unit mass	
E	field strength	
E_e	internal energy of explosive	
E_λ	energy density	(noted)
ΔE_1	Arrhenius constants	
ΔF	free energy of reaction	
H	Mach stem height	(ft)
H_A	depth of apparent crater	(ft)
H_L	height of crater lip	(ft)
H_T	depth of true crater	(ft)
ΔH	heat of activation	
I	radiation intensity	(noted)
I_p^+	positive overpressure impulse	
I_p^-	negative overpressure impulse	
I_u^+	positive dynamic impulse	
I_u^-	negative dynamic impulse	
K	Boltzmann's constant	
K_e	mobility of electrons	
K_s	mobility of charge carriers	
KE	energy per unit length	(ft-lb/in.)
K'	specific reaction rate constant	
L	length of shell casing	(in.)
M	mass	(slugs, grams)
M_o	constant	(as noted)
N	number of fragments	
N	neutron dose	(noted)
N_o	constant	(as noted)
N_t	thermal neutron flux	(neutrons/sq cm)
N_u	neutron flux above Uranium threshold	(neutrons/sq cm)
N_{NP}	neutron flux above Neptunium threshold	(neutrons/sq cm)
N_{PU}	neutron flux above Plutonium threshold	(neutrons/sq cm)
N_s	neutron flux above sulphur threshold	(neutrons/sq cm)
P	thermal power	(cal/sec.)
P	pressure	(psi)
P	path of piston motion	
P_m	peak pressure	(psi)
Q	radiant exposure	(cal/sq cm)
Q	specific heat of reaction	
Q_e	electron atom collision cross section	
R	gas constant	

R	radius of fireball	(ft)
R	target resistance to penetration	(lb)
R	distance from blast center	(ft)
S	tensile strength	(lb/sq in.)
ΔS	entropy of activation	
T	absolute temperature	(°K)
T	total kinetic energy	(ft-lb)
T	atmospheric transmissivity	
U	velocity	(ft/sec.)
U_i	ionization energy	
V	specific volume	
V	velocity	(ft/sec.)
V_c	volume of apparent crater	(cu ft)
W	energy yield	(KT)
W	energy per unit area	(ft-lb/sq in.)
X	field strength	
XU	wave length	(X-units)
α_i	ratio of ionized particles to the total number of particles	
γ	ratio of specific heat	
e	electron charge	
ϵ	expansion ratio	
θ	angle of obliquity between projectile and target at impact	(deg)
θ_c	ambient temperature of fluid before blast	
θ_s	static angle of fragment ejection	(deg)
λ	thermal conductivity	
λ	wave length	(noted)
λ_m	wave length for max energy density	(noted)
μ	amount of matter detonating per second	
μ	one-half the mean fragment mass	(slugs, grams)
μ	wave length	(microns)
μ_a	linear absorption coefficient	
ρ	density	
σ	electrical conductivity	
ϕ	fragment ejection angle	(deg)
ϕ	radiant energy flux	(noted)
Σ	mascropic cross section	
τ	ignition time	

4–22. REFERENCES

1. S. Glasstone, *The Effects of Nuclear Weapons*, United States Atomic Energy Commission, June 1957, (Unclassified).
2. L. Prandtl and O. Tietjens, *Fundamentals of Hydro- and Aeromechanics*, McGraw-Hill, New York, 1934, (Unclassified).
3. K. Owsatitsch, *Gas Dynamics*, Academic Press, New York, 1956, (Unclassified).
4. Sir Horace Lamb, *Hydrodynamics*, Dover, New York, 1945, (Unclassified).
5. R. Cole, *Underwater Explosions*, Princeton University Press, Princeton, 1948, (Unclassified).
6. C. Lampson, *Resume of the Theory of Plane Shock and Adiabatic Waves with Applications to the Theory of the Shock Tube*, BRL Technical Notice No. 139, BRL, Aberdeen Proving Ground, Maryland, March 1950, (Unclassified).
7. H. Bethe, K. Fuchs, J. von Neumann, et al, *Blast Wave*, Los Alamos Scientific Laboratory Report No. LA2000, Los Alamos, New Mexico, August 1947. (Unclassified).
8. J. Kirkwood and S. Brinkley, *Theory of the Propagation of Shock Waves from Explosive Sources in Air and Water*, NDRC Report A 318, OSRD Report 4814, Office of Scientific Research and Development, March 1945, (Unclassified).
9. J. von Neumann and R. Richtmyer, "A Method for the Numerical Calculation of Shocks," Journal of Applied Physics, Vol. 21, March 1950 (Unclassified).
10. W. Weibull, *Explosion of Spherical Charges in Air: Travel Time, Velocity of Front, and Duration of Shock Waves*, BRL Report No. X–127, BRL, Aberdeen Proving Ground, Maryland, February 1950. (Unclassified).
11. Lord Rayleigh, *Proc. Roy. Soc.*, A 84, page 247, 1910, (Unclassified).
12. G. T. Taylor, *Proc. Roy. Soc.*, A 84, page 371, 1910, (Unclassified).
13. R. Becker, *Zeits. F. Physik*, Vol. 8, page 321, 1922, (Unclassified).
14. L. H. Thomas, *Journal of Chemistry and Physics*, Vol. 12, page 449, 1944, (Unclassified).
15. H. Brode, "Numerical Solutions of Spherical Blast Waves," Journal of Applied

Physics, Vol. 26, June 1955, (Unclassified).

16. H. Brode, *A Calculation of the Blast Wave From a Spherical Charge of TNT*, Rand Report RM-1965, Rand Corporation, Santa Monica, California, August 1957, (Unclassified).

17. R. Sachs, *The Dependence of Blast on Ambient Pressure and Temperature*, BRL Report No. 466, BRL, Aberdeen Proving Ground, Maryland, May 1944, (Unclassified).

18. H. Langharr, *Dimensional Analysis and Theory of Models*, Wiley Book Co., New York, 1951, (Unclassified).

19. D. Ipsen, *Units, Dimensions, and Dimensionless Numbers*, McGraw-Hill Book Co., New York, 1960, (Unclassified).

20. J. Dewey and J. Sperrazza, *The Effect of Atmospheric Pressure and Temperature on Air Shock*, BRL Report No. 721, BRL, Aberdeen Proving Ground, Maryland, May 1950, (Unclassified).

21. —— *Capabilities of Atomic Weapons*, Department of the Army Manual, TM 23-200, November 1957, (Confidential).

22. C. Lampson, *Final Report on Effects of Underground Explosions*, NDRC Report No. A-479, OSRD Report No. 6645, OSRD, 1946, (Unclassified).

23. Ugo Fano, *Methods for Computing Data on the Terminal Ballistics of Bombs, II Estimation of the Air Blast*, BRL Report No. 524, BRL, Aberdeen Proving Ground, Maryland, 7 February 1945, (Confidential).

24. R. W. Gurney, *The Initial Velocities of Fragments from Bombs, Shells, and Grenades*, BRL Report 405, BRL, Aberdeen Proving Ground, Maryland, 14 September 1943, (Unclassified).

25. T. D. Carr and R. G. Sachs, *Air Blast Measurements at the Ballistic Research Laboratories*, BRL Report No. 598, BRL, Aberdeen Proving Ground, Maryland, 1942-1946, 29 January 1946, (Unclassified).

26. A. J. Hoffman, S. D. Schlueter and J. Sperrazza, *Comparative Blast Tests of Thin and Thick Wall Blast-type Warheads, T-2 for Falcon-Guided Missile*, BRL Memorandum Report No. 557, BRL, Aberdeen Proving Ground, Maryland, August 1951, (Confidential).

27. E. M. Fisher, *The Effect of the Steel Case on the Air Blast from High Explosives*, NAVORD 2753, U. S. Naval Ordnance Laboratory, White Oak, Maryland, 19 February 1953, (Confidential), ASTIA No. AD-9708.

28. J. G. Kirkwood and S. R. Brinkley, *Tables and Graphs of the Theoretical Peak Pressures, Energies, and Positive Impulses of Blast Waves in Air*, NDRCA-327, May 1945, (Unclassified).

29. R. Smith and C. Wangerin, *Some Preliminary Results on the Effect of a Steel Case on the Blast from Pentolite Cylinders*, BRL Memorandum Report No. 863, BRL, Aberdeen Proving Ground, Maryland, August 1954, (Confidential).

30. S. Sacks and F. G. King, *Single Shot Probability of an "A" Kill on the B-29 Type Bomber of NIKE I*, BRL Memorandum Report No. 553, BRL, Aberdeen Proving Ground, Maryland, July 1951, (Confidential).

31. R. G. Hippensteel, et al, *Air Blast Measurements of a New Series of Conventional Air Force and Navy Bombs*, BRL Memorandum Report No. 1152, BRL, Aberdeen Proving Ground, Maryland, June 1951, (Confidential).

32. C. L. Adams, J. W. Sarmousakis and J. Sperrazza, *Comparison of Blast from Explosive Charges of Different Shapes*, BRL Report No. 631, BRL, Aberdeen Proving Ground, Maryland, January 1949, (Unclassified).

33. R. C. Makino and H. J. Goodman, *Air Blast Data on Bare Explosives of Different Shapes and Compositions*, BRL Memorandum Report No. 1015, BRL, Aberdeen Proving Ground, Maryland, June 1956, (Confidential).

34. W. D. Kennedy, *The Order of Effectiveness of Explosives in Air Blast*, NDRC Report No. A-374, March 1956, (Unclassified).

35. R. G. Hippensteel, *Air Blast Measurements about 8 Pound Special Charges of Five Different High Explosives*, BRL Memorandum Report No. 1052, BRL, Aberdeen Proving Ground, Maryland, December 1956, (Confidential).

36. J. D. Patterson and J. Wenig, *Air Blast Measurements Around Moving Explosive Charges*, BRL Memorandum Report No. 767, BRL, Aberdeen Proving Ground, Maryland, March 1954, (Confidential).

37. B. F. Armendt, *Air Blast Measurements Around Moving Explosive Charges, Part II*, BRL Memorandum Report No. 900, BRL, Aberdeen Proving Ground, Maryland, May 1955, (Confidential).

38. B. F. Armendt and J. Spetrazza, *Air Blast Measurement Around Moving Explosive Charges, Part III*, BRL Memorandum Report No. 1019, BRL, Aberdeen Proving Ground, Maryland, July 1956, (Confidential).

39. B. F. Armendt, *Qualitative Tests of Dynamic Strength of Various Plastic-Bonded and Fiber-Reinforced Explosives*, BRL Memorandum Report No. 977, BRL, Aberdeen Proving Ground, Maryland, February 1956, (Unclassified).

40. C. K. Thornhill and R. Hetherington, *Some Notes on Explosions of Moving Charges*, ARE Memo 6153, April 1952, (Unclassified).

41. J. J. Meszaros, *Target Response Instrumentation*, BRL, August 1957, BRL, Aberdeen Proving Ground, Maryland, (Unclassified).

42. C. W. Lampson and J. J. Meszaros, *Blast Instrumentation*, BRL, Aberdeen Proving Ground, Maryland, August 1957, (Unclassified).

43. W. E. Baker and J. D. Patterson, II, *Blast Effects Tests of a One-Quarter Scale Model of the Air Force Nuclear Engineering Test Reactor*, BRL Report No. 1011, BRL, Aberdeen Proving Ground, Maryland, March 1957, (Unclassified).

44. R. G. Hippensteel, A. J. Hoffman and W. E. Baker, *Safety Tests of NIKE-HERCULES Missile Sites*, BRL Report No. 1085, BRL, Aberdeen Proving Ground, Maryland, November 1959, (Secret).

45. T. K. Groves, *A Photo-Optical System of Recording Shock Profiles From Chemical Explosions*, Suffield Experimental Station, Ralston, Alberta, Canada, (Unclassified).

46. R. E. Riesler, *The Mechanical Self-Recording Pressure-Time Gage*, BRL, Aberdeen Proving Ground, Maryland, (Unclassified).

47. B. F. Armendt, et al, *The Air Blast from Simultaneously Detonated Explosive Spheres*, BRL Memorandum Report No. 1294, BRL, Aberdeen Proving Ground, Maryland, August 1960, (Secret).

48. W. E. Forsythe, *Measurement of Radiant Energy*, McGraw-Hill Book Company, Inc., New York, 1937, (Unclassified).

49. —— *Radiation, A Tool for Industry*, AL 152, U. S. Atomic Energy Commission, January 1959, (Unclassified).

50. —— *ABC Warfare Defense*, Navy Training Course, NAVPERS 10099, Bureau of Naval Personnel, 1960, (Unclassified).

51. W. A. Biggers, L. J. Brown and K. C. Kohr, *Space, Energy, and Time Distribution at the Ground-Air Interface*, LA-2390, Los Alamos Scientific Laboratory, January 1960, (Unclassified).

52. ——*External Neutron Measurements—1952 through 1958*, CWLR 2377, U. S. Army Chemical Warfare Laboratories, Army Chemical Center, Maryland, (Secret—RD).

53. R. H. Richie and G. S. Hurst, "Penetration of Weapons," *Health Physics*, Volume 1, No. 4, March 1959, (Unclassified).

54. J. E. Rosen, et al, *Nuclear Weapons Radiation Doses in Armored Vehicles*, NR-82, Lockheed Aircraft Corporation, July 1960, (Secret -RD).

55. —— *Nuclear Radiation Handbook*, Armed Forces Special Weapons Project, AFSWP–1100, 1959, (Secret—RD).

56. N. F. Mott and E. H. Linfoot, *A Theory of Fragmentation*, Report 3348, Advisory Council on Scientific Research and Development, Ministry of Supply, London, January 1943, (Confidential).

57. N. F. Mott, *A Theory on the Fragmentation of Shells and Bombs*, Report 4035, Advisory Council on Scientific Research and Development, Ministry of Supply, London, c August 1943.

58. N.F. Mott, *Fragmentation of HE Shells: A Theoretical Formula for the Distribution of Weights of Fragments*, Report 3642, Advisory Council on Scientific Research and Development, Ministry of Supply, London, March 1943, (Secret).

59. R. W. Gurney and J. N. Sarmousakis, *The Mass Distribution of Fragments from Bombs, Shells, and Grenades*, BRL Report No. 448, BRL, Aberdeen Proving Ground, Maryland, February 1944, (Confidential).

60. A. D. Solem, N. Shapiro and B. M. Singleton, Jr., *Explosive Comparison for Fragmentation Effectiveness*, NAVORD R–2933, U. S. Naval Ordnance Laboratory, August 1953, (Confidential).

61. F. A. Weymouth, *The Effect of Metallurgical Properties of Steel upon Fragmentation Characteristics of Shell*, BRL Memorandum Report No. 585, BRL, Aberdeen Proving Ground, Maryland, April 1952.

62. F. A. Weymouth, *Fragmentation Characteristics of Three Grades of Ductile Cast Iron*, BRL Technical Notice 600, BRL, Aberdeen Proving Ground, Maryland, June 1952, (Confidential).

63. —— *Fin Stabilized Fragmentation Warhead*, Engineering Report 788, Aircraft Armaments, Inc., March 13, 1956, (Confidential).

64. —— *Development of 300 Pound T–3 Fragmentation Warheads, Report* C58909, Arthur D. Little, Inc., January 15, 1956, (Confidential).

65. J. E. Shaw, *Principles of Controlling Fragment Masses by the Grooved Ring Method*, BRL Report No. 688, BRL, Aberdeen Proving Ground, Maryland, February 1949, (Unclassified).

66. J. E. Shaw, *The Effect of Cushions in Controlled Fragmentation Shell*, BRL Report No. 732, BRL, Aberdeen Proving Ground, Maryland, August 1950, (Confidential).

67. C. L. Grabarek, *Mass, Spacial, and Velocity Distributions of Fragments from MX–904(T7) Warheads, Wire Wrapped Types*, BRL Memorandum Report No. 550, BRL, Aberdeen Proving Ground, Maryland, June 1951, (Confidential).

68. W. N. Wishard, *Fragmentation Tests of Sparrow Warheads EX 5 Mod 0*, U. S. Naval Proving Ground Report 1370, May 1955, (Confidential).

69. —— *Fragmentation Tests of CBS Steel and Forge Company Warheads*. U. S. Naval Proving Ground Report 1222, December 18, 1953, (Confidential).

70. D. P. Clark, *Fragmentation Tests of Experimental Warheads NOL WH 132–1, –2, and –3*, U. S. Naval Proving Ground Report 1341, March 1955, (Confidential).

71. J. W. Gorman, *A Study of Plastic Liners for Fragmentation Control of 3"/50 Projectiles MK 25–0*, U. S. Naval Proving Ground Report 1372, May 13, 1955, (Confidential).

72. C. L. Grabarek, *Comparative Fragmentation Tests of Single and Multi-Walled Cylindrical Warheads*, BRL Report No. 928, BRL, Aberdeen Proving Ground, Maryland, January 1955, (Confidential).

73. H. N. Shapiro, *A Report on Analysis of the Distribution of Perforating Fragments for the 90 mm, M71, Fuzed T74E6, Bursting Charge TNT*, UNM/T–234, University of New Mexico, (about 1944).

74. S. Sewell, *Effect of End Confinement and Shell Length on Spatial Distribution and Velocity of Fragments*, BRL Memoran-

dum Report No. 862, BRL, Aberdeen Proving Ground, Maryland, January 1955, (Confidential).

75. —— *Ordnance Proof Manual 70-90*, (Vol. I), U. S. Army, June 24, 1959, (Unclassified).

76. W. R. Benson, *The Basic Method of Calculating the Lethal Area of a Warhead*, Technical Report 2044, Picatinny Arsenal, October 1954, (Confidential).

77. T. E. Sterne, *A Note on the Initial Velocities of Fragments from Warheads*, BRL Report No. 648, BRL, Aberdeen Proving Ground, Maryland, September 1947, (Confidential).

78. T. E. Sterne, *The Fragment Velocity of a Spherical Shell Containing an Inert Core*, BRL Report No. 753, BRL, Aberdeen Proving Ground, Maryland, March 1951, (Confidential).

79. G. E. Hauver and B. C. Taylor, *Projection of a Thin Metal Plate by an Explosive*, BRL Technical Note 1168, BRL, Aberdeen Proving Ground, Maryland, January 1958.

80. E. M. Pugh, *Mixnay-Schardin Effect*, Carnegie Institute of Technology Report CIT-ORD-M28, October 1952, (Confidential).

81. C. L. Grabarek, *Characteristics of Fragmentation of MX 904 Warheads Blast with Fluted Liner, Comp B, HBX and Tritonal Loaded*, BRL Memorandum Report No. 700, BRL, Aberdeen Proving Ground, Maryland, July 1953, (Confidential).

82. W. C. F. Sheperd and R. Torry, *Fragmentation of Grenades, VII, Velocities of the Fragments from the No. 70 MK II, No. 36M and No. 71 Grenades*, Report 9028, Advisory Council on Scientific Research and Technical Development, Ministry of Supply, London, April 1946, (Confidential).

83. —— *Fragment Velocity Law Program, 4th Partial Report*, U. S. Naval Proving Ground Report 581, June 1950.

84. —— *Fragment Velocity Law for Cylinders, Cones, and Composite Shapes, 1st Partial Report*, U. S. Naval Proving Ground Report 904, January 1952.

85. R. W. Gurney, *Fragmentation of Bombs, Shells, and Grenades*, BRL Report No. 635, BRL, Aberdeen Proving Ground, Maryland, March 1947.

86. L. H. Thomas, *Theory of the Explosion of Cased Charges of Simple Shape*, BRL Report No. 475, BRL, Aberdeen Proving Ground, Maryland, July 1954.

87. —— *Vulnerability of Manned Aircraft to Guided Missiles*, Ministry of Supply, London, England, August 1956, (Secret-Discreet).

88. L. D. Hepner, *Analytical Laboratory Report on Fragmentation Test Design, Collection, Reduction and Analysis of Data*, APG Memorandum Report No. 306, D and PS, Aberdeen Proving Ground, Maryland, September 1959, (Confidential).

89. H. I. Breidenbach, *Fragment Velocities of Hollow Warheads as Determined from Flash Radiographs*, BRL Report No. 640, BRL, Aberdeen Proving Ground, Maryland, June 28, 1947, (Confidential).

90. —— *The Use of the Rotating Drum Camera for the Measurement of the Velocities of Shell or Bomb Fragments*, Report 3900, Office of Scientific Research and Development, July 1944.

91. J. L. Machamer, *A Method for Measuring Fragment Velocities by the Multiple Break Wire Screen*, BRL Memorandum Report No. 919, BRL, Aberdeen Proving Ground, Maryland, July 1955.

92. A. J. Riechiazzi and J. J. Trimble, *Modifications of the Multiple-Break Wire Screen Technique for Measuring Fragment Velocities*, BRL Memorandum Report No. 1137, BRL, Aberdeen Proving Ground, Maryland, April 1958.

93. S. Timoshenko and D. H. Young, *Advanced Dynamics*, McGraw-Hill Book Company, Inc., 1948.

94. D. J. Dunn, Jr. and W. R. Porter, *Air Drag Measurements of Fragments*, BRL Memorandum Report No. 915, BRL, Aberdeen Proving Ground, Maryland, August 1955, (Confidential).

95. J. E. Shaw, *A Measurement of the Drag Coefficient of High Velocity Fragments and Appendix*, BRL Report No. 744, BRL, Aberdeen Proving Ground, Maryland, October 1950.

96. W. R. Porter, J. L. Machamer, and W. O. Ewing, *Electro-Optic Icosahedron Gage*, BRL Report No. 877, BRL, Aberdeen Proving Ground, Maryland, September 1953.

97. —— *Three Station Fragment Retardation Apparatus at Bruceton*, Report 5619, Office of Scientific Research and Development, December 1945.

98. A. G. Walters and L. Rosenhead, *The Penetration and Perforation of Targets by Bombs, Shells, and Irregular Fragments*, Report 4994, Advisory Council on Scientific Research and Technical Development, Ministry of Supply, London, October 1943, (Secret).

99. A. G. Walters and J. Taylor, *The Penetrating and Perforating Power of Fragments and Projectiles*, Report 9146, Advisory Council on Scientific Research and Technical Development, Ministry of Supply, London, June 1946, (Confidential).

100. —— *Investigation of Variables affecting the Performance of Lightweight Armor*, Midwest Research Institute Final Report for Watertown Arsenal, January 9, 1945, (Confidential).

101. D. J. Dunn, Jr., *A Target for an Effects Field*, BRL Technical Note 1172, BRL, Aberdeen Proving Ground, Maryland, January 1958, (Secret).

102. B. L. Welch, *Notes on the Comparative Performance against Thin Mild Steel Plate of Irregular Fragments and Small Regular Projectiles*, Report 8110, AC 8110, Advisory Council on Scientific Research and Development, Ministry of Supply, London, April 23, 1945, (Secret).

103. T. W. Taylor, *The Perforation of Duralumin Plates by Spherical Fragments at Normal and Oblique Angles of Attack*, Report ARE–WRD Rn52/54, Armament Research Establishment, February 1955, (Confidential).

104. J. H. McMillen, et al., *Ballistics of the Penetration of Human Skin by Small Spheres*, Missile Casualties Report No. 11, 1945.

105. T. E. Sterne, *Provisional Values of the Vulnerability of Personnel to Fragments*, BRL Report No. 758, BRL, Aberdeen Proving Ground, Maryland, May 1951, (Confidential).

106. A. J. Dziemian, *The Penetration of Steel Spheres into Tissue Models*, Army Chemical Center Report ACC/CWLR 2226, Army Chemical Center, Maryland, August 1958.

107. R. L. Jameson and J. S. Williams, *Velocity Losses of Cylindrical Steel Projectiles Perforating Mild Steel Plates*, BRL Report No. 1019, BRL, Aberdeen Proving Ground, Maryland, July 1957.

108. R. J. Eichelberger et al, "Seminar on Hypervelocity Impact," BRL Report No. 1101, BRL, Aberdeen Proving Ground, Maryland, February 1960, (Secret–RD).

109. L. G. Richards and L. S. Holloway, *Study of Hypervelocity of Micro-particle Cratering*, BRL Memorandum Report No. 1283, BRL, Aberdeen Proving Ground, Maryland, June, 1960.

110. —— *Fourth Symposium on Hypervelocity Impact*, APGC–TR–60–39 (Vols. 1–4), Air Proving Ground Center, Eglin Air Force Base, Florida, September, 1960.

111. J. W. Gehring, "An Expendable High-Explosive Light Gas Gun for Projecting Hypervelocity Projectiles," Paper presented to the third Symposium on Hypervelocity Impact, Chicago, 1958.

112. D. C. Vest, *An Experimental Traveling Charge Gun*, BRL Report No. 773, BRL, Aberdeen Proving Ground, Maryland, October 1951.

113. J. H. Kineke, Jr., "An Experimental Study of Crater Formation in Lead," *Proceedings of Third Symposium on Hypervelocity Impact*, Armour Research Foundation of Illinois Institute of Technology, Chicago, Illinois, October 1958, (Unclassified). (See also: "Some Results of Hypervelocity Explosive Charge Investigation," E. N. Clark and A. MacKenzie; and "A Critical Study of the Air Cavity Technique for Projecting Intact Hypervelocity Fragments," L. Zernow, K. N. Kreyenhagen, P. G. McManigal, and A. W. Hall.)

114. J. W. Gehring, Jr. "An Analysis of Micro-Particle Cratering," *Proceedings of Third Symposium on Hypervelocity Impact*, Armour Research Foundation of Illinois Institute of Technology, Chicago, Illinois, October 1958, (Unclassified).

115. —— *A Study of Residual Velocity Data for Steel Fragments Impacting on Four Materials; Empirical Relationships (U)*, Project Thor Technical Report No. 36, Ballistic Analysis Laboratory, Institute for Cooperative Research, The Johns Hopkins University, April 1958, (Confidential).

116. —— *The Resistance of Two Nose-Cone Materials to Perforation by Steel Fragments; Empirical Relationships for Fragment Residual Velocity and Residual Weights (U)*, Project Thor Technical Report No. 44, Ballistic Analysis Laboratory, Institute for Cooperative Research, The Johns Hopkins University, January 1960, (Confidential).

117. —— *A Comparison of the Performance of Fragments of Four Materials Impacting on Various Plates (U)*, Project Thor Technical Report No. 41, Ballistic Analysis Laboratory, Institute for Cooperative Research, The Johns Hopkins University, May 1959, (Confidential).

118. A. W. Campbell and J. A. Hull, et al, "Technique for the Measurement of Detonation Velocity," Second ONR Symposium on Detonation, February 1955, (Unclassified).

119. T. J. Boyd, Jr. and P. Fagan, "A Microwave Technique for Measuring Detonation Velocity," Second ONR Symposium on Detonation, February 1955, (Unclassified).

120. B. Brixner, "A High Speed Rotating Mirror Frame Camera," Journal of the Society of Motion Picture and Television Engineers, High Speed Photography, Vol. 5, 1954, (Unclassified).

121. M. Sultanoff, "Photographic Instrumentation in the Study of Explosive Reactions," *Journal of the Society of Motion Picture and Television Engineers*, High Speed Photography, Vol. 5, 1954, (Unclassified).

122. M. Sultanoff, *An Ultra-High Speed Camera*, BRL Report No. 714, BRL, Aberdeen Proving Ground, Maryland, December 1949, (Unclassified).

123. I. S. Bowen, *The C.I.T. Rotating Mirror Camera, Model 2*, Office of Scientific Research and Design, Contract OE MAR-418, California Institute of Technology, 1945, (Unclassified).

124. H. E. Edgerton and C. W. Wychoff, "A Rapid Action Shutter with No [illegible] Parts," Journal of the Society of Motion Picture and Television Engineers, High Speed Photography, Vol. 4, 1952, (Unclassified).

125. R. B. Collins (Editor), "High Speed Photography," Proceedings of the Third International Congress, Butterworths Scientific Publications, London, 1957, (Unclassified).

126. J. W. Gehring, Jr. and Dewey, *An Experimental Determination of Detonation Pressure in Two Solid High Explosives*, BRL Report No. 935, BRL, Aberdeen Proving Ground, Maryland, April 1955 (Unclassified).

127. G. E. Hauver, "Pressure Profiles in Detonating Solid Explosive," Third Symposium on Detonation, ONR Symposium Report, ACR-52, Vol. I, James Forrestal Research Center, Princeton University, (Co-sponsored by Naval Ordnance Lab-

ments from Shock Wave Measurements to Two Megabars," Journal of Applied Physics, Vol. 31, No. 7, July 1960, (Unclassified).

150. J. M. Walsh, et al, "Shock Compressions of Twenty-Seven Metals," "Equations of State of Metals," Physical Review, Vol. 108, No. 2, October 1957, (Unclassified).

4–23. BIBLIOGRAPHY

1. H. Goodman, *Compiled Free Air Blast Data on Bare Spherical Pentolite*, BRL Report 1092, BRL, Aberdeen Proving Ground, Maryland, February 1960, (Unclassified).

2. A. Hoffman and S. Mills, *Air Blast Measurements about Explosive Charges at Side-On and Normal Incidence*, BRL Report No. 988, BRL, Aberdeen Proving Ground, Maryland, July 1956, (Unclassified).

3. J. Dewey, *Note on the Determination of the Form of Air Shocks from the Decay Curve*, BRL Memorandum Report No. 598, BRL, Aberdeen Proving Ground, Maryland, February 1952, (Unclassified).

4. B. Armendt, et al, *The Initial Decay of Pressure Behind a Shock Front: Comparison of Experimental and Calculated Results*, BRL Memorandum Report No. 997, BRL, Aberdeen Proving Ground, Maryland, April 1956, (Unclassified).

5. W. Olson, et al, *The Effect of Atmospheric Pressure on the Reflected Impulse from Air Blast Waves*, BRL Memorandum Report No. 1241, BRL, Aberdeen Proving Ground, Maryland, January 1960, (Unclassified).

6. P. Bridgman, *Dimensional Analysis*, Yale University Press, New Haven, 1931, (Unclassified).

7. W. I. Duvall and T. C. Atchison, *Rock Breakage by Explosives*, Bureau of Mines Report of Investigations 5356, 1957, (Unclassified).

8. B. F. Grant, et al, *Use of Explosives in Oil and Gas Wells—1949 Test Results*, Bureau of Mines Report of Investigations 4714, 1950, (Unclassified).

9. Hino and Kumao, "Fragmentation of Rock through Blasting," Journal of Industrial Explosives Society, Vol. 17, No. 1, 1956, (Unclassified).

10. L. Obert and W. I. Duvall, *Gage and Recording Equipment for Measuring Dynamic Strain in Rock*, Bureau of Mines Report of Investigations 4581, 1949, (Unclassified).

11. —— *Generation and Propagation of Strain Waves in Rock, Part I*, Bureau of Mines Report of Investigations 4683, 1950, (Unclassified).

12. T. C. Atchison and W. E. Tournay, *Comparative Studies of Explosives in Granite*, Bureau of Mines Report of Investigations 5509, 1959, (Unclassified).

13. J. von Neumann, *Oblique Reflection of Shocks*, Explosive Research Report No. 12, Navy Dept., BuORD, 1943.

14. G. H. Lean, *Experiments on the Reflection of Inclosed Shock Waves*, AC 5348, Phys/Ex 501, Advisory Council on Scientific Research and Technical Development, Great Britain, 1943.

15. W. Doering and G. Burkhardt, *Contributions to the Theory of Detonation*, (Engl. Trans. by Brown Univ.), Technical Report No. F-TS-1227-1A (GDAM-A-9-7-46), Headquarters, Air Materiel Command, Wright-Patterson Air Force Base, Dayton, Ohio, May 1949.

16. R. E. Shear and P. McCane, *Normally Reflected Shock Front Parameters*, BRL Memorandum Report No. 1273, BRL, Aberdeen Proving Ground, Maryland, May 1960.

17. Courant and Friedrichs, *Supersonic Flow and Shock Waves*, Interscience, 1948.

18. H. S. Morton and N. de Haas, *Approximations Applicable to the Study of High Explosive Warheads and Target Damage by Blast*, CF-2301, Applied Physics Laboratory, The Johns Hopkins University, December 1954, (Confidential).

oratory and the Office of Naval Research.) September 1960, (Unclassified).

128. S. Joigneau and J. Thouvenin, *Electrical Conductivity of Sulphur Under the Action of a Shock Wave*, C. R. Academy of Science, Paris, 23 June 1958, (Unclassified).

129. Morland, *Philosophical Transaction of the Royal Society*, London, July 1955, (Unclassified).

130. R. E. Duff and E. Houston, "Measurement of the Chapman-Jouguet Pressure and Reaction Zone Length in a Detonating Explosive," Journal of Chemical Physics, July 1955, (Unclassified).

131. F. C. Gibson, "Measurements of Detonation Temperatures," Second ONR Symposium on Detonation, February 1955, (Unclassified).

132. J. J. Paszek, B. C. Taylor and J. L. Squier, *Low Voltage Flash Radiography*, BRL Memorandum Report No. 645, BRL, Aberdeen Proving Ground, Maryland, February 1953, (Unclassified).

133. Taylor, *Detonation in Condensed Explosives*, Oxford, Clarendon Press, 1952, (Unclassified).

134. Greifer, et al, "Combustion and Detonation in Gases," Journal of Applied Physics, Volume 28, Number 3, 1957, (Unclassified).

135. Belles, "Detonability and Chemical Kinetics," Seventh Symposium (International) on Combustion at London and Oxford, Butterworth's Scientific Publications, August 28 to September 3, 1958, (Unclassified).

136. M. A. Cook, *The Science of High Explosives* Rheinhold Publishing Corp., New York 1958, (Unclassified).

137. J. von Neumann, *Theory of Detonation Wave*, Office of Scientific Research and Development Report 549, 1942, (Unclassified).

138. R. Courant and K. O. Friedrichs, *Supersonic Flow and Shock Waves*, Interscience Publishers, Inc., New York, 1956, (Unclassified).

139. M. A. Cook, "Fundamental Principles of Wave Shaping," Proceedings of Detonation Wave Shaping Conference at Picatinny Arsenal, Pages 1 to 22, June 1956, (Confidential).

140. M. A. Cook and W. O. Ursenbach, "Development of an Axial Initiator for the Production of a Cyindrical Wave," Proceedings of Detonation Wave Shaping Conference at Picatinny Arsenal, Pages 107 to 119, June 1956, (Confidential).

141. S. J. Jacobs, "Principles of Wave Shaping," Proceedings of Detonation Wave Shaping Conference at Picatinny Arsenal, Pages 45 to 65, June 1956, (Confidential).

142. W. A. Bore, R. P. Frazer and W. H. Wheeler, *Transactions of the Philosophical Society*, London, 1935, (Unclassified).

143. A. E. Malinovski, *Journal of Chemical Physics* (USSR), 1924, (Unclassified).

144. M. Birk, A. Erez, Y. Manheimar and G. Nahmani, "On Electrical Conductivity in Detonation and Shock Waves, and the Measurement of Detonation and Shock Velocities," Sulletin of the Research Council of Israel, Vol. 3, Number 4, 1954, (Unclassified).

145. Shao-Chi Lin, E. L. Resler and A. Kantrowitz, "Electrical Conductivity of Highly Ionized Argon Produced by Shock Waves," Journal of Applied Physics, Vol. 26, No. 1, January 1955, (Unclassified).

146. M. A. Cook, et al, *Measurements of Ionization and Electron Densities in the Detonation Wave of Solid Explosives*, TR No. 1, Explosive Research Group, University of Utah, Sept. 15, 1956, (Unclasisfied).

147. D. C. Pack, W. M. Evans and H. S. James, *The Propagation of Shock Waves in Steel and Lead*, Proceedings of Physical Society, Vol. 60, 1948, (Unclassified).

148. J. S. Rinehart and J. Pearson, *Behavior of Metals Under Impulsive Loads*, American Society for Metals, Cleveland, Ohio, 1954, (Unclassified).

149. R. G. McQueen and S. P. Marsh, "Equation of State for Nineteen Metallic Ele-

19. —— *Final Report of Atomic Bomb Tests*, Vol. IV, United States Department of Defense, 27 January to 30 September 1946, (Secret).
20. —— *Report of Test Exercises Desert Rock II and III*, Headquarters, Camp Desert Rock, 15 December 1951, (Secret).
21. —— *A Report on the Prediction of Blast Effects on Ordnance Material at Exercise Desert Rock*, BRL Memorandum Report No. 597, BRL, Aberdeen Proving Ground, Maryland, (Secret-RD).
22. E. J. Bryant, et al, *Statistical Estimation of Damage to Ordnance Equipment Exposed to Nuclear Blasts*, WT–733, Project 3.21, Operation Upshot/Knothole, February 1955, (Secret—RD).
23. E. J. Bryant, et al, *Response of the Drag Type Equipment Targets in the Precursor Zone*, Preliminary Report, ITR–1123, Operation Teapot, May 1955, (Secret).
24. W. W. Berning, *Predictions of the Effects of Atomic Weapons on Ordnance Equipment*, BRL Report No. 847, BRL, Aberdeen Proving Ground, Maryland, May 1953, (Secret).
25. —— *Analysis of Atomic Weapons Effects Upon Army Ground Operations Equipment*, First Quarterly Report, ORD–S–80, Armour Research Foundation, First Quarterly Report, 27 December 1950.
26. —— *Analysis of Atomic Weapons Effects Upon Army Ground Operations Equipment*, Second Quarterly Report, ORD–S–81, Armour Research Foundation, 19 January 1951.
27. —— *Analysis of Atomic Weapons Effects Upon Army Ground Operations Equipment*, Third Phase Report, ORD–S–200, Armour Research Foundation, 18 June 1951.
28. —— *Analysis of Atomic Weapons Effect Upon Army Ground Operations Equipment*, Fourth Phase Report, ORD–S–253, Armour Research Foundation, 20 November 1951.
29. —— *Analysis of Atomic Weapons Effects Upon Army Ground Operations Equipment*, Fifth Phase Report, ORO, Armour Research Foundation, 1 July 1952.
30. —— *The Effects of Atomic Blast of Military Equipment*, ARF No. M041, Final Report, Armour Research Foundation, 28 February 1955.
31. E. J. Bryant, et al, *Basic Blast Measurements for Projects 1.14a, 3.1, and 3.10*, WT–1155, Operation Teapot, (Secret).
32. H. Dr[illegible]ven, "Mechanical Analysis of Survival in Falls from Heights of Fifty to One Hundred Fifty Feet," *War Medicine*, 1942, (Unclassified).
33. W. J. White, *Acceleration and Vision*, WADC Technical Report 48–333, November 1958, (Unclassified).
34. —— "The Effects of Nuclear Radiation," (A series of reports concerning nuclear radiation effects on various materials), Radiation Effects Information Center, Battelle Memorial Institute, Contract No. AF 33(616)–6564, (Continuation of AF 33(616)–5171) Task No. 60001, Project No. 2133.
35. —— *Nuclear Weapons Employment*, Department of the Army Pamphlet No. 39–1, May 1959, (Unclassified).
36. William J. Price, *Nuclear Radiation Detection*, McGraw-Hill Book Company, Inc., New York, 1958, (Unclassified).
37. J. K. Crosby, *Fragment Range Modifications for Synchronized Smear Pictures*, SRI Technical Report No. 1, Stanford Research Institute, October 1959.
38. A. D. Solem, *The NOL Fragment Velocity Range*, NAVORD R–2766, February 1953.
39. —— *Photographic Determination of Fragment Velocities and Recovery of Velocity Identified Fragments of Controlled Fragmentation Shells, Grooved Ring Type*, Aberdeen Proving Ground Photographic Laboratory Report 80, Aberdeen Proving Ground, Maryland, September 1948.
40. L. D. Hepner, *Analytical Laboratory Report on a Fragmentation Test to Improve Fragment Velocity Data*, Report No. DPS/APG M 290, D&PS, Aberdeen Proving

Ground, Maryland, June 1959, (Confidential).

41. D. J. Dunn, Jr. "Some Notes on the Determination of Initial Fragment Velocity by the Moving Picture Camera Method," BRL Memorandum Report No. 658, BRL, Aberdeen Proving Ground, Maryland, March 1953, (Unclassified).
42. G. M. Gaydos and S. Stein, *Non-Nuclear Warhead Design Guide for FABMDS*, Tech Memo No. DW 329, Warhead and Special Projects Laboratory, Picatinny Arsenal, Dover, New Jersey, March 1961, (Secret).
43. —— "Explosion Effects Data Sheets," U. S. Naval Ordnance Laboratory, White Oak, Maryland, June 1955, (Confidential).
44. —— "First Partial Report on Fragmentation Tests of Experimental Warheads with Small Length/Diameter Ratios, NPG Report 339, July 1948. U. S. Naval Proving Ground, Dahlgren, Virginia.

GLOSSARY
of Terminal Ballistics Terms (U)

A

air burst. Any burst in the air, but usually having reference to the bursting of a projectile or bomb above the ground with resulting spray of fragments.

aircraft. 1. In a broad sense, any machine or craft designed to go through the air (including, in some instances, outer space), given lift by its own buoyancy (as with airships), or by dynamic reaction of air particles over and about its surfaces, or by reaction to a jet stream or other fluid jet. 2. *Restrictive*—A powered, fixed-wing airplane.

airframe. The structural components of an airplane or missile, including the frame work and skin of such parts as the fuselage, empennage, wings, landing gear (minus tires), and engine mounts.

airspeed. The velocity at which an aircraft is traveling through the atmosphere (air). It is entirely independent of any distance covered on the surface of the earth.

aluminized explosive. An explosive to which aluminum has been added. The aluminum, in flaked or powdered form, is incorporated into the explosive to increase the blast effect. Examples of aluminized explosives include ammonal, HBX's, and tritonal.

ambient. Surrounding, encompassing, as in ambient air, ambient temperature.

ammunition. 1. A generic term which includes all manner of missiles to be thrown against an enemy, such as bullets, projectiles, rockets, grenades, torpedoes, bombs, and guided missiles, along with their necessary propellants, primers, fuzes, detonators and charges of conventional explosive, nuclear explosive, chemical or other materials. 2. In the broadest sense the term is not limited to those materials to be thrown, nor to use against an enemy, but includes, in addition to the items and materials given in sense 1, all explosives, explosive devices, pyrotechnics and pyrotechnic devices. The purpose is not limited and includes, in addition to direct use against an enemy, such uses as illumination, signaling, saluting, mining, digging, cutting, accelerating, decelerating, separating, catapulting personnel or materiel, operating or stopping mechaniams, demolition, decoying, practice, training, guarding, game hunting, and pure sport. 3. In the most restricted sense the term includes a complete round and all its components; that is, the material required for firing a weapon such as a pistol, rifle, or cannon, from which a projectile is thrown for inflicting damage upon an enemy. Generally the term is used or taken in its broadest sense (sense 2) unless a more restricted sense is indicated or is implied by the context.

antiarmor. Of ammunition, bombs, bullets, projectiles, or the like: Designed to defeat armor and other resistant targets.

antimechanized defense. All means used for defense against armored combat vehicles. It may include such means as armored units, antitank weapons and grenades, field artillery, antiaircraft artillery, ditches, traps, mine fields, and any other means available. Also known as antitank defense.

antipersonnel. (apers) Of projectiles, bombs, mines, grenades, or the like: Designed to kill, wound, or obstruct personnel.

antitank. (AT) Used, or designed to be used, against tanks.

antitank weapon. Any weapon designed or suitable for use against tanks or other armored vehicles. Antitank rockets, antitank grenades, and antitank guns are examples of antitank weapons.

applique armor. Material or attachment which can be installed on a tank to give it additional protection against kinetic or nonkinetic energy ammunition.

area target. A target consisting of an area, such as an entire munitions factory, rather than a single building or similar point target.

armor. 1. Any physical protective covering, such as metal, used on tanks, airplanes, etc., or on persons, against projectiles or fragments. *See:* armor, body, fragmentation protective; steel armor plate. 2. Armored units or forces. 3. In a weapon system, that component that gives protection to the vehicle or the weapon on its way to the target. In sense 1, conventional steel armor is classified according to its physical and metallurgical structure, as face hardened or homogeneous. It is also classified according to its method of fabrication, as cast or rolled. In sense 3, the armor may consist of armor (sense 1) or any other protective device or technique, such as "chaff," diversionary attack, speed, etc.

armor, body, fragmentation protective. Armor especially designed to provide fragmentation protection to vital areas of the body. Usually provided in the form of garments which may contain steel, nylon, or other resistant materials.

armor castings. A type of armor frequently used when complicated shapes are involved. Such castings are made of high alloy steel and are so heat treated as to have the properties of armor plate. May be either the homogeneous or face-hardened type. *See:* armor.

armor defeating. A term similar to antiarmor, sometimes applied to any of several types of ammunition, having for its principal purpose the defeat of armor protection of armored vehicles or ships. Types of such ammunition are armor-piercing, HEAT, etc.

armored personnel carrier. An armored vehicle which provides protection from small arms fire and shell fragments; used to transport personnel both on and off the battlefield.

armored vehicle. A wheeled or track-laying vehicle mounting armor plate, used for combat security or cargo. Armored vehicles include tanks, personnel carriers, armored cars, self-propelled artillery and various special purpose vehicles.

armored vehicle damage. *See:* damage categories.

armor-piercing. (AP) Of ammunition, bombs, bullets, projectiles, or the like: Designed to penetrate armor and other resistant targets.

armor-piercing, capped. (APC) Of armor-piercing projectiles: Having an armor-piercing cap over the nose. *See:* cap, armor-piercing.

armor, spaced. *See:* spaced armor.

Army complete penetration. Penetration in which it is possible to see light through the hole made by the projectile, or in which it is possible to see a portion of the projectile in the plate when viewed from the rear.

arrow projectile. *See:* projectile, arrow.

aspect angle. The angle formed between the longitudinal axis of a projectile in flight and the axis of a radar beam.

atomic air burst. The explosion of an atomic weapon in the air, at a height greater than the maximum radius of the fireball.

atomic device. Any explosive device that makes use of active nuclear material to cause a chain reaction upon detonation.

atomic surface burst. Atomic missile burst at an elevation such that the fireball touches the ground.

atomic underground burst. The explosion of an atomic weapon with its center beneath the surface of the ground.

atomic underwater burst. The explosion of an atomic weapon with its center beneath the surface of the water.

attitude. The aspect that an aircraft or missile presents at any given moment, as determined by its inclinations about its three axes.

B

ball ammunition. Non-armor-piercing small arms ammunition in which the projectile is solid. It is intended for use against personnel, light material targets, or for training purposes.

ballistic. Pertaining to *ballistics* (which see) or the motion of missiles.

ballistic coefficient. The numerical measure of the ability of a missile to overcome air resistance. It is dependent upon the mass, the diameter, and the *form factor* (which see).

ballistic limit. The minimum velocity at which a particular armor-piercing projectile is expected to consistently, completely, penetrate armor plate of given thickness and physical properties, at a specified angle of obliquity. Because of the expense of firing tests and the impossibility of controlling striking velocity precisely, plus the existence of a zone of mixed results in which a projectile may completely penetrate or only partially penetrate under apparently identical conditions, statistical approaches are necessary, based upon limited firings. Certain approaches lead to approximation of the V_{50} Point, that is, the velocity at which complete penetration and incomplete penetration are equally likely to occur. Other methods attempt to approximate the V_0 Point; that is, the maximum velocity at which no complete penetration will occur. Other methods attempt to approximate the V_{100} Point; that is, the minimum velocity at which all projectiles will completely penetrate.

ballistic missile. Specifically, any missile guided especially in the upward part of its trajectory, but becoming a free falling body in the latter stages of its flight through the atmosphere. This missile contains guiding devices, such as preset mechanisms; but it is distinguished from a guided missile in that it becomes a free falling body, subject to ballistic reactions as it descends through the atmosphere. Currently, the term has a strong connotation of a missile designed to travel outside, or in the outer reaches of, the atmosphere, before plunging toward its target.

ballistics. Branch of applied mechanics which deals with the motion and behavior characteristics of missiles; that is, projectiles, bombs, rockets, guided missiles, etc., and of accompanying phenomena. It can be conveniently divided into three branches: interior ballistics, which deals with the motion of the projectile in the bore of the weapon; exterior ballistics, which deals with the motion of the projectile while in flight; and terminal ballistics, which is concerned with the effect and action of the projectile when it impacts or bursts.

bazooka. Popular name applied to the 2.36-inch rocket launcher. The later model 3.50-inch rocket launcher was termed the "super bazooka."

biological warfare. (biowar) 1. Warfare waged by the employment of living organisms, toxic bacteriological products, and chemical plant-growth inhibitors to produce death or casualties in man, animals, or plants. 2. Defense against such warfare.

black powder. A low explosive consisting of an intimate mixture of potassium or sodium nitrate, charcoal, and sulfur. It is easily ignited and is friction sensitive, but is not of the same sensitivity as primer mixes, and is not intended to be initiated by friction in ammunition items. Formerly, extensively used as a military propellant, but now its military use is almost exclusively in propellant igniters and primers, in fuzes to give short delay, in powder-train time fuzes, in blank ammunition, and as spotting charges in practice ammunition.

blast. The brief and rapid changes in air pressure, density, temperature, and particle velocity resulting from the detonation of any explosive matter.

blast contour. A graphical representation of the results of tests of bare explosive charges against a given target structure. The contour represents the maximum distance from the center of detonation at

which some level of damage. *See:* **damage categories**, to the structure would occur, from charges of a certain weight, and in a given orientation. A given blast contour applies to only one target structure.

blast wave. *See:* **shock wave.** The shock wave transmitted through the air as the result of an explosion. Through usage, the term shock wave often is referred to as a blast wave, or air blast.

body armor. *See:* **armor, body, fragmentation protective.**

bomb. 1. In a broad sense, an explosive or other lethal agent, together with its container or holder, which is planted or thrown by hand, dropped from an aircraft, or projected by some other slow-speed device (as by lobbing it from a mortar), and is used to destroy, damage, injure, or kill. 2. Anything similar to this object in appearance, operation, or effect, as a leaflet bomb, smoke bomb, photoflash bomb, a bomb-like container or chamber, etc.

bomb, atomic. (A-bomb) *Meaning formerly* limited to a bomb in which the explosive consists of a nuclear-fissionable, radioactive material, as uranium 235 or plutonium 239. Now accepted as synonymous with the term bomb, nuclear.

bomb, cobalt. A theoretical atomic or hydrogen bomb encased in cobalt, the cobalt of which would be transmuted into deadly radioactive dust upon detonation.

bomb, hydrogen. (H-bomb) A fusion bomb in which an isotope of hydrogen is made to fuse under intense heat, with a resultant loss of weight and release of energy.

bomb, nuclear. A bomb that releases explosive energy either through nuclear fission or nuclear fusion. This term is applied either to the atomic bomb or the hydrogen bomb.

booster. Assembly of metal parts and explosive charge provided to augment the explosive component of a fuze, to cause detonation of the main explosive charge of the munition. May be an integral part of the fuze. The explosive in the booster must be sufficiently sensitive to be actuated by the small explosive elements in a fuze, and powerful enough to cause detonation of the main explosive filling.

brisance. The ability of an explosive to shatter the medium which confines it; the shattering effect of the explosive. (Adjective: brisant.)

bullet, incendiary. A bullet having an incendiary charge, used especially against flammable targets.

C

***calorimetric* test.** As applied to interior ballistics, the use of a calorimeter to determine the thermochemical characteristics of propellants and explosives. The properties normally determined are heat of combustion, heat of explosion, heat of formation, and heat of reaction.

casualty agent. A toxic or lethal chemical agent that can be used effectively in the field.

casualty criteria. Standards by means of which may be classified the ability of ammunition items, or fragments therefrom, to inflict disabling wounds on personnel.

casualty gas. War gas capable of producing serious injury or death when used in effective concentrations.

CEP (*abbr.*) Circular probable error. The original expression appears to have been circular error probability.

chaff, countermeasures. A thin, flat, piece of metal foil, plain or backed, specifically designed to act as a countermeasure against enemy radar when released into the atmosphere.

Chapman-Jouguet plane. For a hypothetical, infinite-plane detonation wave: A moving reference plane, behind the initial shock front, in which it is variously assumed that: (a) reaction (and energy releases) has been effectively completed; (b) reaction product gases have reached thermodynamic equilibrium; (c) reaction gases, streaming backward out of the detonation, have reached such a condition that a forward-moving soundwave located at this

precise plane would remain a fixed distance behind the initial shock.

charge. 1. A given quantity of explosive either by itself, or contained in a bomb, projectile, mine, or the like, or used as the propellant for a bullet or projectile. 2. That with which a bomb, projectile, mine, or the like is filled, as a charge of explosive, thermite, etc. Also called the "fill," "filler," or "filling." 3. In small arms, a cartridge or round of ammunition. 4. To fill with a charge. 5. To place a charge in a gun chamber.

charge, bare. An explosive charge without casing, prepared for use in determining explosive blast characteristics.

charge, bursting. The main explosive charge in a mine, bomb, projectile, or the like that breaks the casing and produces fragmentation or demolition.

charge, cased. 1. Propelling charge within a cartridge case. 2. Any explosive charge within a case, as opposed to a bare charge.

charge, shaped. (SC) An explosive charge with a shaped cavity. Sometimes called cavity charge. Called hollow charge in Great Britain. Use of the term shaped charge generally implies the presence of a lined cavity.

chemical agent. *military.* A chemical item either solid, liquid, or gas divided into three principal categories: war gases, smokes, and incendiaries. It is developed for the purpose of conducting defensive and/or offensive warfare. Through its chemical properties it produces: lethal, injurious, or irritant effects resulting in casualties; a screening or colored smoke; or acts as an incendiary agent.

chronograph. 1. *general.* An instrument for measuring time. 2. As applied to ballistics, an instrument for determining velocity by measuring the time required for a projectile to travel a known distance, thus furnishing the data for determination of the velocity. A complete chronograph usually consists of two main systems: one for detecting the projectile as it passes two (or more) points whose distance apart and distance from the muzzle are known accurately; and a second system for recording these passages on a time scale, thus supplying information that is readily converted into velocity. The velocity obtained in this manner is the average velocity between the recorded points. This is converted to muzzle velocity by adding to it the velocity lost, which is obtained from tables or charts which take into account the form factor (shape) of the projectile and the distance which it has traveled.

circular error. 1. A bombing error measured by the radial distance of a point of bomb impact, or mean-point of impact, from the center of the target, excluding gross errors. 2. With an airburst atomic bomb, this is the bombing error measured from the point on the ground, immediately below the bomb burst, to the desired ground zero. *See:* **ground zero.**

circular probable error. (CEP) 1. The probable bombing error expressed in terms of the radius of a circle centered on the desired mean point of impact (DMPI) of a bombfall, and containing half of the expected bombfall, excluding gross errors; also sometimes applied to the actual bombing error. 2. With an airburst atomic bomb, this is the probable bombing error expressed in terms of the radius of a circle centered upon the desired ground zero (DGZ), the radius from that point being projected horizontally to the point below the bomb burst. Gross errors are also excluded in atomic bombing. 3. With reference to guided missiles, this is a probable error expressed in terms of the radius of a circle within which one-half of a given number of missiles can be expected to fall. Gross errors are usually excluded. *See:* **CEP.**

cobalt bomb. *See:* **bomb, cobalt.**

complete penetration. 1. In Army terminology, penetration obtained when the projectile in the target, or light through the target, can be seen from the rear of the target. 2. In Navy terminology, penet -

tion obtained when the projectile passes through the target intact, or a major portion of the projectile passes through. 3. Protection complete penetration (which see).

controls. A general term applied to the means provided to enable the pilot to control the speed, direction of flight, attitude, power, etc., of an aircraft control surface.

control surface. 1. In a broad sense, any movable airfoil used to guide or control an aircraft, guided missile, or the like in the air, including the rudder, elevators, ailerons, spoiler flaps, trim tabs, and the like. 2. In restricted usage, one of the main control surfaces; i.e., the rudder, an elevator, or an aileron.

cover function. A function of the presented area of a target, based upon the shielding or cover afforded the target by the surrounding terrain.

critical mass. The minimum mass of a fissionable material, when related to a specific shape and environment, necessary to sustain a nuclear chain reaction.

D

damage. (dam.) 1. An injury short of complete destruction inflicted upon persons, equipment, or installations. 2. To cause damage, sense 1. 3. *See:* damage categories.

damage assessment. The result of examination of combat materiel, particularly aircraft and armored vehicles, after a simulated attack, to determine the category in which the damage resulting from the attack would be placed. *See:* damage categories. By the assessment, the individual or team making the examination, determine as accurately as possible the probability, in percentage points, that the inflicted damage would produce a result corresponding to a certain damage category.

damage categories. Two damage category classifications, applying to combat materiel subject to attack, have been accepted for use in evaluation damage and damage potential of ammunition. The first classification, applied to aircraft, employs the following damage evaluation terms:

K damage—damage such that the aircraft will fall out of control immediately after the damage occurs.

KK damage—damage such that the aircraft will disintegrate immediately after the damage occurs.

A damage—damage such that the aircraft will fall out of control within five minutes after damage occurs.

B damage—damage such that the aircraft will be unable to return to its base.

C damage—damage that will prevent the aircraft from completing its mission. The second classification, applied to armored vehicles, employs the following damage evaluation terms:

K damage—damage that will cause the vehicle to be destroyed.

F damage—damage causing complete or partial loss of the ability of the vehicle to fire its main armament and machine guns.

M damage—damage causing immobilization of the vehicle.

damage radius. 1. The distance at which, in terms of experience or theoretical calculations, certain types of damage can be expected from a specified type of explosive item. 2. Atomic explosion—the distance from ground zero at which there is a 50 percent probability that a target element susceptible to the weapon effect considered will be damaged.

decay. The spontaneous disintegration of radioactive nuclei to a more stable form, generally accomplished by the emission of particles and/or gamma radiation. Decay also refers to the decrease in intensity of radioactivity with passage of time.

decay factor. A constant which is multiplied by the value of dose rate at one hour, to give the rate at some other time.

desired ground zero. (DGZ) For a surface burst, the point on the earth's surface where atomic detonation is desired. For

an air burst or underground burst, the point is on the earth's surface directly below or directly above the desired point of detonation.

detonation. An exothermic chemical reaction that propagates with such rapidity, that the rate of advance of the reaction zone into the unreacted material exceeds the velocity of sound in the unreacted material; that is, the advancing reaction zone is preceded by a shock wave. A detonation is classed as an explosion. The rate of advance of the reaction zone is termed detonation rate or detonation velocity. When this rate of advance attains such a value that it will continue without diminution through the unreacted material, it is termed the stable detonation velocity. The exact value of this term is dependent upon a number of factors, principally the chemical and physical properties of the material. When the detonation rate is equal to or greater than the stable detonation velocity of the explosive, the reaction is termed a high-order detonation. When the detonation rate is lower than the stable detonation velocity of the explosive, the reaction is termed a low-order detonation.

detonation front. The reaction zone of a detonation.

detonation wave. The shock wave which precedes the advancing reaction zone in a high-order detonation.

detonator. An explosive train component which can be activated by either a nonexplosive impulse, or the action of a primer, and is capable of reliably initiating high-order detonation in a subsequent, high-explosive component of train. When activated by a nonexplosive impulse, a detonator includes the function of a primer. In general, detonators are classified in accordance with the method of initiation, such as percussion, stab, electric, flash, etc.

DGZ (*abbr.*) Desired ground zero.

discarding petal. A part of a discarding sabot in which the sabot is composed of a base and attached pieces extending from it. These pieces, called petals, surround the core. They peel back under centrifugal and aerodynamic forces and are discarded just in front of a gun muzzle.

discarding sabot. *See:* **sabot.**

dose. The total amount of nuclear radiation received by an individual, expressed in roentgens. Usually used to mean total dose. Also expressed as RAD (which see).

dose rate. A measurement of the intensity of persistent or residual radio-activity expressed in terms of roentgens per hour. Also expressed as RAD.

drag force or component. (stress analysis) A force or component, in the drag direction; i.e., parallel to the relative wind.

dynamic pressure. *See:* **pressure, dynamic.**

dynamics. A branch of mathanics that treats of the motion of bodies, and of the forces acting upon bodies in motion or in process of changing motion.

dynamite. A high explosive, consisting of nitroglycerin and/or nitroglycol and/or ammonium nitrate and other materials with or without an inert base, packed in cylindrical paper cartridges or in bags. It is set off by a detonator and is generally used to break rocks, move dirt, or demolish buildings.

E

electronic countermeasures. (ECM) Usually pl. Any of various offensive or defensive tactics using electronic and reflection devices to reduce the military effectiveness of enemy equipment, or tactics, employing or affected by electromagnetic radiations.

electronic jamming. An action involved in electronic countermeasures, being the radiation or re-radiation of electromagnetic waves to impair the use of a specific segment of the radio spectrum. Usually shortened to "jamming."

energy, radiant. Energy consisting of electromagnetic waves, such as light, infrared, radio, and radar.

explosion. (explo) 1. A chemical reaction or change of state, effect in an exceed-

ingly short space of time, with the generation of a high temperature and, generally, a large quantity of gas. An explosion produces a shock wave in the surrounding medium. 2. Now also used with reference to the explosive effects of nuclear weapons. 3. In general sense, any violent bursting or expansion, with noise, following a sudden production of great pressure or a release of great pressure.

explosion, chemical. *See:* **explosion, sense 1.**

explosive. (explo) 1. A substance or mixture of substances which may be made to undergo a rapid chemical change, without an outside supply of oxygen, with the liberation of large quantities of energy, generally accompanied by the evolution of hot gases. Explosives are divided into two classes, high explosives, and low explosives, according to their rate of reaction in normal usage. Certain mixtures of fuels and oxidizers that can be made to explode are considered to be explosives. However, a substance such as a fuel which requires an outside source of oxidizer to explode, or an oxidizer which requires an outside source of fuel to explode, is not considered an explosive. 2. Now used loosely with reference to nuclear weapons.

explosive, conventional. A nonatomic explosive.

F

fallback. That part of the material carried into the air by an atomic explosion that ultimately drops back to the earth, or water, at the site of the explosion.

fallout. The process of precipitation to earth of particulate matter from an atomic cloud; also applied in a collective sense to the particulate matter itself. Although not necessarily so, such particulate matter is generally radioactive.

fallout area. The area on which radioactive materials have settled out, or the area on which it is predicted from weather conditions that radioactive materials may settle out.

film badge. A photographic film packet to to be carried by personnel, in the form of a badge, for measuring and permanently recording (usually) gamma ray dosage.

fin stabilization. Method of stabilizing a projectile, as a rocket bomb or missile, during flight, by the aerodynamic use of protruding fins.

fission. Of radioactive material: To split apart within the atomic nucleus, as in, "cobalt would neither fission nor fuse."

fissionable. Of a material such as uranium: Subject to nuclear fission.

fission bomb. A bomb intended to derive its explosive force from nuclear fission. *See:* **bomb, atomic.**

fission, nuclear. The splitting of an atomic nucleus, as by neutron bombardment. *See:* **bomb, atomic.**

flash radiography. Method of high-speed, X-ray photography. Used in analysis of ammunition functioning.

flechette. 1. An aerial dart. 2. A small fin-stabilized missile, a large number of which can be loaded in artillery canister.

flutter. A vibrating and oscillating movement of a wing, control surface, or the like, caused by aerodynamic forces acting upon an airfoil or surface having elastic and inertial qualities.

form factor. Factor introduced into the ballistic coefficient of a projectile, based on the shape of the projectile. Sometimes called "coefficient of form." *See:* **ballistic coefficient.**

fragment. (frag) 1. A piece of an exploding or exploded bomb, projectile, or the like. 2. To break into fragments.

fragmentation. (frag) A term applied to ammunition, indicating that the item is primarily intended to produce a fragmentation effect.

fragmentation test. Test conducted to determine the number and weight distribution, and where the method used permits, the

velocity and spatial distribution, of the fragments produced by a projectile or other munition upon detonation. Recovery of fragments, without determination of velocity or spatial distribution, can be accomplished by fragmenting in sand or sawdust, or over water. Determination of velocity and spatial distribution requires elaborate recovery means and instrumentation.

fragment density distribution. The number of fragments per unit solid angle (steradian).

fragment mass distribution. Spectrum of fragment weights produced by a shell or warhead.

fuse. (not to be confused with the term fuze) 1. An igniting or explosive device in the form of a cord, consisting of a flexible fabric tube and a core of low or high explosive. Used in blasting and demolition work, and in certain munitions. Fuse with black powder or other low explosive core is called: fuse, blasting, time. Fuse with PETN or other high explosive core is called: cord, detonating. 2. An electrical fuse.

fuselage. The body, of approximately streamline form, of an aircraft or missile. It is the part to which the tail unit and wings (if included) are attached.

fusion. 1. *atomic energy.* Fusion, nuclear. 2. *optics.* The mental blending of the right and left eye images into a single, clear image by stereoscopic action.

fusion, nuclear. The fusing or uniting of the atomic nuclei of an isotope, as those of deuterium, to form other nuclei under the influence of intense heat. *See:* bomb, hydrogen.

fuze. 1. A device with explosive components designed to initiate a train of fire or detonation in an item of ammunition, by an action such as hydrostatic pressure, electrical energy, chemical action, impact, mechanical time, or a combination of these. Excludes: fuse (as modified). 2. A non-explosive device designed to actuate another component by atmospheric pressure and/or temperature change, electrical energy, chemical action, physical impact, acceleration and/or deceleration forces, electromagnetic waves or pulses, and external forces. 3. To equip an item of ammunition with a fuze.

G

gain. 1. *radio.* In an amplifying system, the increase of output power, voltage, or current over the input power, voltage, or current, expressed in terms of a ratio. 2. *radar.* The difference, expressed as a ratio, between the power radiated by a directional antenna and the power radiated by an isotropic antenna, when both have an equal power output.

gelatin block. A block of transparent gelatin, the consistency of which is approximately similar to human tissue. It is used to compare the lethality of bullets, fragments, and flechettes.

Geneva Convention. An international agreement dealing with the humane treatment of combatants and noncombatants in time of war. The original Convention, signed at Geneva in 1864, concerned wounded soldiers and prisoners of war. Later amendments and revisions extended the provisions to victims of maritime actions and to civilian populations. In 1949 existing provisions were reformulated into four conventions for the protection of war victims. The U. S. has been a signatory of the successive conventions, and since 1864 the Convention has been the charter of the International Red Cross.

grenade. A small exposive or chemical missile, originally designed to be thrown by hand, but now also designed to be projected from special grenade launchers, usually fitted to rifles or carbines. Grenades may be classified in a broad sense as: grenade, hand; and grenade, rifle. Many varieties and variations of these have been used, including a number of improvised ones.

ground zero (GZ). The point on the earth's surface at which, above which, or below

which, an atomic detonation has actually occurred.

guided missile. An unmanned self-propelled vehicle, with or without a warhead designed to move in a trajectory or flight path all or partially above the earth's surface, and whose trajectory or course, while in flight, is capable of being controlled remotely, or by homing systems, or by inertial and/or programmed guidance from within. Excludes drones, torpedos, and rockets and other vehicles whose trajectory or course cannot be controlled while in flight.

gun. 1. *General.* A piece of ordnance consisting essentially of a tube or barrel, for throwing projectiles by force, usually the force of an explosive, but sometimes that of compressed gas, spring, etc. The general term embraces such weapons as are sometimes specifically designated as gun, howitzer, mortar, cannon, firearm, rifle, shotgun, carbine, pistol, revolver. 2. *Specif.* A gun with relatively long barrel, usually over 30 calibers, with relatively high initial velocity, and capable of being fired at low angles of elevation.

Gurney constant. A factor for use in Gurney formulas, which is constant for each explosive, but which varies with different explosives. It is expressed in feet per second. *See:* **Gurney formulas.**

Gurney formulas. A series of formulas, each formula corresponding to a particular geometry of the container, which enables quite accurate prediction of the initial fragment velocity. The velocity is dependent on the geometry, the explosive used, and the ratio of the explosive charge and metal weights.

GZ (*abbr.*). Ground Zero.

H

HE (*abbr.*). High explosive.

HEAT, HE, AT (*abbr.*). (often pronounced as a word) Originally an abbreviation for high explosive antitank. A term used to designate high explosive ammunition containing a shaped charge. *See:* **charge, shaped.**

HEP (*abbr.*). (often pronounced as a word) An abbreviation for high-explosive plastic, sometimes called a "squash charge". A term used to designate ammunition (usually used against tanks and reinforced structures) which resembles an ordinary HE shell, but the explosive component is a plastic explosive. This plastic deforms on impact, resulting in an intimate contact of the explosive with the target surface, thereby causing much greater shock waves than other types of explosives, resulting in spalling of the opposite surface.

high explosive. (HE) An explosive which, when used in its normal manner, detonates rather than deflagrating or burning; that is, the rate of advance of the reaction zone into the unreacted material exceeds the velocity of sound in the unreacted material. Whether an explosive reacts as a high explosive or as a low explosive depends on the manner in which it is initiated and confined. For example, a double-base propellant when initiated in the usual manner is a low explosive. However, this material can be made to detonate if the propellant is initiated by an intense shock. Conversely, a high explosive like TNT, under certain conditions, can be ignited by flame and will burn without detonating. High explosives are divided into two classes: primary high explosives and secondary high explosives, according to their sensitivity to heat and shock.

high-order detonation. *See:* **detonation.**

I

illuminant composition. A mixture of materials suitable for use in the candle of a pyrotechnic device, having production of high intensity light as its principal function. The materials used include a fuel (reducing agent), an oxidizing agent, and a binder, plus color intensifier and waterproofing agent. The mixture is loaded

under pressure in a container to form the illuminant candle.

illuminating. Indicates, in ammunition nomenclature, that the munition is intended primarily for illuminating purposes. Usually contains a flare, and may contain a parachute for suspension in the air.

impulse. A vector quantity defined by the time integral of the force F acting on a particle over a finite interval,

for example, $\int_{t_1}^{t_2} F dt$

for the interval from t_1 to t_2.

Specifically, with respect to blast waves, "impulse" refers to the time integral of pressure.

initial radiation. The nuclear radiation accompanying an atomic explosion and emitted from the resultant fireball; immediate radiation. It includes the neutrons and gamma rays given off at the instant of the explosion, and the alpha, beta, and gamma rays emitted in the rising fireball and the column of smoke. In contrast to residual radiation, its delivery to persons and objects on the earth's surface is terminated by the removal of the source (fission products in the atomic cloud), from within effective radiation range of the earth, by the rising cloud.

J

jam. 1. Of a machine gun, full-automatic, semiautomatic or other firearm: To stick or become inoperative because of improper loading, ejection, or the like. 2. To make the transmissions of a radio unintelligible; to make a radio or radar set ineffective, either by the use of counter-transmissions or by the use of a confusion reflector. *See:* electronic jamming.

jet. 1. As pertains to shaped charge ammunition: a. From a lined charge: The slender, generally fastest-moving part of a liner after collapse. b. From an unlined shaped charge: The central stream of high-velocity gases produced upon detonation. 2. A jet engine. 3. A jet airplane

jet breakup. As pertains to shaped charge ammunition: Breaking of jet into discrete particles. The time of breakup is a factor in effective penetration. Bifurcation: radial breakup of the jet into two distinct jets. Polyfurcation: radial breakup of the jet resulting in three or more distinct jets.

K

Kelvin scale. (K) A temperature scale that uses centigrade degrees, but makes the zero degree signify absolute zero. In this scale, water freezes at plus 273.16 degrees and boils at 373.16 degrees. This scale is named after the first Baron Kelvin (1824-1907), an English mathematical physicist.

kiloton. (KT) Refers to the energy released of a thousand tons of TNT, where 1 ton equals 2,000 pounds, and where the energy content of TNT is defined as 1,100 calories/gram.

kinetic energy ammunition. Ammunition designed to inflict damage to fortifications, armored vehicles, or ships by reason of the kinetic energy of the missile upon impact. The damage may consist of shattering, spalling (which see), or piercing. The missile may be solid, or may contain an explosive charge intended to function after penetration.

Kirkwood-Brinkley's theory. In terminal ballistics, a theory formulating the scaling laws from which the effect of blast at high altitudes may be inferred, based upon observed results at ground level. *See:* scaling law, and Sach's theory.

L

lethal area. In terminal ballistics, a figure of merit, having the dimension of area, which permits prediction of the number of casualties a missile may be expected to produce when employed under specified conditions. An equation has been evolved stating the relationship between the lethal area and the numerous factors affecting its numerical value.

lethality criteria. *See:* casualty criteria.

low-order detonation. *See:* detonation.

M

Mach front. A Mach stem.

Mach stem. A shock wave or front formed above the surface of the earth by the fusion of direct and reflected shock waves resulting from an airburst bomb. Also called "Mach wave" and "Mach front."

megaton. (MT) Refers to the energy release of a million tons of TNT (10^{15} calories).

Mev (*abbr.*). Million electron-volts. Sometimes abbr. MEV.

mine. 1. An encased explosive or chemical charge designed to be placed in position so that it detonates when its target touches it, or moves near it, or when touched-off by remote control. General types are: land mine, and underwater mine. 2. An explosive charge placed in a subterranean tunnel under a fortification. 3. To place mines or prepared charges.

missile (msl). 1. Any object that is, or is designed to be, thrown, dropped, projected, or propelled, for the purpose of making it strike a target. 2. A guided missile (which see). 3. A ballistic missile (which see).

Mismay-Schardin effect. The acceleration of a solid end-plate (usually metal) from the face of an explosive charge under detonation, such that the end-plate remains a solid and is usable as a missile.

monocoque. A type of airplane construction in which the skin of the fuselage bears the primary stresses arising in the fuselage.

N

Napalm. (NP) 1. Aluminum soap in powder form, used to gelatinize oil or gasoline for use in Napalm bombs or flame throwers. 2. The resultant, gelatinized substance.

nuclear energy. Energy held within the nucleus of an atom, released in part in certain other elements by the process of nuclear fusion. In the restrictive sense, that part of this energy that is released by fission or fusion. In nuclear fission, the energy released comes from the atomic nucleus being split, resulting in the emission of nuclear particles, such as neutrons, the alpha particle, or the beta particle. In nuclear fusion, the combining atomic nuclei fail to utilize their entire atomic mass in forming the new nucleus, the unused mass being converted into energy.

nuclear fission. *See:* **fission, nuclear.**

nuclear fusion. *See:* **fusion, nuclear.**

nuclear weapon. A bomb, projectile, missile, or the like that carries a nuclear warhead. Also, the warhead itself.

O

ogive. The curved or tapered front of a projectile. As a geometrical body, a convex solid of revolution in which the generating area is bounded by an arc of a circle, the center of which lies on the side of the axis of revolution opposite to the arc. When applied to a projectile contour, the radius of the arc is expressed in calibers, such as a "7-caliber ogive." With a bullet, bomb, or other projectile having a fuze forming the nose, the ogive is included between a point where the projectile begins to curve, or taper, and a point on the line where fuze and body meet. In other types of projectiles, the nose of the projectile is included as a part of the ogive.

Ordnance Proof Manual. (OPM) A manual whose purpose is to simplify, codify, and standardize proof technique and to provide a guide for those who plan, execute, or analyze proof work on ordnance materiel. The manual includes a discussion, in detail, of basic principles, related facts, and specific instructions relating to: classification of tests; examples of test programs on all classes or types of ordnance materiel; proof technique, including the detail operation of proof facilities; the methods of reductions of proof data, calculations performed, the evaluation of tests, and instructions for preparation of proof reports.

overmatching plate. Armor plate whose thickness exceeds the diameter of the projectile.

overmatching projectile. A projectile whose diameter exceeds the thickness of the armor plate.

P

partial penetration. Penetration obtained when a projectile fails to pass through the target far enough for either the projectile itself, or light from its penetration, to be seen from the back of the target; Army partial penetration. *See:* complete penetration, protection complete penetration.

passive armor. A protective device against shaped charge ammunition. Designed to absorb the energy of a shaped charge. Examples: spaced armor, homogeneous materials, plastic armors, composite designs.

peak overpressure. The highest overpressure resulting from the blast wave. Peak overpressures near the fireball of an atomic explosion are very high, but drop off rapidly as the blast wave travels along the ground outward from ground zero.

penumbra. The space of partial illumination, as in an eclipse, between the umbra (perfect shadow) and the full light.

piezoelectric. The property of certain crystals to develop electrical charge or potential difference across certain crystal faces, when subjected to a strain by mechanical forces or, conversely, to produce a mechanical force when a voltage is applied across the material. Examples of piezoelectric materials are quartz, tourmaline, Rochelle salts, and barium titanate.

pitch. An angular displacement about an axis parallel to the lateral axis of an airframe or vehicle.

presented area. That area of a target normal to the flight path of a projectile.

pressure, dynamic. The pressure exerted by a gas, liquid, or solid solely by virtue of its relative motion when it strikes an object. For example, in a pitot-static tube, dynamic pressure is that part of the impact pressure derived from the relative motion of the air, as distinguished from that derived from atmospheric pressure.

primary blast injuries. Those injuries incurred as a direct result of the pressures of the blast or shock wave.

projectile. (proj) 1. *General.* A body projected by exterior force and continuing in motion by its own inertia. 2. *Specif.* A missile (which see) for use in any type of gun (which see). In the general sense, the term is sometimes applied to rockets and guided missiles, although they may not fall within the stated definition. In sense 2, the term projectile is preferred over shell, shot, and the like, in official nomenclature.

projectile, arrow. A relatively long projectile which is designed to be fired from a gun of a caliber considerably larger than the diameter of the projectile body. It is stabilized by fins having a span approximately that of a caliber of the gun. This design is made for the purpose of increasing the velocity, to decrease the time of flight, and/or increase the striking energy of the projectile.

protection complete penetration. Penetration in which a fragment or fragments of either the impacting projectile or the plate are thrown to the rear of the plate with sufficient energy to perforate a .020-inch aluminum-alloy, 24ST, sheet, or its equivalent, when placed so as to receive those fragments passing from the rear of the plate. The "Protection Criterion." When it is possible to observe that these conditions are being met without the use of the sheet, as in heavier plate testing, the sheet may be omitted.

protection partial penetration. Penetration which approaches but does not fulfill the requirements for protection complete penetration.

R

RAD. (from radiation absorbed dose) A unit of absorbed dose of ionizing radiation. The RAD, 100 ergs/gram, is a measure of the energy imparted to matter by ionizing radiation, per unit mass of irradiated material, at the place of interest.

radiation. 1. The transmission of energy through space in the form of electronic waves. 2. *Nuclear radiation.*

radiation absorbed dose (dosage). (RAD) The total quantity of ionizing radiation absorbed by an individual or any mass of material exposed to radiation. If the radiation is X, or gamma, and the mass is free air, the unit of measure is the roentgen.

radiation dosage. Total quantity of radiation to which a person is exposed over a period of time. It is measured in roentgens.

radiation dose rate. The radiation dose (dosage) absorbed per unit time. The common unit of measure for X or gamma radiation is roentgen or milliroentgen per hour.

radiation intensity. The amount of radiant energy, per unit time, passing through a unit area perpendicular to the line of propagation, at the point in question. This term is often used incorrectly when dose rate is intended.

radiography. Nondestructive examination of matter by means of X-rays or gamma rays. The rays are permitted to impinge on a fluorescent screen for temporary work, or photographic film for permanent record. Used in metal industry, research, and analysis, for purposes such as determining the soundness of castings and welded joints.

radiological warfare. The employment of agents or weapons to produce residual radioactive contamination, as distinguished from the initial effects of a nuclear explosion (blast, thermal, and initial nuclear radiation).

Rankine scale. (R) A thermometer scale which uses Fahrenheit degrees, with zero as absolute zero of the Fahrenheit scale. The freezing point of water is 491.69 degrees.

rarefaction. In an atomic bomb explosion, a condition existing at the center of the explosion, in which the pressure, after a rise induced by the explosion, drops below that which existed prior to the explosion.

rarefaction wave. A pressure wave, or rush of air or water, induced by rarefaction. The rarefaction wave (also called a suction wave) travels in the opposite direction to that of the shock wave directly following the explosion.

raster. A system of lumineacent lines traced on the phosphor of a cathode-ray tube by motion of the cathode-ray beam. The changes of brightness in the lines produce a picture as a television picture or a radar map. This word is of German origin and is used particularly in television.

REM (*abbr.*). Roentgen equivalent mammal.

residual radiation. Nuclear radiation emitted by the radioactive material deposited after an atomic burst, or after an attack with radiological warfare agents. Following an atomic burst, the radioactive residue is in the form of fission products, unfissioned nuclear material, and material, such as earth, water, and exposed equipment, in which radioactivity may have been induced by neutron bombardment.

rocket. An unmanned, self-propelled vehicle with or without a warhead, designed to travel above the surface of the earth, and whose trajectory or course, while in flight, cannot be controlled. Excludes guided missile and other vehicles whose trajectory or course, while in flight, can be controlled remotely, or by homing systems, or by inertial and/or programmed guidance from within.

roentgen. A measure of ionization produced by X-ray or gamma radiation. The unit of measurement of radiation in terms of its effect on human beings. This is technically defined as the amount of X or gamma radiation which as a result of ionization will produce, in 1 cubic centimeter of dry air at standard conditions of temperature and pressure, ions carrying 1 electrostatic unit of electricity of either sign.

roentgen equivalent mammal. (REM) The quantity of any type of ionising radiation which, when absorbed by a mammal, produces an effective equivalent to the ab-

sorption by the mammal of one roentgen of X or gamma radiation.

roll. An angular displacement about an axis parallel to the longitudinal axis of an airframe or a missile.

S

sabot. Lightweight carrier in which a subcaliber projectile is centered to permit firing the projectile in the larger caliber weapon. The sabot diameter fills the bore of the weapon from which the projectile is fired. One type of sabot, discarded a short distance from the muzzle, is known as a "discarding sabot." A sabot is used with a high velocity armor-piercing projectile having a tungsten carbide core; in this case, the core may be considered as the subcaliber projectile.

Sach's theory. An alternate theory to Kirkwood-Brinkley's theory, embodying scaling laws by which the effect of blast at high altitudes may be inferred from the results at ground level.

scaling law. A formula which permits the calculation of some property for a given article based on data obtained from a similar, but different size, article; e.g., crater size, nuclear radiation, etc., for a nuclear warhead of any yield, from the known values for another yield.

secondary blast injuries. Those injuries sustained from the indirect effects of a blast; such as falling rubble from a collapsed building, or missiles (debris or objects) which have been picked up by the blast winds generated and hurled against an individual. Also includes injuries resulting from individuals being hurled against stationary objects.

shock resistance. Armor. That property which prevents cracking or general rupture when impacted by fragments, irregular projectiles, or glancing blows from overmatching projectiles. *See:* shock test.

shock test. Armor plate. The test to determine if the armor will fail under impacts of overmatching projectiles. Also called ballistic shock test.

shock wave. The steep, frontal compression, or pressure discontinuity, rapidly advancing through a medium as the consequence of a sudden application of pressure to the medium. Its form depends on the magnitude of the pressure, and the displacement of the medium, as the wave progresses. In soil, the shock wave is commonly referred to as the ground shock; in water, the water shock; and in air, the air blast or blast wave.

shock wave, reflected. A shock wave resulting from an explosion, especially from the explosion of an airburst bomb, which is reflected from a surface or object.

shot. 1.a. A solid projectile for cannon, without a bursting charge. b. A mass or load of numerous, relatively small, lead pellets used in a shotgun, as birdshot or buckshot. 2. That which is fired from a gun as "the first shot was over the target." In sense 1.a., the term "projectile" is preferred for uniformity in nomenclature.

side spray. Fragments of a bursting projectile thrown sidewise from the line of flight, in contrast with base spray, thrown to the rear, and nose spray, thrown to the front.

skirting armor. *See:* skirting plate, spaced armor.

skirting plate. A thin plate, which is spaced a considerable distance in front of the main armor plate and which acts as a passive form of resistance to the jet of shaped charge ammunition.

spaced armor. An arrangement of armor plate, using two or more thicknesses, each thickness spaced from the adjoining one. Used as protective device, particularly against shaped charge ammunition.

spall. Fragment(s) torn from either surface of armor plate, such as might result from the impact of kinetic energy ammunition or the functioning of shaped charge ammunition.

spalling. Production of a spall(s).

spall resistance. That property of armor which prevents the armor from projecting spalls into the armored vehicle when struck by a projectile.

spar. Any principal structural member in an airfoil; esp. in a wing, running from tip to tip or from root to tip.

spectroscope. An optical instrument designed to break up the light from a source into its constituent wave lengths for the observation of spectra, thus providing a means of qualitative or quantitative study of the spectrum formed. The instrument essentially consists of a slit, a lens system, a dispersion system, and an observation system.

spin stabilization. Method of stabilizing a projectile during flight by causing it to rotate about its own longitudinal axis.

stabilizer. Any airfoil, or any combination of airfoils considered as a single unit, the primary function of which is to give stability to an aircraft or missile.

Standard Atmosphere. Since the resistance of the air to a projectile depends upon the wind, the density, and the temperature, it is convenient to assume, as a point of departure in computing firing tables, a wind, density and temperature structure for this purpose. A sort of average or representative air structure so derived is called "a standard atmosphere." The standard atmosphere for the United States Armed Services is the U. S. Standard Atmosphere, which is that of the International Civil Aviation Organization (ICAO). This standard atmosphere assumes a ground pressure of 760 millimeters of mercury and a ground temperature of 15° C. The temperature throughout the troposphere, that is, the region where turbulent mixing takes place, extending up to 11 kilometer, is given by the formula

$$\text{absolute temperature } T\ (^\circ\text{ K}) = 288.16 - 6.5\,H$$

where H is the height above sea level measured in kilometers. In the stratosphere, extending from 11 kilometers to 25 kilometers, the temperature is assumed to be a constant 216.66° K. Above the stratosphere, other laws are assumed. Although the ICAO atmosphere makes no assumptions about wind structure, for firing table purposes it is assumed that there is no wind.

standard deviation. In the field of testing, a measure of the deviation of the individual values of a series from their mean value. The standard deviation is expressed algebraically by the formula

$$\sqrt{\frac{\Sigma x^2}{N}}$$

where Σ (sigma) means the sum of, x equals the deviation from the mean, and N equals the number of scores or individuals in the distribution. For example, let us assume a distribution of 5, with scores of 2, 4, 6, 8, and 10. The mean of these scores is 6, the deviations −4, −2, 0, +2, and +4. Each, squared, gives 16, 4, 0, 4, and 16. The sum of these is 40, which divided by 5 makes 8. The square root of 8 is 2.82. This is the standard deviation. Other methods of arriving at the standard deviation are used, but they go back to the formula shown.

standoff distance. The distance between the base of a shaped charge liner and the surface of a target.

T

terminal ballistics. The study of terminal ballistics is concerned with developing an understanding of the fundamental principles underlying the destructive effects of weapons on targets. Knowledge so gained is applied, offensively, to the improvement of various weapons systems, ranging from rifles and hand grenades carried by soldiers to nuclear warheads carried by ICBM's, and defensively, to the improvement of protective devices, such as body armor for soldiers, protective armor for ground, air-borne and space vehicles, and ground structures, permanent and tem-

porary. Both experimental and theoretical investigations are carried out in the fields of blast, detonation phenomena, penetration of fragments and bullets into various media under study, and ground shock, combustion, and nuclear radiation.

thermonuclear. Of or pertaining to nuclear reactions or processes caused by heat, esp. to nuclear fusion caused by the intense heat of an atomic bomb explosion. (*See:* fusion, nuclear.)

TNT. (*abbr*). Trinitrotoluene (trinitrotoluol). This explosive is better known by its abbreviation than by its chemical name. *See:* **trinitrotoluene.**

trinitrotoluene. (TNT) High explosive widely used as explosive filler in munitions and by engineers; trinitrotoluol; TNT.

tungsten carbide core. The heavy, hard core used in high-velocity armor-piercing type projectiles.

turbulence. A condition in the airflow about a wing, or other airfoil, in which different velocities and pressures are laterally mixed between layers of the airflow.

U

ultraviolet. Outside the visible spectrum, at the violet end; higher in frequency than visible light. The opposite of "infrared." Said of light, rays, frequencies; hence, "ultraviolet light."

V

vulnerable area. The product of: (1) the probability that a projectile striking a target will cause disabling damage; and (2) the presented area of the target.

W

war gas. Toxic or irritant chemical agent regardless of its physical state, whose properties may be effectively exploited in the field of war.

warhead. Rocket and guided missile: That portion which is the payload the vehicle is to deliver to a predetermined point in space and time. In a general sense, it includes the payload plus the missile section surrounding the payload, and its related components. In a specific sense, it refers to the payload only; in which case the complete missile payload assembly is called a warhead section. Warheads may be categorized as high explosive, chemical, nuclear, ballast, etc. In the case of nuclear warheads (sometimes referred to as special warheads), the term warhead refers to the nuclear weapon proper. This, along with the kit which adapts the nuclear weapon proper to the missile warhead application, and the missile warhead compartment, makes up the complete warhead section.

wave length. The distance traveled in one period or cycle by a periodic disturbance. It is the distance between corresponding phases of two consecutive waves of a wave train. A wave length is the quotient of velocity divided by frequency.

wave shaper. Pertaining to explosives, an insert or core of inert material, or of explosives having different detonation rates, used for changing the shape of the detonation wave.

wound ballistics. That portion of terminal ballistics specializing in the effect of bullets and fragments in wounding personnel, and in the factors producing disabling injuries. *See:* **casualty criteria.**

Y

yaw. 1. The angle between the direction of motion of a projectile and the axis of the projectile, referred to either as "yaw," or, more completely, as "angle of yaw." The angle of yaw increases with time of flight in an unstable projectile, and decreases to a constant value called the "yaw of repose," or the "repose angle of yaw," in a stable projectile. 2. Angular displacement about an axis parallel to the normal axis of an aircraft, guided missile or the like.

yield. Also known as energy yield. The total

673922 O-43—25

effective energy released in a nuclear (or atomic) explosion. It is usually expressed in terms of the equivalent tonnage of TNT required to produce the same energy release in an explosion. The total energy yield is manifested as nuclear radiation, thermal radiation, and shock (or blast) energy; the actual distribution being dependent upon the medium in which the explosion occurs (primarily), and also upon the type of weapon and the time after detonation.

INDEX

[redacted]